

Fall 12-21-2018

Pyrrolo[2,3-d]pyrimidine Classical Antifolates for Targeted Cancer Chemotherapy- Applications of Bioisosteric and Regioisomeric Substitutions for Improved Tumor-Selectivity and Potency

Manasa Punaha Ravindra

Follow this and additional works at: <https://dsc.duq.edu/etd>

 Part of the [Medicinal Chemistry and Pharmaceutics Commons](#)

Recommended Citation

Punaha Ravindra, M. (2018). Pyrrolo[2,3-d]pyrimidine Classical Antifolates for Targeted Cancer Chemotherapy- Applications of Bioisosteric and Regioisomeric Substitutions for Improved Tumor-Selectivity and Potency (Doctoral dissertation, Duquesne University). Retrieved from <https://dsc.duq.edu/etd/1747>

This One-year Embargo is brought to you for free and open access by Duquesne Scholarship Collection. It has been accepted for inclusion in Electronic Theses and Dissertations by an authorized administrator of Duquesne Scholarship Collection.

PYRROLO[2,3-*d*]PYRIMIDINE CLASSICAL ANTIFOLATES FOR TARGETED
CANCER CHEMOTHERAPY- APPLICATIONS OF BIOISOSTERIC AND
REGIOISOMERIC SUBSTITUTIONS FOR IMPROVED TUMOR-SELECTIVITY
AND POTENCY

A Dissertation

Submitted to the Graduate School of Pharmaceutical Sciences

Duquesne University

In partial fulfillment of the requirements for
the degree of Doctor of Philosophy

By

Manasa Punaha Ravindra

December 2018

Copyright by
Manasa Punaha Ravindra

2018

PYRROLO[2,3-*d*]PYRIMIDINE CLASSICAL ANTIFOLATES FOR TARGETED
CANCER CHEMOTHERAPY- APPLICATIONS OF BIOISOSTERIC AND
REGIOISOMERIC SUBSTITUTIONS FOR IMPROVED TUMOR-SELECTIVITY
AND POTENCY

By

Manasa Punaha Ravindra

Approved August 28, 2018

Aleem Gangjee, Ph. D.
Distinguished Professor of Medicinal
Chemistry
Graduate School of Pharmaceutical Sciences,
Duquesne University
(Committee Chair)

Marc W. Harrold, Ph. D.
Professor of Medicinal Chemistry
Graduate School of Pharmaceutical Sciences,
Duquesne University,
(Committee member)

Patrick T. Flaherty, Ph. D.
Associate Professor of Medicinal Chemistry
Graduate School of Pharmaceutical Sciences,
Duquesne University,
(Committee member)

Kevin Tidgewell, Ph. D.
Associate Professor of Medicinal Chemistry
Graduate School of Pharmaceutical Sciences,
Duquesne University,
(Committee member)

Lauren O'Donnell, Ph. D.
Associate Professor, Pharmacology
Graduate School of Pharmaceutical Sciences
(Committee member)

Carl Anderson
Associate Professor
Division Head, Pharmaceutical,
Administrative & Social Sciences
Graduate School of Pharmaceutical Sciences,
Duquesne University, Pittsburgh, PA

J. Douglas Bricker, Ph. D.
Dean, School of Pharmacy and the Graduate
School of Pharmaceutical Sciences
Duquesne University, Pittsburgh, PA

ABSTRACT

PYRROLO[2,3-*d*]PYRIMIDINE CLASSICAL ANTIFOLATES FOR TARGETED CANCER CHEMOTHERAPY- APPLICATIONS OF BIOISOSTERIC AND REGIOISOMERIC SUBSTITUTIONS FOR IMPROVED TUMOR-SELECTIVITY AND POTENCY

By

Manasa Punaha Ravindra

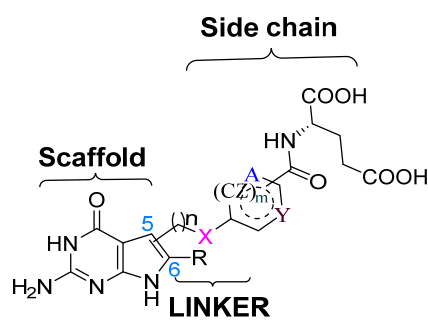
December 2018

Dissertation supervised by Dr. Aleem Gangjee

In 2018, it is estimated that 1,735,350 new cases of cancer and 609,640 deaths from the disease will be diagnosed in the United States alone. Conventional chemotherapy is by far the most successful category of clinical oncology, having cured (complete remission (CR), without return) or provided clinical benefit to millions of people. However, since its earliest discovery, the major causes of failure of conventional cancer chemotherapy have been dose-limiting toxicities and development of resistance. There is a desperate ongoing search for new cancer therapies as tumor-targeted agents (without harming normal cells or tissues) with low propensity for the development of resistance.

Clinically used antifolates methotrexate (**MTX**; DHFR inhibitor), pemetrexed (**PMX**; TS and GARFTase inhibitor), pralatrexate (**PTX**; DHFR inhibitor), and raltitrexed (**RTX**; TS inhibitor), have two major disadvantages: (1) dose-limiting toxicities due to

ubiquitous transport via the reduced folate carrier (RFC) and (2) drug-resistance; mutation and/or overexpression of RFC and target enzymes resulting in inadequate transport, reduced cellular retention, and decreased potency. However, two other folate transporters that are narrowly expressed in healthy tissue while overexpressed in many different types of cancer are the folate receptors (FRs) (epithelial ovarian cancer (EOC), NSCLC, renal, endometrial, colorectal, breast cancers, hematologic malignancies, etc.) and the proton-coupled folate transporter (PCFT) (ovarian and NSCLC). Our aim is to design classical antifolates for selective uptake by FRs and PCFT over RFC and inhibition of multiple folate metabolizing enzymes in their monoglutamate forms. Successful identification of such small molecule single agents will potentially (a) have tumor-targeting action and (b) combat resistance development.



General structure I

This dissertation discusses the bioisosteric and regioisomeric optimization of 5- and/or 6-substituted pyrrolo[2,3-*d*]pyrimidine antifolates for improved tumor-targeted activity. Molecular modeling with the help of known X-ray crystal structures of the transporters and the intracellular enzymes was used to rationalize the design of the analogs. NMR studies that were performed to provide structural evidence for the presence of a conformationally restricting intramolecular fluorine hydrogen bond have been described.

The dissertation also discusses the synthetic efforts for obtaining the pyrrolo[2,3-*d*]pyrimidine analogs with regioisomeric substitutions, modified linkers and bioisosteric replacements (general structure **I**) for selective uptake, and inhibition of one or more enzymes in the de novo purine and/or pyrimidine biosynthetic pathway. The present work identified that, depending on the regioisomeric position, fluorine substitution on the side-chain (het)aryl ring improves both potency as well as selectivity, most significantly towards PCFT-expressing cell lines. NMR-based structural evidence led to one of our hypotheses that entropic benefit due to conformational restriction caused by an intramolecular fluorine hydrogen bond may partly be responsible for improved biological activity. The current work led to the identification of a fluorinated pyrrolo[2,3-*d*]pyrimidine analog **184**, the most potent inhibitor of PCFT-expressing Chinese hamster ovarian (CHO) cells (PCFT4 IC₅₀ = 1.5 (0.4) nM). Another important contribution of the current work is the discovery of multi-enzyme inhibitor **201**, a C6-methylated version of the clinically used anticancer agent **PMX**, which showed selectivity over RFC (**PMX** PC43-10 IC₅₀ = 26.2 nM; **201** PC43-10 IC₅₀ > 1000 nM). Such selectivity can potentially help overcome the dose-limiting toxicities of **PMX**. The fluorinated and methylated analogs described herein are testimonials for the profound effects that minor structural changes can have on polypharmacology.

Dedicated to my family

ACKNOWLEDGEMENT

I would like to acknowledge and convey my gratitude to the individuals who were instrumental for the initiation, persistence and completion of my Ph.D. research. First and foremost, I am most grateful to my mother, P. R. Swarnalatha for her unconditional love and support. I would not have made this far if not for her sacrifices and protection. I owe my nature as well as nurture to my late grandfather V. R. Ramachary, grandmother V. R. Laxmi, my maternal uncle V. R. Srinivas, my aunt M. Sangeetha Raman and my late uncle M. S. Raman and I am eternally grateful to them for shaping my future. My deepest appreciation belongs to my beloved father P. K. Ravindra, for making me his number one priority, and making sure that my focus was always on my education while he took care of my day-to-day responsibilities. I will be forever indebted to my advisor, Professor Dr. Aleem Gangjee, for accepting me into his group, and for his guidance and support which made the research presented in this dissertation possible. I am indebted to him for his scientific guidance, training, and for the financial support by providing graduate assistantship.

I would also like to acknowledge the valuable lessons taught and suggestions provided from the Duquesne University faculty members: Dr. Michael Cascio, Dr. Lauren O'Donnell, Dr. Patrick T. Flaherty, Dr. Fraser Fleming, Dr. David J. Lapinsky, Dr. Marc W. Harrold, and Dr. Aleem Gangjee. I would like to express my gratitude to Dr. Kevin Tidgewell for agreeing to be a part of my committee during the tail end of my Ph.D. I cannot forget to express my gratitude towards the University of Pittsburgh chemistry faculty, Dr. Scott Nelson and Dr. Peter Wipf from whom I have learnt some of the most

interesting, relevant and invaluable lessons. I wish to express my sincere appreciation to Mary Caruso, Jackie Farrer, Nancy Hosni, Amelia Stroyne and Deborah Willson for their kind heart, help and assistance. The acknowledgements would not be complete without mentioning my friends, Suravi Chakrabarty, Dr. Shruti Choudhary, Arpit Doshi, Dr. Rishabh Mohan and Dr. Khushbu Shah who became my family and made my stay in Pittsburgh colorful. I am thankful to my friend, philosopher and guide Dr. Poovaiah Palangappa for coming into my life and sticking with me. I cannot forget to thank my friend and one man solution to every problem, Mohit Gupta. I would like to thank all of my graduate school friends, Dr. Shaili Aggarwal, Tanvir Ahmed, Ankur Dashputre, Dr. Taylor Gentile, Som Ghosh, Michele Herneisey, Farhana Islam, Krishna Kaku, Faqiang Liu, Shikhar Mohan, Md Junaid Nayeem, Saloni Patel, Dr. Sudhir Raghavan, Tasdique Mohammed Quadery, Dhruv Shah and Dr. Sameer Talwar for their irreplaceable help when I was in need and for all the stimulating discussions, and fun we had. I will carry the memories with me wherever I go henceforth. I am forever indebted to Dr. Roheeth Kumar Pavana, Dr. Nilesh Zaware and Dr. Ravi Kumar Devambatla Vyas who mentored me during several stages of my initial Ph.D. life. I would also like to thank Dr. James Drennen and the Graduate School of Pharmaceutical Sciences for financial support.

I would like to thank my cousin aunt, Prof. Uma Vuruputuri and her daughter Anupama Kande for being the beacon and sowing the seed in my mind to pursue Ph.D. in the USA and also for introducing Duquesne University to me. I would also like to thank my extended families in the United States with whom I have spent many a wonderful evening; My cousin uncles Venkata Ramana Chaganty and Venu Tirumalai, my cousin

aunts, Nalini Chaganty and Bargavi Tirumalai and finally my brother-in-law to be Vamsi Codadu and co-sister to be Praneeta Yellakarra.

I would like to convey my deepest and heartfelt gratitude to my partners in crime and my brothers Meghraj Ravindra and Prudhvi Bharat. It was their sacrifices, and support that gave me the strength to leave my family behind and move away for further studies.

Finally, I can never thank the city of Pittsburgh enough for not only introducing to me my closest of friends and family and for being my Utopia where I have become the person that I am today, but mainly for bringing into my life my favorite person, Dr. Neela Krushna Codadu. As I finish my graduate life, it gives me enormous amount of happiness and excitement to enter a new phase of life with him and explore the rest of our lives together.

TABLE OF CONTENTS

I.	BIOCHEMICAL REVIEW	1
II.	CHEMICAL REVIEW	58
III.	STATEMENT OF THE PROBLEM	80
IV.	CHEMICAL DISCUSSION	131
V.	EXPERIMENTAL	188
VI.	BIBLIOGRAPHY	276
VII.	APPENDIX	305

LIST OF TABLES

Table 1. Comparison of the affinities of RFC for different folates	9
Table 2. Cell proliferation assays with pyrrolo[2,3- <i>d</i>]pyrimidine antifolates.	21
Table 3. Comparison of the affinities of PCFT for different folates	23
Table 4. Cell proliferation assays with pyrrolo[2,3- <i>d</i>]pyrimidine antifolates.	29
Table 5. IC ₅₀ Values (nM) for 5-substituted pyrrolo[2,3- <i>d</i>]pyrimidine antifolates	56
Table 6. Key Properties and applications of the C–F Bond	86
Table 7. Cell proliferation assays with pyrrolo[2,3- <i>d</i>]pyrimidine antifolates.	95
Table 8. Changes in properties upon substitution of a CH (sp ²) group with an N (sp ²)	97
Table 9. Changes in relative angles of substitution and dipole moments	102
Table 10. Changes in volume and dipole moment upon bioisosteric replacement	104
Table 11. Changes in volume and dipole moment	106
Table 12. Changes in volume and dipole moment upon isosteric replacement	110
Table 13. Predicted bond angle variations of benzylic substitutions (X) in 194-197	117
Table 14. IC ₅₀ Values (nM) and FR-and PCFT-expressing CHO cell selectivity ratios	123
Table 15. Reaction conditions for the synthesis of 212 .	134
Table 16 The variation of $J_{(F-H)}$ in 179 with temperature	154
Table 17. Reaction conditions for the synthesis of 293 .	160
Table 18. Reaction conditions for the synthesis of 317 and 318 .	168
Table 19. Reaction conditions for the synthesis of 325-329 and 334 .	171
Table 20. Partial charges and p <i>K</i> _a of compounds 313 and 326-329	172
Table 21. Halogenating agents used for the synthesis of intermediates 373 and 380	184

Table 22. Reagents and conditions for the synthesis of intermediate 381 .	185
Table 23. Docked scores of proposed compounds	271

LIST OF FIGURES

Figure 1. The chemical structures of physiologically relevant folate derivatives	2
Figure 2. Biochemical transformations of folates.	3
Figure 3. RFC-, FR- and PCFT-mediated internalization of folates.	4
Figure 4. Compartmentalization of folate-mediated 1C metabolism.	5
Figure 5. Structures of classical antifolates.	7
Figure 6. Predicted and experimentally validated membrane topology of the hRFC.	10
Figure 7. Transcripts for RFC in (A) leukemia and (B) solid tumor cell lines.	12
Figure 8. Two views of the FR α bound to folic acid.	14
Figure 9. Ligand interaction map of folic acid with FR ligand-binding-pocket	15
Figure 10. Schematic model of biological trafficking states of human folate receptors	17
Figure 11. Cartoon models representing proposed states I-III of folate transport.	17
Figure 12. Predicted membrane topology of the hPCFT.	25
Figure 13. Transcripts for PCFT in solid tumor cell lines.	27
Figure 15. The folate-dependent 1C unit transfers in the purine biosynthetic process.	32
Figure 16. The dTMP cycle.	34
Figure 17. Methionine salvage.	35
Figure 18. hDHFR in complex with folic acid.	36
Figure 19. The catalytic mechanism of human DHFR.	38
Figure 20. hTS in complex with dUMP and PMX.	40
Figure 22. hGARFTase in complex with compound 11 .	45

Figure 23. Compound 11 co-crystallized as a complex with hGARFTase.	45
Figure 24. Proposed mechanism for formyl transfer by human GARFTase.	47
Figure 25. Crystal structure of human AICARFTase.	49
Figure 26. Compound BW1540U88UD complex with hAICARFTase.	49
Figure 27. Proposed mechanism for formyl transfer by human AICARFTase.	51
Figure 28. Second generation GARFTase inhibitors.	53
Figure 29. 6-substituted pyrrolo- and thieno[2,3- <i>d</i>]pyrimidine antifolates.	54
Figure 30. AICARFTase inhibiting Antifolates.	55
Figure 31. 5-substituted pyrrolo[2,3- <i>d</i>]pyrimidine linker extension analogs of PMX .	55
Figure 32. PMX , lead compounds 1-3 , and target compounds 179-181 .	84
Figure 33. Conformational restriction of the side-chain L-glutamate in 1031U89 .	85
Figure 34. Pictorial representation of molecular recognition interactions of fluorine.	87
Figure 35. Chemical structures of benzanilides with N-H ···F molecular interactions.	88
Figure 36. Intramolecular fluorine–hydrogen bond.	88
Figure 37. Molecular modeling with hFR α of 179 , 180 and 3 .	89
Figure 38. Molecular modeling with hFR β of 179 , 180 and 3 .	92
Figure 39. Molecular modeling with hGARFTase of 179 , 180 and 3 .	93
Figure 40. Changes in molecular properties upon N (sp ²) substitution of a CH (sp ²).	96
Figure 41. Lead compounds 2-4 , and target compounds 182-183 .	98
Figure 42. Molecular modeling studies of 182 , 3 and 4 with hFr α .	99
Figure 43. Molecular modeling studies of 182 , 3 and 4 with human GARFTase	100
Figure 44. Lead compounds 2 , 3 , 7 and 9 and target compounds 184-185 .	101
Figure 45. Lead compounds 179-180 and target compounds 186-188 .	103

Figure 46. Lead compounds 3 and 179 and target compounds 189-191 .	105
Figure 47. Molecular modeling studies of 191 with human Fr α .	107
Figure 48. Molecular modeling studies of 191 with human GARFTase.	108
Figure 49. Lead compounds 3 and target compounds 192 .	109
Figure 50. Lead compound 13 and target compound 193 .	111
Figure 51. Molecular modeling studies of 193 with human Fr α .	113
Figure 52. Molecular modeling studies of 193 with human GARFTase.	114
Figure 53. Molecular modeling studies of 193 with human AICARFTase.	115
Figure 54. Lead compounds 13 and 14 and target compounds 194-197 .	116
Figure 55. Molecular modeling studies of 194-197 with human Fr α .	118
Figure 56. Molecular modeling studies of 194-197 with human GARFTase.	119
Figure 57. Molecular modeling studies of 194-197 with human AICARFTase.	120
Figure 58. Lead compounds 13 and target compound 198 .	121
Figure 59. Lead compounds 2, 3, PMX, 12 and 13 and target compounds 200-201 .	122
Figure 60. Molecular modeling studies of 199-201 with human Fr α .	126
Figure 61. Molecular modeling studies of 199-201 with human GARFTase.	127
Figure 62. Molecular modeling studies of PMX and 200 with human TS.	128
Figure 63. Molecular modeling studies of 199 and 201 with human TS.	129
Figure 64. Structure of non-fluorinated compound 266 .	147
Figure 65. NH signals of 266, 9, 179 and 185 in ^1H NMR.	149
Figure 66. Representative example compound 179 and its NH signal by ^1H NMR.	150
Figure 67. The nuclear spin coupling between fluorine and NH can transmitted.	151
Figure 68. D $_2$ O exchange studies of representative example 179 .	152

Figure 69. Proposed retrosynthesis of target compounds 194-197.	165
Figure 70. The other possible Fischer indole cyclization product 368.	180
Figure 71. Proposed retrosynthesis of target compound 201.	182

LIST OF SCHEMES

Scheme 1. Synthesis of pyrrolo[2,3- <i>d</i>]pyrimidines 18-19.	58
Scheme 2. Synthesis of 2-methylthio-4-oxo-pyrrolo[2,3- <i>d</i>]pyrimidine 21.	59
Scheme 3. Synthesis of 2-amino-4-oxo-pyrrolo[2,3- <i>d</i>]pyrimidines 27.	59
Scheme 4. Synthesis of furo[2,3- <i>d</i>]pyrimidines 30 and pyrrolo[2,3- <i>d</i>]pyrimidines 31.	60
Scheme 5. Synthesis of pyrrolo[2,3- <i>d</i>]pyrimidines 35.	61
Scheme 6. Synthesis of 2-amino-4-methyl-pyrrolo[2,3- <i>d</i>]pyrimidine 46.	61
Scheme 7. Synthesis of 48.	62
Scheme 8. Synthesis of 50.	62
Scheme 9. Synthesis of 54-55.	63
Scheme 10. Synthesis of 5-substituted pyrrolo[2,3- <i>d</i>]pyrimidine 58.	63
Scheme 11. Synthesis of 6-amino-5-pyrimidylacetaldehydes 62.	64
Scheme 12. Synthesis of PMX from α -bromo aldehyde 67.	65
Scheme 13. Synthesis of 7-substituted pyrrolo[2,3- <i>d</i>]pyrimidines 75.	66
Scheme 14. Synthesis of pyrrolo[2,3- <i>d</i>]pyrimidine 79.	66
Scheme 15. Synthesis of 4-methyl pyrrolo[2,3- <i>d</i>]pyrimidines 82.	67
Scheme 16. Synthesis of 2,4-dimethyl pyrrolo[2,3- <i>d</i>]pyrimidines 89.	67
Scheme 17. Synthesis of pyrrolo[2,3- <i>d</i>]pyrimidines 91 via Fischer indole cyclization.	68
Scheme 18. Synthesis of pyrrolo[2,3- <i>d</i>]pyrimidines 94 and furo[2,3- <i>d</i>]pyrimidines 93.	69
Scheme 19. Synthesis of 2,5,6-trisubstituted-4-amino-pyrrolo[2,3- <i>d</i>]pyrimidines 98.	69
Scheme 20. Synthesis of 4-amino-5-cyanopyrrolo[2,3- <i>d</i>]pyrimidine 107.	70
Scheme 21. Synthesis of 4-amino-5-substituted pyrrolo[2,3- <i>d</i>]pyrimidine 112.	70

Scheme 22. Synthesis of 5,6-disubstituted pyrrolo[2,3- <i>d</i>]pyrimidine 115 .	71
Scheme 23. Synthesis of 2,5,6-trimethyl pyrrolo[2,3- <i>d</i>]pyrimidine 120 .	71
Scheme 24. Synthesis of 2,5-dimethyl- <i>N</i> ⁷ -substituted pyrrolo[2,3- <i>d</i>]pyrimidine 128 .	72
Scheme 25. Synthesis of 2,5-dimethyl pyrrolo[2,3- <i>d</i>]pyrimidine 133 .	72
Scheme 26. Synthesis of <i>N</i> ⁷ -substituted analogs of PMX .	73
Scheme 27. Synthesis of PMX via guanidine cyclization.	74
Scheme 28. Synthesis of 2-methyl-4-amino-pyrrolo[2,3- <i>d</i>]pyrimidine 148 .	74
Scheme 29. Synthesis of 151 .	75
Scheme 30. A general transformation of Sonogashira coupling.	75
Scheme 31. General mechanism of Sonogashira cross-coupling.	76
Scheme 32. Synthesis of 161 .	76
Scheme 33. Synthesis of 164 by Sonogashira coupling.	77
Scheme 34. General transformation of Heck coupling.	77
Scheme 35. Heck coupling to synthesize aldehyde 169 and 170 .	78
Scheme 36. A proposed mechanism of Heck coupling to synthesize aldehyde 169 .	78
Scheme 37. Improved Heck coupling for aldehyde synthesis	79
Scheme 38. Heck coupling with thiophenyl bromide 178 .	79
Scheme 39. Synthesis of 162 .	133
Scheme 40. Synthesis of 210-211 .	133
Scheme 41. Synthesis of 212-213 .	134
Scheme 42 Synthesis of target compounds 179-180	136
Scheme 43 Synthesis of intermediate 219	137
Scheme 44 Possible mechanism of allene formation instead of α -diazoketone	137

Scheme 45. Synthesis of target compound 181 .	139
Scheme 46 Possible mechanism for unsuccessful oxidation of 224 to 225	140
Scheme 47. Synthesis of target compounds 182 .	140
Scheme 48. Synthesis of 250 .	142
Scheme 49. Synthesis of target compounds 183 .	143
Scheme 50. Synthesis of 184 .	144
Scheme 51. Synthesis of 263 .	145
Scheme 52. Synthesis of 185 .	146
Scheme 53. Synthesis of 270-272 .	155
Scheme 54. Synthesis of target compounds 186-188 .	155
Scheme 55. Synthesis of intermediates 282-284 .	156
Scheme 56. Synthesis of intermediates 285-287 .	157
Scheme 57. Synthesis of target compound 189-191 .	157
Scheme 58. Synthesis of intermediate 293 .	159
Scheme 59. Alternate method for the synthesis of intermediate 293 .	159
Scheme 60. CDMT peptide coupling for the synthesis of intermediate 293 .	159
Scheme 61. Synthesis of of target compound 192 .	162
Scheme 62. Synthesis of target compound 193 .	163
Scheme 63. Synthesis of intermediate 305 .	165
Scheme 64. Synthesis of intermediates 306 and 307 .	167
Scheme 65. Synthesis of intermediate 316 .	167
Scheme 66. Synthesis of intermediates 317 and 318 .	168
Scheme 67. Synthesis of intermediate 319 .	169

Scheme 68. Synthesis of intermediates 320-323.	169
Scheme 69. Synthesis of intermediates 325-330, 332 and 334.	170
Scheme 70. Synthesis of intermediates 339-342.	175
Scheme 71. Synthesis of intermediates 344, 345, 347 and 348.	175
Scheme 72. Synthesis of target compounds 194-197.	176
Scheme 73. Synthesis of target compound 198.	177
Scheme 74. Synthesis of intermediate 360.	179
Scheme 75. Synthesis of target compound 200.	180
Scheme 76. Synthesis of intermediate 372	181
Scheme 77. Synthesis of intermediates 374, 376 and 377.	183
Scheme 78. Synthesis of intermediates 373 and 380.	183
Scheme 79. Synthesis of intermediate 381.	184
Scheme 80. Synthesis of intermediate 382.	185

LIST OF ABBREVIATIONS

AICA 5-aminoimidazole-4-carboxamide

AICAR AICA-ribonucleotide

AICARFTase AICAR transformylase

ALL acute lymphoblastic leukemia

ATP adenosine triphosphate

BBFO broad band fluorine observation

C carbon

CDMT 2,4-dimethoxy-6-chloro-triazine

CHO Chinese hamster ovary

CNS central nervous system

CSF cerebral spinal fluid

DHF dihydrofolate

DHFR DHF reductase

DNA deoxyribonucleic acid

dTMP deoxythymidine monophosphate

dUMP deoxyuridine monophosphate

EOC epithelial ovarian cancer

FBS fetal bovine serum

FDA Food and Drug Administration

FPGS folate polyglutamate synthetase

FR folate receptor

GAR glycinamide ribonucleotide

GARFTase GAR transformylases

GI gastro intestine

GPI glycosyl phosphatidylinositol

HBS HEPES-buffered saline

HOESY heteronuclear Overhauser effect spectroscopy

IC₅₀ fifty percent inhibitory concentration

K_i inhibitor constant

K_t transport affinity

LCV leucovorin

LMX lometrexol

MFS major facilitator superfamily

MHz megahertz

MOE Molecular Operating Environment

MRP multidrug resistance-associated protein

MTR methionine synthase

MTR methionine synthase

MTX methotrexate

NADPH nicotinamide adenine dinucleotide phosphate

NMM *N*-methyl morpholine

NMR nuclear magnetic resonance

NOESY nuclear Overhauser effect spectroscopy

NSCLC non-small cell lung cancer

P₂O₅ phosphorus pentoxide

PABA para-amino benzoic acid

PCC pyridinium chlorochromate

PCFT proton-coupled folate transporter

pH potential of hydrogen

PMX pemetrexed

ppm parts per million

PTX pralatrexate

RFC reduced folate carrier

RMSD root mean square deviation

RNA ribonucleic acid

RTX raltitrexed

SAM S-adenosylmethionine

SAR structure-activity relationship

SCID severe combined immunodeficiency

SHMT serine hydroxymethyltransferase

SLC solute carrier

TAMs tumor-associated macrophages

THF tetrahydrofolate

TLC thin-layer chromatography

TMD transmembrane domain

TMS trimethylsilane

tRNA transfer RNA

TYMS Thymidylate synthase

UV ultraviolet

V_{max} maximum velocity

I. BIOCHEMICAL REVIEW

A. Folate receptor and/or proton-coupled folate receptor targeting antifolates with multiple enzyme inhibition as tumor-targeted antimetabolites

A.1. Folates

A.1.1. Introduction

Folates is a generic term given to the group of vitamin B cofactors (Figure 1); folate metabolism is a universal process that falls into a broader set of transformations known as one-carbon (1C) metabolism.¹ It allows for the activation and transfer of 1C units for metabolic processes including purine and thymidine synthesis, and homocysteine re-methylation (Figure 2). Animals cannot synthesize folates and require dietary folate intake. Insufficient dietary folate leads to birth defects/death in developing fetuses and pathologic conditions such as anemia, cardiovascular diseases, cognitive decline, neurologic disorders, and cancer in adults.²⁻³

Folates share a common core structure consisting of a pteridine ring (reduced/oxidized), a para-amino benzoic acid (*p*ABA) linker, and a polyglutamate tail with variable chain length (Figures 1 and 2). Tetrahydrofolate (THF) with the reduced pteridine species, is the biologically active form. The 1C units are covalently bound to THF in three different carbon oxidation states to the 5-position nitrogen atom as 5-methyl-THF or 5-formyl-THF and/or the 10-position nitrogen atom as 5,10-methylene-THF or 10-formyl-THF (Figure 1).^{1, 4} Typically, 5-methyl-THF is the natural dietary folate (Figure 1).⁵ The synthetic dietary supplement for folates, folic acid (essential vitamin B9,

developed in the 1940s for the treatment of anemia) is sequentially reduced to dihydrofolate (DHF) and then to THF for entry into the folate cycle.⁶

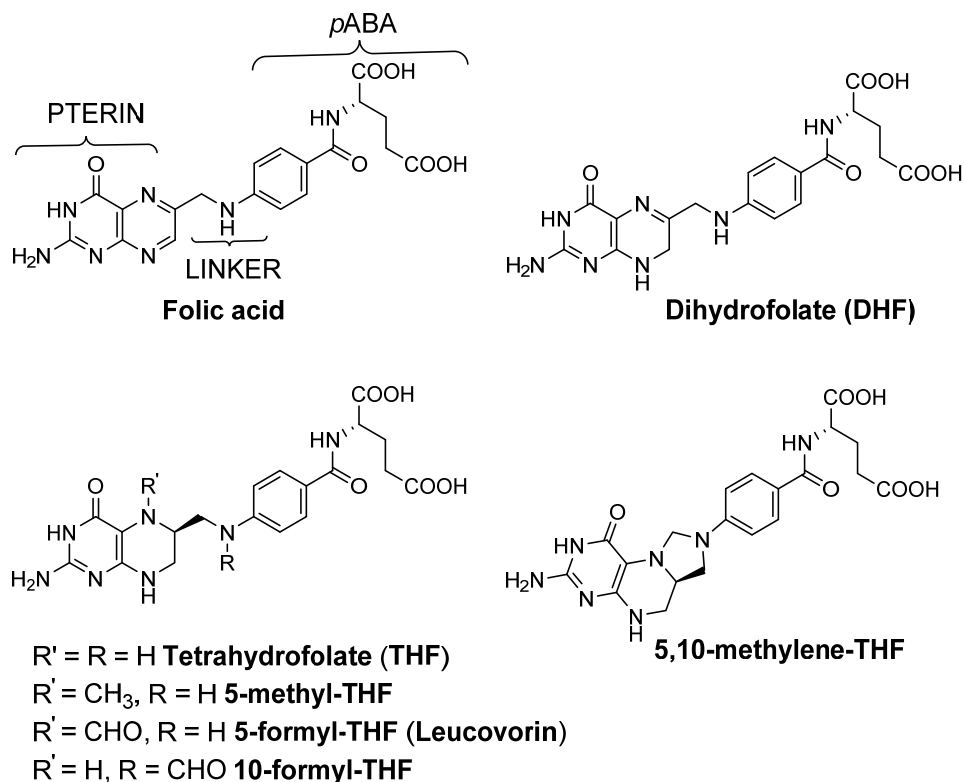


Figure 1. The chemical structures of physiologically relevant folate derivatives with different carbon oxidation states.¹

Since folates are anionic at physiologic pH, mammals express folate specific transporters namely the reduced folate carriers (RFC), folate receptors (FRs) and proton-coupled folate transporters (PCFT) for uptake across cell membranes (Figure 3). Within the cell, the 1C units of 5,10-methylene-THF, 5-methyl-THF, and 10-formyl-THF are interconverted between different oxidation states and compartmentalized for distinct biosynthetic functions. 5-formyl-THF serves as a 1C reserve (Figures 2 and 4).

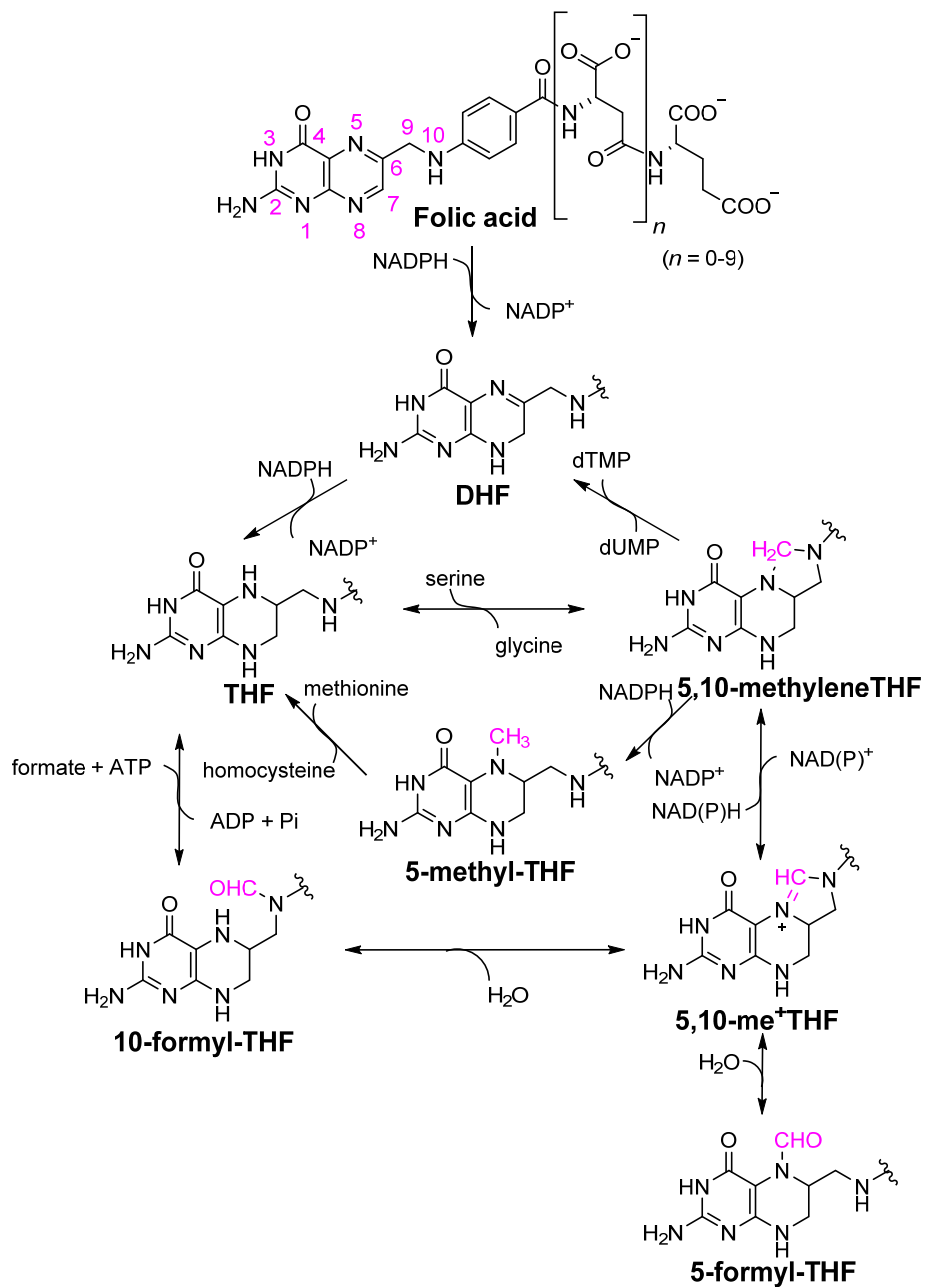


Figure 2. Biochemical transformations of folates. Folic acid is reduced to DHF and ultimately to THF. THF accepts 1C units and undergoes a series of oxidative/reductive transformations to 5-methyl-THF, 5,10-methylene-THF, 5-formyl-THF and 10-formyl-THF.¹

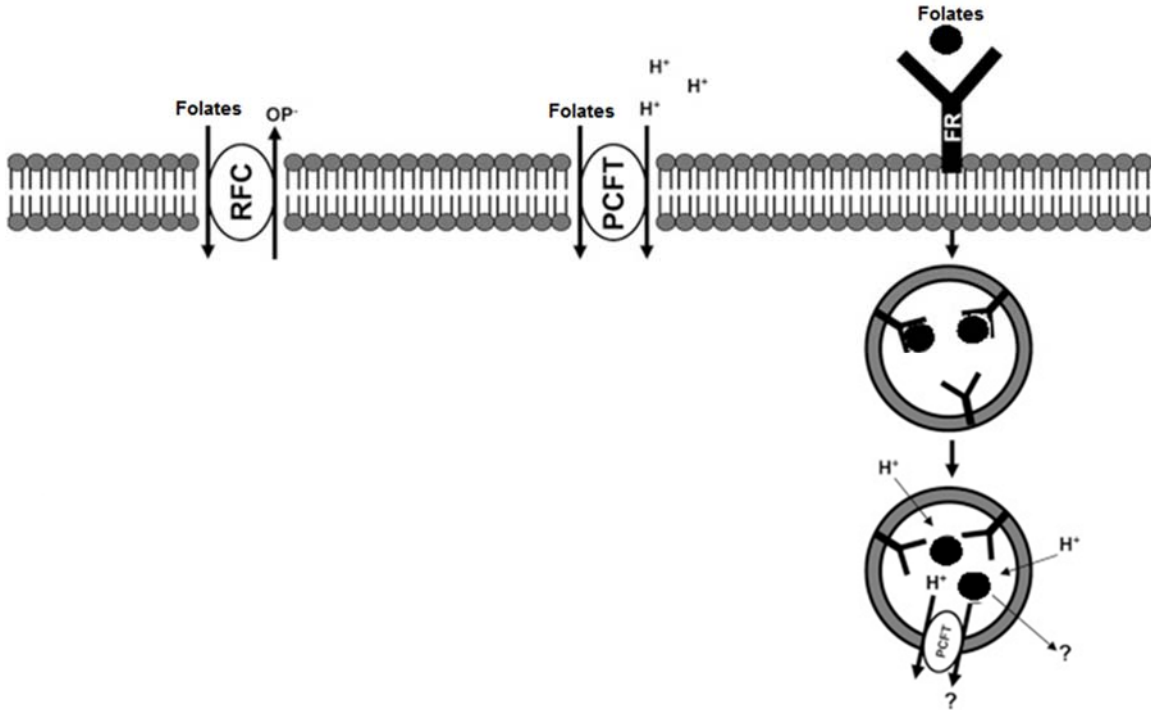


Figure 3. RFC-, FR- and PCFT-mediated internalization of folates. 1) Concentrative uphill uptake of folate substrates by RFC is directly linked to organic phosphates gradients across the plasma membrane 2) PCFT-mediated transport of folates is electrogenic with net translocation of positive charges for each negatively charged folate (the coupling ratio is unknown as at acidic pH as the proton flux is uncoupled from folate transport) 3) The FRs are high affinity GPI-anchored folate binding proteins that mediate cellular folate uptake by endocytosis to form early endosomes, which undergo acidification to release folates.⁷

A.1.2 Folate metabolism in development and proliferative adult tissues:

Research over several decades has long-established the essential requirement for dietary folates during development.¹ Nucleic acid biosynthesis in proliferating tissues is the best characterized essential function of folate metabolism. The anabolic process of folate metabolism also generates methionine, glycine, or serine (Figure 2). Recently, the

specific roles of individual folate-utilizing enzymes in supporting growth and development, folate pathways activated in fetal development, immune proliferation, and tissue homeostasis have also been uncovered.⁸⁻¹¹ Particularly, the role and importance of mitochondrial folate metabolism is probably the most important discovery over the last decade. Mitochondrial folate metabolism intrinsically supplies 1C units in highly proliferative tissues such as the embryo, and deletion of these enzymes lead to neural tube defects and loss of viability (Figure 4).¹²⁻¹³ Defects in the function of the mitochondrial folate enzymes cannot be rescued metabolically.

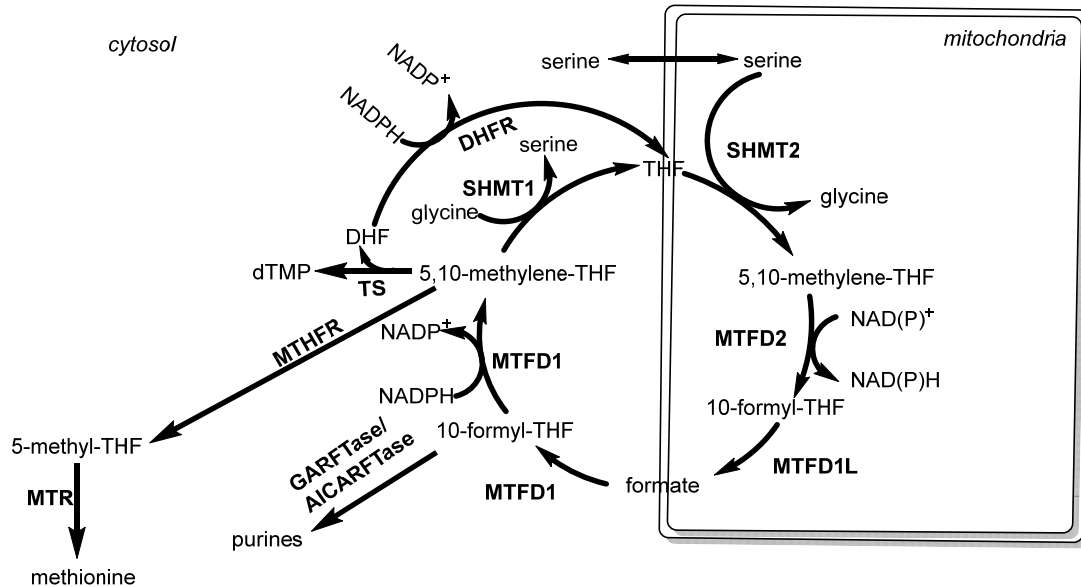


Figure 4. Compartmentalization of folate-mediated 1C metabolism.¹ Folate metabolism supports 1C anabolic reactions through an interlinked set of mitochondrial and cytosolic reactions.¹ All abbreviations are standard gene names. SHMT1/2, serine hydroxymethyl transferase, cytosolic (1)/mitochondrial (2); MTHFD1, methylenetetrahydrofolate dehydrogenase, cyclohydrolase, and formyltetrahydrofolate synthetase 1; MTFD2, methylenetetrahydrofolate dehydrogenase 2; MTHFD1L, monofunctional tetrahydrofolate

synthase, mitochondrial; TYMS, thymidylate synthetase; MTHFR, methylenetetrahydrofolate reductase; MTR, methionine synthase; DHFR, dihydrofolate reductase; GARFTase, glycinamide ribonucleotide formyl transferase; AICARFTase, 5-aminoimidazole-4-carboxamide ribonucleotide formyl transferase.

A.1.3. Folate metabolism in non-proliferative adult tissues

Anabolic 1C reactions among non-proliferative adult tissues are predominantly localized to the liver and kidney for the synthesis of creatine and choline, the major sinks for SAM-bound 1C units.¹ In rest of the non-proliferative tissues, folate metabolism maintains the homeostasis of nucleotides and amino acids (methionine, serine, and glycine), and generates ATP and NADPH from dietary choline, serine, and glycine (Figures 2 and 4).¹⁴

A.1.4. Dietary folate intake and adult disease

Insufficient dietary folate or reduced intestinal folate absorption results in folate deficiency. Increased homocysteine levels because of folate deficiency has been correlated with pathologic conditions such as cardiovascular diseases, cognitive decline, neurologic disorders, and cancer.³ Supplemental vitamin B intake in clinical trials have not shown any benefit in these conditions. Across various experimental and epidemiological studies, incidence of gastrointestinal cancers, particularly colorectal cancer, was observed to be inversely correlated with folate consumption.¹⁵ Population-based studies of breast and pancreatic cancers have also shown similar results.¹⁶⁻¹⁷ However, in a clinical study, supplemental folic acid while not suppressing the recurrence of colon polyps in patients with at least one adenoma, showed a trend toward both more polyps and carcinoma.¹⁸ As

such, while adequate long-term folate intake is essential for genome integrity, the growth of existing lesions may be fueled by added folates.

A.1.5. Folate-based antimetabolite therapies for cancer

Folate metabolism is important for cancer cell growth due to its essential role in nucleic acid synthesis and cellular proliferation (concurrent with increases in folate uptake and folate-metabolic enzymes). Inhibitors of folate transformations are widely used as antimetabolites for treating cancer.

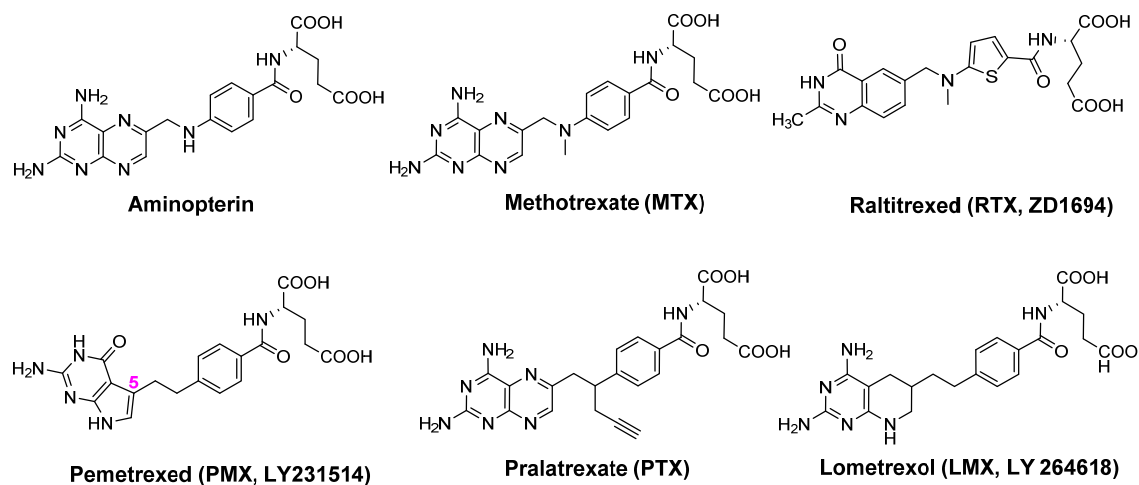


Figure 5. Structures of classical antifolates.

The discovery of antifolate aminopterin, the 4-amino derivative of folic acid, in pediatric leukemia marked the beginning of modern science of chemotherapy (Figure 5).¹⁹ Antifolates inhibit folate cofactors-using cellular enzymes to treat a variety of cancer types and have been in use for over >60 years.²⁰⁻²⁴ Though aminopterin caused remission of childhood leukemia, it showed substantial toxicity and led to the development of methotrexate (**MTX**), a N10-methylated version of aminopterin that inhibits dihydrofolate reductase, currently used widely in the treatment of many malignant conditions including

acute lymphoblastic leukemia (ALL), osteosarcoma, lymphoma, and breast cancer.^{19, 22, 25} Pemetrexed (**PMX**, Alimta, LY231514), a 5-substituted pyrrolo[2,3-*d*]pyrimidine analog is another antifolate used as a first-line treatment for non-small cell lung cancer (NSCLC) which was FDA-approved in 2004 for the treatment of malignant pleural mesothelioma.²⁶⁻²⁷ **PMX** primarily inhibits thymidylate synthase. Other clinically used antifolates include the most recently approved (2009) pralatrexate (**PTX**), a 10-deazaaminopterin analog of **MTX** which is a DHFR inhibitor used for the treatment of relapsed or refractory peripheral T-cell lymphoma. Raltitrexed (**RTX**), a thymidylate synthase inhibitor has been approved outside of the US, for treating advanced colorectal cancer.²⁸⁻³⁰

A.2. Folate uptake

Folate cofactors are hydrophilic anions at physiologic pH and diffuse poorly across cell membranes. Consequently, folate transport systems have evolved in mammalian cells to facilitate cellular uptake.

In mammalian cells, folate transport is facilitated by genetically distinct systems.^{7,}
31-33

A.2.1. Reduced folate carrier (RFC; Solute Carrier (SLC) 19A1)

RFC, a ubiquitously expressed transport system, facilitates the majority of the folate uptake in mammalian healthy cells as well as malignant tissue.³⁴

A.2.1.1. RFC: basic biology and physiology

RFC is the best characterized folate transporter.³⁴⁻³⁹ RFC has high affinity (~50-100-fold) for reduced folates ($K_i \sim 1-5 \mu\text{M}$) and a low affinity for folic acid ($K_i \sim 150 \mu\text{M}$) for transport from the blood into cells of peripheral tissues (Table 1).⁴⁰

Table 1. Comparison of the affinities of RFC for different folates at acidic or neutral pH.⁴⁰

Folate	RFC Influx K_i or K_t (μM)	
	pH = 5.5	pH = 7.4
Folic acid	125	142
(6 <i>S</i>)5-formyl-THF		~2
(6 <i>R</i>)5-formyl-THF		40
(6 <i>S</i>)5-methyl-THF		1-5

RFC transport is temperature- and pH-dependent, characterized by a neutral optimum which decreases dramatically below pH 7 (Table 1).⁴¹ Concentrative uphill uptake of folate substrates by RFC is directly linked to organic phosphates gradient across the plasma membrane that are transported out via RFC (Figure 3).^{38, 42} Highly elevated human RFC (hRFC) transcripts have been detected in the placenta and liver, while significant levels in leukocytes, kidneys, lungs, bone marrow, intestines, and portions of the CNS and brain were also detected.⁴³⁻⁴⁴ RFC is essential for development; inactivating both its alleles is embryonic lethal and causes failure of the hematopoietic organs (bone marrow, the thymus, or the spleen).⁴⁵ Although RFC is exposed to the cerebral spinal fluid (CSF), its role in folate transport in the central nervous system (CNS) is not clear.

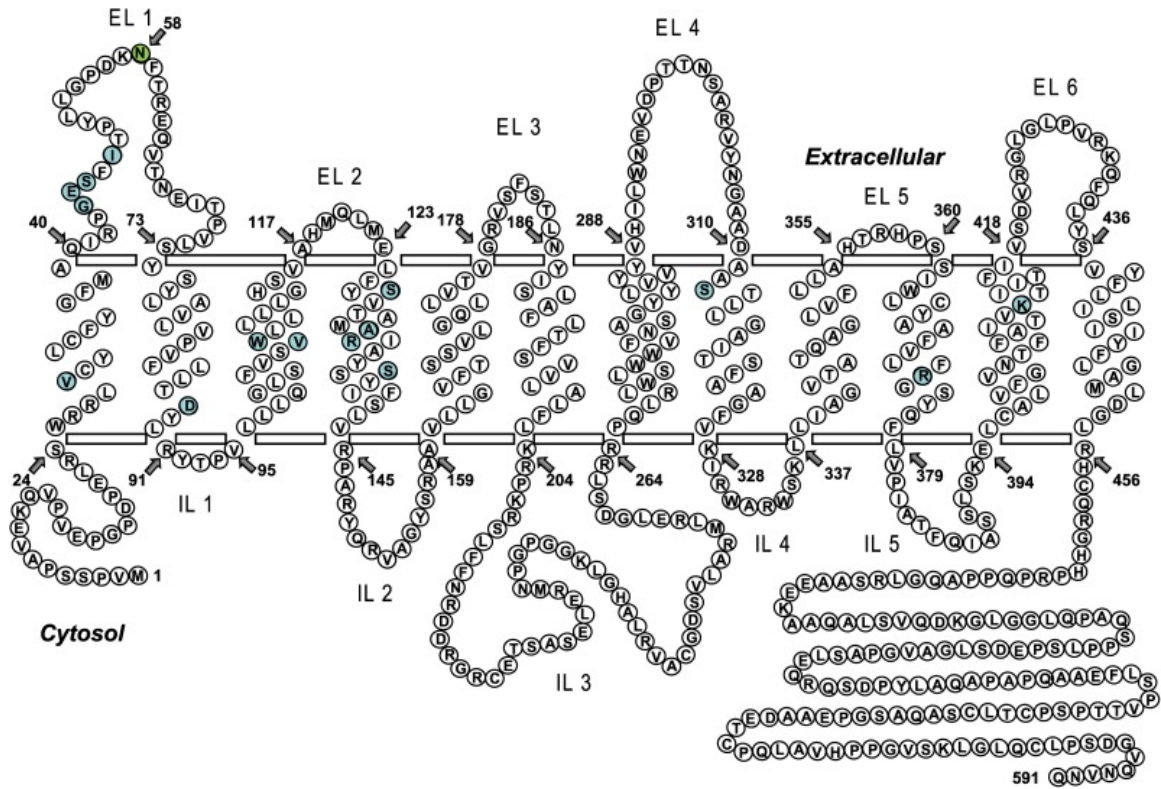


Figure 6. Predicted and experimentally validated membrane topology of the human reduced-folate carrier (hRFC) is shown.⁴⁶ Functionally important residues are highlighted in blue, and the N-glycosylation site is in green. EL, extracellular loop; IL, intracellular loop.

RFC belongs to the major facilitator superfamily (MFS) of transporters and hRFC has a typical MFS protein structure with 591 amino acids arranged in 12 transmembrane domains (TMDs) (Figure 6).^{35, 47-48} The N- and C-termini and a large non-conserved loop domain between TMDs 6 and 7 face the cytosol.^{34-35, 46} Neither the termini, nor the intracellular loop domain participate in the binding and translocation of folate substrates.⁴⁹⁻⁵¹ In the extracellular loop domain connecting TMDs 1 and 2, hRFC is glycosylated at Asn58, mutation of which abolishes N-glycosylation with minimal effect on both membrane targeting and transport activity.⁵²⁻⁵³ The TMD6–7 loop domain provides

appropriate spacing between the TMD1–6 and TMD7–12 segments for optimal transport activity. Arg133, Ile134, Ala135, Tyr136, Ser138 of TMD4 and TMD5, Tyr281 in TMD7, Ser313 in TMD8, Arg373 in TMD10, and TMD11 form the membrane translocation pathway for the anionic folate substrates. Studies of nonfunctional hRFC and site-directed mutagenesis implicated functional or structural importance of some of these amino acids (Ser313, Arg133, Arg373).⁵⁴⁻⁵⁶ Other residues including Val29, Gly44, Glu45, Ser46, Ile48, Val106, Trp107, Ser127, and Ala132 were implicated as functionally important from studies in mouse and hRFCs.⁴⁶ The γ -carboxylates of folate analogs form an ionic bond with Lys411 in TMD11 of hRFC, which is critical for binding and transport.⁵⁷ It was suggested recently that, typical of MFS proteins, hRFC exists as a homo-oligomer with each hRFC monomer functioning independently via individual translocation pathways for folate substrates.⁵⁸⁻⁵⁹ Formation of oligomeric RFC may be necessary for intracellular trafficking and surface expression of the functional transporter.

A.2.1.2. The role of RFC-mediated folate transport in tumors

Not only is hRFC the predominant folate transporter in normal tissues, but hRFC transcripts measured by real-time polymerase chain reaction (qPCR), detected hRFC expression in almost all leukemia cell lines (Figure 7a) and all solid tumor cell lines (Figure 7b).⁶⁰

All of the antifolates in clinic are transported primarily via RFC. In spite of their demonstrated clinical efficacy, none of these agents are selectively targeted to the diseased tissue, resulting in substantial dose-limiting toxicity toward normal tissues drawing no net therapeutic gain.³⁴ The substantial toxicities encountered with these inhibitors are at least

partly due to their RFC-mediated transport with low micromolar K_t (Michaelis constant) into both tumors and normal tissues.^{34-35, 46, 61-64}

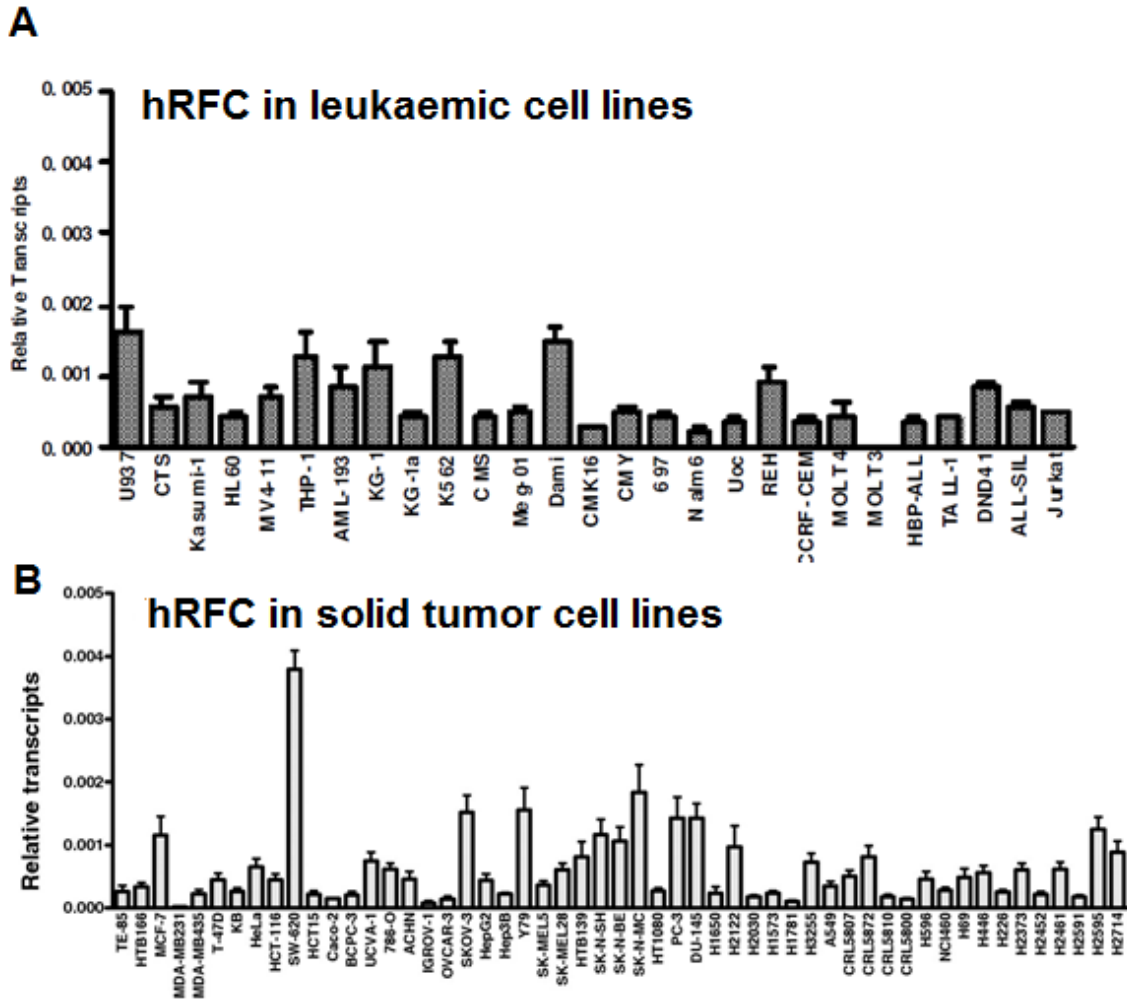


Figure 7. Transcripts for RFC in (A) leukemia and (B) solid tumor cell lines. Transcript levels were normalized to GAPDH transcripts.⁶⁰

Additionally, loss of RFC transport is an important contributing factor for antifolate resistance development. Loss of RFC-mediated antifolate transport results from decreased RFC expression, or synthesis of mutant RFC with impaired transport function.^{34, 65-66} Clinical resistance to **MTX** in ALL and osteogenic sarcoma has been implicated due to

loss of RFC transport. While **PMX** is argued to have superior activity in solid tumors, toxicities are caused by inhibition of 1C metabolism in non-transformed cells, including those of the intestinal epithelium and bone marrow, resulting in gastric complications, anemia, and immune deficiency. While rescue therapy with 5-formyl-THF (folinic acid, marketed as leucovorin) (Figure 1) decreases toxicity, their therapeutic index remains modest.^{1, 22, 65}

A.2.2. The folate receptors (FRs)

One other type of important folate uptake systems in mammalian cells and tissues include the glycosyl phosphatidylinositol (GPI)-tethered FRs α and β anchored at the plasma membrane, and FR γ (secreted due to the lack of GPI anchoring signal sequence).^{32, 67-77}

A.2.2.1. FRs: basic biology and physiology

The FRs are high affinity folate binding proteins that mediate cellular folate uptake by endocytosis.⁷⁸ FR α is expressed in the choroid plexus, proximal renal tubules, retinal pigment epithelium, uterus, and placenta.⁶⁷ In the proximal renal tubules, FR α is expressed at the apical brush-border membrane (not exposed to circulation, whereas RFC expressed at the basolateral membrane is exposed to circulation).^{32, 39, 67} During glomerulus filtration of urine, folates are reabsorbed and reenter the circulation primarily by FR α -mediated process at the apical membrane. Along with PCFT, folates are suggested to be actively transported via the FR α localized at the basal and apical membranes of the choroid plexus into the CSF.^{32, 79-80} In children with cerebral folate deficiency, loss of function mutations in FR α were described.⁸¹⁻⁸² FR β is expressed in placenta and hematopoietic cells, as well

as inactivated macrophages.^{67, 83-84} Human FR β (hFR β) is a differentiation marker co-expressed at relatively low levels with cluster of differentiation (CD) 14 in monocytes.⁸⁵⁻
⁸⁶ Low levels of human FR γ (hFR γ) is secreted by the lymphoid cells in the spleen, thymus, and bone marrow. The biological functions of hFR β and hFR γ in normal tissue are unclear.^{74, 78, 84-90}

A.2.2.2. Structure of FRs

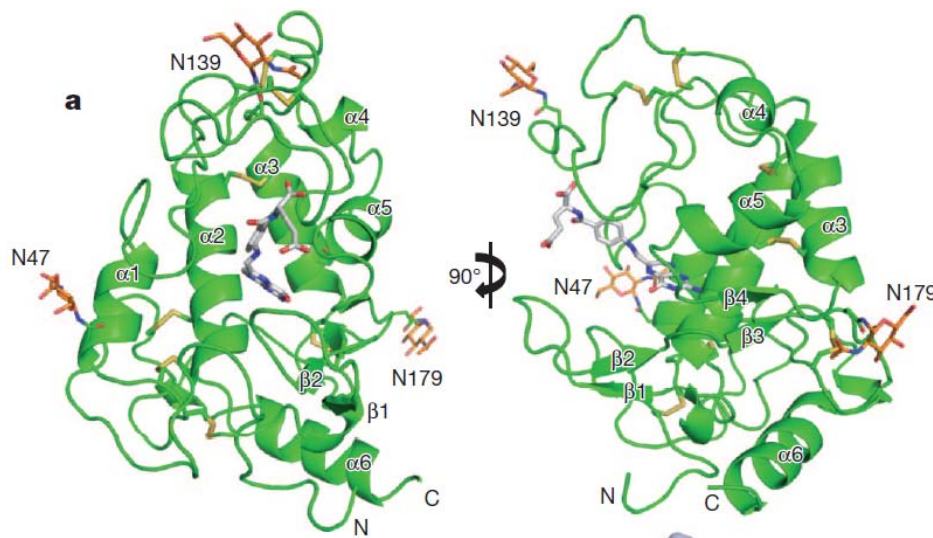


Figure 8. Two views of the complex structure of FR α (green) bound to folic acid (grey).⁹¹ The disulphide bonds are depicted as yellow sticks and *N*-acetyl glucosamine (NAG) is in orange. The N- and C- termini are labelled.

Folate receptors are cysteine-rich, highly homologous proteins (68-79% identical amino acid sequence) with 229 to 236 amino acids and two (β , γ) or three (α) N-glycosylation sites.⁹¹ The cysteine rich crystal structure of human FR α (deglycosylated) in complex with folic acid was recently resolved at 2.8 Å resolution (Figures 8 and 9).⁹¹ It consists of ~205 residues that form a globular tertiary structure, comprising of four

long α -helices ($\alpha 1$, $\alpha 2$, $\alpha 3$, $\alpha 6$), two short α -helices ($\alpha 4$, $\alpha 5$), four short β -strands ($\beta 1$ – $\beta 4$) and many loop regions (Figure 8). The tertiary structure is stabilized by eight disulphide bonds and has three N-glycosylation sites at N47, N139 and N179.^{70-71, 92} The long and open folate-binding pocket is formed by $\alpha 1$, $\alpha 2$ and $\alpha 3$ in the back; the amino-terminal loop, $\beta 1$ and $\beta 2$ in the bottom; the $\alpha 1$ – $\alpha 2$ and $\alpha 3$ – $\alpha 4$ loops in the left and top; and $\alpha 4$, $\alpha 5$, $\beta 4$ and $\beta 3$ in the right (Figure 8).

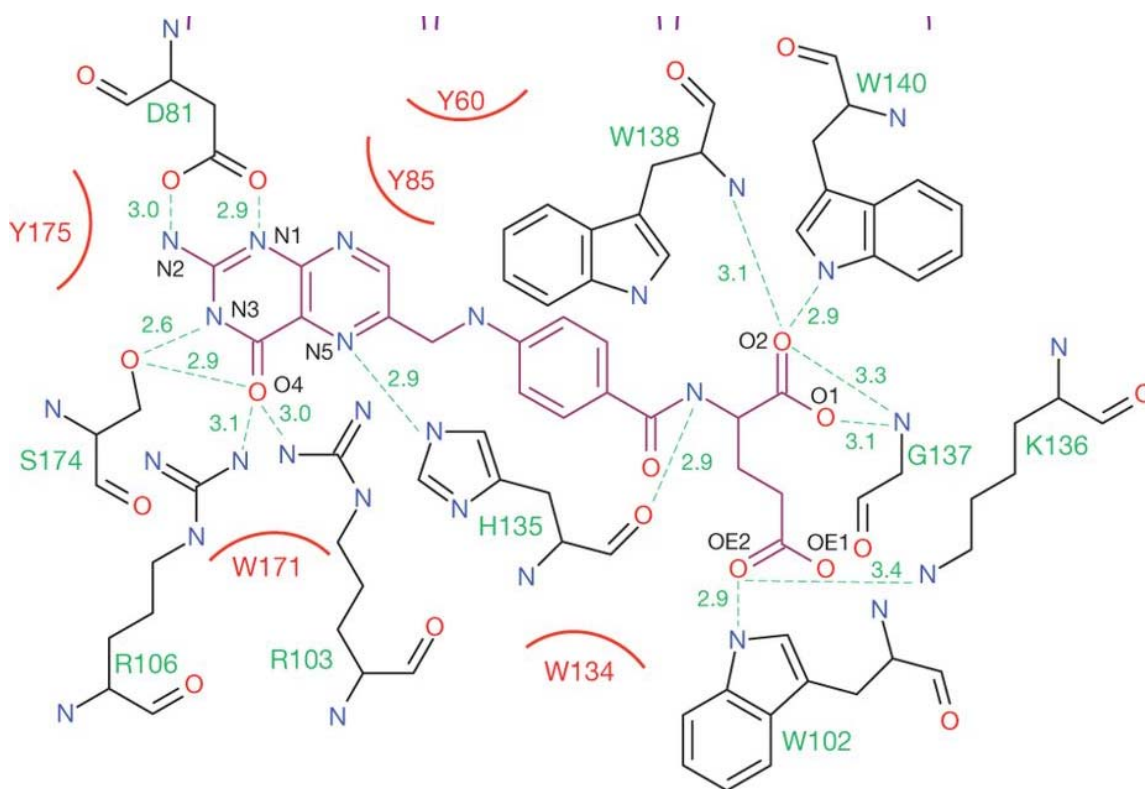


Figure 9. Ligand interaction map of folic acid (magenta) with FR ligand-binding-pocket residues (black).⁹¹ Hydrogen bonds are shown as green dashed lines with bond distances (Å). Hydrophobic interactions are shown as curved red lines.

The residues that form the folate-binding pocket in hFR α and hFR β are conserved and only one residue in the binding pocket that makes a polar contact with the ligands

differs (Lys136 α /Arg152 β) (Figure 9). The folate-binding interactions are conserved among the subtypes. Folate cofactors are oriented with the basic pterate moiety buried within the negatively charged pocket whereas the negatively charged glutamate moiety is solvent-exposed and sticks out of the positively charged pocket entrance. The pterin ring, stacked in between hydrophobic residues Tyr85 and Trp171, and Tyr175 is engaged in a series of hydrogen bonds with receptor residues (Figure 9). The N1 and N2 atoms form hydrogen bonds with the side-chain carboxyl of Asp81. This interaction is a key contributor to high-affinity ligand binding as replacement of Asp81 decreased affinity by more than one order of magnitude. The N3 and O4 atoms engage in hydrogen bonds with the hydroxyl group of Ser174, and the O4 atom additionally makes two hydrogen bonds with the Arg103 and Arg106 guanidinium groups. The N5 atom forms a hydrogen bond with the side-chain of His135. The CH₂ linker and the aminobenzoyl side-chain extend through the central region of the elongated ligand-binding pocket formed by the hydrophobic residues Tyr60, Trp102 and Trp134. The glutamate tail, also involved in extensive interactions, engages in six hydrogen bonds with the side-chains of Trp102, Lys136 and Trp140, and the backbone amide of His135, Gly137 and Trp138. These receptors transport folate via a cell division cycle 42 protein-dependent endocytic mechanism.^{75, 93-94} FRs transport function is proposed to occur via three discrete pH-dependent biological trafficking states (Figures 10 and 11).⁹⁵

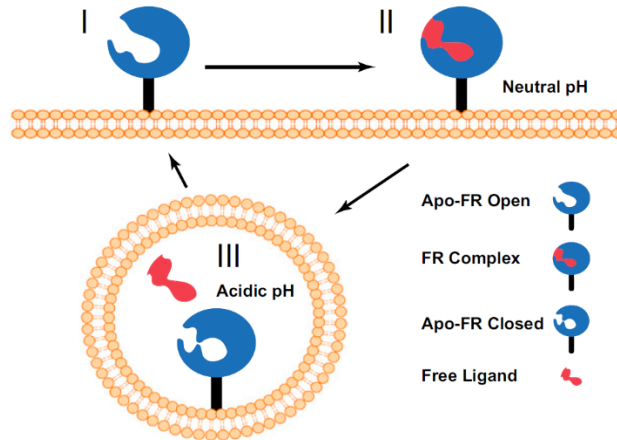


Figure 10. Schematic model of three biological trafficking states of human folate receptors for ligand endocytosis.⁹⁵ Apo-FR conformation at the cell surface, at neutral to slightly basic pH (state I). Structural transition occurs upon ligand binding leading to complex formation (state II). After endocytosis, the mildly acidic microenvironment of the recycling endosome promotes ligand release. A third distinct conformation (state III) is likely to form under acidic conditions after ligand release, before recycling to the cell surface.

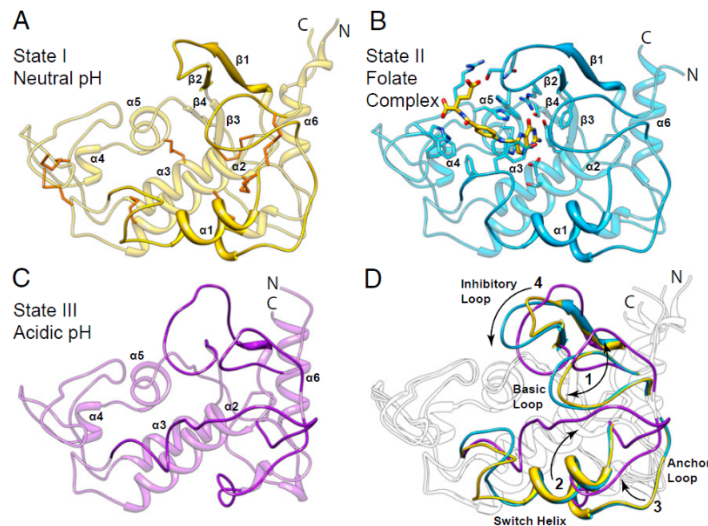


Figure 11. Cartoon models representing proposed states I-III (A-C respectively) of folate transport.⁹⁵ (A) apo-hFR β structure with conserved disulfides colored orange. (B)

hFR β /FOL complex (interacting residues shown as sticks). (C) The apo-hFR α model with global conformational differences in the structure of apo-hFR at pH 5.5. (D) Conformational differences between the three trafficking states are illustrated (numbered with arrows in the order of movement). Regions varying in each individual model are a shade darker of the same color.

The three conformational states of FR are the apo-receptor and folate bound receptor at the cell surface and the apo-receptor within the endosome (Figures 9 and 10). The apo-receptor in an open conformation at neutral pH, at the cell surface undergoes minor rearrangements in loop regions (1) connecting the β 1 and β 2 strands and (2) following the α 1 helix. Changes in sidechain rotamer conformations (e.g., His151, Arg152, Ser190, not shown here) facilitate specific contacts with folate, thus forming the folate bound conformational state (Figures 9 and 10). Subsequently, FRs are encapsulated into an endosome and endocytosed, wherein folate release occurs. This release is due to a conformational change in the hFR/folate complex within the acidic microenvironment of the endosome (pH range of 5.6–7.2 with an average value of 6.5).^{68, 78, 93, 96} The receptor undergoes several conformational changes wherein the movement of four surface loops (basic loop, switch helix, anchor loop, and inhibitory loop) ultimately occlude the folate binding site to prevent reassociation of the released folate (Figure 10). Several basic residues (Arg125/Arg119 (Fr α /FR β), His54/His48 (Fr α /FR β), His36, His37) facilitate these global structural rearrangements due to ionization at acidic pH. In addition, the changes in electrostatic surface potential of hFR/folate complex with varying pH may in part trigger ligand release. After endocytosis, the folates are released into the cytoplasm by PCFT.⁹⁷

A.2.2.3. The role of FR-associated folate transport in tumors

FR α is the most widely overexpressed FR isoform in tumors such as, nonmucinous adenocarcinomas of the ovary (up to 90% of ovarian cancers), uterus, breast, cervix, kidney, and colon, as well as testicular choriocarcinoma, ependymal brain tumors, malignant pleural mesothelioma, and nonfunctioning pituitary adenocarcinoma and is exposed to the circulation significantly contributing to the folate uptake.^{33, 67, 90, 98-100} hFR β is overexpressed in certain leukemias, (chronic myelogenous leukemia and acute myelogenous leukemia) and tumor-associated macrophages (TAMs).^{85, 101} TAMs may play an important role in tumor metastasis and angiogenesis by releasing proangiogenic factors, (e.g., vascular endothelial growth factor, matrix metalloproteinase).

More recently, the emphasis in folate-mediated drug therapy has shifted towards the development of therapeutic molecules specifically transported via the FRs over RFC.^{67, 102-103} The substantial levels of FR-overexpression in many tumors compared to most normal tissues, and their significant transport activity combined with the efficacy of clinically available classical antifolates as first line therapy for several types of cancers, call for the design of FR-selective tumor-targeted therapeutics. FR-selective cytotoxic agents are expected to exhibit reduced toxicity toward normal tissues than the clinically available antifolates.

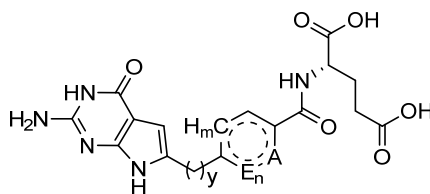
The overexpression of FR α and FR β in several types of cancers as mentioned above, warrants the development of folate receptor selective tumor-targeting cytotoxic agents.^{83, 96, 102, 104-107} The FRs in healthy cells are presented on the apical surface of polarized epithelial cells, which renders them mostly inaccessible to the circulating antifolates following intravenous administration.^{32, 67, 90} This principle has been utilized for

the design of several cytotoxic folate conjugates that selectively target FR expressing tumors.^{24, 108} Furthermore, monoclonal anti-FR antibodies could promote clearance of FR-positive cells by the immune system, folate-conjugated drugs/imaging agents can deliver cytotoxic cargo or imaging agents to FR-positive cells, and FR-targeted antifolates are expected to circumvent the cytotoxic side effects of current antifolates (due to ubiquitous uptake via RFC).^{23, 104, 109-112} Additionally, FR β -positive TAMs constitute an additional potential therapeutic target in assorted cancers.^{84-85, 89}

A.2.2.4. Structural requirements for antifolate binding to FRs

The structural and mutational analyses of FRs provide rationale for the absolute requirement of the folate anchoring pterin group for binding to the receptor. Replacement of O4 with an amino group (**MTX** and aminopterin have reduced affinity for FR α) is not tolerated due to loss of the hydrogen bonds made with Arg103 and Arg106, along with steric/electronic clash of the amino group into the side-chain of Arg103.¹¹²⁻¹¹³ However, such a replacement is tolerated for uptake by RFC. **PMX** is a 5-substituted 2-amino-4-oxo-pyrrolo[2,3-*d*]pyrimidine antifolate with a 2C linker connecting the bicyclic scaffold to the *p*ABA sidechain (Figure 5). It is a potent KB human tumor subline (expresses hRFC, hFRs and hPCFT) inhibitor ($IC_{50} = 68$ (12) nM) and is a non-selective inhibitor of engineered CHO sublines; PC43–10 (expresses hRFC), RT16 (expresses hFR α) and D4 (expresses hFR β). **PMX** is one- to two-fold more selective towards RFC-overexpressing CHO cells over those that overexpress FRs (Table 2).¹¹⁴

Table 2. Cell proliferation assays with 6-substituted pyrrolo[2,3-*d*]pyrimidine antifolates.¹¹⁴⁻¹¹⁸



1 $y = 2, E = CH, n = 1, A = CH, m = 1$ **6** $y = 4, n = 0, A = S, m = 1$
2 $y = 3, E = CH, n = 1, A = CH, m = 1$ **7** $y = 3, E = CH, n = 1, A = S, m = 0$
3 $y = 4, E = CH, n = 1, A = CH, m = 1$ **8** $y = 3, E = S, n = 1, A = CH, m = 0$
4 $y = 4, E = CH, n = 1, A = N, m = 1$ **9** $y = 4, E = CH, n = 1, A = S, m = 0$
5 $y = 3, n = 0, A = S, m = 1$ **10** $y = 4, E = S, n = 1, A = CH, m = 0$

Antifolate	CHO (IC _{50s}) (nM)			KB (IC _{50s}) (nM)
	PC43-10 (RFC)	RT16 (FR α)	D4 (FR β)	
1	>1000	199	48	10.4
2	304 (89)	4.1 (1.6)	5.6 (1.2)	1.7 (0.4)
3	>1000	6.3 (1.6)	10 (2.0)	1.0 (0.7)
4	>1000	1.3 (0.1)	0.51 (0.09)	0.37 (0.08)
5	106 (17)	0.31(0.15)	0.16 (0.02)	0.26 (0.03)
6	>1000	1.82 (0.28)	0.57 (0.09)	0.55 (0.1)
7	197 (49)	0.33 (0.15)	0.34 (0.03)	0.17 (0.05)
8	189 (51)	0.61 (0.11)	0.1 (0.01)	0.09 (0.02)
9	>1000	2.5 (0.5)	0.43 (0.14)	0.17 (0.02)
10	>1000	2.6 (0.59)	0.515	0.27 (0.07)
PMX	26.2 (5.5)	42 (9)	60 (8)	68 (12)
MTX	12 (1.1)	114 (31)	106 (11)	6.0 (0.6)
RTX	6.3 (1.3)	15 (5)	22 (10)	5.9 (2.2)
PTX	0.69 (0.07)	168 (50)	ND	0.47 (0.20)

While the 6-regioisomer of **PMX** was inert toward tumor cells in culture, the conformationally extended and more flexible 3C (**2**) or 4C (**3**) linked analogs showed improved inhibition of proliferation of KB human tumor subline with IC₅₀s of 1.7 and 1 nM respectively.^{114, 119-120} Studies with the engineered PC43-10, RT16 and D4 CHO sublines convincingly showed that compounds **2** and **3** were highly selective inhibitors of proliferation of FR-expressing cells at nanomolar (nM) concentrations (Table 2).¹¹⁴ Both compounds **2** and **3** were ~6 to 11-fold more active toward hFR-expressing RT16 and D4 cells and >100-fold selective for FRs over RFC, than **PMX**. These compounds are also more potent and selective than other clinically used folates, **MTX**, **PTX**, or **RTX** which showed no selectivity for hFRs over hRFC (Table 2). Furthermore, thienyl-for-phenyl/pyridyl-for-phenyl sidechain replacements afforded some of the most potent FR-selective antifolate compounds **4-10**.^{104, 107, 115-116, 121} Pyrrolo[2,3-*d*]pyrimidine thienoyl regioisomers, **5** and **10** with 3C and 4C linkers are few of the most potent and selective inhibitors respectively (Table 2). Compound **5**, **7** and **8** with 3C linked regioisomers are the most potent RT16, D4 and KB cell inhibitors but with submicromolar activity against PC43-10, whereas the 4C linked regioisomeric compounds **6**, **9** and **10** are relatively less potent RT16, D4 and KB cell inhibitors but with >1 μM IC₅₀s against PC43-10. Activity generally declined dramatically as the linker lengths were increased beyond 4C.

A.2.3. Proton-coupled folate transporter (PCFT, SLC46A1)

PCFT, identified in 2006 is a facilitative high affinity transporter of dietary folates in the duodenum.¹²²

A.2.3.1. PCFT: basic biology and physiology

PCFT is distantly related to RFC (~ 14% amino acid identity), belongs to the major facilitator superfamily (MFS) of secondary transporters, but with distinct substrate specificities, mechanism, pH optimum, and patterns of expression in tissues and tumors.⁴⁶

122-124

Table 3. Comparison of the affinities of PCFT for different folates at acidic or neutral pH.

Folates	PCFT	
	Influx K_t or K_i (μ M)	
	pH = 5.5	pH = 7.4
Folic acid	1.3	56.2
(6S)5-formyl-THF	0.13	
(6R)5-formyl-THF	0.87	
(6S)5-methyl-THF	0.53	

Whereas RFC is optimally active at neutral, physiologic pH (pH 7.2–7.4), PCFT is a folate-proton symporter with an acidic maximal activity at pH 4.5–5.5, with appreciable activity up to pH 6.8 and dramatic loss with further increase (above pH 7).^{40, 123, 125-127} PCFT is highly expressed in the apical brush border membranes in the proximal part of small intestine (jejunum and duodenum) where despite the presence of RFC, the acidic pH optimum of the upper gastro intestine (GI) (pH 5.8–6.0) permits PCFT-, but not RFC-mediated membrane transport.^{32, 39, 112, 122, 126, 128-129} From the enterocytes, folates are transported across the surface of basolateral membrane [most likely by multidrug resistance-associated protein (MRP) 3] into the bloodstream for delivery to the liver by the

hepatic portal vein. From the liver, folates (primarily as 5-methyl THF) are released into the blood. PCFT also shows significant folate uptake in the CNS.^{97, 130} Unlike the ubiquitously expressed RFC, PCFT expression is elevated in only certain tissues (e.g., the kidney, the sinusoidal membrane of the liver, the basolateral membrane of the choroid plexus, retinal pigment epithelium, the placenta and spleen) and its broader physiologic role for folate uptake in these tissues is still uncertain and seems unlikely due to the characteristic non-acidic conditions (except transport across the choroid plexus due to a localized low pH at the basolateral membrane of ependymal cells).^{7, 32, 39, 97, 122, 126, 130-131} The K_t (Michaelis constant) values of folate transport by PCFT changes with pH for individual substrates (Table 3).^{60, 104, 119, 132-133} While folic acid is poorly transported by RFC, it is a reasonably good PCFT substrate.¹²⁷ Loss or mutations in human PCFT (hPCFT) as can be recapitulated in PCFT knockout mice, result in hereditary folate malabsorption syndrome, a rare autosomal recessive disorder characterized by the onset of macrocytic folate deficiency, anemia, and failure to thrive within the first few months of life.^{40, 80, 122, 134-141} Loss of hPCFT function also leads to gait disorders, peripheral neuropathies and seizures, and impaired folate uptake across the choroid plexus into the CNS.

A.2.3.2. Structure of PCFT and biology of transport

PCFT is composed of 459 amino acids (Figure 12) and the predicted molecular mass is 49.8 kDa. It has 12 TMDs with cytosolic N and C termini.¹⁴²⁻¹⁴³ The extracellular loop domain connecting TMDs 1 and 2 has two N-glycosylation sites (Asn58 and Asn68). Single mutation of either Asn58 or Asn68 does not affect the expression and function, while Asn58/Asn68 double mutation reduces transport activity by 40%. Carboxyl-terminal

amino acids (up to position 449) are not involved in either targeting or transport activity. Also, the disulfide bond between Cys66 (first extracellular loop) and Cys298 (fourth extracellular loop) connecting TMDs 7 and 8 is not essential for transport activity.

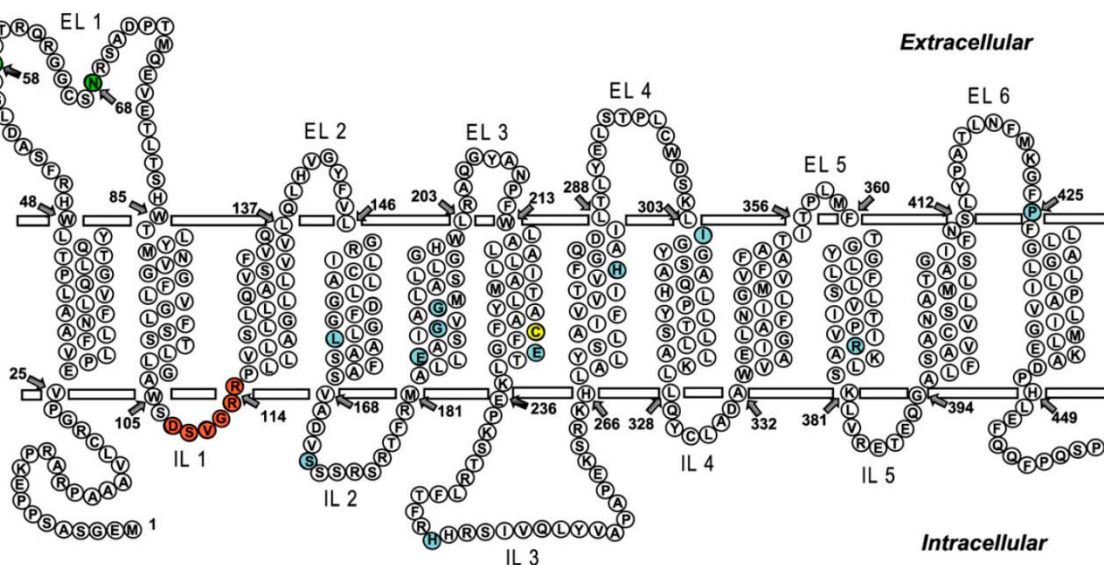


Figure 12. Predicted membrane topology of the hPCFT. Functionally important residues are highlighted in blue and the β -turn formed by residues 109–114 is in orange.⁴⁶ Cys229 is highlighted in yellow. Asn58 and Asn68, the two N-glycosylation sites are highlighted in green. EL, extracellular loop; IL, intracellular loop.¹⁴³

Functionally important hPCFT residues include Glu185 (TMD5, proton coupling), His281 (TMD7, PCFT protonation for enhanced substrate binding), Arg376 (TMD10, proton and substrate binding), a conserved stretch of amino acids linking TMDs 2 and 3 (DXXGRR; positions 109–114) including a β -turn, Asp109, Arg113, His247 [decreased rates of transport (V_{max}), and increased affinities (K_t)], Leu161 (TMD4, substrate affinities), Glu232 (TMD6, rate of carrier translocation), Ile304 (TMD8, substrate affinities), and Pro425 (flanks TMD12, substrate affinities), Gly189 and Gly192,

(TMD5).^{40, 134, 137, 139, 142, 144-148} Residues Phe157, Gly158, and Leu161 in TMD4 and Ile188 in TMD5 are predicted to lie within or nearby the folate binding site in hPCFT.¹⁴⁸⁻¹⁴⁹ Like the other MFS proteins, hPCFT is proposed to exist as a functionally significant homooligomer with TMD6 providing a structural interface between individual hPCFT monomer.^{148, 150-152} PCFT-mediated transport of folates is electrogenic with net translocation of positive charges for each negatively charged folate (Figure 3).^{122, 137, 142}

A.2.3.3. The role of facilitative folate transport by PCFT in tumors

Within the tumor microenvironment, the extracellular pH (pH_e) can be as low as ~ 6.7–7.1, and intracellular pH (pH_i) is ≥ 7.4 (a hallmark of cancer) while pH_e is ~ 7.3 and pH_i is ~ 7.2 in a normal differentiated cell.¹⁵³⁻¹⁵⁷ Since PCFT transports folates and related molecules under low pH conditions and is significantly active at pH 6.5–6.8, it is a major folate-proton symporter in the acidic microenvironment of many solid tumors.^{7, 60} In the acidic pH of tumors, the elevated electrochemical proton gradient favors high levels of membrane transport of cytotoxic PCFT. There is growing evidence supporting an association between PCFT levels and function with the malignant phenotype. Substantial PCFT expression in 52 of 53 human solid tumors ($n = 53$) was detected in a comprehensive analysis of folate transporter expression (Figure 13).⁶⁰ Elevated PCFT transcript levels and transport activity at pH 5.5 are observed in hepatoma cells, epithelial ovarian cancer, malignant pleural mesothelioma, non-small cell lung cancer and pancreatic cancer cells.^{60, 119, 158-160} PCFT levels are low-to-undetectable in leukemias (including ALL and acute myeloid leukemia).^{60, 161}

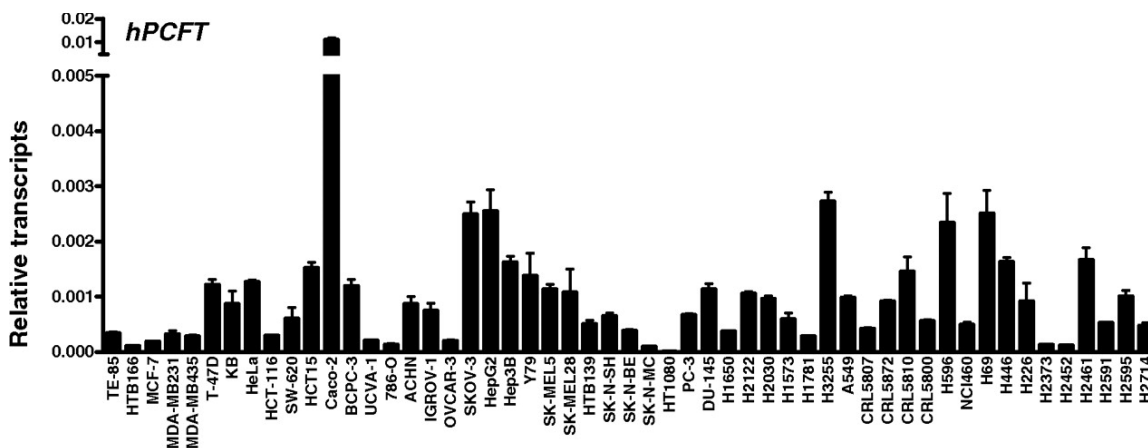


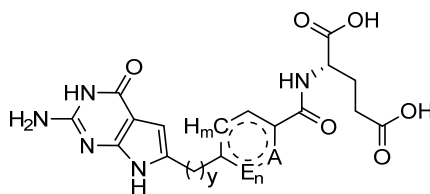
Figure 13. Transcripts for PCFT in solid tumor cell lines. Transcript levels were normalized to GAPDH transcripts.⁶⁰

Even if PCFT is present in the normal tissue milieu, neutral pH and reduced electrochemical proton gradient favors membrane transport by RFC, limited PCFT-mediated uptake of cytotoxic antifolates, and limited cytotoxicity toward normal tissues. Depending upon the substrates specificities for PCFT and/or RFC, PCFT/ RFC expression levels, their localization in the tumor/tissue which determines their access to circulating drug, and the pH of the tumor/tissue microenvironment relative to the pH for optimal transport by PCFT or RFC, net uptake of classical antifolate drugs by tumor and tissue confers antitumor efficacy and toxicity respectively. Antifolates such as **MTX**, **PMX**, **RTX** and **PTX** which are RFC substrates are also transported by PCFT, albeit to different extents.^{7, 22, 40, 46, 96, 112, 122-123, 127, 132, 135, 162-165} In mesothelioma patients treated with **PMX**, patients with low PCFT transcripts had significantly lower rates of disease control and shorter overall survival, strongly implying that PCFT is an important determinant of **PMX** clinical efficacy in malignant mesothelioma.¹⁶⁰

The clinical successes of **PMX**, along with evidence that hPCFT can potentially offer tumor-targeted antifolate delivery, has steered drug discovery efforts to develop novel PCFT-selective cytotoxic antifolates over RFC. More recently, the emphasis in folate-mediated drug therapy has shifted towards the development of therapeutic molecules specifically transported via PCFT over RFC.^{7, 60, 104, 107, 119, 121, 158-159, 166-167} The (1) substantial levels of FRs and PCFT-expression in many tumors compared to most normal tissues, and (2) significant transport activity of PCFT at tumor microenvironment specific acidic pH, combined with (3) the efficacy of clinically available classical antifolates as first line therapy for several types of cancers, call for the design of selective tumor-targeted therapeutics with high level substrate activity and selectivity for PCFT over RFC. PCFT-selective cytotoxic agents are expected to exhibit reduced toxicity toward normal tissues than the clinically available antifolates.

While **PMX**, a 5-substituted 2-amino-4-oxo-pyrrolo[2,3-*d*]pyrimidine antifolate with a 2C linker is a PCFT substrate, (Figure 5) the 6-sustituted regioisomer of **PMX** was inert toward tumor cells in culture (Table 4). Upon extension of the linker to 3C and 4C in compounds **2** and **3** respectively, activity was regained with much higher potency when compared to **PMX**. Compound **2** was ~40-fold more active and compound **3** was ~70-fold more potent than **PMX** (IC₅₀s of 1.7, 1 and 68 (12) nM respectively) toward KB cells (Table 4).

Table 4. Cell proliferation assays with 6-substituted pyrrolo[2,3-*d*]pyrimidine antifolates.¹¹⁴⁻¹¹⁷



- 1** $y = 2$, $E = CH$, $n = 1$, $A = CH$, $m = 1$ **6** $y = 4$, $n = 0$, $A = S$, $m = 1$
2 $y = 3$, $E = CH$, $n = 1$, $A = CH$, $m = 1$ **7** $y = 3$, $E = CH$, $n = 1$, $A = S$, $m = 0$
3 $y = 4$, $E = CH$, $n = 1$, $A = CH$, $m = 1$ **8** $y = 3$, $E = S$, $n = 1$, $A = CH$, $m = 0$
4 $y = 4$, $E = CH$, $n = 1$, $A = N$, $m = 1$ **9** $y = 4$, $E = CH$, $n = 1$, $A = S$, $m = 0$
5 $y = 3$, $n = 0$, $A = S$, $m = 1$ **10** $y = 4$, $E = S$, $n = 1$, $A = CH$, $m = 0$

Antifolate	CHO (IC _{50s}) (nM)		KB (IC _{50s}) (nM)
	PC43-10 (RFC)	R2/PCFT4 (PCFT)	
1	>1000	>1000	10.4
2	304 (89)	23.0 (3.3)	1.7 (0.4)
3	>1000	213 (28)	1.0 (0.7)
4	>1000	30.4 (10.7)	0.37 (0.08)
5	106 (17)	3.3 (0.5)	0.26 (0.03)
6	>1000	43.4 (4.1)	0.55 (0.1)
7	197 (49)	5.4 (1.3)	0.17 (0.05)
8	189 (51)	6.51 (1.3)	0.09 (0.02)
9	>1000	41.5 (3.1)	0.17 (0.02)
10	>1000	63.82 (16.23)	0.27 (0.07)
PMX	26.2 (5.5)	8.3 (2.7)	68 (12)
MTX	12 (1.1)	121 (17)	6.0 (0.6)
RTX	6.3 (1.3)	99.5 (11.4)	5.9 (2.2)
PTX	0.69 (0.07)	57 (12)	0.47 (0.20)

Studies with the engineered PC43–10 and PCFT expressing R2/hPCFT4 CHO sublines convincingly showed that these compounds were selective inhibitors of proliferation of hPCFT over RFC expressing cells unlike **PMX**.¹¹⁴ Compound **2** was ~9-fold more active than compound **3** (IC₅₀s of 23 (3.3) and 213 (28) nM respectively) toward hPCFT-expressing R2/hPCFT4 cells. A similar trend of improved potency as well as selectivity were observed when compared with the other clinically used antifolates **MTX**, **PTX**, or **RTX** (Table 4). Similar to improvement in FR mediated potency and selectivity, thienyl-for-phenyl/pyridyl-for-phenyl sidechain replacements afforded some of the most potent PCFT-selective antifolate compounds **4-10** (Table 4). Pyrrolo[2,3-*d*]pyrimidine thienoyl regioisomers with 3C linkers, **5** (2',5'-substituted thiophene), **7** (2',4'-substituted thiophene) and **8** (3',5'-substituted thiophene), showed the best PCFT-targeted activity with IC₅₀s of 3.3 (0.5) and 5.4 (1.3), and 6.51 (1.3) nM respectively against R2/hPCFT4 cells. Activity generally declined dramatically for analogs with linker lengths longer than 4C.

A.3. Folate compartmentalization

A.3.1. Polyglutamylation encoded compartmentalization

Folates, once inside a cell, are distributed between mitochondria, cytoplasm and nucleus.¹⁶⁸⁻¹⁶⁹ Up to 40% of the intracellular folate is concentrated in the mitochondria, (transported in the mono-glutamylated form by a folate specific mitochondrial transporter SLC25A2).¹⁷⁰⁻¹⁷¹ Furthermore, the intracellular folates are polyglutamylated (2–8 glutamate moieties) by the addition of glutamate residues via a γ -peptide linkage catalyzed by folate polyglutamate synthetase (FPGS) (Figure 14).¹⁷²⁻¹⁷⁵ Polyglutamylation reduces

folate affinity for the transporters/efflux pumps and are thereby retained within. It also enhances the affinity of folates towards the target enzymes, and is essential for cell proliferation.^{172, 176-178}

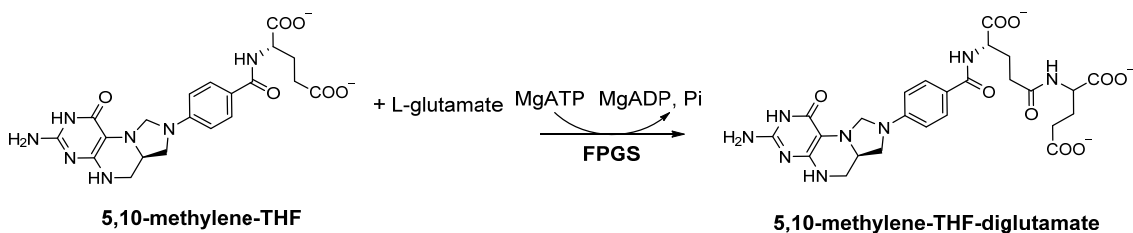


Figure 14. Polyglutamylation reaction catalyzed by folylpolyglutamate synthetase. Representative example shown is diglutamylation of 5,10-methylene-THF.¹⁷⁹

Antifolate inhibitors such as **MTX** or **PMX** that are transported into tumors sustain potent antitumor activity upon polyglutamylation. Polyglutamyl antifolates typically bind to their cellular targets with much higher affinities than their non-polyglutamyl drug forms.^{22, 63, 165, 180-181} For example, **PMX** inhibits thymidylate synthase ~100-fold more effectively following its polyglutamylation.¹⁸² Upregulated FPGS function in tumors likely contributes to the differences in the extent of antifolate polyglutamylation between normal tissues and tumors, drug selectivity and antitumor efficacy. Reduced FPGS activity is a known mechanism of resistance developed by tumor cells towards antifolates.⁶⁶ However, antifolates with sufficiently potent folate-metabolizing enzyme inhibition independent of polyglutamylation could be efficient against antifolate resistant tumors with changes in FPGS function and expression.^{65, 183}

A.4. Folate Metabolism

A.4.1. Products of 10-formyl-THF

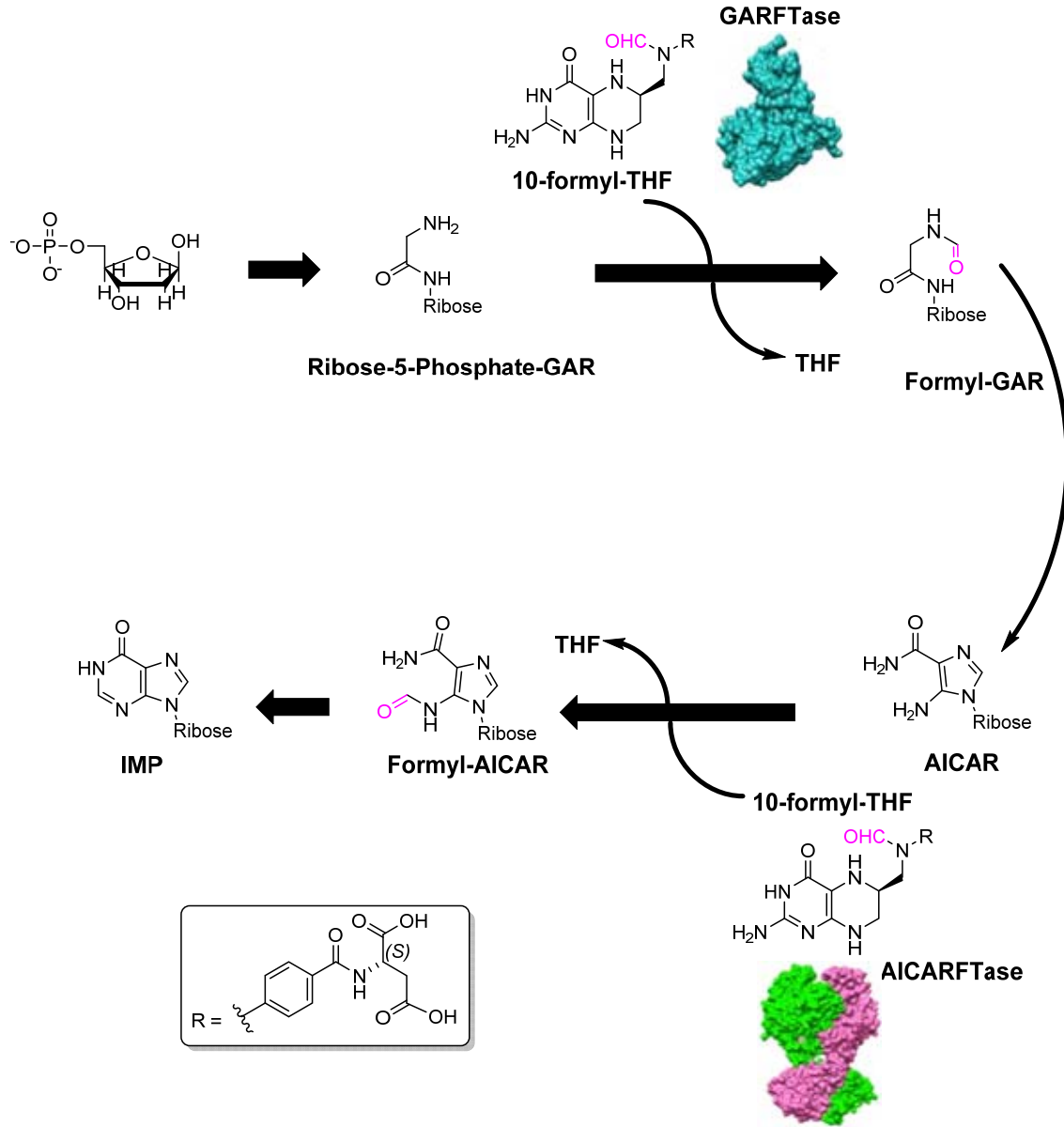


Figure 15. The two folate-dependent 1C unit transfers in the purine biosynthetic process.

De novo synthesis of purines in proliferating mammalian cells demands for the largest proportion of the folate 1C units in the form of 10-formyl-THF. The folate-

dependent enzymes, glycinamide ribonucleotide formyl transferase and 5-aminoimidazole-4-carboxamide ribonucleotide formyl transferase (GARFTase and AICARFTase) that catalyze the 1C unit transfer are a part of a putative multi-enzyme complex termed the purinosome that are co-localized in the cytoplasm outside of mitochondria.¹⁸⁴⁻¹⁸⁵ In the 11-reaction purine biosynthetic process, two 10-formyl-THF units are incorporated into the purine backbone (Figure 15). As such, on an average, for every newly synthesized DNA or RNA base, one 10-formyl-THF is required.

In the mitochondria, 10-formyl-THF formylates the initiator methionine transfer RNAs (tRNAs) for translation of mitochondrially encoded proteins.¹⁸⁶ 10-formyl-THF is reversibly hydrolyzed in an ATP-generating reaction to free formate by mitochondrial methylenetetrahydrofolate dehydrogenase 1 like (MTHFD1L) to enable transfer of 1C units between compartments.¹⁸⁷ Additionally, the elimination of the 1C unit of 10-formyl-THF via oxidation to CO₂ by mitochondrial 10-formyltetrahydrofolate dehydrogenase (FDH) is coupled to NADPH-generation. As per recent findings, folate-mediated NADPH production may be vital for mitochondrial redox homeostasis.¹⁸⁸⁻¹⁸⁹

A.4.2 Products of 5,10-methylene-THF:

Catalyzed by Thymidylate synthase (TS), 5,10-methylene-THF methylates deoxyuridine monophosphate (dUMP) to deoxythymidine monophosphate (dTMP) in the cytoplasm (Figure 16). In this process, two electrons are abstracted from 5,10-methylene-THF producing DHF as the product. DHF is reduced back to THF by the NADPH-dependent activity of dihydrofolate reductase (DHFR). For every 4 newly synthesized DNA or RNA base, an average of one 5,10-methylene-THF is needed for DNA synthesis.

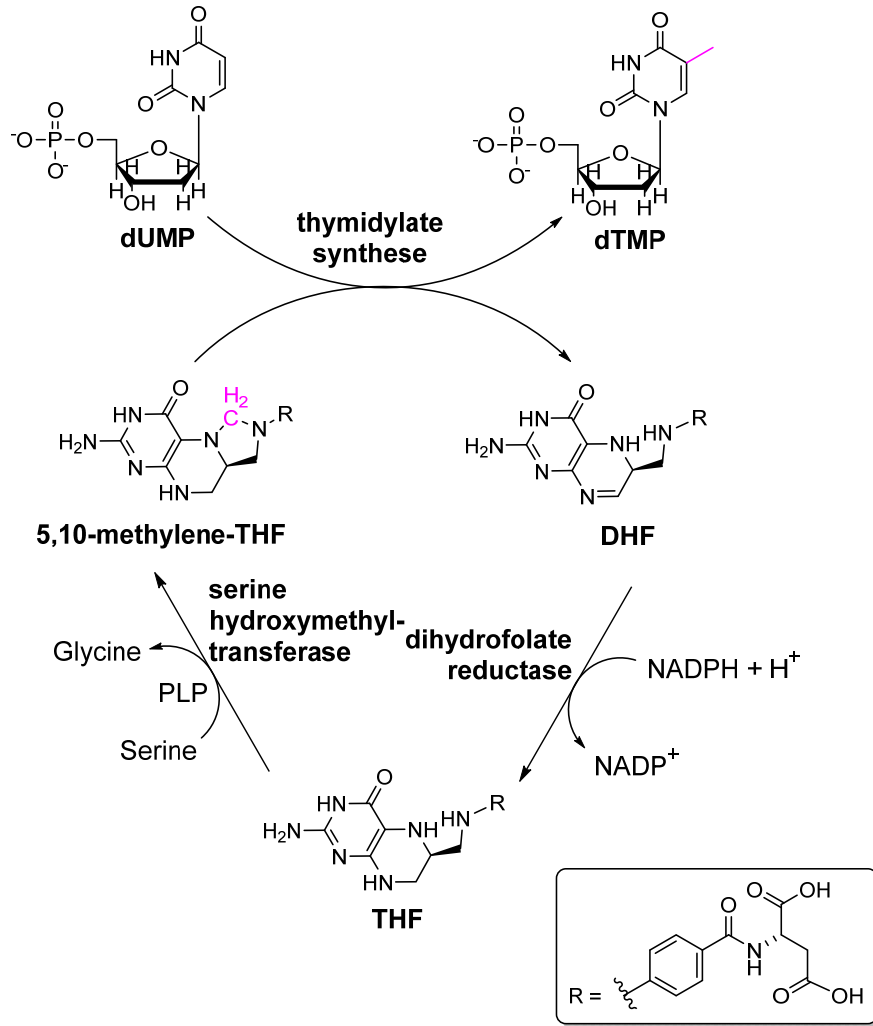


Figure 16. The dTMP cycle.

5,10-methylene-THF-dependent hydroxymethylation of glycine to serine is synthesized in a reversible reaction by serine hydroxymethyltransferase (SHMT) (Figure 16). SHMT-mediated metabolism of serine is compartmentalized between the mitochondria and cytoplasm, depending upon the supply and demand of 1C units (Figure 4).¹⁹⁰

A.4.3 Product of 5-methyl-THF:

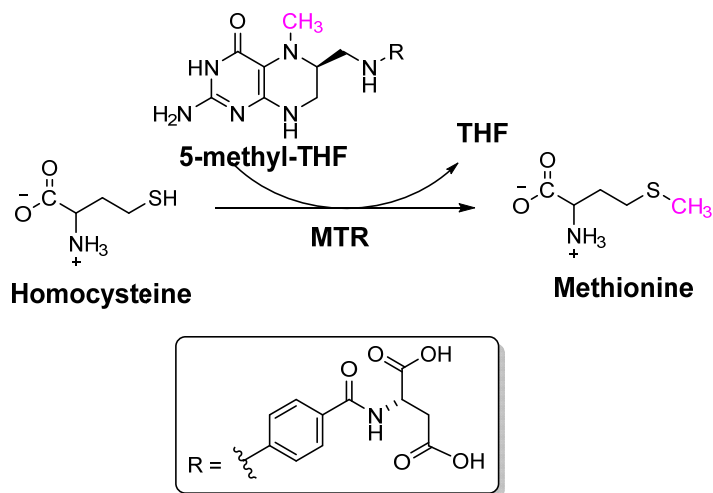


Figure 17. Methionine salvage.

5-Methyl-THF is the 1C unit transferring cofactor of methionine synthase (MTR) used for remethylation of homocysteine to methionine (Figure 17).¹⁹¹⁻¹⁹⁴ Methionine is the substrate for the synthesis of physiologically important reactive methyl carrier *S*-adenosylmethionine (SAM) by SAM synthetase. SAM, the second most common enzymatic cofactor after ATP, plays a key role in epigenetics (histone methylation); biosynthetic processes including phosphatidylcholine (likely the largest 1C sink in adult mammals), creatine, and polyamine synthesis; and sulfur metabolism.

A.5. Folate metabolizing enzymes

A.5.1. Dihydrofolate reductase (DHFR)

DHFR catalyzes the NADPH-dependent reduction of folic acid to DHF and THF. THF is an essential cofactor for the biosynthesis of purines, thymidylate, and several amino

acids, and biological methylation reactions.¹⁹⁵ Altered enzymatic activity of DHFR due to *DHFR* gene polymorphisms alters the THF pool for 1C metabolism which may contribute towards diseases dependent on folate status, such as cancer and spina bifida.

A.5.1.1. Structure of DHFR

DHFR is a small monomeric enzyme with 159-250 amino acids. It has an α/β structure with the core made up of eight-stranded β -sheet (seven parallel and one antiparallel strands). It also has four α -helices. The active site for substrate and cofactor (nicotinamide portion of NADPH) binding is located in a hydrophobic pocket indicating an important role of van der Waals interactions in ligand binding. The polar residues and the backbone carbonyls in the hydrophobic pocket however, do complement the polar pteridine and glutamate portions of the folate substrate (Figure 18).¹⁹⁶

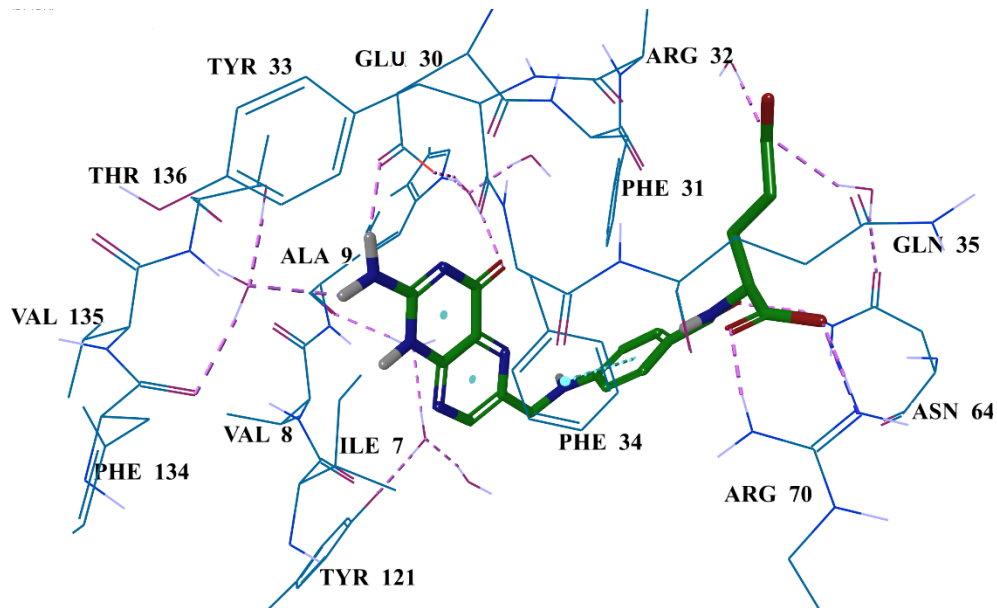


Figure 18. hDHFR in complex with folic acid (green) (PDB 1DRF) visualized using Maestro 11.2.¹⁹⁶⁻¹⁹⁷

As the reduced folates DHF and THF are susceptible to oxidative degradation, folic acid bound crystallographic structure of DHFR was resolved to gather structural information on protein-substrate interactions and substrate reduction by NADPH (Figure 18).¹⁹⁸ The 2-amino group of the pteridine moiety hydrogen bonds specifically with the carbonyl side-chain of Glu30. It also forms a network of hydrogen bond via a conserved water molecule with the side-chain oxygen of Thr136 and the backbone carbonyl of Phe134. The lactam O4 is hydrogen bonded to side-chain carboxylate of Glu30 and the indole nitrogen of Trp24 via the conserved water molecule. The *p*ABA moiety is positioned in a hydrophobic subsite, and van der Waals contacts exist between the benzoyl ring and the sidechains of Phe31 and Phe34. The amide carbonyl oxygen forms a hydrogen bond with the sidechain amide nitrogen of Asn64. The α -carboxyl of the L-glutamate interacts strongly via a salt bridge with the side-chain guanidinium of the Arg70. In contrast, the γ -carboxylate does not interact with any residue and is exposed to the bulk-solvent interface. This suggests that the folate polyglutamates polymerized via the γ -carboxylate could readily extend into the surrounding solvent for improved binding to hDHFR.¹⁹⁹⁻²⁰⁰

A.5.1.2. Catalytic mechanism

One side of the pteridine ring faces the binding site of the nicotinamide moiety of the coenzyme from where a hydride ion is transferred during catalysis.²⁰¹ Neither N5 nor N8 interact with the enzyme or to any of the water molecules. In the first step of folate reduction, a proton must be transferred from solution to N8, and to N5 after dihydrofolate reduction (after hydride transfer). Although no intermediates have been experimentally observed or characterized, multiple evidence point towards the first step of reduction to

7,8-DHF.^{196, 202-203} The proposed catalytic mechanism of 7,8-DHF reduction to THF by DHFR is shown in Figure 19.

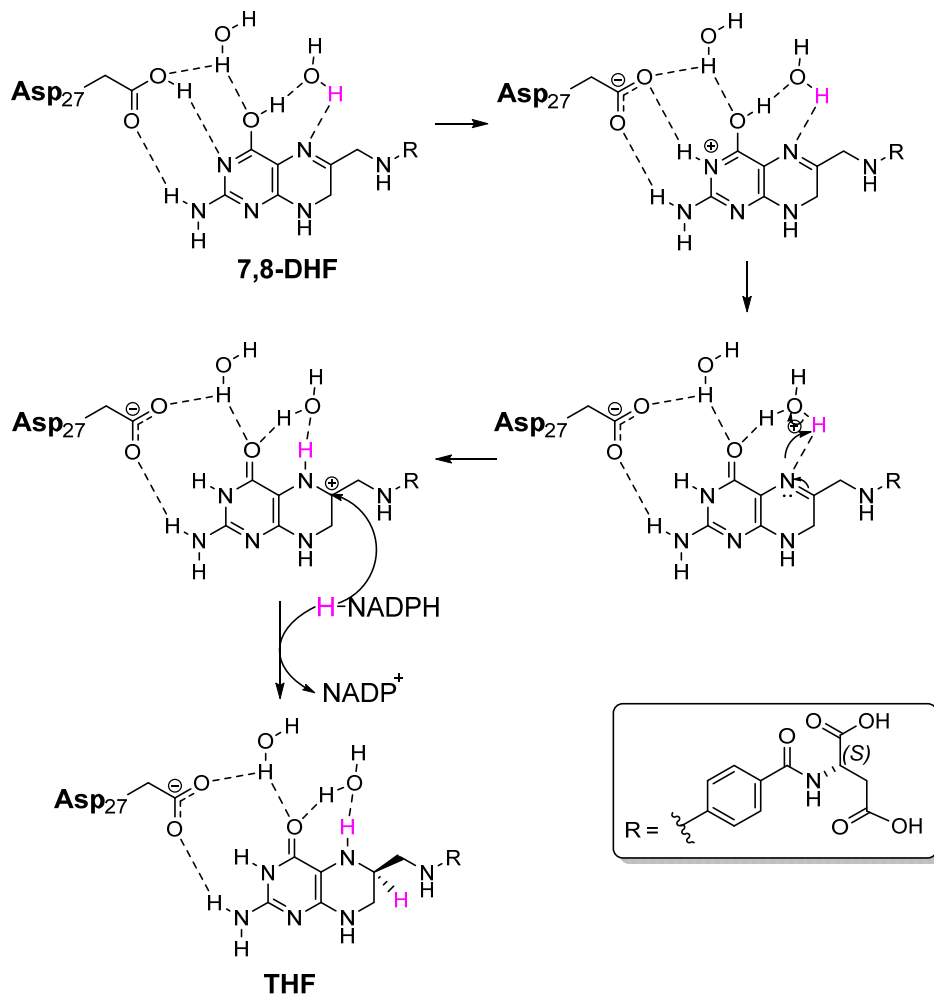


Figure 19. The catalytic mechanism of human DHFR.

The dissociation of THF is the rate-determining stage of the catalytic cycle for all forms of DHFR, and occurs only after NADP⁺ is replaced by NADPH due to negative cooperative effect upon the formation of the ternary complex. X-ray diffraction studies confirmed that the final step of reduction afforded (6*S*)-THF.²⁰⁴

A.5.1.3. Role of DHFR in cancer

THF shuttles carbon atoms for the action of folate-dependent enzymes and is thus essential for DNA synthesis and methylation. After a carbon unit is transferred, the folate is sequentially recycled by DHFR. Depleting THF levels by inhibiting DHFR, slows DNA synthesis and cell proliferation. Mutations and abnormal protein expression of DHFR has been related to specific cancers such as ALL, breast cancer, uterine sarcoma, cervical cancer etc.²⁰⁵⁻²⁰⁶

A.5.2. Thymidylate synthase (TS)

TS uses 5,10-methylene-THF as the 1C methyl donor for the catalytic reductive methylation of dUMP to dTMP, an essential precursor for DNA synthesis (Figure 16).²⁰⁷

A.5.2.1. Structure of TS

TS is a homodimeric enzyme (30-35kDa each) and contains about 316 amino acids. The overall fold of the enzyme is defined by 8 α -helices, 10 strands of β sheet, and several segments of coil that connect the secondary structural elements. Each subunit has a deep active site cavity that contains residues donated from both the subunits providing a structural basis for obligate dimerization of TS.²⁰⁸

Sayre *et al.* reported a 2.89 Å X-ray crystal structure of the ternary complex of hTS :dUMP:PMX.²⁰⁹ dUMP which binds first, forms part of the binding site for folates which bind to the active site on top of the nucleotide (Figure 20). The pterin ring of the folates adopt a folded conformation when bound to TS and is placed roughly perpendicular to the *p*ABA side-chain. The largest contact of the pterin scaffold is made with the bound pyrimidine of dUMP in which the ring systems of the two ligands are stacked against each

other by nonpolar interactions with Trp109. The backbone carbonyl of Ala313 and the side-chain carbonyl of Asp112 accept hydrogen bonds from the 2-NH₂ group and the pyrrole 7-NH respectively. The aromatic ring of the *p*ABA sidechain is placed in a hydrophobic pocket lined with the sidechains of Phe225, Leu221 and Ile108. The α -carboxyl of the glutamate forms an ionic interaction with Lys77. The binary crystal structures of TS with folate analogs confirm that folates can bind to the enzyme in the absence of the substrate.²¹⁰⁻

215

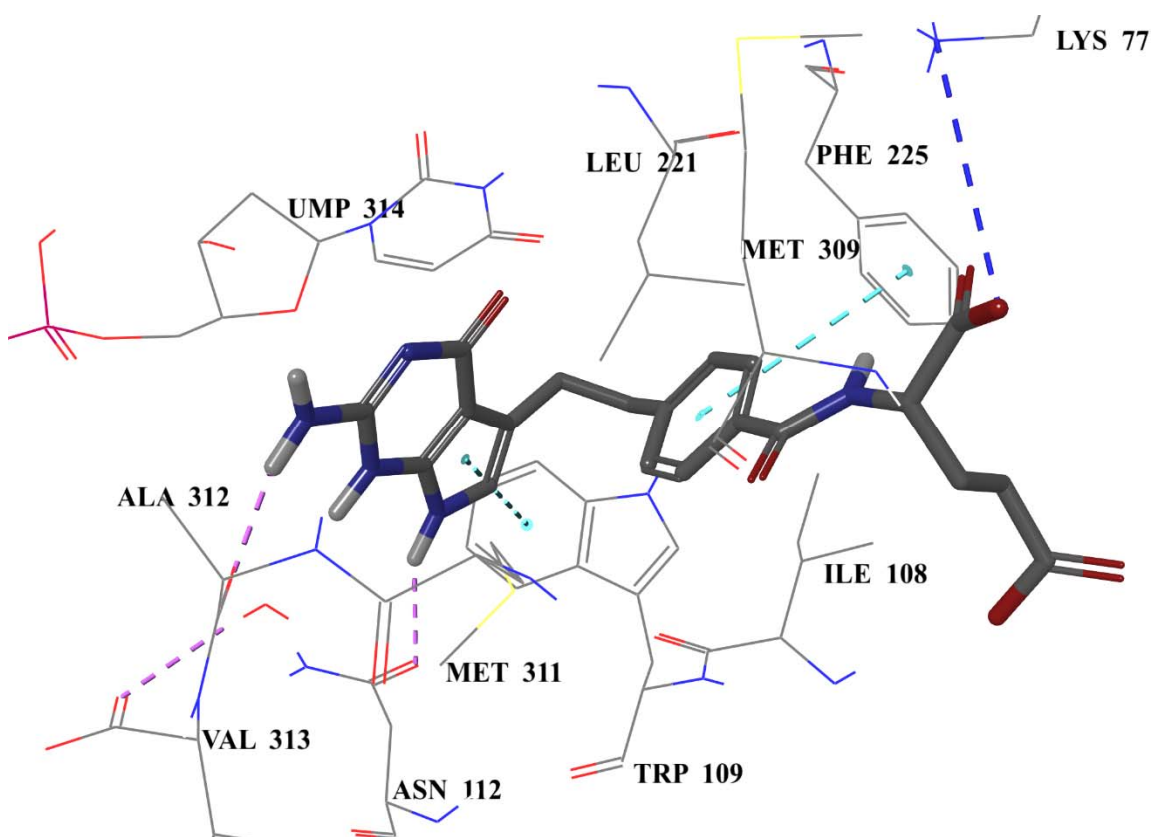


Figure 20. hTS in complex with dUMP and PMX (grey) (PDB 1JU6) visualized using Maestro 11.2.^{197, 208}

A.5.2.2. Catalytic mechanism

Figure 21 shows the salient features of the chemical mechanism of TS. A reversible ternary complex of TS is formed after sequential binding of the substrate dUMP followed by cofactor 5,10-methylene-THF.²⁰⁷ A Michael-type adduct formed by the nucleophilic attack of the sulfhydryl of Cys195 of human TS (hTS) on the C6-position of the uracil ring in dUMP activates the C5-position.

Protonation of the N10-position opens the tricyclic ring of the cofactor forming the N5-imminium ion in the bicyclic form. The N5-imminium of the unstable, covalent ternary complex is then trapped by the C5 Michael-type adduct to form the intermediate, which is followed by abstraction of C5-proton by a yet to be identified base in the active site. Its conjugate base is resonance delocalized through the pyrimidine ring of the substrate, eventually leading to the elimination of the covalently bound folate and formation of the intermediate with an exocyclic methylene. Due its high carbonium ion character, the C7 methylene readily accepts a hydride from C6 of the noncovalently bound folate. The final β -elimination of the enzyme from C6 of the pyrimidine occurs without any assistance.²⁰⁷

A.5.2.3. Implications of Surface Charge Pattern on Polyglutamylation

The folate-binding region of TS active site exhibits the largest area of positively charged surface as observed from the molecular electrostatic potential map. This is the region where the polyglutamate tail of the folate cofactor binds.²¹⁶ The polyglutamyl moiety does not form fixed interactions with the protein except for the first glutamate residue. The additional glutamate chains are progressively more disordered and are

expected to bind to Lys50, Lys51, His-53, Arg55 Lys58 and Lys311 residues in the regions of positive electrostatic potential.²¹⁷⁻²¹⁹

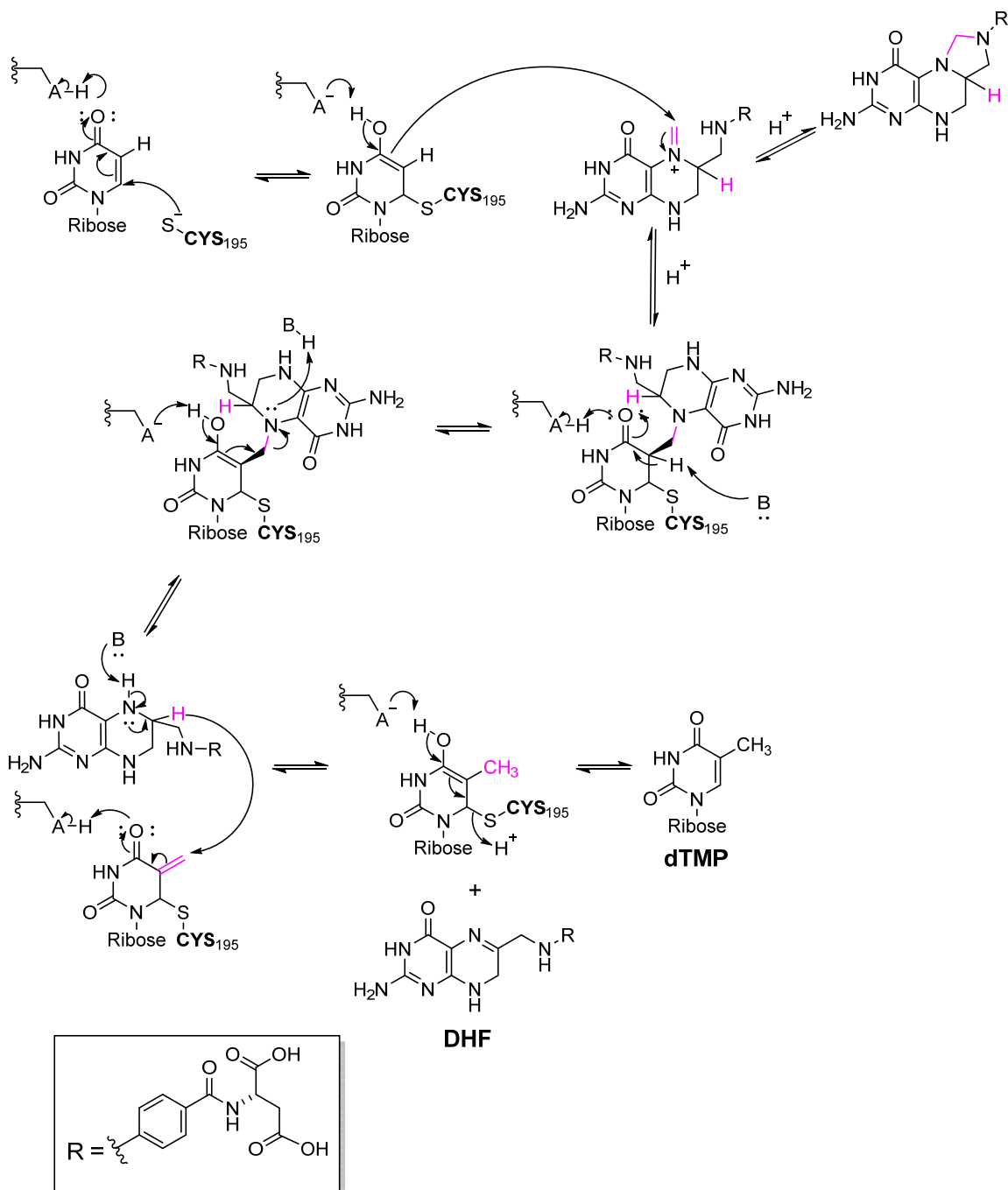


Figure 21. The catalytic mechanism of human TS.

A.5.2.4. Role of TS in cancer

TS protein and mRNA levels are elevated in many human cancers such as colorectal, breast, cervical, bladder, kidney, and non-small cell lung cancers, which correlates with poor patient prognosis.²²⁰⁻²²⁴ 2'-deoxythymidine-5'-triphosphate (dTTP) depletion due to inhibition of TS leads to dUTP misincorporation in to DNA, DNA fragmentation and growth prevention of actively dividing cells and finally apoptosis, referred to as “thymineless death”.²²⁵⁻²²⁶

A.5.3. The purinosome

The enzymes of the de novo purine biosynthetic pathway compartmentalize in the cytoplasm under conditions of purine depletion to form a functional complex termed the purinosome.^{184, 205} Purines are essential molecules that are components of a myriad of vital biomolecules such as DNA (cellular processes such as genetic transfer), RNA (translation and transcription), ATP and GTP (energy storage and transfer), cyclic AMP and GMP (signaling), and NADH, NADPH and coenzyme A (cofactors).²²⁷ Cells procure purine nucleotides either from de novo biosynthesis of inosine monophosphate (IMP) or by salvage from hypoxanthine, adenine or guanine. Increased de novo purine biosynthesis is linked to malignant transformation as purines are preferentially salvaged in a healthy cell.²²⁸⁻²³¹

The de novo biosynthesis of purines is a highly conserved pathway that forms inosine monophosphate (IMP) from 5-phosphoribosyl- α -1-pyrophosphate (PRPP) and glutamine. Ten enzymatic activities required to carry out this conversion in humans are catalyzed by six enzymes.²³²⁻²³³ A trifunctional enzyme (TGART) composed of

glycinamide ribonucleotide synthetase (GARS), GARFTase and aminoimidazole ribonucleotide synthetase (AIRS), and a bifunctional enzyme (ATIC) which is composed of AICARFTase and inosinemonophosphate cyclohydrolase (IMPCH) utilize folate cofactors for 1C transfer (a formyl group from 10-formyl-THF is transferred to the intermediate (Figure 15). X-ray crystal structures have been solved for TGART as well as ATIC.²³⁴⁻²³⁸

The interplay of the purinosome with other metabolic pathways and its impact is only just beginning to be understood. The growth of cancer cells is dependent upon increased glucose uptake and lactic acid fermentation via a metabolic reprogramming phenomenon called the Warburg effect.^{156, 239} This process is tightly regulated by cellular purine levels. Pyruvate kinase, involved in glycolysis, plays a vital role in the growth and metabolic reprogramming of cancer cells and is allosterically stimulated by the purine biosynthetic pathway intermediate, succinyl-5-aminoimidazole-4-carboxamide-1-ribose-5'-phosphate (SAICAR).²⁴⁰ This allosteric stimulation may then generate energy and metabolic flux in response to nutritional and energetic demands of rapidly multiplying cells. AICAR, a de novo purine biosynthetic intermediate and substrate of AICARFTase is an AMP analog and a known activator of AMP kinase (AMPK). AMPK is a regulatory switch for several intracellular processes such as glucose uptake, glycolysis, insulin signaling, lipogenesis, and cell cycle control among others.²⁴¹⁻²⁴³

A.5.3.1. GARFTase

In higher eukaryotes, the enzyme GARFTase comprising the C-terminal domain of a trifunctional enzyme TGART catalyzes formylation of glycinamide ribonucleotide (GAR) to *N*-formyl glycinamide ribonucleotide (FGAR) (the first of two formyl transfer

reactions) in the de novo biosynthetic pathway of purines.^{236, 244-247} This is accompanied by the conversion of the cosubstrate, 10-formyl-THF, to THF.^{244, 248}

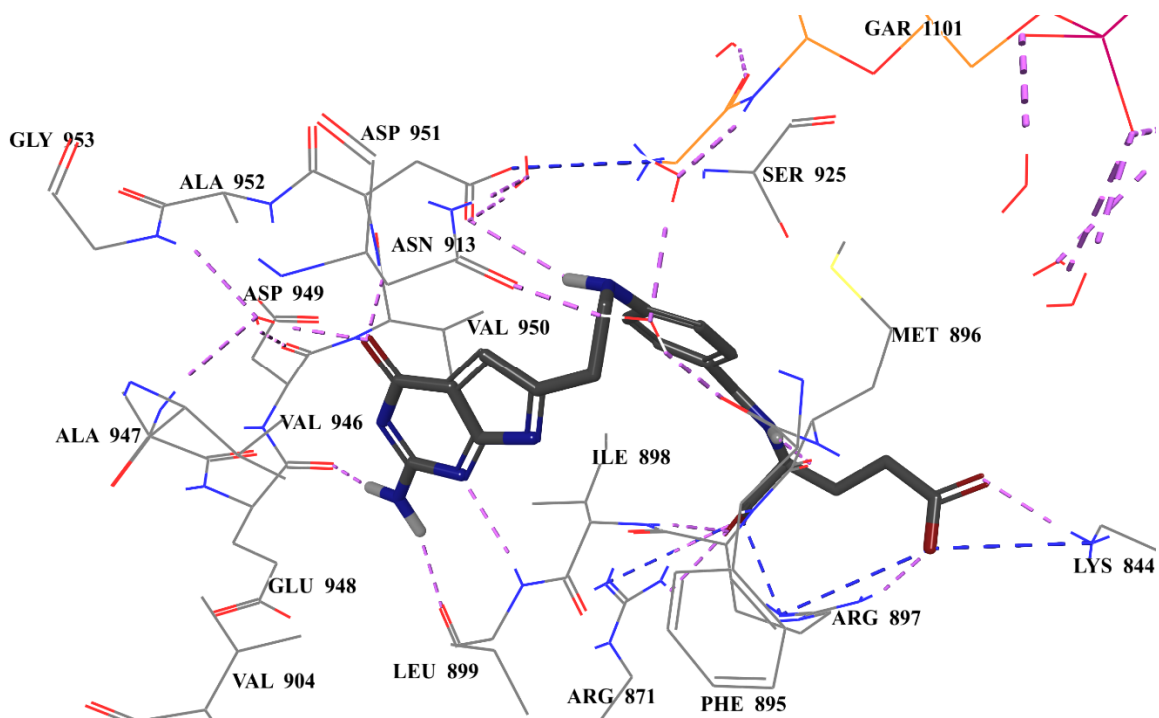


Figure 22. hGARFTase in complex with compound **11** (grey) (PDB 5J9F) visualized using Maestro 11.2.^{167, 197} Partial structure of GAR is shown in orange.

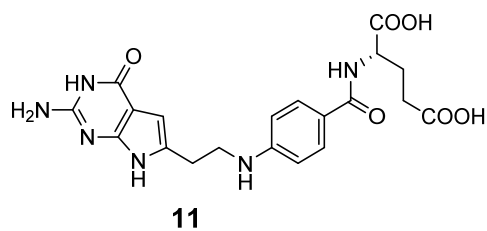


Figure 23. Compound **11** co-crystallized as a complex with hGARFTase (PDB 5J9F).¹⁶⁷

A.5.3.1.1. Structure of GARFTase

The apo protein, binary and ternary structures of human GARFTase (hGARFTase) with antifolates have been reported.^{167, 236, 249-251} Figure 22 shows the interactions made by

a co-crystallized GARFTase inhibitor, compound **11** in the folate binding pocket.¹⁶⁷ The scaffold is stabilized in the binding site by multiple interactions, hydrogen bonds between (1) the N1 nitrogen and the backbone NH of Leu899, (2) 2-NH₂ and the backbone carbonyl of Leu899 and Glu948, and (3) the 4-oxo and the backbone NH of Asp951 (Figure 22). Additionally, the 4-oxo form a water-mediated hydrogen bonding network via a conserved water molecule with Ala947, Gly953, and Asp949. The pyrrolo[2,3-*d*]pyrimidine bicyclic scaffold is also placed appropriately for van der Waals interactions with Val950. The N10 hydrogen forms a hydrogen bond with the sidechain carboxyl of Asp951. The amide NH of the L-glutamate form a hydrogen bond with the carbonyl of Met896. The L-glutamates are oriented with the α -carboxylates forming a salt bridge with the side-chain of Arg871 and a hydrogen bond interaction with the backbone amide NH of Ile898 and with the side-chain of Arg897. The γ -carboxylate forms salt bridges with the side-chains of Lys844 and Arg897.

A.5.3.1.2. Catalytic Mechanism

Kinetic studies of hGARFTase suggest a random sequential binding and a direct nucleophilic attack of the GAR amino group on the formyl carbon of 10-formyl-THF for formyl group transfer.²⁵² The formyl group in the bound 10-formyl-THF is suggested to twist out of the delocalized planar structure and relieve the resonance stabilization thereby increasing its electrophilicity.²⁵³ Further, a random-collision mechanism between the pre-activated cosubstrate and the flexible nucleophilic end of GAR at extremely high local concentrations has been suggested for catalysis. A tetrahedral intermediate has been proposed that collapses to product via proton transfer relay between GAR (NH₂) and

His915 (electrostatic interaction to GAR (NH₂) through Asn913 and ultimately Asp951 and His915) (Figure 24).

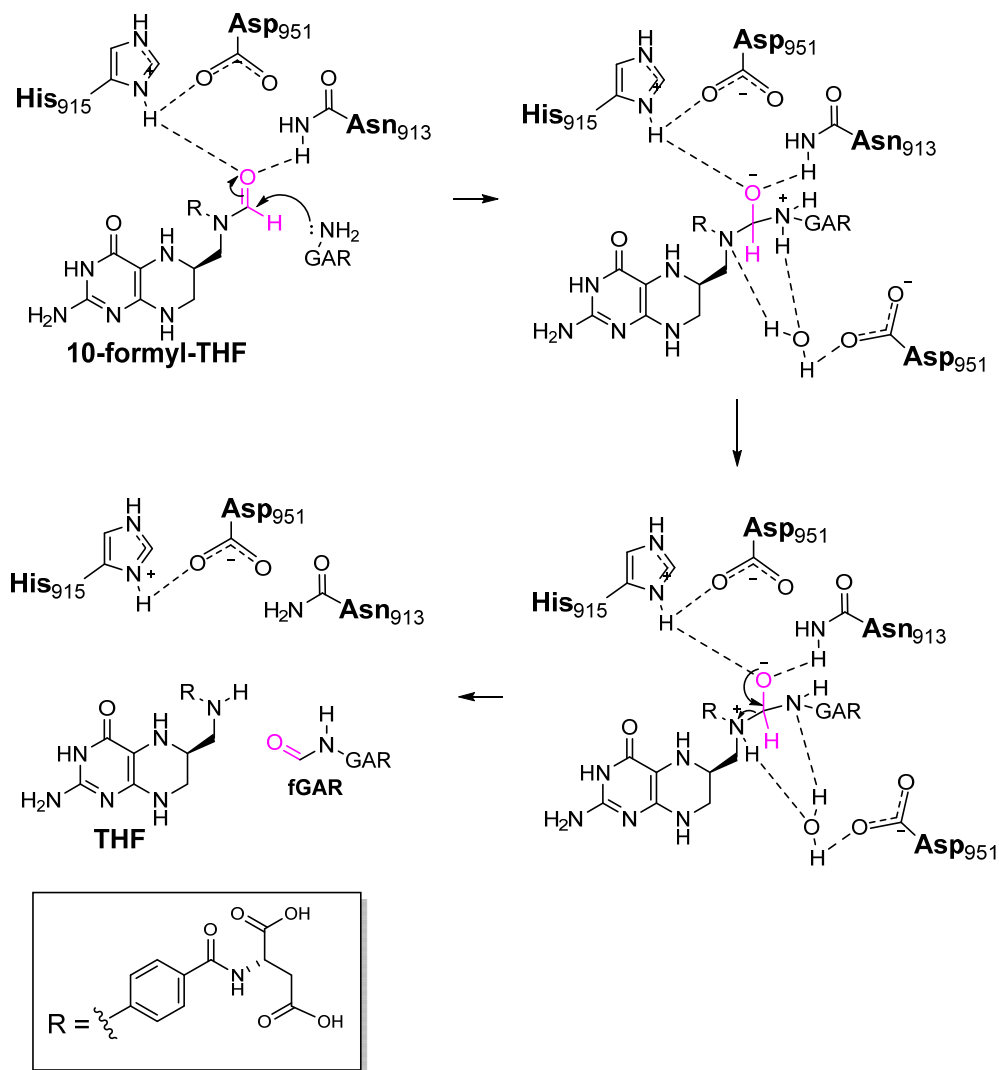


Figure 24. Proposed mechanism for formyl transfer by human GARFTase.

A.5.3.1.3. Implications of Surface Charge Pattern on Polyglutamylation.

Polyglutamylation enhances affinity of folates by orders of magnitude towards hGARFTase.²⁵⁴⁻²⁵⁵ Surface potential of the ternary complex of the hGARFTase depicts that the electrostatic potential at its surface extending away from the γ -carboxylate of the

monoglutamate to the folate binding loop is either neutral or positively charged. Therefore, it would be complementary to the charge pattern of a polyglutamate (neutral and negatively charged regions) and may explain the improved binding affinity.

A.5.3.1.4. Role of GARFTase in cancer

GARFTase which catalyzes the first of the two folate-dependent 1C transfer reactions plays a pivotal role in the de novo purine biosynthetic pathway overexpressed in most tumor cells. A majority of cancer tissues such as hepatocellular carcinoma, renal cancer, head and neck cancer, liver cancer, pancreatic cancer, testicular- and urothelial cancer display moderate to strong GARFTase cytoplasmic expression. High mRNA expression correlates with shorter survival times with mostly unfavorable prognosis.²⁵⁶⁻²⁵⁷

A.5.3.2. AICARFTase

AICARFTase catalyzes the formylation of 5-aminoimidazole-4-carboxamide-ribonucleotide (AICAR) to produce formyl-AICAR (fAICAR) accompanied by the conversion of the cosubstrate, 10-formyl-THF, to THF (Figure 15). AICARFTase has no significant homology with GARFTase. Homodimerization of ATIC is a requisite for transformylase activity of AICARFTase as the active sites form at the interface of the interacting proteins, with each monomer contributing residues to the folate and AICAR binding pockets.

A.5.3.2.1. Structure of AICARFTase

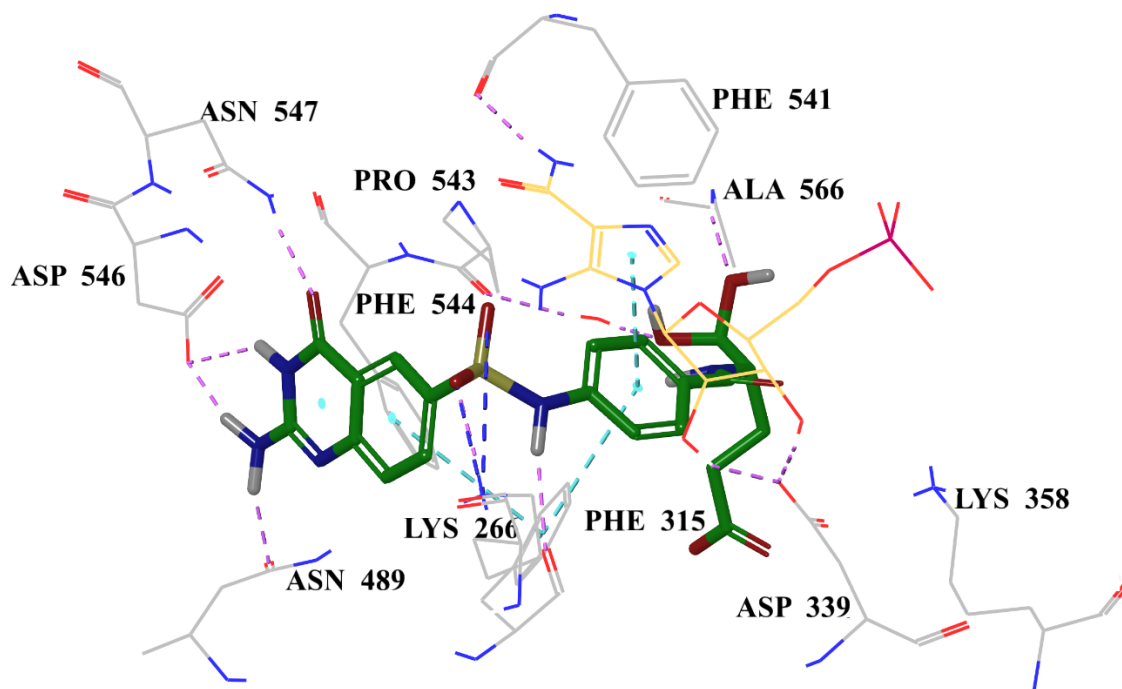


Figure 25. Crystal structure of human AICARFTase in complex with folate-based inhibitor **BW1540U88UD** (green) (PDB 1P4R), visualized using Maestro 11.2.^{197, 258} AICAR is shown in yellow.

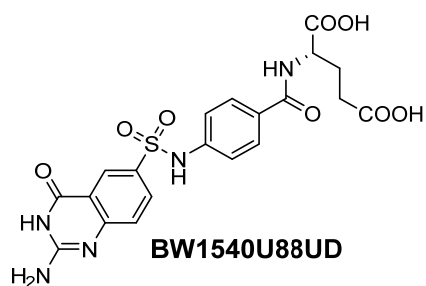


Figure 26. Compound **BW1540U88UD** co-crystallized as a complex with hAICARFTase (PDB 1P4R).²⁵⁸

AICARFTase is the functional, C-terminal domain (residues 200–593) of a bifunctional homodimer enzyme ATIC.²⁵⁸ Two sulfamido-linked 5,8-dideazafolate folate-

based inhibitors that are specific for human ATIC were co-crystallized with human ATIC in the presence of the substrate AICAR. The AICARFTase active site is located at the dimer interface in a long, narrow cleft where AICAR and folate interact primarily with the opposing subunits (Figure 25).²⁵⁹ The 5,8-position of the dideazafolate ring of co-crystallized **BW1540U88UD** (Figure 26) (homologous to the pterin ring in 10-formyl-THF) is fixed within a hydrophobic environment Pro543, Phe544, above and side chain of Phe315 below. Hydrogen bond interactions are formed between the 2-amino group and side chain carbonyls of Asn489 and Asp546, N3 and side-chain carbonyl of Asp546, and 4-oxo and side-chain carbonyl of Asn547. The AICAR imidazole and the phenyl moiety of *p*ABA form π -stacking interactions with each other as well as with the side-chains of Phe541 and Phe315. The sulfonyl oxygen and NH (N10-formyl group mimic) form hydrogen bonds with the side-chain of Lys266. The glutamate tail is oriented such that a hydrogen bond is made by the α -glutamate with the backbone amide of Ala566 and a water-mediated hydrogen bond is made with the backbone of Pro543.

Extensive electropositive surface near the active site likely accounts for binding to the negatively charged polyglutamate tail, for increased affinity to ATIC.²⁶⁰⁻²⁶¹

A.5.3.2.2. Catalytic mechanism

The AICARFTase ternary complex formation is ordered and sequential and the folate cofactor binds first to the active site.²⁶² The formyl group is transferred directly to AICAR without any enzyme-bound formylated intermediate (Figure 27).^{238, 259, 263} His267 is the proposed catalytic base that deprotonates the AICAR amino group, thus increasing the nucleophilicity for concomitant nucleophilic attack on the formyl group of 10-formyl-

THF. The oxyanion transition state is stabilized in the oxyanion hole and protons are shuttled to the N10 of THF by Lys266.²⁶⁴⁻²⁶⁵

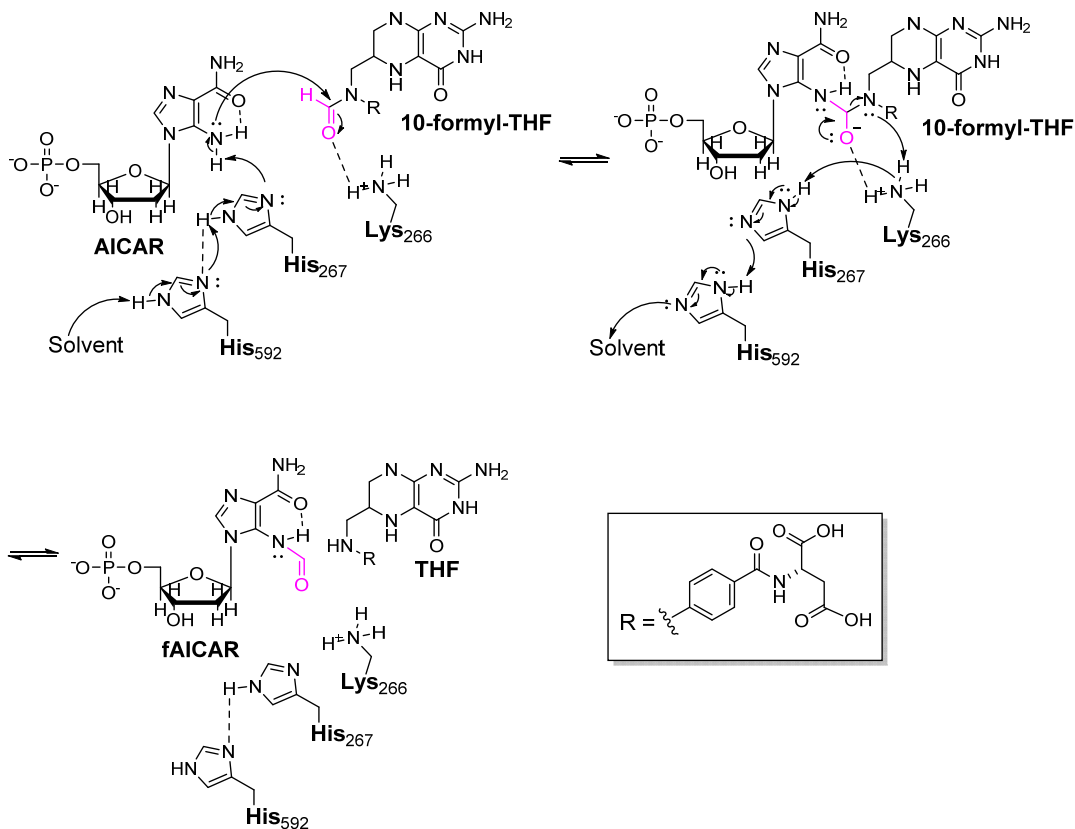


Figure 27. Proposed mechanism for formyl transfer by human AICARFTase.

A.5.3.2.3. Role of AICARFTase in cancer

AICARFTase, which catalyzes the second folate-dependent 1C transfer reactions plays a pivotal role in the de novo purine biosynthetic pathway overexpressed in most tumor cells. A majority of cancer tissues such as colorectal, testicular, breast, stomach and pancreatic cancers, and melanomas, display strong AICARFTase cytoplasmic expression. High mRNA expression correlates with shorter survival times with mostly unfavorable prognosis.²⁶⁶

The de novo biosynthetic pathways of purine and pyrimidine nucleotides produce ATP, GTP, UTP, and CTP, precursors for DNA, precursors for RNA, and activated metabolites such as UDP-glucose and CDP-choline.²⁶⁷ More than 20% of all approved oncology drugs are purine or pyrimidine antimetabolites.²⁶⁸ TS is the primary target of clinically used antifolate anticancer agents **PMX** and **RTX**, while DHFR is the canonical target of the antifolate anticancer agents **MTX** and **PTX** and a secondary target of **PMX** (Figure 5).^{22, 165, 180, 269-271}

Currently, there are no clinically used inhibitors of the folate-dependent enzymes of the purinosome. Inhibitors of the enzymes of these pathways may be effective as drugs for treatment of cancer. Depletion of purines by targeting de novo purine nucleotide biosynthesis with folate analogs can limit nucleotide levels for DNA synthesis and repair, while also influencing the ATP and GTP cellular energetics stores. The folate-dependent enzymes GARFTase and/or AICARFTase are primary targets of “second generation” antifolates (Figure 28). Inhibition of glycinamide ribonucleotide GARFTase and/or AICARFTase, is a potential chemotherapeutic intervention that can provide both potency and selectivity due to two main reasons: 1) rapidly dividing tumors produce purines via de novo synthesis, whereas normal cells salvage them, and 2) common cellular folate transport systems can be used for dual targeting of both the folate-dependent enzymes.^{228-230, 272}

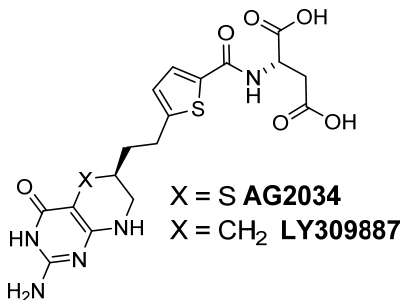


Figure 28. Second generation GARFTase inhibitors.^{63, 273-274}

The discovery of a C6 *R* isomer of potent antipurine antifolate 5,10-dideazatetrahydrofolate (DDATHF, lometrexol, **LMX**) in the mid-1980s as the inhibitor of GARFTase validated GARFTase as a viable anticancer target (Figure 5).²⁷³ It entered clinical trials and demonstrated antitumor activity against a wide range of solid tumors. GARFTase in de novo purine nucleotide biosynthesis is a secondary target of PMX.^{165, 180, 270-271} **LY309887** and **AG2034** (Figure 28) are the 2nd generation inhibitors which exclusively target de novo purine nucleotide biosynthesis at GARFTase and showed promising in vitro and in vivo antitumor activities in assorted preclinical tumor models associated with depletion of purine nucleotide pools.^{63, 273-275} Unfortunately, in phase I clinical trials, these inhibitors showed dose-limiting myelosuppression and mucositis toxicities due to RFC uptake thus hampering further clinical development.^{63-64, 276-277}

Gangjee and coworkers reported ternary crystallographic structures of the formyltransferase domain of hGARFTase complexed with the β -GAR substrate and eight structurally diverse 6-substituted pyrrolo- and thieno[2,3-*d*]pyrimidine antifolates (monoglutamates) that are relatively potent (compared to the clinically available antifolates) tumor-targeted inhibitors (Figure 29).²⁵¹ Collectively, the results provide a rational basis for understanding the in vitro activity profiles of FR- and PCFT-targeted

antifolates that inhibit GARFTase. Differences in the positioning and number of contacts formed by the L-glutamyl tail, and the hydrogen bonding capability of the bicyclic ring correlate with the inhibitor potencies. The ideal positioning of the glutamyl tail is influenced by the inherent length and flexibility of the linkers, and the regioisomeric substitution on the side-chain (het)aryl ring. A 4C linker connected to a planar aromatic sidechain maximizes the number of contacts of L-glutamate tails atoms with the GARFTase binding pocket. A hydrogen bond interaction with Arg897 carboxyl by the pyrrolo[2,3-*d*]pyrimidine antifolates correlates with the loss of activity upon bioisosteric replacement of the pyrrole ring with a non-hydrogen bonding thiophene in the thieno[2,3-*d*]pyrimidine antifolates. These structural determinants involved in GARFTase inhibition aid in the design of future generations of novel targeted antifolates that inhibit GARFTase.

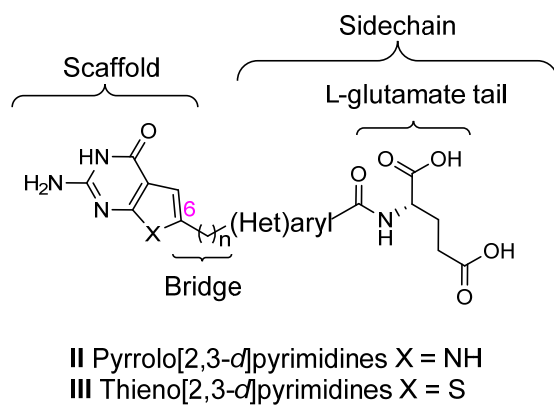


Figure 29. 6-substituted pyrrolo- and thieno[2,3-*d*]pyrimidine antifolates.²⁵¹

Along with inhibition of the de novo purine biosynthesis, AICARFTase inhibition also demonstrates inhibition of cell proliferation and cell cycle progression in human carcinomas by indirectly activating the AMP activated protein kinase (AMPK), Modulation of AICAR levels represents a novel means to AMPK signaling and cell cycle

control.²⁷⁰⁻²⁷¹ The inhibition of AICARFTase activity along with RFC uptake displays non-specific activity and undesirable side effects.²⁶⁷ The 6(*S*)-diastereomer of **LMX** and the tetraglutamyl derivative of **dmAMT** are potent AICARFtase inhibitors (Figures 5 and 31).²⁷⁴ Little published information is available about another classical antifolate, **AG2009** (Figure 30), which is an AICARFTase specific inhibitor.²⁷⁸ Notably, AICARFTase, is a secondary target of **PMX**.^{165, 180, 270-271} Inhibition of AICARFTase in **PMX**-treated tumor cells causes accumulation of its substrate ZMP, ZMP-mediated activation of 5' adenosine monophosphate-activated protein kinase (AMPK), AMPK-mediated phosphorylation of RapTOR and TSC2 and p53 independent mTOR inhibition.²⁷⁹

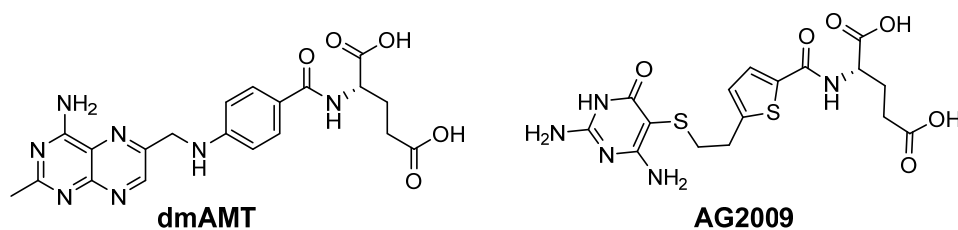


Figure 30. AICARFTase inhibiting Antifolates.^{274, 278}

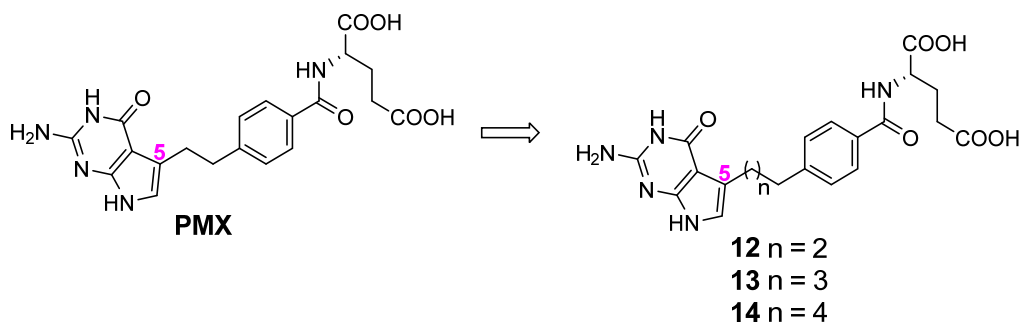


Figure 31. 5-substituted pyrrolo[2,3-*d*]pyrimidine linker extension analogs of **PMX**.¹²⁰

Gangjee and coworkers have reported relatively more potent tumor-targeted 5-substituted pyrrolo[2,3-*d*]pyrimidine 3C-5C linker extension analogs of **PMX** which

displayed dual GARFTase and AICARFTase activity (Figure 31 and Table 5).^{117, 120} Unlike **PMX**, which is a pyrimidine biosynthesis inhibitor, they primarily inhibit the purine biosynthetic pathway as dual inhibitors. These novel, dual inhibitors will not only have reduced propensity for resistance development (another caveat of cancer chemotherapy) but will also circumvent the current TS resistance developed against **PMX**.

Table 5. IC₅₀ Values (nM) for 5-substituted pyrrolo[2,3-*d*]pyrimidine antifolates and classical antifolates.¹²⁰ For KB cells, data are shown for the protective effects of nucleoside additions, including adenosine (Ade), thymidine (Thd), or AICA.

Antifolate	CHO (IC ₅₀ s) (nM)			KB (IC ₅₀ s) (nM)	KB (+Thd/Ade/AICA)
	PC43-10 (RFC)	RT16 (FR α)	PCFT4 (PCFT)		
12	68.8 (21.2)	72.0 (27.1)	329 (61)	49.5 (13.2)	Ade
13	56.6 (5.8)	8.6 (2.1)	840 (90)	12.7 (5.4)	Ade
14	196.4 (55)	33.5(2.5)	>1000	17.3(8.9)	Ade/AICA
PMX	26.2 (5.5)	42 (9)	8.3 (2.7)	68 (12)	Thd/Ade
MTX	12 (1.1)	114 (31)	121 (17)	6.0 (0.6)	Thd/Ade
RTX	6.3 (1.3)	15 (5)	99.5 (11.4)	5.9 (2.2)	Thd
PTX	0.69 (0.07)	168 (50)	57 (12)	0.47 (0.20)	Ade/Thd

Currently, there are no tumor targeted cytotoxic agents in clinical use; all the chemotherapeutic agents display dose-limiting toxicity. Clinically used antifolates not only have dose-limiting toxicities but also suffer from drug-resistance. As such, to circumvent these drawbacks, novel antifolates that block purine biosynthesis by targeting either or both the folate-utilizing enzymes selectively by virtue of their specificities for FRs and /or PCFT are needed. Inhibition of purine biosynthesis not only provides a novel mechanism of

action but also circumvents resistance developed by the currently clinically relevant antifolate enzyme targets; TS as well as DHFR. Moreover, targeting more than one purine metabolizing enzyme reduces the probability of resistance towards the additional target, thus preserving the cytotoxic activity of the inhibitors.

The novel mechanisms of action, and improved potency and selectivity of the 5-and 6-substituted pyrrolo[2,3-*d*]pyrimidine antifolates over the currently marketed counterparts call for the optimization of these analogs as a viable approach for the development of novel cancer chemotherapeutics.

II. CHEMICAL REVIEW

The synthetic methodologies related to the present work is reviewed and includes the approaches to the following general structures:

B.1. Synthesis of pyrrolo[2,3-*d*]pyrimidines

B.2. Synthesis of alkyl benzoates by Sonogashira coupling

B.3. Synthesis of alkyl benzoates by domino Heck reactions

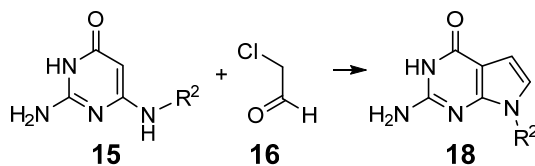
B.1. Synthesis of pyrrolo[2,3-*d*]pyrimidines

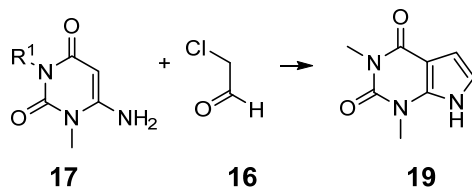
The pyrrolo[2,3-*d*]pyrimidine scaffold finds application in medicinal chemistry design as a deazapurine analog. As such, its syntheses has been extensively reported using various strategies that can be classified into the following:

1. Synthesis from pyrimidine precursors
2. Synthesis from furan precursors
3. Synthesis from pyrrole precursors

B.1.1. From pyrimidine precursors

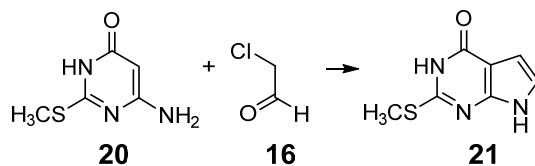
Scheme 1. Synthesis of pyrrolo[2,3-*d*]pyrimidines **18-19**.





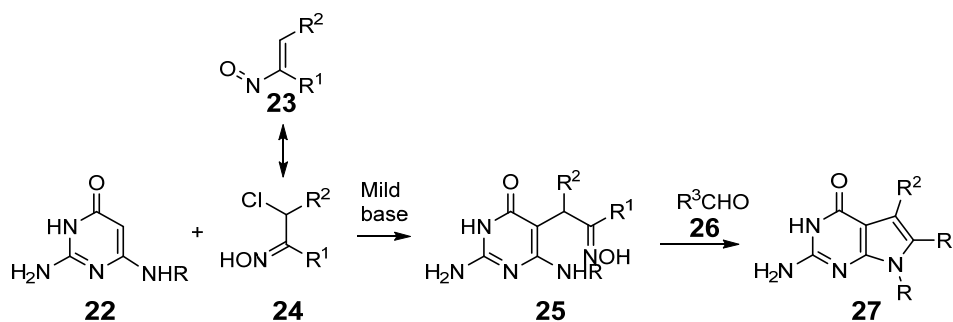
Noell and Robins²⁸⁰ originally reported the synthesis of pyrrolo[2,3-*d*]pyrimidines **18** and **19** (Scheme 1) via condensation of chloroacetaldehyde **16** with 2-amino-6-alkylamino-4-oxypyrimidines **15** and 6-amino-1,3-dimethyluracil **17** respectively.

Scheme 2. Synthesis of 2-methylthio-4-oxo-pyrrolo[2,3-*d*]pyrimidine **21**.



Noell and Robins²⁸⁰ also reported the synthesis of 2-methylthio-4-oxo-pyrrolo[2,3-*d*]pyrimidine **21** (Scheme 2) in the same report, from 2-methylthio-6-amino-4-pyrimidone **20** and chloroacetaldehyde **16**.

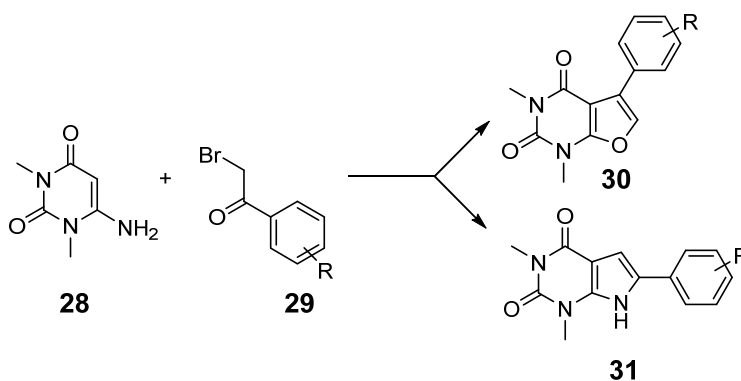
Scheme 3. Synthesis of 2-amino-4-oxo-pyrrolo[2,3-*d*]pyrimidines **27**.



Gibson et al.²⁸¹ reported a synthetic approach for the preparation of 2-amino-4-oxo-pyrrolo[2,3-*d*]pyrimidines **27** (Scheme 3) from condensation of an oxime **24** with 2,6-

diamino-4-pyrimidone **22** in mildly basic conditions (sodium carbonate, sodium acetate, or triethylamine) to the intermediate adduct **25**. Thermal cyclization/cyclization under acid-catalyzed transoximation of **25** with substituted aldehydes **26** afforded the pyrrolo[2,3-*d*]pyrimidine scaffolds substituted **27** at the C5 and C6 positions.

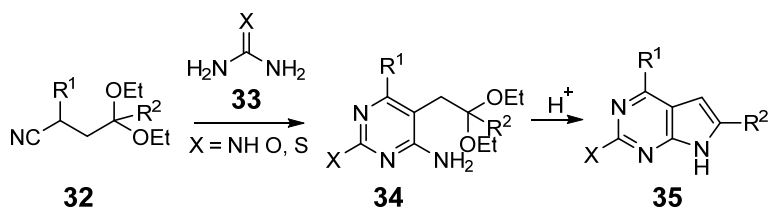
Scheme 4. Synthesis of furo[2,3-*d*]pyrimidines **30** and pyrrolo[2,3-*d*]pyrimidines **31**.



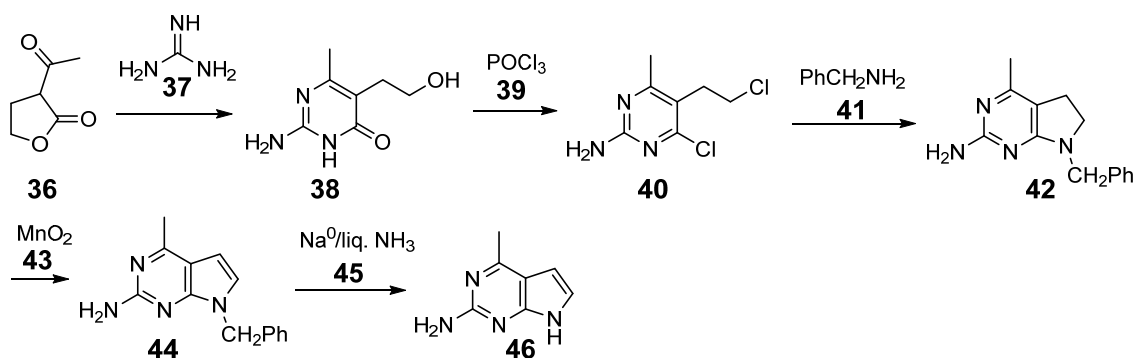
Fumio *et al.*²⁸² reported that the condensation of 6-amino-1,3-dimethyluracil **28** (Scheme 4) with phenacyl bromides **29** in DMF afforded 1,3-dimethyl-6-phenylpyrrolo[2,3-*d*]pyrimidines **31**. However, running the reaction in acetic acid also afforded the 1,3-dimethyl-5-phenylfuro[2,3-*d*]pyrimidine-2,4-(1*H*,3*H*)-diones **31** as a side product.

Davoll and coworkers²⁸³ reported an acid mediated cyclization of acetals or ketal derivatives of pyrimidine 5-acetaldehyde or acetone **34** (Scheme 35) to various pyrrolo[2,3-*d*]pyrimidines **35**. The intermediate **34** were obtained from the cyclization of the substituted nitrile **32** with guanidine, urea and thiourea **33**.

Scheme 5. Synthesis of pyrrolo[2,3-*d*]pyrimidines **35**.

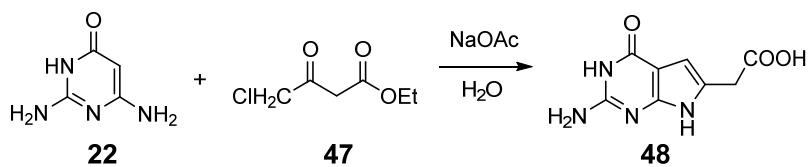


Scheme 6. Synthesis of 2-amino-4-methyl-pyrrolo[2,3-*d*]pyrimidine **46**.



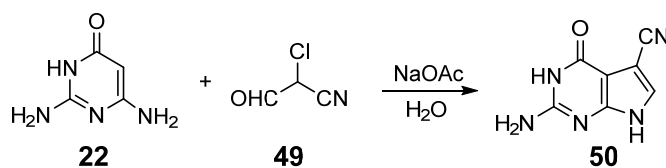
Gangjee and coworkers²⁸⁴ reported a novel ring closure method for the synthesis of 2-amino-4-methyl-pyrrolo[2,3-*d*]pyrimidine **46** (Scheme 6). Condensation of 2-acetylbutyrolactone **36** with guanidine **37** afforded the substituted pyrimidine **38**. Chlorination with POCl₃ to the dichloro derivative **40** and subsequent condensation with benzylamine **41** afforded the 7-benzyl-4-methyl-6,7-dihydro-5*H*-pyrrolo[2,3-*d*]pyrimidin-2-amine **42**. Oxidative aromatization of the dihydropyrrole ring in **42** with MnO₂, followed by debenzylation with metallic sodium in ammonia provided the 2-amino-4-methyl-pyrrolo[2,3-*d*]pyrimidine **46**.

Scheme 7. Synthesis of 2-(2-amino-4-oxo-4,7-dihydro-1*H*-pyrrolo[2,3-*d*]pyrimidin-6-yl)acetic acid **48**.



Gangjee and coworkers²⁸⁵ also reported the synthesis of 2-(2-amino-4-oxo-4,7-dihydro-1*H*-pyrrolo[2,3-*d*]pyrimidin-6-yl)acetic acid **48** (Scheme 7). Condensation of 2,6-diaminopyrimidin-4(1*H*)-one **22** with ethyl 4-chloro-3-oxobutanoate **47** in the presence of sodium acetate (Scheme 7) afforded the pyrrolo[2,3-*d*]pyrimidine **48**.

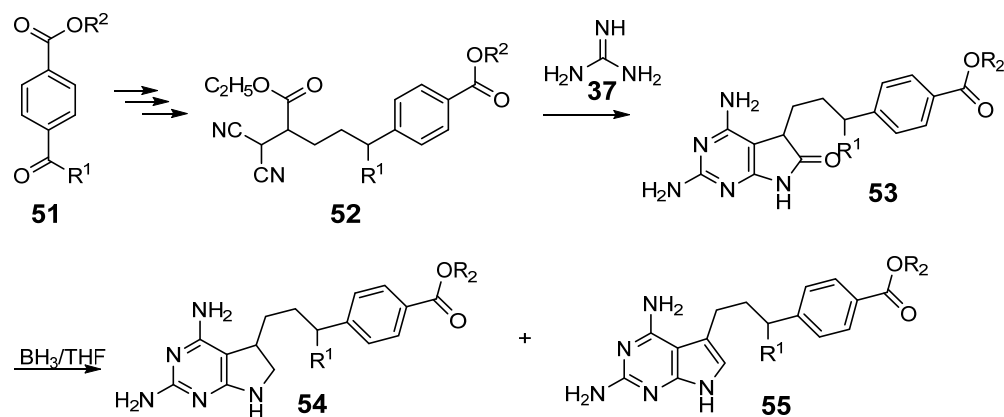
Scheme 8. Synthesis of 2-amino-4-oxo-4,7-dihydro-1*H*-pyrrolo[2,3-*d*]pyrimidine-5-carbonitrile **50**.



In another report, Gangjee and coworkers²⁸⁶ also reported the synthesis of 2-amino-4-oxo-4,7-1*H*-pyrrolo[2,3-*d*]pyrimidine-5-carbonitrile **50** (Scheme 8) from the condensation of pyrimidine **22** with 2-chloro-3-oxopropanenitrile **49** under basic conditions.

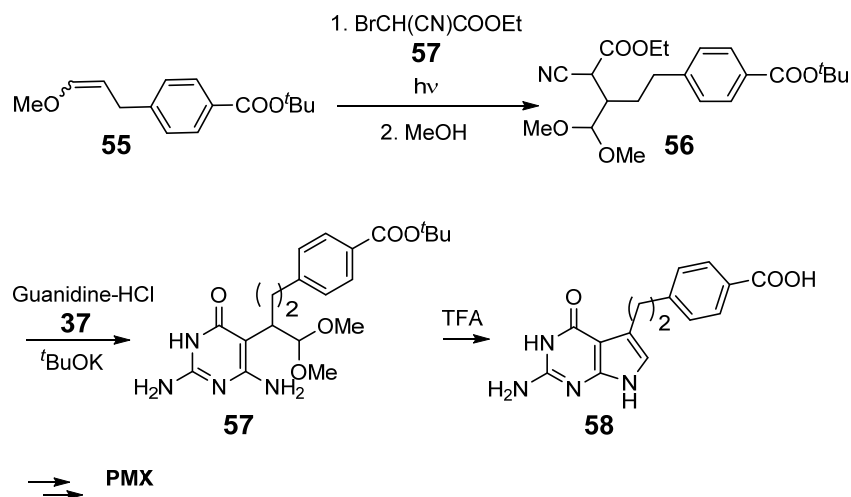
Scheme 9. Synthesis of 2,4-diamino-5-arylalkyl substituted pyrrolo[2,3-*d*]pyrimidines

54-55.



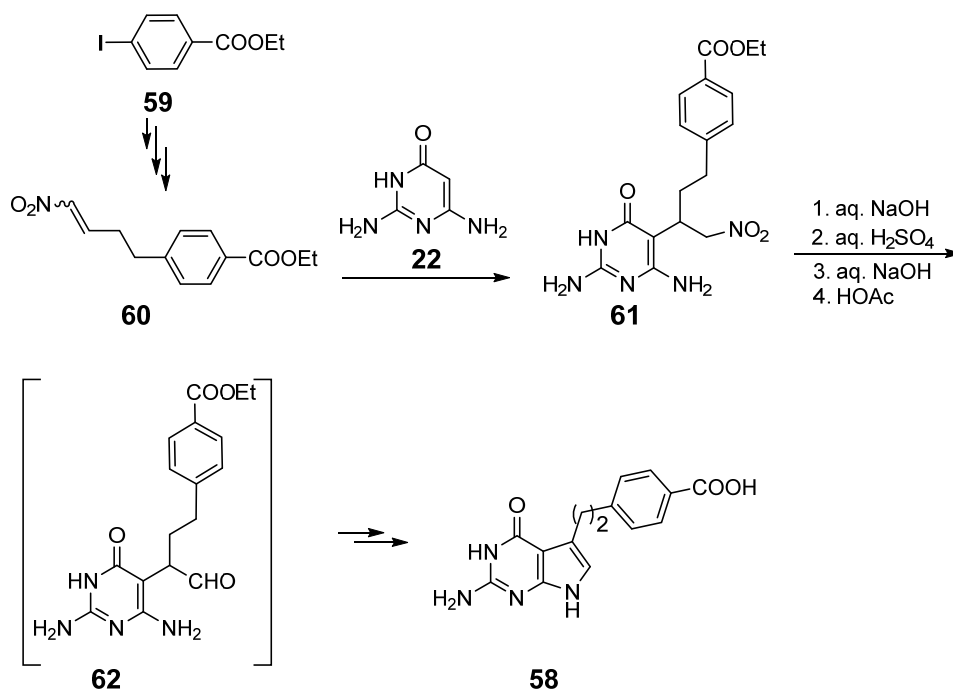
Miwa and coworkers²⁸⁷ reported the synthesis of a series of 2,4-diamino-5-arylalkyl substituted classical pyrrolo[2,3-*d*]pyrimidine antifolates in 1991. Condensation of guanidine **37** (Scheme 9) and the malonodinitrile derivative **52** afforded the bicyclic ring **53**. The lactam in **53** was reduced in the presence of borane to provide the pyrrolo[2,3-*d*]pyrimidine intermediate **55** along with its 5,6-dihydro analog **54**.

Scheme 10. Synthesis of 5-substituted pyrrolo[2,3-*d*]pyrimidine **58**.



A procedure for the synthesis of **PMX** was reported by Miwa and coworkers²⁸⁷ utilizing the spontaneous cyclization of 6-amino-5-pyrimidylacetaldehyde (Scheme 10). The enol ether **55** was reacted with ethyl bromocyanoacetate in methanol under UV irradiation for photo-initiated free radical addition to regioselectively afford the acetal functionalized ethyl cyanoacetate **56**. Guanidine **37** and cyanoacetate **56** were condensed at reflux to form the acetal protected 6-amino-5-pyrimidylacetaldehyde **57**. The dimethyl acetal and *t*-butyl moieties were deprotected under acid catalyzed conditions to afford 4-[2-(2-amino-4-oxo-pyrrolo[2,3-*d*]pyrimidin-5-yl)-ethyl]-benzoic acid **58**. Acid **58** was peptide coupled to L-glutamate ester and subsequently saponified to get to the target compound **PMX**.

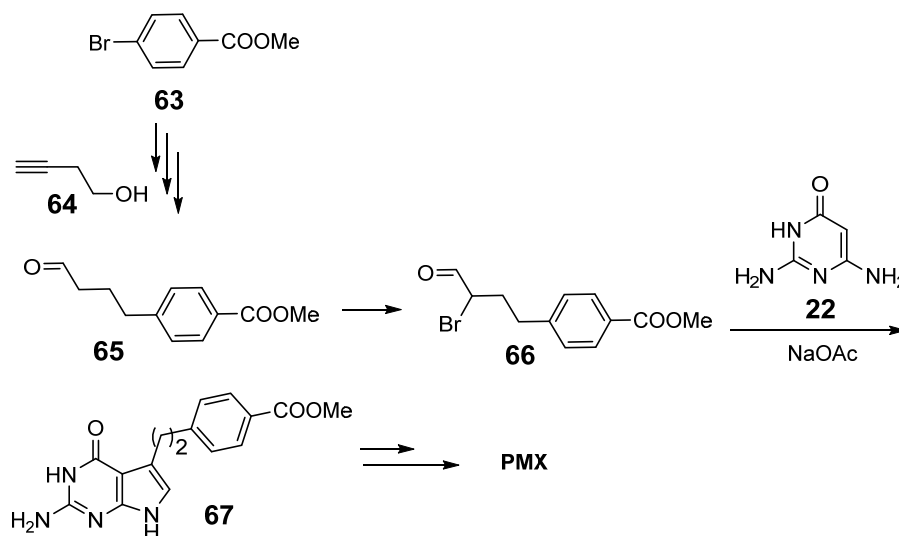
Scheme 11. Synthesis of 6-amino-5-pyrimidylacetaldehydes **62**.



Taylor and coworkers²⁸⁸ reported a concise method for the synthesis of **PMX** which involved the spontaneous cyclization of 6-amino-5-pyrimidylacetaldehydes **62** (Scheme 11). The acid **58** was synthesized via the intermediate **62** by a one-pot five-step Nef reaction

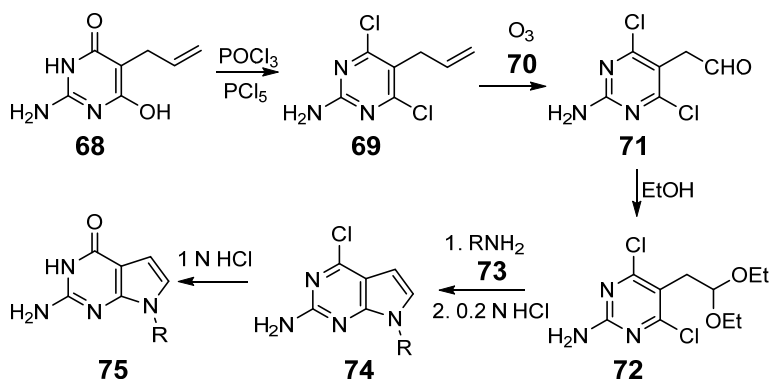
of compound **61**. Michael addition reaction between the C5 of pyrimidine **22** and the Michael acceptor **60** produced the compound **61**. The synthesis of the Michael acceptor involved palladium-catalyzed cross-coupling of methyl 4-iodobenzoate **59** with an allyl alcohol, aldol condensation with nitromethane followed by dehydration using methanesulfonyl chloride in basic conditions. **PMX** was synthesized from the acid **58** in additional two steps that involved peptide coupling with diethyl L-glutamate ester and saponification.

Scheme 12. Synthesis of **PMX** from α -bromo aldehyde **67**.



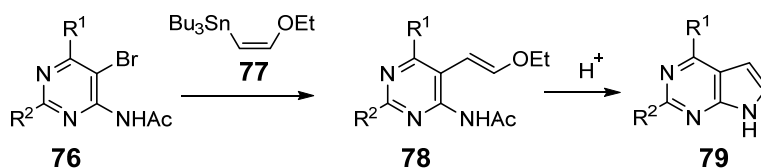
Another method for the synthesis of **PMX** was reported by Barnett and coworkers²⁸⁹ which involved the cyclization of 2-bromo-4-arylbutanal **66** (Scheme 12) with 2,4-diamino-6-oxo-pyrimidine **22**. The cyclization regioselectively afforded the 5-substituted pyrrolo[2,3-*d*]pyrimidine **67**. The key α -bromo aldehyde intermediate was synthesized via Sonogashira coupling of methyl 4-bromobenzoate **63** with 3-butyn-1-ol **64**, reduction of the alkyne coupled product and oxidation of the alcohol to aldehyde **65** and subsequent α -bromination to **66**.

Scheme 13. Synthesis of 7-substituted pyrrolo[2,3-*d*]pyrimidines **75**.



Legraverend and coworkers²⁹⁰ reported the synthesis of *N*7-substituted pyrrolo[2,3-*d*]pyrimidine **75** (Scheme 13) from 2-amino-4,6-dichloro-5-(2,2-diethoxyethyl)pyrimidine **72**. Conversion of 5-allyl-2-amino-4,6-dihydroxypyrimidine **68** to the 4,6-dichloro derivative **69** was carried out in the presence of POCl₃, PCl₅. Compound **69** was then subjected to ozonolysis of the allyl group to afford the intermediate 2-(2-amino-4,6-dichloropyrimidin-5-yl)acetaldehyde **71**. The aldehyde was then converted to the diethylacetal **72** and subsequently cyclized under acidic conditions to 4-chloro-7*R*-pyrrolo[2,3-*d*]pyrimidin-2-amine **74**. The 4-chloro group was then hydrolyzed in the presence of 1 N HCl to afford the final compound **75**.

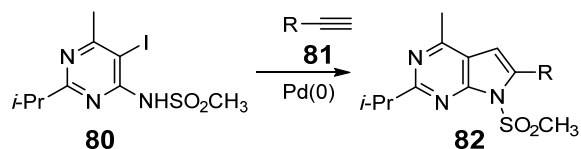
Scheme 14. Synthesis of pyrrolo[2,3-*d*]pyrimidine **79**.



Sakamoto and coworkers²⁹¹ reported the synthesis of pyrrolo[2,3-*d*]pyrimidines **79** (Scheme 14) from acid catalyzed cyclization of protected 5-acetaldehyde pyrimidines **78**.

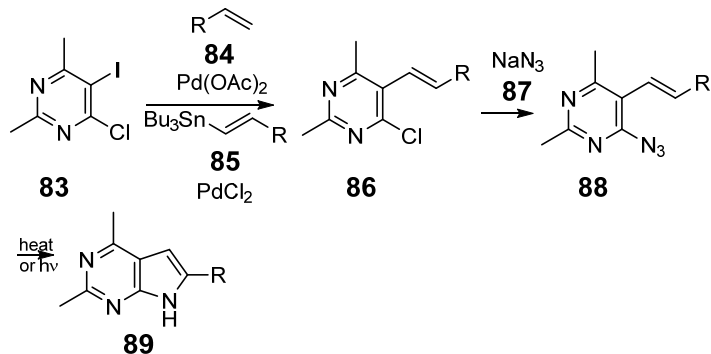
Palladium catalyzed coupling of appropriate 2,4-disubstituted-5-bromo-6-acetamido pyrimidine **76** with (*Z*)-tributyl(2-ethoxyvinyl)stannane **77** afforded intermediate **78**.

Scheme 15. Synthesis of 4-methyl pyrrolo[2,3-*d*]pyrimidines **82**.



Another method for the synthesis of 4-methyl pyrrolo[2,3-*d*]pyrimidine **82** (Scheme 15) was reported by Kondo et al.²⁹² via a palladium(0) catalyzed cross-coupling of terminal alkynes **81** with *N*-(5-iodo-2-isopropyl-6-methylpyrimidin-4-yl)methanesulfonamides **80**.

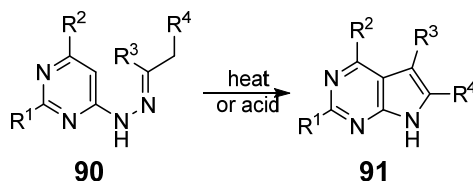
Scheme 16. Synthesis of 2,4-dimethyl pyrrolo[2,3-*d*]pyrimidines **89**.



Kondo et al.²⁹² in the same report discussed the synthesis of 2,4-dimethyl pyrrolo[2,3-*d*]pyrimidine **89** (Scheme 16) via thermal or photoinduced cyclization of the C5 olefinic functionality of 4-azidopyrimidines **88**. The olefinic moiety was introduced by a palladium catalyzed cross-coupling between the 5-iodopyrimidine **83** and appropriate

alkenes **84/85**, and the azide functionality was introduced via nucleophilic displacement of the 4-chloro in the pyrimidine **86** by sodium azide **87**.

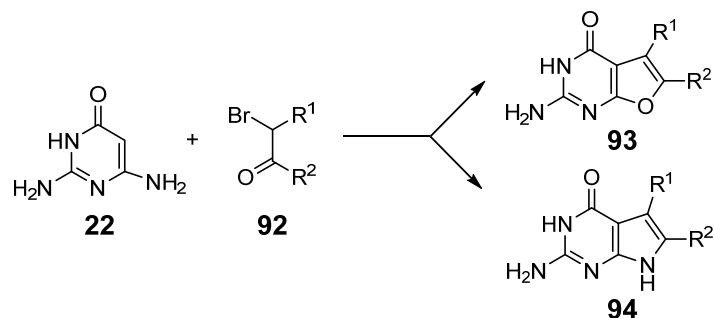
Scheme 17. Synthesis of pyrrolo[2,3-*d*]pyrimidines **91** via Fischer indole cyclization.



Several reports employed the Fischer indole cyclization for the synthesis of pyrrolo[2,3-*d*]pyrimidines **91** (Scheme 17) from 4-pyrimidinylhydrazones **90**.²⁹³⁻²⁹⁷ However, the applicability of the method is limited by high reaction temperatures and the steric constraints for [3,3] sigmatropic rearrangement involved in the mechanism.

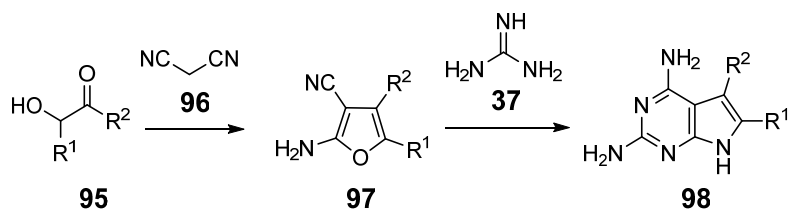
Secrist and Liu²⁹⁸ provided a detailed structural study of the cyclization products afforded upon reacting 2,6-diamino-4-pyrimidone **22** (Scheme 18) with various types of α -halo aldehydes and ketones **92**. They reported that the cyclization with α -halo ketones could occur via two different mechanisms to produce either the furo[2,3-*d*]pyrimidine **93** and pyrrolo[2,3-*d*]pyrimidine **94**. Electron density at the C5 of the pyrimidine nucleus is critical for it to displace the leaving group at the α -carbon atom of the α -halo ketones to give specifically the pyrrolo[2,3-*d*]pyrimidines **94**.

Scheme 18. Synthesis of pyrrolo[2,3-*d*]pyrimidines **94** and furo[2,3-*d*]pyrimidines **93**.



B.1.2. From furan precursors

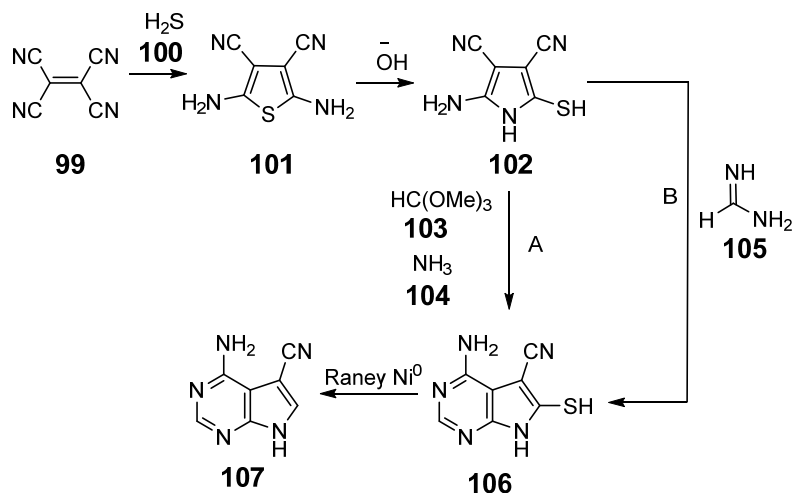
Scheme 19. Synthesis of 2,5,6-trisubstituted-4-amino-pyrrolo[2,3-*d*]pyrimidines **98**.



Taylor et al.²⁹⁹ reported a general method to obtain the 2,5,6-trisubstituted-4-amino-pyrrolo[2,3-*d*]pyrimidine scaffold **98** (Scheme 19) via appropriately substituted 2-amino-3-cyanofurans **97** as the intermediate. Condensation of appropriate α -hydroxyketones **95** with malononitrile **96** afforded the substituted furan **97** which was then cyclized with guanidine **37** to afford the corresponding 2,5,6-trisubstituted-4-amino-pyrrolo[2,3-*d*]pyrimidine rings **98** via a ring transformation/annulation sequence.

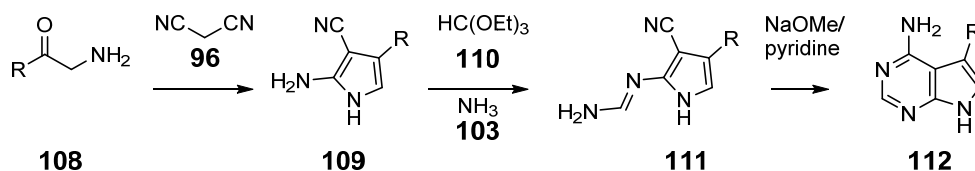
B.1.3. From pyrrole precursors

Scheme 20. Synthesis of 4-amino-5-cyanopyrrolo[2,3-*d*]pyrimidine **107**.



Taylor et al.³⁰⁰⁻³⁰¹ reported the synthesis of 4-amino-5-cyano-pyrrolo[2,3-*d*]pyrimidine **107** (Scheme 20) from tetracyanoethylene **99** via the pyrrole intermediate **102**. Reaction with trimethylorthoformate followed by ammonia or condensation with formamidine acetate resulted in the cyclization of 2-mercapto-3,4-dicyano-5-aminopyrrole **102** to the pyrrolo[2,3-*d*]pyrimidine **106**. The mercapto group was removed by Raney Ni⁰ to afford **107**.

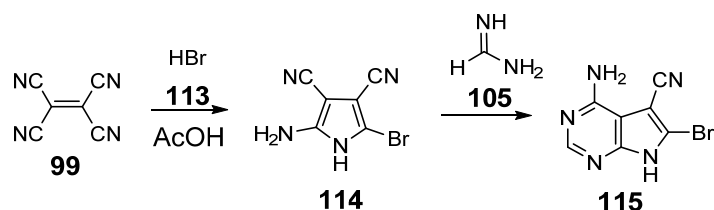
Scheme 21. Synthesis of 4-amino-5-substituted pyrrolo[2,3-*d*]pyrimidine **112**.



Taylor and coworkers³⁰¹ also reported the synthesis of 4-amino-5-substituted pyrrolo[2,3-*d*]pyrimidine **112** (Scheme 21) from 2-amino-3-cyano-5-substituted pyrroles **109**. Appropriate α -aminoketones **108** were condensed with malonodinitrile **96** to afford the pyrroles **109** which were then treated with triethylorthoformate followed by ammonia

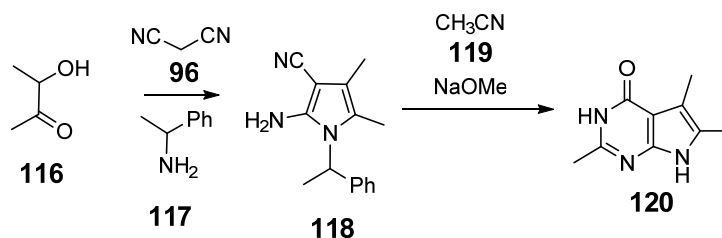
103 to the pyrrole **111**. Cyclization under basic conditions afforded the pyrrolo[2,3-*d*]pyrimidine **112**.

Scheme 22. Synthesis of 5,6-disubstituted pyrrolo[2,3-*d*]pyrimidine **115**.



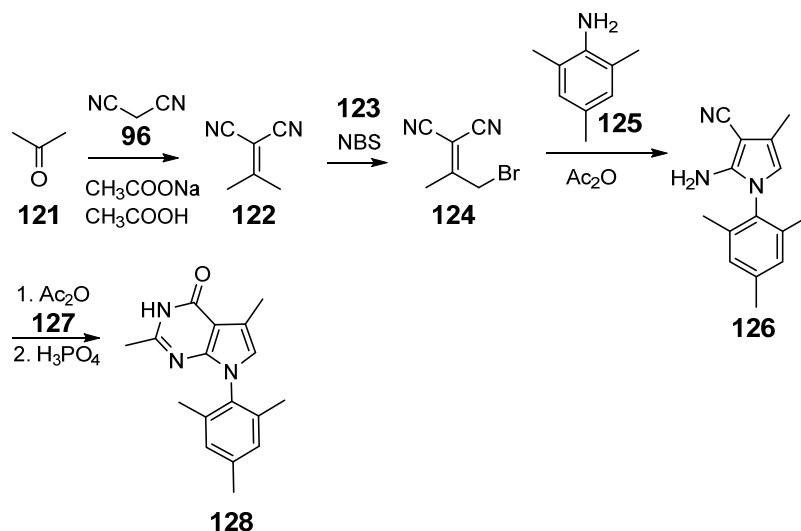
Tolman and coworkers³⁰² reported the cyclization of 2-amino-5-bromo-3,4-dicyanopyrrole **114** (Scheme 22) in the presence of formamidine acetate **105** to pyrrolo[2,3-*d*]pyrimidine **115**. The synthesis of the pyrrole intermediate was reported by Swayze and coworkers³⁰³ in an efficient one-step intramolecular self-condensation reaction from tetracyanoethylene **99** under controlled addition of HBr **113** in acetic acid.

Scheme 23. Synthesis of 2,5,6-trimethyl pyrrolo[2,3-*d*]pyrimidine **120**.



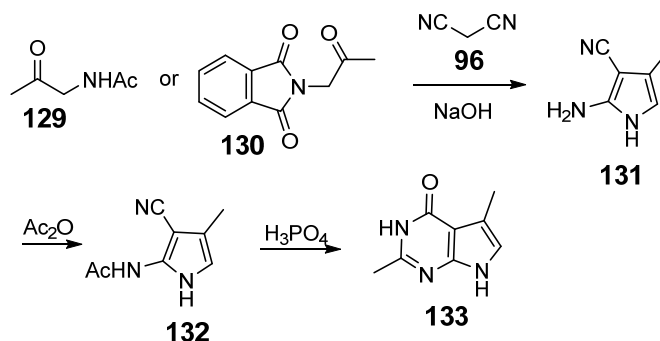
Eger and coworkers³⁰⁴⁻³⁰⁵ reported the cyclization of 3-cyano-4,5-dimethyl-1-(1-phenylethyl)-1*H*-pyrrol-2-amine **118** (Scheme 23) for the synthesis of 2,5,6-trimethyl pyrrolo[2,3-*d*]pyrimidine **120**. The cyclocondensation of 3-hydroxy-2-butanone **116**, 1-phenyl-ethylamine **117** and malonodinitrile **96** afforded the pyrrole intermediate **118**.

Scheme 24. Synthesis of 2,5-dimethyl-*N*⁷-substituted pyrrolo[2,3-*d*]pyrimidine **128**.



Chen and coworkers³⁰⁶ reported a multistep synthesis of pyrrolo[2,3-*d*]pyrimidine **128** (Scheme 24). Condensation of acetone **121** and malonodinitrile **96** afforded **122** which was brominated using NBS **123** to afford 2-(1-bromopropan-2-ylidene)malononitrile **124**. Compound **124** was cyclized with aryl amine **125** to afford the pyrrole **126** which was then cyclized to the pyrrolo[2,3-*d*]pyrimidine derivative **128** under acidic conditions.

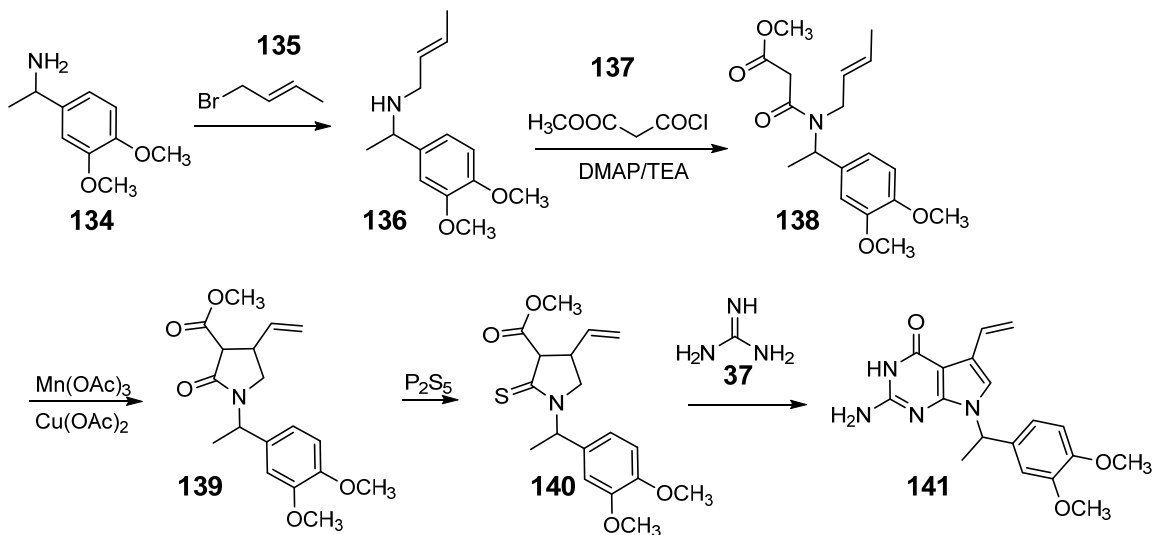
Scheme 25. Synthesis of 2,5-dimethyl pyrrole[2,3-*d*]pyrimidine **133**.



Girgis and coworkers³⁰⁷ reported the synthesis of 2,5-dimethyl pyrrole[2,3-*d*]pyrimidine **133** (Scheme 25) from *N*-(3-cyano-4-methyl-1*H*-pyrrol-2-yl)acetamide **132**

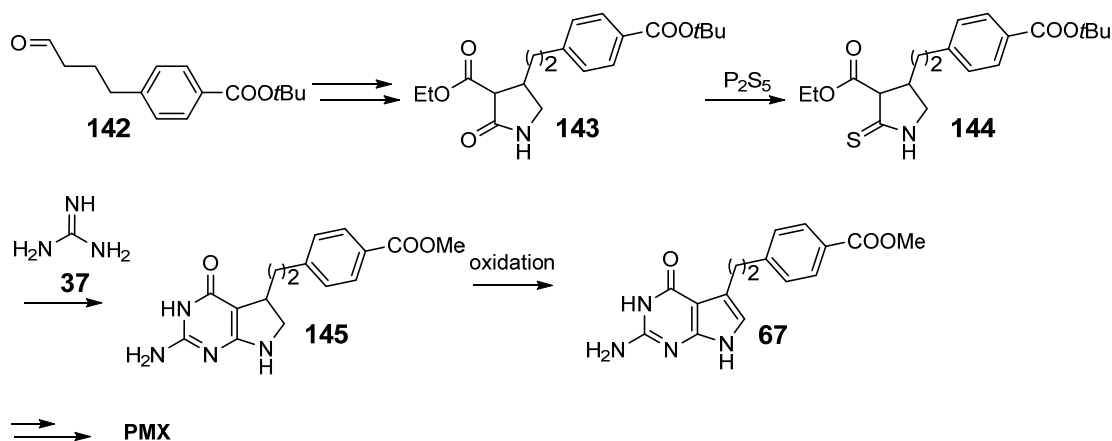
by heating under acidic conditions. The pyrrole **132** was obtained by cyclocondensation of **129** or **130** with malonodinitrile **96** under basic conditions to afford **131** followed by acetylation with acetic anhydride.³⁰⁸⁻³⁰⁹

Scheme 26. Synthesis of N7-substituted analogs of **PMX**.



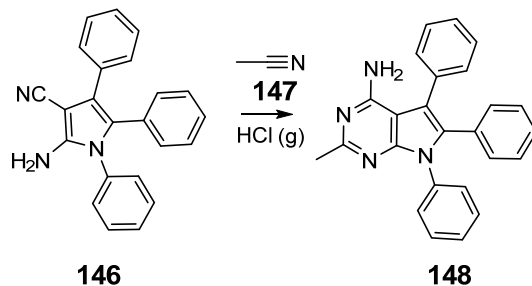
Taylor and coworkers³¹⁰ reported a novel synthetic route of N7-substituted analogs of **PMX** (Scheme 26). A diastereomeric mixture of the 3-carbomethoxy-2-pyrrolidinone **139** was afforded via manganic triacetate catalyzed radical cyclization of methyl (*E*)-3-(but-2-en-1-yl(1-(3,4-dimethoxyphenyl)ethyl)amino)-3-oxopropanoate **138**.³¹¹ The intermediate **138** was afforded by alkylation of racemic 1-(3,4-dimethoxyphenyl)ethan-1-amine **134** with crotyl bromide **135** followed by acylation with methyl malonyl chloride **137** in the presence of catalytic DMAP. P₂S₅ was used to convert the pyrrolidinone **139** to the thiolactam **140** which was then cyclocondensed with guanidine **37** to successfully afford the N7-protected 5,6-dihydro-5-allyl-pyrrolo[2,3-*d*]pyrimidine **141**. The pyrrolo[2,3-*d*]pyrimidine **141** was subsequently utilized to afford **PMX** analogs.

Scheme 27. Synthesis of **PMX** via guanidine cyclization.



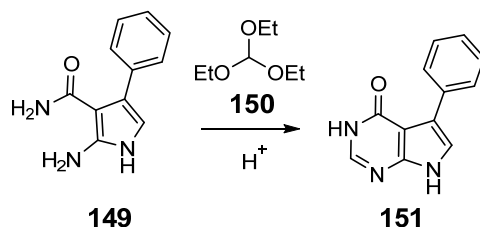
Barnett and coworkers³¹² reported a guanidine cyclization of a preformed 3-carbethoxy-2-thiopyrrolidine **144** (Scheme 27) to 2-amino-4-oxo-5,6-dihydropyrrolo[2,3-*d*]pyrimidine **145**. The intermediate **143** was synthesized in several steps beginning with *tert*-butyl 4-(4-oxobutyl)benzoate **142**. The bicyclic dihydropyrrole compound **145** was oxidized to the pyrrolo[2,3-*d*]pyrimidine intermediate **67** which was subsequently elaborated to **PMX** in three additional steps.

Scheme 28. Synthesis of 2-methyl-4-amino-pyrrolo[2,3-*d*]pyrimidine **148**.



Dave *et al.*³¹³ reported a general procedure for the synthesis of condensed pyrimidines. Acetonitrile **147** (Scheme 28) and substituted pyrrole **146** were condensed under $HCl(g)$ conditions to afford 2-methyl-4-amino-pyrrolo[2,3-*d*]pyrimidine **148**.

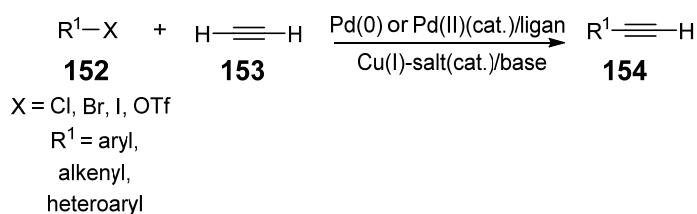
Scheme 29. Synthesis of 5-phenyl-3,7-dihydro-4*H*-pyrrolo[2,3-*d*]pyrimidin-4-one **151**.



Bookser *et al.*³¹⁴ reported the condensation between substituted pyrrole **149** (Scheme 29) and triethylorthoformate **150** under acidic conditions for the synthesis of pyrrolo[2,3-*d*]pyrimidine **151**.

B.2. Synthesis of alkyl benzoates by Sonogashira coupling

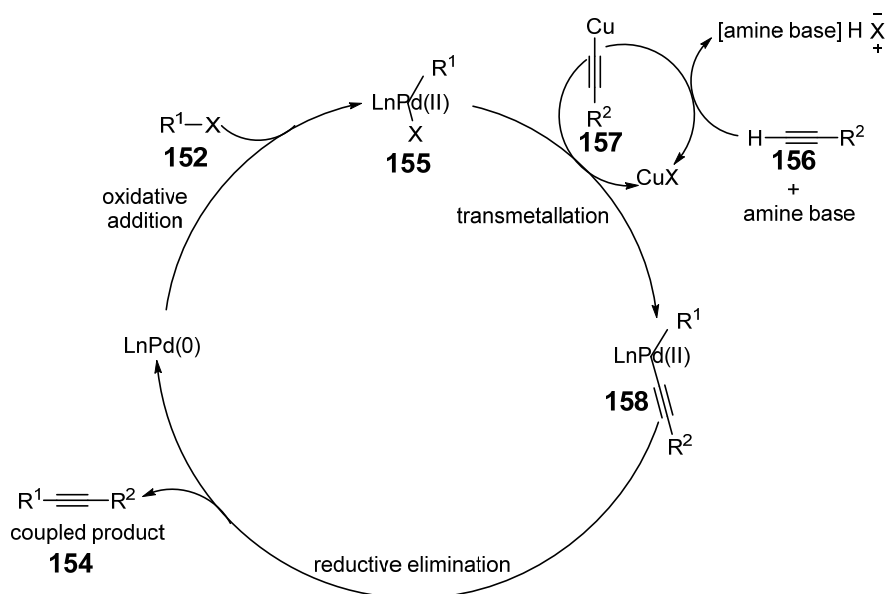
Scheme 30. A general transformation of Sonogashira coupling.³¹⁵⁻³¹⁶



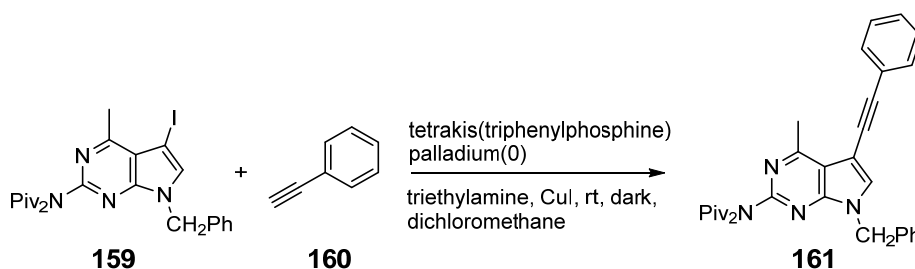
Sonogashira *et al.*³¹⁷ reported a novel method for the synthesis of symmetrically substituted alkynes via a coupling reaction between aryl iodides/vinyl bromides **152** (Scheme 30) and acetylene gas **153** in the presence of catalytic $\text{Pd}(\text{PPh}_3)\text{Cl}_2$ and CuI . This copper-palladium catalyzed cross coupling of terminal alkynes with aryl and vinyl halides (or triflate) to give enynes is termed the Sonogashira coupling. Typically, for the reaction to occur, a $\text{Pd}(0)$ catalyst, a halide salt of copper(I), and a base to neutralize the hydrogen

halide side product are necessary. The reactivity of the aryl/vinyl halides is $I > OTf > Br > Cl$.³¹⁵⁻³¹⁶

Scheme 31. General mechanism of Sonogashira cross-coupling.

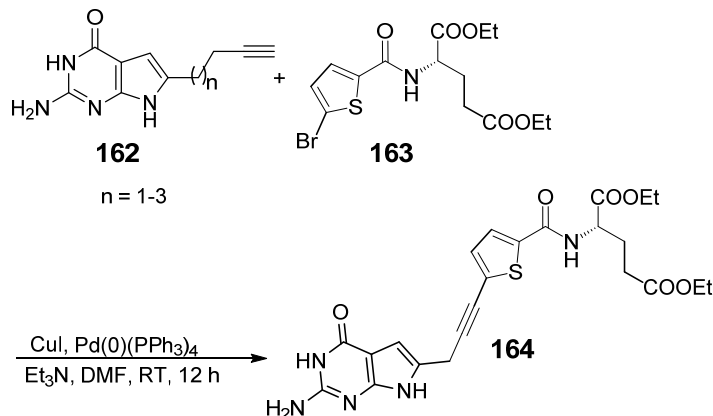


Scheme 32. Synthesis of *N*-(7-benzyl-4-methyl-5-(phenylethynyl)-7*H*-pyrrolo[2,3-*d*]pyrimidin-2-yl)-*N*-pivaloylpivalamide **161**.



Gangjee et al.³¹⁸ reported the synthesis of *N*-(7-benzyl-4-methyl-5-(phenylethynyl)-7*H*-pyrrolo[2,3-*d*]pyrimidin-2-yl)-*N*-pivaloylpivalamide **161** (Scheme 32) from a tetrakis(triphenylphosphine) palladium(0) and CuI catalyzed Sonogashira cross-coupling.

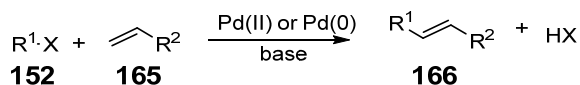
Scheme 33. Synthesis of classical 2-amino-4-oxo-6-substituted-pyrrolo[2,3-*d*]pyrimidine **164** by Sonogashira coupling.



Wang et al.¹³³ reported the synthesis of a classical 2-amino-4-oxo-6-substituted-pyrrolo[2,3-*d*]pyrimidines **164** (Scheme 33) via a tetrakis(triphenylphosphine) palladium(0) and CuI catalyzed Sonogashira cross-coupling between terminal alkynes **162** and thiophenyl bromides **163**.

B.3. Synthesis of alkyl benzoates by domino Heck reactions

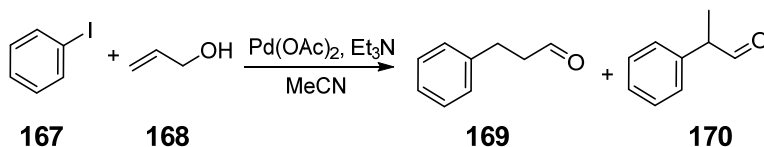
Scheme 34. General transformation of Heck coupling.



The Heck/Mizoroki-Heck reaction is a palladium catalyzed cross-coupling of an aryl/vinyl halides (or triflate) **152** (Scheme 34) with an alkene **165** in the presence of a base

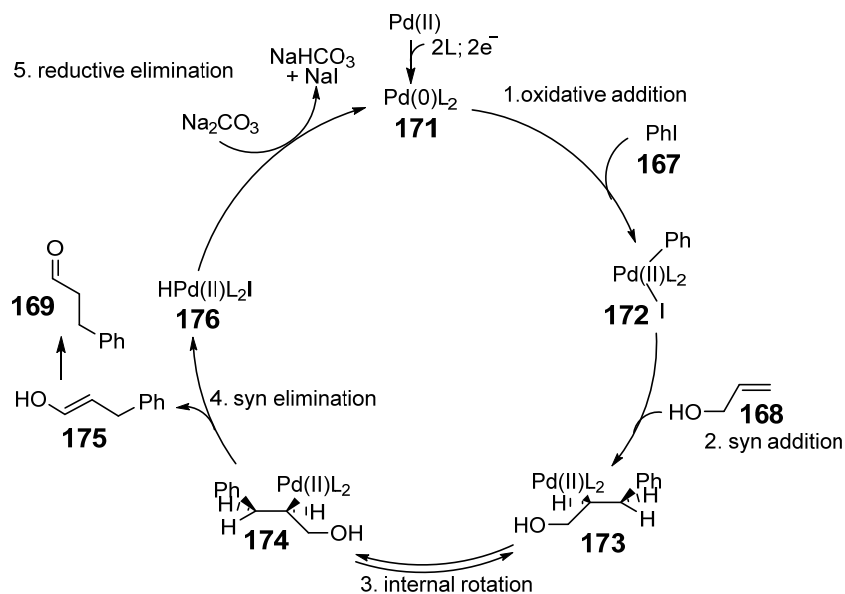
to form a substituted alkene **166**.³¹⁹⁻³²⁰ A general Heck coupling transformation is shown in Scheme 34.

Scheme 35. Heck coupling to synthesize aldehyde **169** and **170**.



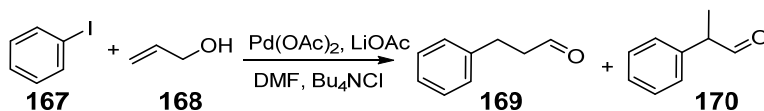
Melpolder et al.³²¹ and Chalk et al.³²² reported the synthesis of aldehydes **169** and **170** (Scheme 35) from phenyl iodide **167** and allyl alcohol **168** in one step reaction in the presence of catalytic palladium acetate.

Scheme 36. A proposed mechanism of Heck coupling to synthesize aldehyde **169**.



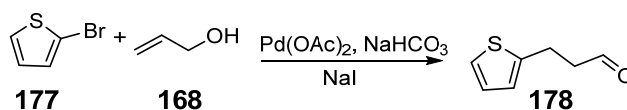
A possible mechanism for Heck coupling synthesis of aldehydes is shown in Scheme 36.

Scheme 37. Improved Heck coupling for aldehyde synthesis



Larock et al.³²³ reported an improved method for Heck coupling for the synthesis of the aldehydes **169** and **170** (Scheme 37). The reported reaction method involves a palladium acetate catalyzed coupling between phenyl iodide **167** and allyl alcohol **168**. Additionally, tetrabutyl ammonium chloride as a phase transfer catalyst and lithium acetate as the base were used to improve the yield and lower the temperature requirement of the reaction. The mild reaction conditions helped in the synthesis of several aldehydes as versatile intermediates.³²⁴⁻³²⁶

Scheme 38. Heck coupling with thiophenyl bromide **178**.



Another method for improved heck coupling was reported by Tamaru et al.³²⁷ and Yoshida et al.³²⁸ which involved the cross-coupling of a thiophenyl bromide **177** (Scheme 38) and allylic alcohol **168**. The coupling occurred in the presence of palladium acetate, sodium iodide, and sodium bicarbonate as base. The successful reaction demonstrated the application of Heck coupling in heteroaromatic systems such as **178**.

III. STATEMENT OF THE PROBLEM

The present section deals with the rationale behind the design of antifolate antimetabolites for tumor targeted chemotherapy via selective uptake and inhibition of 1C metabolism.

C.1. GARFTase inhibitors with selectivity for FRs and/or PCFT over RFC

1. 6-Substituted, 2-amino-4-oxo pyrrolo[2,3-*d*]pyrimidine-fluorophenyl classical antifolates
2. 6-Substituted, 2-amino-4-oxo pyrrolo[2,3-*d*]pyrimidine-3'-fluoropyridyl classical antifolates
3. 6-Substituted, 2-amino-4-oxo pyrrolo[2,3-*d*]pyrimidine-3'-fluorothieryl classical antifolates
4. 6-Substituted, 2-amino-4-oxo pyrrolo[2,3-*d*]pyrimidine-difluorophenyl classical antifolates
5. 6-Substituted, 2-amino-4-oxo pyrrolo[2,3-*d*]pyrimidine-2'-substitutedphenyl classical antifolates
6. 6-Substituted, 2-amino-4-oxo pyrrolo[2,3-*d*]pyrimidine-pyrimidyl classical antifolates

C.2. Multiple enzyme inhibitors (GARFTase and AICARFTase) with selectivity for FRs and/or PCFT over RFC

1. 5-Substituted, 2-amino-4-oxo pyrrolo[2,3-*d*]pyrimidine-3'-butylphenyl classical antifolates
2. 5-Substituted, 2-amino-4-oxo pyrrolo[2,3-*d*]pyrimidine-4'-propyloxy/propylthio/propylamino/butylaminophenyl classical antifolates

3. 5-Substituted, 2-amino-4-oxo pyrrolo[2,3-*d*]pyrimidine-butyl-2'-fluorophenyl classical antifolates

C.3. Multiple enzyme inhibitors (TS, GARFTase, AICARFTase) with selectivity for FRs and/or PCFT over RFC

1. 5-Substituted, 2-amino-4-oxo-6-methyl pyrrolo[2,3-*d*]pyrimidine classical antifolates

RFC is ubiquitously expressed in both healthy as well as tumor cells. Clinically used antifolate agents, such as **MTX**, **PMX**, **PTX** and **RTX**, display dose-limiting toxicities due to predominant uptake by RFC.^{34, 115}

FRs and PCFT are narrowly expressed in healthy tissue and overexpressed in many different types of cancer. FRs expressed in normal tissue are inaccessible to blood circulation and contribute mainly to the reabsorption of folates (FR α expression in proximal tubules of kidney) or are nonfunctional (FR β in thymus).^{32, 39, 67} Several tumors (e.g., epithelial ovarian cancer (EOC), NSCLC, renal, endometrial, colorectal, breast cancers) often overexpress FR α exposed to the blood circulation for transport of folate cofactors.^{33, 67, 90, 98-100} FR β is overexpressed in hematologic malignancies such as acute myeloid leukemia.⁸⁵ In addition, FR β is also overexpressed in tumor-associated macrophages (TAMs) and may play an important role in tumor metastasis and angiogenesis by releasing proangiogenic factors, (e.g., vascular endothelial growth factor, matrix metalloproteinase).¹⁰¹ PCFT is expressed in the upper gastrointestinal tract where it is the predominant transporter of dietary folates at acidic pH (pH 5.8–6.0).^{32, 39, 122, 126, 128-129} While PCFT is expressed in a number of other normal tissues (e.g., liver, kidney), it is

inactive due to loss of transport function at physiological pH (pH 7.4). It functions optimally at pH < 7, reaching its maximum activity at pH 4.5 – 5.5, thus limiting folate transport via PCFT in healthy tissue. PCFT is the predominant transporter in solid tumors (e.g., ovarian, NSCLC), where the pH of the microenvironment is <7.^{7, 60, 161}

Accordingly, selective uptake of antifolate antimetabolites via FRs and/or PCFT over RFC, is an attractive approach for the development of tumor targeted chemotherapy. Additionally, inhibition of FR β overexpressing TAMs by FR β -targeted agents constitutes an additional potential therapeutic target against heterogeneous cancers.¹⁰¹ The principle of FR-targeting has been utilized for the design of cytotoxic folic acid-vindesine conjugate (vintafolide) that is internalized by FRs for intracellular release of the cytotoxic agent.^{24, 108} Though these therapies are considered to have enormous potential, we envision limitations in this therapy with respect to a mechanism of action that requires cleavage of the cytotoxic agent (premature cleavage will result in undesirable side effects) and the use of folic acid as the targeting agent.¹⁰⁸ Our aim is to design small molecule classical antifolates as single agents with tumor-targeting (as well as) cytotoxic potential.

PMX is a 5-substituted 2-amino-4-oxo-pyrrolo[2,3-*d*]pyrimidine antifolate with a 2C linker connecting the bicyclic scaffold to the *p*ABA sidechain (Figures 5 and 32). It is a potent KB human tumor subline (expresses hRFC, hFRs and hPCFT) inhibitor (IC₅₀ = 68 (12) nM) and is a non-selective inhibitor of engineered PC43–10 (expresses hRFC), RT16 (expresses hFR α), D4 (expresses hFR β) and R2/hPCFT4 (expresses hPCFT) CHO sublines indicating its non-selective uptake (**PMX** is one- to two-fold more selective towards RFC expressing CHO sublines over FRs (Table 1)).¹¹⁴⁻¹¹⁵ **PMX** undergoes rapid polyglutamylation and primarily binds to and inhibits TS (K_i = 1.3 \pm 0.3 nM) after entering

normal cells through RFC and tumor cells through RFC and PCFT.¹⁶⁵ **PMX** and its polyglutamate metabolites also inhibit DHFR ($K_i = 72 \pm 0.4$ nM), GARFTase ($K_i = 65 \pm 16$ nM) and AICARFTase ($K_i = 265$ nM). Though it is considered a “multitargeted antifolate”, its principal target is TS (50 to 200 times stronger inhibition than the other targets).^{165, 270} It is currently used for the treatment of non-squamous NSCLC and malignant pleural mesothelioma in combination with cisplatin, among other types of cancers.³²⁹ However, the significant uptake of **PMX** via RFC renders it with severe dose-limiting toxicities (e.g., hematological toxicities, hepatotoxicity, and gastrointestinal toxicity).³³⁰

PMX not only has dose-limiting toxicities but its chemotherapeutic action is hindered due to the development of drug-resistance against its transport, cellular retention and enzyme inhibition.⁶⁶ As such, novel antifolates that circumvent these drawbacks are needed. One such strategy is to selectively block purine biosynthesis by targeting either or both the folate-utilizing enzymes (GARFTase and/or AICARFTase) by virtue of their tumor specificities via FRs and /or PCFT. The optimization of the 5- and 6-substituted pyrrolo[2,3-*d*]pyrimidine antifolates for novel mechanisms of action, and improved potency and selectivity over the currently marketed agents is a viable approach for the development of novel non-toxic cancer chemotherapeutics.

C.1. GARFTase inhibitors with selectivity for FRs and/or PCFT over RFC

C.1.1 Design of 6-substituted, 2-amino-4-oxo pyrrolo[2,3-*d*]pyrimidine-fluorophenyl classical antifolates

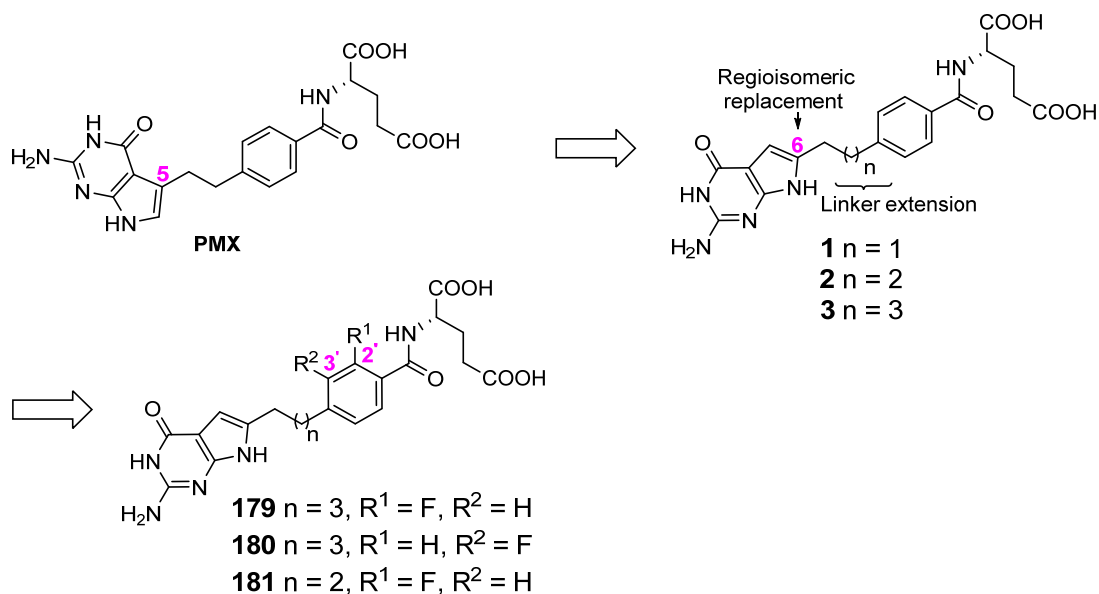


Figure 32. **PMX**, lead compounds **1-3**, and target compounds **179-181**.

Gangjee and coworkers^{114, 118} designed and synthesized the 6-regioisomers of **PMX**. While compound **1**, the 2C linked 6-regioisomer, of **PMX** was inert toward tumor cells in culture, compounds **2** and **3**, the 3C and 4C linked analogs respectively, provided size extension and greater conformational flexibility, that resulted in improved inhibition of proliferation of KB human tumor subline (expresses human RFC (hRFC), FRs (hFR), and PCFT (hPCFT)) with IC_{50} s of 1.7 (0.4) and 1.0 (0.7) nM respectively (>35-fold more potent than **PMX**). Studies with engineered PC43-10, RT16, D4 and R2/hPCFT4 CHO sublines convincingly showed that compounds **2** and **3** were highly selective inhibitors of proliferation of FR- and PCFT-expressing cells at nanomolar (nM) concentrations (Tables 2 and 4). Both compounds **2** and **3** were ~6- to 11-fold more active toward hFR-expressing RT16 and D4 cells and ~100- to 300-fold selective for FRs over RFC, than **PMX**. These compounds are also more potent and selective than any other clinically used antifolates, **MTX**, **PTX**, or **RTX** which show no selectivity for hFRs over hRFC (Tables 2 and 4).

Though the analogs **2** and **3** were more selective due to reduced RFC uptake, they were moderately potent towards the hPCFT-expressing CHO cells when compared to **PMX** (Table 4). The 6-substituted pyrrolo[2,3-*d*]pyrimidine benzoyl L-glutamate antifolates **2** and **3** (Figure 32) inhibit de novo purine nucleotide biosynthesis at GARFTase; a novel mechanism of action devoid of TS inhibition like **PMX**.

Pendergast et al.³³¹⁻³³³ observed that a 2'-fluoro substitution of a benzo[*f*]quinazoline antifolate increased RFC uptake and antitumor activity which was attributed to the conformational restriction of the side-chain L-glutamate via a fluorine-hydrogen bond (Figure 33).

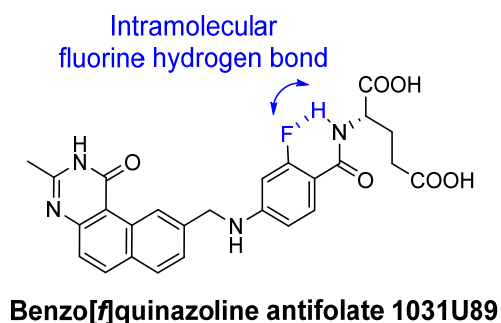


Figure 33. Conformational restriction of the side-chain L-glutamate in benzo[*f*]quinazoline antifolate **1031U89** via an intramolecular fluorine-hydrogen bond.

Introduction of fluorine atoms as a bioisosteric replacement of the hydrogen atom in bioactive molecules is a well-established strategy for modifying the biological properties of drugs, as exemplified by the growing percentage of FDA-approved fluorinated drugs (from 20% in 2010 to about 30% currently).³³⁴⁻³³⁵ Though fluorine is only ~20% larger than hydrogen (van der Waals radii), the C–F bond is longer and larger compared to a C–H bond, has a larger dipole moment in the opposite direction of a C–H, is modestly more

lipophilic and can form strong electrostatic interactions including fluorine-hydrogen bonds (Table 6).³³⁶⁻³⁴⁵ These properties provide fluorine with considerable versatility, however that is also very much dependent upon the biochemical context in which the fluorine substituted analog is to function.

Table 6. Key Properties and applications of the C–F Bond Compared to the C–H bond.

EN = electronegativity.³⁴¹

Properties	C-H	C-F	Applications
Bond length (Å)	1.09	1.35	Hydrophobic interactions, lipophilicity, conformational effects
Total size (Å ³)	2.29	2.82	
EN of the element	2.2	3.98	Molecular recognition (hydrogen bonding, dipole interactions), conformational effects.
Dipole moment (μ)	-0.4	1.4	

Owing to extensive development of RFC resistance mechanisms and heterogeneity of tumor subtypes (varying levels of folate transporters), potent as well as selective inhibitors of both FR and PCFT overexpressing tumor cells are expected to have wider applications.^{34, 65-66} The previous efforts of Gangjee and coworkers have been focused on the design and synthesis of antifolates that are superior to the currently marketed antifolates by virtue of (i) selective tumor-targeting as a result of reduced RFC uptake (ii) selective tumor-targeting and improved antitumor potency as a result of increased FRs/PCFT uptake,

and (ii) improved antitumor potency due to GARFTase inhibition (novel mechanism of action).

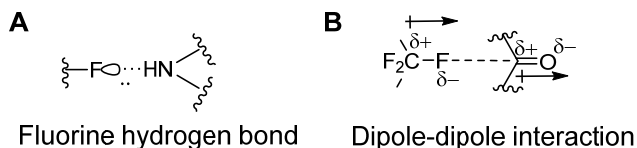


Figure 34. Pictorial representation of molecular recognition interactions of fluorine. (A) Fluorine hydrogen bond and (B) dipole-dipole interaction of a C-F bond with carbonyl C=O.

In order to test the improvement in tumor-targeted activity (selective uptake and GARFTase inhibition) upon fluorination of the previously reported 6-substituted pyrrolo[2,3-*d*]pyrimidine benzoyl L-glutamate antifolates **2** and **3**, compounds **179**, **180**, and **181** with a fluorine on either the 2' [*ortho* (*o*-) to the L-glutamate] (**179** and **181**) or 3' [*meta* (*m*-) to the L-glutamate] position (**180**) were designed (Figure 32). The proposed analogs will evaluate (i) the influence of modified steric/electronic effects at the 2'- and 3'-position (Table 6) and (ii) the presence of an intra-molecular fluorine-hydrogen bond and the significance of the resulting conformational restriction (Figures 33 and 34).

Two dimensional heteronuclear ^{15}N - ^1H double quantum-single quantum correlation experiment (relative signs and magnitudes of through space couplings), ^{19}F and ^1H -NMR spectroscopic techniques together with density functional theoretical (DFT) calculations, and single crystal X-ray diffraction studies provided direct evidence for the existence of intra-molecular N-H \cdots F-C(sp^2) hydrogen bond in 2-fluorobenzamide organofluorine derivatives, in the liquid state (Figure 35).³⁴⁶⁻³⁴⁸ Since the fluorinated analogs **179** and **181** (Figure 32) have a 2'-fluoroarylamide sidechain, it is of interest to

establish the presence of an intra-molecular N-H \cdots F-C(sp²) hydrogen bond in the fluorinated analogs. Such an interaction is expected to be energetically important for target binding as it will restrict the number of conformations of the aromatic side-chain and the amide group, thus potentially providing entropic benefit upon binding.³⁴⁹⁻³⁵⁰

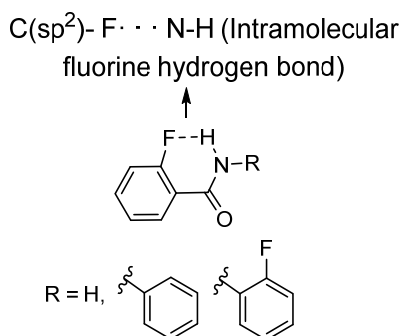


Figure 35. Chemical structures of benzanilides in which weak N-H \cdots F molecular interactions were observed.³⁴⁶⁻³⁴⁸

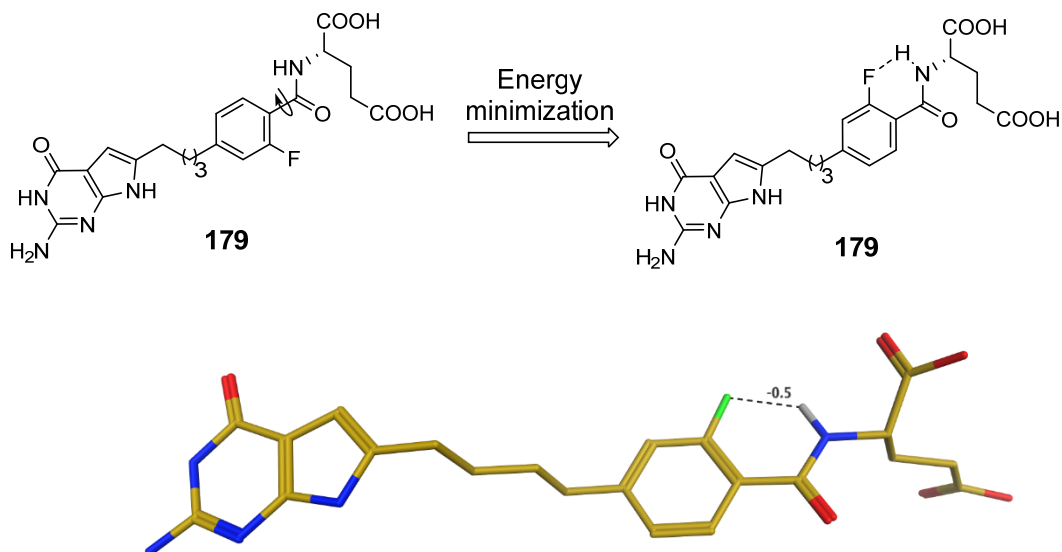


Figure 36. Intramolecular fluorine–hydrogen bond (bond energy = -0.5 kcal·mol⁻¹) detected in energy-minimized free ligand **179** using MOE 2016.08.³⁵¹

To evaluate the presence of an intramolecular interaction between the fluorine atom and the amide NH (N-H \cdots F), energy minimization of the ligand **179** (Figure 36) was performed in its unbound solution state. The energy minima structure shows rotation about the C1'-C(O) bond and orients the fluorine and the amide NH in a syn conformation, facilitating a weak intramolecular fluorine-hydrogen bond (bond energy = -0.5 kcal.mol⁻¹).

Molecular modeling studies of the fluorinated analogs **179** and **180** were carried out using X-ray crystal structures of human FR α (5IZQ), FR β (4KN2) and GARFTase (5J9F) to explore the binding interactions compared to the lead analog **3** to validate their drug targets (Figures 37-39). The compounds display similar interactions as the native crystal structure ligands (not shown here for clarity) and **3**, by maintaining key interactions involving the bicyclic scaffolds and the benzoyl L-glutamate tail.

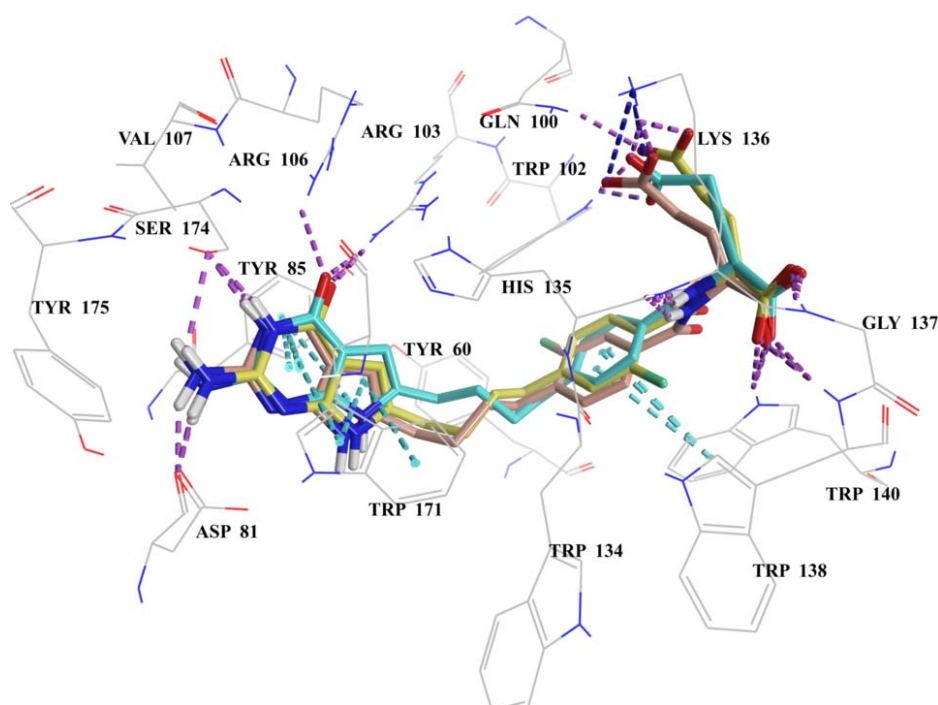


Figure 37. Molecular modeling studies with human FR α (PDB 5IZQ).¹⁶⁷ Superimposition of the docked pose of **179** (yellow, -53 kJ/mol), **180** (light pink, -56 kJ/mol) with the

docked pose of **3** (teal, -55 kJ/mol). Docking studies were performed using LeadIT 2.1.6 and visualized using Maestro 11.2.^{197, 352}

The docked poses of **179** and **180** in FR α (Figure 37) show the 2-NH₂ group interacting in a hydrogen bond with Asp103 (81) (for FR α , full-length gene product numbers are designated along with numbering of the mature protein in parentheses). The 3-NH of **179** and **180** form a hydrogen bond each with the side-chain hydroxyl of Ser196 (174) and the 4-oxo moieties make a hydrogen bond each with the side-chain nitrogen of Arg125 (103). Though hydrogen bond interaction with the side-chain of Arg128 (106) is not maintained as in **3** (teal), the 4-oxo of **179** and **180** are at a distance of 3.5 to 3.7 Å respectively, that can induce a hydrogen bond in situ (2.8 Å in **3**, distances not shown for clarity). The pyrrolo[2,3-*d*]pyrimidine scaffolds are stacked amid the hydrophobic aromatic side-chains of Tyr82 (60), Tyr107 (85) and Trp193 (171) (for π - π , van der Waals and hydrophobic interactions). The L-glutamate moieties of **179** and **180** occupy a similar binding space as the corresponding L-glutamate of the native ligand. The amide NH forms a hydrogen bond with the backbone carbonyl of His157 (135). The α -carboxylates form a network of hydrogen bonds involving the backbone NH of Gly159 (137) and Trp160 (138), and the side-chain NH of Trp162 (140), while the γ -carboxylic acids form salt bridge interactions with the side-chain protonated amine of Lys158 (136) and hydrogen bonds with the side-chain NH of Gln122 (100) and Trp124 (102). The four carbon linkers and the fluorinated phenyl side-chains are positioned in a hydrophobic region formed by Tyr82 (60), Trp124 (102), and His157 (135).

The docked poses of **179** and **180** in FR β are shown (Figure 38). The 2-NH₂ of the ligands interact in a hydrogen bond with the side-chain carboxyl of Asp99 (97) (again for FR β , the full-length gene product numbers are designated with numbering of the mature protein in parentheses), and the 4-oxo moieties form two hydrogen bonds, one each with the side-chain nitrogens of Arg121 (119) and His153 (151). The pyrrolo[2,3-*d*]pyrimidine scaffolds are stacked amid the hydrophobic aromatic side-chains of Tyr103 (101) and Tyr189 (187) (for π - π , van der Waals and hydrophobic interactions) similar to the bicyclic ring of the crystallized ligand. The L-glutamate moieties occupy a similar binding space as the corresponding L-glutamate of the native ligand. The amide NH form a hydrogen bond with the backbone carbonyl of His153 (151). The α -carboxylate of **179** forms a salt bridge with the side-chain of Arg154 (152) and hydrogen bonds with the backbone NH of Gly155 (153) and a conserved water molecule. The α -carboxylate of **180** forms hydrogen bonds with the backbone NH of Gly155 (153) and side-chain of Trp158 (156). The γ -carboxylic acid of **179** forms a salt bridge with the side-chain of Arg138 (136) and hydrogen bonds with the backbone NH of Ser119 (117) and the backbone NH of Gln118 (116), while the γ -carboxylic acid of **180** forms a salt bridge with the side-chain of Arg138 (136) and hydrogen bonds with the backbone NH of Ser119 (117), side chain NH of Gln118 (116) and side-chain NH of Trp120 (118). The four carbon linkers and the fluorinated phenyl rings are positioned in a hydrophobic region formed by Tyr78 (76), Trp120 (118), and Trp158 (156).

The docked poses of fluorinated compounds **179-180** in the GARFTase active site show that the pyrrolo[2,3-*d*]pyrimidine scaffolds bind in the same region as that occupied

by the bicyclic scaffold of the native ligand in the GARFTase crystal structure (PDB 5J9F, native ligand not shown for clarity) (Figure 39).

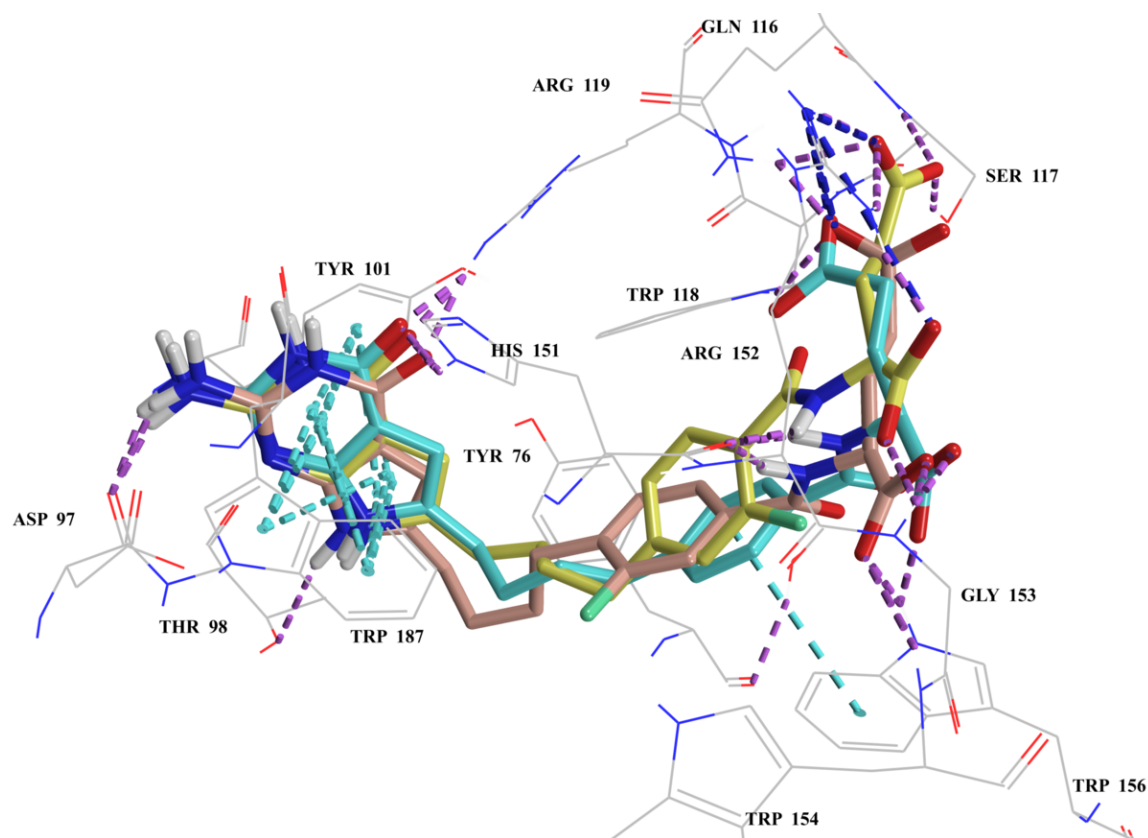


Figure 38. Molecular modeling studies with human FR β (PDB 4KN2).⁹⁵ Superimposition of the docked pose of **179** (yellow, -62.5 kJ/mol), **180** (pink, -57.3 kJ/mol) with the docked pose of **3** (teal, -56.9 kJ/mol). Docking studies were performed using LeadIT 2.1.6 and visualized using Maestro 11.2.^{197, 352}

The scaffold is stabilized in the binding site by multiple interactions, hydrogen bonds between (1) the N1 nitrogens and the backbone NH of Leu899, (2) 2-NH₂ and the backbone carbonyl of Leu899 and (3) the 4-oxo and the backbone NH of Asp951. Additionally, the 4-oxo form a water-mediated hydrogen bonding network via a conserved water molecule with Ala947, Ala952, and Asp949. The N7-nitrogens form a hydrogen

bond with the backbone carbonyl of Arg897. The pyrrolo[2,3-*d*]pyrimidine bicyclic scaffolds are also positioned appropriately for van der Waals interactions with Val950. The amide NH of the L-glutamate form a hydrogen bond with the carbonyl of Met896. The L-glutamates are oriented with the α -carboxylates forming a salt bridge with the side-chain of Arg897 and a hydrogen bond interaction with the backbone amide NH of Ile898 and/or with the side-chain of Arg871. The γ -carboxylate forms salt bridge interactions with the side-chains of Lys844 and Arg897.

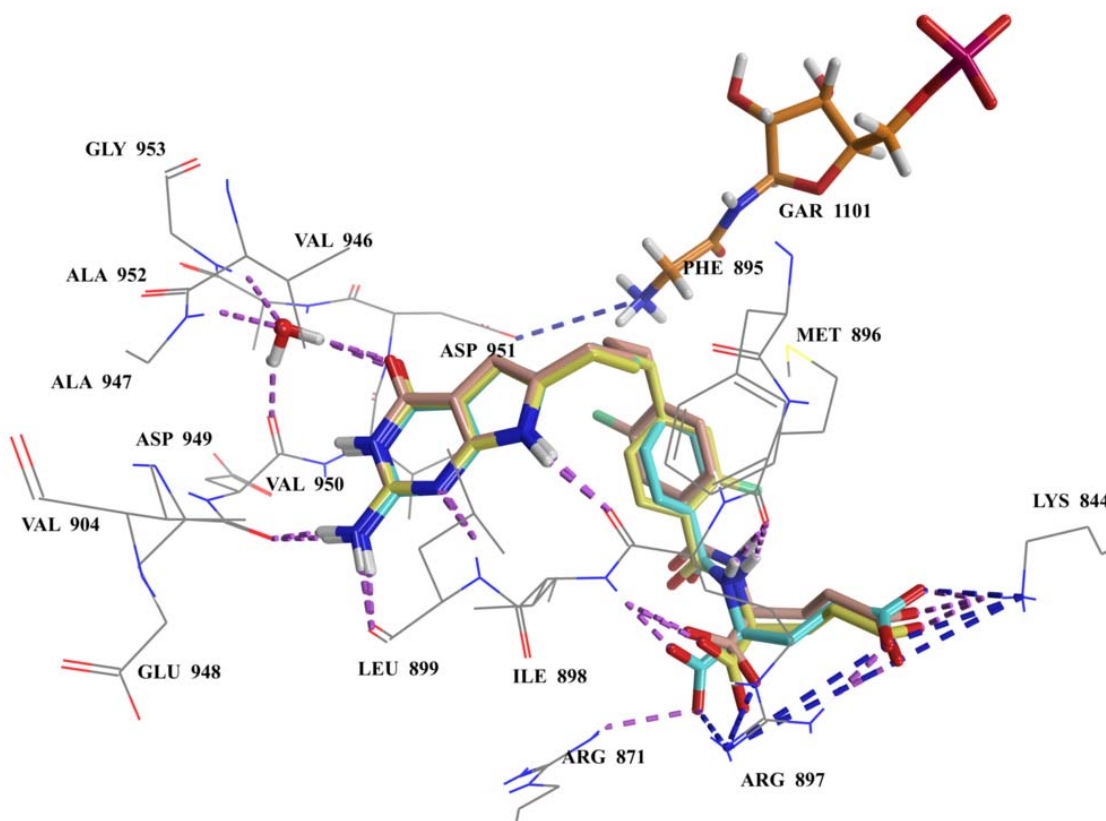


Figure 39. Molecular modeling studies with human GARFTase (PDB 5J9F).¹⁶⁷ Superimposition of the docked pose of **179** (yellow, -51.7 kJ/mol), **180** (blue, -53.3 kJ/mol)

with the docked pose of **3** (brown, -55.4 kJ/mol). Docking studies were performed using LeadIT 2.1.6 and visualized using Maestro 11.2.^{197, 352} Shown in orange is the substrate GAR.

Comparing the docked poses of the parent desfluoro analog **3** and the fluorinated analogs **179** and **180** in FR α , FR β , and in GARFTase (Figures 37-39), the slight increase in size at the 2'- (**179**) or 3'-position (**180**) due to C(sp²)F (1.32 Å) replacement of a C(sp²)H (1 Å) bond, preserved the required orientation and interactions of the scaffold and side-chain groups. However, no interactions were observed by either of the fluorine atoms with the amino acids in the binding sites. A noteworthy observation is that, in a majority of the poses generated for each of the protein targets (Figures 37-39 are the best docked poses of the 10 generated poses within each protein, w.r.t docked scores, root mean square deviation (RMSD) and conserved interactions) with the 2'-fluorinated (*o*- to the L-glutamate) analog **179**, the fluorine atom and the amide NH are positioned in a syn conformation (-0.1° to -30° dihedral angles). As such, an intramolecular N-H · · · F interaction in the low energy state of the unbound ligand as predicted by the energy minima of **179** (Figure 36), could stabilize the bound conformation and provide an entropic benefit upon binding. However, this N-H · · · F hydrogen bond observed in the unbound state is required to break upon binding, as the amide NH is involved in a much stronger and conserved hydrogen bond with the backbone carbonyl of the target proteins (Figures 37-39).

Table 7. Cell proliferation assays with 6-substituted pyrrolo[2,3-*d*]pyrimidine antifolates.¹¹⁴

Antifolate	CHO (IC ₅₀ s) (nM)				KB (IC ₅₀ s) (nM)
	RFC PC43-10	FR α RT16	FR β D4	PCFT R2/PCFT4	
3	>1000	6.3 (1.6)	10.0 (2)	213 (28)	1.9 (0.7)
179	>1000	0.58 (0.12)	1.6 (0.44)	23 (2)	0.59
180	>1000	1.4	0.93	207	1.67

In the cell proliferation assays, the 3'-fluorinated compound **180** showed ~5- to 10-fold improved inhibition of the FR-expressing CHO cells (RT16 and D4) but retained similar activity as the parent desfluoro **3** in PCFT-expressing CHO cells (PCFT4) and KB cells. The 2'-fluoro substitution in **179** improved activity/selectivity across all cell lines with the largest impact (11- and 9-fold, respectively) on the FR α - and PCFT-expressing CHO cell lines (Table 7).¹¹⁴ These results indicate that fluorine substitution influences the activity depending on its regioisomeric position. As dual PCFT- and FR-targeting provides the greatest utility of our targeted analogs, these results prompted further systematic studies of the impact of *o*-fluoro substitutions on the growth inhibitory activities of our previously

reported 6-substituted pyrrolo[2,3-*d*]pyrimidine compounds toward FR- and PCFT-expressing cells (Tables 2, 4 and 5).

C.1.2 Design of 6-substituted, 2-amino-4-oxo pyrrolo[2,3-*d*]pyrimidine-3'-fluoropyridyl classical antifolates

Substituting a CH (sp^2) group with an N (sp^2) atom can lead to improvements in functional activities as N-substitution redistributes the electron density in the aromatic ring, and introduces a dipole moment, hydrogen bond capability and polarity into the molecule (Figure 40 and Table 8).³⁵³

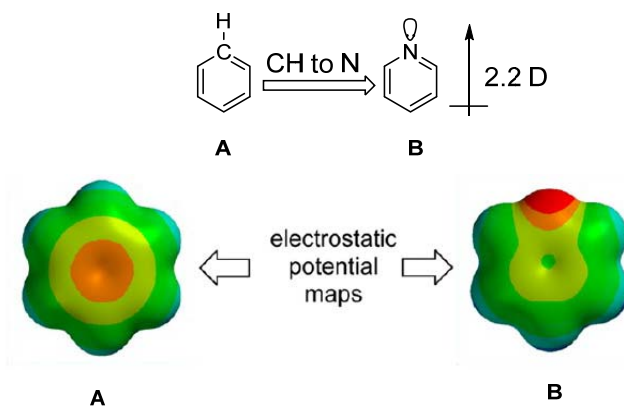


Figure 40. Changes in molecular properties upon substitution of a CH (sp^2) group with an N (sp^2) atom.³⁵³

Each of the modified properties (Figure 40 and Table 8) could influence the biological activity.³⁵³ A pyridyl-for-phenyl replacement of the 6-substituted pyrrolo[2,3-

d]pyrimidine benzoyl L-glutamate antifolate **3** afforded tumor-targeted GARFTase inhibitor **4** with improved activity (Tables 2 and 4).¹¹⁵ The phenyl side-chain was replaced with 3',6'; 2',5'; and 2',6' pyridyls, and proliferation inhibition of CHO, KB and NCI-IGROV1 EOC cells were analyzed. The 2',5'-substituted compound **4** was ~20-fold more active against FR β -expressing CHO cells and ~4- to 5-fold more active against FR α - and PCFT-expressing CHO cells than the lead **3**. Compound **4** was ~3-fold more potent than **3** in in situ GARFTase assays (GARFTase IC₅₀ value of **3** and **4** were 5.6 nM and 1.8 nM respectively). Antitumor efficacy of **4** in vivo with subcutaneous IGROV1 tumor xenografts in severe combined immunodeficiency (SCID) mice showed potent efficacy, as reflected in tumor growth delay (T-C to reach 1000 mg in days was 45 days for compound **4** and 0 days for **PMX**).¹¹⁵

Table 8. Changes in molecular and physicochemical properties upon substitution of a CH (sp²) group with an N (sp²) atom.³⁴¹

Properties	A	B
Polar surface area (tPSA)	-	12.9 Å ²
Lipophilicity (CLogP)	2.142	0.645
Basicity (pK _a)	-	5.2
C/N electronegativity (χ)	2.55	3.04
Dipole moment (μ)	-	2.2 D
CH/N van der Waals radius (r_w)	1.77 Å	1.55 Å
A-A/A-B π -stacking energy (ΔE)	-2.71 kcal/mol	-3.23 kcal/mol

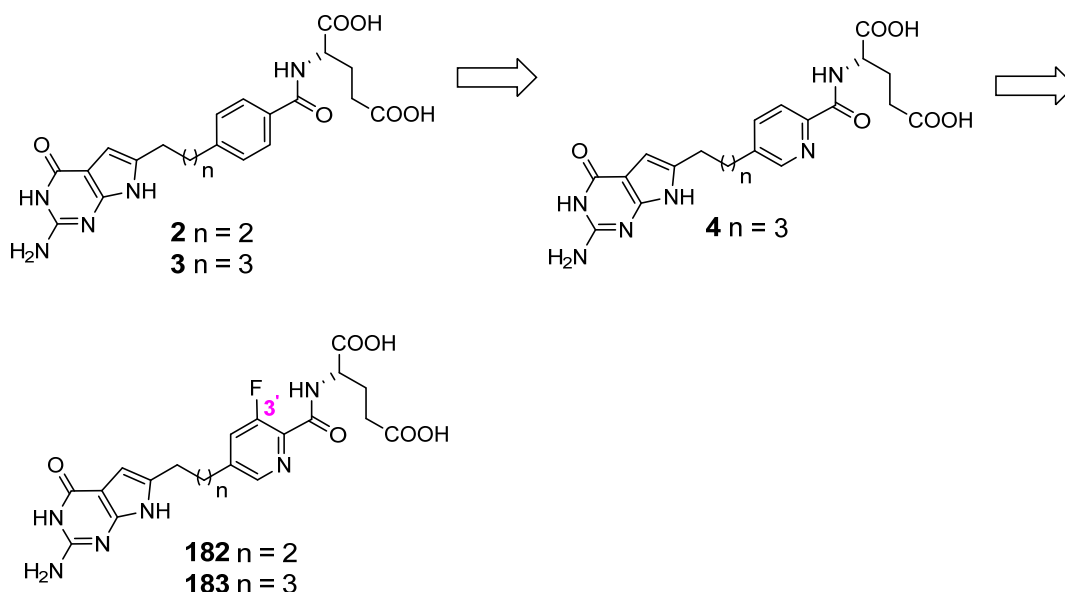


Figure 41. Lead compounds **2-4**, and target compounds **182-183**.

From previous SAR studies it is evident that the 3C linker analogs of 6-substituted pyrrolo[2,3-*d*]pyrimidines are more potent while the 4C linkers are more selective inhibitors of CHO cells expressing human FR α (RT16), FR β (D4) and PCFT (R2/PCFT4) (over CHO cells expressing human RFC (PC43-10)) (Tables 2 and 4). Fluorine substitution *o*- to the L-glutamate dramatically increased the tumor-targeted antiproliferative activity of the phenyl series, mediated through selective transport (especially PCFT). Consequently, it is of interest to investigate the contribution of the 3'-[*ortho* (*o*-) to the L-glutamate] fluorine substitution in the pyridyl series for a single agent with improved tumor potency as well as selectivity. The SAR study from 3'-fluorinated compounds **182** and **183** with 3C and 4C linkers respectively will determine the steric and electronic influence of *o*-fluorination on tumor-targeted activity (especially PCFT over RFC transport) in the 2',5'-substituted pyridyl analogs (Figure 41).

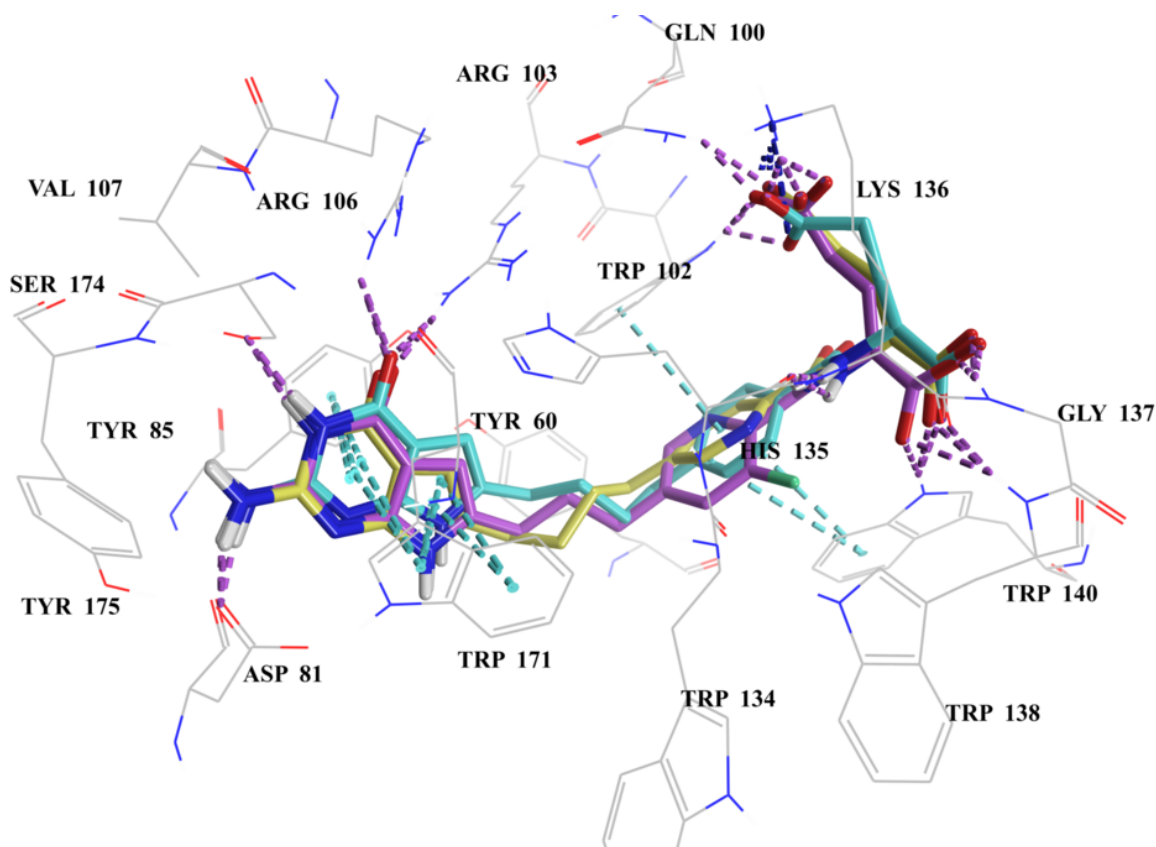


Figure 42. Molecular modeling studies with human FR α (PDB 5IZQ).¹⁶⁷ Superimposition of the docked pose of **182** (violet, -56 kJ/mol) with the docked pose of **3** (teal, -55 kJ/mol) and **4** (yellow, -51 kJ/mol). Docking studies were performed using LeadIT 2.1.6 and visualized using Maestro 11.2.^{197, 352}

Molecular modeling studies of lead compounds **3**, and **4** along with 3'-fluorinated compounds **182** did not detect any additional interactions of the 2',5'-pyridyl ring compared to the parent phenyl analog **3** (Figures 42 and 43). The improvement in potency of **4** (e.g., GARFTase IC₅₀ value of **3** and **4** were 5.6 nM and 1.8 nM respectively) perhaps is a result of improved energies due to additional hydrophobic/van der Waals/CH- π / π - π /hydrogen bond interactions of the differentially polarized pyridyl ring (compared to the phenyl ring

in **3**) with the side-chains of the aromatic amino acids (Trp124 (102) and Trp162 (140) in FR α /Trp120 (118), Trp158 (156) in FR β) in the FRs (Figures 38, and 42-43).

Compounds **182** and **183** (Figure 41) were tested against CHO cells expressing human FR α (RT16), FR β (D4), RFC (PC43-10), and PCFT (R2/PCFT4), KB, and HeLa cells and, IGROV1 and A2780 epithelial ovarian cancer cells, for drug potency and transport selectivity.

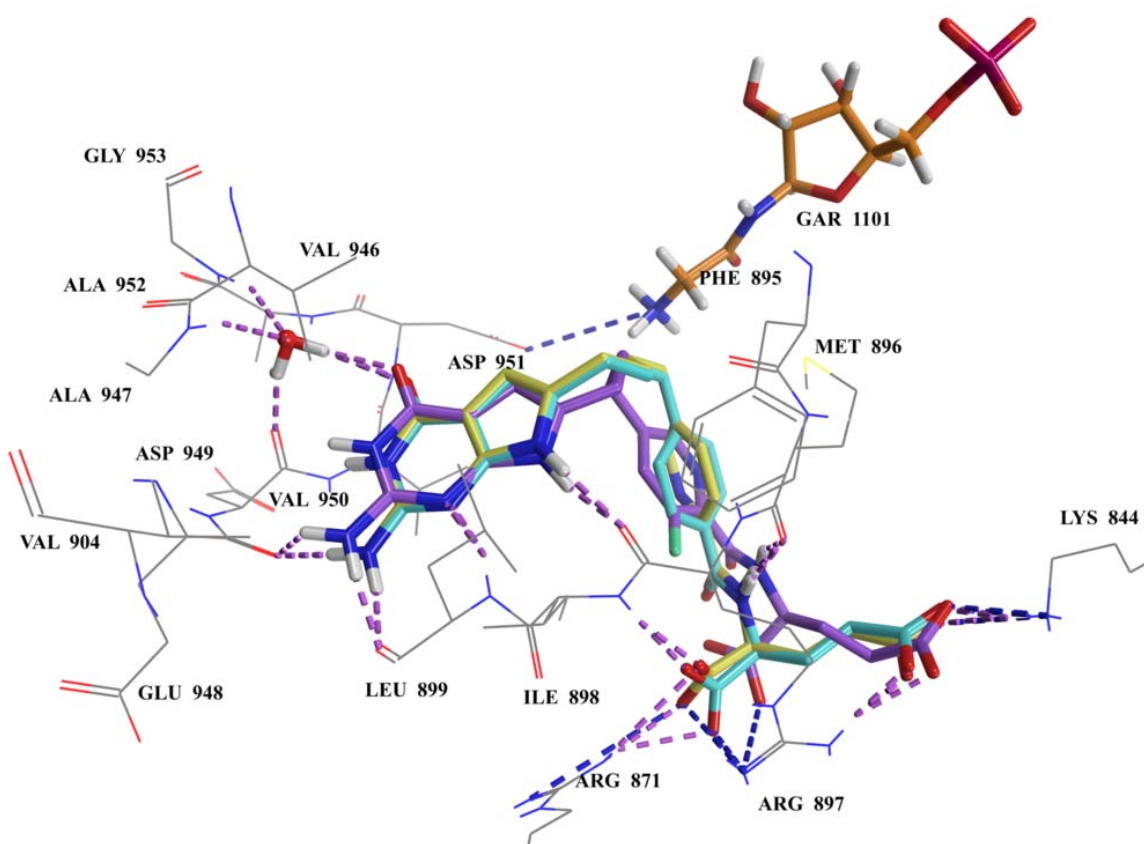


Figure 43. Molecular modeling studies with human GARFTase (PDB 5J9F).¹⁶⁷ Superimposition of the docked pose of **182** (violet, -57 kJ/mol) with the docked pose of **3** (teal, -55.4 kJ/mol) and **4** (yellow, -53 kJ/mol). Docking studies were performed using LeadIT 2.1.6 and visualized using Maestro 11.2.^{197, 352} Shown in orange is the substrate GAR.

C.1.3 Design of 6-substituted, 2-amino-4-oxo pyrrolo[2,3-*d*]pyrimidine-3'-fluorothieryl classical antifolates

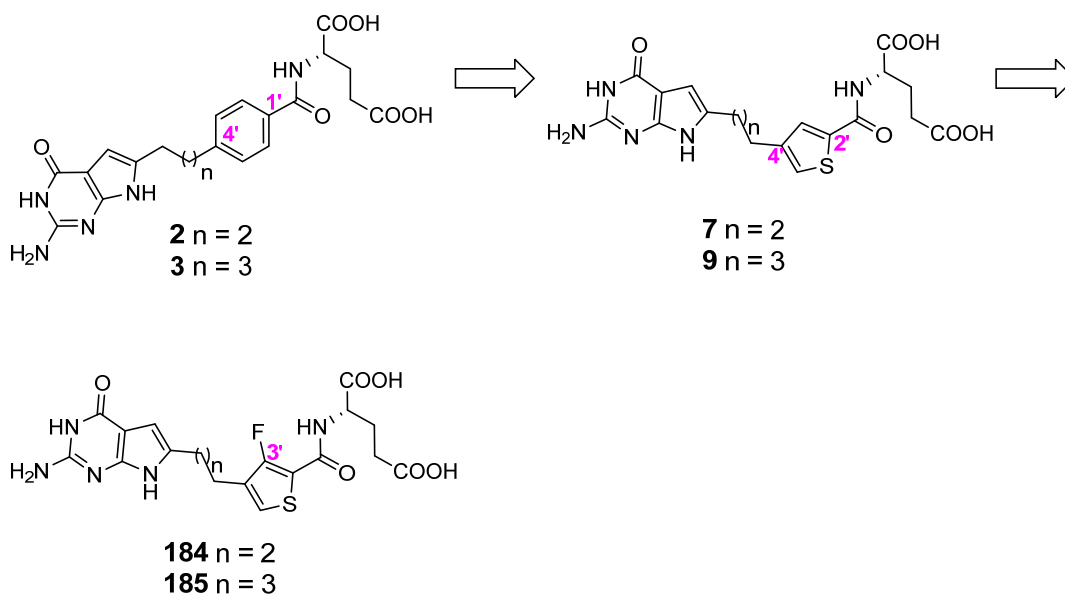


Figure 44. Lead compounds **2**, **3**, **7** and **9** and target compounds **184-185**.

A thienyl-for-phenyl replacement (based on the previous GARFTase inhibitors **LY309887** and **AG2034**, Figure 28) of the 6-substituted pyrrolo[2,3-*d*]pyrimidine benzoyl L-glutamate antifolates not only restored PCFT potency, but also afforded the most potent PCFT-selective antifolates known (Tables 2 and 4).^{60, 104, 107, 116, 119, 121, 158-159, 166, 354} Among the various thienyl ring regioisomeric substitutions tested (2',5'-, 2',4'-, and 3',5'-), the 2',4'-substituted antifolates **7** and **9** with 3C and 4C linkers respectively, showed substantial PCFT-targeted activity towards R2/hPCFT4 CHO cells, with IC₅₀s of 5.4 (1.3) and 41.5 (3.1) nM, respectively (Table 4). While **7** is one of the most potent hPCFT4 cell inhibitors, it has significant non-selective activity against hRFC-expressing PC43-10 CHO cells (Tables 2 and 4). Though **8** is not as potent as its 3C linker analog, it is the most potent hPCFT4 cell inhibitor amongst the analogs that are inactive toward PC43-10 CHO cells

(IC₅₀ = >1000 nM) (Table 4). Consequently, it is of interest to explore the thienyl series for a single agent with both potency and selectivity towards PCFT-expressing cells (the crystal structure of the membrane bound transporters, RFC and PCFT, have not been resolved yet). Molecular modeling studies in FRs and GARFTase did not detect any additional interactions made by the thiophene ring. Compared to a phenyl ring, thiophene ring is differentially polarized and the bond angle between the substitutions on the ring vary (Table 9). As such, the improved potency of the thienyl series could be a result of: (a) improved energies of ligand-protein interactions in the transport protein and enzyme binding pockets due to better alignment of the scaffold and the L-glutamate side-chain and/or (b) additional hydrophobic/van der Waals/CH- π / π - π / interactions with the side-chains of the aromatic amino acids (e.g., Trp102, Trp140 in FR α /Trp 118, Trp156 in FR β) in the FRs.

Table 9. Changes in relative angles of substitution and dipole moments upon bioisosteric replacement of phenyl with thienyl ring. Dipole moments were calculated using QikProp, Maestro 11.2.^{197, 355}

Compd. No.	Regioisomeric substitution	Relative orientation of the substituents	Dipole μ (D)
3	1',4'	Linear (180°)	5.7
7/9	2',4'	Non-linear	6.7

Fluorine substitution *o*- to the L-glutamate dramatically increased tumor-targeted antiproliferative activity of the phenyl series, mediated through selective transport (particularly PCFT) (Table 7).¹¹⁴ It is therefore of interest to investigate the contribution of a 3' [*ortho* (*o*-) to the L-glutamate] fluorine substitution on tumor-targeted activity

(selective uptake and GARFTase inhibition) in the thienyl analogs **184-185**. The limited SAR study from compounds **184-185** will determine the steric and/or electronic influence of *o*-fluorination on tumor-targeted activity (especially PCFT over RFC uptake) in the 2',4'-substituted thienyl analogs.

Compounds **184-185** were tested against CHO cells expressing human FR α (RT16), FR β (D4), RFC (PC43-10), and PCFT (R2/PCFT4), KB, and HeLa cells and, IGROV1 and A2780 epithelial ovarian cancer cells, for drug potency and transport selectivity.

C.1.4 Design of 6-substituted, 2-amino-4-oxo pyrrolo[2,3-*d*]pyrimidine-difluorophenyl classical antifolates

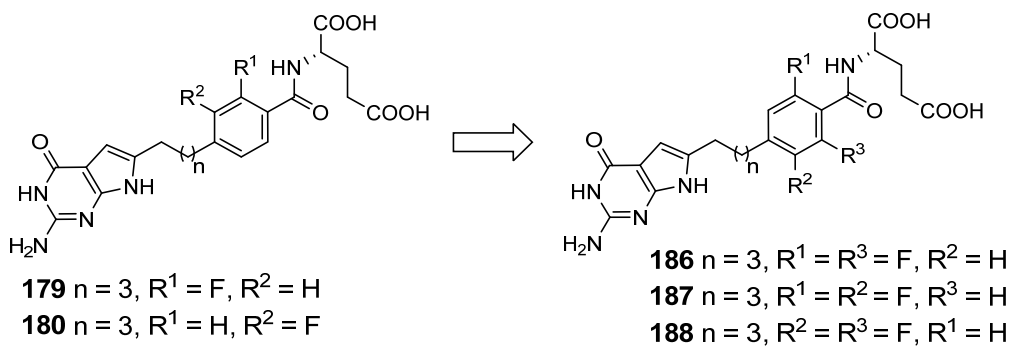
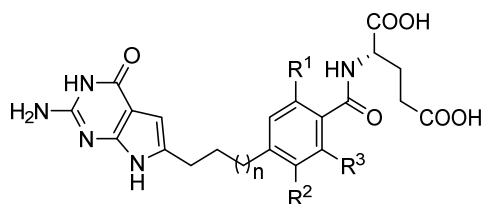


Figure 45. Lead compounds **179-180** and target compounds **186-188**.

The predictability associated with fluorine substitutions in bioactive molecules is not straight forward and often necessitates “fluorine scanning” approaches for the discovery of optimized fluorine-substituted drugs.³⁴¹ From the biological activity of the fluorinated phenyl series it is apparent that fluorine substitutions either on the 2'- or 3'-position (*o*- or *m*-substitution to the L-glutamate respectively) of the aryl ring are tolerated in the binding sites of FRs and GARFTase (Table 7).¹¹⁴

Table 10. Changes in volume and dipole moment upon bioisosteric replacement of CH (sp²) with CF (sp²). Physicochemical properties were calculated using QikProp, Maestro 11.2.^{197, 355}



Compd. No.	R ¹	R ²	R ³	Volume (Å ³) 	Dipole μ (D) 	Intra-molecular N-H...F bond
3	H	H	H	380	5.7	-
179	F	H	H	396	5.3	+
180	H	F	H	396	4	-
186	F	H	F	412	7.11	+
187	F	F	H	412	5.7	+
188	H	F	F	412	4.2	+

Therefore, systematic structure-activity relationship (SAR) study of tumor-targeted antifolates was extended by strategic fluorine scanning on the side-chain phenyl ring. Compounds **186-188** include a 4C linker with the possible (*o*-/*m*-) combinations of difluorinated analogs (Figure 45). The proposed analogs will determine if more than one fluorine atom substitution is beneficial/detrimental to activity and if a specific difluoro

regioisomeric substitution is more tolerated over the others owing to modified (i) sterics and/or (ii) electronics (Table 10).

Compounds **186** and **187** (Figure 45) were tested against CHO cells expressing human FR α (RT16), FR β (D4), RFC (PC43-10), and PCFT (R2/PCFT4) as well as KB tumor cells in culture, for drug potency and transport selectivity.

C.1.5 Design of 6-substituted, 2-amino-4-oxo pyrrolo[2,3-*d*]pyrimidine-2'-substitutedphenyl classical antifolates

From the biological activity of the fluorinated phenyl series, the 2'-fluoro substitution dramatically increased antiproliferative activity mediated through FR α , FR β and PCFT transport with the largest impact (11- and 9-fold, respectively) on the FR α - and PCFT-expressing CHO cell lines (Table 7).¹¹⁴ These results indicate that not only does fluorine substitution influence the activity but its regioisomeric position on the phenyl ring dictates the improvement/loss of activity.

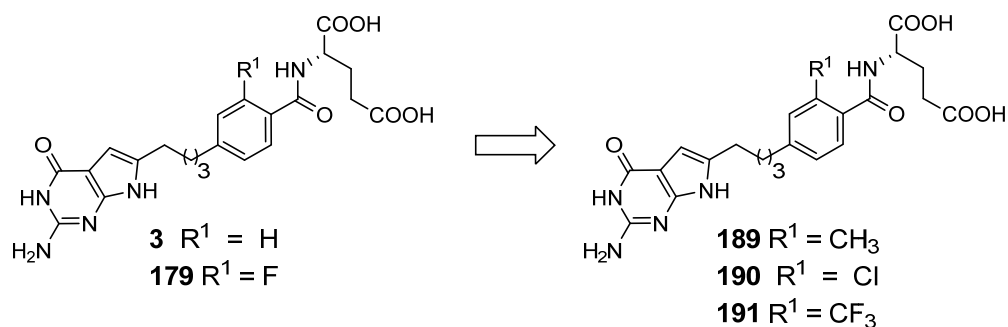
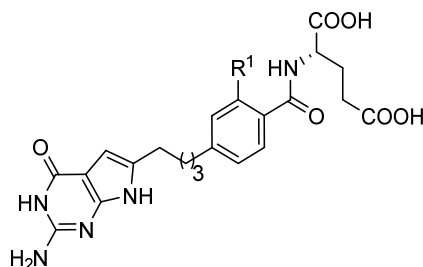


Figure 46. Lead compounds **3** and **179** and target compounds **189-191**.

Table 11. Changes in volume and dipole moment upon replacement of CH (sp²) with C(CH₃) (sp²), C(CF₃) (sp²), C(Cl) (sp²). Physicochemical properties were calculated using QikProp, Maestro 11.2.^{197, 355}



Compd. No.	R ¹	Volume (Å ³)	Dipole μ (D)	Intra-molecular N-H \cdots F bond
3	H	380	5.7	-
179	F	396	5.3	+
189	CH ₃	440	5.9	-
190	Cl	424	5.6	-
191	CF ₃	477	7.2	+

As dual PCFT- and FR-targeting provides the greatest utility of our targeted analogs, these results prompted further systematic evaluation of the impact of *ortho*-substitutions on the growth inhibitory activities of the 6-substituted pyrrolo[2,3-*d*]pyrimidine compounds. To separate the influence of the steric property from the electronic (electron withdrawing effect, hydrogen bonding and dipole interactions) properties on tumor-targeted activity, compounds **189-191** were designed (Figure 46). Compounds **189** and **190** with bulkier 2'-CH₃ and 2'-Cl substitutions respectively on the

phenyl side-chain occupy larger volumes than the unsubstituted phenyl but have similar dipole moment at the side-chain benzamide as the parent **3** (Table 11). In compound **191**, a 2'-CF₃ substituted analog occupies a larger volume and has a larger dipole as well, in the direction of the carbonyl of the amide (Table 11).

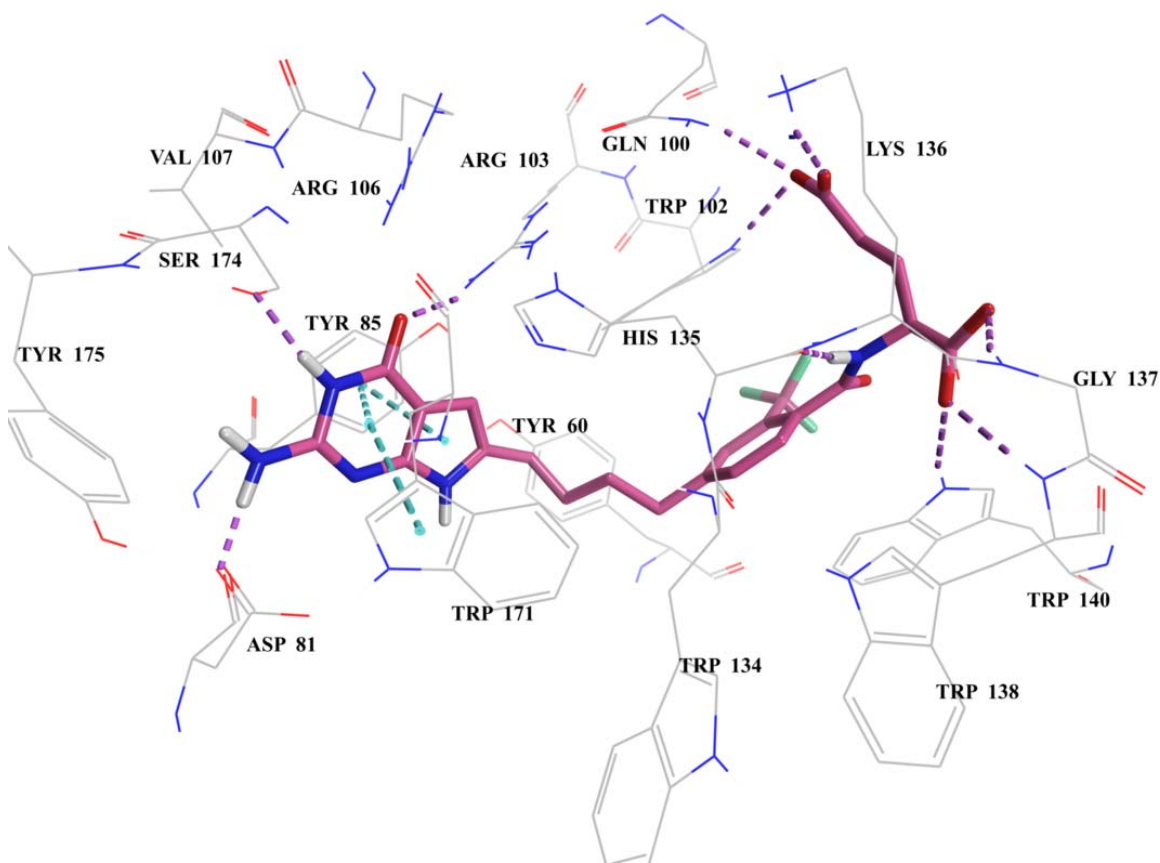


Figure 47. Molecular modeling studies with human FR α (PDB 5IZQ).¹⁶⁷ Docked pose of **191** (pink, -54.2 kJ/mol). Docking studies were performed using LeadIT 2.1.6 and visualized using Maestro 11.2.^{197, 352}

The analog with the largest 2'-substitution (2'-CF₃), compound **191**, was modeled in FR α and GARFTase to identify the presence of steric clashes of the larger substitutions (compared to a H substitution) with the neighboring amino acids (Figure 47-48).

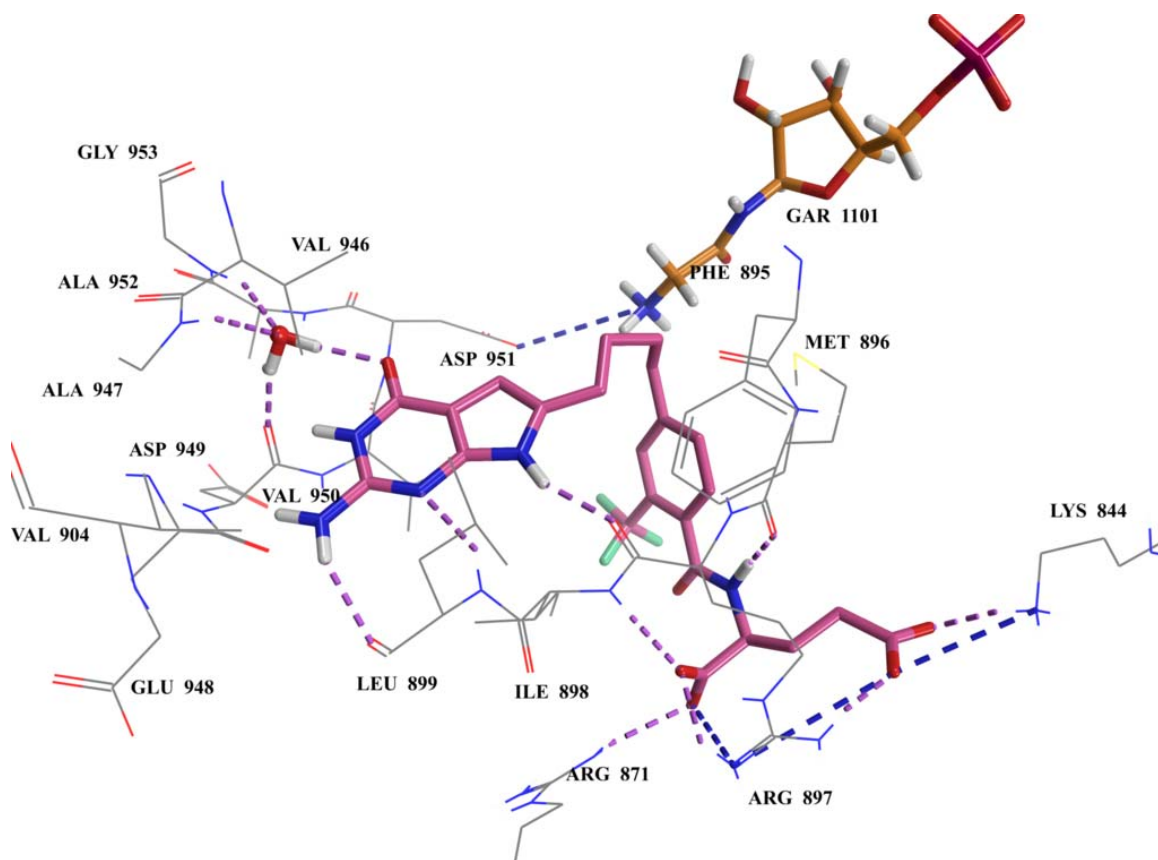


Figure 48. Molecular modeling studies with human GARFTase (PDB 5J9F).¹⁶⁷ Docked pose of **191** (dark grey, -54.7 kJ/mol). Docking studies were performed using LeadIT 2.1.6 and visualized using Maestro 11.2.^{197, 352} Shown in orange is the substrate GAR.

All the interactions are maintained and the binding pockets of both the transporter FRs (only FR α is shown) and the enzyme GARFTase have sufficient space to accommodate the larger 2'-substitutions, however oriented *anti* to the sidechain amide NH. The CF₃ group is placed favorably to form van der Waals interactions with the surrounding hydrophobic residues (Tyr82 (60) and Trp162 (140) in FR α , and Ile898 in GARFTase, Figure 48). The *anti* conformation can be stabilized in **191** due to the capability of the CF₃ group to form an intramolecular dipole-dipole interaction with the carbonyl of the amide (Figure 34).³⁵⁶

The modifications in these three compounds **189-191** will systematically evaluate the influence of size and electronics (individually and in combination) of the side-chain phenyl, on tumor-targeted activity.

Compounds **189** and **191** (Figure 46) were tested against CHO cells expressing human FR α (RT16), FR β (D4), RFC (PC43-10), and PCFT (R2/PCFT4) as well as KB tumor cells in culture, for drug potency and transport selectivity.

C.1.6 Design of 6-substituted, 2-amino-4-oxo pyrrolo[2,3-*d*]pyrimidine-pyrimidyl classical antifolates.

Thienyl-for-phenyl and pyridyl-for-phenyl sidechain replacements afforded some of the most potent, and FR- and PCFT-selective antifolate compounds known (Tables 2 and 4).¹⁰⁴

107, 115-116, 121

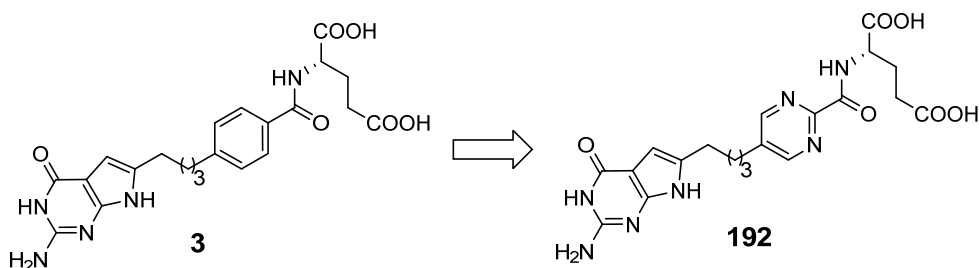
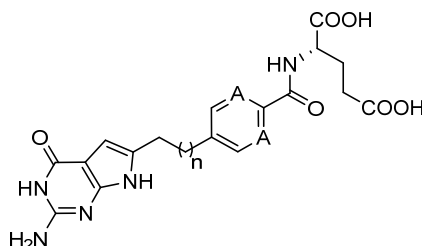


Figure 49. Lead compounds **3** and target compounds **192**.

Table 12. Changes in volume and dipole moment upon isosteric replacement of the phenyl ring with a pyrimidyl. Physicochemical properties were calculated using QikProp, Maestro 11.2.^{197, 355}



Compd. No.	A	Volume (Å ³)	Dipole μ (D)
3	CH	380	5.7
192	N	351	7.02

From the biological activity of the fluorinated phenyl analogs **179** and **180** (Table 7), the 2'-fluoro substitution dramatically increased antiproliferative activity mediated through FR α , FR β and PCFT transport with the largest impact (11- and 9-fold, respectively) on the FR α - and PCFT-expressing CHO cell lines (Table 7).¹¹⁴ These results indicate that stereoelectronic modification of the phenyl ring positively influences the potency and selectivity of the 6-substituted, pyrrolo[2,3-*d*]pyrimidine classical antifolates. As dual PCFT- and FR-targeting provides increased utility of our targeted analogs, these results prompted further systematic studies into the impact of isosteric sidechain replacements on the growth inhibitory activities of the 6-substituted pyrrolo[2,3-*d*]pyrimidine compounds. To elucidate the influence of electronic (electron withdrawing

effect, hydrogen bonding and dipole interactions) properties on tumor-targeted activity, compound **192** was designed as a pyrimidyl-for-phenyl replacement which has similar size but with a larger dipole in the direction of the amide carbonyl (Figure 49 and Table 12).

Compound **192** (Figure 49) was tested against CHO cells expressing human FR α (RT16), FR β (D4), RFC (PC43-10), and PCFT (R2/PCFT4) as well as KB tumor cells in culture, for drug potency and transport selectivity.

C.2. Multiple enzyme inhibitors (GARFTase and AICARFTase) with selectivity for FRs and/or PCFT over RFC

C.2.1. Design of 5-substituted, 2-amino-4-oxo pyrrolo[2,3-*d*]pyrimidine-3'-butylphenyl classical antifolates

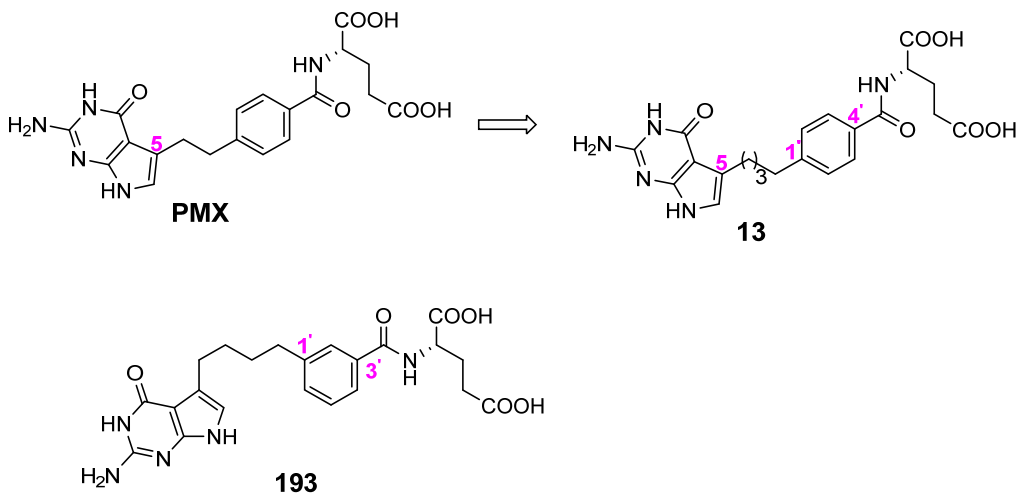


Figure 50. Lead compound **13** and target compound **193**.

Gangjee et al.¹²⁰ previously reported 5-substituted pyrrolo[2,3-*d*]pyrimidine antifolate **13** with 4C linker and a phenyl L-glutamate sidechain as a chain extension

analog of the clinically used **PMX** for improved tumor cell potency as well as tumor-selectivity (Figure 31 and Table 5). Compound **13** is a first-in-class examples of antifolates that act via dual inhibition of AICARFTase and GARFTase alone (Table 5). Compared to **PMX**, extension to 4C linker in compound **13** improved inhibition of proliferation of KB human tumor as well as FR α -expressing CHO cells (RT16). However, **13** had reduced activity toward PCFT-expressing CHO cells (PCFT4). Additionally, high activity toward RFC-expressing CHO cells renders it only moderately selective for FR α over RFC and selective for RFC over PCFT. Previous studies of related 6-substituted pyrrolo[2,3-*d*]pyrimidines established that the conformation of the scaffold and side-chain, as a consequence of linker length and flexibility, plays an important role in determining tumor cell potency and selectivity. Thus, it was of interest to synthesize the regioisomeric, 1',3'-substituted analog **193** of the most potent analog **13** to evaluate its influence on selectivity and potency (Figure 50). The 1',3'-substitution provides a non-linear conformational orientation of the substitutions on the phenyl ring and subsequently influences the orientation of the scaffold and the L-glutamate sidechain in the binding pockets (RFC, FRs, PCFT, GARFTase and AICARFTase).

Molecular modeling studies of **193** compared to the parent analog **13** (Figures 51 and 52) in the FR and GARFTase pockets showed that the binding poses are superimposable and **193** retained all the important interactions (all the key interactions have been explained in detail in Figures 37 and 39).

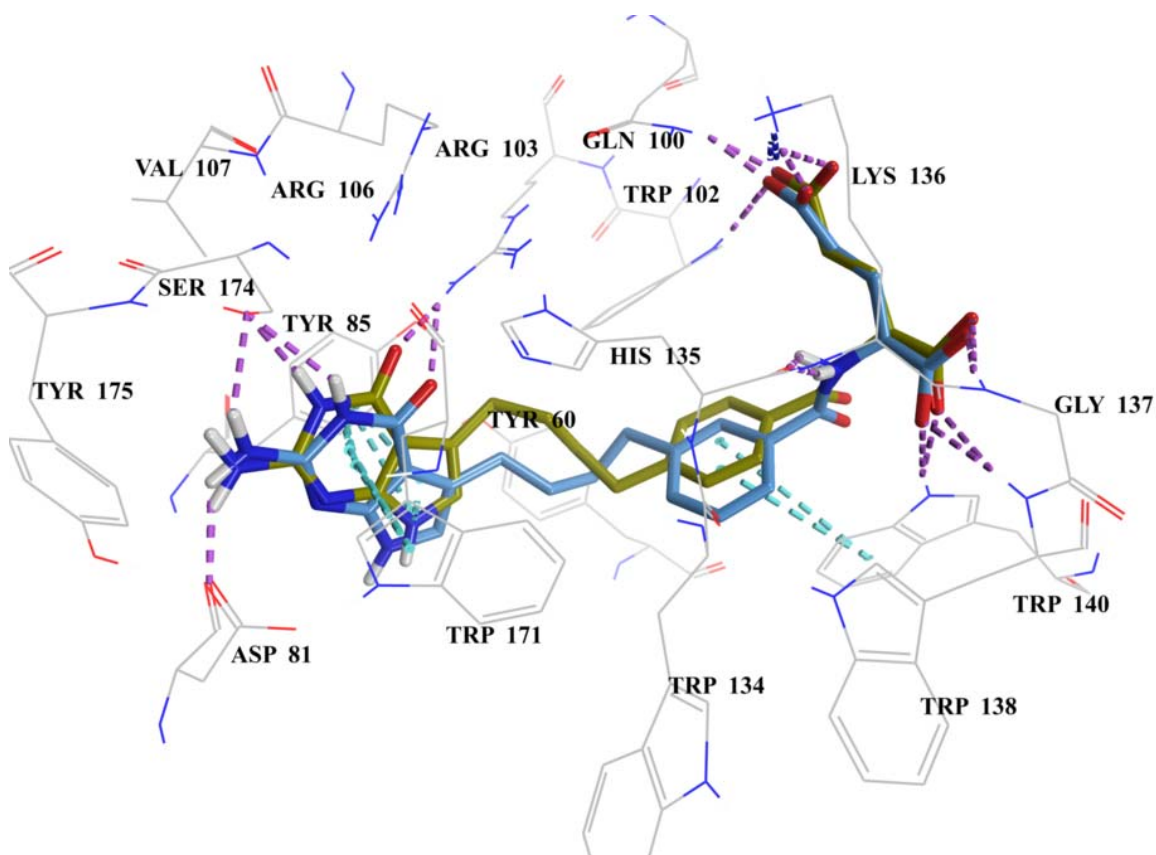


Figure 51. Molecular modeling studies with human FR α (PDB 5IZQ).¹⁶⁷ Superimposition of the docked poses of **193** (blue, -55 kJ/mol) and **13** (green, -56.8 kJ/mol). Docking studies were performed using LeadIT 2.1.6 and visualized using Maestro 11.2.^{197, 352}

In the AICARFTase active site, the pyrrolo[2,3-*d*]pyrimidine scaffolds of compound **193** and lead **13** are superimposable and are fixed within the hydrophobic environment of Pro543 and Phe544 above, and the side chain of Phe315 below (Figure 53).²⁵⁹ Hydrogen bond interactions are formed between the 2-amino group and side chains of Asn489 and Asp546, N-3 and side chain of Asp546, and 4-oxo and side chain of Asn547. The phenyl moieties of the side-chain form π -stacking interactions with the side-chain of Phe315. The orientation of the L-glutamate tail of the docked compounds vary due to the para/meta variation in the phenyl substitution pattern. The α -glutamates of both docked

analogs interact via a salt bridge with the protonated Lys358. In **13**, the γ -glutamate makes a hydrogen bond with the backbone NH of Ala566 and a water mediated hydrogen bond with the backbone NH of Pro543 while the γ -glutamate of **193** makes a hydrogen bond only with the backbone NH of Ala566.

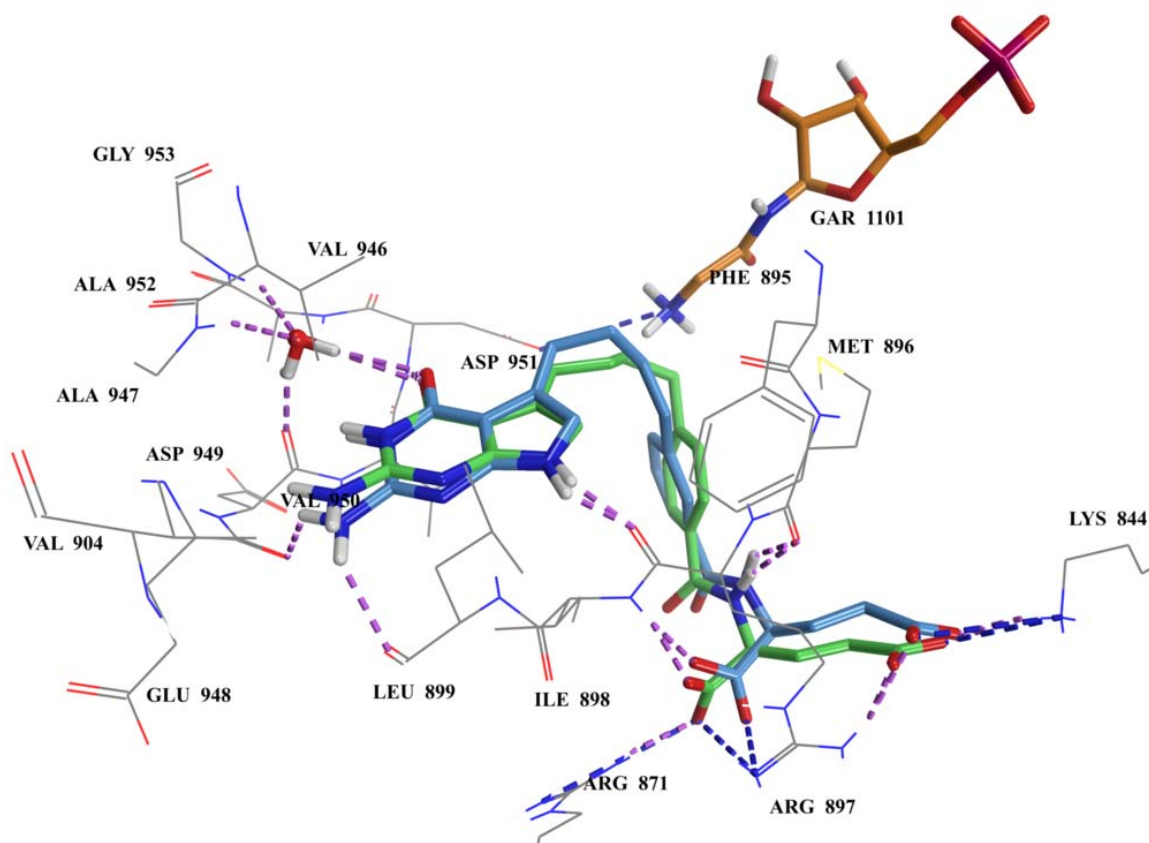


Figure 52. Molecular modeling studies with human GARFTase (PDB 5J9F).¹⁶⁷ Superimposition of the docked poses of **193** (blue, -42.7 kJ/mol) and **13** (green, -48.6 kJ/mol). Docking studies were performed using LeadIT 2.1.6 and visualized using Maestro 11.2.^{197, 352} Partial structure of substrate GAR is shown in orange.

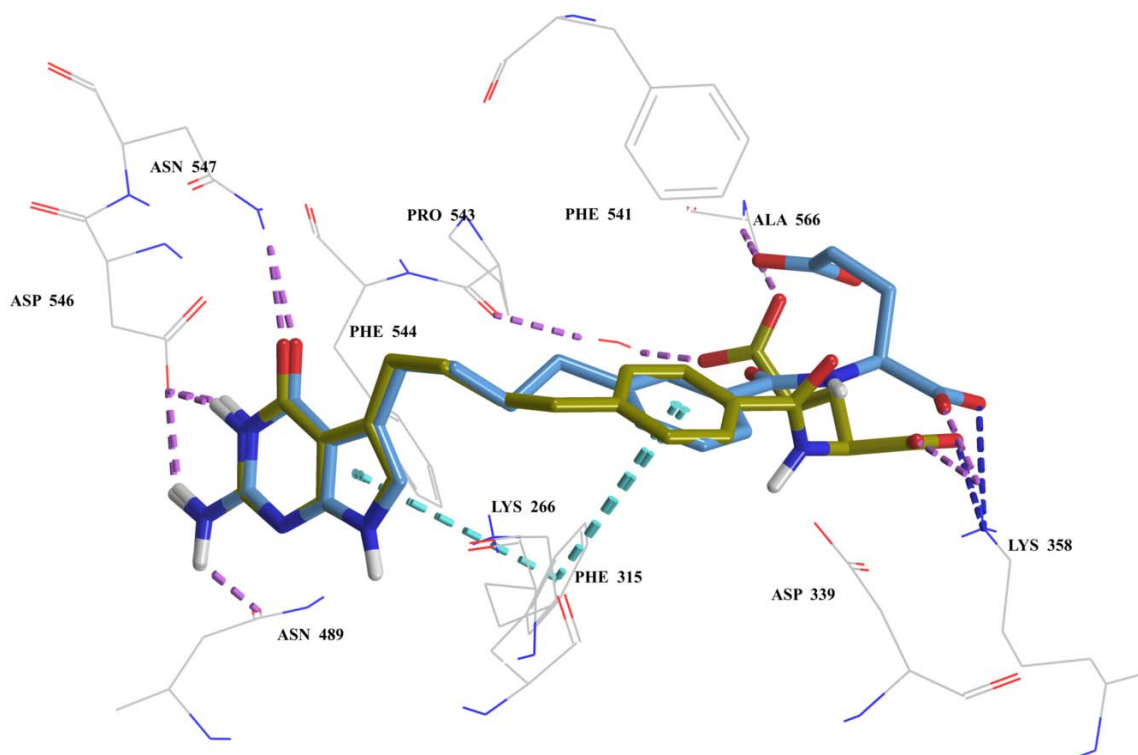


Figure 53. Molecular modeling studies with human AICARFTase (PDB 1P4R).²⁵⁸ Docked poses of **193** (blue, -42.3 kJ/mol) and **13** (green, -36.5 kJ/mol). Docking studies were performed using LeadIT 2.1.6 and visualized using Maestro 11.2.^{197, 352}

Compound **193** (Figure 50) were tested against CHO cells expressing human FR α (RT16), FR β (D4), RFC (PC43-10), and PCFT (R2/PCFT4) as well as KB tumor cells in culture, for drug potency and transport selectivity.

C.2.2. Design of 5-substituted, 2-amino-4-oxo pyrrolo[2,3-*d*]pyrimidine-4'-propyloxy/propylthio/propylamino/butylaminophenyl classical antifolates

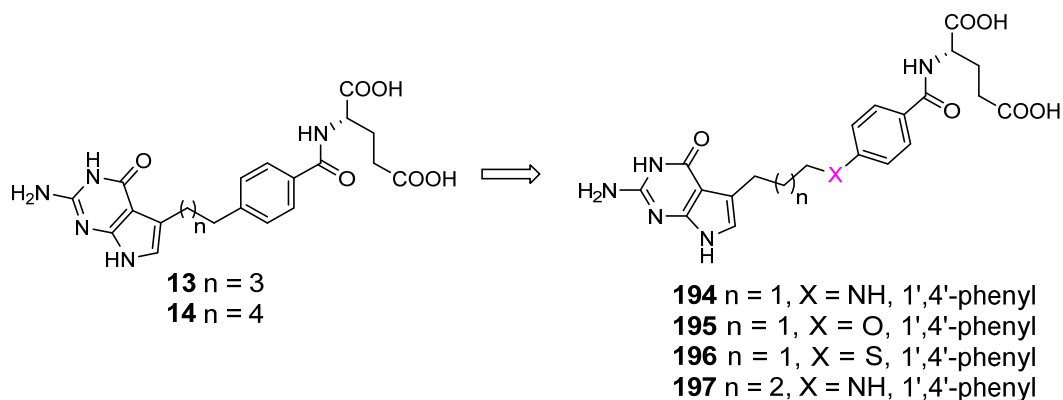
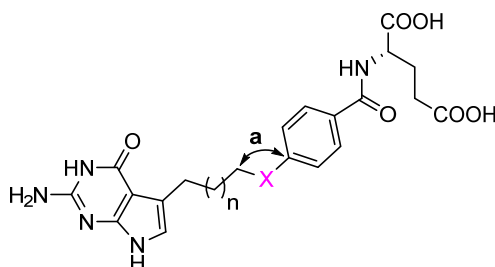


Figure 54. Lead compounds **13** and **14** and target compounds **194-197**.

Gangjee et al.¹²⁰ previously reported 5-substituted pyrrolo[2,3-*d*]pyrimidine antifolates **13** and **14** with 4C and 5C linkers respectively, and a phenyl L-glutamate sidechain (Table 5) as a series of chain extension analogs of clinically used **PMX** for improved tumor cell potency as well as tumor selectivity. Compounds **13** is a first-in-class examples of antifolates that act via dual inhibition of AICARFTase and GARFTase alone (Table 5). Extension to a 4C linker in compound **13** not only improved potency in KB human tumor compared to **PMX**, but also improved inhibition of proliferation of FR α -expressing CHO cells (RT16). However, **13** had reduced activity toward PCFT-expressing CHO cells (PCFT4). Additionally, high activity toward RFC-expressing CHO cells (PC43-10) renders it moderately selective for FR α over RFC and selective for RFC over PCFT. While compound **14** with 5C linker was moderately active, it showed the least uptake by RFC-expressing CHO cells (PC43-10 IC₅₀ > 1000 nM) (Table 5).

Table 13. Predicted bond angle variations of benzylic substitutions (X) in **194-197**. Bond angles were measured using energy-minimized conformations of compounds with Maestro 11.2.¹⁹⁷



Compd. No.	X	Angle (a)
13	CH	112.2°
194/197	NH	120.9°
195	O	118.3°
196	S	106.8°

Previous studies of related 6-substituted pyrrolo[2,3-*d*]pyrimidines established that the distance between the scaffold and side-chain as a consequence of linker length and flexibility, plays an important role in determining tumor cell inhibitory potency and selectivity (Tables 2 and 4).^{104, 107, 115-116, 121} Thus, it was of interest to introduce heteroatoms (NH, O or S substitutions of the benzylic CH₂) in the most potent carbon analog **13**, to evaluate the influence of varied bond angles of the benzylic position on selectivity and potency (Table 13). The varied bond angles of the C–X–C bonds in ligands **194-196** provide different conformational orientations of the scaffold and the L-glutamate sidechain and could impact transport selectivity, as well as dual GARFTase and AICARFTase inhibition (Figure 54).

Though analog **14** with a 5C-linker is less potent than compound **13**, it has ~4-fold reduced activity toward CHO cells expressing RFC (Table 5). As a preliminary study, analog **197** with a 5-atom linker and a benzylic NH substitution was also designed to investigate the contribution of further conformational flexibility towards potency and selectivity in the 5C-linker series of 5-substituted pyrrolo[2,3-*d*]pyrimidine antifolates (Figure 54).

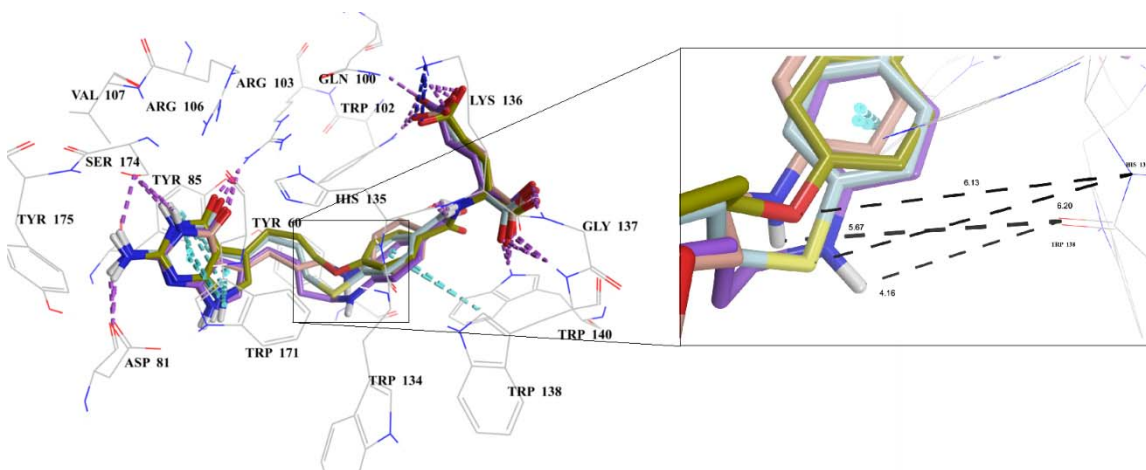


Figure 55. Molecular modeling studies with human FR α (PDB 5IZQ).¹⁶⁷ Superimposition of the docked poses of **194** (pink, -57.8 kJ/mol), **195** (green, -58 kJ/mol), **196** (blue, -58 kJ/mol), and **197** (violet, -58 kJ/mol). Docking studies were performed using LeadIT 2.1.6 and visualized using Maestro 11.2.^{197, 352}

Molecular modeling studies of the heteroatom analogs **194-197** were carried out using X-ray crystal structures of human FR α (5IZQ), GARFTase (5J9F) and AICARFTase (1P4R) to explore the binding interactions (Figures 55-57). The compounds display similar interactions as the native crystal structure ligands and the lead compounds **13** or **14** (not shown here for clarity), by maintaining key interactions involving the bicyclic scaffolds and the benzoyl L-glutamate tail.

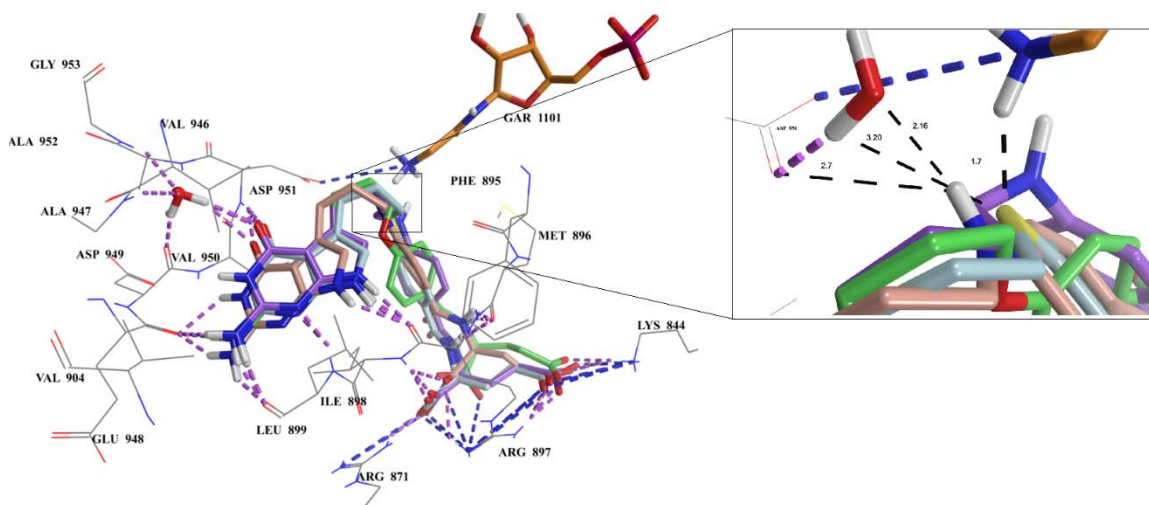


Figure 56. Molecular modeling studies with human GARFTase (PDB 5J9F).¹⁶⁷ Superimposition of the docked poses of **194** (pink, -52.6 kJ/mol), **195** (green, -46.3 kJ/mol), **196** (blue, -50 kJ/mol), and **197** (violet, -52.5 kJ/mol). Docking studies were performed using LeadIT 2.1.6 and visualized using Maestro 11.2.^{197, 352} Substrate GAR is shown in orange.

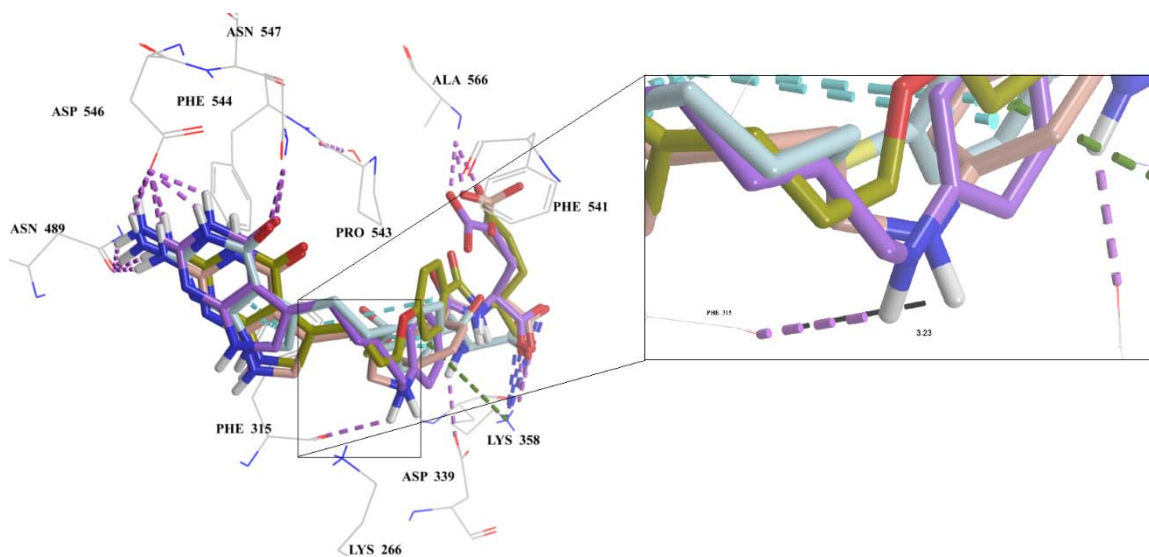


Figure 57. Molecular modeling studies with human AICARFTase (PDB 1P4R).²⁵⁸ Superimposition of the docked poses of **194** (pink, -39.3 kJ/mol), **195** (green, -34.9 kJ/mol), **196** (blue, -32 kJ/mol), and **197** (violet, -41.1 kJ/mol). Docking studies were performed using LeadIT 2.1.6 and visualized using Maestro 11.2.^{197,352} Substrate AICAR is not shown for clarity.

Zooming into the docked poses of **194-197** in FR α (Figure 55) shows that the benzylic heteroatom substitutions not only influence linker conformations due to varied bond angles but are also near (\sim 4 to 6 Å away) the backbone amide formed by Trp134 and His135. Within the flexible environment of a protein, such distances may be shortened (ideal distance required for hydrogen bond formation is \sim 3 Å) to promote hydrogen bond interactions for improved binding energies.

Similarly, the docked poses of compounds **196** and **197** in the GARFTase active site show that the region occupied by the benzylic heteroatomic substitutions are \sim 2 to 4 Å away from hydrogen donors (conserved water, side-chain protonated amine of GAR) and acceptor (side-chain carbonyl of Asp951) (Figure 56).

In the AICARFTase active site, the docked pose of compounds **197** forms an additional hydrogen bond interaction formed between the benzylic NH and the side-chain carbonyl of the Phe315 (Figure 57). Additionally, the benzylic NH of **194** is \sim 3.23 Å away from the backbone carbonyl (hydrogen bond acceptor) of Phe315.

The hydrogen bond interactions that are not recognized in the docking studies are plausible within the constantly moving, flexible environment of a protein in aqueous solution in vivo which can further stabilize binding for better transport and/or inhibition.

The novel analogs **195** and **196** were tested as growth inhibitors against CHO cells expressing human FR α (RT16), FR β (D4), RFC (PC43-10), and PCFT (R2/PCFT4) as well as KB tumor cells in culture.

C.2.3 Design of 5-substituted, 2-amino-4-oxo pyrrolo[2,3-*d*]pyrimidine-butyl-2'-fluorophenyl classical antifolates

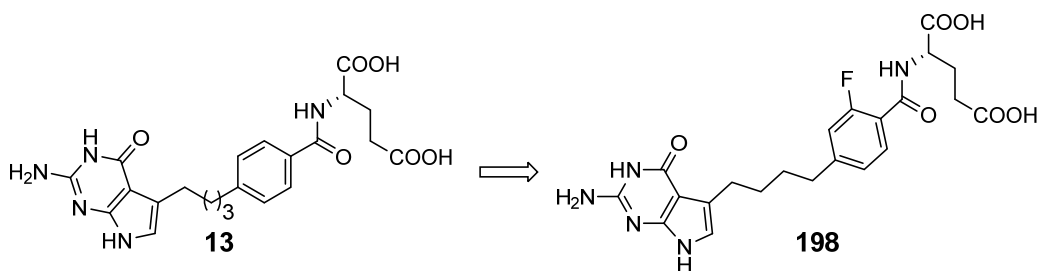


Figure 58. Lead compounds **13** and target compound **198**.

Extension of the 2C-linker in **PMX** to a 4C-linker in compound **13** not only improved potency against KB human tumor but also the inhibition of proliferation of FR α -expressing CHO cells. However, **13** had reduced activity toward PCFT-expressing CHO cells. Additionally, high activity toward RFC- expressing CHO cells renders selective for RFC over PCFT. 2'-[*ortho* (*o*-) to the L-glutamate] fluorine substitution in 6-substituted pyrrolo[2,3-*d*]pyrimidines dramatically increased tumor-targeted antiproliferative activity of the phenyl series mediated through selective transport (especially PCFT) (Table 7).¹¹⁴ Consequently, it is of interest to investigate the contribution of 2'-fluorine substitution in the phenyl series of 5-substituted pyrrolo[2,3-*d*]pyrimidines for improved PCFT-targeted potency as well as selectivity. Compound **198** (Figure 58) was designed and its impact on drug potency and transport selectivity was determined.

The novel analog **198** was tested as growth inhibitors against CHO cells expressing human FR α (RT16), FR β (D4), RFC (PC43-10), and PCFT (R2/PCFT4) as well as KB tumor cells in culture.

C.3. Multiple enzyme inhibitors (TS, GARFTase, AICARFTase) with selectivity for FRs and/or PCFT over RFC

C.3.1. Design of 5-substituted, 2-amino-4-oxo-6-methyl pyrrolo[2,3-*d*]pyrimidine classical antifolates

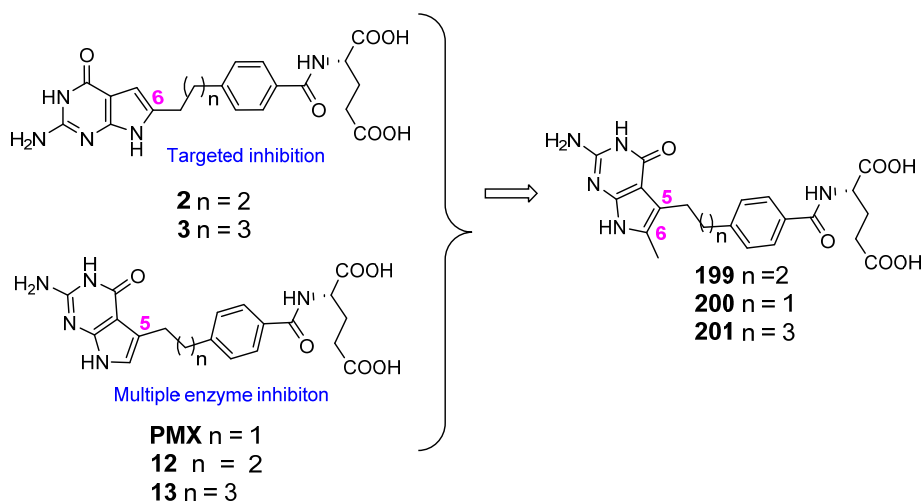


Figure 59. Lead compounds **2**, **3**, **PMX**, **12** and **13** and target compounds **200** and **201**.

Although the methyl group often considered as chemically inert, only participates in London dispersion interactions, it plays a very important role in the molecular recognition of endogenous and exogenous ligands by bioreceptors.³⁵⁷ The stereoelectronic effects of a methyl leads to selective binding and increased potency, among various other pharmacological effects.^{330, 358-359} As such, it is a useful tool used in medicinal chemistry design to modify aspects related to conformation, electronic factors, pharmacokinetics, among other factors.³⁵⁸⁻³⁵⁹

Table 14. IC₅₀ Values (nM) and FR-and PCFT-expressing CHO cell selectivity ratios over RFC-expressing CHO cells for **12**, **199**, and **PMX**. For KB cells, data are shown for the protective effects of nucleoside additions, including adenosine (Ade), thymidine (Thd), or AICA.

Compd. No.	KB IC₅₀ (nM) Potency	RFC/FRα Selectivity ratios (IC₅₀) for FRα over RFC	RFC/FRβ Selectivity ratios (IC₅₀) for FRβ over RFC	RFC/PCFT Selectivity ratios (IC₅₀) for PCFT over RFC	KB (+Thd/Ade /AICA)
PMX	9.94 (3.11)	0.62	0.44	3.15	Thd/Ade
12	49.5 (13.2)	0.95	-	0.2	Ade
199	49.9	>15	>385	>17	Ade/AICA/ Thd

Studies of 5- and 6-substituted pyrrolo[2,3-*d*]pyrimidines established that while the 6-substituted analogs are selective (>100 fold for FR and/or PCFT expressing CHO cells over those that express RFC) and potent GARFTase inhibitors, the related 5-substituted pyrrolo[2,3-*d*]pyrimidines are non-selective (<10 fold for FR and/or PCFT expressing CHO cells over those that express RFC) dual GARFTase and AICARFTase inhibitors (Tables 2, 4 and 5).^{104, 107, 116, 120-121} A superior inhibitor to the above two series of analogs would be a compound that is a FR- and PCFT-selective (over RFC), dual GARFTase and AICARFTase inhibitor. Thus, it was of interest to synthesize and evaluate 6-methylated, 2-amino-4-oxo-pyrrolo[2,3-*d*]pyrimidines **200** and **201** as the hybrids of 5- and 6-

substituted analogs, to evaluate for improved selectivity and dual enzyme inhibitory activity.

Gangjee *et al*³⁶⁰ performed a preliminary study of a 5-substituted, 2-amino-4-oxo-6-methyl pyrrolo[2,3-*d*]pyrimidine **199** with a 3C-linker and found that the hypothesis for selectivity due to a 6-methyl substitution was supported by the biological activity. Compound **200** is a multi-enzyme inhibitor of purine and pyrimidine biosynthesis (Table 14); in vitro growth inhibition of IGROV1 tumor cells was completely protected only in the presence of both Ade (adenine) and Thd (thymidine) (Table 14). The potency of compound **199** towards KB cells (49.9 nM) was identical to its parent desmethyl analog **12** (Table 14). Unlike **12** (equally selective for RFC- and FR α -expressing CHO cells, and ~5-fold selective for RFC- over PCFT-expressing CHO cells), it is selective for FR α , FR β and PCFT over RFC- expressing CHO cells (>15-, >385- and >17-fold respectively) primarily due to loss of uptake by RFC (Table 14). This study led to the discovery of a compound that was ~5-fold less potent against KB cell proliferation and ~5-(PCFT) to 900-(FR β) fold more selective than **PMX**.

The pharmacological influences of a methyl substitution for the observed loss of RFC binding is perhaps due to steric repulsion. The crystal structure of hRFC is not known and hence the arrangement of the amino acids that line the folate binding pocket and the binding interactions remain unidentified. However, based on the general trend of reduced RFC binding by the 6-substituted pyrrolo[2,3-*d*]pyrimidine series of analogs, a possible steric repulsion in the scaffold binding subsite caused by the alkyl group at 6-position is proposed.

To investigate the contribution of 6-methyl substitution in the phenyl series of 5-substituted pyrrolo[2,3-*d*]pyrimidine series for improved potency as well as selectivity, compounds **200** and **201** with 2C- (6-methyl analog of **PMX**) and 4C-linkers respectively were designed (Figure 59).

Molecular modeling studies of the 6-methylated analogs **199-201** were carried out using X-ray crystal structures of human FR α (5IZQ), GARFTase (5J9F) and TS (1JU6) to explore the binding interactions and to validate their drug targets (Figures 60-63). The compounds display similar interactions as the native crystal structure ligands (not shown here for clarity)

The docked poses of the 2C-, 3C- and 4C-linker analogs **200**, **199** and **201** respectively, in FR α (Figure 60) display similar interactions as the native crystal structure ligands (not shown here for clarity) by maintaining key interactions involving the bicyclic scaffolds and the benzoyl L-glutamate tail. However, due to its shorter length, the 2C-linker analog **200** does not fully occupy the extended pocket of FR α . In order to accommodate energetically favorable ionic interactions of the side-chain L-glutamate, the bicyclic scaffold is shifted to the right, away from the scaffold binding region. As a result, the hydrogen bond interactions of the 3-NH with the side-chain hydroxyl of Ser196 (174) and the 4-oxo moiety with the side-chain nitrogen of Arg125 (103) are lost, reducing the energy of binding. Apart from shifting the bicyclic ring away from the scaffold binding region, the 6-methyl substitution neither sterically clashes with the binding site of FR α , nor does it alter the conformation of the scaffold when compared to the desmethyl analog.

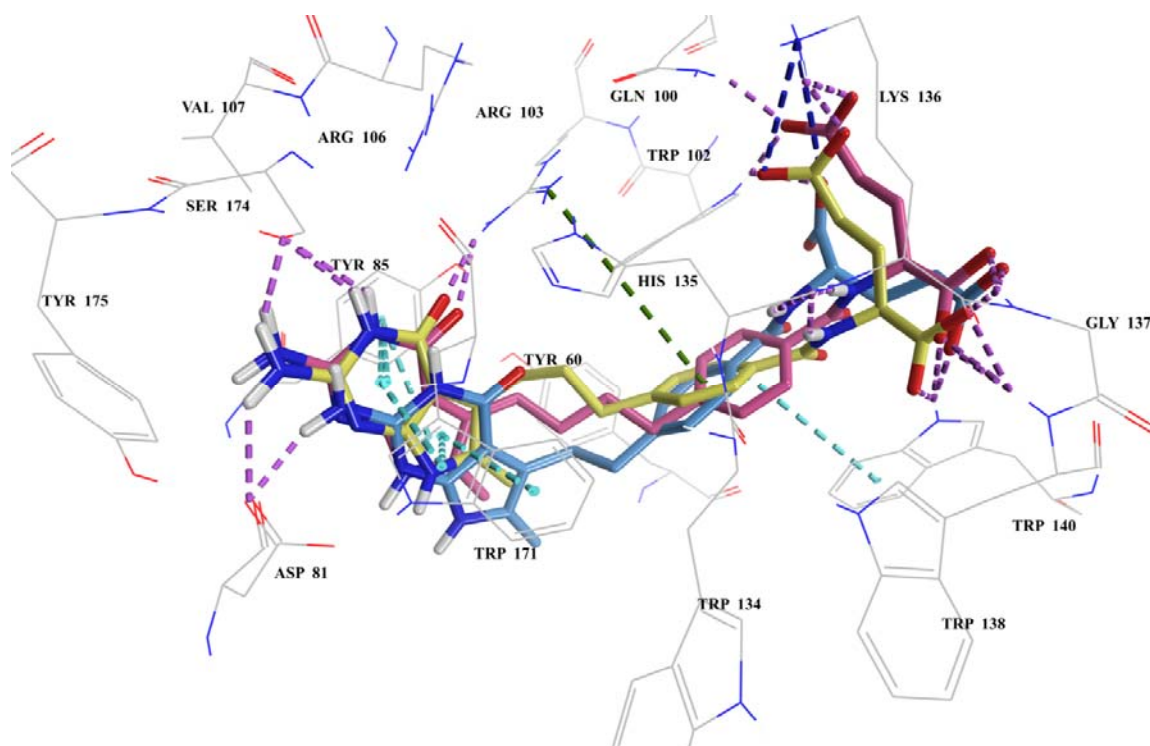


Figure 60. Molecular modeling studies with human FR α (PDB 5IZQ).¹⁶⁷ Superimposition of the docked poses of **199** (yellow, -61.5 kJ/mol), **200** (blue, -49.2 kJ/mol) and **201** (pink, -55.8 kJ/mol). Docking studies were performed using LeadIT 2.1.6 and visualized using Maestro 11.2.^{197, 352}

The docked poses of the 6-methyl compounds **199-201** in the GARFTase active site show that they bind in the same region as native ligand in the GARFTase crystal structure (PDB 5J9F, native ligand not shown for clarity) (Figure 61).

Unlike the extended pocket of the FRs, the binding pocket in GARFTase is curved and forces a conformation such that the linker projects the sidechain aryl almost at a 90°

angle. As such the binding pocket accommodates and maintains key interactions with classical folate analogs that have linkers ranging from 2-atoms to 5-atoms. For the 6-methyl analogs, the bent conformation forces the bulky 6-methyl group in **199-201** close to its sidechain aryl ring (~ 2 Å, not shown for clarity). This steric hindrance may destabilize the bound conformation, thus drastically reducing the binding energies.

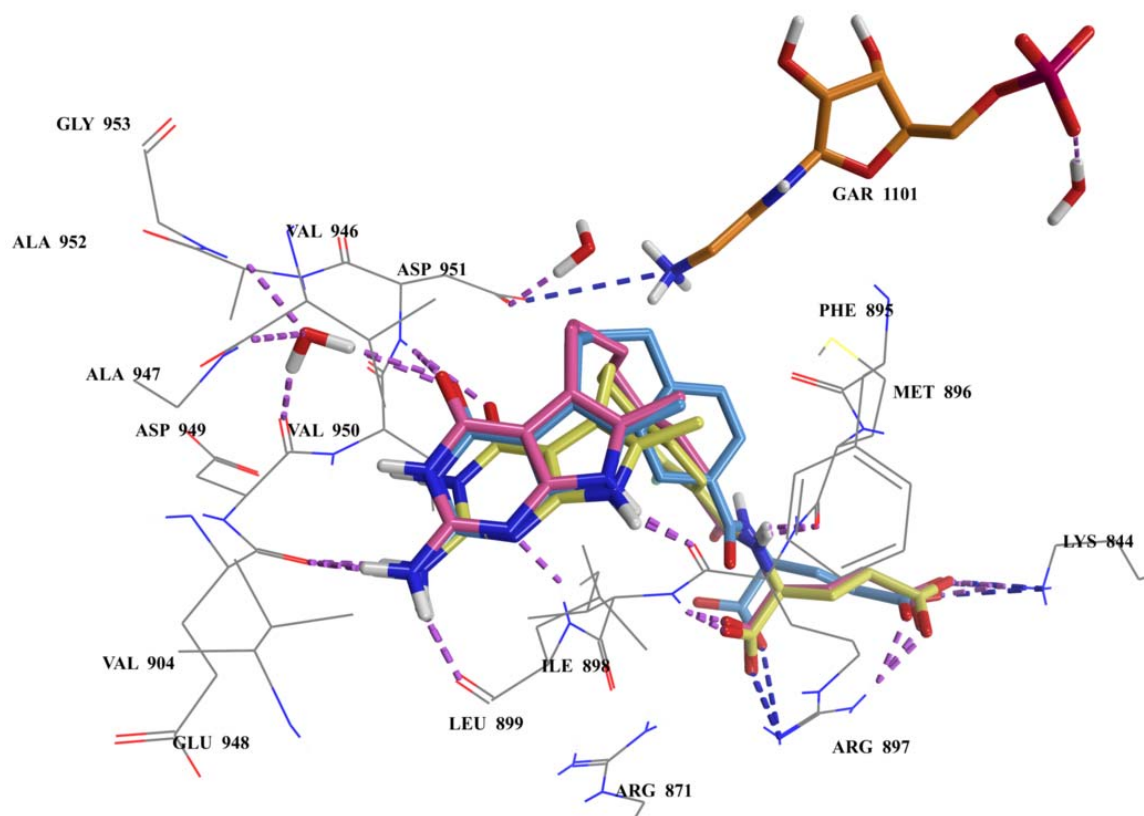


Figure 61. Molecular modeling studies with human GARFTase (PDB 5J9F).¹⁶⁷ Superimposition of the docked poses of **199** (yellow, -40.9 kJ/mol), **200** (blue, -35.5 kJ/mol) and **201** (pink, -48.7 kJ/mol). Docking studies were performed using LeadIT 2.1.6 and visualized using Maestro 11.2.^{197, 352} Substrate GAR is shown in orange.

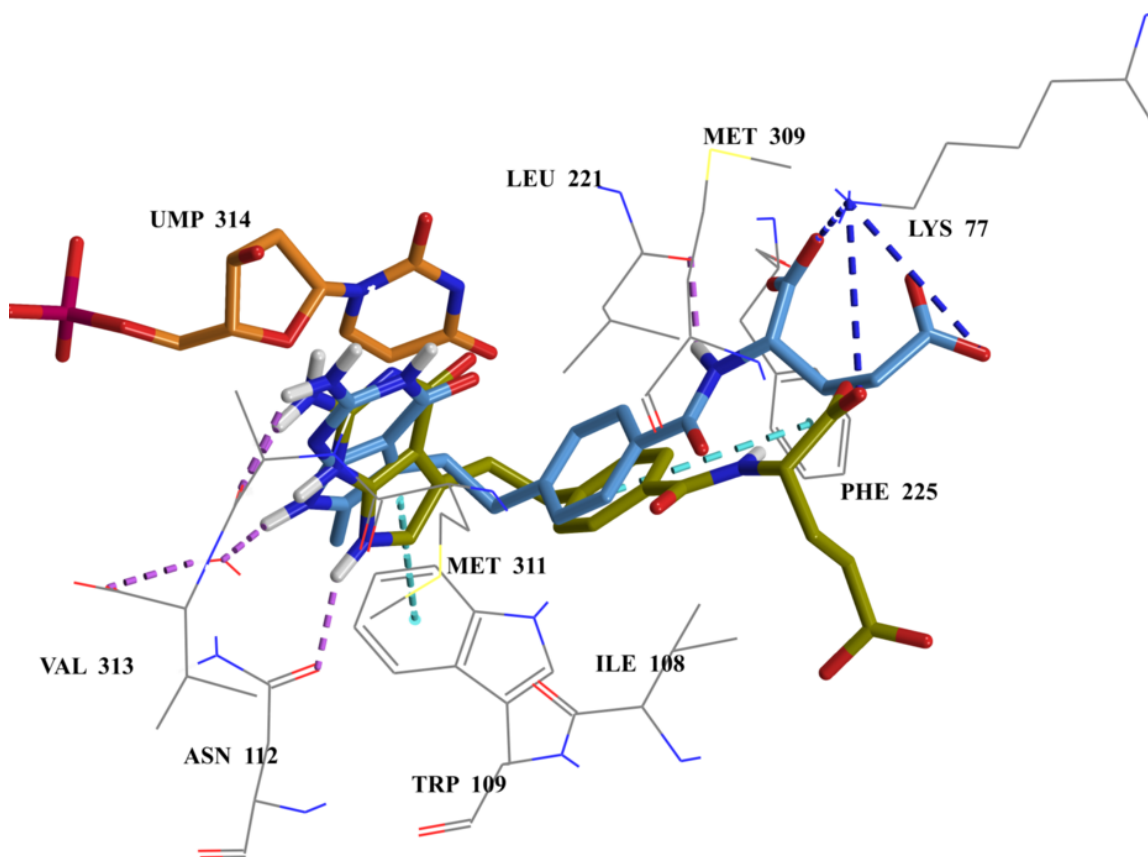


Figure 62. Molecular modeling studies with human TS (PDB 1JU6).²⁰⁹ Superimposition of the docked poses of **200** (blue, -38.2 kJ/mol) and **PMX** (green, -40.4 kJ/mol). Substrate UMP is shown in orange. Docking studies were performed using LeadIT 2.1.6 and visualized using Maestro 11.2.^{197, 352}

Protection studies show that Thd by itself does not protect KB cells from the cytotoxic action of compound **199** and Ade by itself is partially protective. However, a combination of Ade and Thd are fully protective, implying a weak/secondary inhibition of TS. Docking studies were performed to validate TS as one of the drug targets. The analogs **199-201** bind in the same region as **PMX** (Figures 62 and 63) and the interactions are maintained with docked scores in the order of **PMX** (2C linker) > **200** (2C linker) > **201** (3C linker) > **199** (4C linker).

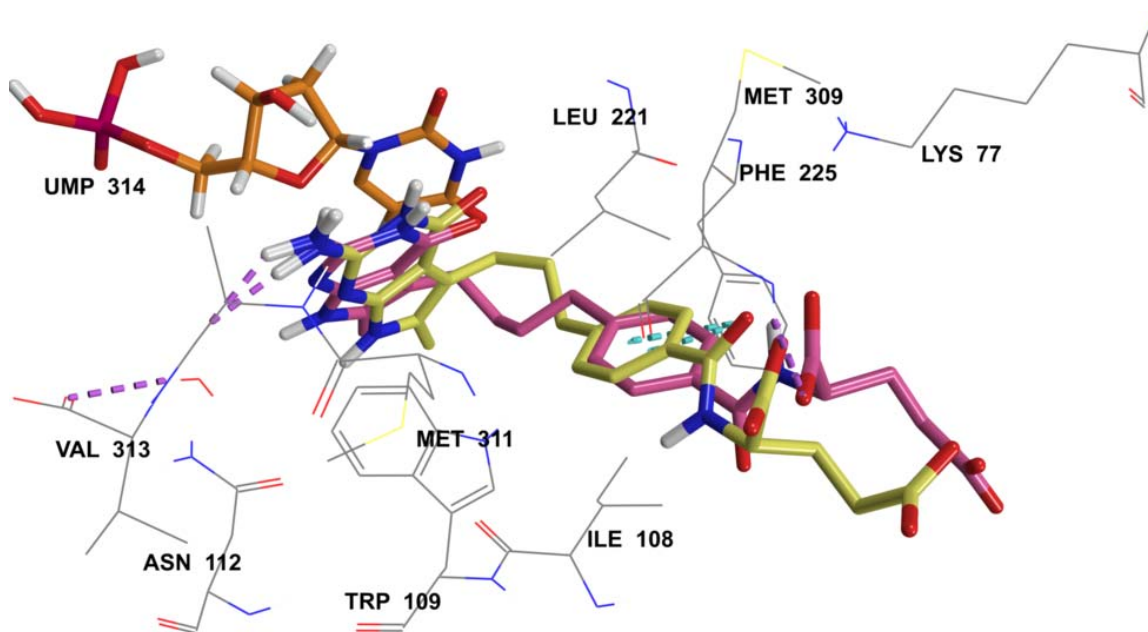


Figure 63. Molecular modeling studies with human TS (PDB 1JU6).²⁰⁹ Superimposition of the docked poses of **199** (yellow, - 36.8 kJ/mol) and **201** (pink, -37.5 kJ/mol). Substrate UMP is shown in orange. Docking studies were performed using LeadIT 2.1.6 and visualized using Maestro 11.2.^{197, 352}

The bicyclic pyrrolo[2,3-*d*]pyrimidine ring of the analogs **199-201** make van der Waals contacts with the bound pyrimidine of dUMP in which the ring systems of the two ligands are stacked against each other by nonpolar interactions with Trp109 (Figures 62 and 63). The backbone carbonyl of Ala312 accepts a hydrogen bond from the 2-amino group. The N7 of **PMX** forms a hydrogen bond with the side-chain carbonyl of Asn112 (Figure 62). Its 6-methylated analog **200** twists out of plane and instead forms a water mediated hydrogen bond with the backbone carbonyl of Val313 while the N7 nitrogens of the 3C- and 4C-analogs are not involved in any interactions (Figure 62). The aromatic rings of the *p*ABA sidechains in all the analogs are placed in a hydrophobic pocket lined with the sidechains of Phe225, Leu221 and Ile108 (Figures 62 and 63). Similar to **PMX**, the

glutamate α -carboxyl of its 6-methyl analog **200** forms an ionic interaction with Lys77. Compound **200** additionally orients its γ -carboxylate for a favorable ionic interaction with Lys77. The 3C- and 4C-linker extended analogs **199** and **201**, being longer than the pocket, extend their L-glutamate chain outside the pocket, and do not make any of the standard ionic interactions (Figure 63). Based on the docking studies, it is anticipated that **200**, the 6-methyl analog of **PMX** would inhibit TS more efficiently than **199**. In addition, **200**, an isosterically modified **PMX**, should potentially circumvent the **PMX**-associated dose-limiting toxicities against healthy cells thus exemplifying the “magic-methyl effect” where a simple methylation results in improved selectivity (loss of RFC binding and uptake, Table 14).³³⁰

The novel analogs were tested as growth inhibitors against CHO cells expressing human FR α (RT16), FR β (D4), RFC (PC43-10), and PCFT (R2/PCFT4) as well as KB tumor cells in culture.

IV. CHEMICAL DISCUSSION

This section contains the synthetic schemes developed for the compounds in the following three projects:

D.1. GARFTase inhibitors with selectivity for FRs and/or PCFT over RFC

1. 6-substituted, 2-amino-4-oxo pyrrolo[2,3-*d*]pyrimidine-fluorophenyl classical antifolates
2. 6-substituted, 2-amino-4-oxo pyrrolo[2,3-*d*]pyrimidine-3'-fluoropyridyl classical antifolates
3. 6-substituted, 2-amino-4-oxo pyrrolo[2,3-*d*]pyrimidine-3'-fluorothieryl classical antifolates
4. 6-substituted, 2-amino-4-oxo pyrrolo[2,3-*d*]pyrimidine-difluorophenyl classical antifolates
5. 6-substituted, 2-amino-4-oxo pyrrolo[2,3-*d*]pyrimidine-2'-substitutedphenyl classical antifolates
6. 6-substituted, 2-amino-4-oxo pyrrolo[2,3-*d*]pyrimidine-pyrimidyl classical antifolates

D.2. Multiple enzyme inhibitors (GARFTase and AICARFTase) with selectivity for FRs and/or PCFT over RFC

1. 5-substituted, 2-amino-4-oxo pyrrolo[2,3-*d*]pyrimidine-3'-butylphenyl classical antifolates
2. 5-substituted, 2-amino-4-oxo pyrrolo[2,3-*d*]pyrimidine-4'-propyloxy/propylthio/propylamino/butylaminophenyl classical antifolates

3. 5-substituted, 2-amino-4-oxo pyrrolo[2,3-*d*]pyrimidine-butyl-2'-fluorophenyl classical antifolates

D.3. Multiple enzyme inhibitors (TS, GARFTase, AICARFTase) with selectivity for FRs and/or PCFT over RFC

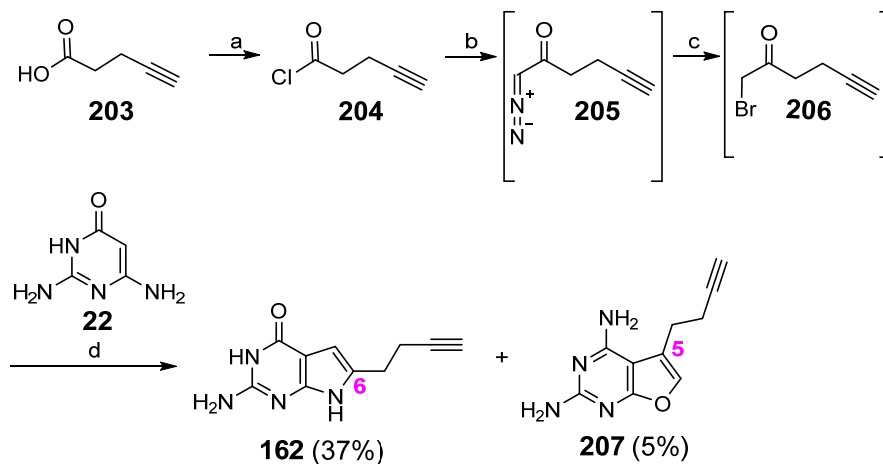
1. 5-substituted, 2-amino-4-oxo-6-methyl pyrrolo[2,3-*d*]pyrimidine classical antifolates

D.1.1 The synthesis of 6-substituted, 2-amino-4-oxo pyrrolo[2,3-*d*]pyrimidine-fluorophenyl classical antifolates (**179-181**).

The synthesis of target compounds was achieved via key intermediate diethyl (4-(3-(2-amino-4-oxo-4,7-dihydro-3*H*-pyrrolo[2,3-*d*]pyrimidin-6-yl)alk-1-yn-1-yl)fluorobenzoyl)-L-glutamates, **212-213**.

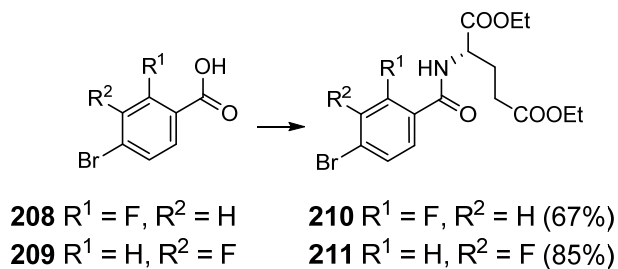
Following a reported procedure, the commercially available terminal acetylene pent-4-ynoic acid **203** (Scheme 39) was converted to its acid chloride **204** which was reacted with in situ synthesized diazomethane to form the α -diazoketone **205**.¹²¹ The unstable diazoketone **205** was immediately reacted with 48% aq. HBr to give the desired α -bromo-methylketone **206** by displacing N₂ gas. Condensation of the α -bromo-methylketone **206** with 2,4-diamino-6-hydroxypyrimidine **22** at room temperature for 72 h afforded the 6-substituted pyrrolo[2,3-*d*]pyrimidine with a terminal acetylene **162** in 37% yield and the 5-substituted 2,4-diamino-furo[2,3-*d*]pyrimidines **207** in 5% yield.²⁹⁸ The structures were confirmed via clear differences in the magnitude of chemical shift of the C5-CH and C6-CH protons and the number of exchangeable 2-NH₂ protons in ¹H NMRs of pyrrolo and furo[2,3-*d*]pyrimidines **162** and **207** respectively.

Scheme 39. Synthesis of 162.



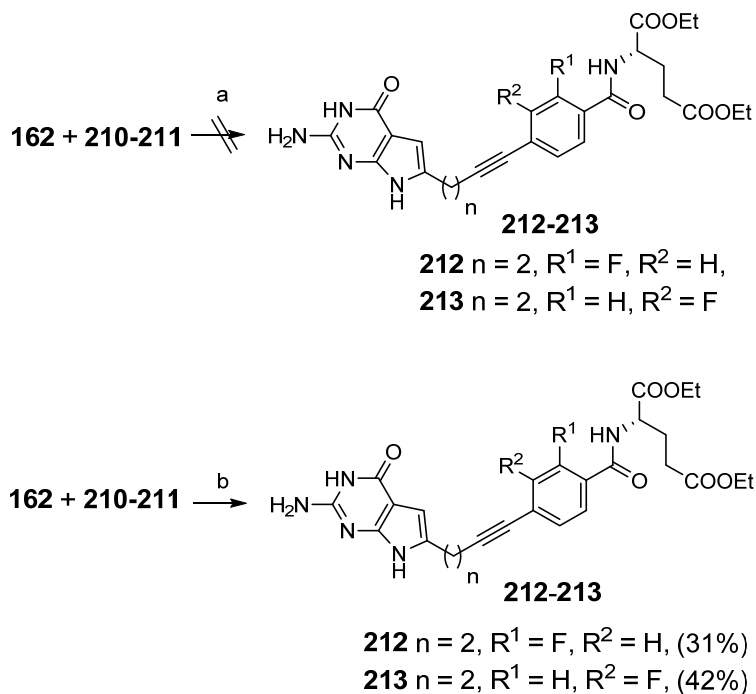
Reagents and conditions: (a) oxalyl chloride, CH_2Cl_2 , reflux, 1 h; (b) diazomethane, Et_2O , 0°C -rt, 1 h; (c) 48% HBr, 80°C , 2 h; (d) DMF, rt, 72 h, 5-37% yields.

Scheme 40. Synthesis of 210-211.



Reagents and conditions: *N*-methylmorpholine (NMM), 2-chloro-4,6-dimethoxy-1,3,5-triazine (CDMT), L-glutamate diethyl ester hydrochloride, DMF, rt, 12 h, 67-85% yields.

Scheme 41. Synthesis of 212-213.



Reagents and conditions: (a) CuI, Pd(0)(PPh₃)₄, Et₃N, DMF, rt, 12 to 72 h; (b) CuI, Pd(0)(PPh₃)₄, Et₃N, DMF, 70 °C, μ W, 12 h, 31-42% yields.

Table 15. Reaction conditions for the synthesis of **212**.

Reaction conditions	Progress of the reaction
rt, 12 h to 72 h, benchtop	No reaction
rt, 12 h, μ W	No reaction
50 °C, 12 h, μ W	New nonpolar TLC spot observed; starting material remaining
70 °C, 12 h, μ W	New nonpolar TLC spot observed; starting material disappeared

For the synthesis of the intermediates 2-amino-6-(but-3-yn-1-yl)-3,7-dihydro-4H-pyrrolo[2,3-*d*]pyrimidin-4-one, **212-213** (Scheme 41), the reported procedure was

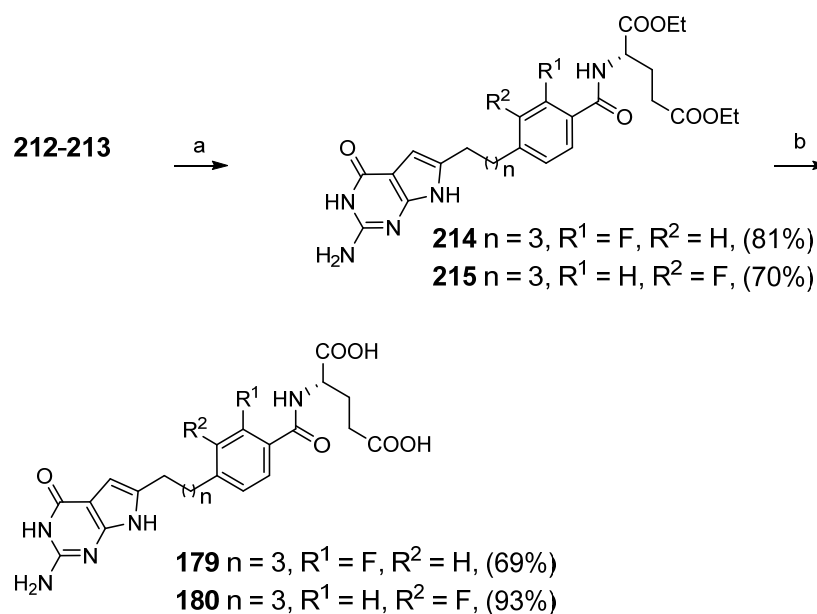
followed for Sonogashira coupling of the alkyne **162** with the bromo-glutamate esters **210-211**.¹¹⁶ However, the room temperature reaction with tetrakis(triphenylphosphine)palladium(0) (0.16 eq) and copper(I) iodide (0.16 eq) as catalysts and triethylamine (10 eq) as base did not yield the coupled product even after extending the reaction from 12 h to 3 days. To improve the scope and repeatability of the reaction, the method was moved from benchtop to microwave (Table 15). As a test reaction, Sonogashira coupling of **162** with **210** was run over a range of temperatures starting from room temperature till 70 °C for 12 hours at which point the starting material **162** was completely used up affording **212** in 31% yield. Repeating the reaction conditions with **211** gave **213** in 42% yield. Reduced yields despite complete disappearance of starting material is attributed to the compound lost during column chromatography because of its basic polarity (sticks to the slightly acidic silica).

As per the reported procedure, hydrogenation of **212** and **213** (Scheme 42) at 55 psi gave the saturated analogs **214** and **215** respectively in 81% and 70% yields. Subsequent saponification of the glutamate esters in **214** and **215** afforded the target compounds **179** and **180**, respectively in 69% and 93% yields respectively.

Compounds **210-211** (Scheme 40) were synthesized in 67-85% yields by peptide coupling of the commercially available bromo-carboxylic acids **208-209** and L-glutamate diethyl ester hydrochloride in the presence of *N*-methylmorpholine (NMM) and 2-chloro-4,6-dimethoxy-1,3,5-triazine (CDMT) as the coupling agents.

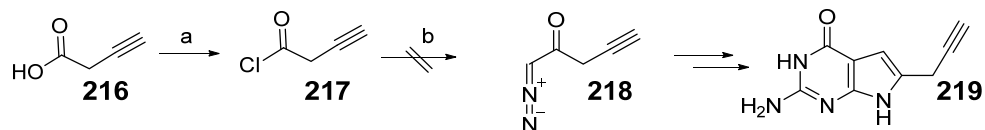
Following a similar procedure (Schemes 39-42) for the synthesis of target compound **181**, would require the generation of the intermediate **219** (Scheme 43). However, the reaction did not proceed from the conversion of acid chloride **217** to the α -diazoketone **218**. The reduced pKa (~ 15) (calculated using Chemicalize)³⁶¹ of the CH₂-proton of the acid chloride **217** along with resonance stabilization of the electron pair (Scheme 44) could provide an explanation for the failed conversion.

Scheme 42 Synthesis of target compounds **179-180**



Reagents and conditions: (a) 10% Pd/C, H₂, 55 psi, EtOH, MeOH, 12 h, 70-92%; (b) (i) 1 N NaOH, rt, 1 h; (ii) 0-4 °C, 1 N HCl, 69-80% yields.

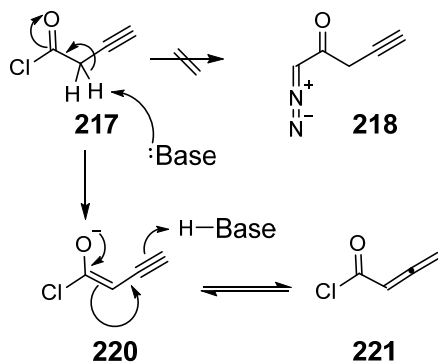
Scheme 43 Synthesis of intermediate **219**



Reagents and conditions: (a) oxalyl chloride, CH_2Cl_2 , reflux, 1 h; (b) diazomethane, Et_2O , KOH, EtOH , 0°C -rt, 1 h.

We speculate that an allene **221** (Scheme 44) is generated from the acid chloride at reflux conditions which is in conjugation with the carbonyl group. This reduces the electron deficiency of the acid chloride thus interfering with the displacement of the chloride ion by diazomethane. This strategy was abandoned and an alternate procedure was used.

Scheme 44 Possible mechanism of allene formation instead of α -diazoketone



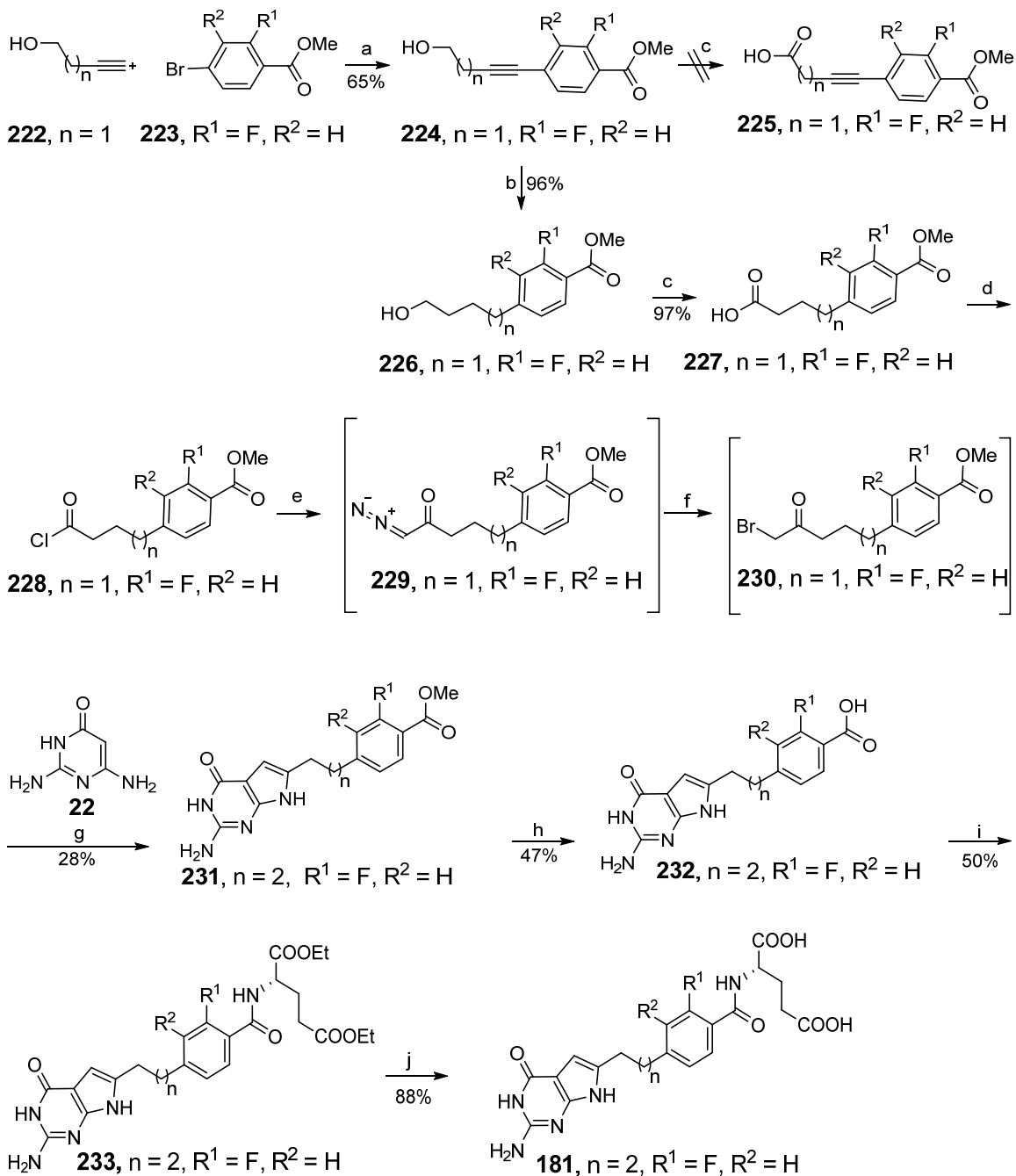
Reagents and conditions: diazomethane, Et_2O , 0°C -rt, 1 h.

The synthesis of target compound **181** (Scheme 45) was initiated by following a reported procedure of a palladium(II)-catalyzed Sonogashira coupling of but-3-yn-1-ol **222**

with methyl 4-bromo-2-fluorobenzoate, **223**, to afford the butynyl alcohol **224** in 65% yield.¹²¹ The reported procedure was slightly altered and periodic acid/PCC oxidation of the butynyl alcohol was (repeatedly) attempted, but the conversion of **224** to acid **225** was unsuccessful. Upon monitoring the reaction progress on TLC (12 h), the starting material remained and no new fluorescent spot was observed. We hypothesize that the complex formed by the alcohol with the powerful oxidizing agent, chlorochromatoperiodate (CCP) **236** (Scheme 46), is a reversible process in which the equilibrium is shifted towards left.³⁶² This could be because of an energetically costing unstable oxidized product, the alpha-alkynyl aldehyde **238**. Our hypothesis is supported by literature evidence in which an alternate TEMPO oxidation of butyn-1-ol to its aldehyde failed to work.³⁶³

Hence, as per reported procedure, the alkyne was first reduced by catalytic hydrogenation to the saturated alcohol **226** (Scheme 45) in 96% yield and subsequently oxidized using periodic acid/PCC to the carboxylic acid **227** in 97% yield.¹²¹ The acid was converted to the acid chloride **228**, immediately reacted with in situ synthesized diazomethane followed by 48% aq. HBr to give the α -bromomethylketone **230**. The bis-electrophile was condensed with 2,4-diamino-6-hydroxypyrimidine **22** at room temperature for 3 days to afford the crude 6-substituted pyrrolo[2,3-*d*]pyrimidine **231** in 28% yield over 4 steps, which was hydrolyzed to yield the acid **232** in 47% yield. The free acid was subsequently peptide coupled with L-glutamate diethyl ester hydrochloride in the presence of NMM and CDMT as the coupling agents to afford the diesters **233** in 50% yield. Final saponification of the diesters gave the desired final compound **181** in 88% yield.

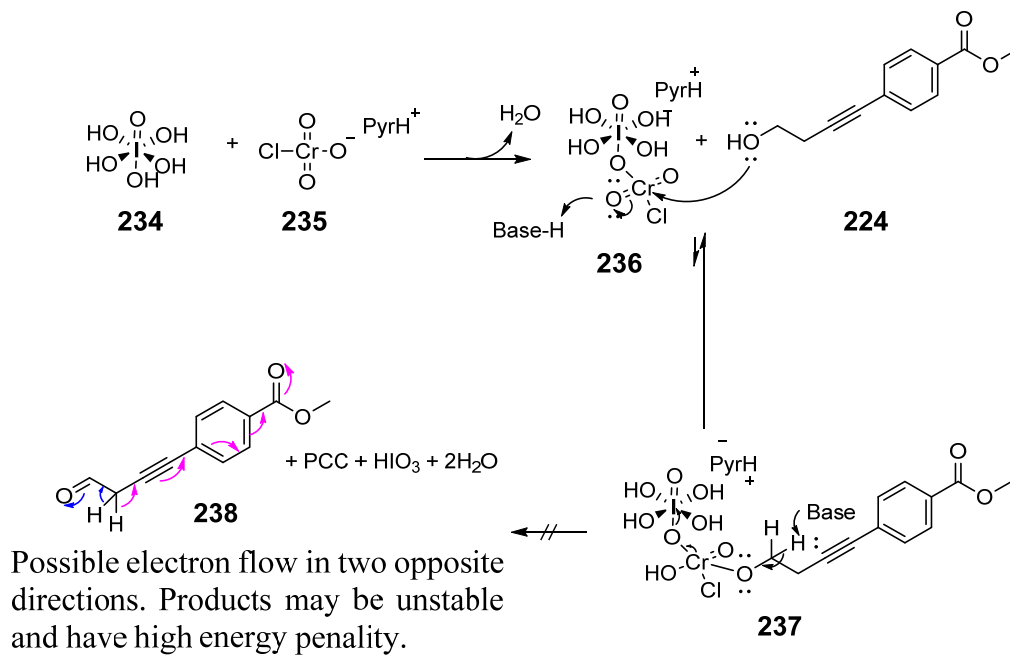
Scheme 45. Synthesis of target compound 181.



Reagents and conditions: (a) $\text{PdCl}_2, \text{Ph}_3\text{P}, \text{TEA}, \text{CuI}, \text{ACN}, \mu\text{W}, 100^\circ\text{C}, 30 \text{ min}, 65\%$; (b) $10\% \text{ Pd/C}, \text{H}_2, 55 \text{ psi}, \text{EtOH}, \text{MeOH}, 96\%$; (c) $\text{H}_5\text{IO}_6, \text{PCC}, \text{ACN}, 0^\circ\text{C} - \text{rt}, 3 \text{ h}, 97\%$; (d) (i) oxalyl chloride, CH_2Cl_2 , reflux, 1 h; (e) diazomethane, $(\text{Et})_2\text{O}, 0^\circ\text{C} - \text{rt}, 1 \text{ h}$; (f) 48%

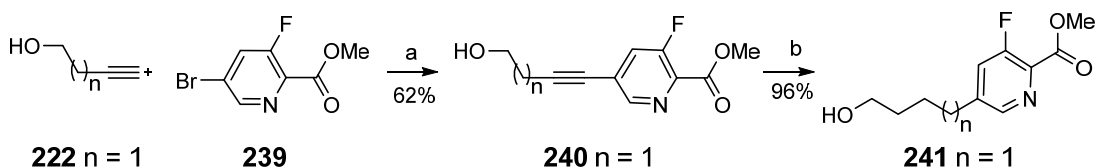
HBr, (Et)₂O, 50 °C, 2 h; (g) DMF, rt, 3 days, 28% over 4 steps; (h) (i) 1N, NaOH, rt, 12 h, (ii) 1N HCl, 47%; (i) NMM, CDMT, diethyl-L-glutamate, DMF, rt, 12 h, 50%; (j) (i) 1N, NaOH, rt, 1 h; (ii) 1N HCl, 88%.

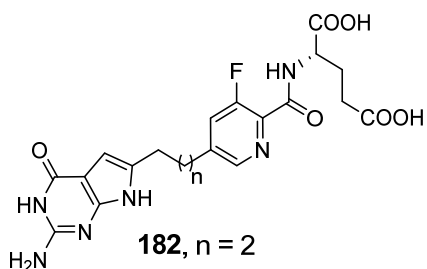
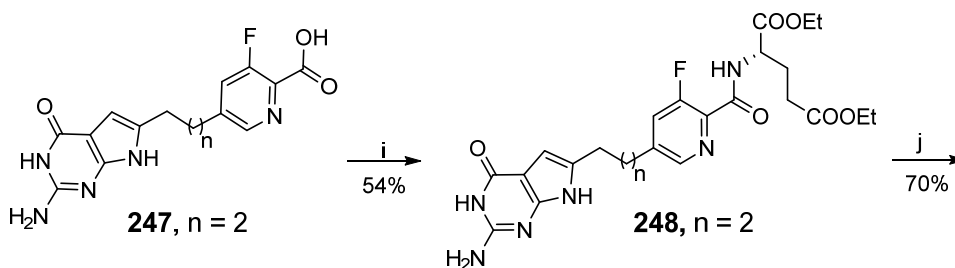
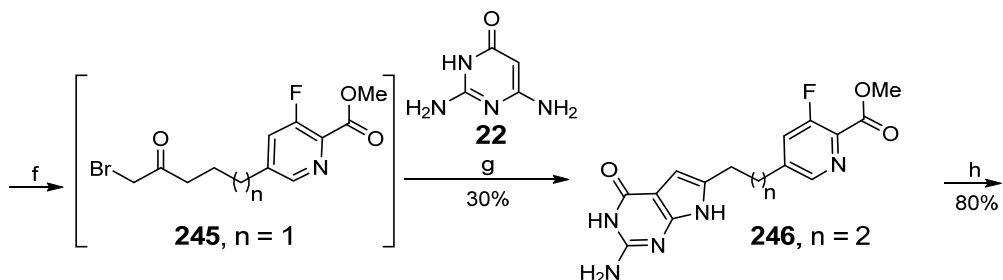
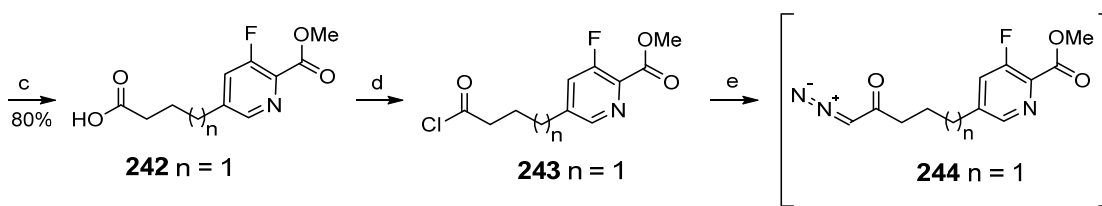
Scheme 46 Possible mechanism for unsuccessful oxidation of butynol **224** to acid **225**



D.1.2. The synthesis of 6-substituted, 2-amino-4-oxo pyrrolo[2,3-*d*]pyrimidine-3'-fluoropyridyl classical antifolates (**182-183**).

Scheme 47. Synthesis of target compounds **182**.

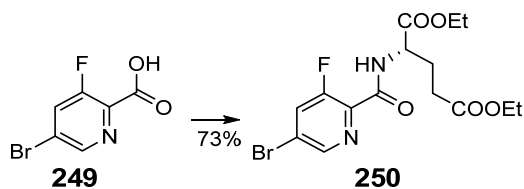




Reagents and conditions: (a) PdCl₂, Ph₃P, TEA, CuI, ACN, μ W, 100 °C, 30 min, 62%; (b) 10% Pd/C, H₂, 55 psi, EtOH, MeOH, 96%; (c) H₅IO₆, PCC, ACN, 0 °C - rt, 12 h, 80%; (d) 10% Pd/C, H₂, 55 psi, EtOH, MeOH, 96%; (e) diazomethane, (Et)₂O, 0 °C - rt, 1 h; (f) 48% HBr, (Et)₂O, 50 °C, 2 h; (g) DMF, rt, 3 days, 30% yield over 4 steps; (h) (i) 1N, NaOH, rt, 12 h, (ii) 1N HCl, 80%; (i) NMM, CDMT, diethyl-L-glutamate, DMF, rt, 12 h, 54%; (j) (i) 1N, NaOH, rt, 1 h; (ii) 1N HCl, 70%.

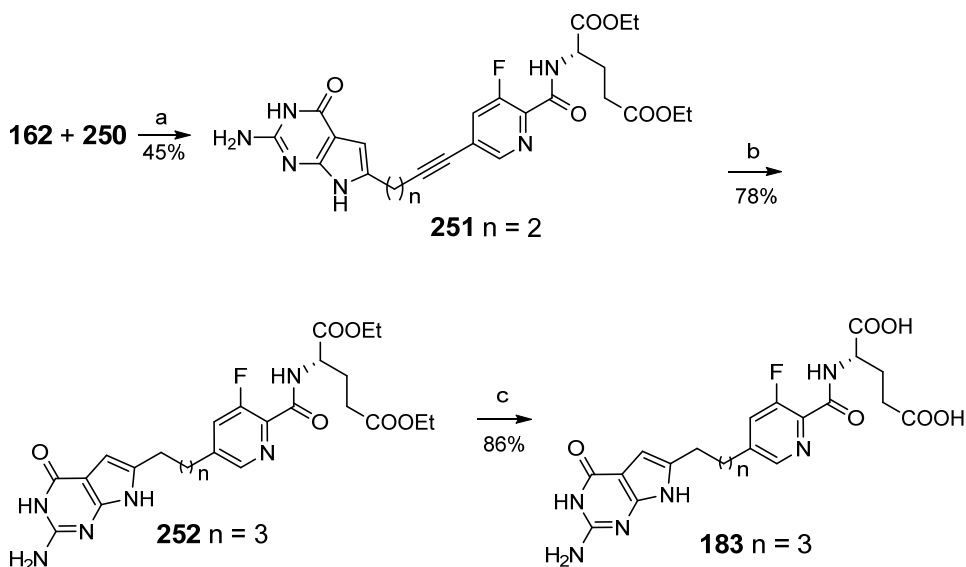
The synthesis of target compound **182** (Scheme 47) was initiated by following a reported procedure of a palladium(II)-catalyzed Sonogashira coupling of but-3-yn-1-ol, **222** with methyl 5-bromo-3-fluoropicolinate, **239** to afford the butynyl alcohol **240** in 62% yield.¹²¹ The alkyne **240** was first reduced by palladium catalyzed hydrogenation to the saturated alcohol **241** in 96% yield and subsequently oxidized using periodic acid/PCC to the carboxylic acid **242** in 80% yield. The acid was converted to the acid chloride **243**, immediately reacted with in situ synthesized diazomethane followed by 48% aq. HBr to give the α -bromomethylketone **245**. During the extraction of **245**, it was observed that the intermediate was mostly concentrated in the acidic aqueous layer due to protonation of the pyridine sidechain ($pK_a \sim 1$). The aqueous layer was cooled to 0 °C and neutralized with 10% aq. sodium carbonate (Na_2CO_3) to extract the α -bromomethylketone **245**. The bis-electrophile was condensed with 2,4-diamino-6-hydroxypyrimidine **22** at room temperature for 3 days to afford the 6-substituted pyrrolo[2,3-*d*]pyrimidine **246** in 30% yield over 4 steps, which was hydrolyzed to yield the acid **247** in 80% yield. The free acid was subsequently peptide coupled with L-glutamate diethyl ester hydrochloride in the presence of NMM and CDMT as the coupling agents to afford the diesters **248** in 54% yield. Final saponification of the diesters gave the desired final compound **182** in 70% yield.

Scheme 48. Synthesis of **250**.



Reagents and conditions: NMM, CDMT, L-glutamate diethyl ester hydrochloride, DMF, rt, 12 h, 73% yield.

Scheme 49. Synthesis of target compounds **183**.

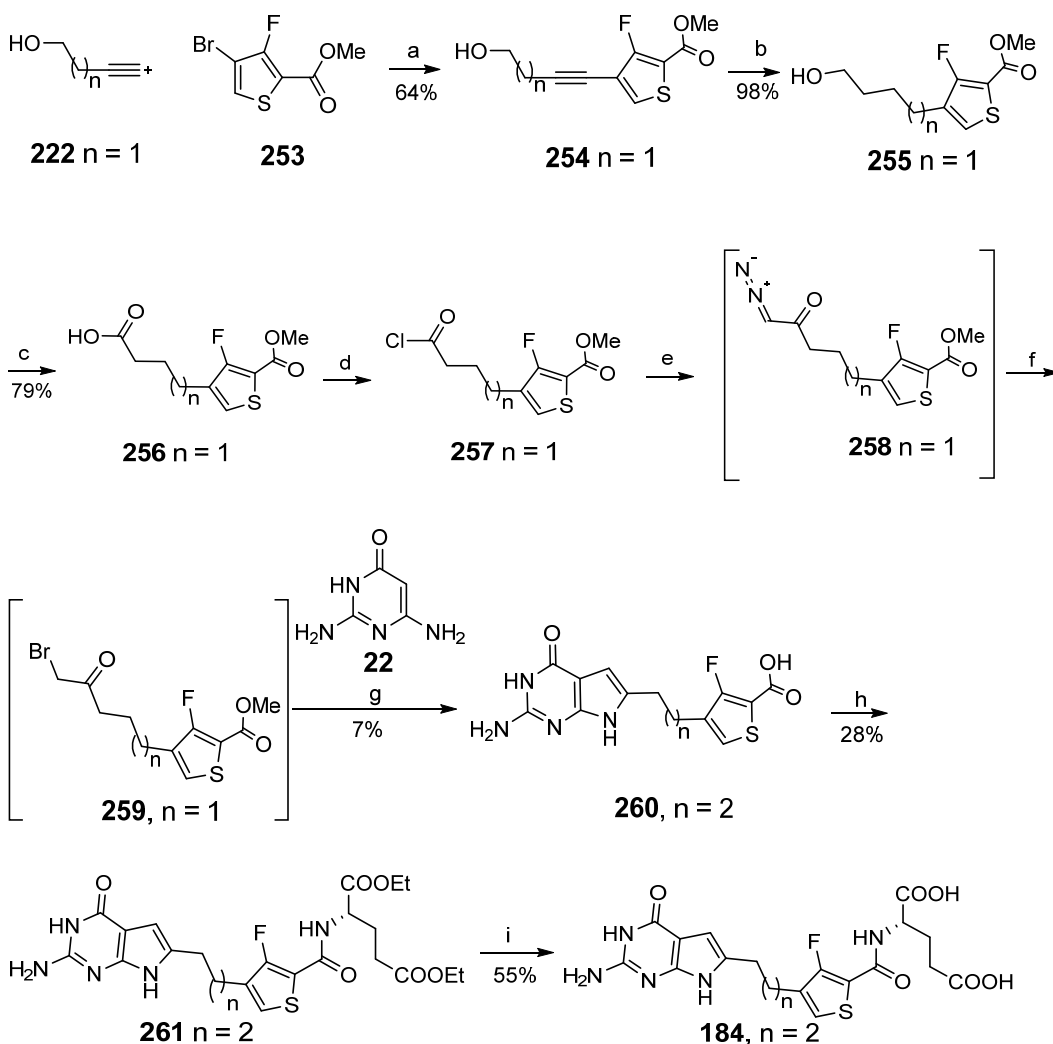


Reagents and conditions: (a) CuI, Pd(0)(PPh₃)₄, Et₃N, DMF, 70 °C, μ W, 12 h, 45% yield; (b) 10% Pd/C, H₂, 55 psi, EtOH, MeOH, 12 h, 78%; (c) (i) 1 N NaOH, rt, 1 h; (ii) 0-4 °C, 1 N HCl, 86% yield.

The synthesis of target compound **183** (Scheme 49) started from the reported intermediate **162** (Scheme 39).¹¹⁶ Sonogashira coupling of **162** with diethyl (5-bromo-3-fluoropicolinoyl)-L-glutamate **250** utilizing the optimized microwave reaction (Table 15), afforded **251** in 45% yield. Subsequent palladium catalyzed hydrogenation to **252** in 78% yield and saponification afforded the target compound **183** in 86% yield. Compound **250** (Scheme 48) was synthesized by peptide coupling of the commercially available 5-bromo-3-fluoropicolinic acid **249** with L-glutamate diethyl ester hydrochloride in 73% yield.

D.1.3 The synthesis of 6-substituted, 2-amino-4-oxo pyrrolo[2,3-*d*]pyrimidine-3'-fluorothienyl classical antifolates (**184-185**).

Scheme 50. Synthesis of **184**.

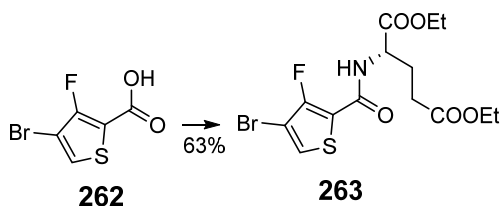


Reagents and conditions: (a) PdCl_2 , Ph_3P , TEA, CuI, ACN, μW , 100°C , 30 min, 64%; (b) 10% Pd/C, H_2 , 55 psi, EtOH, MeOH, 98%; (c) H_5IO_6 , PCC, ACN, 0°C - rt, 12 h, 79%; (d) (i) oxalyl chloride, CH_2Cl_2 , reflux, 1 h; (e) diazomethane, $(\text{Et})_2\text{O}$, 0°C - rt, 1 h; (f) 48% HBr, $(\text{Et})_2\text{O}$, 50°C , 2 h; (g) (i) **22**, DMF, rt, 3 days; (ii) 1N, NaOH, rt, 12 h, (iii) 1N HCl,

7% yield over 5 steps; (h) NMM, CDMT, diethyl-L-glutamate, DMF, rt, 12 h, 28%; (i) (i) 1N, NaOH, rt, 1 h; (ii) 1N HCl, 55%.

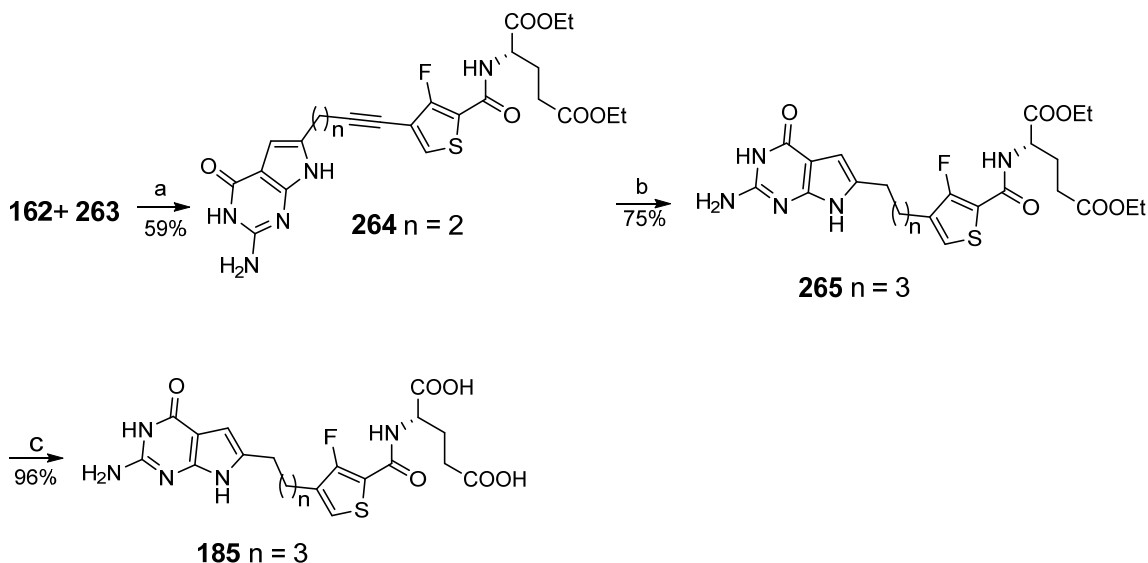
The synthesis of target compound **184** (Scheme 50) was initiated by following a reported procedure of a palladium(II)-catalyzed Sonogashira coupling of but-3-yn-1-ol, **222** with methyl 4-bromo-3-fluorothiophene-2-carboxylate **253**, to afford the butynyl alcohol **254** in 64% yield.¹²¹ The alkyne of **254** was first reduced by palladium catalyzed hydrogenation to the saturated alcohol **255** in 98% yield and subsequently oxidized using periodic acid/PCC to the carboxylic acid **256** in 79% yield. The acid was converted to the acid chloride **257**, immediately reacted with in situ synthesized diazomethane followed by 48% aq. HBr to give the α -bromomethylketone **259**. The bis-electrophile was condensed with 2,4-diamino-6-hydroxypyrimidine **22** at room temperature for 3 days and ester hydrolyzed to yield the pterioic acid **260** in 7% yield over 5 steps. The free acid was subsequently peptide coupled with L-glutamate diethyl ester hydrochloride in the presence of NMM and CDMT as the coupling agents to afford the diesters **261** in 28% yield. Final saponification of the diesters gave the desired final compound **184** in 55% yield.

Scheme 51. Synthesis of 263.



Reagents and conditions: NMM, CDMT, L-glutamate diethyl ester hydrochloride, DMF, rt, 12 h, 63% yield.

Scheme 52. Synthesis of 185.



Reagents and conditions: (a) CuI, Pd(0)(PPh₃)₄, Et₃N, DMF, 70 °C, μ W, 12 h, 59% yield; (a) 10% Pd/C, H₂, 55 psi, EtOH, MeOH, 12 h, 75% yield; (b) (i) 1 N NaOH, rt, 1 h; (ii) 0-4 °C, 1 N HCl, 96% yield.

The synthesis of target compound **185** (Scheme 52) started from the reported intermediate **162** (Scheme 39).¹¹⁶ Sonogashira coupling utilizing the optimized microwave reaction of **162** with diethyl (4-bromo-3-fluorothiophene-2-carbonyl)-L-glutamate **263** afforded **264** in 59% yield. Subsequent palladium catalyzed hydrogenation to **265** in 75% yield and saponification of **265** afforded the target compound **185** in 96% yield. Compound **263** (Scheme 51) was synthesized by peptide coupling of the commercially available 4-bromo-3-fluorothiophene-2-carboxylic acid **262** with L-glutamate diethyl ester hydrochloride in 63% yield.

**NMR Evidence for the Presence of Intramolecular N–H···F–C(sp²) Hydrogen Bond
in Solution State of the Fluorinated Analogs**

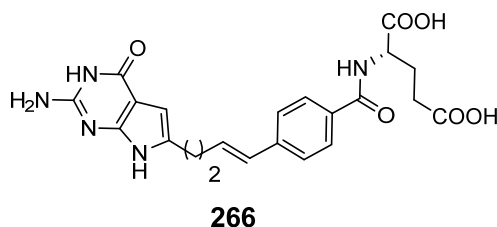
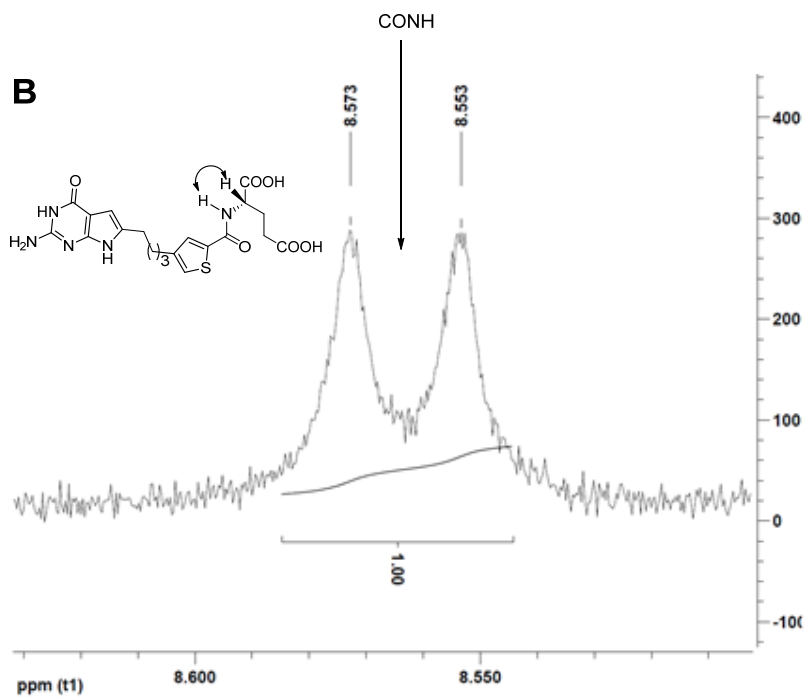
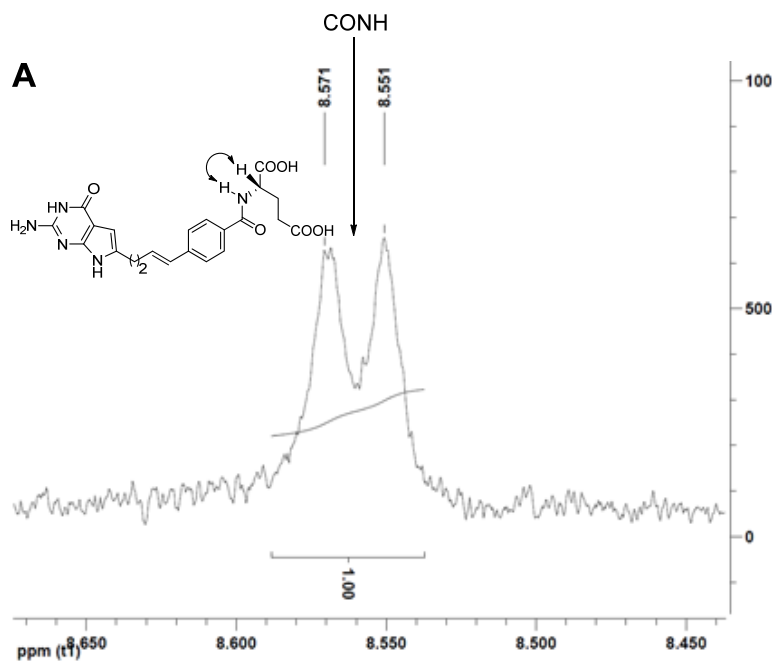


Figure 64. Structure of non-fluorinated compound **266**.

In the ¹H NMR spectra (in DMSO-*d*₆) of the benzoyl-L-glutamate and thiophene-2-carbonyl-L-glutamate of the desfluoro analogs **266** (Figure 64) and **9** (Table 2), the amide NH protons split into a doublet due to coupling with the α-CH proton (Figures 65A: ³*J*_(H-H) = 7.98 Hz and 65B ³*J*_(H-H) = 10.51 Hz).¹¹⁶ The corresponding protons in the 2-fluorobenzoyl-L-glutamate and 3-fluorothiophene-2-carbonyl-L-glutamate (*o*- to L-glutamate) of fluorinated analogs **179/** and **184** respectively, are split into doublet of a doublet, indicating the presence of spin-spin coupling between fluorine and the amide NH (Figures 65C: *J*_(F-H) = 2.08 Hz, ³*J*_(H-H) = 7.83 Hz and 65D: *J*_(F-H) = 2.91 Hz, ³*J*_(H-H) = 7.88 Hz).

In target compound **179** (representative example), the amide NH doublet of a doublet collapsed to a doublet either when decoupled from the α-CH proton (Figure 66, *J*_(H,F) = 1.54 Hz), or in ¹H{¹⁹F}



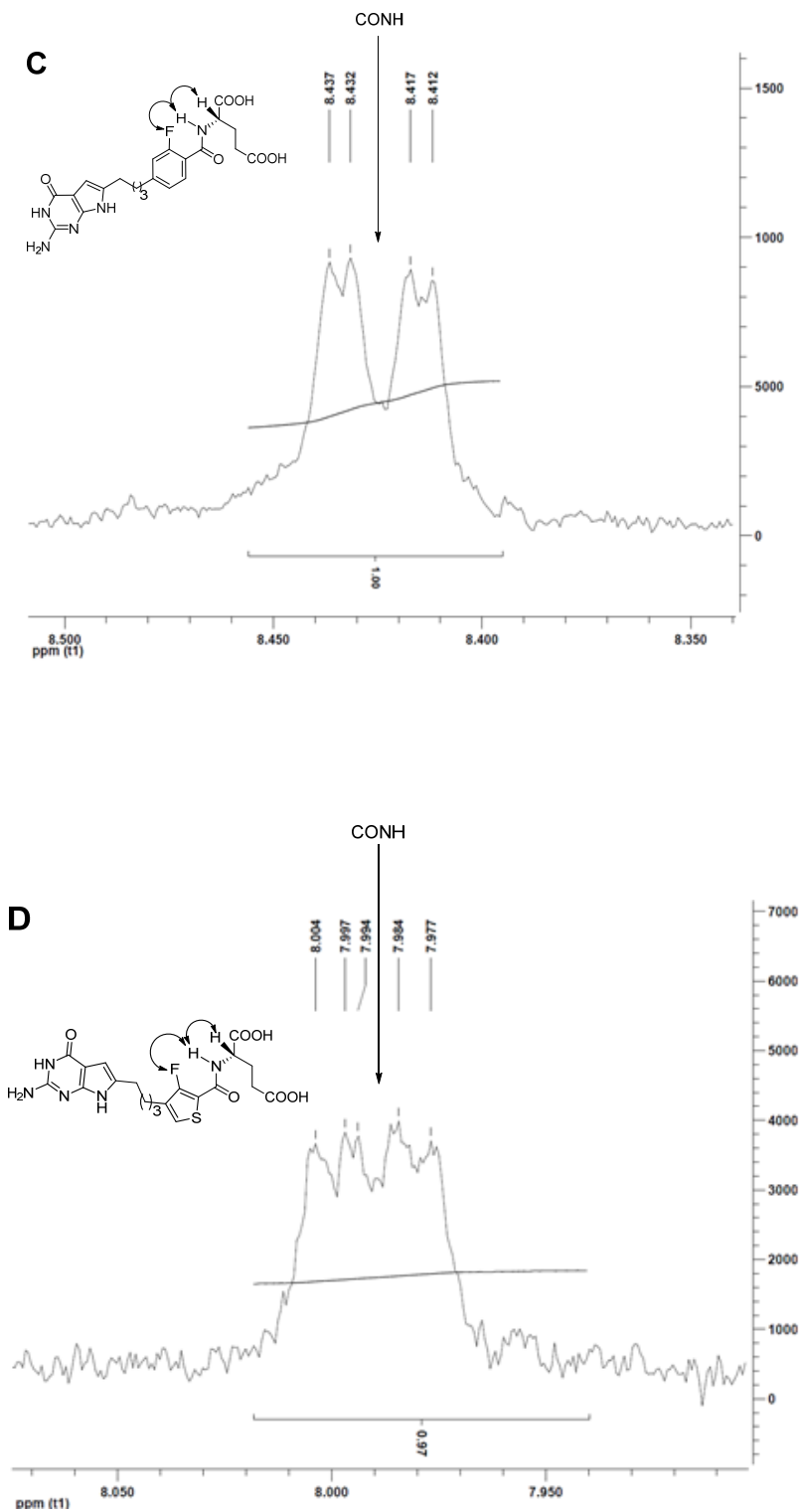


Figure 65. NH signals of **266**, **9**, **179** and **185** in ^1H NMR. (A) 400 MHz ^1H NMR, doublet peak of L-glutamate CONH (arrow pointed) of **266**. (B) 400 MHz ^1H NMR, doublet peak

of L-glutamate CONH (arrow pointed) of **9**. (C) 400 MHz ^1H NMR, doublet of a doublet peak of L-glutamate CONH (arrow pointed) of **179**. (D) 400 MHz ^1H NMR, doublet of a doublet peak of L-glutamate CONH (arrow pointed) of **185**. NMR studies were carried out in $\text{DMSO-}d_6$.

NMR (Figure 66, $^3J_{(\text{H-H})} = 7.11$ Hz) indicating nuclear spin coupling of the NH proton with the fluorine atom as well as the α -CH proton. Such coupling between a fluorine atom and the amide proton of the side-chain L-glutamate was generalized in previous reports as a $\text{N-H} \cdots \text{F-C}(\text{sp}^2)$ hydrogen bond.³³²⁻³³³

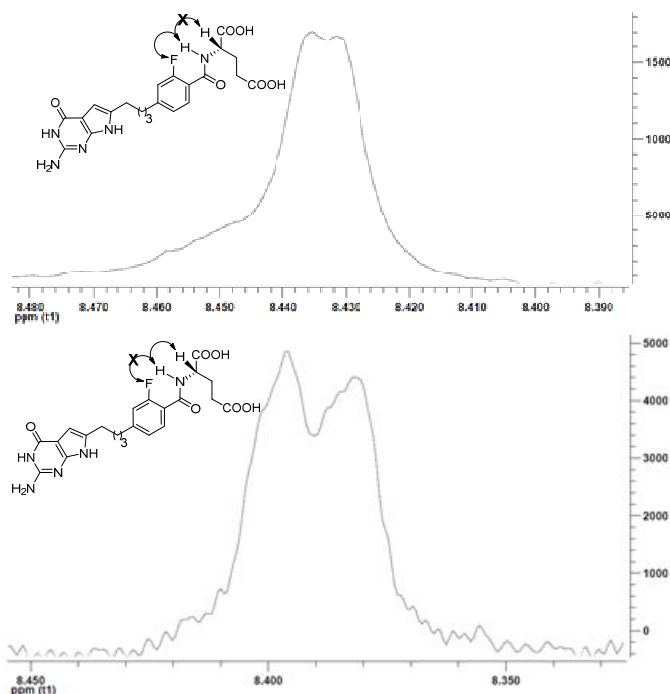


Figure 66. Representative example compound **179** and its NH signal by ^1H NMR. (A) 400 MHz ^1H NMR α -CH decoupled signal of NH proton ($^1J_{(\text{F-H})} = 1.54$ Hz). (C) 500 MHz ^1H NMR, $^1\text{H}\{^{19}\text{F}\}$ NMR signal of NH proton ($^3J_{(\text{H-H})} = 7.11$ Hz). NMR studies were carried out in $\text{DMSO-}d_6$ and the excessive broadening of the NH signal is due to ^{14}N quadrupolar relaxation.

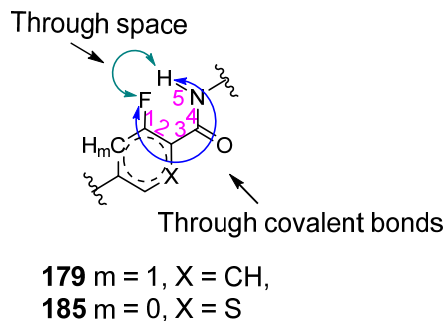


Figure 67. The two directions in which nuclear spin coupling between fluorine and the amide NH can be transmitted is shown. Shown in green is the through space N–H···F–C(sp²) hydrogen bond and shown in blue is nuclear spin information transmitted through covalent bonds.

Though the collapse of the doublet of doublets in $^1\text{H}\{^{19}\text{F}\}$ NMR spectra confirm coupling between ^{19}F and ^1H , it is still ambiguous whether nuclear spin information is transmitted through covalent bonds or through space (hydrogen bond) (Figure 67). When equal concentrations of the corresponding compounds **266** and **179**, dissolved in DMSO-*d*₆ were D₂O exchanged, the amide NH proton of the fluorinated analog **179** took longer time periods (>1 h) to exchange completely compared to the non-fluorinated analog **266** (<5 mins) (Figure 68). This observation supports, in part, the notion of a significant involvement of the NH proton of the fluorinated analog **179** in a fluorine-hydrogen bond.³⁶⁴

The detection of “through-space” couplings between the nuclei directly involved in hydrogen-bonding can establish the presence of a -NH···F-C(sp²) hydrogen bond.³⁴⁸ However, the ^1H - ^{19}F HOESY (heteronuclear NOESY) NMR of **179** (representative example) did not detect any through-space coupling between the fluorine and the NH

proton. This observation is ambiguous as the absence of an observable interaction in the 2D HOESY NMR does not necessarily rule out the presence of a weak hydrogen bond.³⁶⁵

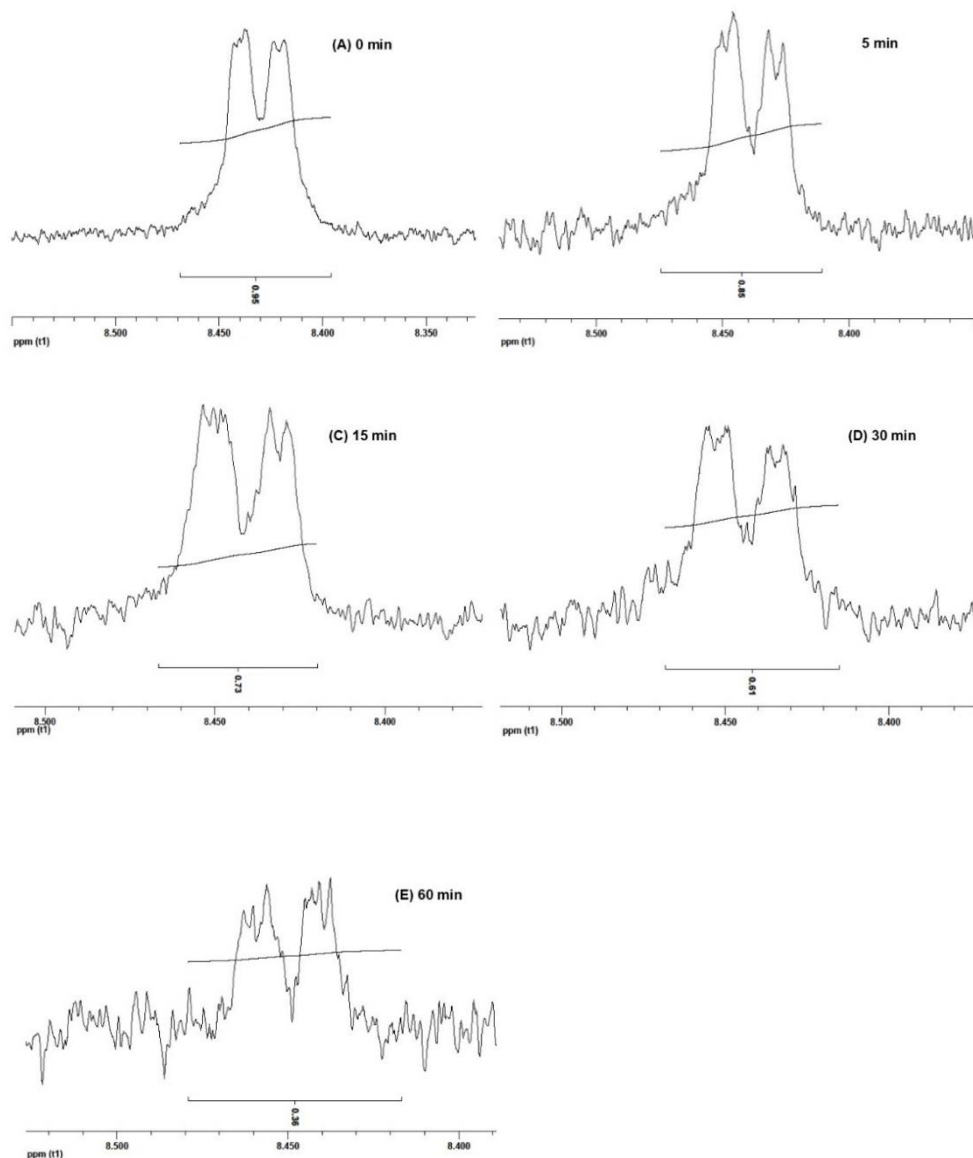


Figure 68. D₂O exchange studies of representative example **179**. The integration of NH signal over 60 minutes upon exchange of 0.8 mg of compound **179** in 0.7 mL DMSO-*d*₆

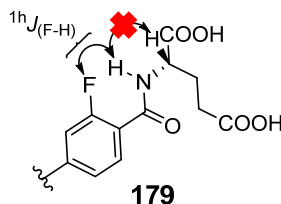
with 0.01 mL D₂O. (A) Integration of NH signal before exchange with D₂O (B) Integration of NH signal 5 minutes after exchange with D₂O. (C) Integration of NH signal 15 minutes after exchange with D₂O. (D) Integration of NH signal 30 minutes after exchange with D₂O. (E) Integration of NH signal 60 minutes after exchange with D₂O.

Temperature-induced perturbations of $^1\text{H}J_{(\text{F-H})}$ are of particular interest as increased temperature disrupts intramolecular hydrogen bonds and consequently diminishes the intensity of the observable $^1\text{H}J_{(\text{F-H})}$ coupling.³⁴⁶ Compound **179** was subjected to temperature perturbations over the range of 292-352 K in DMSO-*d*₆ and $\Delta J_{(\text{F-H})}$ were monitored (Table 16). The $J_{(\text{F-H})}$ varied from 1.54 (292 k) to 3.12 (352 k) Hz, which is uncommon for spin-spin couplings across covalent bonds. This clear variation of $J_{(\text{F-H})}$ with temperature is a strong indicator of through space scalar $^1\text{H}J_{(\text{F-H})}$ coupling (the observable spin-spin coupling constants of the other protons in the ¹H NMR did not change significantly). The numerical values of $^1\text{H}J_{(\text{F-H})}$ at varied temperatures are reported (Table 16). However, contrary to an expected loss, increased $^1\text{H}J_{(\text{F-H})}$ interaction at higher temperatures was observed. It remains to be determined if the -NH · · · F-C(sp²) hydrogen bond in **179** is stabilized at higher temperatures owing to a conformational shift to a more linear -NH · · · F bond angle and geometric proximity.

Exceptionally, in the fluorinated pyridyl analogs **182** and **183**, the amide NH protons are observed as doublets similar to the corresponding proton in the desfluoro analog **4** (not shown, refer to Experimental, compounds **182** and **183**).¹¹⁵ Though the reasons for the absence of fluorine hydrogen coupling ($J_{(\text{F-H})}$) in **182** and **183** are yet to be determined, it however provides supplementary evidence that the coupling between the

fluorine and amide NH, where observed, occurs through space and not across covalent bonds.

Table 16 The variation of $J_{(F-H)}$ in **179** with temperature



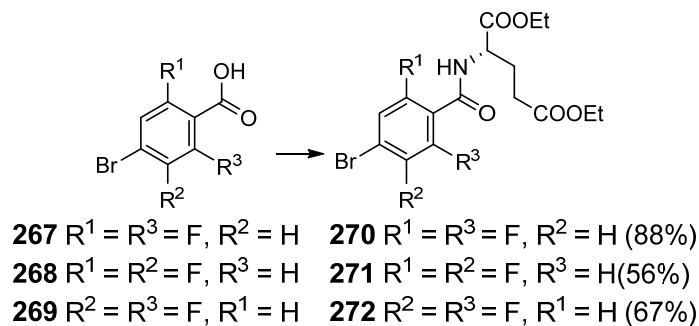
Temperature (K)	$^1hJ_{(F-H)}$ (Hz)
292	1.54
312	2.38
332	2.70
352	3.12

The presence of an intramolecular -NH \cdots F-C(sp²) hydrogen bond in the solution state of the free ligands **179**, **181**, **184** and **185** indicates that the fluorine and amide NH are in a relative *syn* orientation in its energy minimized conformations similar to their docked (bound) conformations (in the target proteins FR α / β and GARFTase).

D.1.4. 6-substituted, 2-amino-4-oxo pyrrolo[2,3-*d*]pyrimidine-difluorophenyl classical antifolates (**186-189**).

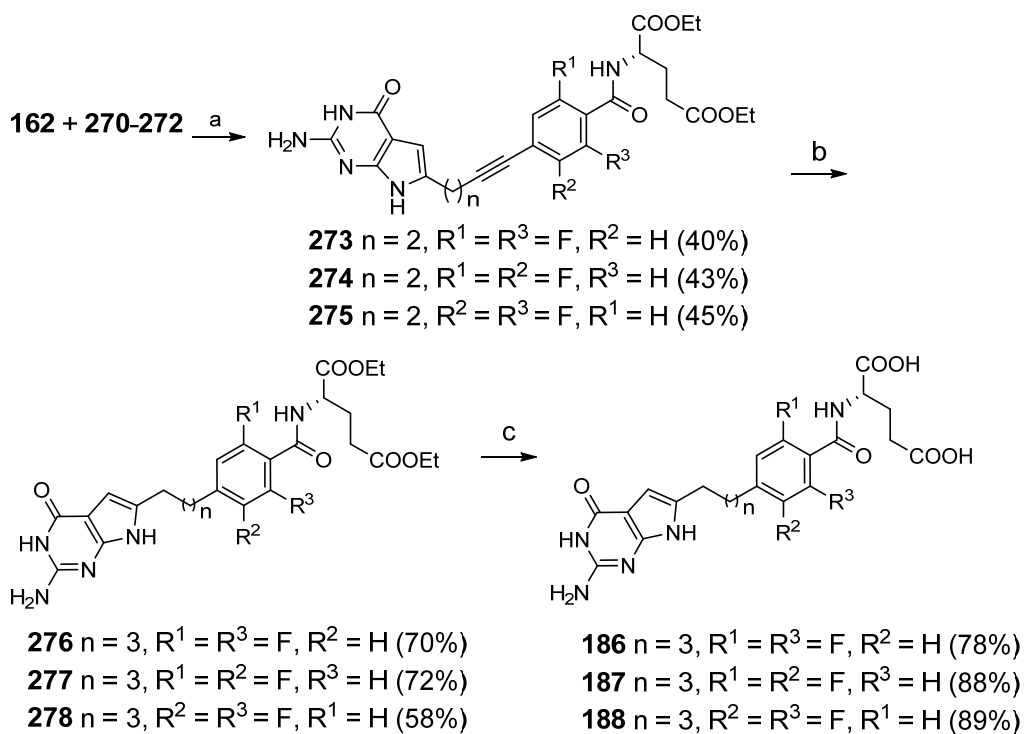
The synthesis of target compounds **186-188** (Scheme 54) started from the synthesis of reported intermediate **162** (Scheme 39).¹¹⁶

Scheme 53. Synthesis of 270-272.



Reagents and conditions: NMM, CDMT, L-glutamate diethyl ester hydrochloride, DMF, rt, 12 h, 56-88% yields.

Scheme 54. Synthesis of target compounds 186-188.

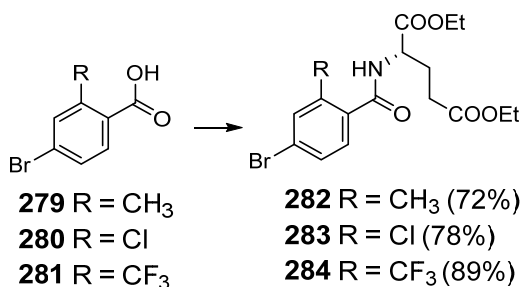


Reagents and conditions: (a) CuI, Pd(0)(PPh₃)₄, Et₃N, DMF, 70 °C, μ W, 12 h, 40-45% yields; (a) 10% Pd/C, H₂, 55 psi, EtOH, MeOH, 12 h, 58-72% yields; (b) (i) 1 N NaOH, rt, 1 h; (ii) 0-4 °C, 1 N HCl, 78-89% yields.

Sonogashira coupling of **162** with diethyl-L-glutamates **270-272** afforded **273-275** respectively, in 40-45% yields. Subsequent palladium catalyzed hydrogenation to **276-278** in 58-72% yields and saponification afforded the target compounds **186-188** in 78-89% yields. Compounds **270-272** (Scheme 53) were synthesized by peptide coupling of the commercially available acids **267-269** with L-glutamate diethyl ester hydrochloride in 56-88% yields.

D.1.5. 6-substituted, 2-amino-4-oxo pyrrolo[2,3-*d*]pyrimidine-2'-substitutedphenyl classical antifolates (**189-191**).

Scheme 55. Synthesis of intermediates **282-284**.

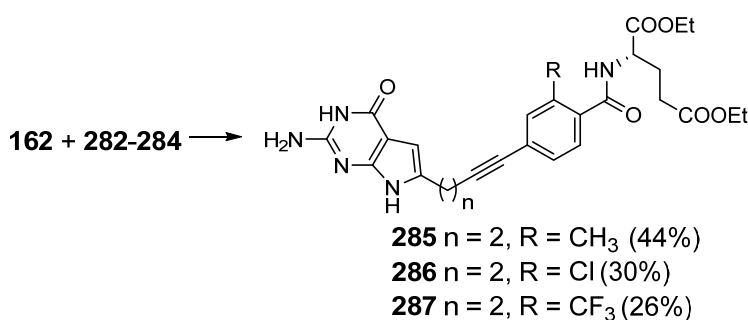


Reagents and conditions: NMM, CDMT, L-glutamate diethyl ester hydrochloride, DMF, rt, 12 h, 72-89% yields.

The synthesis of target compounds **189-191** (Scheme 57) started from the reported intermediate **162** (Scheme 39).¹¹⁶ Sonogashira coupling of **162** with diethyl-L-glutamates **282** and **284** afforded the alkynes **285** and **287** respectively, in 44 and 26% yields

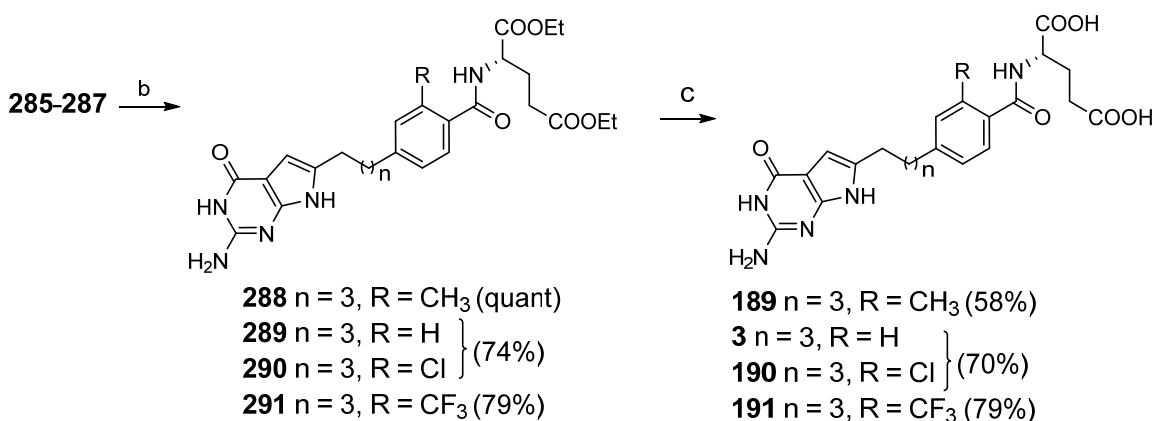
respectively (Scheme 56). Sonogashira coupling of glutamate **283** (2'-chloro substituent; R = Cl) selectively afforded the desired bromo-coupled product **286** in 30% yield (Scheme 56). Subsequent palladium catalyzed hydrogenation of **285** and **287** (Scheme 57) afforded the reduced glutamate esters **288** and **291** in quantitative and 79% yields respectively. Saponification of **288** and **291** afforded the target compounds **189** and **191** in 58% and 79% yields respectively.

Scheme 56. Synthesis of intermediates **285-287**.



Reagents and conditions: CuI, Pd(0)(PPh₃)₄, Et₃N, DMF, 70 °C, μ W, 12 h, 26-44% yields.

Scheme 57. Synthesis of target compound **189-191**.

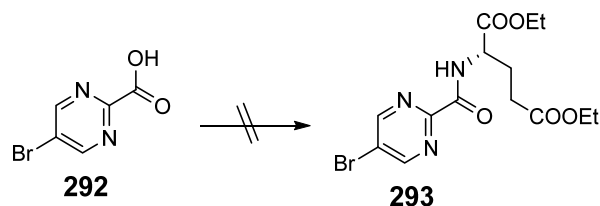


Reagents and conditions: (a) 10% Pd/C, H₂, 55 psi, EtOH, MeOH, 1-12 h 74%-quant. yields; (b) (i) 1 N NaOH, rt, 1 h; (ii) 0-4 °C, 1 N HCl, 58-79% yields.

When the alkyne **286** with 2'-chloro substituent (R = Cl) was reduced by palladium catalyzed hydrogenation at 55 psi H₂, dehalogenation ensued to give a mixture of compounds **289** and **290** (Scheme 57) in 74% yield. Reduction of **286** was attempted several times with reduced time duration each time (1 h to 12 h). Irrespective of the number of hours, dehalogenation was non-selective and occurred simultaneously with alkyne reduction to give a mixture of chlorinated and non-chlorinated intermediates. The presence of a mixture of compounds was confirmed by ¹H NMR as well as CHN analysis of the mixture of diacid compounds **190** and **3**. ¹H NMR of **190** and **3** showed clear doublets (indicating dehalogenation) within the multiplets near the aromatic region that integrated to more than 4 protons (should have ideally integrated to 3 protons). Dehalogenation was additionally confirmed by >4% decrease in the required chlorine percentage of **190**, from the CHN analysis of the hydrolyzed mixture **190** and **3**. Since the synthesis of the target compound **190** using the reported procedure involves unavoidable hydrogenation of the alkyne, attempts to make **190** were terminated. It remains to be tested if decreasing the pressure variable would selectively reduce the alkyne. Compounds **282-284** (Scheme 55) were synthesized by peptide coupling of the commercially available acids **279-281** with L-glutamate diethyl ester hydrochloride in 72-89% yields.

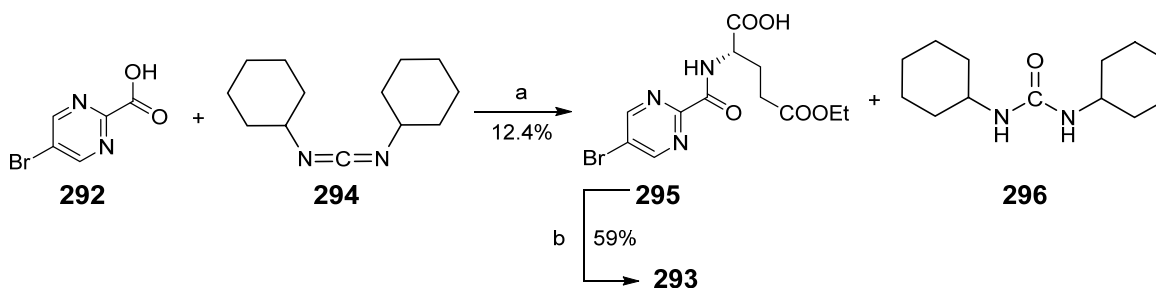
D.1.6. 6-substituted, 2-amino-4-oxo pyrrolo[2,3-*d*]pyrimidine-pyrimidyl classical antifolates (**192**).

Scheme 58. Synthesis of intermediate **293**.



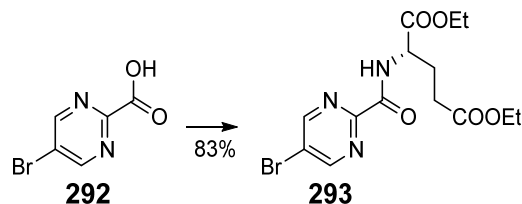
Reagents and conditions: *N*-methylmorpholine, 2-chloro-4,6-dimethoxy-1,3,5-triazine, L-glutamate diethyl ester hydrochloride, DMF, rt, 12 h.

Scheme 59. Alternate method for the synthesis of intermediate **293**.



Reagents and conditions: (a) (i) Pyridine, rt, 96 h; (ii) 2N HCl, sat. Na₂CO₃, 12.4% yield; (b) (i) SOCl₂, EtOH, 75 °C, 12 h, 59% yield.

Scheme 60. Alternate CDMT peptide coupling conditions for the synthesis of intermediate **293**.



Reagents and conditions: (a) NMM, CDMT, L-glutamate diethyl ester hydrochloride, DMF, rt, 12 h, 83% yield.

The synthesis of target compounds **192** (Scheme 61) started from the reported intermediate **162** (Scheme 39).¹¹⁶ Sonogashira coupling of **162** with diethyl-L-glutamate **293** afforded **297** in 40% yield.

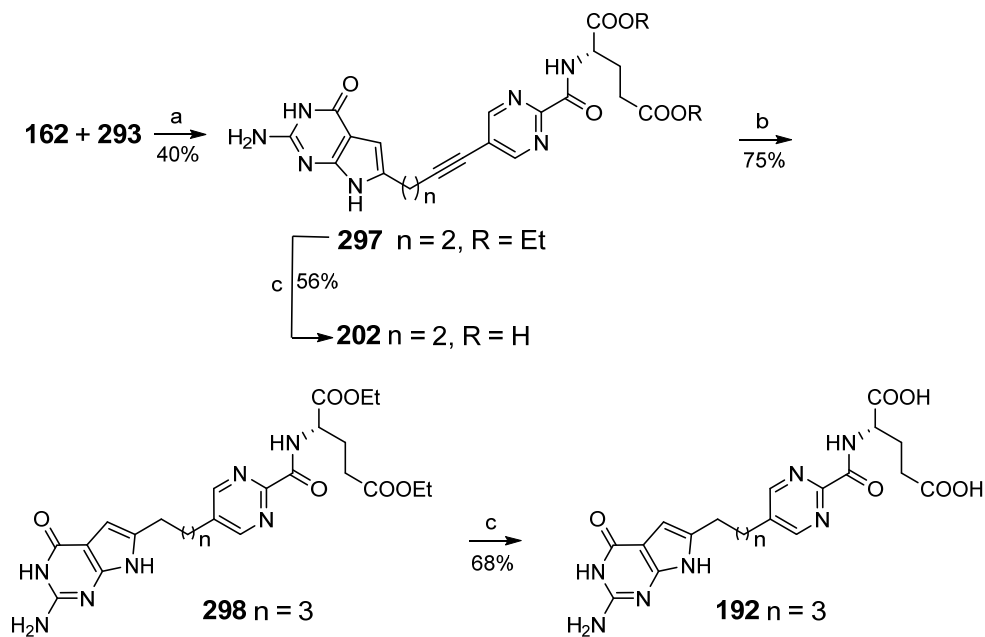
Table 17. Reaction conditions for the synthesis of **293**.

Reagents and conditions	Sequence of addition	Product (301)
CDMT, NMM, DMF, rt, 12 h	Amine added after carboxylic acid activation	x
CDMT, NMM	All together	83%

Palladium catalyzed hydrogenation of 6-substituted pyrrolo[2,3-*d*]pyrimidines with a pyrimidyl side chain, at 55 psi of H₂, reduces the pyrimidine side-chain along with the alkyne (data not shown). Pyrimidine ring and alkyne reductions occur simultaneously at 55 psi of H₂ but decreasing the H₂ pressure from 55 psi to 15 psi (~1 atm) selectively reduces the alkyne but not the side-chain pyrimidine ring. As such, palladium catalyzed hydrogenation of **297** at 15 psi of H₂ gave the alkyne reduced product **298** in 75% yield. Subsequent saponification of **298** afforded the target compound **192** in 68% yield. The L-glutamate ester of alkyne **297** was also hydrolyzed to afford the final compound **202** to test the influence of modified flexibility on biological activity, due to the presence of a conformationally restricting alkyne group in the linker. The synthesis of L-glutamate ester intermediate **293** (Scheme 58) was initially attempted using the reported procedure of peptide coupling of the commercially available acid **292** with L-glutamate diethyl ester hydrochloride in the presence of *N*-methylmorpholine (NMM) and 2-chloro-4,6-dimethoxy-1,3,5-triazine (CDMT) as the coupling agents. The reaction proceeds with

initial activation of the acid (for 2 hours) followed by addition of the amine. However, this procedure failed to produce the peptide coupled product and the starting material was recovered. Alternatively, the reaction was carried out using *N,N'*-dicyclohexylcarbodiimide in pyridine as the peptide coupling agents (Scheme 59).³⁶⁶ However, peptide coupled monoacid product **293** (Scheme 59) was formed in 12.4% yield due to hydrolysis of the α -carboxylate ester during the acid/base workup with 2N HCl followed by sat. NaHCO₃. Difficulty in separating the polar *N,N'*-dicyclohexylurea side product **296** and re-esterification using SOCl₂ in ethanol to afford **293** in 59% yield, collectively reduced the overall yield of **293** to 7.3%.

Scheme 61. Synthesis of target compound **192**.

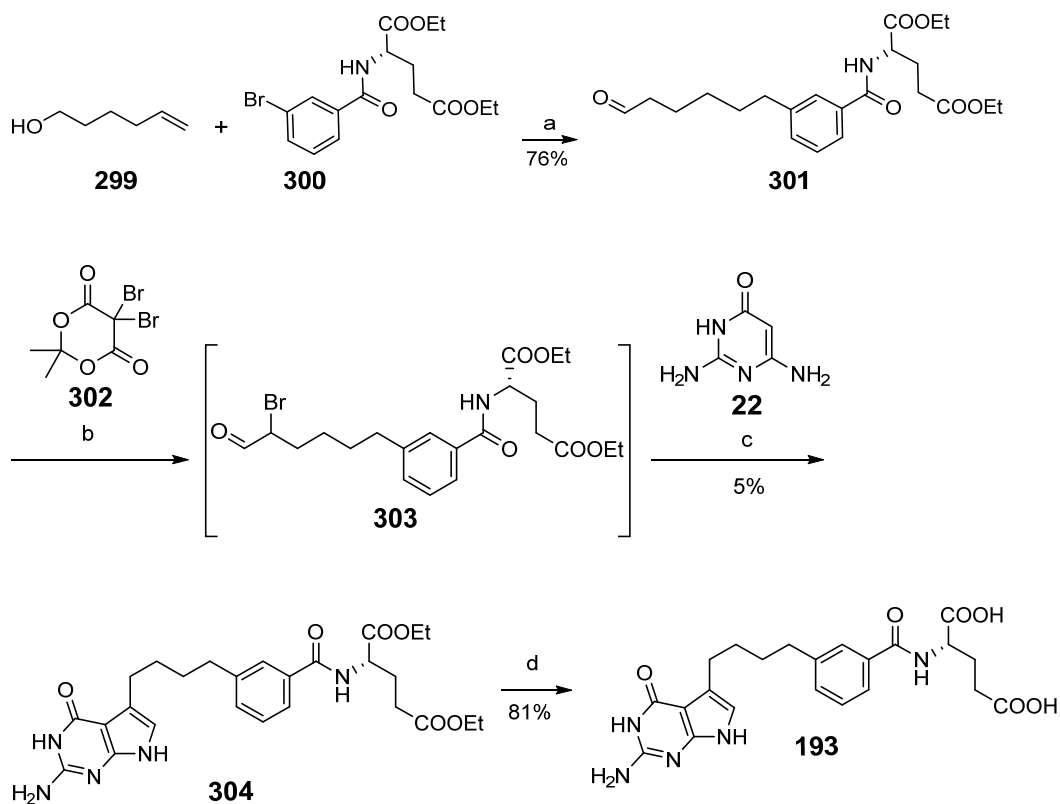


Reagents and conditions: (a) CuI, Pd(0)(PPh₃)₄, Et₃N, DMF, 70 °C, μ W, 12 h, 40% yield. (b) 10% Pd/C, H₂, 15 psi, 7 h, 75% yield; (c) (i) 1 N NaOH, rt, 1 h; (ii) 0-4 °C, 1 N HCl, 56-68% yield.

Peptide coupling with NMM and CDMT was revisited in order to rationalize the failure of a predominantly successful reaction that worked with several (het)aryl carboxylic acids. Following an alternate reported method for peptide coupling using CDMT and NMM, when the reacting groups, activating agent (CDMT) and base (NMM) were added all at once (instead of sequential addition), compound **293** (Scheme 60) formed in 83% yield.³⁶⁷ The synthesis of **293** was achieved under similar conditions (Scheme 58) with the only variation of sequence of addition. This indicates that the successful reaction necessitates immediate nucleophilic attack by the amine of the L-glutamate on the activated carboxylic acid.

D.2.1. 5-substituted, 2-amino-4-oxo pyrrolo[2,3-*d*]pyrimidine-3'-butylphenyl classical antifolates (**193**)

Scheme 62. Synthesis of target compound **193**.



Reagents and conditions: (a) Pd(OAc)₂, LiCl, LiOAc, Bu₄NCl, DMF, 80 °C, 3 h, 76%; (b) 5,5-dibromo-2,2-dimethyl-4,6-dioxo-1,3-dioxane, 1N HCl in (Et)₂O, (Et)₂O, rt, 48 h; (c) CH₃COONa, MeOH, H₂O, 45 °C, 4 h, 5 % yield over 2 steps; (d) (i) 1 N NaOH, rt, 1 h; (ii) 0-4 °C, 1 N HCl, 81 % yield.

Compound **193** (Scheme 62) was obtained using a reported procedure in which condensation of the α -bromo aldehyde **303** with 2,6-diamino-4-oxo-pyrimidine **22** is the key step.¹²⁰ As reported by Larock et al.,³²³ Heck coupling reaction of commercially available hex-5-en-1-ol **299** with diethyl (3-bromobenzoyl)-L-glutamate **300**, afforded the

unsaturated, coupled alcohol that rearranged to the vinyl alcohol and tautomerised to afford the aldehyde **301** in 76% yield. Subsequent α -bromination of **301** with 5,5-dibromo-2,2-dimethyl-4,6-dioxo-1,3-dioxane (DBMA) **302** at room temperature afforded corresponding α -bromo aldehyde **303** which was immediately condensed with 2,6-diamino-4-oxo-pyrimidine **22** in the presence of sodium acetate to afford the 5-substituted pyrrolo[2,3-*d*]pyrimidine **304** in 5% yield over 2 steps. Final saponification of the diesters with 1 N NaOH and neutralization to pH 4, provided target compound **193** in 81% yield. Compound **300** (Scheme 62) was obtained from the repository of intermediates synthesized by Dr. Yiqiang Wang.

D.2.2. 5-substituted, 2-amino-4-oxo pyrrolo[2,3-*d*]pyrimidine-4'-propyloxy/propylthio/propylamino/butylaminophenyl classical antifolates (**194-197**).

Syntheses of **194-197** were envisioned to occur via Sonogashira coupling of intermediate iodide **305** and alkynes **306-308** (Figure 69). *N*-(5-iodo-4-oxo-4,7-dihydro-3*H*-pyrrolo[2,3-*d*]pyrimidin-2-yl)pivalamide **305** can be synthesized following a reported procedure and the intermediates **306-308** could be synthesized via nucleophilic substitutions of propargyl bromides with nucleophilic heteroatom substituted benzoate ester.³⁶⁸⁻³⁷¹

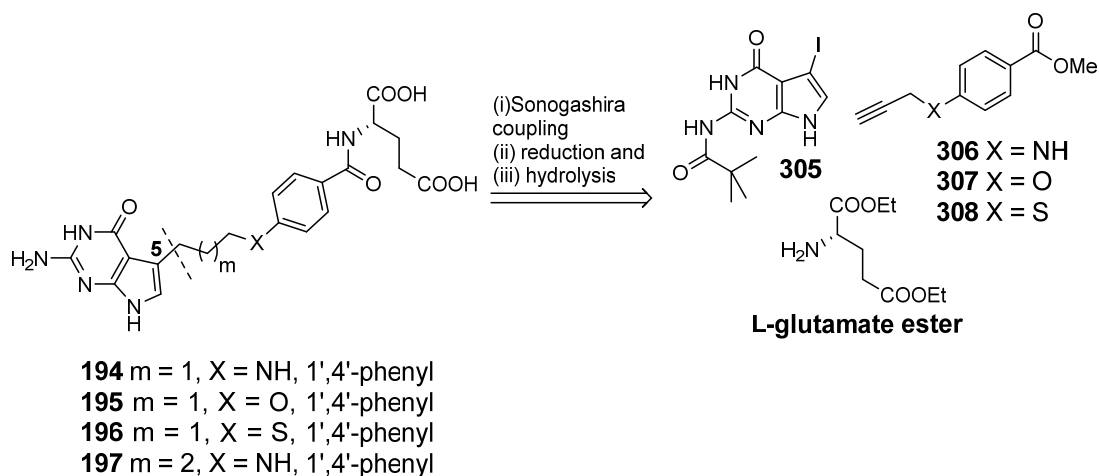
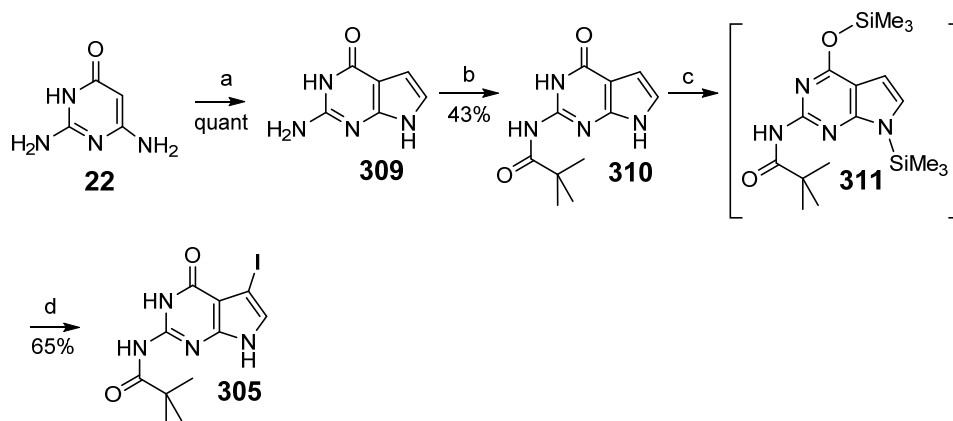


Figure 69. Proposed retrosynthesis of target compounds **194-197**.

This convergent procedure not only will improve the overall yield in lesser number of steps, but can also be applied for the synthesis of homologous compounds.

Scheme 63. Synthesis of intermediate **305**.



Reagents and conditions: (a) Chloroacetaldehyde, CH_3COONa , MeOH , H_2O , $45\text{ }^\circ\text{C}$, 4 h, quant.; (b) pivaloyl chloride, pyridine, $90\text{ }^\circ\text{C}$, 30 min, 43%; (c) bis(trimethylsilyl)acetamide, DMF , $40\text{ }^\circ\text{C}$, 2 h; (d) NIS, DMF , rt, 12 h, 65%.

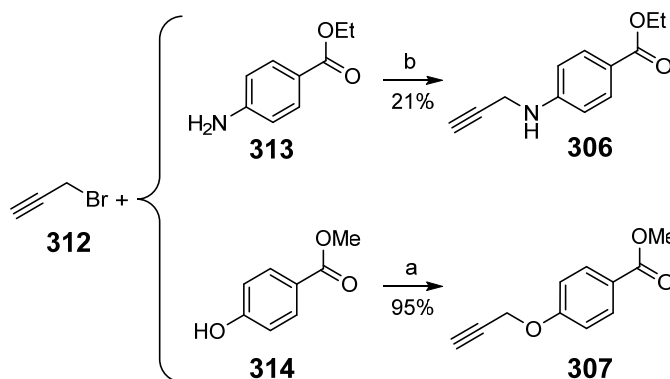
Synthesis of the key intermediate **305** (Scheme 63) began with the condensation of 2,4-diamino-6-hydroxypyrimidine **22** with chloroacetaldehyde in the presence of sodium acetate yielding the cyclized product 2-amino-3,7-dihydro-4*H*-pyrrolo[2,3-*d*]pyrimidin-4-one **309** in quantitative yield.³⁶⁸ The pyrrolo[2,3-*d*]pyrimidine **309** was treated with trimethylacetyl chloride to yield the *N*(2)-monoacylated compound **310** in 43% yield. The procedure reported by Barnett *et al.*³⁷¹ was adopted for the regiospecific C5 iodination of **310**. The 4-oxo and N-7 groups were silylated using bis(trimethylsilyl)acetamide to a silylated intermediate **311**, followed immediately by C5 iodination using *N*-iodosuccinimide (NIS). The unstable silyl protecting groups were deprotected under aqueous work-up conditions to yield the intermediate **305** in 65% yield.

The key Sonogashira coupling partners **306** and **307** (alkynyl esters) (Scheme 64) were synthesized by reacting propargyl bromide **312** with ethyl 4-aminobenzoate **313** and methyl 4-hydroxybenzoate **314** in the presence of potassium carbonate in 95% and 21% yields respectively.³⁶⁹ An alkyne glutamate coupling partner **316** (Scheme 65) was also synthesized by hydrolyzing the methyl 4-hydroxybenzoate **307** to the acid **315** in 83% yield. The free acid was subsequently peptide coupled with L-glutamate diethyl ester hydrochloride in the presence of *N*-methylmorpholine (NMM) and 2-chloro-4,6-dimethoxy-1,3,5-triazine (CDMT) as the coupling agents to afford the alkyne glutamate ester **316** in 85% yield.

However, the Sonogashira coupling reactions of **305** (Scheme 66, Table 18) with the alkynyl esters **306** and **307** to afford **317** and **318** were unsuccessful under various coupling conditions. Predominantly, no new product spots were observed on TLC and the starting material was recovered as the dehalogenated intermediate **310**. It was evident that

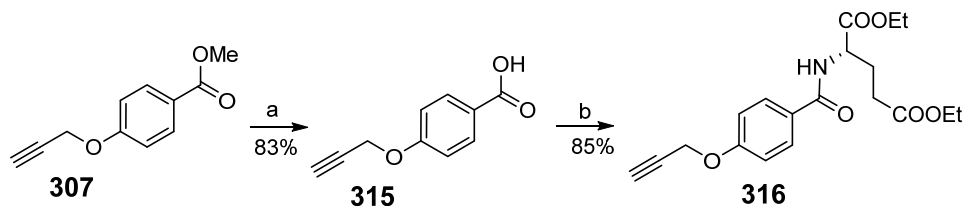
independent of temperature and the oxidation state of the palladium catalyst, the competitive reaction of Sonogashira coupling of *N*-(5-iodo-4-oxo-4,7-dihydro-3*H*-pyrrolo[2,3-*d*]pyrimidin-2-yl)pivalamide **305** was C5 deiodination. In one case, Sonogashira coupling of **305** (Scheme 67) with the alkynyl glutamate **316** besides deiodination, resulted in acetylenic Glaser coupling of **316** to the homodimer **319** in 9% yield, a common side product observed in Cu (I) cocatalyzed Sonogashira reaction conditions.³⁷² Deiodination depletes the key coupling partner **305** and therefore this method was abandoned and an alternate procedure was considered.

Scheme 64. Synthesis of intermediates **306** and **307**.



Reagents and conditions: (a) K_2CO_3 , EtOH, reflux, 18 h, 21%; (b) K_2CO_3 , acetone, reflux, 3 h, 95% (b)

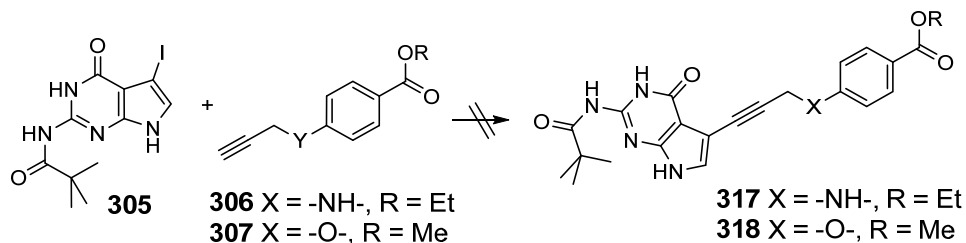
Scheme 65. Synthesis of intermediate **316**.



Reagents and conditions: (a) 1 N NaOH, MeOH, reflux, 2.5 h. (ii) 1 N HCl, 83 % yield.

(b) *N*-methylmorpholine, 2-chloro-4,6-dimethoxy-1,3,5-triazine, L-glutamate diethyl ester hydrochloride, DMF, rt, 12 h, 85% yield.

Scheme 66. Synthesis of intermediates **317** and **318**.



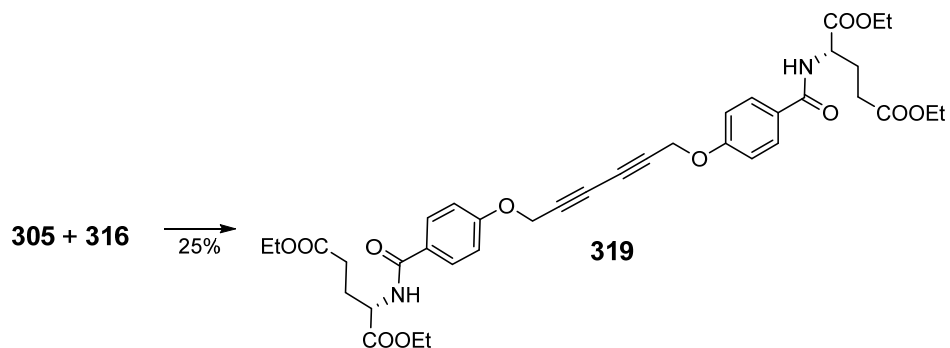
Reagents and conditions: Pd catalyst, CuI, TEA, Solvent, temp, 12 h.

Table 18. Reaction conditions for the synthesis of **317** and **318**.

Catalyst	Solvent	Temp. (°C)
Pd[(C ₆ H ₅) ₃ P] ₄	DMF	21, 50, 80
Pd[(C ₆ H ₅) ₃ P] ₄	TEA	21, 50, 80
Pd(OAc) ₂	ACN	21, 50, 80
PdCl ₂ (PPh ₃) ₂	DMF	21, 50, 80
Pd ₂ (dba) ₃	DMF	21, 50, 80

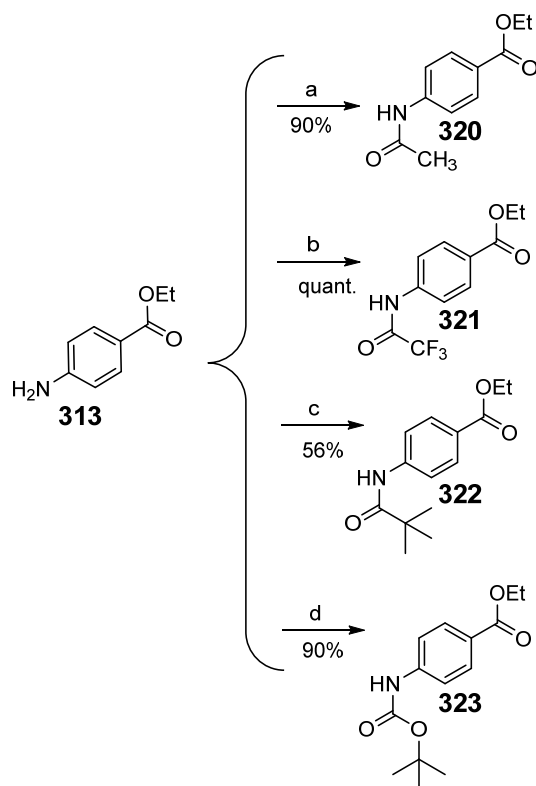
Compound **194-197** (Scheme 72) was obtained using a reported procedure in which condensation of the α -bromo aldehydes **339-342** with 2,6-diamino-4-oxo-pyrimidine **22** is the key step.¹²⁰

Scheme 67. Synthesis of intermediate **319**.



Reagents and conditions: (a) CuI, Pd(0)(PPh₃)₄, Et₃N, DMF, rt, 12 h, 25% yield.

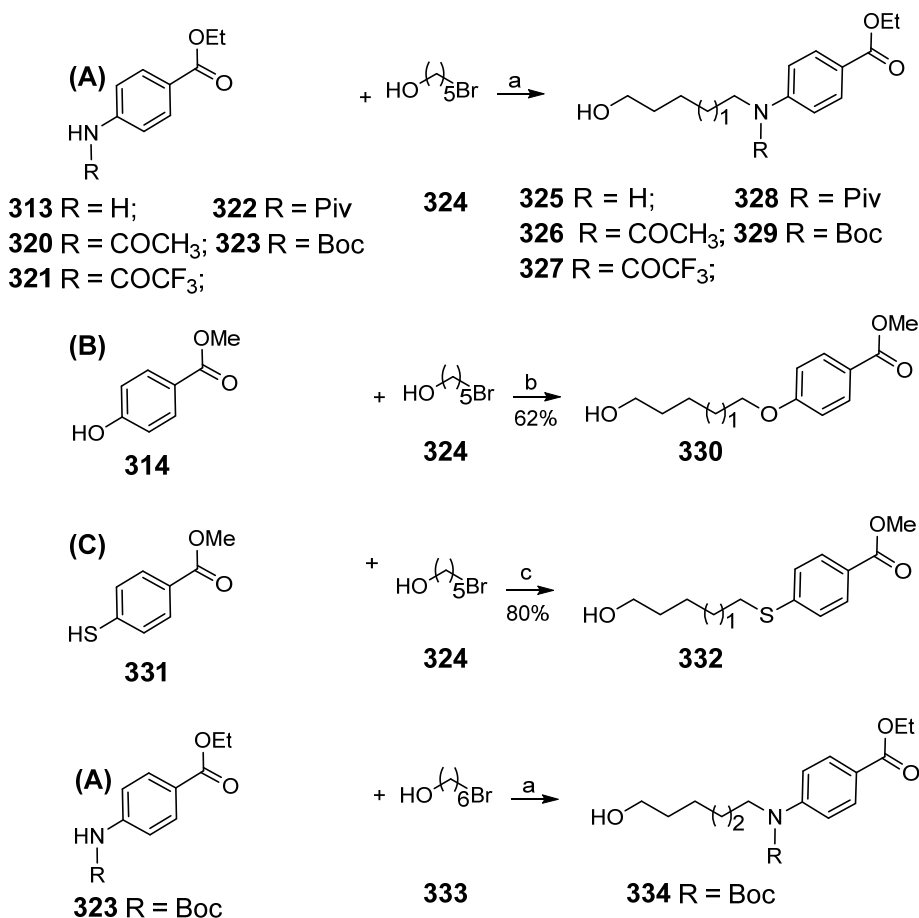
Scheme 68. Synthesis of intermediates **320-323**.



Reagents and conditions: (a) Ac₂O, CH₂Cl₂, rt, 12 h, 90%; (b) (CF₃CO)₂O, rt, 2 h, quant;

(c) Piv₂O, 80 °C, 8 h, 56%; (d) Boc₂O, 1,4-dioxane, 80 °C, 24 h, 90%.

Scheme 69. Synthesis of intermediates **325-330**, **332** and **334**.



Reagents and conditions: (a) base, solvent, temp, time (Table 19); (b) K₂CO₃, acetone, 80 °C, 24 h, 62%; (c) Cs₂CO₃, TBAI, DMF, 0-rt, 4 h, 80%.

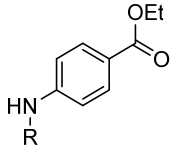
Nucleophilic substitution reactions of heteroatom substituted aromatic esters **314**, **323** and **331** (Scheme 69) with commercially available bromo alkanols **324** and **333** under basic conditions, afforded the hydroxyalkyl benzoates **329**, **330**, **332** and **334**. Several basic conditions were attempted for the nucleophilic displacement of **324** (Scheme 69, Table 19) by ethyl 4-aminobenzoate **313** and its N-protected derivatives **320-323**.

Table 19. Reaction conditions for the synthesis of **325-329** and **334**.

Compd. No.	Reagents and conditions			
	Base	Solvent	Temp.	Yield
325	NaH	DMF	rt - 50 °C	-
325	TEA	DMF	80 °C	20%
325	Cs ₂ CO ₃	DMF	0 °C - 70 °C	-
325	2,6-lutidine	DMF	0 °C - 70 °C	-
326	NaH	DMF	rt - 50 °C	-
327	Cs ₂ CO ₃ /TBAI	DMF	0 °C - 70 °C	-
328	Cs ₂ CO ₃ /TBAI	DMF	0 °C - 70 °C	-
329	Cs ₂ CO ₃ /TBAI	DMF	0 °C - 70 °C	74%
334	Cs ₂ CO ₃ /TBAI	DMF	0 °C - 70 °C	51%

Initial efforts for the synthesis of intermediate **325** from ethyl 4-aminobenzoate **313** in the presence of NaH (rt-50 °C), Cs₂CO₃ (0 °C-70 °C) and 2,6-lutidine (0 °C-70 °C), in DMF failed to work. When triethylamine (TEA) was used as base, the reaction proceeded to give **325** in 20% yield. It was anticipated that increasing the acidity of the 4-NH₂ proton of ethyl 4-aminobenzoate could promote the reaction by facilitating its ease of extraction by a mild base. The *N*-acetyl protecting group decreased the p*K*_a of the NH proton but the reaction was unsuccessful in the presence of NaH (Tables 19 and 20).³⁷³

Table 20. Partial charges and pK_a of compounds **313** and **326-329** were calculated using Maestro 11.2 and Chemicalize respectively.^{208, 361}

Compd. No.	R	Partial charge of N (electron unit)	pK_a
			
313	H	-0.9	~30
326	CH ₃ CO	-0.38	13.6
327	CF ₃ CO	-0.38	10.4
328	Piv	-0.38	13.5
329	Boc	-0.52	12.6

Though the early attempt for N-alkylation using Cs₂CO₃ failed, but based upon numerous reports of efficient N-alkylation using cesium bases, another set of reactions with the N-protected ethyl 4-aminobenzoates **320-323** were examined with Cs₂CO₃ as the base accompanied by TBAI (phase transfer agent).³⁷⁴⁻³⁷⁶ Cesium reagents are generally far superior to their alkali metal counterparts with respect to reaction time, yield, chemoselectivity and are highly compatible with a wide range of functional groups. The improved reactivity under mild conditions is defined as the "cesium effect" that stems from better solubility and the generation of highly reactive "naked anions" (due to weak coordination of the cesium cation). TBAI not only acts as a phase transfer catalyst but may also facilitate an internal Finkelstein-type reaction for the in situ generation of 5-iodopentanol from bromide **324**, hence producing high product yields. Among **320-323**, the *N*-boc protected ethyl-4-aminobenzoate **323** was favorably alkylated to ethyl 4-((*tert*-

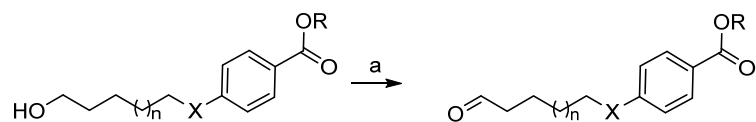
butoxycarbonyl)(5-hydroxypentyl)amino)benzoate **329** in 74% yield. We hypothesize that, along with the presence of naked anions (cesium effect) and phase transfer agent (TBAI), a balance between reduced pK_a and availability of lone pair of electrons was struck in the *N*-boc protected derivative **329** due to reduced resonance stabilization of the lone pair of electrons (compared **326-328**) for the efficient nucleophilic displacement of 5-bromopentanol (Table 20). The synthesis of ethyl 4-((5-hydroxypentyl)oxy)benzoate **330** (Scheme 69) was accomplished via a straightforward displacement of 5-bromopentanol **324** by ethyl 4-hydroxybenzoate **314** in the presence of potassium carbonate.³⁶⁹ When similar reagents and conditions were used for the synthesis of **332** from the nucleophilic displacement of **324** by ethyl 4-mercaptobenzoate **331**, the reaction failed to proceed. Consequently, the procedure reported by Salvatore et al.,³⁷⁷ was adopted wherein Cs_2CO_3 as base and tetrabutylammonium iodide (TBAI) as a phase transfer agent, in DMF was successfully utilized to facilitate the synthesis of **332** in 80% yield (Scheme 69). The successful reaction conditions used for the synthesis of **329** (Scheme 69) were repeated for the synthesis of ethyl 4-((*tert*-butoxycarbonyl)(5-hydroxyhexyl)amino)benzoate **334** via nucleophilic displacement of 6-bromohexanol **333** by **323**.

Intermediates **320-323** (Scheme 68) were synthesized by following reported procedures. *N*-acetyl, *N*-piv and *N*-boc protections in **320**, **322** and **323** were carried out in the presence of Ac_2O , Piv_2O and Boc_2O in 90%, 56% and 90% yields respectively.^{373, 378} The *N*-trifluoroacetyl protecting group in **321** (Scheme 68) was introduced in quantitative yield by reacting ethyl 4-aminobenzoate **313** with excess trifluoroacetic acid as per reported procedure.¹⁶⁷

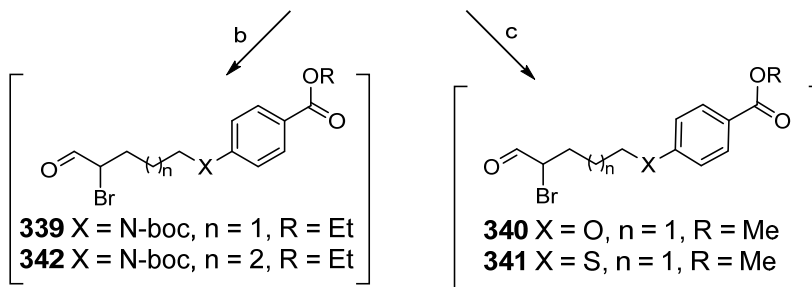
The terminal alcohols **329**, **330**, **332** and **334** (Scheme 70) were subjected to oxidation using Dess-Martin periodinane to afford the aldehydes **335-338** in 60-84% yields.³⁷⁹ α -bromination of the *N*-*boc*-protected aldehydes **335** and **338** with bromine (Br₂) in 1,4-dioxane at room temperature failed. The unsuccessful α -bromination is attributed to depletion of bromine due to a potential electrophilic substitution of the aniline ring. Therefore, an alternate bromination procedure described earlier for the synthesis of target compound **193** was utilized. Freshly bought 5,5-dibromo-2,2-dimethyl-4,6-dioxo-1,3-dioxane (DBMA) **302** successfully yielded the α -bromo aldehydes **339** and **342** from **335** and **338** respectively. The aldehydes of ether and thioether linker analogs **336** and **337** were α -brominated with bromine (Br₂) in 1,4-dioxane at room temperature to the corresponding α -bromo aldehydes **340** and **341**.³⁸⁰

The corresponding α -bromo aldehydes **339-342** (Scheme 71) were immediately condensed with 2,6-diamino-4-oxo-pyrimidine **22** in the presence of sodium acetate for 4 hours followed by base catalyzed hydrolysis to afford the 5-substituted pyrrolo[2,3-*d*]pyrimidine pteronic acids with heteroatom linkers **343-346** in 16-27% yields over 3 steps. Intermediates **343** and **346** were subjected to hydrolysis under acidic conditions to yield the *N*-*boc* deprotected pteronic acids **347** and **348** in 93% and 97% yields respectively. The acids **347**, **344**, **345** and **348** were subsequently peptide coupled with L-glutamate diethyl ester hydrochloride in the presence of *N*-methylmorpholine (NMM) and 2-chloro-4,6-dimethoxy-1,3,5-triazine (CDMT) as the coupling agents to afford the diesters **349**, **350**, **351** and **352** respectively in 37-76% yields (Scheme 72). Final saponification of the diesters gave the desired final compounds **194-197** in 45-90% yields.

Scheme 70. Synthesis of intermediates **339-342**.

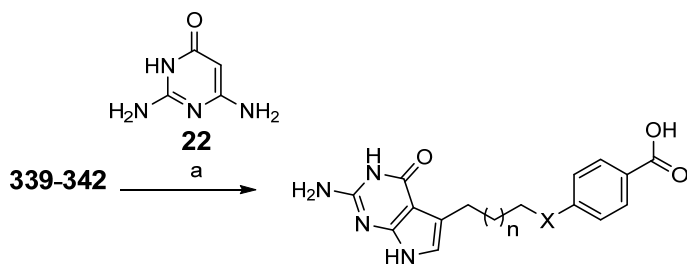


- | | |
|-------------------------------------|---|
| 329 X = N-boc, n = 1, R = Et | 335 X = N-boc, n = 1, R = Et (60%) |
| 330 X = O, n = 1, R = Me | 336 X = O, n = 1, R = Me (60%) |
| 332 X = S, n = 1, R = Me | 337 X = S, n = 1, R = Me (84%) |
| 334 X = N-boc, n = 2, R = Et | 338 X = N-boc, n = 2, R = Et (67%) |

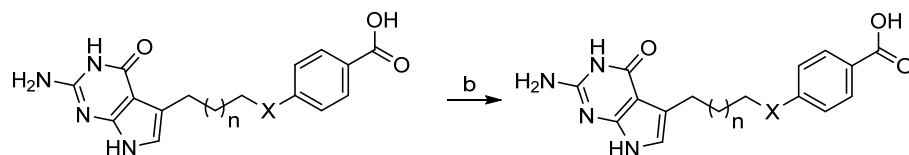


Reagents and conditions: (a) Dess-Martin periodinane, CH₂Cl₂, 0 °C-rt, 0.5-4 h, 60-84%;
 (b) 5,5-dibromo-2,2-dimethyl-4,6-dioxo-1,3-dioxane **302**, 1N HCl in (Et)₂O, (Et)₂O, rt, 48 h;
 (c) Br₂, 1,4-dioxane, CH₂Cl₂, 5 h.

Scheme 71. Synthesis of intermediates **344**, **345**, **347** and **348**.



- | |
|--|
| 343 X = N-boc, n = 1 (23% over 3 steps) |
| 344 X = O, n = 1 (27% over 3 steps) |
| 345 X = S, n = 1 (18% over 3 steps) |
| 346 X = N-boc, n = 2 (16% over 3 steps) |



343 X = N-boc, n = 1 (29% over 2 steps)

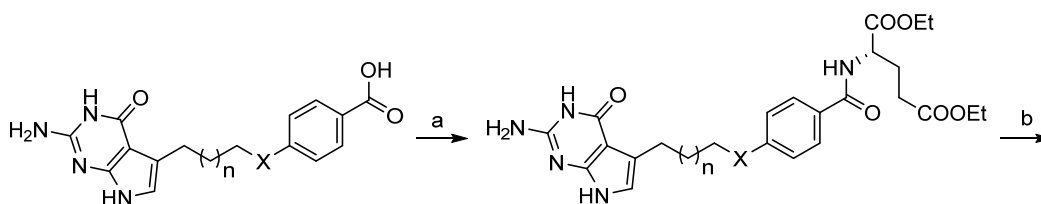
346 X = N-boc, n = 2 (19% over 2 steps)

347 X = NH, n = 1, (93%)

348 X = NH, n = 2, (97%)

Reagents and conditions: (a) (i) CH₃COONa, MeOH, H₂O, 45 °C, 4 h; (ii) (i) 1 N NaOH, rt, 12 h, 16-27% yields over 3 steps; (b) (i) 3N HCl, 1,4-dioxane, rt, 16 h; (ii) 1 N NaOH, rt, -10 °C; (iii) 0-4 °C, 1 N HCl, 93-97% yields.

Scheme 72. Synthesis of target compounds 194-197.



347 X = NH, n = 1

344 X = O, n = 1

345 X = S, n = 1

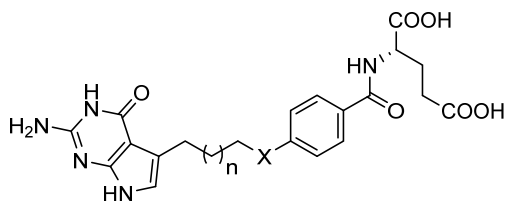
348 X = NH, n = 2

349 X = NH, n = 1, (76%)

350 X = O, n = 1, (67%)

351 X = S, n = 1, (37%)

352 X = NH, n = 2, (50%)



194 X = NH, n = 1, (90%)

195 X = O, n = 1, (78%)

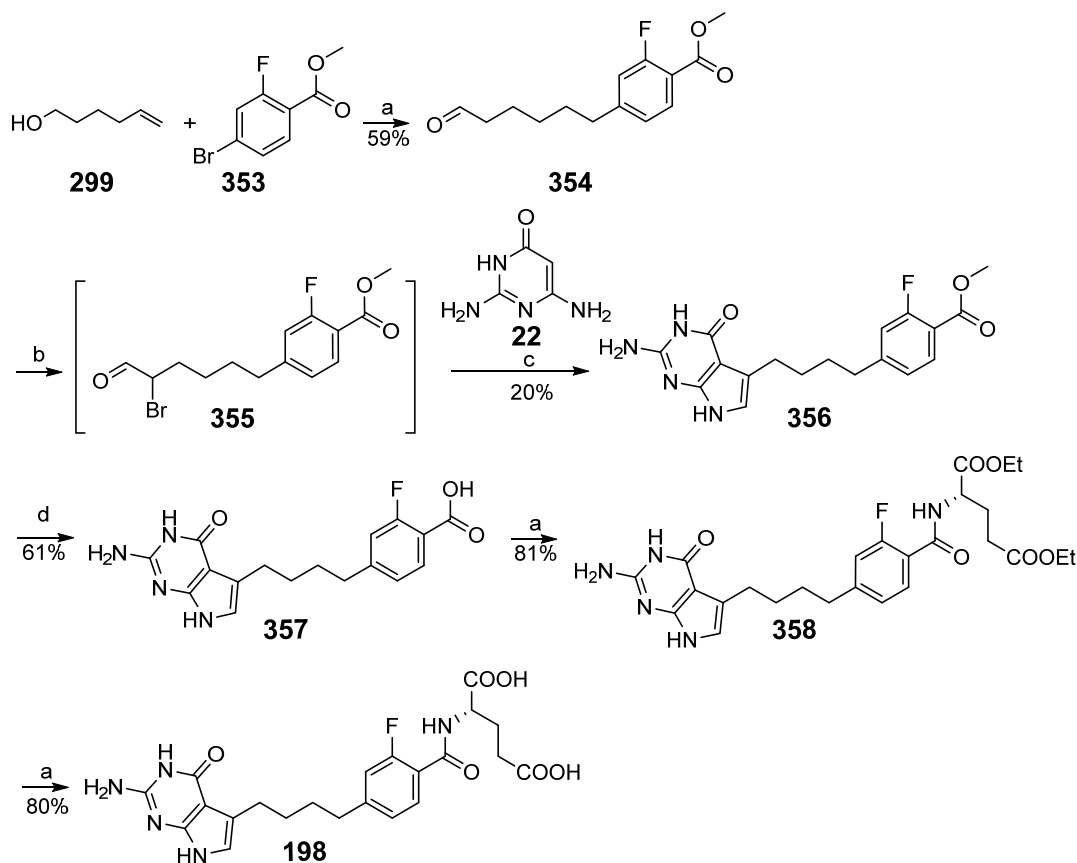
196 X = S, n = 1, (45%)

197 X = NH, n = 2, (67%)

Reagents and conditions: (a) NMM, CDMT, diethyl-L-glutamate, DMF, rt, 12 h, 37-76% yields; (b) (i) 1N, NaOH, rt, 1 h; (ii) 0-4 °C, 1 N HCl, 45-90% yields.

D.2.3. Synthesis of 5-substituted, 2-amino-4-oxo pyrrolo[2,3-*d*]pyrimidine-butyl-2'-fluorophenyl classical antifolates **198.**

Scheme 73. Synthesis of target compound **198.**



Reagents and conditions: (a) Pd(OAc)₂, LiCl, LiOAc, Bu₄NCl, DMF, 90 °C, 2.5 h, 59%; (b) 5,5-dibromo-2,2-dimethyl-4,6-dioxo-1,3-dioxane **302**, 1N HCl in (Et)₂O, (Et)₂O, rt, 48 h; (c) CH₃COONa, MeOH, H₂O, 45 °C, 4 h, 20 % yield over 2 steps; (d) (i) 1 N NaOH, rt, 12 h; (ii) 1 N HCl, 61% yield; (e) NMM, CDMT, diethyl-L-glutamate, DMF, rt, 12 h, 81%; (f) (i) 1N, NaOH, rt, 1 h; (ii) 0-4 °C, 1 N HCl, 80%.

Compound **198** (Scheme 73) was obtained using a reported procedure in which condensation of the α -bromo aldehyde **355** with 2,6-diamino-4-oxo-pyrimidine **22** is the

key step.¹²⁰ As reported by Larock et al.,³²³ Heck coupling reaction of commercially available hex-5-en-1-ol **299** and methyl 4-bromo-2-fluorobenzoate **353** afforded the unsaturated, coupled alcohol that rearranged to the vinyl alcohol and tautomerized to afford the aldehyde **354** in 59% yield. It was observed that the Heck coupling of the fluorinated benzoate **353** does not proceed at temperatures below 90 °C, unlike the non-fluorinated analogs such as **300** (Scheme 62) which undergo Heck coupling at temperatures >70 °C. Subsequent α -bromination of **354** with 5,5-dibromo-2,2-dimethyl-4,6-dioxo-1,3-dioxane (DBMA) **302** at room temperature afforded corresponding α -bromo aldehyde **355** which was immediately condensed with 2,6-diamino-4-oxo-pyrimidine **22** in the presence of sodium acetate to afford the 5-substituted pyrrolo[2,3-*d*]pyrimidine **356** in 20% yield over 2 steps. The terminal ester of **356** was subjected to base catalyzed hydrolysis to afford the pteronic acid **357** in 61% yield. The acid **357** was subsequently peptide coupled with L-glutamate diethyl ester hydrochloride in the presence of NMM and CDMT as the coupling agents to afford the diester **358** in 81% yield. Final saponification of the diesters with 1 N NaOH and neutralization to pH 4, provided target compound **198** in 80% yield.

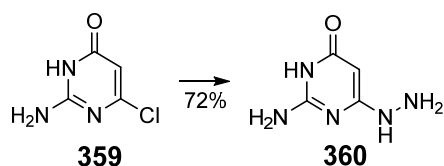
D.3. Multiple enzyme inhibitors (TS, GARFTase, AICARFTase) with selectivity for FRs and/or PCFT over RFC

D.3.1. 5-substituted, 2-amino-4-oxo-6-methyl pyrrolo[2,3-*d*]pyrimidine classical antifolates (**200-201**)

A key step in the synthesis of the 5-substituted, 2-amino-4-oxo-6-methyl pyrrolo[2,3-*d*]pyrimidine classical antifolates involved thermal indolization of the hydrazone **364** (Scheme 75) using a reported method.³⁸¹ Palladium-catalyzed Heck coupling of commercially available starting materials methyl 4-bromobenzoate **361** (Scheme 75) and

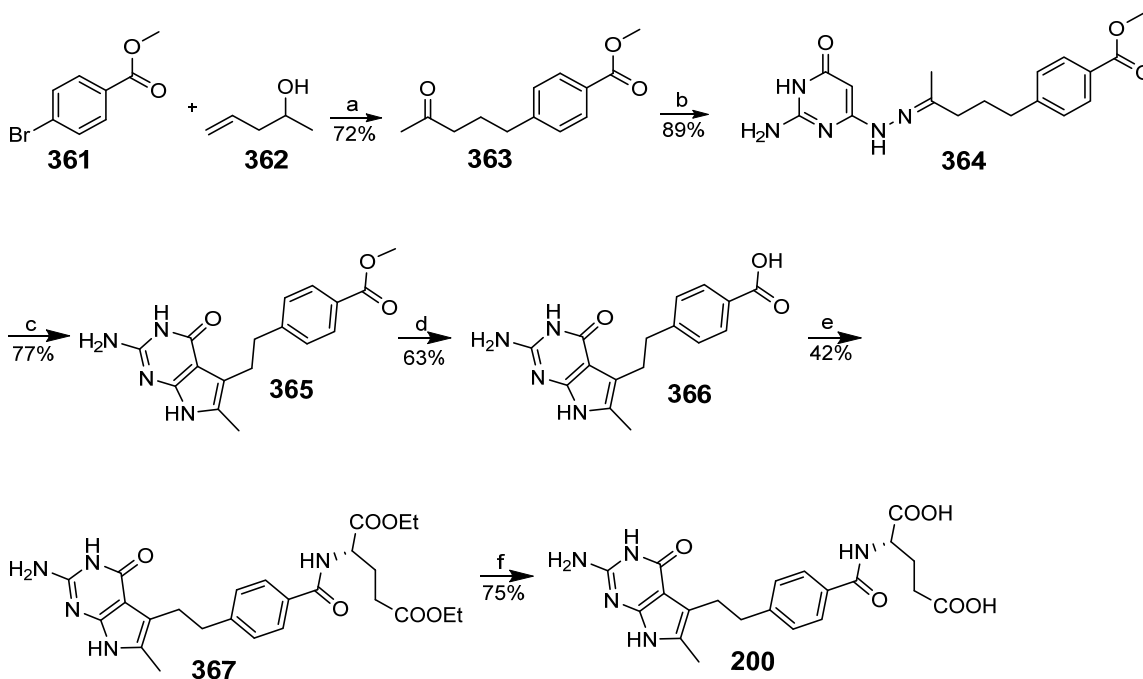
4-penten-2-ol **362** gave the coupled, unsaturated secondary alcohol that rearranged to the vinyl alcohol and tautomerized to afford the ketone **363** in 72% yield.³²³ Condensation of the ketone **363** with the hydrazine **360** under reflux conditions in 2-methoxyethanol afforded the key intermediate hydrazonepyrimidine **364** in 89% yield.³⁸¹ The Fischer indole cyclization of hydrazone **364** was accomplished regioselectively to the 5-substituted, 2-amino-4-oxo-6-methyl pyrrolo[2,3-*d*]pyrimidine **365** in 77% yield by thermolysis in diphenyl ether at reflux conditions. ¹H NMR did not show any evidence for the presence of the other possible regioisomer **368** (Figure 70) (a key determinant is the presence of C6-C(CH₃) peak at δ 1.8 ppm). The aromatic ester of **365** was subjected to base catalyzed hydrolysis to afford the pteric acid **366** in 63% yield. The acid **366** was subsequently peptide coupled with L-glutamate diethyl ester hydrochloride in the presence of *N*-methylnmorpholine (NMM) and 2-chloro-4,6-dimethoxy-1,3,5-triazine (CDMT) as the coupling agents to afford the diester **367** in 42% yield. Final saponification of the diesters with 1 N NaOH and neutralization to pH 4, provided the 2C linker target compound **200** in 75% yield. Nucleophilic aromatic substitution of the commercially available 2-amino-6-chloropyrimidin-4(3*H*)-one **359** (Scheme 74) with hydrazine hydrate afforded the intermediate hydrazine **360** in 72% yield.³⁸¹

Scheme 74. Synthesis of intermediate **360**.



Reagents and conditions: Hydrazine hydrate, H₂O, reflux, 3 h, 72%.

Scheme 75. Synthesis of target compound **200**.



Reagents and conditions: (a) $\text{Bu}_4\text{NH}_4\text{Cl}$, $\text{Pd}(\text{OAc})_2$, LiCl , LiOAc , DMF, 80°C , 3 h, 72%, (b) **360**, methoxyethanol, 145°C , 14 h, 89%; (c) Ph_2O , 270°C , 6 h, 77%; (d) 1N, NaOH, rt, 12 h, 63%; (e) Diethyl-L-glutamate, NMM, CDMT, DMF, rt, 12 h, 42%; (f) (i) 1N, NaOH, rt, 1 h; (ii) $0-4^\circ\text{C}$, 1 N HCl, 75%.

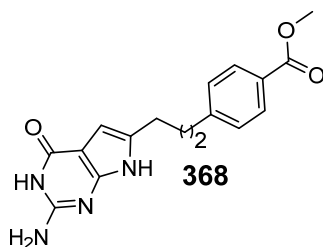
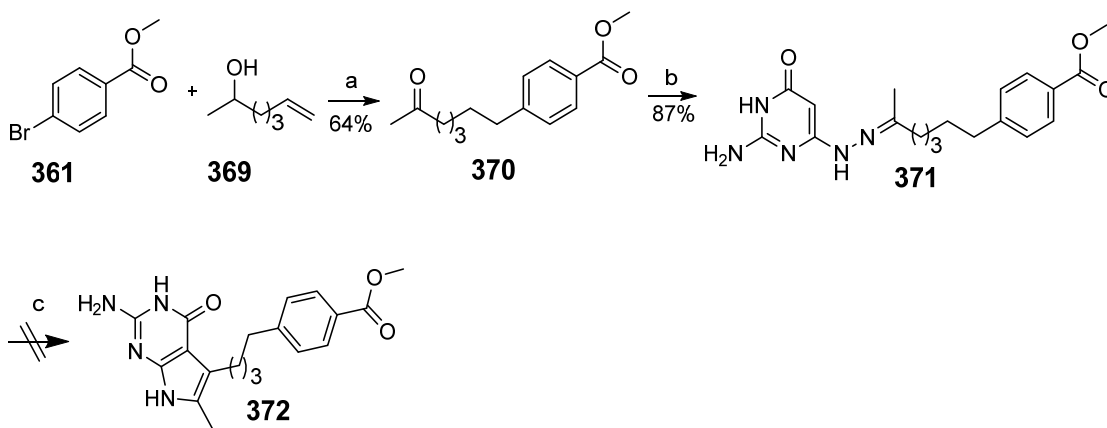


Figure 70. The other possible Fischer indole cyclization product **368**.

When a similar procedure was pursued for the synthesis of 5-substituted, 2-amino-4-oxo-6-methyl pyrrolo[2,3-*d*]pyrimidine classical antifolate **201** with a 4C linker, the

thermal indolization of the hydrazone **371** was repeatedly unsuccessful (Scheme 76). Palladium-catalyzed Heck coupling of commercially available starting material methyl 4-bromobenzoate **361** with 6-hexen-2-ol **369** gave the coupled, unsaturated secondary alcohols that rearranged to the vinyl alcohol and tautomerized to afford the ketone **370** in 64% yield.³²³ Condensation of the ketone **370** with the hydrazine **360** under reflux conditions in 2-methoxyethanol afforded the key intermediate hydrazonepyrimidine **371** in 87% yield. The Fischer indole cyclization of hydrazone **371** to the 5-substituted, 2-amino-4-oxo-6-methyl pyrrolo[2,3-*d*]pyrimidine **372** was unsuccessful due to degradation of the reaction mixture as confirmed by ¹H NMR. It is speculated that the reduced melting point of the longer, 7C alkyl chain linked intermediate **371** (mp 152 °C) when compared with the 5C linker counterpart **364** (mp 240 °C) causes degradation of the intermediate **371** under thermolytic conditions of the cyclization reaction (270 °C) to **372**.

Scheme 76. Synthesis of intermediate **372**



Reagents and conditions: (a) Bu₄NH₄Cl, Pd(OAc)₂, LiCl, LiOAc, DMF, 80 °C, 3 h, 64%; (b) **372**, methoxyethanol, 145 °C, 14 h, 87%; (c) Ph₂O, 270 °C, 6 h.

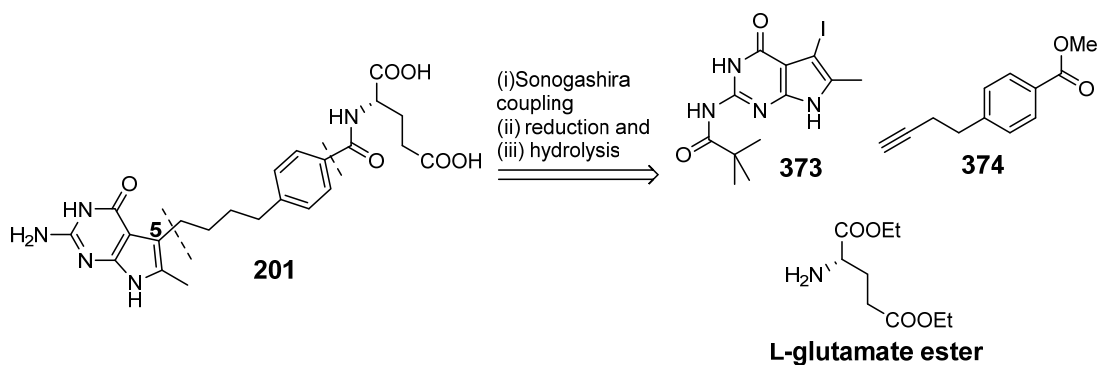


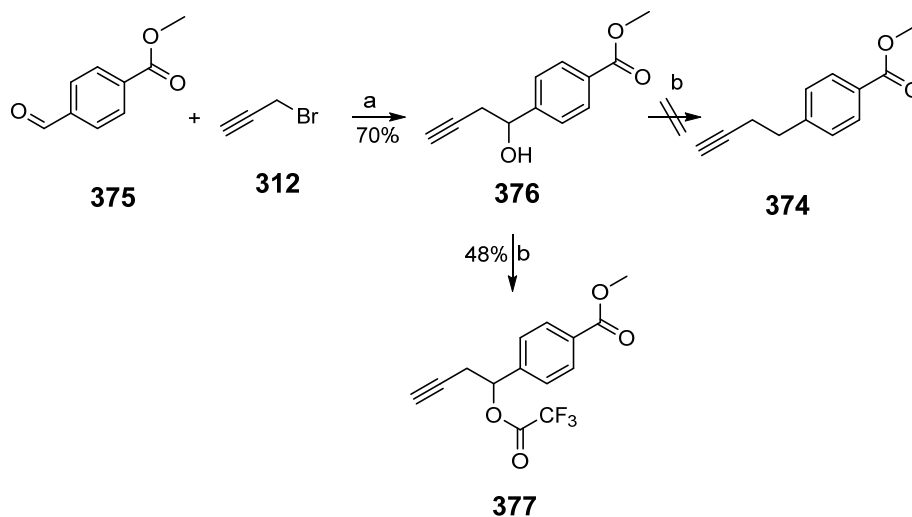
Figure 71. Proposed retrosynthesis of target compound **201**.

Alternate procedure for the synthesis of the 5-substituted, 2-amino-4-oxo-6-methyl pyrrolo[2,3-*d*]pyrimidine classical antifolates with a 4C linker was envisioned to be accomplished via a Sonogashira coupling of intermediate iodide **373** and alkyne **374** (Figure 71). *N*-(5-iodo-6-methyl-4-oxo-4,7-dihydro-3*H*-pyrrolo[2,3-*d*]pyrimidin-2-yl)pivalamide **373** can be synthesized by following a reported procedure³⁸² and the intermediate **374** could be synthesized via a reported Barbier reaction³⁸³ of propargyl bromides with 4-formylbenzoate. This convergent procedure not only will improve the overall yield in lesser number of steps, but can also be applied for the synthesis of homologous compounds.

The key intermediate, secondary homopropargyl alcohol **376** (Scheme 77) was synthesized as per a reported Barbier type synthesis.³⁸³ Aromatic aldehyde **375** and propargyl bromide **312** in the presence of activated zinc and saturated aqueous NH₄Cl afforded the secondary homopropargyl alcohol **376** in 70% yield. Having obtained **376**, deoxygenation of the benzyl alcohol using triethylsilane (TES) was carried out. However, instead of the deoxygenated product methyl 4-(but-3-yn-1-yl)benzoate **374**, the trifluoroacetyl protected intermediate **377** (Scheme 77) was obtained in 48% yield. The

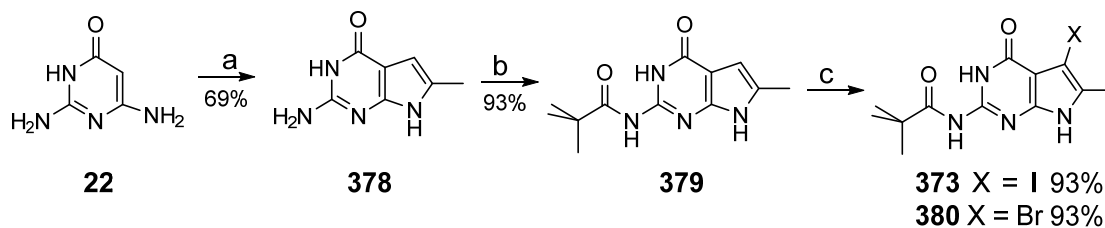
deoxygenation step was temporarily abandoned and the homopropargyl alcohol **376** was taken forward to test the feasibility of Sonogashira coupling of the alkynes **376** with intermediate halide **373**.

Scheme 77. Synthesis of intermediates **374**, **376** and **377**.



Reagents and conditions: (a) Zn, sat. aq, NH₄Cl, THF, 0 °C - rt, 24 h, 70%; (b) TFA, TES, CH₂Cl₂, 0 °C - rt, 7 days, 48%.

Scheme 78. Synthesis of intermediates **373** and **380**.



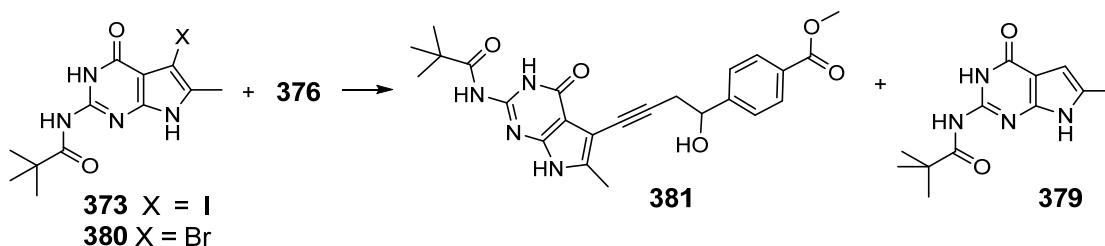
Reagents and conditions: (a) chloroacetone, CH₃COONa, DMF, reflux, 3.5 h, 69%; (b) (Piv)₂O, 120 °C, 12 h, 93%; (c) halogenating reagent, CH₂Cl₂, 40 °C, 30 min, 93%.

Table 21. Halogenating agents used for the synthesis of intermediates **373** and **380** (Scheme 78).

Halogenating reagent	Product
NIS	373
NBS	380

Synthesis of the key halogenated intermediates **373** and **380** (Scheme 78) began with the condensation of 2,4-diamino-6-hydroxypyrimidine **22** with bromoacetone in the presence of sodium acetate yielding the cyclized product 2-amino-6-methyl-3,7-dihydro-4*H*-pyrrolo[2,3-*d*]pyrimidin-4-one **378** in 51% yield.³⁸² Compound **378** was treated with trimethylacetic anhydride to yield the *N*(2)-monoacylated compound **379** in 93% yield. Aromatic iodination or bromination using NIS or NBS afforded the C5 halogenated intermediates **373** or **380** respectively in 93% yields (Table 21). Halogenation at the benzylic position was not observed.³⁸⁴

Scheme 79. Synthesis of intermediate **381**.

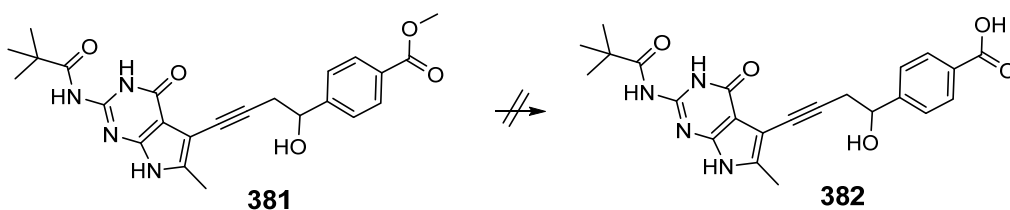


Reagents and conditions: Pd[P(Ph)₃]₄, CuI, TEA, Solvent, temp, time.

Table 22. Reagents and conditions for the synthesis of intermediate **381**. Wherever iodinated and brominated intermediates yielded different results under similar coupling conditions, the products are correspondingly color coded with the starting material halide.

Solvent	X	Reagents and conditions					Product	% Yield of compd. 381
		CuI (eq)	Pd(0) (eq)	TEA (eq)	Temp.	Time		
DMF	I/Br	0.2	0.5	10	rt	72 h	379/NA	-
DMF	I/Br	0.2	0.5	10	55 °C	12 h	379	-
DMF	I/Br	0.2	0.5	10	90 °C	12 h	379	-
DMF	I/Br	0.2	0.5	10	150 °C	3 min	379	-
3:1 THF:DMF	I/Br	0.4	0.1	1	rt	72 h	381 and 379 /NA	30%
3:1 THF:DMF	I/Br	0.4	0.1	1	90 °C	12 h	381 and 379 / 387	10%
3:1 THF: DMF	I/Br	0.4	0.1	1	150 °C	3 min	379	-
THF	I	0.4	0.1	1	rt	72 h	381 and 379	70%

Scheme 80. Synthesis of intermediate **382**.



Reagents and conditions: 1N, NaOH, rt, 12 h.

Sonogashira coupling reactions of halides **373** and **380** (Scheme 79, Table 22) with the alkyne **376** were carried out under various coupling conditions. Upon varying the reacting halide (iodo or bromo), solvents, and equivalents of catalysts and base, it was observed that the solvent in which the reaction was carried out was the most vital variable. The Sonogashira coupling method optimized for the synthesis of **212-213** (Scheme 41) produced no new product spots on TLC in the presence of iodo **373** and alkyne **376**. Majority of the starting material was deiodinated to the intermediate **379** (Table 22). Similar results were observed at lower temperatures (55 °C and rt) or higher temperature (150 °C), analogous to the results obtained in the Sonogashira coupling of the iodo **305** with alkynes **306** and **307** (Scheme 66). Though a palladium complex is formed with the 6-methyl pyrrolo[2,3-*d*]pyrimidine scaffold (confirmed from ¹H NMR studies), however the consecutive reaction step appears to be the temperature independent C5 deiodination. Repeating the reactions with the brominated analog **380** either proceeded without any depletion of starting material (rt) or resulted in dehalogenation at higher temperatures. In another set of reactions, a reported procedure of Sonogashira coupling where the catalysts Pd[(PPh)₃]₄, CuI and base TEA were used in modified equivalents in THF:DMF solvent ratio of 3:1 at room temperature in 4 hours (4 h) was followed.³⁸⁵ The coupling of the alkyne **376** with the iodo **373** at room temperature did not proceed to form any new spot over a period of 4 h and was therefore continued for additional period of time. After 8 h a new polar spot was observed on the TLC. The reaction did not go to completion and the intensity of the new spot did not increase beyond 72 h at which point, the reaction spots were separated on a column chromatograph to afford the required Sonogashira coupled product **381** (confirmed by ¹H NMR) in 30% yield. However, the product was difficult to

purify (due to formation of multiple unidentified side products with similar R_f) and warranted further optimization of the reaction procedure. Replacing **373** with bromo **380** at rt and/or increasing the reaction temperature was detrimental to the palladium complex formation and/or resulted in dehalogenation. Since replacing DMF with 3:1 ratio of THF and DMF afforded the required intermediate **381**, the next logical step was to examine the scope of the reaction in pure THF. This was feasible due to the improved solubility of *N*(2)-monoacylated **373**. The reaction in THF not only improved the yield to 70% (crude), but the separation of the reaction mixture was easier. However, base catalyzed hydrolysis of **381** to **382** (Scheme 80) at room temperature failed to work and instead resulted in degradation of the starting material. Our hypothesis is that under basic conditions, the CH_2 protons (diastereotopic) next to the alkyne may have been deprotonated to produce a carbanion that is resonance stabilized by the neighboring pi orbitals. In the future attempts for the synthesis of **201**, it will be worthwhile to reduce the triple bond in **373** before carrying it forward for base-catalyzed hydrolysis.

V. EXPERIMENTAL

All evaporations were carried out in vacuum with a rotary evaporator. Analytical samples were dried in vacuo in a CHEM-DRY drying apparatus over P₂O₅ at 50 °C. Melting points were determined either using a MEL-TEMP II melting point apparatus with FLUKE 51 K/J electronic thermometer or using an MPA100 OptiMelt automated melting point system and are uncorrected. Nuclear magnetic resonance spectra for proton (¹H NMR) were recorded on the Bruker Avance II 400 (400 MHz) or Bruker Avance II 500 (500 MHz) NMR systems with TopSpin processing software. ¹⁹F NMR were recorded using a Bruker WH-400 (400 MHz) spectrometer or a Bruker AV-III 700 MHz spectrometer using a BBFO-Plus probe. The ¹H homonuclear decoupling experiments were carried out individually at each elevated temperature (data acquisition each time was delayed until the temperature was stabilized). The 2D HOESY NMR was carried out using a standard ¹H/¹⁹F HOESY experiment with ¹⁹F detection. ¹H and ¹⁹F spectra were referenced to TMS and trifluoroacetic acid, respectively, as the internal standards to express the chemical shift values (δ) in ppm (parts per million): s, singlet; d, doublet; dd, doublet of doublet; t, triplet; q, quartet; m, multiplet; br, broad singlet; td, triplet of doublet; dt, doublet of triplet; quin, quintet. ¹H NMR of alkyl CH₂s of target compounds merged with DMSO and water peaks have been omitted from the experimental whenever not visible in ¹H NMR. ¹H NMR of alkyl CH₂s of intermediate compounds within DMSO and water peaks and D₂O exchangeable peaks that were exchanged due to excess moisture have also been omitted from the experimental whenever not visible in ¹H NMR. Thin-layer chromatography (TLC) was performed on Whatman® PE SIL G/UV254 flexible silica gel plates and the spots were visualized under 254 and 365 nm ultraviolet illumination. Proportions of solvents

used for TLC are by volume. All analytical samples were homogeneous on TLC in at least two different solvent systems. Column chromatography was performed on the silica gel (70 to 230 meshes, Fisher Scientific) column. Flash chromatography was carried out on the CombiFlash® *Rf* systems, model COMBIFLASH *RF*. Pre-packed RediSep® *Rf* normal-phase flash columns (230 to 400 meshes) of various sizes were used. The amount (weight) of silica gel/celite for column chromatography was in the range of 5-10 times the amount (weight) of the crude reaction mixture being separated. Elemental analyses were performed by Atlantic Microlab, Inc., Norcross, GA. Element compositions are within \pm 0.4% of the calculated values. Fractional moles of water or organic solvents frequently found in some analytical samples could not be prevented despite 24 to 48 hours of drying in vacuo and were confirmed where possible by their presence in the ^1H NMR spectra. High Performance Liquid Chromatography (HPLC) was performed on Waters® 600E Multisolute Delivery System, components: Waters® 600 Controller (model code: 600), 600E Pump (model code: 60F), Waters® 2487 Dual λ Absorbance Detector. Mobile phase was an aqueous blend of water with a miscible, polar organic solvent acetonitrile.

General Procedure for the Synthesis of Compounds 162 and 207.

To the solution of commercially available 4-pentynoic acid **203** (1 eq) in anhydrous CH_2Cl_2 was added oxalyl chloride (6 eq) and stirred at reflux for 1 h to form the acid chloride **204**. After cooling to room temperature, the solvent was evaporated under reduced pressure and the residue was dissolved in Et_2O without further characterization. The solution was added in a dropwise manner to an ice-cooled (ice-bath) diazomethane solution (generated in situ from diazald (5 eq) by using Aldrich Mini Diazald apparatus). The resulting mixture was

allowed to stand for 30 min after which it was stirred for 1 h to give the unstable α -diazoketone **205**. Subsequently, 48% HBr in water (20 eq) was added to this solution, and stirred at reflux temperature for 1.5 h. The solution was then brought down to room temperature and the organic layer was separated. The aqueous layer was extracted twice with Et₂O and combined with the organic layer. The Et₂O extract was washed twice with 10% Na₂CO₃ solution, dried over Na₂SO₄, filtered and solvent was evaporated under reduced pressure to afford α -bromoketone **206** a light-yellow/orange syrup. Without further characterization, the residue was dissolved in anhydrous DMF to which 2,6-diamino-3*H*-pyrimidin-4-one **22** (1 eq), was added. The resulting mixture was stirred at room temperature for 72 h under N₂, until a new spot was observed under TLC (CHCl₃/MeOH) after which the solvent was evaporated to afford a sticky crude solid. A silica plug was prepared by adding silica gel and methanol followed by evaporation of the solvent in vacuo, which was then loaded on to a silica gel column and eluted with CHCl₃ followed by gradual increase in polarity to 10% MeOH in CHCl₃. The desired fractions (TLC) were pooled and evaporated to afford the alkyne intermediates.

2-Amino-6-(but-3-yn-1-yl)-3,7-dihydro-4*H*-pyrrolo[2,3-*d*]pyrimidin-4-one (162)

Following the general procedure described for the synthesis of **162** and **207**, cyclization of **203** (1.96 g, 20 mmol) at room temperature for 72 h afforded the intermediate **162** (1.5 g, 7.42 mmol, 37% yield after 4 steps) as a pink colored powder. TLC R_f = 0.45 (CHCl₃/MeOH 5:1); mp 269 °C dec. ¹H NMR (DMSO-*d*₆, 400 MHz): δ 2.44-2.48 (dt, J = 2.53, 7.51, 7.47 Hz, 2H, CH₂), 2.66-2.7 (t, J = 7.45, 7.45 Hz, 2 H, CH₂), 2.8-2.81 (t, J = 2.59, 2.59 Hz, 1 H, CH), 5.98-5.99 (d, J = 2.20 Hz, 1 H, C5-CH), 6.21 (s, br, 2 H, 2-NH₂, exch),

10.37 (s, 1 H, 3-NH, exch), 10.95 (s, 1 H, 7-NH, exch). The ^1H NMR matches the ^1H NMR of the reported compound.¹⁰⁷

5-(but-3-yn-1-yl)furo[2,3-*d*]pyrimidine-2,4-diamine (207)

Following the general procedure described for the synthesis of **162** and **207**, cyclization of **203** (1.96 g, 20 mmol) at room temperature for 72 h afforded the intermediate **207** as a side product (200 mg, 1 mmol, 5% yield after 4 steps) as a buff colored powder. TLC R_f = 0.56 ($\text{CHCl}_3/\text{MeOH}$ 5:1); mp 189.2 °C dec. ^1H NMR ($\text{DMSO-}d_6$, 400 MHz): δ 2.34-2.38 (dt, J = 2.63, 7.32, 6.97 Hz, 2 H, CH_2), 2.7-2.74 (t, J = 7.30, 7.30 Hz, 2 H, CH_2), 2.82-2.83 (t, J = 2.66, 2.66 Hz, 1 H, CH), 4.95 (s, 2 H, 2- NH_2 , exch), 5.4 (s, 1 H, C6-CH), 7.7 (s, br, 2 H, 4- NH_2 , exch). The intermediate **207** was not characterized further.

General Procedure for the Synthesis of Compounds 210–211.

A mixture of bromo-fluoro-arylcarboxylic acids (**208-209**) (1 eq), *N*-methylmorpholine (1.2 eq), 2-chloro-4,6-dimethoxy-1,3,5-triazine (1.2 eq) in anhydrous DMF in a round bottomed flask, was stirred for 1.5 h, at room temperature. Subsequently, *N*-methylmorpholine (1.2 eq) and L-glutamic acid diethylester hydrochloride (1.5 eq) was added to the mixture and stirred at room temperature for 5 h until disappearance of the starting material and a new major non-polar spot was observed on TLC (hexane/EtOAc). After evaporation of the solvent in vacuo, MeOH was added followed by silica gel and the solvent was evaporated by further drying. The resulting plug was loaded on to a silica gel column and eluted with hexanes followed by gradual increase of EtOAc to 50% EtOAc in hexanes. Fractions with the desired R_f (TLC) were pooled and evaporated to afford glutamate esters **210-211** as colorless syrups.

Diethyl (4-bromo-2-fluorobenzoyl)-L-glutamate (**210**).

Compound **210** was prepared using the general method described for the preparation of **210-211**, from 4-bromo-2-fluorobenzoic acid, **208** (2 g, 9 mmol), to give **210** (2.45 g, 67%) as a colorless syrup. TLC R_f = 0.45 (hexane/EtOAc, 1:1); ^1H NMR (500 MHz, CDCl_3): δ 1.24-1.27 (t, J = 7.15, 7.15 Hz, 3 H, γ - $\text{COOCH}_2\text{CH}_3$), 1.32-1.35 (t, J = 7.14, 7.14 Hz, 3 H, α - $\text{COOCH}_2\text{CH}_3$), 2.12-2.53 (m, 4 H, β - CH_2 , γ - CH_2), 4.11-4.16 (dq, J = 0.60, 7.12, 7.07, 7.07 Hz, 2 H, γ - $\text{COOCH}_2\text{CH}_3$), 4.24-4.3 (dq, J = 1.70, 7.14, 7.12, 7.12 Hz, 2 H, α - $\text{COOCH}_2\text{CH}_3$), 4.83-4.87 (ddt, J = 2.02, 5.11, 7.33, 7.33 Hz, 1 H, α -CH), 7.33-7.39 (m, 2 H, Ar, CONH, exch), 7.43-7.45 (dd, J = 1.71, 8.44 Hz, 1 H, Ar), 7.95-7.99 (t, J = 8.38 Hz, 1 H, Ar). The intermediate **210** was used for the next reaction without further characterization.

Diethyl (4-bromo-3-fluorobenzoyl)-L-glutamate (**211**).

Compound **211** was prepared using the general method described for the preparation of **210-211**, from 4-bromo-3-fluorobenzoic acid, **209** (500 mg, 2.3 mmol), to give **211** (780 mg, 85%) as a colorless syrup. TLC R_f = 0.45 (hexane/EtOAc 1:1); ^1H NMR (400 MHz, CDCl_3): δ 1.24-1.28 (dd, J = 0.78, 7.09 Hz, 3 H, γ - $\text{COOCH}_2\text{CH}_3$), 1.32-1.35 (dd, J = 0.76, 7.12 Hz, 3 H, α - $\text{COOCH}_2\text{CH}_3$), 2.14-2.58 (m, 4 H, β - CH_2 , γ - CH_2), 4.10-4.19 (dq, J = 2.95, 7.11, 7.04, 7.04 Hz, 2 H, γ - $\text{COOCH}_2\text{CH}_3$), 4.23-4.3 (q, J = 6.37, 6.37, 6.50 Hz, 2 H, α - $\text{COOCH}_2\text{CH}_3$), 4.73-4.78 (dt, J = 4.97, 7.51, 7.63 Hz, 1 H, α -CH), 7.25-7.27 (d, J = 7.31 Hz, 1 H, Ar), 7.49-7.51 (dd, J = 1.77, 8.27 Hz, 1 H, Ar), 7.63-7.69 (m, 2 H, Ar, CONH, exch). The intermediate **211** was used for the next reaction without further characterization.

General Procedure for the Synthesis of Compounds 212-213.

To a round-bottomed flask equipped with a magnetic stirrer and purged with N₂, was added a mixture of tetrakis(triphenylphosphine)palladium(0) (0.16 eq), triethylamine (10 eq), **210-211** (1.5 eq) and anhydrous DMF. To the stirred mixture, under N₂, was added copper(I) iodide (0.16 eq) and **162** (1 eq) and the reaction mixture was stirred at 70 °C for 12 h in a microwave. TLC showed the disappearance of the starting material and one a new non-polar spot (CHCl₃/MeOH). After evaporation of solvent under reduced pressure, MeOH was added followed by silica gel and the solvent was evaporated. The resulting plug was loaded on to a silica gel column and eluted with CHCl₃ followed by 10% MeOH in CHCl₃. Fractions with desired R_f(TLC) were pooled and evaporated to afford the alkynes **212-213**.

Diethyl (4-(4-(2-amino-4-oxo-4,7-dihydro-3H-pyrrolo[2,3-d]pyrimidin-6-yl)but-1-yn-1-yl)-2-fluorobenzoyl)-L-glutamate (**212**).

Compound **212** was prepared using the general method described for the preparation of **212-213**, from **162** (100 mg, 0.5 mmol) and diethyl (4-bromo-2-fluorobenzoyl)-L-glutamate, **210** (300 mg, 0.74 mmol) to give **212** (80 mg, 31%) as a golden-brown sticky solid. TLC R_f = 0.5 (CHCl₃/MeOH 5:1); ¹H NMR (400 MHz, DMSO-*d*₆): δ 1.15-1.20 (m, 6 H, COOCH₂CH₃), 1.87-2.14 (m, 2 H, β-CH₂), 2.4-2.45 (m, 2 H, γ-CH₂), 4.02-4.13 (m, 4 H, COOCH₂CH₃), 4.38-4.49 (m, 1 H, α-CH), 6.02-6.05 (m, 3 H, C5-CH, 2-NH₂, exch), 7.26-7.32 (m, 1 H, Ar), 7.51-7.81 (m, 2 H, Ar), 8.75-8.77 (dd, *J* = 2.08, 7.83 Hz, 1 H, CONH, exch), 10.22 (s, 1 H, 3-NH, exch), 10.92 (s, 1 H, 7-NH, exch). The intermediate **212** was used for the next reaction without further characterization.

Diethyl (4-(4-(2-amino-4-oxo-4,7-dihydro-3*H*-pyrrolo[2,3-*d*]pyrimidin-6-yl)but-1-yn-1-yl)-3-fluorobenzoyl)-L-glutamate (213).

Compound **213** was prepared using the general method described for the preparation of **212-213**, from **162** (100 mg, 0.5 mmol) and diethyl (4-bromo-3-fluorobenzoyl)-L-glutamate, **211** (300 mg, 0.74 mmol) to give **213** (110 mg, 42%) as a brown sticky solid. TLC $R_f = 0.5$ ($\text{CHCl}_3/\text{MeOH}$ 5:1); $^1\text{H NMR}$ (400 MHz, $\text{DMSO-}d_6$): δ 1.12-1.18 (m, 6 H, $\text{COOCH}_2\text{CH}_3$), 1.95-2.13 (m, 2 H, $\beta\text{-CH}_2$), 2.40-2.44 (m, 2 H, $\gamma\text{-CH}_2$), 2.65-2.67 (m, 2H, CH_2), 4.01-4.12 (m, 4H, $\text{COOCH}_2\text{CH}_3$), 4.38-4.43 (m, 1 H, $\alpha\text{-CH}$), 5.88 (s, 1 H, C5-CH), 6.0 (s, 2 H, 2-NH₂, exch), 7.37-7.41 (m, 1 H, Ar), 7.59-7.64 (m, 2 H, Ar), 8.77-8.80 (d, $J = 8.26$ Hz, 1 H, CONH, exch), 10.23 (s, 1 H, 3-NH, exch), 10.83 (s, 1 H, 7-NH, exch). The intermediate **213** was used for the next reaction without further characterization.

General procedure for the synthesis of compounds 214-215.

To a Parr flask with 10% palladium on activated carbon (0.5 wt eq) soaked in ethanol was added a methanolic solution of **212-213**. Hydrogenation was carried out at 55 psi of H₂ for 12 h. TLC showed the disappearance of the starting material and one a new slightly non-polar spot ($\text{CHCl}_3/\text{MeOH}$). The reaction mixture was filtered through celite, washed with MeOH and concentrated under reduced pressure to give the reduced alkanes **214-215** as sticky solids.

Diethyl (4-(4-(2-amino-4-oxo-4,7-dihydro-3*H*-pyrrolo[2,3-*d*]pyrimidin-6-yl)butyl)-2-fluorobenzoyl)-L-glutamate (214).

Compound **214** was prepared using the general method described for the preparation of **214-215**, from **212** (80 mg, 0.13 mmol) to give **214** (65 mg, 81%) as a light yellow sticky

solid. TLC $R_f = 0.52$ ($\text{CHCl}_3/\text{MeOH}$ 5:1); $^1\text{H NMR}$ (400 MHz, $\text{DMSO-}d_6$): δ 1.16-1.22 (m, 6 H, $\text{COOCH}_2\text{CH}_3$), 1.57-1.61 (m, 4 H, CH_2CH_2), 1.92-2.13 (m, 2 H, $\beta\text{-CH}_2$), 2.44-2.48 (m, 2 H, $\gamma\text{-CH}_2$), 2.63-2.68 (m, 2 H, Ar- CH_2), 4.03-4.08 (dd, $J = 6.98, 14.09$ Hz, 2 H, $\text{COOCH}_2\text{CH}_3$), 4.1-4.15 (m, 2 H, $\text{COOCH}_2\text{CH}_3$), 4.41-4.43 (m, 1 H, $\alpha\text{-CH}$), 5.84-5.85 (d, $J = 2.05$ Hz, 1 H, C5-CH), 5.96 (s, 2 H, 2-NH₂, exch), 7.11-7.16 (m, 2 H, Ar), 7.48-7.52 (t, $J = 7.80, 7.80$ Hz, 1 H, Ar), 8.57-8.58 (dd, $J = 0.82, 5.91$ Hz, 1 H, CONH, exch), 10.12 (s, 1 H, 3-NH, exch), 10.80 (s, 1 H, 7-NH, exch). The intermediate **214** was used for the next reaction without further characterization.

Diethyl (4-(4-(2-amino-4-oxo-4,7-dihydro-3H-pyrrolo[2,3-d]pyrimidin-6-yl)butyl)-3-fluorobenzoyl)-L-glutamate (215).

Compound **215** was prepared using the general method described for the preparation of **214-215**, from **213** (100 mg, 0.19 mmol) to give **215** (70 mg, 70%) as a light yellow sticky solid. TLC $R_f = 0.52$ ($\text{CHCl}_3/\text{MeOH}$ 5:1); $^1\text{H NMR}$ (400 MHz, $\text{DMSO-}d_6$): δ 1.12-1.18 (m, 6 H, $\text{COOCH}_2\text{CH}_3$), 1.54-1.61 (m, 4 H, CH_2CH_2), 1.95-2.12 (m, 2 H, $\beta\text{-CH}_2$), 2.4-2.44 (m, 2 H, $\gamma\text{-CH}_2$), 2.66-2.68 (m, 2 H, Ar- CH_2), 4.0-4.12 (m, 4 H, $\text{COOCH}_2\text{CH}_3$), 4.38-4.42 (m, 1 H, $\alpha\text{-CH}$), 5.88 (s, 1 H, C5-CH), 6.1 (s, 2 H, 2-NH₂, exch), 7.38-7.43 (m, 1 H, Ar), 7.59-7.64 (m, 2 H, Ar), 8.77-8.81 (m, 1 H, CONH, exch), 10.23 (s, 1 H, 3-NH, exch), 10.83 (s, 1 H, 7-NH, exch). The intermediate **215** was used for the next reaction without further characterization.

General procedure for the synthesis of compounds 179-180.

To the reduced alkanes **214-215** was added 1 N NaOH and the mixture was stirred at room temperature for 1 h. TLC showed the disappearance of the starting material and one major

spot at the origin (CHCl₃/ MeOH 5:1). The solution was cooled in an ice bath and the pH was adjusted to 3-4 with dropwise addition of 1 N HCl. The resulting suspension was cooled to 4-5 °C in the refrigerator overnight and filtered. The residue was thoroughly washed with cold water and dried in vacuum using P₂O₅ to afford the target compounds **179-180**.

(4-(4-(2-Amino-4-oxo-4,7-dihydro-3H-pyrrolo[2,3-d]pyrimidin-6-yl)butyl)-2-fluorobenzoyl)-L-glutamic acid (179).

Compound **179** was prepared using the general method described for the preparation of **179-180**, from **214** (65 mg, 0.12 mmol) to give **179** (40 mg, 69%) as a light yellow powder. mp 137.4 °C dec. ¹H NMR (400 MHz, DMSO-*d*₆): δ 1.57-1.58 (m, 4 H, CH₂CH₂), 1.85-2.11 (m, 2 H, β-CH₂), 2.33-2.37 (m, 2 H, γ-CH₂), 2.63-2.66 (t, *J* = 6.40, 6.40 Hz, 2 H, Ar-CH₂), 4.36-4.41 (m, 1 H, α-CH), 5.85-5.86 (d, *J* = 2.10 Hz, 1 H, C5-CH), 6.02 (s, 2 H, 2-NH₂, exch), 7.10-7.15 (m, 2 H, Ar), 7.50-7.54 (t, *J* = 7.86, 7.86 Hz, 1 H, Ar), 8.41-8.43 (dd, *J* = 2.08, 7.83 Hz, 1 H, CONH, exch), 10.18 (s, 1 H, 3-NH, exch), 10.83 (s, 1 H, 7-NH, exch). Anal. Calcd for C₂₂H₂₄FN₅O₆ · 0.82 H₂O: C, 54.12; H, 5.29; N, 14.34; F, 3.89. Found: C, 54.19; H, 5.13; N, 14.05; F, 3.76.

(4-(4-(2-Amino-4-oxo-4,7-dihydro-3H-pyrrolo[2,3-d]pyrimidin-6-yl)butyl)-3-fluorobenzoyl)-L-glutamic acid (180).

Compound **180** was prepared using the general method described for the preparation of **179-180**, from **215** (60 mg, 0.13 mmol) to give **180** (50 mg, 93%) as a light yellow powder. ¹H NMR (400 MHz, DMSO-*d*₆): δ 1.5-1.60 (m, 4 H, CH₂CH₂), 1.89-2.12 (m, 2 H, α-CH₂), 2.32-2.35 (m, 2H, β-CH₂), 2.65-2.68 (m, 2 H, Ar-CH₂), 4.35-4.43 (m, 1 H, α-CH), 5.8 (s,

1 H, C5-CH), 5.99 (s, 2 H, 2-NH₂, exch), 7.37-7.41 (m, 1 H, Ar), 7.6-7.65 (m, 2 H, Ar), 8.61-8.63 (d, *J* = 8.2 Hz, 1 H, CONH, exch), 10.2 (s, 1 H, 3-NH, exch), 10.80 (s, 1 H, 7-NH, exch). Anal. Calcd for C₂₂H₂₄FN₅O₆ · 1.15 H₂O: C, 53.46; H, 5.36; N, 14.17; F, 3.84. Found: C, 53.54; H, 5.11; N, 13.83; F, 3.64. mp 163.1 °C dec.

Methyl 2-fluoro-4-(4-hydroxybut-1-yn-1-yl)benzoate (224).

To a solution of 3-butynol **222** (508 g, 8.25 mmol) and methyl 4-bromo-2-fluorobenzoate **223** (2 g, 8.6 mmol, 1.04 eq) in anhydrous acetonitrile (10 mL) was added palladium chloride (59 mg, 0.33 mmol, 0.04 eq), triphenylphosphine (86.6 mg, 0.33 mmol, 0.04 eq), copper iodide (251.4 mg, 1.32 mmol, 0.16 eq), and triethylamine (11.5 mL, 86mmol, 10 eq). The reaction mixture was heated to 100 °C and run for 0.5 h under microwave heating until the starting material disappeared a new polar spot was observed on TLC (hexane/EtOAc). A silica plug was prepared by adding silica gel and methanol followed by evaporation of the solvent in vacuo, which was then loaded on to a silica gel column and eluted with hexane followed by 50% EtOAc in hexane. The fractions with the desired *R_f* were pooled and evaporated to afford **224** (1.2 g, 65%) of **19a** as a colorless syrup. TLC *R_f* = 0.2 (hexane/EtOAc, 1:1). ¹H NMR (400 MHz, CDCl₃): δ 1.8 (s, br, OH, exch), 2.73-2.76 (t, *J* = 6.02, 6.02 Hz, 2 H, CH₂), 3.85–3.88 (t, *J* = 6.09, 6.09 Hz, 2 H, CH₂), 3.95 (s, 3 H, COOCH₃), 7.18-7.29 (m, 2 H, Ar), 7.87-7.91 (t, *J* = 7.77, 7.77 Hz, 1 H, Ar). The intermediate **224** was used for the next reaction without further characterization.

Methyl 2-fluoro-4-(4-hydroxybutyl)benzoate (226).

To 10% palladium on activated carbon (600 mg, 0.5 wt eq) in a Parr flask, ethanol (10 mL) was added to quench. Methanolic solution of alcohols **224** (1.2 g, 5.4 mmol) was added

and hydrogenation was carried out at 55 psi of H₂ for 12 h until the disappearance of starting material and formation of a slightly non-polar spot in TLC. The reaction mixture was filtered through celite, washed with MeOH, passed through a short silica gel column (3 cm × 5 cm) and concentrated under reduced pressure to give **226** (1.17 g, 96%) as a colorless syrup. TLC R_f = 0.22 (hexane/EtOAc, 1:1); ¹H NMR (400 MHz, CDCl₃): δ 1.5-1.79 (m, 5 H, CH₂CH₂, OH, exch), 2.67-2.71 (t, *J* = 7.60, 7.60 Hz, 2 H, CH₂), 3.65-3.69 (t, *J* = 6.37, 6.37 Hz, 2 H, CH₂), 3.92 (s, 3 H, COOCH₃), 6.95-6.99 (d, *J* = 1.32 Hz, 1 H, Ar), 7.01-7.04 (dd, *J* = 1.50, 8.02 Hz, 1 H, Ar), 7.83-7.87 (t, *J* = 7.84, 7.84 Hz, 1 H, Ar). The intermediate **226** was used for the next reaction without further characterization.

4-(3-Fluoro-4-(methoxycarbonyl)phenyl)butanoic acid benzoate (227).

To acetonitrile (35mL), periodic acid (3.12g, 13.7 mmol, 2.65 eq), was added and stirred for 15 min. To this solution at 0 °C (in an ice-water bath), compound **226** (1.17 g, 5.17 mmol, 1 eq) was added followed by the addition of PCC (33.44 mg, 0.16 mmol, 0.03 eq). The mixture was then stirred for 6 h until no starting material was detected on TLC a new non-polar spot was observed (hexane/EtOAc). The solvent was evaporated in vacuo to a residue which was dissolved in EtOAc, washed successively with brine-water, satd. aq. NaHSO₃ solution, and brine, dried over anhydrous Na₂SO₄, and concentrated to give **227** (1.2 g, 97%) as a colorless syrup. TLC R_f = 0.58 (hexane/EtOAc 1:1); ¹H NMR (400 MHz, CDCl₃): δ 1.97-2.04 (m, 2 H, CH₂), 2.39-2.43 (t, *J* = 7.31, 7.31 Hz, 2 H, CH₂), 2.72-2.76 (m, 2 H, CH₂), 3.94 (s, 3 H, COOCH₃), 6.98-7.01 (d, *J* = 1.23 Hz, 1 H, Ar), 7.04-7.07 (dd, *J* = 1.37, 8.01 Hz, 1 H, Ar), 7.87-7.91 (t, *J* = 7.82, 7.82 Hz, 1 H, Ar). The intermediate **227** was used for the next reaction without further characterization.

Methyl 4-(3-(2-amino-4-oxo-4,7-dihydro-3H-pyrrolo[2,3-d]pyrimidin-6-yl)propyl)-2-fluorobenzoate (231).

To the solution of acid **227** (500 mg, 2.08 mmol, 1 eq) in anhydrous CH₂Cl₂ (10 mL) was added oxalyl chloride (1.1 mL, 12.5 mmol, 6 eq) and stirred at reflux for 1 h to the acid chloride **228**. After cooling to room temperature, the solvent was evaporated under reduced pressure and without further characterization, the residue was dissolved in Et₂O (10 mL). This was added in a dropwise manner to an ice-cooled (ice-bath) diazomethane solution (generated in situ from diazald (5 eq) by using Aldrich Mini Diazald apparatus). The resulting mixture was allowed to stand for 30 min after which it was stirred for 1 h to afford the unstable α -diazoketone **229**. Subsequently, 48% HBr in water (5 mL, 20 eq) was added to this solution, and stirred at reflux temperature for 1.5 h. The solution was then brought down to room temperature and the organic layer was separated. The aqueous layer was extracted twice with Et₂O (10 mL) and combined with the organic layer. The Et₂O extract was washed twice with 10% Na₂CO₃ (10 mL) solution and dried over Na₂SO₄. Solvent was evaporated under reduced pressure to afford the α -bromoketone **230** as an orange syrup. Without further characterization, the residue was dissolved in anhydrous DMF (5 mL) to which 2,6-diamino-3H-pyrimidin-4-one **22** (275 mg, 2.18 mmol, 1.05 eq), was added. The resulting mixture was stirred at room temperature for 72 h under N₂ until no starting material was detected on TLC a new non-polar spot was observed (CHCl₃/MeOH). The solvent was evaporated to afford a sticky crude solid. MeOH was added to it followed by silica gel and the solvent was evaporated. The resulting plug was loaded on to a silica gel column and eluted with 10% MeOH in CHCl₃. Fractions with desired R_f were pooled and evaporated to afford the crude pterotic ester **231** (200 mg, 28%) as a pink sticky solid. NMR

of the crude **231** clearly had the required peaks of the bicyclic pyrrolo[2,3-*d*]pyrimidine scaffold and the side chain phenyl confirming successful cyclization to **231**. TLC $R_f = 0.45$ (CHCl₃/MeOH 5:1); ¹H NMR (400 MHz, DMSO-*d*₆): δ 1.77-1.94 (m, 2 H, CH₂), 2.45-2.48 (m, 2 H, Ar-CH₂), 2.62-2.74 (m, 2 H, Ar-CH₂), 3.9 (s, 3 H, COOCH₃), 5.72 (s, 1 H, C5-CH), 6.33 (s, 2 H, 2-NH₂, exch), 7.14-7.15, (m, 2 H, Ar), 7.77-8.17, (m, 1 H, Ar), 10.77 (s, 1 H, 3-NH, exch), 11.54 (s, 1 H, 7-NH, exch). The intermediate **231** was used for the next reaction without further characterization.

4-(3-(2-Amino-4-oxo-4,7-dihydro-3H-pyrrolo[2,3-*d*]pyrimidin-6-yl)propyl)-2-fluorobenzoic acid (232).

Saturated methanolic solutions of the crude ester **231** (200 mg, 0.58 mmol) was dissolved in 1 N NaOH (3 mL) and stirred under N₂ for 12 h. Upon consumption of the starting materials and one major polar spot on TLC was obtained, the pH was adjusted to 3–4 with dropwise addition of 1 N HCl to form a precipitate. The resulting suspensions were cooled in the refrigerator overnight and filtered, washed with cold water and dried under reduced pressure using P₂O₅ to afford the crude acid **232** (90 mg, 47%) as a yellow powder. TLC $R_f = 0.4$ (CHCl₃/MeOH 5:1); ¹H NMR (400 MHz, DMSO-*d*₆): δ 1.79-1.92 (m, 2 H, CH₂), 2.63-2.69 (m, 2 H, CH₂), 5.94 (s, 1 H, C5-CH), 7.16-7.21 (m, 2 H, Ar), 7.79-7.84 (m, 1 H, Ar), 10.3 (s, 1 H, 3-NH, exch), 10.97 (s, 1 H, 7-NH, exch). The intermediate **232** was used for the next reaction without further characterization.

Diethyl (4-(3-(2-amino-4-oxo-4,7-dihydro-3H-pyrrolo[2,3-d]pyrimidin-6-yl)propyl)-2-fluorobenzoyl)-L-glutamate (233).

A mixture of the crude acid **232** (90 mg, 0.3 mmol, 1 eq), *N*-methyilmorpholine (33.07 mg, 0.33 mmol, 1.2 eq) and 2-chloro-4,6-dimethoxy-1,3,5 triazine (57.40 mg, 0.33 mmol, 1.2 eq) in anhydrous DMF (5 mL) was stirred at room temperature for 2 h. *N*-methyilmorpholine (33.07 mg, 0.33 mmol, 1.2 eq) and L-glutamate diethyl ester hydrochloride (83.06 mg, 0.4 mmol, 1.5 eq) were then added to the mixture and stirred for an additional 4 h at room temperature until disappearance of starting material and formation of a new non-polar major spot (CHCl₃/MeOH). The residue obtained after evaporation of the solvent under reduced pressure was dissolved in MeOH followed by addition of silica gel. The solution was evaporated to from a silica plug and chromatographed on a silica gel column and eluted with CHCl₃ followed by gradual increase of polarity to 5% MeOH in CHCl₃. Fractions that showed the desired R_f were pooled and the solvent was evaporated to dryness under reduced pressure to afford the intermediate glutamate esters **233** (70 mg, 50%) as an orange sticky solid. TLC R_f = 0.5 (CHCl₃/MeOH 5:1); ¹H NMR (400 MHz, DMSO-*d*₆): δ 1.15-1.20 (m, 8H, COOCH₂CH₃, CH₂), 1.91-2.13 (m, 2 H, β-CH₂), 2.40-2.44 (m, 2 H, γ-CH₂), 3.54-3.56 (t, *J* = 4.28, 4.28 Hz, 2 H, CH₂), 4.02-4.12 (m, 4 H, COOCH₂CH₃), 4.38-4.43 (m, 1 H, α-CH), 5.69 (s, 1 H, C5-CH), 6.3 (s, 2 H, 2-NH₂, exch), 7.13-7.17 (m, 2 H, Ar), 7.46-7.50 (t, *J* = 7.75, 7.75 Hz, 1 H, Ar), 8.59-8.61 (d, *J* = 6.97 Hz, 1 H, CONH, exch), 10.75 (s, 1H, 7-NH, exch). The intermediate **233** was used for the next reaction without further characterization.

(4-(3-(2-Amino-4-oxo-4,7-dihydro-3H-pyrrolo[2,3-d]pyrimidin-6-yl)propyl)-2-fluorobenzoyl)-L-glutamic acid (181).

Compound **181** was prepared using the general method described for the preparation of **179-180** (70 mg, 0.15 mmol) to give 55 mg (88%) of **9** as a light yellow powder. mp 139.4 °C dec. ¹H NMR (500 MHz, DMSO-*d*₆): δ 1.87-2.11 (m, 4 H, CH₂, β-CH₂), 2.33-2.37 (dt, *J* = 2.92, 7.89, 8.12 Hz, 2 H, γ-CH₂), 2.64-2.67 (t, *J* = 7.53, 7.53 Hz, 2 H, Ar-CH₂), 4.37-4.41 (m, 1 H, α-CH), 5.89-5.90 (d, *J* = 2.11 Hz, 1 H, C5-CH), 6.01 (s, 2 H, 2-NH₂, exch), 7.13-7.17 (m, 2 H, Ar), 7.53-7.56 (t, *J* = 7.80, 7.80 Hz, 1 H, Ar), 8.44-8.46 (dd, *J* = 2.12, 7.64 Hz, 1 H, CONH, exch), 10.17 (s, 1 H, 3-NH, exch), 10.86 (s, 1 H, 7-NH, exch). Anal. Calcd for C₂₁H₂₂FN₅O₆ · 1.11 H₂O: C, 52.60; H, 5.09; N, 14.60; F, 3.96. Found: C, 52.58; H, 5.02; N, 14.68; F, 3.88.

Ethyl 3-fluoro-5-(4-hydroxybut-1-yn-1-yl)picolinate (240).

To a solution of 3-butynol **222** (243 mg, 3.47 mmol, 1 eq) and ethyl 5-bromo-3-fluoropicolinate **239** (895 mg, 3.61 mmol, 1.04 eq) in anhydrous acetonitrile (10 mL) was added palladium chloride (24.6 mg, 0.14 mmol, 0.04 eq), triphenylphosphine (36.4 mg, 0.14 mmol, 0.04 eq), copper iodide (106 mg, 0.55 mmol, 0.16 eq), and triethylamine (5 mL, 35 mmol, 10 eq). The reaction mixture was heated to 100 °C and run for 30 min under microwave heating until the starting material disappeared and a new polar spot was observed under TLC (hexane/EtOAc). A silica plug was prepared by adding silica gel and methanol followed by evaporation of the solvent in vacuo, which was then loaded on to a silica gel column and eluted with hexane followed by 50% EtOAc in hexane. The desired fractions (TLC) were pooled and evaporated to afford **240** (511 mg, 62%) as a yellow

syrup. TLC R_f = 0.25 (hexane/EtOAc, 3:1); ^1H NMR (400 MHz, CDCl_3): δ 1.3-1.34 (t, J = 7.14, 7.14 Hz, 3 H, $\text{COOCH}_2\text{CH}_3$), 2.63-2.66 (t, J = 6.30, 6.30 Hz, 2 H, CH_2), 3.6-3.63 (m, 2 H, CH_2), 4.34-4.38 (q, J = 7.15, 7.15, 7.14 Hz, 2 H, $\text{COOCH}_2\text{CH}_3$), 4.98 (s, br, 1 H, OH), 7.98-8.01 (dd, J = 1.48, 10.59 Hz, 1 H, Ar) 8.55 (s, 1 H, Ar). The intermediate **240** was used for the next reaction without further characterization.

Ethyl 3-fluoro-5-(4-hydroxybutyl)picolinate (241).

To 10% palladium on activated carbon (250 mg, 0.5 wt eq) in a Parr flask, ethanol (5 mL) was added to quench. Methanolic solution of alcohols **240** (511 mg, 2.15 mmol) was added and hydrogenation was carried out at 55 psi of H_2 for 6 h until the disappearance of starting material and formation of a slightly non-polar spot in TLC. The reaction mixture was filtered through celite, washed with MeOH, passed through a short silica gel column (3 cm \times 5 cm) and concentrated under reduced pressure to give **241** (500 mg, 96%) as a yellow syrup. TLC R_f = 0.27 (hexane/EtOAc, 3:1); ^1H NMR (400 MHz, $\text{DMSO}-d_6$): δ 1.3-1.34 (t, J = 7.11, 7.11 Hz, 3 H, $\text{COOCH}_2\text{CH}_3$), 1.38-1.47 (td, J = 6.45, 6.45, 13.24 Hz, 2 H, CH_2), 1.6-1.68 (td, J = 7.64, 7.64, 15.37 Hz, 2 H, CH_2), 2.7-2.73 (m, 2 H, Ar- CH_2), 3.39-3.43 (m, 2 H, OH- CH_2), 4.3-4.37 (q, J = 7.09, 7.09, 7.11 Hz, 2 H, $\text{COOCH}_2\text{CH}_3$), 4.4-4.43 (t, J = 5.19, 5.19 Hz, 1 H, OH, exch), 7.77-7.8 (dd, J = 1.28, 11.70 Hz, 1 H, Ar), 8.41-8.44 (s, 1 H, Ar). The intermediate **240** was used for the next reaction without further characterization.

4-(6-(ethoxycarbonyl)-5-fluoropyridin-3-yl)butanoic acid (242).

To acetonitrile (6 mL), periodic acid (1.25 g, 5.5 mmol, 2.65 eq) was added and stirred for 15 min. To this solution at 0°C (in an ice-water bath), compound **241** (500 mg, 2.07 mmol,

1 eq) was added followed by the addition of PCC (11.2 mg, 0.06 mmol, 0.03 eq). The mixture was then stirred for 6 h until no starting material and a non-polar spot was detected on TLC (hexane/EtOAc). The solvent was evaporated in vacuo to a residue which was dissolved in EtOAc, washed successively with brine–water, satd. Aq. NaHSO₃ solution, and brine, dried over anhydrous Na₂SO₄, and concentrated to give **242** (425 mg, 80%) as a yellow syrup. TLC R_f = 0.6 (hexane/EtOAc 1:1); ¹H NMR (400 MHz, CDCl₃): δ 1.31-1.33 (t, *J* = 7.09, 7.09 Hz, 3 H, COOCH₂CH₃), 1.83-1.89 (m, 2 H, CH₂), 2.24-2.27 (t, *J* = 7.37, 7.37 Hz, 2 H, CH₂), 2.71-2.75 (t, *J* = 7.68, 7.68 Hz, 2 H, CH₂), 4.33-4.38 (q, *J* = 7.07, 7.07, 7.08 Hz, 2 H, COOCH₂CH₃), 7.78-7.8 (dd, *J* = 1.14, 11.61 Hz, 1 H, Ar), 8.41 (s, 1 H, Ar), 12.09 (s, br, 1 H, COOH, exch). The intermediate **240** was used for the next reaction without further characterization.

Ethyl 5-(3-(2-amino-4-oxo-4,7-dihydro-3*H*-pyrrolo[2,3-*d*]pyrimidin-6-yl)propyl)-3-fluoropicolinate (246).

To the solution of acid **242** (426 mg, 1.67 mmol, 1 eq) in anhydrous CH₂Cl₂ (5 mL) was added oxalyl chloride (1.43 mL, 16.7 mmol, 10 eq) and stirred at reflux for 1 h to the acid chloride **243**. After cooling to room temperature, the solvent was evaporated under reduced pressure and without further characterization, the residue was dissolved in Et₂O. This was added in a dropwise manner to an ice-cooled (ice-bath) diazomethane solution (generated in situ from diazald (5 eq) by using Aldrich Mini Diazald apparatus). The resulting mixture was allowed to stand for 30 min after which it was stirred for 1 h to afford the unstable α-diazoketone **244**. Subsequently, 48% HBr (5 mL, 20 eq) in water was added to this solution, and stirred at reflux temperature for 1.5 h. The solution was then brought down to room temperature and the organic layer was separated. The aqueous layer was extracted twice

with Et₂O (10 mL) and combined with the organic layer. Furthermore, the pH of the aqueous layer was carefully neutralized using 10% Na₂CO₃ and extracted with Et₂O (2X10 mL). The organic layers were combined and were washed twice with 10% Na₂CO₃ (10 mL) solution and dried over Na₂SO₄. Solvent was evaporated under reduced pressure to afford the α -bromoketone **245** as an orange syrup. Without further characterization, the residue was dissolved in anhydrous DMF (5 mL) to which 2,6-diamino-3*H*-pyrimidin-4-one **22** (211 mg, 1.67 mmol, 1 eq), was added. The resulting mixture was stirred at room temperature for 72 h under N₂ until a new non-polar spot was observed under TLC (CHCl₃/MeOH), after which the solvent was evaporated to afford a sticky crude solid. MeOH was added to it followed by silica gel and the solvent was evaporated. The resulting plug was loaded on to a silica gel column and eluted with 10% MeOH in CHCl₃. Fractions with desired R_f were pooled and evaporated to afford the crude pterioic ester **246** (180 mg, 30%) as a orange-brown sticky solid. TLC R_f = 0.4 (CHCl₃/MeOH 5:1); ¹H NMR (400 MHz, DMSO-*d*₆): δ 1.3-1.34 (t, *J* = 7.10, 7.10 Hz, 3 H, COOCH₂CH₃), 1.91-1.99 (td, *J* = 7.53, 7.53, 14.92 Hz, 2 H, CH₂), 2.72-2.76 (m, 2 H, Ar-CH₂), 4.32-4.38 (q, *J* = 7.10, 7.10, 7.08 Hz, 2 H, COOCH₂CH₃), 5.99-6.01 (d, *J* = 1.70 Hz, 1 H, C5-CH), 6.59 (s, br, 2 H, 2-NH₂, exch), 7.79-7.82 (d, *J* = 11.73 Hz, 1 H, Ar), 8.41 (s, 1 H, Ar), 10.67 (s, br, 1 H, 3-NH, exch), 11.1 (s, br, 1 H, 7-NH, exch). The intermediate **246** was used for the next reaction without further characterization.

5-(3-(2-amino-4-oxo-4,7-dihydro-3*H*-pyrrolo[2,3-*d*]pyrimidin-6-yl)propyl)-3-fluoropicolinic acid (247).

Saturated methanolic solutions of the crude ester **246** (150 mg, 0.42 mmol) was dissolved in 1 N NaOH (3 mL) was added and stirred under N₂ for 12 h. Upon consumption of the

starting materials and one major polar spot (CHCl₃/MeOH) on a TLC was obtained, the pH adjusted to 3–4 with dropwise addition of 1 N HCl to form a precipitate. The resulting suspensions were cooled in the refrigerator overnight and filtered, washed with cold water and dried under reduced pressure using P₂O₅ to afford the crude acid **247** (110 mg, 80%) as a yellow powder. TLC R_f = 0.3 (CHCl₃/MeOH 5:1); ¹H NMR (400 MHz, DMSO-*d*₆): δ 1.93-1.98 (m, 2 H, CH₂), 2.70-2.74 (m, 2 H, Ar-CH₂), 5.91-5.913 (d, *J*=1.21 Hz, 1 H, C5-CH), 6.08 (s, 2 H, 2-NH₂, exch), 7.75-7.78 (d, *J*=11.61 Hz, 1 H, Ar), 8.39 (s, 1 H, Ar), 10.23 (s, 1 H, 3-NH, exch), 10.84 (s, 1 H, 7-NH, exch). The intermediate **247** was used for the next reaction without further characterization.

Diethyl (5-(3-(2-amino-4-oxo-4,7-dihydro-3*H*-pyrrolo[2,3-*d*]pyrimidin-6-yl)propyl)-3-fluoropicolinoyl)-L-glutamate (248).

A mixture of the crude acid **247** (95 mg, 0.29 mmol, 1 eq), *N*-methylmorpholine (0.04 mL, 0.34 mmol, 1.2 eq) and 2-chloro-4,6-dimethoxy-1,3,5 triazine (60.40 mg, 0.34 mmol, 1.2 eq) in anhydrous DMF (5 mL) was stirred at room temperature for 2 h. *N*-methylmorpholine (0.04 mL, 0.34 mmol, 1.2 eq) and L-glutamate diethyl ester hydrochloride (87.4 mg, 0.43 mmol, 1.5 eq) were then added to the mixture and stirred for an additional 4 h at room temperature until disappearance of starting material and formation of a new non-polar major spot on TLC (CHCl₃/MeOH). The residue obtained after evaporation of the solvent under reduced pressure was dissolved in MeOH followed by addition of silica gel. The solution was evaporated to from a silica plug and chromatographed on a silica gel column with CHCl₃ as the eluent and gradual increase in polarity to 5% MeOH in CHCl₃ as the eluent. Fractions that showed the desired R_f were pooled and the solvent was evaporated to dryness under reduced pressure to afford the

intermediate glutamate esters **248** (80 mg, 54%) as an orange sticky solid. TLC $R_f = 0.5$ ($\text{CHCl}_3/\text{MeOH}$ 5:1); $^1\text{H NMR}$ (400 MHz, $\text{DMSO}-d_6$): δ 1.14-1.24 (m, 6 H, $\text{COOCH}_2\text{CH}_3$), 1.93-2.18 (m, 4 H, CH_2 , $\beta\text{-CH}_2$), 2.38-2.42 (m, 2 H, $\gamma\text{-CH}_2$), 2.72-2.75 (m, 2 H, Ar- CH_2), 4.01-4.06 (dd, $J=7.00$, 14.10 Hz, 2 H, $\text{COOCH}_2\text{CH}_3$), 4.1-4.16 (m, 2 H, $\text{COOCH}_2\text{CH}_3$), 4.45-4.52 (m, 1 H, $\alpha\text{-CH}$), 5.91-5.92 (d, $J=1.47$ Hz, 1 H, C5-CH), 5.98 (s, 2 H, 2- NH_2 , exch), 7.75-7.78 (dd, $J = 0.76$, 12.20 Hz, 1 H, Ar), 8.38 (s, 1 H, Ar), 8.89-8.91 (d, $J = 7.92$ Hz, 2 H, CONH, exch), 10.15 (s, 1 H, 3-NH, exch), 10.83 (s, 1 H, 7-NH, exch). The intermediate **248** was used for the next reaction without further characterization.

(5-(3-(2-amino-4-oxo-4,7-dihydro-3H-pyrrolo[2,3-d]pyrimidin-6-yl)propyl)-3-fluoropicolinoyl)-L-glutamic acid (182).

Compound **182** was prepared using the general method described for the preparation of **179-180** (80 mg, 0.15 mmol) to give **182** (50 mg, 70%) as a light yellow powder. mp 161.9 °C. $^1\text{H NMR}$ (400 MHz, $\text{DMSO}-d_6$): δ 1.91-2.17 (m, 4 H, CH_2 , $\alpha\text{-CH}_2$), 2.3-2.33 (t, $J=7.33$, 7.33 Hz, 2 H, $\beta\text{-CH}_2$), 2.71-2.75 (t, $J=7.33$, 7.33 Hz, 2 H, Ar- CH_2), 4.44-4.49 (m, 1 H, $\alpha\text{-CH}$), 5.92 (s, 1 H, C5-CH), 5.97 (s, 2 H, 2- NH_2 , exch), 7.75-7.78 (d, $J=11.88$ Hz, 1 H, Ar), 8.37 (s, 1 H, Ar), 8.76-8.78 (d, $J=8.20$ Hz, 1 H, CONH, exch), 10.13 (s, 1 H, 3-NH, exch), 10.83 (s, 1 H, 7-NH, exch). Anal. Calcd for $\text{C}_{20}\text{H}_{21}\text{FN}_6\text{O}_6 \cdot 1.08 \text{H}_2\text{O}$: C, 50.05; H, 4.86; N, 17.5; F, 3.95. Found: C, 50.15; H, 5.17; N, 17.37; F, 3.81.

Diethyl (5-bromo-3-fluoropicolinoyl)-L-glutamate (250).

Compound **250** was prepared using the general method described for the preparation of **210-211**, from 5-bromo-3-fluoropicolinic acid **249** (2 g, 9 mmol), to give **250** (2.7 g, 73%) of as a yellow syrup. TLC $R_f = 0.45$ (hexane/EtOAc, 1:1). $^1\text{H NMR}$ (400 MHz, CDCl_3): δ

1.26-1.29 (t, $J = 7.14, 7.14$ Hz, 3 H, γ -COOCH₂CH₃) 1.31-1.35 (t, $J = 7.13, 7.13$ Hz, 3 H, α -COOCH₂CH₃), 2.08-2.57 (m, 4 H, β -CH₂ and γ -CH₂), 4.13-4.18 (q, $J = 7.15, 7.15, 7.14$ Hz, 2 H, COOCH₂CH₃) 4.24-4.29 (q, $J = 7.14, 7.14, 7.13$ Hz, 2 H, COOCH₂CH₃), 4.80-4.86 (dt, $J = 4.95, 7.70, 7.63$ Hz, 1 H, α -CH), 6.78-6.80 (d, $J = 7.52$ Hz, 1 H, CONH, exch), 7.18-7.2 (m, 2 H, Ar). The intermediate **250** was used for the next reaction without further characterization.

Diethyl (5-(4-(2-amino-4-oxo-4,7-dihydro-3H-pyrrolo[2,3-d]pyrimidin-6-yl)but-1-yn-1-yl)-3-fluoropicolinoyl)-L-glutamate (251).

Compound **251** was prepared using the general method described for the preparation of **212-213**, from **162** (100 mg, 0.5 mmol) and diethyl (5-bromo-3-fluoropicolinoyl)-L-glutamate, **250** (300 mg, 0.74 mmol) to give **251** (116.6 mg, 45%) as a brown sticky solid; TLC $R_f = 0.5$ (CHCl₃/MeOH 5:1); ¹H NMR (400 MHz, DMSO-*d*₆): δ 1.14-1.21 (m, 6 H, COOCH₂CH₃), 1.95-2.18 (m, 2 H, β -CH₂), 2.38-2.42 (t, $J = 8.07, 8.07$ Hz, 2 H, γ -CH₂), 4.01-4.06 (q, $J = 7.11, 7.11, 7.10$ Hz, 2 H, γ -COOCH₂CH₃), 4.09-4.16 (dq, $J = 1.80, 7.02, 6.93, 6.93$ Hz, 2 H, α -COOCH₂CH₃), 4.44-4.49 (m, 1 H, α -CH), 6.01-6.04 (m, 3 H, C5-CH, 2-NH₂, exch), 7.92-7.96 (dd, $J = 1.53, 11.24$ Hz, 1 H, Ar), 8.47 (s, 1 H, Ar), 8.98-9.00 (d, $J = 7.89$ Hz, 1 H, CONH, exch), 10.18 (s, 1 H, 3-NH, exch), 10.91-10.92 (d, $J = 1.71$ Hz, 1H, 7-NH, exch). The intermediate **251** was used for the next reaction without further characterization.

Diethyl (5-(4-(2-amino-4-oxo-4,7-dihydro-3H-pyrrolo[2,3-d]pyrimidin-6-yl)butyl)-3-fluoropicolinoyl)-L-glutamate (252).

Compound **252** was prepared using the general method described for the preparation of **214-215**, from **251** (116 mg, 0.13 mmol) to give **252** (91 mg, 78%) as a light yellow sticky solid. TLC $R_f = 0.51$ ($\text{CHCl}_3/\text{MeOH}$ 5:1); ^1H NMR (400 MHz, $\text{DMSO-}d_6$): δ 1.11-1.25 (m, 6 H, $\text{COOCH}_2\text{CH}_3$), 1.53-1.65 (m, 4 H, CH_2CH_2), 1.99-2.17 (m, 2 H, $\beta\text{-CH}_2$), 2.38-2.42 (m, 2 H, $\gamma\text{-CH}_2$), 2.65-2.75 (m, 2 H, Ar- CH_2), 3.96-4.16 (m, 4 H, $\text{COOCH}_2\text{CH}_3$), 4.40-4.54 (m, 1 H, $\alpha\text{-CH}$), 5.84-5.88 (m, 1 H, C5-CH), 6.08 (s, 2 H, 2-NH₂, exch), 7.71-7.8 (d, $J=10.98$ Hz, 1 H, Ar), 8.38 (s, 1 H, Ar), 8.84-8.98 (m, 1 H, CONH, exch), 10.79 (s, 1 H, 7-NH, exch). The intermediate **252** was used for the next reaction without further characterization.

(5-(4-(2-Amino-4-oxo-4,7-dihydro-3H-pyrrolo[2,3-d]pyrimidin-6-yl)butyl)-3-fluoropicolinoyl)-L-glutamic acid (183).

Compound **183** was prepared using the general method described for the preparation of **179-180**, from **252** (91 mg, 0.17 mmol) to give **183** (70 mg, 86%) as a brown powder. ^1H NMR (400 MHz, $\text{DMSO-}d_6$): δ 1.56-1.69 (m, 4 H, CH_2CH_2), 1.96-2.34 (m, 4 H, $\beta\text{-CH}_2$, $\gamma\text{-CH}_2$), 2.70-2.73 (m, 2 H, Ar- CH_2), 4.31-4.37 (m, 1 H, $\alpha\text{-CH}$), 5.87-5.88 (d, $J = 2.12$ Hz, 1 H, C5-CH), 5.98 (s, 2 H, 2-NH₂, exch), 7.71-7.75 (dd, $J=1.37, 11.85$ Hz, 1 H, Ar), 8.37 (s, 1 H), 8.68-8.70 (d, $J = 7.81$ Hz, 1 H, CONH, exch), 10.15 (s, 1 H, 3-NH, exch), 10.81 (s, 1 H, 7-NH, exch). Anal. Calcd for $\text{C}_{21}\text{H}_{23}\text{FN}_6\text{O}_6 \cdot 2.02 \text{H}_2\text{O} \cdot 0.21 \text{NaCl}$: C, 48.21; H, 5.21; N, 16.06; F, 3.63, Cl, 1.40. Found: C, 48.12; H, 5.21; N, 16.37; F, 3.50, Cl, 1.14. mp 200.6 °C dec.

Methyl 3-fluoro-4-(4-hydroxybut-1-yn-1-yl)thiophene-2-carboxylate (254).

To a solution of 3-butynol **222** (0.5 g, 7.13 mmol) and ethyl 4-bromo-3-fluorothiophene-2-carboxylate **253** (1.9 g, 7.42 mmol) in anhydrous acetonitrile (10 mL) was added palladium chloride (51 mg, 0.28 mmol, 0.04 eq), triphenylphosphine (75 mg, 0.28 mmol, 0.04 eq), copper iodide (218 mg, 1.14 mmol, 0.16 eq), and triethylamine (10 mL, 71.3 mmol, 10 eq). The reaction mixture was heated to 100 °C and run for 30 min under microwave heating until the starting material disappeared and a new polar spot was detected on TLC (hexane/EtOAc). A silica plug was prepared by adding silica gel and methanol followed by evaporation of the solvent in vacuo. The plug was then loaded on to a silica gel column and eluted with hexane followed by gradual increase to 50% EtOAc in hexane. The fractions with desired R_f were pooled and evaporated to afford **254** (1.1 g, 64%) as a yellow syrup. TLC R_f = 0.25 (hexane/EtOAc, 1:1); $^1\text{H NMR}$ (400 MHz, CDCl_3): δ 2.70-2.73 (t, J = 6.23, 6.23 Hz, 2 H, CH_2), 3.83-3.86 (t, J = 6.23, 6.23 Hz, 2 H, CH_2), 3.81 (s, 3 H, COOCH_3), 7.46-7.47 (d, J = 4.15 Hz, 1 H, Ar). The intermediate **254** was used for the next reaction without further characterization.

Methyl 3-fluoro-4-(4-hydroxybutyl)thiophene-2-carboxylate (255).

To 10% palladium on activated carbon (500 mg, 0.5 wt eq) in a Parr flask, ethanol (10 mL) was added to quench. Methanolic solution of alcohol **254** (1.4 g, 5.78 mmol) was added and hydrogenation was carried out at 55 psi of H_2 for 12 h until the disappearance of starting material and formation of a slightly non-polar spot on TLC (hexane/EtOAc). The reaction mixture was filtered through celite, washed with MeOH, passed through a short silica gel column (3 cm \times 5 cm) and concentrated under reduced pressure to give **255** (1.1 g, 98%) as a yellow syrup. TLC R_f = 0.25 (hexane/EtOAc 1:1); $^1\text{H NMR}$ (400 MHz,

DMSO-*d*₆): δ 1.39-1.46 (td, $J = 6.47, 6.47, 13.30$ Hz, 2 H, CH₂), 1.54-1.62 (td, $J = 7.63, 7.63, 15.45$ Hz, 2 H, CH₂), 3.8 (s, 3 H, COOCH₃), 3.38-3.42 (dd, $J = 6.32, 11.63$ Hz, 2 H, CH₂), 4.4-4.43 (t, $J=5.15, 5.15$ Hz, 1 H, OH, exch), 7.65-7.67 (d, $J = 4.80$ Hz, 1 H, Ar).

The intermediate **255** was used for the next reaction without further characterization.

4-(4-Fluoro-5-(methoxycarbonyl)thiophen-3-yl)butanoic acid (256).

To acetonitrile (20 mL), periodic acid (3 g, 13.3 mmol, 2.65 eq), was added and stirred for 15 min. To this solution at 0 °C (in an ice–water bath), compound **255** (1.4 g, 6 mmol, 1 eq) was added followed by the addition of PCC (26 mg, 0.12 mmol, 0.02 eq). The mixture was then stirred for 6 h until no starting material was detected and a new non-polar spot was detected on TLC (hexane/EtOAc). The solvent was evaporated in vacuo to a residue which was dissolved in EtOAc, washed successively with brine–water, satd. Aq. NaHSO₃ solution, and brine, dried over anhydrous Na₂SO₄, and concentrated to give **256** (1.2 g, 79%) as a yellow syrup. TLC $R_f = 0.65$ (hexane/EtOAc 1:1). ¹H NMR (400 MHz, CDCl₃): δ 1.94-2.01 (td, $J = 7.34, 7.34, 14.47$ Hz, 2 H, CH₂), 2.41-2.45 (t, $J = 7.29, 7.29$ Hz, 2 H), 2.62-2.66 (t, 2 H, CH₂), 3.91 (s, 3 H, COOCH₃), 7.11-7.17 (d, $J = 4.29$ Hz, 1 H). The intermediate **256** was used for the next reaction without further characterization.

4-(3-(2-amino-4-oxo-4,7-dihydro-3H-pyrrolo[2,3-d]pyrimidin-6-yl)propyl)-3-fluorothiophene-2-carboxylate (260).

To the solution of acid **256** (1.18 g, 4.79 mmol, 1 eq) in anhydrous CH₂Cl₂ (10 mL) was added oxalyl chloride (2.5 mL, 28.75 mmol, 6 eq) and stirred at reflux for 1 h to the acid chloride **257**. After cooling to room temperature, the solvent was evaporated under reduced pressure and without further characterization the residue was dissolved in Et₂O. This was

added in a dropwise manner to an ice-cooled (ice-bath) diazomethane solution (generated in situ from diazald (5 eq) by using Aldrich Mini Diazald apparatus). The resulting mixture was allowed to stand for 30 min after which it was stirred for 1 h to afford the unstable α -diazoketone **258**. Subsequently, 48% HBr (10 mL, 20 eq) in water was added to this solution, and stirred at reflux temperature for 1.5 h. The solution was then brought down to room temperature and the organic layer was separated. The aqueous layer was extracted twice with Et₂O and combined with the organic layer. The Et₂O extract was washed twice with 10% Na₂CO₃ solution and dried over Na₂SO₄. Solvent was evaporated under reduced pressure to afford the α -bromoketone **259** as an orange syrup. Without further characterization, the residue was dissolved in anhydrous DMF (5 mL) to which 2,6-diamino-3*H*-pyrimidin-4-one **22** (604 mg, 4.79 mmol, 1 eq), was added. The resulting mixture was stirred at room temperature for 72 h under N₂, until a new non-polar spot was observed under TLC (CHCl₃/MeOH) The solvent was evaporated to afford a sticky crude solid to which MeOH was added followed by silica gel and subsequently evaporated. The resulting plug was loaded on to a silica gel column and eluted with 10% MeOH in CHCl₃. The collected fractions were pooled and evaporated to afford a pink sticky solid (TLC R_f = 0.4; CHCl₃/MeOH 5:1) which was without further characterization, dissolved in minimal amount of methanol and 1 N NaOH (3 mL) and stirred for 12 h. Upon completion of base-catalyzed hydrolysis and consumption of the starting materials and appearance of one major polar spot on a TLC was obtained (CHCl₃/MeOH), the pH adjusted to 3–4 with dropwise addition of 1 N HCl to form a precipitate. The resulting suspensions were cooled in the refrigerator overnight and filtered, washed with cold water and dried under reduced pressure using P₂O₅ to afford the crude acid **260** (100 mg, 7%) as a buff colored powder.

TLC $R_f = 0.3$ ($\text{CHCl}_3/\text{MeOH}$ 5:1); $^1\text{H NMR}$ (400 MHz, $\text{DMSO}-d_6$): δ 1.81-1.89 (td, $J = 7.50, 7.50, 15.20$ Hz, 2 H, CH_2), 2.46-2.5 (m, 2 H, Ar- CH_2), 5.89-5.90 (d, $J = 2.10$ Hz, 1 H, C5-CH), 6.08 (s, 1 H, 2- NH_2 , exch), 7.40-7.41 (m, 1 H, Ar), 10.26 (s, 1 H, 3-NH, exch), 10.85 (s, 1 H, 7-NH, exch). The intermediate **260** was taken forward without further characterization.

Diethyl (4-(3-(2-amino-4-oxo-4,7-dihydro-3H-pyrrolo[2,3-d]pyrimidin-6-yl)propyl)-3-fluorothiophene-2-carbonyl)-L-glutamate (261).

A mixture of the crude acid **260** (70 mg, 0.2 mmol, 1 eq), *N*-methylmorpholine (0.02 mL, 0.25 mmol, 1.2 eq) and 2-chloro-4,6-dimethoxy-1,3,5 triazine (44 mg, 0.25 mmol, 1.2 eq) in anhydrous DMF (5 mL) was stirred at room temperature for 2 h. *N*-methylmorpholine (0.02 mL, 0.25 mmol, 1.2 eq) and L-glutamate diethyl ester hydrochloride (63 mg, 0.3 mmol, 1.5 eq) were then added to the mixture and stirred for an additional 4 h at room temperature until disappearance of starting material and formation of a new non-polar major spot ($\text{CHCl}_3/\text{MeOH}$). The residue obtained after evaporation of the solvent under reduced pressure was dissolved in MeOH followed by addition of silica gel. The solution was evaporated to from a silica plug and chromatographed on a silica gel column and eluted initially with CHCl_3 followed by gradual increase to 10% MeOH in CHCl_3 . Fractions with the desired R_f were pooled and the solvent was evaporated to dryness under reduced pressure to afford the intermediate glutamate esters **261** (30 mg, 28%) as an orange sticky solid. TLC $R_f = 0.5$ ($\text{CHCl}_3/\text{MeOH}$ 5:1); $^1\text{H NMR}$ (400 MHz, $\text{DMSO}-d_6$): δ 1.11-1.21 (m, 6H, $\text{COOCH}_2\text{CH}_3$), 1.86-1.91 (m, 2 H, CH_2) 1.96-2.17 (m, 2 H, $\beta\text{-CH}_2$), 2.38-2.42 (t, $J = 7.65$ Hz, 2H, $\gamma\text{-CH}_2$), 4.01-4.14 (m, 4H, $\text{COOCH}_2\text{CH}_3$), 4.38-4.44 (m, 1H, $\alpha\text{-CH}$), 5.91-5.92 (d, $J = 2.07$ Hz, 1 H, C5-CH), 5.99 (s, 1 H, 2- NH_2 , exch), 7.55-7.56 (d, $J = 4.65$ Hz,

1 H, Ar), 8.15-8.17 (dd, $J = 2.98, 7.38$ Hz, 1 H, CONH, exch), 10.16 (s, 1 H, 3-NH, exch), 10.86 (s, 1 H, 7-NH, exch). The intermediate **261** was used for the next reaction without further characterization.

(4-(3-(2-Amino-4-oxo-4,7-dihydro-3H-pyrrolo[2,3-d]pyrimidin-6-yl)propyl)-3-fluorothiophene-2-carbonyl)-L-glutamic acid (184).

Compound **184** was prepared using the general method described for the preparation of **179-180** from **261** (30 mg, 0.15 mmol) to give **184** (20 mg, 75%) as a yellow powder. mp 207.8 °C dec. ¹H NMR (400 MHz, DMSO-*d*₆): δ 1.84-2.14 (m, 4 H, CH₂, β -CH₂), 2.30-2.34 (t, $J = 7.37, 7.37$ Hz, 2 H, γ -CH₂), 2.52-2.55 (m, 2 H, Ar-CH₂), 4.35-4.41 (m, 1 H, α -CH), 5.91-5.92 (d, $J = 1.69$ Hz, 1 H, C5-CH), 5.99 (s, 2 H, 2-NH₂, exch), 7.55-7.56 (d, $J = 4.53$ Hz, 1 H, Ar), 7.98-8.01 (dd, $J = 3.47, 7.42$ Hz, 1 H, CONH, exch), 10.15 (s, 1 H, 3-NH, exch), 10.86 (s, 1 H, 7-NH, exch). Anal. Calcd for C₁₉H₂₀FN₅O₆S · 1.15 H₂O: C, 46.93; H, 4.62; N, 14.40; F, 3.90; S, 6.59. Found: C, 46.99; H, 4.68; N, 14.33; F, 3.85; S, 6.41.

Diethyl (4-bromo-3-fluorothiophene-2-carbonyl)-L-glutamate (263).

Compound **263** was prepared using the general method described for the preparation of **210-211**, from 4-bromo-3-fluorothiophene-2-carboxylic acid, **262** (1.75 g, 7.8 mmol) to afford **263** (2 g, 63%) as a colorless syrup. TLC $R_f = 0.44$ (hexane/EtOAc, 1:1); ¹H NMR (400 MHz, DMSO-*d*₆): δ 1.15-1.21 (m, 6H, COOCH₂CH₃), 1.95-2.16 (m, 2 H, β -CH₂), 2.38-2.42 (m, 2 H, γ -CH₂), 4.02-4.14 (m, 4 H, COOCH₂CH₃), 4.34-4.43 (m, 1 H, α -CH), 7.45 (s, 1 H, Ar), 8.26-8.29 (dd, $J = 2.22, 7.49$ Hz, 1 H, CONH, exch). The intermediate **263** was used for the next reaction without further characterization.

Diethyl (5-(4-(2-amino-4-oxo-4,7-dihydro-3H-pyrrolo[2,3-d]pyrimidin-6-yl)but-1-yn-1-yl)-2-fluorothiophene-3-carbonyl)-L-glutamate (264).

Compound **264** was prepared using the general method described for the preparation of **212-213**, from **162** (60 mg, 0.3 mmol) and **263** (180 mg, 0.44 mmol) to give **264** (92 mg, 59%) as a brown sticky solid; TLC $R_f = 0.5$ ($\text{CHCl}_3/\text{MeOH}$ 5:1); $^1\text{H NMR}$ (400 MHz, $\text{DMSO}-d_6$): δ 1.15-1.24 (m, 6 H, $\text{COOCH}_2\text{CH}_3$), 1.96-2.15 (m, 2 H, β - CH_2), 2.39-2.42 (t, $J = 8.0$ Hz, 2 H, γ - CH_2), 2.72-2.77 (m, 2 H, Ar- CH_2), 4.01-4.14 (m, 4 H, $\text{COOCH}_2\text{CH}_3$), 4.37-4.43 (m, 1 H, α -CH), 6-6.02 (m, 3 H, C5-CH, 2-NH₂, exch), 7.94-7.95 (d, $J = 4.13$ Hz, 1 H, Ar), 8.35-8.36 (dd, $J = 0.66, 7.87$ Hz, 1 H, CONH, exch), 10.17 (s, 1 H, 3-NH, exch), 10.88 (s, 1H, 7-NH, exch). The intermediate **264** was used for the next reaction without further characterization.

Diethyl (4-(4-(2-amino-4-oxo-4,7-dihydro-3H-pyrrolo[2,3-d]pyrimidin-6-yl)butyl)-3-fluorothiophene-2-carbonyl)-L-glutamate (265).

Compound **265** was prepared using the general method described for the preparation of **214-215**, from **264** (92 mg, 0.17 mmol) to give **265** (70 mg, 75%) as a brown sticky solid; TLC $R_f = 0.55$ ($\text{CHCl}_3/\text{MeOH}$ 5:1); $^1\text{H NMR}$ (400 MHz, $\text{DMSO}-d_6$): δ 1.13-1.24 (m, 6 H, $\text{COOCH}_2\text{CH}_3$), 1.54-1.65 (m, 4 H, CH_2CH_2), 1.96-2.17 (m, 2 H, β - CH_2), 2.37-2.43 (t, $J = 7.36$, $J = 7.36$ Hz, 2 H, γ - CH_2), 3.15-3.17 (m, 2 H, Ar- CH_2), 4-4.16 (m, 4 H, $\text{COOCH}_2\text{CH}_3$), 4.38-4.46 (m, 1 H, α -CH), 5.87-5.9 (m, 1 H, C5-CH), 5.97 (s, 1H, 2-NH₂, exch), 7.5-7.55 (m, 1 H, Ar), 8.13-8.24 (m, 1 H, CONH, exch), 10.16 (s, 1 H, 3-NH, exch), 10.84 (s, 1 H, 7-NH, exch). The intermediate **265** was used for the next reaction without further characterization.

(5-(4-(2-Amino-4-oxo-4,7-dihydro-3H-pyrrolo[2,3-d]pyrimidin-6-yl)butyl)-2-fluorothiophene-3-carbonyl)-L-glutamic acid (185).

Compound **185** was prepared using the general method described for the preparation of **179-180**, from **265** (70 mg, 0.13 mmol) to give **185** (60 mg, 96%) as a yellow powder. mp 162 °C dec. ¹H NMR (400 MHz, DMSO-*d*₆): δ 1.59-1.6 (m, 4 H, CH₂CH₂), 1.91-2.16 (m, 2 H, β-CH₂), 2.30-2.34 (t, *J* = 7.36, *J* = 7.36 Hz, 2 H, γ-CH₂), 4.35-4.44 (m, 1 H, α-CH), 5.86-5.87 (d, *J* = 1.80 Hz, 1 H, C5-CH), 5.97 (s, 1H, 2-NH₂, exch), 7.51-7.52 (d, *J* = 4.85 Hz, 1 H, Ar), 7.97-8.0 (dd, *J* = 2.91, 7.88 Hz, 1 H, CONH, exch), 10.14 (s, 1 H, 3-NH, exch), 10.83 (s, 1 H, 7-NH, exch). Anal. Calcd for C₂₀H₂₂FN₅O₆S · 1.26 H₂O: C, 47.83; H, 4.92; N, 13.94; F, 3.78; S, 6.38. Found: C, 47.85; H, 4.83; N, 13.85; F, 3.59; S, 6.46.

Diethyl (4-bromo-2,6-difluorobenzoyl)-L-glutamate (270).

Compound **270** was prepared using the general method described for the preparation of **210-211**, from 4-bromo-2,6-difluoro benzoic acid **267** (128 mg, 0.13 mmol), to give **270** (200 mg, 88%) as a colorless syrup. TLC *R*_f = 0.5 (hexane/EtOAc 1:1); ¹H NMR (400 MHz, DMSO-*d*₆): δ 1.16-1.23 (m, 6 H, COOCH₂CH₃) 1.82-2.12 (m, 2 H, β-CH₂), 2.4-2.45 (m, 2 H, γ-CH₂), 4.04-4.07 (q, *J*=7.11, 7.11, 7.10 Hz, 2 H, γ-COOCH₂CH₃), 4.1-4.16 (dq, *J*=2.36, 7.11, 7.10, 7.10 Hz, 2 H, α-COOCH₂CH₃), 4.44-4.48 (ddd, *J*=5.14, 7.72, 9.49 Hz, 1 H, α-CH), 7.60-7.62 (d, *J*=6.95 Hz, 2 H, Ar), 9.2-9.21 (d, *J*=7.62 Hz, 1 H, CONH, exch). The intermediate **270** was used for the next reaction without further characterization.

Diethyl (4-bromo-2,5-difluorobenzoyl)-L-glutamate (271).

Compound **271** was prepared using the general method described for the preparation of **210-211** from 4-bromo-2,5-difluoro benzoic acid **268** (1 g, 4.22 mmol) to give **271** (1 g,

56%) as a colorless syrup. TLC R_f = 0.5 (hexane/EtOAc 1:1). $^1\text{H NMR}$ (400 MHz, CDCl_3): δ 1.24-1.35 (m, 6 H, $\text{COOCH}_2\text{CH}_3$), 2.13-2.55 (m, 4 H, $\beta\text{-CH}_2, \gamma\text{-CH}_2$), 4.11-4.3 (m, 4 H, $\text{COOCH}_2\text{CH}_3$), 4.83-4.88 (m, 1 H, $\alpha\text{-CH}$), 7.43 (s, 2 H, Ar), 7.83-7.87 (m, 1 H, CONH, exch). The intermediate **271** was used for the next reaction without further characterization.

Diethyl (4-bromo-2,3-difluorobenzoyl)-L-glutamate (272).

Compound **272** was prepared using the general method described for the preparation of **210-211** from 4-bromo-2,3-difluoro benzoic acid **269** (1 g, 4.22 mmol) to give **272** (1.2 g, 67%) as a colorless syrup. TLC R_f = 0.45 (hexane/EtOAc 1:1). $^1\text{H NMR}$ (400 MHz, CDCl_3): δ 1.25-1.28 (t, J = 6.85, 6.85 Hz, 3 H, $\gamma\text{-COOCH}_2\text{CH}_3$), 1.32-1.36 (t, J = 7.15, 7.15 Hz, 3 H, $\alpha\text{-COOCH}_2\text{CH}_3$), 2.12-2.55 (m, 4 H, $\beta\text{-CH}_2, \gamma\text{-CH}_2$) 4.12-4.17 (q, J = 7.07, 7.07, 7.07 Hz, 2 H, $\gamma\text{-COOCH}_2\text{CH}_3$), 4.24-4.3 (q, J = 7.00 Hz, 2 H, $\alpha\text{-COOCH}_2\text{CH}_3$), 4.81-4.86 (m, 1 H, $\alpha\text{-CH}$) 7.32-7.35 (m, CONH, exch) 7.44-7.48 (m, 1 H, Ar), 7.71-7.75 (m, 1 H, Ar). The intermediate **272** was used for the next reaction without further characterization.

Diethyl (4-(4-(2-amino-4-oxo-4,7-dihydro-3H-pyrrolo[2,3-d]pyrimidin-6-yl)but-1-yn-1-yl)-2,6-difluorobenzoyl)-L-glutamate (273).

Compound **273** was prepared using the general method described for the preparation of **212-213**, from **162** (131 mg, 0.65 mmol) and **270** (412 mg, 0.98 mmol) to give **273** (142 mg, 40%) as a brown sticky solid. TLC R_f = 0.5 ($\text{CHCl}_3/\text{MeOH}$ 5:1); $^1\text{H NMR}$ (400 MHz, $\text{DMSO-}d_6$): δ 1.15-1.23 (m, 6 H, $\text{COOCH}_2\text{CH}_3$), 1.85-1.22 (m, 2 H, $\beta\text{-CH}_2$), 2.32-2.47 (m, 2 H, $\gamma\text{-CH}_2$), 4.04-4.14 (m, 4 H, $\text{COOCH}_2\text{CH}_3$), 4.45-4.51 (m, 1 H, $\alpha\text{-CH}$), 6.49 (m, 1 H, C5-CH), 7.01-7.06 (m, 2 H, Ar), 9.07-9.18-9.23 (d, J = 7.11 Hz, 1 H, CONH, exch). The intermediate **273** was used for the next reaction without further characterization.

Diethyl (4-(4-(2-amino-4-oxo-4,7-dihydro-3*H*-pyrrolo[2,3-*d*]pyrimidin-6-yl)but-1-yn-1-yl)-2,5-difluorobenzoyl)-L-glutamate (274).

Compound **274** was prepared using the general method described for the preparation of **212-213**, from **162** (140 mg, 0.7 mmol) and diethyl (4-bromo-2,5-difluorobenzoyl)-L-glutamate **271** (443 mg, 1.05 mmol) to give **274** (165 mg, 43%) as a brown sticky solid. TLC $R_f = 0.5$ (CHCl₃/MeOH 5:1); ¹H NMR (400 MHz, DMSO-*d*₆): δ 1.14-1.23 (m, 6 H, COOCH₂CH₃), 1.83-2.16 (m, 2 H, β -CH₂), 2.4-2.44 (t, $J=7.81, 7.81$ Hz, 2 H, γ -CH₂), 3.61-3.65 (m, 2 H, Ar-CH₂), 4.03-4.19 (m, 4 H, COOCH₂CH₃), 4.4-4.44 (m, 1 H, α -CH), 6.01-6.02 (m, 3 H, C5-CH, 2-NH₂, exch), 7.44-7.5 (m, 2 H, Ar), 8.83-8.85 (d, $J=7.55$ Hz, 1 H, CONH, exch), 10.17 (s, 1 H, 3-NH, exch), 10.91-10.92 (d, $J=1.79$ Hz, 1 H, 7-NH, exch). The intermediate **274** was used for the next reaction without further characterization.

Diethyl (4-(4-(2-amino-4-oxo-4,7-dihydro-3*H*-pyrrolo[2,3-*d*]pyrimidin-6-yl)but-1-yn-1-yl)-2,3-difluorobenzoyl)-L-glutamate (275).

Compound **275** was prepared using the general method described for the preparation of **212-213**, from **162** (140 mg, 0.7 mmol) and diethyl (4-bromo-2,3-difluorobenzoyl)-L-glutamate **272** (443 mg, 1.05 mmol) to give **275** (170 mg, 45%) as a brown sticky solid. TLC $R_f = 0.5$ (CHCl₃/MeOH 5:1); ¹H NMR (400 MHz, DMSO-*d*₆): δ 1.16-1.22 (m, 6 H, COOCH₂CH₃), 1.9-2.12 (m, 2 H, β -CH₂), 2.42-2.46 (t, $J=7.69, 7.69$ Hz, 2 H, γ -CH₂), 4.03-4.15 (m, 4 H, COOCH₂CH₃), 4.38-4.44 (m, 1 H, α -CH), 6.02 (m, 3 H, C5-CH, 2-NH₂, exch) 7.34-7.35 (d, $J = 5.02$ Hz, 1 H, Ar), 7.72-7.74 (m, 2 H, Ar), 8.91-8.93 (d, $J = 6.98$ Hz, 1 H, CONH, exch) 10.17 (s, 1 H, 3-NH, exch) 10.89-10.895 (d, $J=1.51$ Hz, 1 H, 7-NH, exch). The intermediate **275** was used for the next reaction without further characterization.

Diethyl (4-(4-(2-amino-4-oxo-4,7-dihydro-3H-pyrrolo[2,3-d]pyrimidin-6-yl)butyl)-2,6-difluorobenzoyl)-L-glutamate (276).

Compound **276** was prepared using the general method described for the preparation of **214-215**, from **273** (142 mg, 0.26 mmol) to give **276** (100 mg, 70%) as an orange sticky solid. TLC R_f = 0.51 (CHCl₃/MeOH 5:1); ¹H NMR (400 MHz, DMSO-*d*₆): δ 1.15-1.21 (m, 6 H, COOCH₂CH₃), 1.56-1.6 (m, 4 H, CH₂CH₂), 1.81-2.1 (m, 2 H, β -CH₂), 2.40-2.43 (m, 2 H, γ -CH₂), 2.61-2.65 (m, 2 H, CH₂), 4.02-4.17 (m, 4 H, COOCH₂CH₃), 4.37-4.46 (m, 1 H, α -CH), 5.92-5.925 (d, J = 1.76 Hz, 1 H, C5-CH), 7.01-7.06 (m, 2 H, Ar), 9.07-9.09 (d, J = 7.66 Hz, 1 H, CONH, exch) 11.03 (s, 1 H, 7-NH, exch). The intermediate **276** was used for the next reaction without further characterization.

Diethyl (4-(4-(2-amino-4-oxo-4,7-dihydro-3H-pyrrolo[2,3-d]pyrimidin-6-yl)butyl)-2,5-difluorobenzoyl)-L-glutamate (277).

Compound **277** was prepared using the general method described for the preparation of **214-215**, from **274** (165 mg, 0.3 mmol) to give **277** (120 mg, 72%) as an orange sticky solid. TLC R_f = 0.51 (CHCl₃/MeOH 5:1); ¹H NMR (400 MHz, DMSO-*d*₆): δ 1.16-1.22 (m, 6 H, COOCH₂CH₃), 1.55-1.62 (m, 4 H, CH₂CH₂), 1.89-2.14 (m, 2 H, β -CH₂), 2.41-2.46 (t, J = 7.51, 2 H, γ -CH₂), 2.65-2.68 (m, 2 H, Ar-CH₂), 4.03-4.15 (m, 4 H, COOCH₂CH₃), 4.39-4.44 (m, 1 H, α -CH), 5.84-5.85 (d, J = 2.05 Hz, 1 H, C5-CH), 6.01 (s, 2 H, 2-NH₂, exch) 7.29-7.37 (m, 2 H, Ar), 8.69-8.70 (dd, J = 1.05, 7.50 Hz, 1 H, CONH, exch) 10.22 (s, 1 H, 3-NH, exch) 10.8 (d, J = 1.26 Hz, 1 H, 7-NH, exch). The intermediate **277** was used for the next reaction without further characterization.

Diethyl (4-(4-(2-amino-4-oxo-4,7-dihydro-3*H*-pyrrolo[2,3-*d*]pyrimidin-6-yl)butyl)-2,3-difluorobenzoyl)-L-glutamate (278).

Compound **278** was prepared using the general method described for the preparation of **214-215**, from **275** (170 mg, 0.3 mmol) to give **278** (100 mg, 58%) as an orange sticky solid. TLC $R_f = 0.51$ (CHCl₃/MeOH 5:1); ¹H NMR (400 MHz, DMSO-*d*₆): δ 1.1-1.22 (m, 6 H, COOCH₂CH₃), 1.55-1.61 (m, 4 H, CH₂CH₂), 1.89-2.13 (m, 2 H, β -CH₂), 2.39-2.45 (m, 2 H, γ -CH₂), 2.67-2.72 (m, 2 H, CH₂), 4.03-4.15 (m, 4 H, COOCH₂CH₃), 4.37-4.47 (m, 1 H, α -CH), 5.87-5.88 (d, $J=2.05$ Hz, 1 H, C5-CH) 6.01 (s, 2 H, 2-NH₂, exch), 7.16-7.21 (m, 1 H, Ar), 7.27-7.32 (m, 1 H, Ar), 8.8-8.83 (m, 1 H, CONH, exch) 10.22 (s, 1 H, 3-NH, exch) 10.82-10.83 (m, 1 H, 7-NH, exch). The intermediate **278** was used for the next reaction without further characterization.

(4-(4-(2-amino-4-oxo-4,7-dihydro-3*H*-pyrrolo[2,3-*d*]pyrimidin-6-yl)butyl)-2,6-difluorobenzoyl)-L-glutamate (186).

Compound **186** was prepared using the general method described for the preparation of **179-180**, from **276** (100 mg, 0.18 mmol) to give **186** (70 mg, 78%) as a yellow powder. mp 159.6 °C dec. ¹H NMR (400 MHz, DMSO-*d*₆): δ 1.54-1.62 (m, 4 H, CH₂CH₂) 1.76-2.1 (m, 2 H, β -CH₂), 2.32-2.36 (m, 2 H, γ -CH₂), 2.63-2.65 (m, 2 H, Ar-CH₂), 4.36-4.43 (m, 1 H, α -CH), 5.86 (s, 1 H, C5-CH), 5.97 (s, 2 H, 2-NH₂, exch) 7.02-7.04 (d, $J=8.54$ Hz, 2 H, Ar), 8.92-8.95 (d, $J=7.99$ Hz, 1 H, CONH, exch) 10.14 (s, 1 H, 3-NH, exch), 10.82 (s, 1 H, 7-NH, exch). Anal. Calcd for C₂₂H₂₃F₂N₅O₆ · 1.85 H₂O: C, 50.34; H, 5.12; N, 13.34; F, 7.23. Found: C, 50.33; H, 4.83; N, 13.21; F, 7.31.

(4-(4-(2-amino-4-oxo-4,7-dihydro-3H-pyrrolo[2,3-d]pyrimidin-6-yl)butyl)-2,5-difluorobenzoyl)-L-glutamate (187).

Compound **187** was prepared using the general method described for the preparation of **179-180**, from **277** (120 mg, 0.22 mmol) to give **187** (95 mg, 88%) of as an orange powder. mp 169.12 °C dec. ¹H NMR (400 MHz, DMSO-*d*₆): δ 1.56-1.61 (m, 4 H, CH₂CH₂) 1.83-2.12 (m, 2 H, β-CH₂), 2.33-2.37 (t, *J*=7.61, 7.61 Hz, 2 H, γ-CH₂), 2.66-2.68 (t, *J*=5.53, 5.53 Hz, 2 H, Ar-CH₂), 4.35-4.44 (m, 1 H, α-CH), 5.84-5.85 (d, *J*=2.13 Hz, 1 H, C5-CH), 5.97 (s, 2 H, 2-NH₂, exch) 7.29-7.37 (m, 2 H, Ar), 8.53-8.56 (dd, *J*=2.32, 7.67 Hz, 1 H, CONH, exch) 10.13 (s, 1 H, 3-NH, exch) 10.81-10.82 (d, *J*=1.77 Hz, 1 H, 7-NH, exch). Anal. Calcd for C₂₂H₂₃N₅F₂O₆ · 1.11 H₂O: C, 51.65; H, 4.97; N, 13.69; F, 7.42. Found: C, 51.77; H, 4.98; N, 13.38; F, 7.19.

(4-(4-(2-amino-4-oxo-4,7-dihydro-3H-pyrrolo[2,3-d]pyrimidin-6-yl)butyl)-2,3-difluorobenzoyl)-L-glutamate (188).

Compound **188** was prepared using the general method described for the preparation of **179-180**, from **278** (100 mg, 0.18 mmol) to give **188** (80 mg, 89%) as a buff powder. mp: 150.5 °C dec. ¹H NMR (400 MHz, DMSO-*d*₆): δ 1.53-1.64 (m, 4 H, CH₂CH₂), 1.9-2.12 (m, 2 H, β-CH₂), 2.32-2.38 (t, *J*=7.25, 7.25 Hz, 2 H, γ-CH₂), 2.67-2.73 (t, *J*=6.41, 6.41 Hz, 2 H, Ar-CH₂), 4.32-4.44 (m, 1 H, α-CH), 5.8-5.88 (s, 1 H, C5-CH) 5.92-6.0 (s, 2 H, 2-NH₂, exch) 7.13-7.23 (t, *J*=7.61, 7.61 Hz, 1 H, Ar), 7.26-7.35 (t, *J*=6.99, 6.99 Hz, 2 H, Ar), 8.56-8.7 (s, br, 1 H, CONH, exch) 10.18 (s, br, 1 H, 3-NH, exch) 10.83 (s, br, 1 H, 7-NH, exch). HPLC analysis: retention time, 8.5 min; peak area, 95.12%; eluent A, H₂O; eluent B, ACN; gradient elution (95% H₂O to 100% ACN) over 10 mins with flow rate of 0.5 mL/min and

detection at 254 nm; column temperature, rt. LRMS calculated for C₂₂H₂₃F₂N₅O₆ = 491.16, found [M+H]⁺ 492.1 and [M-H]⁻ 490.2.

Diethyl (4-bromo-2-methylbenzoyl)-L-glutamate (282).

Compound **282** was prepared using the general method described for the preparation of **210-211**, from 4-bromo-2-methylbenzoic acid **279** (1.5 g, 7 mmol), to give **282** (2 g, 72%) as a colorless syrup. TLC R_f = 0.5 (hexane/EtOAc, 1:1); ¹H NMR (400 MHz, DMSO-*d*₆): δ 1.25-1.29 (t, *J* = 7.14, 7.14 Hz, 3 H, γ-COOCH₂CH₃), 1.32-1.35 (t, *J* = 7.14, 7.14 Hz, 3 H, α-COOCH₂CH₃), 2.07-2.37 (m, 2 H, β-CH₂), 2.42-2.57 (m, 5 H, γ-CH₂, Ar-CH₃), 4.12-4.17 (q, *J* = 7.10, 7.10, 7.14 Hz, 2 H, γ-COOCH₂CH₃), 4.24-4.29 (q, *J* = 7.09, 7.09, 7.10 Hz, 2 H, α-COOCH₂CH₃), 4.76-4.81 (dt, *J* = 5.00, 7.96, 7.94 Hz, 1 H, α-CH), 6.56-6.58 (d, *J* = 7.63 Hz, 1 H, CONH, exch), 7.28-7.42 (m, 3 H, Ar). The intermediate **282** was used for the next reaction without further characterization.

Diethyl (5-bromo-2-chlorobenzoyl)-L-glutamate (283).

Compound **283** was prepared using the general method described for the preparation of **210-211**, from 4-bromo-2-chlorobenzoic acid **280** (1 g, 4.25 mmol), to give **283** (1.4 g, 78%) as a colorless syrup. TLC R_f = 0.5 (hexane/EtOAc, 1:1); ¹H NMR (400 MHz, DMSO-*d*₆): δ 1.17-1.23 (m, 6 H, COOCH₂CH₃), 1.85-2.13 (m, 2 H, β-CH₂), 2.44-2.48 (m, 2 H, γ-CH₂), 4.03-4.09 (m, 2 H, γ-COOCH₂CH₃), 4.1-4.19 (m, 2 H, α-COOCH₂CH₃), 4.4-4.45 (m, 1 H, α-CH), 7.37-7.39 (d, *J* = 8.18 Hz, 1 H, Ar), 7.65-7.67 (dd, *J* = 1.43, 8.14 Hz, 1 H, Ar), 7.83-7.834 (d, *J* = 1.51 Hz, 1 H, Ar), 8.93-8.95 (d, *J* = 7.53 Hz, 1 H, CONH, exch). The intermediate **283** was used for the next reaction without further characterization.

Diethyl (4-bromo-2-(trifluoromethyl)benzoyl)-L-glutamate (284).

Compound **284** was prepared using the general method described for the preparation of **210-211** from 4-bromo-2-(trifluoromethyl)benzoic acid **281** (1 g, 3.72 mmol) to give **284** (1.50 g, 89%) as a colorless syrup. TLC $R_f = 0.25$ (H:E, 3:1). $^1\text{H NMR}$ (400 MHz, DMSO- d_6): δ 1.16-1.23 (6 H, COO $\underline{\text{CH}_2}$ CH $_3$), 1.84-2.13 (m, 2 H, β -CH $_2$), 2.41-2.45 (t, $J=7.81$, 7.81 Hz, 2 H, γ -CH $_2$) 4.04-4.09 (q, $J=7.09$, 7.09, 7.11 Hz, 2 H, COO $\underline{\text{CH}_2}$ CH $_3$), 4.1-4.16 (dq, $J=1.70$, 7.08, 7.03, 7.03 Hz, 2 H, COO $\underline{\text{CH}_2}$ CH $_3$), 4.39-4.45 (ddd, $J=5.12$, 7.70, 9.62 Hz, 1 H, α -CH), 7.47-7.5 (d, $J=8.80$ Hz, 1 H, Ar), 8-8.02 (m, 2 H, Ar), 9-9.02 (d, $J=7.70$ Hz, 1 H, CONH, exch). The intermediate **284** was used for the next reaction without further characterization.

Diethyl (4-(4-(2-amino-4-oxo-4,7-dihydro-3H-pyrrolo[2,3-d]pyrimidin-6-yl)but-1-yn-1-yl)-2-methylbenzoyl)-L-glutamate (285).

Compound **285** was prepared using the general method described for the preparation of **212-213**, from **162** (100 mg, 0.5 mmol) and diethyl (4-bromo-2-methylbenzoyl)-L-glutamate, **282** (300 mg, 0.74 mmol) to give **285** (70 mg, 44%) as a golden-brown sticky solid. TLC $R_f = 0.56$ (CHCl $_3$ /MeOH 5:1); $^1\text{H NMR}$ (400 MHz, DMSO- d_6): δ 1.17-1.23 (6 H, COOCH $_2$ $\underline{\text{CH}_3}$), 1.84-2.11 (m, 2 H, β -CH $_2$), 2.3 (s, 3 H, Ar-CH $_3$) 2.42-2.46 (m, 2 H, γ -CH $_2$), 4.03-4.16 (m, 4 H, COO $\underline{\text{CH}_2}$ CH $_3$), 4.36-4.45 (m, 1 H, α -CH), 6.02-6.022 (m, 3 H, C5-CH, 2-NH $_2$), 7.24-7.35 (m, 3 H, Ar), 8.69-8.7 (d, $J = 7.19$ Hz, 1 H, CONH, exch), 10.18 (s, 1 H, 3-NH, exch), 10.9 (s, 1 H, 7-NH, exch). The intermediate **285** was used for the next reaction without further characterization.

Diethyl (4-(4-(2-amino-4-oxo-4,7-dihydro-3*H*-pyrrolo[2,3-*d*]pyrimidin-6-yl)but-1-yn-1-yl)-2-chlorobenzoyl)-L-glutamate (286).

Compound **286** was prepared using the general method described for the preparation of **212-213**, from **162** (70 mg, 0.35 mmol) and diethyl (4-bromo-2-chlorobenzoyl)-L-glutamate, **283** (218 mg, 0.52 mmol) to give **286** (55 mg, 30%) as a brown sticky solid. TLC $R_f = 0.5$ (CHCl₃/MeOH 5:1); ¹H NMR (400 MHz, DMSO-*d*₆): δ 1.17-1.24 (6 H, COOCH₂CH₃), 1.86-2.15 (m, 2 H, β -CH₂), 2.3 (m, 2 H, γ -CH₂) 4.04-4.2 (m, 4 H, COOCH₂CH₃), 4.4-4.46 (m, 1 H, α -CH), 6.02 (s, 1 H, C5-CH), 7.38-7.4 (m, 2 H, Ar), 7.5 (s, 1 H, Ar), 8.9-8.92 (d, $J=7.48$ Hz, 1 H, CONH, exch), 10.18 (s, 1 H, 3-NH, exch), 10.9 (s, 1 H, 7-NH, exch). The intermediate **286** was used for the next reaction without further characterization.

Diethyl (4-(4-(2-amino-4-oxo-4,7-dihydro-3*H*-pyrrolo[2,3-*d*]pyrimidin-6-yl)but-1-yn-1-yl)-2-(trifluoromethyl)benzoyl)-L-glutamate (287).

Compound **287** was prepared using the general method described for the preparation of **212-213**, from **162** (200 mg, 0.99 mmol) and diethyl (4-bromo-2-trifluoromethyl)-L-glutamate, **284** (674 mg, 1.48 mmol) to give **287** (150 mg, 26%) as a brown sticky solid. TLC $R_f = 0.5$ (CHCl₃/MeOH 5:1); ¹H NMR (400 MHz, DMSO-*d*₆): δ 1.16-1.23 (6 H, COOCH₂CH₃), 1.82-2.12 (m, 2 H, β -CH₂), 2.4-2.44 (t, $J=7.81$, 7.81 Hz, 2 H, γ -CH₂) 4.04-4.19 (m, 4 H, COOCH₂CH₃), 4.39-4.44 (m, 1 H, α -CH), 6.02 (s, 3 H, C5-CH, 2-NH₂, exch), 7.48-7.5 (d, $J=7.66$ Hz, 2 H, Ar), 7.72-7.95 (m, 2 H, Ar), 8.9-9.0 (d, $J=7.55$ Hz, 1 H, CONH, exch), 10.2 (s, 1 H, 3-NH, exch), 10.92-10.923 (d, $J=1.79$ Hz, 7-NH, exch). The intermediate **287** was used for the next reaction without further characterization.

Diethyl (4-(4-(2-amino-4-oxo-4,7-dihydro-3H-pyrrolo[2,3-d]pyrimidin-6-yl)butyl)-2-methylbenzoyl)-L-glutamate (288).

Compound **288** was prepared using the general method described for the preparation of **214-215**, from **285** (70 mg, 0.22 mmol) to give **288** (70 mg, quant) as a light yellow sticky solid. TLC $R_f = 0.56$ ($\text{CHCl}_3/\text{MeOH}$ 5:1); ^1H NMR (400 MHz, $\text{DMSO-}d_6$): δ 1.15-1.23 (m, 6 H, $\text{COOCH}_2\text{CH}_3$), 1.42-1.5 (m, 2 H, CH_2), 1.62-1.7 (m, 2 H, CH_2), 1.87-2.13 (m, 2 H, $\beta\text{-CH}_2$), 2.34 (s, 3 H, Ar-CH_3), 2.43-2.47 (m, 2 H, $\gamma\text{-CH}_2$), 4.02-4.17 (m, 4 H, $\text{COOCH}_2\text{CH}_3$), 4.37-4.44 (m, 1 H, $\alpha\text{-CH}$), 6.95 (m, 1 H, C5-CH), 7.17-7.36 (m, 3 H, Ar), 8.64-8.65 (d, $J=7.43$ Hz, 1 H, CONH, exch). The intermediate **288** was used for the next reaction without further characterization.

Diethyl (4-(4-(2-amino-4-oxo-4,7-dihydro-3H-pyrrolo[2,3-d]pyrimidin-6-yl)butyl)-2-benzoyl)-L-glutamate mixtures (289) and (290).

Using the general method described for the preparation of **214-215**, hydrogenation of **286** (40 mg, 0.07 mmol) gave a mixture of **289** and **290** (30 mg, 74%) as a yellow sticky solid. TLC $R_f = 0.52$ ($\text{CHCl}_3/\text{MeOH}$ 5:1); ^1H NMR (400 MHz, $\text{DMSO-}d_6$): δ 1.15-1.23 (6 H, $\text{COOCH}_2\text{CH}_3$), 1.54-1.65 (m, 4 H, CH_2CH_2), 1.94-2.16 (m, 2 H, $\beta\text{-CH}_2$), 2.42-2.46 (m, 2 H, $\gamma\text{-CH}_2$), 2.63-2.66 (m, 2 H, Ar-CH_2), 4.02-4.11 (m, 4 H, $\text{COOCH}_2\text{CH}_3$), 4.37-4.47 (m, 1 H, $\alpha\text{-CH}$), 5.85 (s, 1 H, C5-CH), 6.09 (s, 2 H, 2-NH₂, exch), 7.23-7.35 (m, 3 H, Ar), 7.78-7.8 (m, Ar), 8.65-8.69 (m, CONH, exch), 10.37 (s, 1 H, 3-NH, exch), 10.8 (s, 1 H, 7-NH, exch). The intermediate mixture of **289** and **290** were used for the next reaction without further characterization.

Diethyl (4-(4-(2-amino-4-oxo-4,7-dihydro-3*H*-pyrrolo[2,3-*d*]pyrimidin-6-yl)butyl)-2-(trifluoromethyl)benzoyl)-L-glutamate (291).

Compound **291** was prepared using the general method described for the preparation of **214-215**, from **287** (120 mg, 0.21 mmol) to give **291** (95 mg, 79%) as a yellow sticky solid. TLC $R_f = 0.5$ (CHCl₃/MeOH 5:1); ¹H NMR (400 MHz, DMSO-*d*₆): δ 1.16-1.23 (6 H, COOCH₂CH₃), 1.53-1.65 (m, 4 H, CH₂CH₂), 1.86-2.12 (m, 2 H, β -CH₂), 2.41-2.45 (t, $J=8.19, 8.19$ Hz, 2 H, γ -CH₂) 2.71-2.73 (s, 2H, Ar-CH₂), 4.04-4.15 (m, 4 H, COOCH₂CH₃), 4.37-4.43 (m, 1 H, α -CH), 5.84 (s, 1 H, C5-CH), 6.1 (s, 2 H, 2-NH₂, exch), 7.42-7.44 (d, $J = 7.61$ Hz, 1 H, Ar), 7.57-7.61 (m, 2 H, Ar), 8.88-9.0 (d, $J = 7.16$ Hz, 1 H, CONH, exch), 10.3 (s, 1 H, 3-NH, exch), 10.82 (s, 1 H, 7-NH, exch). The intermediate **291** was used for the next reaction without further characterization.

(4-(4-(2-amino-4-oxo-4,7-dihydro-3*H*-pyrrolo[2,3-*d*]pyrimidin-6-yl)butyl)-2-methylbenzoyl)-L-glutamic acid (189).

Compound **189** was prepared using the general method described for the preparation of **179-180**, from **288** (50 mg, 0.09 mmol) to give **189** (26 mg, 58%) as a light yellow powder. mp 170.2 °C dec. ¹H NMR (400 MHz, DMSO-*d*₆): δ 1.52-1.61 (m, 4 H, CH₂CH₂), 1.8-2.1 (m, 2 H, β -CH₂), 2.32 (s, 3 H, Ar-CH₃), 2.36-2.38 (m, 2 H, γ -CH₂), 2.57-2.61 (s, 2 H, Ar-CH₂), 4.3-4.37 (m, 1 H, α -CH), 5.85 (m, 1 H, C5-CH), 5.98 (s, 2 H, 2-NH₂, exch), 7.05-7.06 (d, $J = 4.42$ Hz, 2 H, Ar), 7.25-7.27 (d, $J = 8.16$ Hz, 1 H, Ar), 8.41-8.43 (d, $J = 7.45$ Hz, 1 H, CONH, exch), 10.16 (s, 1 H, 3-NH, exch), 10.82 (s, 1 H, 7-NH, exch). Anal. Calcd for C₂₃H₂₇N₅O₆ · 0.78 H₂O: C, 57.11; H, 5.95; N, 14.48. Found: C, 57.18; H, 5.89; N, 14.2.

(4-(4-(2-amino-4-oxo-4,7-dihydro-3H-pyrrolo[2,3-d]pyrimidin-6-yl)butyl)-2-benzoyl)-L-glutamate mixture (3) and (190).

Using the general method described for the preparation of **179-180**, hydrolysis of compound mixture of **289** and **290** (40 mg, 0.07 mmol) gave a mixture of **3** and **190** (25 mg, 70%) as a light yellow powder. ¹H NMR (400 MHz, DMSO-*d*₆): δ 1.54-1.66 (m, 6 H, CH₂CH₂), 1.89-2.14 (m, 3 H, β-CH₂), 2.34-2.37 (t, *J*=6.92, 6.92 Hz, 3 H, γ-CH₂) 2.65 (s, 3 H, Ar-CH₃), 4.36-4.41 (m, 2 H, α-CH), 5.85 (s, 1 H, C5-CH), 5.98 (s, 2 H, 2-NH₂, exch), 7.22-7.35 (m, 3 H, Ar), 7.79-7.8 (m, 2 H, Ar), 8.53-8.55 (d, *J*=6.7 Hz, 1 H, CONH, exch), 8.65-8.67 (d, *J* = 7.33 Hz, 1 H, CONH, exch), 10.14 (s, 1 H, 3-NH, exch), 10.81 (s, 1 H, 7-NH, exch). Anal. Calcd for C₂₂H₂₄ClN₅O₆: C, 53.94; H, 4.94; N, 14.30; Cl, 7.24; Found. C, 54.64; H, 5.59; N, 14.34; Cl, 2.74; The elemental analysis had a >4% deviation in Cl percentage, indicating dechlorination during hydrogenation of **286**. The mixture was not characterized further.

(4-(4-(2-amino-4-oxo-4,7-dihydro-3H-pyrrolo[2,3-d]pyrimidin-6-yl)butyl)-2-(trifluoromethyl)benzoyl)-L-glutamate (191).

Compound **191** was prepared using the general method described for the preparation of **179-180**, from **291** (70 mg, 0.12 mmol) to give **191** (50 mg, 79%) as a yellow powder. TLC *R_f* = 0.3 (CHCl₃/MeOH 5:1); mp 185 °C dec. ¹H NMR (400 MHz, DMSO-*d*₆): δ 1.56-1.66 (m, 4 H, CH₂CH₂), 1.8-2.11 (m, 2 H, β-CH₂), 2.31-2.39 (s, 2 H, γ-CH₂), 2.7-2.77 (m, 2 H, Ar-CH₂) 4.33-4.43 (m, 1 H, α-CH), 5.84 (m, 1 H, C5-CH) 5.99 (s, 1 H, 2-NH₂, exch) 7.42-7.44 (d, *J*=7.98 Hz, 1 H, Ar), 7.57-7.61 (m, 2 H, Ar) 8.74-8.76 (d, *J* = 8.2 Hz, 1 H, CONH, exch) 10.15 (s, 1 H, 3-NH, exch) 10.82 (s, 1 H, 7-NH, exch). HPLC analysis: retention time, 2 min; peak area, 98.49%; eluent A, H₂O; eluent B, ACN; gradient elution (100%

H₂O to 10% H₂O) over 10 mins with flow rate of 0.5 mL/min and detection at 254 nm; column temperature, rt. LRMS calculated for C₂₃H₂₄F₃N₅O₆ = 523.17, found [M+H]⁺ 524.20.

Diethyl (5-bromopyrimidine-2-carbonyl)-L-glutamate (293).

Compound **293** was prepared using the general method described for the preparation of **210-211**. However, the amine and second equivalent of NMM were also added at once with the acid **292** (1.05 g, 4.77 mmol) and the reaction proceeded to completion in 1 h to give **293** (1.67 g, 83%) as a yellow syrup. TLC R_f = 0.15 (hexane/EtOAc 3:1); ¹H NMR (400 MHz, DMSO-*d*₆): δ 1.14-1.21 (m, 6 H, COOCH₂CH₃), 1.99-2.2 (m, 2 H, β-CH₂) 2.38-2.41 (t, *J* = 7.14, 7.14 Hz, 2 H, γ-CH₂), 4.01-4.06 (q, *J* = 7.11, 7.11, 7.10 Hz, 2 H, COOCH₂CH₃), 4.06-4.16 (dq, *J* = 2.14, 7.07, 7.01, 7.01 Hz, 1 H, COOCH₂CH₃), 4.51 (m, 1 H, α-CH), 9.17-9.21 (m, 3 H, Ar, CONH, exch). The intermediate **293** was used for the next reaction without further characterization.

(S)-2-(5-bromopyrimidine-2-carboxamido)-5-ethoxy-5-oxopentanoic acid (295). To a solution of 5-bromopyrimidine-2-carboxylic acid **292** (1 g, 4.93 mmol, 1 eq) and diethyl L-glutamate hydrochloride (1 g, 4.93 mmol, 1 eq) in pyridine (10 mL) was added dicyclohexylcarbodiimide **294** (1.02 g, 4.93 mmol, 1 eq) and the mixture was stirred at room temperature for 96 h until the formation of a new non-polar spot on TLC R_f = 0.1 (hexane/EtOAc 3:1). The reaction mixture was filtered to decant the dicyclohexylurea side product **296** and the filtrate was evaporated. The residue of the filtrate was washed with 2 N HCl followed by sat. NaHCO₃ to afford **295** (220 mg, 12.4%) as a yellow syrup. ¹H NMR (400 MHz, CDCl₃): δ 1.23-1.27 (t, *J*=7.14, 7.14 Hz, 3 H, γ-COOCH₂CH₃), 2.14-2.54 (m, 4 H, α-CH₂, β-CH₂), 4.1-4.16 (dq, *J*=3.38, 7.13, 7.12, 7.12 Hz, 2 H, γ-

COOCH₂CH₃), 4.89-4.94 (dt, $J=4.82, 8.05, 7.94$ Hz, 1 H, α -CH), 8.45-8.47 (d, $J=8.34$ Hz, 2 H, CONH, exch), 8.96 (s, 2 H, Ar). The intermediate **295** was not characterized further.

Diethyl (5-(4-(2-amino-4-oxo-4,7-dihydro-3H-pyrrolo[2,3-d]pyrimidin-6-yl)but-1-yn-1-yl)pyrimidine-2-carbonyl)-L-glutamate (297).

Compound **297** was prepared using the general method described for the preparation of **211-212**, from **162** (200 mg, 0.99 mmol) and diethyl (5-bromopyrimidine-2-carbonyl)-L-glutamate **293** (576 mg, 1.48 mmol) to give **297** (200 mg, 40%) as an orange sticky solid. TLC $R_f = 0.4$ (CHCl₃/MeOH 5:1); ¹H NMR (400 MHz, DMSO-*d*₆): δ 1.14-1.21 (m, 6 H, COOCH₂CH₃), 2.03-2.2 (m, 2 H, β -CH₂), 2.37-2.41 (t, $J=7.60, 7.60$ Hz, 2 H, γ -CH₂), 4-4.06 (q, $J=7.11, 7.11, 7.13$ Hz, 2 H, COOCH₂CH₃), 4.08-4.16 (dq, $J=2.15, 7.11, 7.05, 7.05$ Hz, 2 H, COOCH₂CH₃), 4.47-4.54 (m, 1 H, α -CH) 6.04 (m, 3 H, C5-CH, 2-NH₂, exch) 8.98 (s, 2 H, Ar) 9.16-9.18 (d, $J=7.90$ Hz, 1 H, CONH, exch), 10.18 (s, 1H, 3-NH, exch) 10.93-10.94 (d, $J=1.65$ Hz, 1 H, 7-NH, exch). The intermediate **297** was used for the next reaction without further characterization.

Diethyl (5-(4-(2-amino-4-oxo-4,7-dihydro-3H-pyrrolo[2,3-d]pyrimidin-6-yl)butyl)pyrimidine-2-carbonyl)-L-glutamate (298).

To a Parr flask with 10% palladium on activated carbon (0.5 wt eq) soaked in ethanol was added a methanolic solution of **297** (160 mg, 0.3 mmol). Hydrogenation was carried out at 15 psi of H₂ for 12 h. TLC showed the disappearance of the starting material and one a new non-polar spot (CHCl₃/ MeOH). The reaction mixture was filtered through celite, washed with MeOH and concentrated under reduced pressure to give the reduced alkane **298** (120

mg, 75%) as a brown sticky solid. TLC $R_f = 0.5$ ($\text{CHCl}_3/\text{MeOH}$ 5:1); $^1\text{H NMR}$ (400 MHz, $\text{DMSO}-d_6$): δ 1.14-1.21 (m, 6 H, $\text{COOCH}_2\text{CH}_3$), 1.57-1.68 (m, 4 H, CH_2CH_2), 2.03-2.2 (m, 2 H, $\beta\text{-CH}_2$), 2.37-2.41 (t, $J=7.83$, 7.83 Hz, 2 H, $\gamma\text{-CH}_2$), 2.7-2.74 (t, $J=7.16$, 7.16 Hz, 2 H, CH_2), 4-4.06 (q, $J=7.12$, 7.12, 7.13 Hz, 2 H, $\text{COOCH}_2\text{CH}_3$), 4.09-4.15 (dq, $J=2.19$, 7.12, 7.08, 7.08 Hz, 2 H, $\text{COOCH}_2\text{CH}_3$), 4.47-4.54 (m, 1 H, $\alpha\text{-CH}$) 5.87 (s, 1 H, C5-CH), 5.97 (m, 3 H, C5-CH, 2-NH₂, exch) 8.85 (s, 2 H, Ar) 9.08-9.10 (d, $J = 7.95$ Hz, 1 H, CONH, exch), 10.13 (s, 1H, 3-NH, exch) 10.82-10.825 (d, $J = 2.05$ Hz, 1 H, 7-NH, exch). The intermediate **298** was used for the next reaction without further characterization.

(5-(4-(2-amino-4-oxo-4,7-dihydro-3H-pyrrolo[2,3-d]pyrimidin-6-yl)butyl)pyrimidine-2-carbonyl)-L-glutamic acid (192).

Compound **192** was prepared using the general method described for the preparation of **179-180** from **298** (50 mg, 0.1 mmol) to give **192** (30 mg, 68%) as an orange powder. TLC $R_f = 0.3$ ($\text{CHCl}_3/\text{MeOH}$ 5:1); mp 121.8 °C dec. $^1\text{H NMR}$ (400 MHz, $\text{DMSO}-d_6$): δ 1.6-1.65 (m, 4 H, CH_2CH_2), 1.99-2.19 (m, 2 H, $\beta\text{-CH}_2$), 2.29-2.33 (t, $J=7.20$, 7.20 Hz, 2 H, $\gamma\text{-CH}_2$), 2.7-2.74 (t, $J=6.91$, 6.91 Hz, 2 H, Ar- CH_2), 4.42-4.48 (m, 1 H, $\alpha\text{-CH}$) 5.87-5.88 (d, $J = 2.18$ Hz, 1 H, C5-CH), 5.97 (s, 2 H, 2-NH₂, exch) 8.84 (s, 2 H, Ar) 8.93-8.95 (d, $J = 7.94$ Hz, 1 H, CONH, exch), 10.14 (s, 1H, 3-NH, exch) 10.82-10.825 (d, $J = 1.71$ Hz, 1 H, 7-NH, exch). Anal. Calcd for ($\text{C}_{20}\text{H}_{23}\text{N}_7\text{O}_6 \cdot 0.81 \text{H}_2\text{O}$) C, 50.87; H, 5.25; N, 20.76. Found C, 50.94; H, 5.26; N, 20.61.

Diethyl (3-(6-oxohexyl)benzoyl)-L-glutamate (301).

To a solution of diethyl (3-bromobenzoyl)-L-glutamate **300** (2.16 g, 5 mmol, 1 eq) in anhydrous DMF (20 mL) was added hex-2-en-1-ol **299** (1.31 g, 5 mmol, 1 eq), LiCl (210

mg, 5 mmol, 1 eq), LiOAc (850 mg, 12.5 mmol, 2.5 eq), Bu₄NCl (1.4 g, 5 mmol, 1 eq), Pd(OAc)₂ (60 mg, 0.3 mmol, 0.06 eq) and the mixture was stirred at 70 °C for 3 hours. TLC showed the disappearance of the starting material and formation of one major non-polar spot (hexane/EtOAc). To the reaction mixture cooled to room temperature was added EtOAc. The resulting solution was extracted with H₂O and dried over Na₂SO₄. After evaporation of solvent, the residue was loaded on a silica gel column and eluted with hexane followed by gradual increase to 50% EtOAc and the desired fractions were pooled and evaporated to afford **301** (1.54 g, 76%), as colorless syrup. TLC R_f = 0.8 (hexane/EtOAc, 1:1); ¹H NMR (400 MHz, DMSO-*d*₆): δ 0.99-1.14 (m, 2 H, CH₂), 1.20-1.24 (t, *J*=7.13, 7.13 Hz, 2 H, COOCH₂CH₃), 1.26-1.3 (, *J*=7.13, 7.13 Hz, 2 H, COOCH₂CH₃), 1.69-1.71 (m, 4 H, CH₂CH₂), 2.09-2.35 (m, 2 H, β-CH₂), 2.5-2.53 (t, *J*=7.25, 7.25 Hz, 2 H, γ-CH₂), 2.68-2.72 (m, 2 H, Ar-CH₂), 4.08-4.13 (q, *J*=7.12, 7.12, 7.13 Hz, 2 H, COOCH₂CH₃), 4.18-4.24 (q, *J*=7.10, 7.10, 7.12 Hz, 2 H, COOCH₂CH₃), 4.63-4.66 (dd, *J*=5.20, 9.43 Hz, 1 H, α-CH), 7.34-7.35 (m, 2 H, Ar), 7.64-7.67 (m, 1 H, Ar), 7.7 (s, 1 H, Ar), 7.91 (s, 2 H, CHO, CONH, exch). The intermediate **301** was used for the next reaction without further characterization.

Diethyl (3-(4-(2-amino-4-oxo-4,7-dihydro-3H-pyrrolo[2,3-d]pyrimidin-5-yl)butyl)benzoyl)-L-glutamate (304).

To a solution of aldehyde **301** (1.54 g, 3.8 mmol, 1 eq) in anhydrous Et₂O was added 5,5-dibromo-2,2-dimethyl-4,6-dioxo-1,3-dioxane **302** (572 mg, 1.9 mmol, 0.5 eq), 2 N HCl in Et₂O solution (0.02 mL, 0.1 eq) and the mixture was stirred at room temperature for 24 hours. TLC showed the disappearance of the starting material and formation of one major non-polar spot (hexane/EtOAc). The reaction solution was washed with 5% NaHCO₃

solution and extracted with H₂O and dried over Na₂SO₄. After evaporation of solvent, the residue **303** was used directly in the next step without further characterization. TLC R_f = 0.9 (hexane/EtOAc 1:1)

To a solution of 2,6-diaminopyrimidin-4(3*H*)-one **22** (479 mg, 3.8 mmol, 1 eq) and sodium acetate (623 mg, 7.6 mmol, 2 eq) in water (5 mL) and methanol (5 mL) was added α -bromo aldehyde **303** (1.54 g, 3.8 mmol, 1 eq). The reaction mixture was stirred at 45 °C for 3 hours. TLC showed the disappearance of starting materials and the formation of one major spot (CHCl₃/MeOH). After evaporation of solvent, CH₃OH was added followed by silica gel and solvent was evaporated to afford a plug. The plug was loaded onto a silica gel column and eluted initially with CHCl₃ followed by gradual increase of 10% MeOH in CHCl₃. Fractions with the required R_f were pooled and evaporated to afford **304** (100 mg, 5% over two steps) as a light pink sticky solid. TLC R_f = 0.3 (CHCl₃/MeOH, 10:1); ¹H NMR (400 MHz, DMSO-*d*₆); δ 1.14-1.2 (m, 6 H, COOCH₂CH₃), 1.64 (s, 4 H, CH₂CH₂), 1.96-2.14 (m, 2 H, β -CH₂), 2.42-2.45 (t, J =7.16, 7.16 Hz, 2 H, γ -CH₂), 2.58-2.6 (m, 2 H, Ar-CH₂), 2.61-2.65 (s, 2 H, Ar-CH₂), 4.02-4.06 (m, 2 H, COOCH₂CH₃), 4.08-4.12 (m, 2 H, COOCH₂CH₃), 4.4-4.45 (td, J =5.94, 5.94, 7.94 Hz, 1 H, α -CH) 5.96 (s, 2 H, 2-NH₂, exch) 6.32 (s, 1 H, C6-CH), 7.35-7.36 (m, 2 H, Ar) 7.66-7.69 (m, 2 H, Ar), 8.67-8.68 (d, J =7.04 Hz, 1 H, CONH, exch), 10.09 (s, 1H, 3-NH, exch) 10.59 (s, 1 H, 7-NH, exch). The intermediate **304** was used for the next reaction without further characterization.

(3-(4-(2-amino-4-oxo-4,7-dihydro-3*H*-pyrrolo[2,3-*d*]pyrimidin-5-yl)butyl)benzoyl)-L-glutamic acid (193).

To **304** (51 mg, 0.1 mmol), was added 1 N NaOH (2 mL) and the resulting mixture was stirred at rt for 1 h. TLC indicated the disappearance of starting material and the formation

of one major spot at the origin. The solution was cooled in an ice bath, and the pH was adjusted 3 to 4 using 1 N HCl. The resulting suspension was chilled in a dry ice/acetone bath and thawed to 4 °C overnight in a refrigerator. The precipitate was filtered, washed with cold water, and dried in a desiccator under reduced pressure using P₂O₅ to yield **193** (37 mg, 81%) as a yellow powder. TLC R_f = 0.3 (CHCl₃/MeOH, 10:1 in a drop of CH₃COOH); mp 139.5 °C dec. ¹H NMR (400 MHz, DMSO-*d*₆): δ 1.57-1.69 (m, 4 H, CH₂CH₂), 1.91-2.14 (m, 2 H, β-CH₂), 2.34-2.37 (t, *J*=7.52, 7.52 Hz, 2 H, γ-CH₂), 2.58-2.64 (m, 4 H, CH₂, CH₂), 4.37-4.42 (td, *J*=5.94, 5.94, 7.94 Hz, 1 H, α-CH) 5.96 (s, 2 H, 2-NH₂, exch) 6.34 (s, 1 H, C6-CH), 7.35-7.37 (m, 2 H, Ar) 7.65-7.74 (m, 2 H, Ar), 8.56-8.58 (d, *J* = 7.72 Hz, 1 H, CONH, exch), 10.11 (s, 1H, 3-NH, exch) 10.6 (s, 1 H, 7-NH, exch). HPLC analysis: retention time, 19 min; peak area, 95.11%; eluent A, H₂O; eluent B, ACN; gradient elution (100% H₂O to 100% ACN) over 60 mins with flow rate of 0.5 mL/min and detection at 254 nm; column temperature, rt. LRMS calculated for C₂₂H₂₅N₅O₆: 455.18, found [M+H]⁺ 456.1887.

2-Amino-3,7-dihydro-pyrrolo[2,3-*d*]pyrimidin-4-one (309).

2,4-Diamino-6-hydroxypyrimidine **22** (2.1 g, 16.65 mmol, 1 eq), sodium acetate (2.73 g, 33.3 mmol, 2 eq) and chloroacetaldehyde (1.05 mL, 16.65 mmol, 1 eq) were dissolved in MeOH (25 mL) and water (25 mL) and the resulting yellow solution was stirred at 45 °C for 4 h until a new non-polar spot was observed on TLC (CHCl₃/MeOH). The reaction mixture was then concentrated in vacuo and MeOH was added followed by silica gel. Evaporation of the solvent afforded a plug, which was loaded onto a silica gel column and eluted initially with CHCl₃ followed by gradual increase of polarity to 10% MeOH in CHCl₃. Fractions with the required R_f were pooled and evaporated to afford **309** (2.5 g,

quant.) as a light pink powder. TLC R_f = 0.5 (CHCl₃/MeOH, 5:1); mp >300 °C.³⁸⁶ ¹H NMR (400 MHz, DMSO-*d*₆): δ 6.04 (s, 2 H, 2-NH₂, exch), 6.17-6.19 (dd, J =2.16, 3.27 Hz, 1 H, C5-CH), 6.6-6.62 (dd, J =2.30, 3.23 Hz, 1 H, C6-CH), 10.21 (s, 1 H, 3-NH, exch), 10.97 (s, 1 H, 7-NH, exch). ¹H NMR matches with the ¹H NMR of reported compound.³⁸⁷

***N*-(4-oxo-4,7-dihydro-3*H*-pyrrolo[2,3-*d*]pyrimidin-2-yl)pivalamide (310).**

A solution of **309** (2.4 g, 16 mmol, 1 eq) in pyridine (30 mL) was treated with trimethylacetyl chloride (7 mL, 56 mmol, 3.5 eq) at 90 °C for 0.5 h. The solvent was evaporated and the residue was dissolved in MeOH and precipitated in 10% aqueous ammonia for 30 min to selectively cleave the *N*(7)- pivaloyl group. The precipitate was filtered, washed with cold MeOH, and dried on high vacuum to give **310** (1.6 g, 43% yield) as a pink powder. TLC R_f = 0.7 (CHCl₃/MeOH 5:1); mp 297 °C.³⁸⁸ ¹H NMR (400 MHz, DMSO-*d*₆): δ 1.2 (s, 9 H, (CH₃)₃), 6.4-6.42 (dd, J =2.05, 3.38 Hz, 1 H, C5-CH), 6.95-6.96 (dd, J =2.4, 3.33 Hz, 1 H, C6-CH), 10.81 (s, 1 H, 2-NH, exch), 11.62 (s, 1 H, 3-NH, exch), 11.85 (s, 1 H, 7-NH, exch). ¹H NMR matches with the ¹H NMR of reported compound.³⁸⁸

***N*-(5-iodo-4-oxo-4,7-dihydro-3*H*-pyrrolo[2,3-*d*]pyrimidin-2-yl)pivalamide (305).**

To the solution of **310** (1.6 g, 6.83 mmol, 1 eq) in DMF (40 mL), bis(trimethylsilyl)acetamide (4.2 mL, 17.1 mmol, 2.5 eq) was added and the resulting solution was stirred at 40 °C for 1 h to give the intermediate **311**. The reaction was cooled to room temperature after which, NIS (1.84 g, 8.2 mmol, 1.2 eq) was added to the reaction. The reaction vessel was protected from light and stirred overnight at room temperature. The mixture was then poured into water (100 mL) and stirred for another 2 h to form a precipitate, which was filtered to afford **305** (1.6 g, 65%) as a pink powder. TLC R_f = 0.47

(CHCl₃/MeOH 10:1); mp 151.3 °C dec. ¹H NMR (400 MHz, DMSO-*d*₆) δ 1.24 (s, 9 H, (CH₃)₃), 7.15-7.16 (d, *J*=2.44 Hz, 1 H, C6-CH), 10.84 (s, 1 H, 2-NH, exch), 11.83 (s, 1 H, 3-NH, exch), 11.93 (s, 1 H, 7-NH, exch). ¹H NMR matches with the ¹H NMR of reported compound.³⁸⁹

Ethyl 4-(prop-2-yn-1-ylamino)benzoate (306).

To ethyl 4-aminobenzoate **313** (1.52 g, 10 mmol, 1 eq) dissolved in EtOH (30 mL), K₂CO₃ (1.4 g, 10.1 mmol, 1.01 eq) and propargyl bromide (80% wt in toluene) **312** (1.11 mL, 10 mmol, 1 eq) were added, and the mixture was refluxed for 18 h until a new non-polar spot was observed on TLC (hexane/EtOAc). The solvent was removed in vacuo, MeOH was added followed by silica gel and evaporated to afford a plug. The plug was loaded onto a silica gel column and eluted initially with hexane followed by gradual increase of polarity to 100% EtOAc. Fractions with the required R_f were pooled and evaporated to afford **306** (420 mg, 21%) as a yellow powder. TLC R_f = 0.7 (hexane/EtOAc, 1:1); mp 58.3 °C. ¹H NMR (400 MHz, DMSO-*d*₆): ¹H NMR (500 MHz, CDCl₃): δ 1.26-1.3 (t, *J*=7.09, 7.09 Hz, 3 H, COOCH₂CH₃), 3.13-3.15 (t, *J*=2.21, 2.21 Hz, 1 H, CH), 3.94-3.96 (d, *J* = 2.38 Hz, 2 H, CH₂), 4.19-4.25 (q, *J*=7.07, 7.07, 7.08 Hz, 2 H, COOCH₂CH₃), 6.66-6.68 (d, *J*=8.73 Hz, 2 H, Ar), 6.86-6.89 (t, *J*=5.85, 5.85 Hz, 1 H, NH, exch), 7.72-7.74 (d, *J*=8.69 Hz, 2 H, Ar). The intermediate **306** was used for the next reaction without further characterization.

Methyl 4-(2-propynyloxy)-benzoate (307).

To methyl 4-hydroxybenzoate **314** (1.32 g, 8.7 mmol, 1 eq) dissolved in dry acetone (15 mL), and K₂CO₃ (2.77 g, 2.77 mmol, 2.3 eq) was added, propargyl bromide (80% wt in toluene) **312** (1.54 mL, 17.4 mmol, 2 eq), and the mixture was refluxed for 3 h until a new

non-polar spot was observed on TLC (hexane/EtOAc). The mixture was then diluted with CH₂Cl₂ (50 mL), washed with H₂O (25 mL) and brine (25 mL), dried over Na₂SO₄, and the solvent was removed in vacuo. To the residue, MeOH was added followed by silica gel and evaporated to afford a plug, which was loaded onto a silica gel column and eluted initially with hexane followed by gradual increase to 100% EtOAc. Fractions with the required R_f were pooled and evaporated to afford **307** (1.56 g, 95%) as a white powder. TLC R_f = 0.8 (hexane/EtOAc, 1:1); mp 58 °C.³⁹⁰ ¹H NMR (400 MHz, DMSO-*d*₆): δ 3.64-3.65 (t, *J* = 2.36, 2.36 Hz, 1 H, CH), 3.82 (s, 3 H, COOCH₃), 4.90-4.91 (d, *J* = 2.38 Hz, 2 H, CH₂), 7.09-7.1 (d, *J* = 8.91 Hz, 2 H, Ar), 7.92-7.94 (d, *J* = 8.94 Hz, 2 H, Ar). ¹H NMR matches with the ¹H NMR of reported compound.³⁹⁰

4-(prop-2-yn-1-yloxy)benzoic acid (315).

To a solution of methyl 4-(2-propynyloxy)-benzoate **307** (225 mg, 1.18 mmol, 1 eq) dissolved in MeOH (1 mL) and THF (1 mL), was added 1 N NaOH (1 mL). The resultant mixture was refluxed for 2.5 h until disappearance of starting material and a new polar spot was observed on TLC (hexane/EtOAc). The organic solvents were removed in vacuo and the pH of the solution was adjusted to 2-3 using 1 N HCl to afford a white precipitate. The precipitate was filtered, washed with water and dried overnight in vacuo to afford **315** (173 mg, 83%) as a white powder. TLC R_f = 0.7 (hexane/EtOAc, 1:1); ¹H NMR (400 MHz, DMSO-*d*₆): δ 3.63-3.64 (t, *J* = 2.29, 2.29 Hz, 1 H, CH), 4.89-4.90 (d, *J* = 2.32 Hz, 2 H, CH₂), 7.06-7.08 (d, *J* = 8.84 Hz, 2 H, Ar), 7.9-7.92 (d, *J* = 8.86 Hz, 2 H, Ar). ¹H NMR matches with the ¹H NMR of reported compound.³⁹¹ The intermediate **315** was used for the next reaction without further characterization.

Diethyl (4-(prop-2-yn-1-yloxy)benzoyl)-L-glutamate (316).

Compound **316** was prepared using the general method described for the preparation of **210-211**, from 4-(prop-2-yn-1-yloxy)benzoic acid **315** (175 mg, 1 mmol), to give **316** (308 mg, 85%) as a colorless liquid. TLC R_f = 0.4 (hexane/EtOAc, 3:1); ^1H NMR (400 MHz, DMSO- d_6): δ 1.14-1.2 (m, 6 H, $\text{COOCH}_2\text{CH}_3$), 1.94-2.14(m, 2 H, β - CH_2), 2.41-2.445 (t, $J=7.53$, 7.53 Hz, 2 H, γ - CH_2), 3.59-3.6 (t, $J = 2.28$, 2.28 Hz, 1H, CH), 4.01-4.13 (m, 4 H, $\text{COOCH}_2\text{CH}_3$), 4.39-4.4 (dd, $J=5.23$, 9.63 Hz, 1 H, α -CH), 4.87-4.88 (d, $J = 2.30$ Hz, 2 H, CH_2), 7.05-7.07 (d, $J = 8.83$ Hz, 2 H, Ar), 7.85-7.87 (d, $J=8.77$ Hz, 2 H, Ar). The intermediate **316** was used for the next reaction without further characterization.

Tetraethyl 2,2'-((4,4'-(hexa-2,4-diyne-1,6-diylbis(oxy))bis(benzoyl))bis(azanediy))-(2S,2'S)-diglutarate (319).

A mixture of **316** (26 mg, 0.09 mmol, 1.3 eq), $\text{Pd}(\text{PPh}_3)_4$ (5.6 mg, 0.005 mmol, 7 mol %), and TEA (0.02 mL, 0.14 mmol, 2 equiv) in DMF (1 mL) was stirred at room temperature, away from light for 15 min to. *N*-(5-iodo-4-oxo-4,7-dihydro-3*H*-pyrrolo[2,3-*d*]pyrimidin-2-yl)pivalamide **305** (26 mg, 0.07 mmol, 1 eq) and CuI (2 mg, 15 mol %) were added to this reaction mixture, which was then stirred at room temperature for 12 h. The solvent was removed in vacuo and MeOH followed by silica gel was added to the residue, and evaporated to afford a plug. The plug was loaded onto a silica gel column and eluted initially with CHCl_3 followed by gradual increase to 1% CHCl_3 in MeOH. Fractions with required R_f were pooled and evaporated to afford the Glaser coupling product **319** (13 mg, 25%) as an orange sticky solid. TLC R_f = 0.8 ($\text{CHCl}_3/\text{MeOH}$ 5:1); ^1H NMR (400 MHz, DMSO- d_6): δ 1.14-1.2 (m, 12 H, $\text{COOCH}_2\text{CH}_3$), 1.96-2.16 (m, 4 H, β - CH_2), 2.41-2.46 (m, 4 H, γ - CH_2), 4.02-4.13 (m, 8 H, $\text{COOCH}_2\text{CH}_3$), 4.38-4.47 (m, 2 H, α -CH), 6.99-7.01 (d, J

= 8.82 Hz, 4 H, Ar), 7.84-7.86 (d, $J=8.77$ Hz, 4 H, Ar), 8.56-8.57 (d, $J=7.73$ Hz, 2 H, CONH, exch). LRMS calculated for $C_{38}H_{44}N_2O_{12}$ = 720.29, found $[M+Na]^+$ 743.2792 .

The intermediate **319** was not characterized further.

Ethyl 4-acetamidobenzoate (320).

To ethyl 4-aminobenzoate **313** (1 g, 6 mmol, 1 eq) in dry CH_2Cl_2 (20 mL) was added acetic anhydride (0.7 mL, 7.26 mmol, 1.2 eq) and the reaction was stirred at room temperature and monitored by TLC. Upon completion of the reaction after 12 h and appearance of a new non-polar spot on TLC (hexane/EtOAc), the reaction mixture was washed with sat. Na_2CO_3 , dried over Na_2SO_4 and the solvent was removed under reduced pressure. The product **320** (1.13 g, 90%), was obtained as a white powder. TLC R_f = 0.4 (hexane/EtOAc 1:1); 1H NMR (400 MHz, $DMSO-d_6$): δ 1.29-1.32 (t, $J=7.05$, 7.05 Hz, 3 H, $COOCH_2CH_3$), 2.08 (s, 3 H, CH_3), 4.25-4.31 (q, $J=7.10$, 7.10, 7.09 Hz, 2 H, $COOCH_2CH_3$), 7.7-7.72 (d, $J=8.74$ Hz, 2 H, Ar), 7.89-7.91 (d, $J=8.75$ Hz, 2 H, Ar), 10.29 (s, 1 H, NH, exch). 1H NMR matches with the 1H NMR of reported compound.³⁹² mp 101 °C.³⁹³

Ethyl 4-(2,2,2-trifluoroacetamido)benzoate (321).

A suspension of ethyl 4-aminobenzoate **313** (5 g, 30 mmol) in trifluoroacetic anhydride (50 mL) was stirred under anhydrous conditions at room temperature for 2 h, and was subsequently allowed to stand at room temperature overnight. Excess trifluoroacetic anhydride was removed under reduced pressure and the residue was dissolved in CH_2Cl_2 (70 mL), washed with cold 2% HCl (50 mL), cold 5% $NaHCO_3$ (50 mL), and cold water (2×100 mL). The organic layer was dried over Na_2SO_4 , filtered, and the solvent was evaporated under reduced pressure to afford **321** (7.9 g, quant.) as a buff colored powder.

TLC R_f = 0.6 (hexane/EtOAc 1:1); mp 128 °C dec.³⁹⁴ ^1H NMR (400 MHz, DMSO- d_6) δ 1.31-1.34 (t, J =6.98, 6.98 Hz, 3 H, $\text{COOCH}_2\text{CH}_3$), 4.29-4.33 (q, J =6.92, 2 H, $\text{COOCH}_2\text{CH}_3$), 7.83-7.85 (d, J =7.63 Hz, 2 H, Ar), 8-8.01 (d, J =7.64 Hz, 2 H, Ar). ^1H NMR matches with the ^1H NMR of reported compound.³⁹⁴ LRMS calculated for $\text{C}_{13}\text{H}_9\text{F}_6\text{NO}_4$ = 261.06, found $[\text{M}-\text{H}]^-$ 260.0.

Ethyl 4-pivalamidobenzoate (322).

A solution of ethyl 4-aminobenzoate **313** (3 g, 18.2 mmol, 1 eq) in pivalic anhydride (50 mL) was stirred at 80 °C for 8 h. The reaction was cooled to room temperature and then evaporated to dryness. MeOH followed by silica gel was added to the residue and evaporated to afford a plug which was loaded onto a silica gel column and eluted initially with hexane followed by gradual increase to 100% EtOAc. Fractions with the required R_f were pooled and evaporated to afford **322** (1.4 g, 56%) as a white powder. TLC R_f = 0.6 (hexane/EtOAc 1:1); ^1H NMR (400 MHz, DMSO- d_6): δ 1.24 (s, 9 H, $(\text{CH}_3)_3$), 1.29-1.33 (t, J = 7.09, 7.09 Hz, 3 H, $\text{COOCH}_2\text{CH}_3$), 4.25-4.31 (q, J =7.07, 7.07, 7.08 Hz, 2 H, $\text{COOCH}_2\text{CH}_3$), 7.81-7.83 (d, J = 8.77 Hz, 2 H, Ar), 7.89-7.91 (d, J = 8.80 Hz, 2 H, Ar), 9.52 (s, br, 1 H, NH, exch). ^1H NMR matches with the ^1H NMR of reported compound.³⁹⁵ The intermediate **322** was used for the next reaction without further characterization.

Ethyl 4-((*tert*-butoxycarbonyl)amino)benzoate (323).

To a solution of ethyl 4-aminobenzoate **313** (3 g, 18.2 mmol, 1 eq) in 1,4-dioxane (67 mL), di-*tert*-butyl dicarbonate (6.3 g, 29 mmol, 1.6 eq) was added and the mixture was stirred at 80 °C for 24 h. The reaction was cooled to room temperature, solvent was removed in vacuo and MeOH followed by silica gel was added to the residue and evaporated to afford a plug.

The plug was loaded onto a silica gel column and eluted initially with hexane followed by gradual increase in polarity to 100% EtOAc. Fractions with the required R_f were pooled and evaporated to afford **323** (4.35 g, 90%) as a buff colored powder. TLC R_f = 0.5 (hexane/EtOAc 3:1); mp 135.8 °C dec. ^1H NMR (400 MHz, CDCl_3): δ 1.39-1.42 (m, 3 H, $\text{COOCH}_2\text{CH}_3$), 1.55 (s, 9 H, $(\text{CH}_3)_3$), 4.35-4.4 (q, J = 6.41 Hz, 2 H, $\text{COOCH}_2\text{CH}_3$), 6.7 (s, br, 1 H, NH, exch), 7.44-7.46 (d, J = 8.09 Hz, 2 H, Ar), 7.99-8.01 (d, J = 7.27 Hz, 2 H, Ar). ^1H NMR matches with the ^1H NMR of reported compound.³⁹⁶ The intermediate **323** was used for the next reaction without further characterization.

Ethyl 4-((5-hydroxypentyl)amino)benzoate (325).

To a solution of ethyl 4-aminobenzoate **313** (1 g, 6.05 mmol, 1 eq) in DMF (10 mL), TEA (1.69 g, 12.1 mmol, 2 eq) was added and the mixture was stirred at 80 °C for 18 h. The reaction was cooled to room temperature, solvent was removed in vacuo and MeOH followed by silica gel was added to the residue and evaporated to afford a plug. The plug was loaded onto a silica gel column and eluted initially with hexane followed by gradual increase in polarity to 100% EtOAc. Fractions with the required R_f were pooled and evaporated to afford **325** (300 mg, 20%) as a yellow syrup. TLC R_f = 0.3 (hexane/EtOAc 1:1); ^1H NMR (400 MHz, CDCl_3): δ 1.25-1.29 (t, 3 H, J =7.10, 7.10 Hz, $\text{COOCH}_2\text{CH}_3$), 1.38-1.45 (m, 2 H, CH_2), 1.52-1.61 (m, 4 H, CH_2CH_2), 3.04-3.07 (t, J =6.92, 6.92 Hz, 2 H, NH- CH_2), 3.41-3.45 (t, J =6.37, 6.37 Hz, 2 H, OH- CH_2), 3.56 (s, br, 1 H, OH, exch), 4.17-4.23 (q, J =7.08, 7.08, 7.09 Hz, 2 H, $\text{COOCH}_2\text{CH}_3$), 6.56-6.58 (d, J =8.82 Hz, 2 H, Ar), 7.66-7.69 (d, J =8.79 Hz, 2 H, Ar). The intermediate **325** was not characterized further.

Ethyl 4-((*tert*-butoxycarbonyl)(5-hydroxypentyl)amino)benzoate (329).

To a suspension of Cs₂CO₃ (2.46 g, 7.54 mmol, 1 equiv), tetrabutylammonium iodide (2.79 g, 7.54 mmol, 1 equiv) in anhydrous DMF (40 mL), was added ethyl 4-((*tert*-butoxycarbonyl)amino)benzoate **323** (2 g, 7.54 mmol, 1 eq) and the mixture was stirred for 1 h at room temperature. The reaction mixture was subsequently cooled to 0 °C and 5-bromopentanol **324** (1 mL, 8.3 mmol, 1.1 equiv) was added dropwise and the resulting mixture was gradually heated to 70 °C and stirred for an additional 18 h. The resultant suspension was then poured into water (100 mL) and extracted with EtOAc (3 x 100 mL). The organic layer was washed further with water (3 x 100 mL), brine (100 mL), and dried over Na₂SO₄ and the solvent was removed in vacuo. To the residue, MeOH was added followed by silica gel and the solvent was evaporated to afford a plug. The plug was loaded onto a silica gel column and eluted initially with hexane followed by gradual increase in polarity to 100% EtOAc. Fractions with the required R_f were pooled and evaporated to afford **329** (1.96 g, 74%) as a yellow syrup. TLC R_f = 0.15 (hexane/EtOAc, 3:1). ¹H NMR (400 MHz, DMSO-*d*₆): δ 1.23-1.6 (m, 18 H, CH₂CH₂CH₂, COOCH₂CH₃, NHCO(CH₃)₃), 3.32-3.4 (m, 2 H, Ar-CH₂), 3.63-3.68 (m, 2 H, OH-CH₂), 3.99-4.05 (m, 3 H, COOCH₂CH₃, OH, exch), 7.38-7.40 (d, *J*=8.42 Hz, 2 H, Ar), 7.90-7.93 (d, *J*=8.59 Hz, 2 H, Ar). The intermediate **329** was used for the next reaction without further characterization.

Methyl 4-((5-hydroxypentyl)oxy)benzoate (330).

To methyl 4-hydroxybenzoate **314** (2.75 g, 18.07 mmol, 1 eq) dissolved in dry acetone (40 mL), and K₂CO₃ (5 g, 36.15 mmol, 2 eq) was added, 5-bromopentanol **324** (2.2 mL, 18.07 mmol, 1 eq), and the mixture was stirred at 80 °C for 24 h. The solvent was removed in vacuo and to the residue, MeOH was added followed by silica gel and evaporated to afford

a plug. The plug was loaded onto a silica gel column and eluted initially with hexane followed by gradual increase in polarity to 100% EtOAc. Fractions with the required R_f were pooled and evaporated to afford **330** (2.65 g, 62%) as a white syrup. TLC R_f = 0.4 (hexane/EtOAc, 1:1). $^1\text{H NMR}$ (400 MHz, DMSO- d_6): δ 1.4-1.52 (m, 4 H, CH_2CH_2), 1.7-1.77 (m, 2 H, CH_2), 3.39-3.43 (m, 2 H, OH- $\underline{\text{CH}_2}$), 3.81 (s, 3 H, COOCH_3), 4.03-4.06 (t, $J=6.49, 6.49$ Hz, 2 H, ArO- CH_2), 4.38-4.4 (t, $J=5.14, 5.14$ Hz, 1 H, OH, exch), 7.02-7.05 (d, $J=8.90$ Hz, 2 H, Ar), 7.89-7.91 (d, $J=8.88$ Hz, 2 H, Ar). The intermediate **330** was used for the next reaction without further characterization.

Methyl 4-((5-hydroxypentyl)thio)benzoate (332).

To a suspension of Cs_2CO_3 (2.5 g, 7.7 mmol, 1 equiv), tetrabutylammonium iodide (2.83 g, 7.7 mmol, 1 equiv) in anhydrous DMF (40 mL), was added ethyl 4-mercaptobenzoate **331** (1.3 g, 7.7 mmol, 1 eq) and the mixture was stirred for 1 h at room temperature. The reaction mixture was subsequently cooled to 0 °C and 5-bromopentanol **324** (1.04 mL, 8.5 mmol, 1.1 equiv) was added dropwise and the resulting mixture was gradually warmed to room temperature while being stirred for an additional 3 h. The resultant suspension was then poured into water (100 mL) and extracted with EtOAc (3 x 100 mL). The organic layer was washed further with water (3 x 100 mL), brine (100 mL), and dried over Na_2SO_4 and the solvent was removed in vacuo. To the residue, MeOH was added followed by silica gel and the solvent was evaporated to afford a plug. The plug was loaded onto a silica gel column and eluted initially with hexane followed by gradual increase in polarity to 100% EtOAc. Fractions with the required R_f were pooled and evaporated to afford **332** (1.53 g, 80%) as a white syrup. TLC R_f = 0.4 (hexane/EtOAc, 1:1). $^1\text{H NMR}$ (500 MHz, DMSO- d_6): δ 1.42-1.45 (m, 4 H, CH_2CH_2), 1.59-1.65 (m, 2 H, CH_2), 3.03-3.06 (m, 2 H, OH- $\underline{\text{CH}_2}$),

3.83 (s, 3 H, COOCH₃), 4.42-4.44 (m, 1 H, OH, exch), 7.38-7.40 (d, $J=8.53$ Hz, 2 H, Ar), 7.85-7.87 (d, $J=8.52$ Hz, 2 H, Ar). The intermediate **332** was used for the next reaction without further characterization.

Ethyl 4-((*tert*-butoxycarbonyl)(6-hydroxyhexyl)amino)benzoate (334).

To a suspension of Cs₂CO₃ (614 mg, 1.88 mmol, 1 equiv), tetrabutylammonium iodide (695 mg, 1.88 mmol, 1 equiv) in anhydrous DMF (10 mL), was added ethyl 4-((*tert*-butoxycarbonyl)amino)benzoate **323** (500 mg, 1.88 mmol, 1 eq) and the mixture was stirred for 1 h at room temperature. The reaction mixture was subsequently cooled to 0 °C and 6-bromohexanol **333** (0.27 mL, 2.07 mmol, 1.1 equiv) was added dropwise and the resulting mixture was gradually heated to 80 °C and stirred for an additional 18 h. The resultant suspension was then poured into water (100 mL) and extracted with EtOAc (3 x 25 mL). The organic layer was washed further with water (3 x 25 mL), brine (25 mL), and dried over Na₂SO₄ and the solvent was removed in vacuo. To the residue, MeOH was added followed by silica gel and the solvent was evaporated to afford a plug. The plug was loaded onto a silica gel column and eluted initially with hexane followed by gradual increase in polarity to 100% EtOAc. Fractions with the required R_f were pooled and evaporated to afford **334** (350 mg, 51%) as a yellow syrup. TLC R_f = 0.15 (hexane/EtOAc, 3:1). ¹H NMR (400 MHz, CDCl₃): δ 1.32-1.45 (m, 16 H, CH₂CH₂, COOCH₂CH₃, NHCO(CH₃)₃), 1.52-1.72 (m, 4 H, CH₂, CH₂) 3.62-3.71 (m, 4 H, OH-CH₂, N-CH₂), 4.1-4.16 (m, 1 H, OH, exch), 4.36-4.42 (q, $J=7.13, 7.13, 7.12$ Hz, 2 H, COOCH₂CH₃), 7.27-7.29 (d, $J=8.72$ Hz, 2 H, Ar), 8.01-8.04 (d, $J=8.79$ Hz, 2 H, Ar). The intermediate **334** was used for the next reaction without further characterization.

General procedure for the synthesis of aldehydes 335-338.

Alcohols **329**, **330**, **332** and **334** (1 eq) in anhyd. CH₂Cl₂ were added to a stirred solution of Dess-Martin periodinane (1.2 eq) in CH₂Cl₂ at 0 °C and the mixture was allowed to warm to room temperature while being stirred for 0.5-4 h. TLC (hexane/EtOAc) showed formation of one new major non-polar spot. Excess oxidant was destroyed by vigorously stirring the reaction mixture for 5 min with 1 N NaOH (0.2 eq). The mixture was diluted with (Et)₂O and washed with water and brine solution, and dried over Na₂SO₄. The solvent was evaporated, MeOH and celite were added to the residue, and evaporated to dryness. The resultant plug was loaded on a silica gel column and flash-chromatographed with hexanes followed by gradual increase of EtOAc to 50% EtOAc in hexanes. Fractions with the desired R_f (TLC) were pooled and evaporated to afford target compounds **335-338** as syrups.

Ethyl 4-((*tert*-butoxycarbonyl)(5-oxopentyl)amino)benzoate (**335**).

Compound **335** was prepared using the general method described for the preparation of **335-338** in 0.5 h, from **329** (500 mg, 1.42 mmol) to give **335** (300 mg, 60%) as a colorless syrup. TLC R_f = 0.31 (hexane/EtOAc, 3:1); ¹H NMR (400 MHz, CDCl₃): δ 1.39-1.43 (t, *J*=7.13, 7.13 Hz, 3 H, COOCH₂CH₃), 1.45 (s, 9 H, NHCO(CH₃)₃), 1.54-1.68 (m, 4 H, CH₂), 2.45-2.49 (dt, *J*=1.45, 7.03, 7.11 Hz, 2 H, CHO-CH₂), 3.69-3.73 (t, *J*=7.01, 7.01 Hz, 2 H, N-CH₂), 4.36-4.42 (q, *J*=7.13, 7.13, 7.13 Hz, 2 H, COOCH₂CH₃), 7.27-7.29 (d, *J*=8.62 Hz, 2 H, Ar), 8.02-8.04 (d, *J*=8.58 Hz, 2 H, Ar), 9.75-9.76 (t, *J*=1.51, 1.51 Hz, 1 H, CHO). The intermediate **335** was used for the next reaction without further characterization.

Methyl 4-((5-oxopentyl)oxy)benzoate (336).

Compound **336** was prepared using the general method described for the preparation of **335-338** in 4 h, from **330** (1.46 g, 6.11 mmol) to give **336** (859 mg, 60%) as a colorless syrup. TLC R_f = 0.7 (hexane/EtOAc, 1:1); $^1\text{H NMR}$ (400 MHz, DMSO- d_6): δ 1.63-1.78 (m, 4 H, CH_2CH_2), 3.81 (s, 3 H, COOCH_3), 7.02-7.04 (d, $J=8.84$ Hz, 2 H, Ar), 7.89-7.91 (d, $J=8.88$ Hz, 2 H, Ar), 9.69 (m, 1 H, CHO). The intermediate **336** was used for the next reaction without further characterization.

Methyl 4-((5-oxopentyl)thio)benzoate (337).

Compound **337** was prepared using the general method described for the preparation of **335-338** in 4 h, from **332** (447 mg, 1.77 mmol) to give **337** (373 mg, 84%) as a colorless syrup. TLC R_f = 0.7 (hexane/EtOAc, 1:1); $^1\text{H NMR}$ (400 MHz, DMSO- d_6): δ 1.58-1.7 (m, 4 H, CH_2CH_2), 3.05-3.09 (t, $J=6.82$, 6.82 Hz, 2 H, Ar- CH_2), 3.83 (s, 3 H, COCH_3), 7.39-7.41 (d, $J=8.42$ Hz, 2 H, Ar), 7.85-7.87 (d, $J=8.46$ Hz, 2 H, Ar), 9.66 (s, 1 H, CHO). The intermediate **337** was used for the next reaction without further characterization.

Ethyl 4-((tert-butoxycarbonyl)(5-oxohexyl)amino)benzoate (338).

Compound **338** was prepared using the general method described for the preparation of **335-338**, from **334** (1.35 g, 3.69 mmol) to give **338** (900 mg, 67%) as a colorless syrup. TLC R_f = 0.3 (hexane/EtOAc, 3:1); $^1\text{H NMR}$ (400 MHz, CDCl_3): δ 1.31-1.37 (m, 2 H, CH_2), 1.37-1.43 (t, $J=7.13$, 7.13 Hz, 3 H, $\text{COOCH}_2\text{CH}_3$), 1.45 (s, 9 H, $\text{NHCO}(\text{CH}_3)_3$), 1.54-1.67 (m, 4 H, CH_2), 2.4-2.45 (dt, $J=1.66$, 7.30, 7.33 Hz, 2 H, CH_2), 3.67-3.71 (m, 2 H, CH_2), 4.1-4.17 (dd, $J=7.16$, 14.28 Hz, 2 H, CH_2), 4.36-4.43 (q, $J=7.16$, 7.16, 7.12 Hz, 2 H, $\text{COOCH}_2\text{CH}_3$), 7.26-7.28 (m, 2 H, Ar), 8.01-8.04 (d, $J=8.48$ Hz, 2 H, Ar), 9.75-9.76 (t,

$J=1.65, 1.65$ Hz, 1 H, CHO). The intermediate **338** was used for the next reaction without further characterization.

General procedure for the synthesis of 343 and 346.

To the solution of aldehydes **335** and **338** (1 eq) in anhydrous Et₂O was added 5,5-dibromo-2,2-dimethyl-4,6-dioxo-1,3-dioxane **302** (1.2 mmol), 2 N HCl in Et₂O solution (0.1 eq) and the mixture was stirred at room temperature for 48 hours. TLC showed formation of one major non-polar spot (hexane/EtOAc 3:1). The reaction solution was washed with 5% NaHCO₃ solution and extracted with H₂O and dried over Na₂SO₄. Evaporation of the solvent yielded unstable α -bromo aldehyde residues **339** and **342** which were used directly for the next step without purification and further characterization. To a solution of 2,6-diamino-4-oxopyrimidine **22** (1 eq) and sodium acetate (2 eq) in water were added α -bromo aldehydes (1 eq) and the reaction mixture was stirred at 45 °C for 4 hours. TLC showed one major non-polar spot (CHCl₃/MeOH). After evaporation of the solvents, CH₃OH was added followed by celite and methanol was evaporated to afford a plug. The plug was loaded onto a silica gel column and flash chromatographed with 10% MeOH in CHCl₃. Desired fractions (TLC R_f = 0.5 ; CHCl₃/MeOH, 5:1) were pooled and evaporated to afford crude pink sticky solids which were dissolved in minimal amount of MeOH and 1 N NaOH.

The mixture was stirred at room temperature for 12 h. Monitoring the reaction using TLC indicated consumption of the starting materials and generation of one major spot at the baseline (CHCl₃/MeOH). The methanol in the reaction mixture was then evaporated under reduced pressure. The resulting basic solution was cooled in ice bath, and the pH was adjusted to 3–4 with dropwise addition of 1 N HCl. The resulting suspension was cooled at 4–5 °C in the refrigerator for 2 h, and filtered. The residues were washed with a

cold water and dried under reduced pressure using P₂O₅ to afford boc-protected, ester hydrolyzed acids **343** and **346**.

General procedure for the synthesis of 344 and 345.

Bromine (0.9 eq) was added dropwise to 1,4-dioxane and stirred for 10 min. To this mixture, CH₂Cl₂ was added and the resultant solution was added dropwise to an ice-cooled solution of **336** and **337** in CH₂Cl₂. The reaction mixture was then stirred for 3.5 h after which aqueous solution of sat. Na₂CO₃ was added and stirred for an additional 0.5 h. The organic layer was then extracted with chloroform, washed with sat. Na₂S₂O₃ followed by water, dried over Na₂SO₄ and concentrated in vacuo to give crude α -bromo aldehyde residues **340** and **341** as syrups. The intermediates **340** and **341** were used directly for the next step without purification and further characterization. To a solution of 2,6-diamino-4-oxopyrimidine **22** (1 eq) and sodium acetate (2 eq) in water were added α -bromo aldehydes (1 eq) and the reaction mixture was stirred at 45 °C for 4 hours. TLC showed one major non-polar spot (CHCl₃/MeOH). After evaporation of the solvents, MeOH was added followed by celite. Evaporation of the MeOH afforded a plug, which was loaded onto a silica gel column and flash chromatographed with 10% MeOH in CHCl₃. Desired fractions (TLC R_f = 0.5 ; CHCl₃/MeOH, 5:1) were pooled and evaporated to afford crude pink sticky solids which were dissolved in minimal amount of MeOH and 1 N NaOH.

The mixture was stirred at room temperature for 12 h. Monitoring the reaction using TLC indicated consumption of the starting materials and generation of one major spot at the baseline (CHCl₃/MeOH). The methanol in the reaction mixture was then evaporated under reduced pressure. The resulting basic solution was cooled in ice bath, and the pH was adjusted to 3–4 with dropwise addition of 1 N HCl. The resulting suspension was

cooled at 4–5 °C in the refrigerator for 2 h, and filtered. The residues were washed with a cold water and dried under reduced pressure using P₂O₅ to afford acids **344** and **345**.

4-((3-(2-amino-4-oxo-4,7-dihydro-3H-pyrrolo[2,3-d]pyrimidin-5-yl)propyl)(tert-butoxycarbonyl)amino)benzoate (343).

Compound **343** was prepared using the general method described for the preparation of **343** and **346**, from **335** (240 mg, 0.7 mmol) to give crude **343** (70 mg, 23% over three steps) as a light pink powder. TLC R_f = 0.23 (CHCl₃/MeOH, 5:1); ¹H NMR (400 MHz, DMSO-*d*₆): δ 1.37 (s, 9 H, NHCO(CH₃)₃), 1.76-1.84 (m, 2 H, CH₂), 3.62-3.66 (m, 2 H, CH₂), 6.34 (s, 1 H, C6-CH), 6.52 (s, br, 2 H, 2-NH₂, exch) 7.36-7.38 (d, *J*=8.40 Hz, 2 H, Ar), 7.87-7.90 (d, *J*=8.48 Hz, 2 H, Ar), 10.56 (s, 1 H, 3-NH, exch), 10.86 (s, 1 H, 7-NH, exch). The intermediate **343** was used for the next reaction without further characterization.

4-(3-(2-amino-4-oxo-4,7-dihydro-3H-pyrrolo[2,3-d]pyrimidin-5-yl)propoxy)benzoate (344).

Compound **344** was prepared using the general method described for the preparation of **344** and **345**, from **336** (859 mg, 3.4 mmol) to give crude **344** (300 mg, 27% over three steps) as a pink powder. TLC R_f = 0.3 (CHCl₃/MeOH, 5:1); ¹H NMR (400 MHz, DMSO-*d*₆): δ 2.04-2.13 (m, 2 H, CH₂), 2.69-2.73 (m, 2 H, Ar-CH₂), 4.02-4.05 (t, *J*=6.40, 6.40 Hz, 2 H, ArO-CH₂), 6.25-6.42 (s, br, 3 H, C6-CH, 2-NH₂, exch), 6.99-7.01 (d, *J*=8.83 Hz, 2 H, Ar), 7.86-7.88 (d, *J*=8.77 Hz, 2 H, Ar), 10.46 (s, 1 H, 3-NH, exch), 10.81 (s, 1 H, 7-NH, exch). The intermediate **344** was used for the next reaction without further characterization.

4-((3-(2-amino-4-oxo-4,7-dihydro-3H-pyrrolo[2,3-d]pyrimidin-5-yl)propyl)thio)benzoate (345).

Compound **345** was prepared using the general method described for the preparation of **344** and **345**, from **337** (823 mg, 3.6 mmol) to give crude **345** (210 mg, 18% over three steps) as a pink powder. TLC $R_f = 0.3$ ($\text{CHCl}_3/\text{MeOH}$, 5:1); $^1\text{H NMR}$ (500 MHz, $\text{DMSO-}d_6$): δ 1.692-1.695 (m, 2 H, CH_2), 3.01-3.04 (t, $J=6.81$, 6.81 Hz, 2 H, CH_2), 6.74 (s, br, 2 H, 2- NH_2 , exch), 7.33-7.34 (d, $J=7.15$ Hz, 2 H, Ar), 7.82-7.84 (d, $J=7.03$ Hz, 2 H, Ar), 10.42 (s, 1 H, 3-NH, exch), 10.58 (s, 1 H, 7-NH, exch). The intermediate **345** was used for the next reaction without further characterization.

4-((3-(2-amino-4-oxo-4,7-dihydro-3H-pyrrolo[2,3-d]pyrimidin-5-yl)butyl)(tert-butoxycarbonyl)amino)benzoate (346).

Compound **346** was prepared using the general method described for the preparation of **343** and **346**, from **338** (1.06 g, 2.40 mmol) to give crude **346** (85 mg, 16% over three steps) as a pink powder. TLC $R_f = 0.25$ ($\text{CHCl}_3/\text{MeOH}$, 5:1); $^1\text{H NMR}$ (400 MHz, $\text{DMSO-}d_6$): δ 1.37 (s, 9 H, $\text{NHCO}(\text{CH}_3)_3$), 1.42-1.48 (m, 2 H, CH_2), 1.53-1.61 (m, 2 H, CH_2), 3.62-3.66 (m, 2 H, CH_2), 6.0 (s, 2 H, 2- NH_2 , exch), 6.29-6.3 (d, $J = 1.73$ Hz, 1 H, C6-CH), 7.34-7.36 (d, $J = 8.60$ Hz, 2 H, Ar), 7.87-7.90 (d, $J = 8.56$ Hz, 2 H, Ar), 10.15 (s, 1 H, 3-NH, exch), 10.62 (s, 1 H, 7-NH, exch). The intermediate **346** was used for the next reaction without further characterization.

General procedure for the synthesis of 347 and 348.

Solutions of **343** and **346** (1 eq) in hydrochloric acid/dioxane (3 M in 1,4-dioxane, 16 eq.) were stirred at room temperature for 16 h, then the pH was adjusted to 3-4 with NaOH

solution at -10 deg °C. The resulting suspension was warmed to 4–5 °C, refrigerated for 2 h, and filtered. The residues were washed with a cold water and dried under reduced pressure using P₂O₅ to afford crude acids **347** and **348**.

4-((3-(2-amino-4-oxo-4,7-dihydro-3H-pyrrolo[2,3-d]pyrimidin-5-yl)propyl)amino)benzoic acid (347).

Compound **347** was prepared using the general method described for the preparation of **347** and **348**, from **343** (70 mg, 0.16 mmol) to give crude **347** (50 mg, 93%) as a pink powder. TLC R_f = 0.2 (CHCl₃/MeOH, 5:1); ¹H NMR (400 MHz, DMSO-*d*₆): δ 1.83-1.90 (m, 2 H, CH₂), 2.63-2.67 (t, *J*=7.23, 7.23 Hz, 2 H, CH₂), 3.03-3.06 (t, *J*=6.82, 6.82 Hz, 2 H, CH₂), 6.43-6.74 (m, 6 H, C6-CH, Ar, 2-NH₂, exch, Ar-NH, exch), 7.63-7.66 (d, *J*=8.46 Hz, 2 H, Ar), 10.67 (s, 1 H, 3-NH, exch), 10.93 (s, 1 H, 7-NH, exch). The intermediate **347** was used for the next reaction without further characterization.

4-((3-(2-amino-4-oxo-4,7-dihydro-3H-pyrrolo[2,3-d]pyrimidin-5-yl)butyl)amino)benzoic acid (348).

Compound **348** was prepared using the general method described for the preparation of **347** and **348**, from **346** (80 mg, 0.18 mmol) to give crude **348** (60 mg, 97%) as a pink powder. TLC R_f = 0.2 (CHCl₃/MeOH, 5:1); ¹H NMR (400 MHz, DMSO-*d*₆): δ 1.50-1.74 (m, 4 H, CH₂CH₂), 3.06-3.08 (m, 2 H, CH₂), 6.15-6.55 (m, 6 H, C6-CH, Ar, Ar-NH, exch, 2-NH₂, exch), 7.63-7.65 (m, 2 H, Ar), 10.28 (s, br, 1 H, 3-NH, exch), 10.72 (s, br, 1 H, 7-NH, exch). The intermediate **348** was used for the next reaction without further characterization.

General procedure for the synthesis of 349-352.

To the acids **347**, **344**, **345** and **348** (1 eq) in anhydrous DMF were added *N*-methylmorpholine (1.2 eq) and 2-chloro-4,6-dimethoxy-1,3,5 triazine (1.2 eq). The resulting mixture was stirred at room temperature for 2 h. To this mixture were added *N*-methylmorpholine (1.2 eq) and L-glutamate diethyl ester hydrochloride (1.5 eq). The reaction mixture was stirred for an additional 12 h at room temperature until disappearance of the starting material and formation of a new non-polar spot on TLC and then evaporated to dryness under reduced pressure. To the residue, was added minimum amount of MeOH followed by silica gel and evaporated to dryness. The resulting plug was loaded on to a silica gel column and eluted with CHCl₃ followed by gradual increase in polarity to 5% MeOH in CHCl₃. Fractions with required R_f were pooled and evaporated to afford glutamate esters **349-352**.

Diethyl (4-((3-(2-amino-4-oxo-4,7-dihydro-3*H*-pyrrolo[2,3-*d*]pyrimidin-5-yl)propyl)amino)benzoyl)-L-glutamate (**349**).

Compound **349** was prepared using the general method described for the preparation of **349-352**, from **347** (50 mg, 0.22 mmol) and L-glutamate diethyl ester hydrochloride (70 mg, 0.34 mmol) to give **349** (40 mg, 76%) as a yellow sticky solid. TLC R_f = 0.6 (CHCl₃/MeOH, 5:1); ¹H NMR (400 MHz, DMSO-*d*₆): δ 1.15-1.2 (m, 6 H, COOCH₂CH₃), 1.83-2.12 (m, 4 H, β-CH₂, CH₂), 2.39-2.43 (t, 2 H, *J*=7.49, 7.49 Hz, γ-CH₂), 2.63-2.67 (t, *J*=7.30, 7.30 Hz, 2 H, CH₂), 3.03-3.06 (m, 2 H, CH₂), 4.02-4.11 (m, 4 H, COOCH₂CH₃), 4.34-4.4 (m, 1 H, α-CH), 6.00 (s, 2 H, 2-NH₂, exch), 6.30-6.32 (t, *J* = 5.09, 5.09 Hz, 1 H, Ar-NH, exch), 6.38 (s, 1 H, C6-CH), 6.52-6.55 (d, *J* = 8.50 Hz, 2 H, Ar), 7.63-7.66 (d, *J* = 8.48 Hz, 2 H, Ar), 8.22-8.24 (d, *J* = 7.25 Hz, 1 H, CONH, exch), 10.2 (s, 1 H, 3-NH, exch),

10.67 (s, 1 H, 7-NH, exch). The intermediate **349** was used for the next reaction without further characterization.

Diethyl (4-(3-(2-amino-4-oxo-4,7-dihydro-3H-pyrrolo[2,3-d]pyrimidin-5-yl)propoxy)benzoyl)-L-glutamate (350).

Compound **350** was prepared using the general method described for the preparation of **349-352**, from **344** (287 g, 0.87 mmol) and L-glutamate diethyl ester hydrochloride (315.6 g, 1.55 mmol) to give **350** (300 mg, 67%) as a pink sticky solid. TLC R_f = 0.6 (CHCl₃/MeOH, 5:1); ¹H NMR (400 MHz, DMSO-*d*₆): δ 1.15-1.2 (m, 6 H, COOCH₂CH₃), 1.83-2.14 (m, 4 H, β -CH₂, CH₂), 2.41-2.45 (m, 2 H, γ -CH₂), 2.69-2.73 (m, 2 H, CH₂), 4.02-4.13 (m, 4 H, COOCH₂CH₃), 4.36-4.46 (m, 1 H, α -CH), 5.99 (s, 2 H, 2-NH₂, exch), 6.37 (s, 1 H, C6-CH), 6.98-7.0 (d, J = 8.82 Hz, 2 H, Ar), 7.83-7.85 (d, J = 8.79 Hz, 2 H, Ar), 8.55-8.57 (d, J = 7.34 Hz, 1 H, CONH, exch), 10.17 (s, 1 H, 3-NH, exch), 10.66 (s, 1 H, 7-NH, exch). The intermediate **350** was used for the next reaction without further characterization.

Diethyl (4-((3-(2-amino-4-oxo-4,7-dihydro-3H-pyrrolo[2,3-d]pyrimidin-5-yl)propyl)thio)benzoyl)-L-glutamate (351).

Compound **351** was prepared using the general method described for the preparation of **349-352**, from **345** (220 mg, 0.64 mmol) and L-glutamate diethyl ester hydrochloride (195 g, 0.96 mmol) to give **351** (120 mg, 37%) as a pink sticky solid. TLC R_f = 0.6 (CHCl₃/MeOH, 5:1); ¹H NMR (400 MHz, DMSO-*d*₆): δ 1.15-1.22 (m, 6 H, COOCH₂CH₃), 1.68 (m, 2 H, CH₂), 1.8-2.04 (m, 2 H, β -CH₂), 2.42-2.46 (t, J =7.50, 7.50 Hz, γ -CH₂), 3.0-3.04 (t, J = 7.18, 7.18 Hz, 2 H, CH₂), 4.02-4.13 (m, 4 H, COOCH₂CH₃), 4.39-4.44 (m, 1

H, α -CH), 5.99 (s, 2 H, 2-NH₂, exch), 6.72 (s, 1 H, C6-CH), 7.34-7.35 (d, $J = 8.37$ Hz, 2 H, Ar), 7.78-7.80 (d, $J = 8.35$ Hz, 2 H, Ar), 8.68-8.70 (d, $J = 7.36$ Hz, 1 H, CONH, exch), 10.17 (s, 1 H, 3-NH, exch), 10.57 (s, 1 H, 7-NH, exch). The intermediate **351** was used for the next reaction without further characterization.

Diethyl (4-((3-(2-amino-4-oxo-4,7-dihydro-3H-pyrrolo[2,3-d]pyrimidin-5-yl)butyl)amino)benzoyl)-L-glutamate (352).

Compound **352** was prepared using the general method described for the preparation of **349-352**, from **348** (65 mg, 0.19 mmol) and L-glutamate diethyl ester hydrochloride (50 mg, 0.23 mmol) to give **352** (50 mg, 50%) as a yellow sticky solid. TLC $R_f = 0.5$ (CHCl₃/MeOH, 5:1); ¹H NMR (400 MHz, DMSO-*d*₆): δ 1.15-1.2 (m, 6 H, COOCH₂CH₃), 1.52-1.72 (m, 4 H, CH₂CH₂), 1.93-2.12 (m, 2 H, β -CH₂), 2.40-2.43 (t, 2 H, $J=7.42$, 7.42 Hz, γ -CH₂), 2.58-2.61 (m, 2 H, CH₂), 3.04-3.09 (m, 2 H, CH₂), 4.02-4.11 (m, 4 H, COOCH₂CH₃), 4.34-4.41 (m, 1 H, α -CH), 5.98 (s, 2 H, 2-NH₂, exch), 6.21-6.24 (t, $J=4.72$, 4.72 Hz, 1 H, Ar-NH, exch), 6.36 (s, 1 H, C6-CH), 6.53-6.56 (d, $J = 8.48$ Hz, 2 H, Ar), 7.64-7.66 (t, $J = 8.55$ Hz, 2 H, Ar), 8.22-8.24 (d, $J = 7.16$ Hz, 1 H, CONH, exch), 10.14 (s, br, 1 H, 3-NH, exch), 10.64 (d, $J = 0.70$ Hz, 1 H, 7-NH, exch). The intermediate **352** was used for the next reaction without further characterization.

General procedure for the synthesis of 194-197.

To the glutamate esters **349-352** was added 1 N NaOH and the mixture was stirred at room temperature for 1 h. Monitoring the reaction using TLC indicated consumption of the starting material and generation of one major spot at the baseline (CHCl₃/MeOH 5:1). The pH of the solution was then adjusted to 3–4 with 1 N HCl (dropwise addition). The resulting

suspension was refrigerated at 4–5 °C for 2 h and filtered. The residue was washed with a small amount of cold water and dried in vacuum using P₂O₅ to afford acids **194-197**.

(4-((3-(2-amino-4-oxo-4,7-dihydro-3H-pyrrolo[2,3-d]pyrimidin-5-yl)propyl)amino)benzoyl)-L-glutamate (194).

Compound **194** was prepared using the general method described for the preparation of **194-197**, from **349** (25 mg, 0.05 mmol) to give **194** (20 mg, 90%) as a yellow powder. mp 149.4 °C dec. ¹H NMR (400 MHz, DMSO-*d*₆): δ 1.84-2.09 (m, 4 H, β-CH₂, CH₂), 2.32-2.35 (t, *J*=7.52, 7.52 Hz, 2 H, γ-CH₂), 2.64-2.67 (t, *J*=7.04, 7.04 Hz, 2 H, CH₂), 3.02-3.06 (dd, *J* = 6.73, 12.61 Hz, 2 H, CH₂), 4.32-4.36 (m, 1 H, α-CH), 5.99 (s, 2 H, 2-NH₂, exch), 6.26-6.28 (t, *J* = 5.37, 5.37 Hz, 1 H, Ar-NH, exch), 6.37-6.38 (d, *J* = 2.01 Hz, 1 H, C6-CH), 6.52-6.54 (d, *J* = 8.81 Hz, 2 H, Ar), 7.64-7.65 (d, *J* = 8.78 Hz, 2 H, Ar), 8.1-8.12 (d, *J* = 7.74 Hz, 1 H, CONH, exch), 10.19 (s, 1 H, 3-NH, exch), 10.65 (d, *J* = 0.97 Hz, 1 H, 7-NH, exch). HPLC analysis: retention time, 5.4 min; peak area, 95.08%; eluent A, H₂O; eluent B, ACN; gradient elution (95% H₂O to 100% ACN) over 10 mins with flow rate of 0.5 mL/min and detection at 254 nm; column temperature, rt. LRMS calculated for C₂₁H₂₄N₆O₆ = 456.18, found [M+H]⁺ 457.10.

(4-(3-(2-amino-4-oxo-4,7-dihydro-3H-pyrrolo[2,3-d]pyrimidin-5-yl)propoxy)benzoyl)-L-glutamic acid (195).

Compound **195** was prepared using the general method described for the preparation of **194-197**, from **350** (100 mg, 0.19 mmol) to give **195** (50 mg, 78%) as a light green powder. mp 150 °C dec. ¹H NMR (400 MHz, DMSO-*d*₆): δ 1.89-2.11 (m, 4 H, β-CH₂, CH₂), 2.32-2.35 (t, *J*=7.25, 7.25 Hz, 2 H, γ-CH₂), 2.7-2.73 (m, 2 H, CH₂), 4.0-4.03 (t, *J* = 6.27, 6.27

Hz, 2 H, CH₂), 4.33-4.36 (m, 1 H, α-CH), 5.99 (s, 2 H, 2-NH₂, exch), 6.36-6.37 (d, *J* = 1.43 Hz, 1 H, C6-CH), 6.97-6.99 (d, *J* = 8.82 Hz, 2 H, Ar), 7.82-7.84 (d, *J* = 8.81 Hz, 2 H, Ar), 8.38-8.40 (d, *J* = 7.56 Hz, 1 H, CONH, exch), 10.18 (s, 1 H, 3-NH, exch), 10.65 (d, *J* = 0.99 Hz, 1 H, 7-NH, exch). Anal. Calcd for C₂₁H₂₃N₅O₇ · 1.25 H₂O: C, 52.54; H, 5.35; N, 14.58. Found C, 52.58; H, 5.2; N, 14.39.

(4-((3-(2-amino-4-oxo-4,7-dihydro-3*H*-pyrrolo[2,3-*d*]pyrimidin-5-yl)propyl)thio)benzoyl)-L-glutamic acid (196).

Compound **196** was prepared using the general method described for the preparation of **194-197**, from **351** (120 mg, 0.22 mmol) to give **196** (40 mg, 45%) as a buff colored powder. mp 137 °C dec. ¹H NMR (400 MHz, DMSO-*d*₆): δ 1.80-1.99 (m, 4 H, β-CH₂, CH₂), 2.33-2.37 (m, 2 H, γ-CH₂), 2.99-3.03 (t, *J* = 7.05, 7.05 Hz, 2 H, CH₂), 4.36-4.38 (m, 1 H, α-CH), 5.99 (s, 2 H, 2-NH₂, exch), 6.37-6.38 (s, 1 H, C6-CH), 7.32-7.34 (d, *J* = 8.28 Hz, 2 H, Ar), 7.79-7.81 (d, *J* = 8.39 Hz, 2 H, Ar), 8.62 (s, br, 1 H, CONH, exch), 10.18 (s, 1 H, 3-NH, exch), 10.56 (d, *J* = 0.97 Hz, 1 H, 7-NH, exch). Anal. Calcd for C₂₁H₂₃N₅O₇ · 1.39 H₂O: C, 50.58; H, 5.21; N, 14.04; S, 6.43. Found C, 50.65; H, 5.03; N, 13.85; S, 6.16.

(4-((3-(2-amino-4-oxo-4,7-dihydro-3*H*-pyrrolo[2,3-*d*]pyrimidin-5-yl)butyl)amino)benzoyl)-L-glutamate (197).

Compound **197** was prepared using the general method described for the preparation of **194-197**, from **352** (50 mg, 0.09 mmol) to give **197** (30 mg, 67%) as a pink powder. mp 129.7 °C dec. ¹H NMR (400 MHz, DMSO-*d*₆): δ 1.54-1.59 (m, 2 H, CH₂), 1.64-1.72 (m, 2 H, CH₂), 1.87-2.09 (m, 2 H, β-CH₂), 2.31-2.35 (t, *J* = 7.36, 7.36 Hz, 2 H, γ-CH₂), 2.58-2.62 (t, *J* = 7.09, 7.09 Hz, 2 H, CH₂), 3.04-3.09 (dd, *J* = 6.14, 11.91 Hz, 2 H, CH₂), 4.31-4.37 (m,

1 H, α -CH), 5.99 (s, 2 H, 2-NH₂, exch), 6.19-6.22 (t, $J = 5.33, 5.33$ Hz, 1 H, Ar-NH, exch), 6.36-6.362 (d, $J = 1.20$ Hz, 1 H, C6-CH), 6.53-6.56 (d, $J = 8.80$ Hz, 2 H, Ar), 7.64-7.66 (t, $J=8.63$ Hz, 2 H, Ar), 8.08-8.10 (d, $J = 7.16$ Hz, 1 H, CONH, exch), 10.15 (s, br, 1 H, 3-NH, exch), 10.63-10.64 (d, $J=1.62$ Hz, 1 H, 7-NH, exch). HPLC analysis: retention time, 8.29 min; peak area, 96.17%; eluent A, H₂O; eluent B, ACN; gradient elution (95% H₂O to 100% ACN) over 10 mins with flow rate of 0.5 mL/min and detection at 254 nm; column temperature, rt. LRMS calculated for C₂₂H₂₆N₆O₆ = 470.19, found [M+H]⁺ 471.2 and [M-H]⁻ 469.2.

Methyl 2-fluoro-4-(6-oxohexyl)benzoate (354).

To a solution of methyl 4-bromo-2-fluorobenzoate (**353**) (2.33 g, 10 mmol, 1 eq) in anhydrous DMF (20 mL) was added hex-2-en-1-ol **299** (1.18 mL, 10 mmol, 1 eq), LiCl (424 mg, 10 mmol, 1 eq), LiOAc (1.65 g, 25 mmol, 2.5 eq), Bu₄NCl (2.82 g, 10 mmol, 1 eq), Pd(OAc)₂ (135 mg, 0.6 mmol, 0.06 eq) and the mixture was stirred at 90 °C for 2.5 h. TLC showed the disappearance of the starting material and formation of one major non-polar spot. After the reaction mixture was cooled to room temperature, ethyl acetate (3 X 20 mL) was added and the resulting solution was extracted with H₂O (2 X 20 mL) and dried over Na₂SO₄. After evaporation of solvent, the residue was loaded on a silica gel column and flash-chromatographed with hexane followed by gradual increase in polarity to 100% EtOAc and the desired fractions were pooled. After evaporation of solvent the residue was dried in vacuo using P₂O₅ to afford **354** (1.5 g, 59%), as a colorless syrup. TLC $R_f = 0.8$ (hexane/EtOAc, 1:1); ¹H NMR (400 MHz, CDCl₃): δ 1.38 (tt, $J = 6.38, 6.38, 10.15, 10.15$ Hz, 2 H, CH₂), 1.63-1.72 (m, 4 H, CH₂CH₂), 2.44-2.48 (dt, $J = 1.62, 7.30, 7.30$ Hz, 2 H, CHO-CH₂), 2.65-2.69 (m, 2 H, Ar-CH₂), 3.94 (s, 3 H, COOCH₃), 6.94-6.98 (dd, $J =$

1.34, 11.88 Hz, 1 H, Ar), 7.01-7.03 (dd, $J = 1.44, 7.96$ Hz, 1 H, Ar), 7.85-7.89 (t, $J = 7.81, 7.81$ Hz, 1 H, Ar), 9.79 (t, $J = 1.62, 1.62$ Hz, 1 H, CHO). The intermediate **354** was used for the next reaction without further characterization.

Methyl 4-(4-(2-amino-4-hydroxy-7H-pyrrolo[2,3-d]pyrimidin-5-yl)butyl)-2-fluorobenzoate (356).

To a solution of aldehyde **354** (500 mg, 1.88 mmol, 1 eq) in anhydrous Et₂O was added 5,5-dibromo-2,2-dimethyl-4,6-dioxo-1,3-dioxane **302** (283 mg, 0.94 mmol, 0.5 eq), 2 N HCl in Et₂O solution (0.01 mL, 0.18 mmol, 0.1 eq) and the mixture was stirred at room temperature for 48 hours. TLC showed the disappearance of the starting material and formation of one major non-polar spot. The reaction solution was washed with 5% NaHCO₃ solution and extracted with H₂O and dried over Na₂SO₄. After evaporation of solvent, the orange colored syrupy residue, α -bromo aldehyde **355** was used for directly for next step without further characterization. To a solution of 2,6-diamino-4-oxopyrimidine **22** (237 mg, 1.88 mmol, 1 eq) and sodium acetate (308 mg, 3.76 mmol, 2 eq) in water (5 mL) and methanol (5 mL) was added α -bromo aldehyde **355** (649 mg, 1.88 mmol, 1 eq). The reaction mixture was stirred at 45 °C for 4 hours. TLC showed the disappearance of starting materials and the formation of one new major spot (CHCl₃/MeOH, 5:1). After evaporation of solvent, MeOH was added followed by silica gel. Evaporation of the solvent afforded a plug, which was loaded onto a silica gel column and eluted with 10% MeOH in CHCl₃. Fractions with required R_f were pooled and evaporated to afford crude **356** (150 mg, 20%) as a pink sticky solid. TLC $R_f = 0.5$ (CHCl₃/MeOH 5:1); ¹H NMR (500 MHz, DMSO-*d*₆): δ 1.60-1.607 (m, 4 H, CH₂CH₂), 2.57-2.60 (t, $J=6.55, 6.55$ Hz, 2 H, Ar-CH₂), 2.65-2.67 (t, $J=6.79, 6.79$ Hz, 2 H, Ar-CH₂),

3.83 (s, 1 H, COOCH₃), 5.94 (s, 2 H, 2-NH₂, exch), 6.332-6.335 (d, $J = 1.85$ Hz, 1 H, C6-CH), 7.14-7.19 (dd, $J = 7.52, 15.65$ Hz, 2 H, Ar), 7.77-7.8 (t, $J = 7.86, 7.86$ Hz, 1 H, Ar), 10.08 (s, 1 H, 3-NH, exch), 10.59 (s, 1 H, 7-NH, exch). The intermediate **356** was used for the next reaction without further characterization.

4-(4-(2-amino-4-hydroxy-7*H*-pyrrolo[2,3-*d*]pyrimidin-5-yl)butyl)-2-fluorobenzoate (357).

To **356** (150 mg, 0.4 mmol), was added 1 N NaOH (3 mL) and the resulting mixture was stirred under N₂ at room temperature for 12 h. TLC indicated the disappearance of starting material and the formation of one major spot at the origin. The resulting solution was cooled in an ice bath, and the pH was adjusted 3 to 4 using 1 N HCl. The resulting suspension was chilled in a dry ice/acetone bath and thawed to 4 °C overnight in a refrigerator. The precipitate was filtered, washed with cold water, and dried in a desiccator under reduced pressure using P₂O₅ to afford crude acid **357** (88 mg, 61%) as a buff colored powder. TLC $R_f = 0.3$ (CHCl₃/MeOH 5:1); ¹H NMR (400 MHz, DMSO-*d*₆): δ 1.58-1.60 (m, 4 H, CH₂CH₂), 2.45-2.68 (m, 4 H, Ar-CH₂, Ar-CH₂), 6.05-6.08 (s, 2 H, 2-NH₂, exch), 6.35-6.36 (d, $J = 2.15$ Hz, 1 H, C6-CH), 7.11-7.12 (m, 2 H, Ar), 7.77-7.8 (t, $J = 8.09, 8.09$ Hz, 1 H, Ar), 10.19 (s, 1 H, 3-NH, exch), 10.65-10.66 (d, $J = 1.99$ Hz, 1 H, 7-NH, exch). The intermediate **357** was used for the next reaction without further characterization.

Diethyl (4-(4-(2-amino-4-hydroxy-7*H*-pyrrolo[2,3-*d*]pyrimidin-5-yl)butyl)-2-fluorobenzoyl)-L-glutamate (358).

To a solution of **357** (80 mg, 0.23 mmol, 1 eq) in anhydrous DMF (5 mL) was added 6-chloro-2,4-dimethoxy-1,3,5-triazine (49 mg, 0.3 mmol, 1.2 eq) and *N*-methylmorpholine

(0.03 mL, 0.3 mmol, 1.2 eq). After the mixture was stirred at room temperature for 2 h, *N*-methylmorpholine (0.03 mL, 0.3 mmol, 1.2 eq) and dimethyl L-glutamate hydrochloride (71 mg, 0.35 mmol, 1.5 eq) were added all at once. The mixture was stirred at room temperature for 12 h. TLC showed the formation of one major non-polar spot and disappearance of starting material (CHCl₃/MeOH). The reaction mixture was evaporated to dryness under reduced pressure. To the residue, MeOH was added followed by silica gel and the mixture was evaporated to afford a plug. The plug was loaded onto a silica gel column and eluted initially with CHCl₃ followed by gradual increase in polarity to 10% MeOH in CHCl₃. Fractions with required R_f were pooled and evaporated to afford crude **358** (100 mg, 81%) as a pink sticky solid. TLC R_f = 0.5 (CHCl₃/MeOH 5:1); ¹H NMR (500 MHz, DMSO-*d*₆): δ 1.15-1.21 (m, 6 H, COOCH₂CH₃), 1.50-1.54 (m, 2 H, CH₂), 1.71-2.1 (m, 4 H, β-CH₂, CH₂), 2.43-2.46 (m, 2 H, γ-CH₂), 2.54-2.63 (m, 2 H, Ar-CH₂), 4.02-4.14 (m, 4 H, COOCH₂CH₃), 4.41-4.42 (m, 1 H, α-CH), 6.68 (s, br, 1 H, C6-CH), 7.08-7.13 (m, 2 H, Ar), 7.46-7.5 (dt, *J*=3.11, 7.60, 7.61 Hz, 1 H, Ar), 8.56-8.57 (d, *J*=7.09 Hz, 1 H, CONH, exch), 10.51 (s, 1 H, 7-NH, exch). The intermediate **358** was used for the next reaction without further characterization.

(4-(4-(2-amino-4-hydroxy-7*H*-pyrrolo[2,3-*d*]pyrimidin-5-yl)butyl)-2-fluorobenzoyl)-L-glutamate (198).

To **366** (70 mg, 0.13 mmol) was added 1 N NaOH (3 mL) and the resulting mixture was stirred at room temperature for 1 h. TLC indicated the disappearance of starting material and the formation of one major spot at the origin. The solution was cooled in an ice bath, and the pH was adjusted to 3-4 using 1 N HCl. The resulting suspension was chilled in a dry ice/acetone bath and thawed to 4 °C overnight in a refrigerator. The precipitate was

filtered, washed with cold water, and dried in a desiccator under reduced pressure using P₂O₅ to yield **198** (50 mg, 80%) as a yellow powder. mp 131.8 °C dec. ¹H NMR (400 MHz, DMSO-*d*₆): δ 1.60-1.66 (m, 4 H, CH₂ CH₂), 1.82-2.13 (m, 2 H, β-CH₂), 2.3-2.38 (m, 2 H, γ-CH₂), 2.57-2.69 (m, 2 H, Ar-CH₂), 4.33-4.43 (m, 1 H, α-CH), 6.07 (s, br, 2 H, 2-NH₂, exch) 6.32-6.41 (s, br, 1 H, C6-CH), 7.05-7.19 (m, 2 H, Ar), 7.46-7.56 (dt, *J* = 3.11, 7.60, 7.61 Hz, 1 H, Ar), 8.39-8.46 (d, *J* = 7.09 Hz, 1 H, CONH exch), 10.15-10.17 (s, br, 1 H, 3-NH, exch), 10.51 (s, 1 H, 7-NH, exch). Anal. Calcd for C₂₂H₂₄FN₅O₆ · 1.12 H₂O: C, 53.57; H, 5.35; N, 14.2; F, 3.85. Found: C, 53.57, H, 5.23, N, 14.01, F, 3.66

2-Amino-6-hydrazinopyrimidin-4(3*H*)-one (360).

To a stirred suspension of **359** (2 g, 13.74 mmol, 1 eq) in water (20 mL) was added anhydrous hydrazine (1.56 mL, 50 mmol, 3.65 eq), and the mixture was heated to reflux for 3 h. The resulting clear solution was cooled, and the precipitate that separated was collected by filtration, washed with water followed by ethanol and dried to give **360** (1.4 g, 72%) as a buff colored powder. mp 274 °C dec. Compound **360** spots very faintly AND doesn't run on TLC (CHCl₃/MeOH). ¹H NMR (400 MHz, DMSO-*d*₆): δ 4.03 (s, 2 H, NH-NH₂, exch), 4.77 (s, 1 H, 6-NH, exch), 6.10 (s, 2 H, 2-NH₂, exch), 7.25 (s, 1 H, C5-CH), 9.65 (s, 1 H, 3-NH, exch). ¹H NMR matches with the reported NMR.³⁸¹

Methyl 4-(4-oxopentyl)benzoate (363).

To a solution of methyl 4-iodobenzoate (**361**) (1.4 g, 5 mmol, 1 eq) in DMF (20 mL) was added pent-4-en-2-ol **362** (0.52 ml, 5 mmol, 1 eq), LiCl (212 mg, 5 mmol, 1 eq), LiOAc (825 mg, 12.5 mmol, 2.5 eq), Bu₄NCl (1.41 g, 5 mmol, 1 eq), Pd(OAc)₂ (68 mg, 0.3 mmol, 0.06 eq) and the mixture was stirred at 80 °C for 3 hours. TLC showed the disappearance

of the starting material and formation of one major polar spot (hexane/EtOAc). To the reaction mixture cooled to room temperature was added ethyl acetate. The resulting solution was extracted with H₂O and dried over Na₂SO₄. After evaporation of solvent, the residue was loaded on a silica gel column and flash-chromatographed with hexane followed by gradual increase in polarity to 100% EtOAc. The desired fractions were pooled, evaporated and the residue was dried in vacuo using P₂O₅ to afford **363** (788 mg, 72%) as colorless SYRUP. TLC R_f = 0.42 (hexane/EtOAc 3:1); ¹H NMR (400 MHz, DMSO-*d*₆): δ 1.73-1.81 (m, 2 H, CH₂), 2.07 (s, 3 H, COCH₃), 2.42-2.46 (t, *J* = 7.31, 7.31 Hz, 2 H, Ar-CH₂), 2.6-2.64 (m, 2 H, CH₂), 3.84 (s, 3 H, COOCH₃), 7.33-7.36 (d, *J* = 8.33 Hz, 2 H, Ar), 7.87-7.89 (d, *J* = 8.30 Hz, 2 H). ¹H NMR matches with the reported NMR.³⁸¹

Methyl-4-(4-(2-(2-amino-6-oxo-1,6-dihydropyrimidin-4-yl)hydrazineylidene)pentyl)benzoate (364).

A mixture of the ketone **363** (591 mg, 2.52 mmol, 1 eq) and 2-Amino-6-hydrazinopyrimidin-4(3*H*)-one **360** (356 mg, 2.52 mmol, 1 eq) in 2-methoxyethanol (20 mL) was refluxed for 14 h, then cooled to room temperature and filtered. The filtrate was concentrated to which 1:1 ether/hexanes were added, and the resulting brownish powder was collected by filtration to afford **364** (770 mg, 89%) as a light brown powder. TLC R_f = 0.2 (CHCl₃/MeOH, 5:1); mp 240 °C.³⁸¹ ¹H NMR (400 MHz, DMSO-*d*₆): δ 1.78-86 (m, 5 H, CNCH₃, CH₂), 2.2-2.24 (t, *J*=7.35, 7.35 Hz, 2 H, CH₂), 2.66-2.7 (t, *J*=7.58, 7.58 Hz, 2 H, CH₂), 3.84 (s, 3 H, COOCH₃), 5.09 (s, 1 H, C5-CH), 6.18 (s, 2 H, 2-NH₂, exch), 7.36-7.42 (m, 2 H, Ar), 7.88-7.89 (d, *J* = 8.22 Hz, 2 H, Ar), 8.75 (s, 1 H, 6-NH, exch), 9.95 (s, 1 H, 3-NH, exch). ¹H NMR matches with the reported NMR.³⁸¹

Methyl 4-(2-(2-amino-6-methyl-4-oxo-4,7-dihydro-3H-pyrrolo[2,3-d]pyrimidin-5-yl)ethyl)benzoate (365).

A mixture of **364** (350 mg, 1.02 mmol), in diphenyl ether (20 mL) was stirred and heated under reflux for 6 h. After cooling to room temperature, hexanes were added and the precipitated powder was collected by filtration and run through a quick silica column with 5% MeOH in CHCl₃ as the eluent to give cyclized **365** (255 mg, 77%) as a yellow powder. TLC R_f = 0.25 (CHCl₃/MeOH, 5:1); mp 260 °C.³⁸¹ ¹H NMR (400 MHz, DMSO-*d*₆): δ 1.83 (s, 3 H, Ar-CH₃), 2.75-2.79 (t, J = 7.29, 7.29 Hz, 2 H, Ar-CH₂), 2.89-2.93 (m, 2 H, Ar-CH₂), 3.83 (s, 3 H, COOCH₃), 5.96 (s, 2 H, 2-NH₂, exch), 7.26-7.28 (d, J = 8.20 Hz, 2 H, Ar), 7.83-7.85 (d, J = 8.16 Hz, 2 H, Ar), 10.1 (s, 1 H, 3-NH, exch), 10.5 (s, 1 H, 7-NH, exch). ¹H NMR matches with the reported NMR.³⁸¹

4-(2-(2-amino-6-methyl-4-oxo-4,7-dihydro-3H-pyrrolo[2,3-d]pyrimidin-5-yl)ethyl)benzoate (366).

To **365** (250 mg, 0.77 mmol) was added 1 N NaOH (5 mL) and the resulting mixture was stirred under N₂ at room temperature for 12 h. TLC indicated the disappearance of starting material and the formation of one major polar spot (CHCl₃/MeOH). The resulting solution was cooled in an ice bath, and the pH was adjusted to 3-4 using 1 N HCl. The resulting suspension was chilled in a dry ice/acetone bath and thawed to 4 °C overnight in a refrigerator. The precipitate was filtered, washed with cold water, and dried in a desiccator under reduced pressure using P₂O₅ to afford acid **366** (150 mg, 63%) as a buff colored powder. TLC R_f = 0.1 (CHCl₃/MeOH, 5:1); mp 194 °C.³⁸¹ ¹H NMR (400 MHz, DMSO-*d*₆): δ 1.84 (s, 3 H, CH₃), 2.75-2.79 (t, J =7.29, 7.29 Hz, 2 H, Ar-CH₂), 2.87-2.91 (m, 2 H, Ar-CH₂), 6.3 (s, 2 H, 2-NH₂, exch), 7.23-7.25 (d, J = 8.16 Hz, 2 H, Ar), 7.81-7.83 (d, J =

8.13 Hz, 2 H, Ar), 10.4 (s, 1 H, 3-NH, exch), 10.7 (s, 1 H, 7-NH, exch). ¹H NMR matches with the reported NMR.³⁸¹

Ethyl (4-(2-(2-amino-4-hydroxy-6-methyl-7*H*-pyrrolo[2,3-*d*]pyrimidin-5-yl)ethyl)benzoyl)-L-glutamate (367).

To a solution of **366** (150 mg, 0.48 mmol, 1 eq) in anhydrous DMF was added 6-chloro-2,4-dimethoxy-1,3,5-triazine (101 mg, 0.58 mmol, 1.2 eq) and *N*-methylmorpholine (0.06 mL, 0.58 mmol, 1.2 eq). After the mixture was stirred at room temperature for 2 h, *N*-methylmorpholine (0.06 mL, 0.58 mmol, 1.2 eq) and dimethyl L-glutamate hydrochloride (146 mg, 0.72 mmol, 1.5 eq) were added all at once. The mixture was stirred at room temperature for 12 h. TLC showed the formation of one major non-polar spot and disappearance of starting material (CHCl₃/MeOH). The reaction mixture was evaporated to dryness under reduced pressure and the residue was dissolved in MeOH. To the solution, celite was added and the solvent was evaporated to afford a plug. The plug was loaded on a silica gel column and flash-chromatographed with CHCl₃ followed by gradual increase in polarity to 5% MeOH in CHCl₃. The fractions with desired R_f were pooled, evaporated and the residue was dried in vacuo using P₂O₅ to afford the glutamate ester **367** (100 mg, 42%) as a light pink sticky solid. TLC R_f = 0.5 (CHCl₃/MeOH, 5:1); ¹H NMR (400 MHz, DMSO-*d*₆): δ 1.15-1.2 (m, 6 H, COOCH₂CH₃), 1.85 (s, 3 H, Ar-CH₃), 1.96-2.15 (m, 2 H, β-CH₂), 2.42-2.46 (t, *J* = 7.86, 7.86 Hz, 2 H, γ-CH₂), 2.75-2.79 (m, 2 H, Ar-CH₂), 2.87-2.91 (m, 2 H, Ar-CH₂), 4.02-4.16 (m, 4 H, COOCH₂CH₃), 4.39-4.45 (m, 1 H, α-CH), 5.96 (s, 2 H, 2-NH₂, exch), 7.22-7.24 (d, *J* = 8.28 Hz, 2 H, Ar), 7.75-7.77 (d, *J* = 8.07 Hz, 2 H, Ar), 8.64-8.66 (d, *J* = 7.39 Hz, 1 H, CONH exch), 10.1 (s, 1 H, 3-NH, exch), 10.5 (s, 1 H, 7-NH, exch). ¹H NMR matches with the reported NMR.³⁸¹

(4-(2-(2-amino-4-hydroxy-6-methyl-7H-pyrrolo[2,3-d]pyrimidin-5-yl)ethyl)benzoyl)-L-glutamate (200).

To **367** (60 mg, 0.12 mmol), was added 1 N NaOH (3 mL) and the resulting mixture was stirred at room temperature for 1 h. TLC indicated the disappearance of starting material and the formation of one major spot at the origin (CHCl₃/MeOH). The solution was cooled in an ice bath, and the pH was adjusted to 3-4 using 1 N HCl. The resulting suspension was chilled in a dry ice/acetone bath and thawed to 4 °C overnight in a refrigerator. The precipitate was filtered, washed with cold water, and dried in a desiccator under reduced pressure using P₂O₅, to afford **200** (40 mg, 75%) as a buff colored powder. mp 164.6 °C. ¹H NMR (400 MHz, DMSO-*d*₆): δ 1.85 (s, 3 H, Ar-CH₃), 1.94-2.11 (m, 2 H, β-CH₂), 2.33-2.38 (t, *J* = 7.86, 7.86 Hz, 2 H, γ-CH₂) 2.75-2.78 (m, 2 H, Ar-CH₂), 2.86-2.9 (m, 2 H, Ar-CH₂), 4.35-4.42 (m, 1 H, α-CH), 5.97 (s, 2 H, 2-NH₂, exch), 7.2-7.23 (d, *J* = 8.25 Hz, 2 H, Ar), 7.75-7.77 (d, *J* = 8.12 Hz, 2 H, Ar), 8.53-8.55 (d, *J* = 7.64 Hz, 1 H, CONH exch), 10.11 (s, 1 H, 3-NH, exch), 10.5 (s, 1 H, 7-NH, exch). Anal. Calcd for C₂₁H₂₃N₅O₆ · 0.95 H₂O: C, 54.99; H, 5.47; N, 15.27. Found: C, 55.04; H, 5.42; N, 15.09. ¹H NMR matches with the reported NMR.³⁸¹

Methyl 4-(6-oxoheptyl)benzoate (370).

To a solution of methyl 4-bromobenzoate (**361**) (942 mg, 4.48 mmol, 1 eq) in DMF (20 mL) was added hept-6-en-2-ol **377** (0.6 ml, 4.48 mmol, 1 eq), LiCl (186 mg, 4.48 mmol, 1 eq), LiOAc (723 mg, 11 mmol, 2.5 eq), Bu₄NI (1.64 g, 4.48 mmol, 1 eq), Pd(OAc)₂ (59 mg, 0.26 mmol, 0.06 eq) and the mixture was stirred at 80 °C for 3 hours. TLC (hexane/EtOAc) showed the disappearance of the starting material and formation of one major polar spot. To the reaction mixture cooled to room temperature was added ethyl

acetate. The resulting solution was extracted with H₂O and dried over Na₂SO₄. After evaporation of solvent, the residue was dissolved in MeOH followed by the addition of celite. The solution was evaporated to dryness to afford a plug which was loaded on a silica gel column and flash-chromatographed with hexanes followed by gradual increase in polarity to 100% EtOAc. The desired fractions were pooled, evaporated and the residue was dried in vacuo using P₂O₅ to afford **370** (700 mg, 64%) as colorless liquid. TLC R_f = 0.5 (hexane/EtOAc 3:1); ¹H NMR (400 MHz, CDCl₃): δ 1.3-1.38 (m, 2 H, CH₂), 1.58-1.7 (m, 4 H, CH₂CH₂), 2.15 (s, 3 H, COCH₃), 2.4-2.46 (t, *J*=7.41, 7.41 Hz, 2 H, CH₂), 2.66-2.7 (t, *J*=7.69, 7.69 Hz, 2 H, CH₂), 3.92 (s, 3 H, COOCH₃), 7.24-7.26 (d, *J* = 8.04 Hz, 2 H, Ar), 7.96-7.98 (d, *J* = 8.03 Hz, 2 H, Ar). The intermediate **370** was used for the next reaction without further characterization.

Methyl 4-(6-(2-(2-amino-6-oxo-1,6-dihydropyrimidin-4-yl)hydrazineylidene)heptyl)benzoate (371).

A mixture of the ketone **370** (580 mg, 2.34 mmol, 1 eq) and 2-Amino-6-hydrazinopyrimidin-4(3*H*)-one **360** (330 mg, 2.52 mmol, 1 eq) in 2-methoxyethanol (20 mL) was refluxed for 14 h, then cooled to room temperature and filtered. The filtrate was concentrated to which 1:1 ether/hexanes were added, and the resulting brownish powder was collected by filtration to afford **371** (700 mg, 87%) as a light brown powder. TLC R_f = 0.3 (CHCl₃/MeOH, 5:1); ¹H NMR (400 MHz, DMSO-*d*₆): δ 1.26-1.35 (m, 2 H, CH₂), 1.49-1.56 (m, 2 H, CH₂), 1.58-1.66 (m, 2 H, CH₂), 1.82 (s, 3 H, CNCH₃), 2.17-2.21 (m, 2 H, Ar-CH₂), 2.63-2.68 (m, 2 H, Ar-CH₂), 3.84 (s, 3 H, COOCH₃), 5.07 (s, 1 H, C5-CH), 6.16 (s, 2 H, 2-NH₂, exch), 7.34-7.36 (d, *J*=8.18 Hz, 2 H, Ar), 7.86-7.88 (d, *J*=10.28 Hz,

2 H, Ar), 8.7 (s, 1 H, 6-NH, exch), 9.92 (s, 1 H, 3-NH, exch). The intermediate **371** was used for the next reaction without further characterization.

Methyl 4-(1-hydroxybut-3-yn-1-yl)benzoate (376).

To a solution of methyl 4-formylbenzoate **375** (12 g, 73 mmol, 1 eq) in THF (40 mL), sat. aqueous NH₄Cl (160 mL) followed by propargyl bromide bromide (80% wt in toluene) **312** (13.85 mL, 146 mmol, 2.0 equiv) were added. To this mixture, activated zinc dust (9.56 g, 146 mmol, 2.0 equiv) was slowly added portion wise at 0 °C and the resulting solution was stirred for 1 h at 0 °C. The reaction mixture was warmed to room temperature and stirred for additional 24 h until a new major polar spot was observed by TLC analysis (hexane/EtOAc). The reaction mixture was extracted by EtOAc (3 × 100 mL) and the combined organic layers were dried over anhydrous Na₂SO₄, filtered, and the organic phase was concentrated under reduced pressure to afford a colorless syrupy residue. Celite was added to the residue dissolved in MeOH and the solvent was evaporated to afford a celite plug. The plug was loaded onto a silica gel column and flash chromatographed with hexane followed by gradual increase in polarity to 100% EtOAc. The fractions with the required R_f were collected and evaporated to afford **376** (10.5 g, 70%) as a colorless syrup. TLC R_f = 0.2 (hexane/EtOAc 3:1); ¹H NMR (400 MHz, DMSO-*d*₆): δ 2.10-2.12 (t, *J*=2.64, 2.64 Hz, 1 H, CH), 2.50-2.51 (d, *J*=2.42 Hz, 1 H, OH, exch), 2.61-2.74 (m, 2 H, CH₂), 3.94 (s, 3 H, COOCH₃), 4.95-4.99 (m, 1 H, OH-CH), 7.48-7.51 (d, *J* = 8.67 Hz, 2 H, Ar), 8.05-8.07 (d, *J* = 8.36 Hz, 2 H, Ar). ¹H NMR matches with the reported NMR.³⁹⁷ The intermediate **376** was used for the next reaction without further characterization.

Methyl 4-(1-(2,2,2-trifluoroacetoxy)but-3-yn-1-yl)benzoate (377).

TFA (0.15 mL, 1.96 mmol, 2 eq) was added to a solution of **376** (200 mg, 0.98 mmol, 1 eq) in CH₂Cl₂ (8 mL). The solution changed color immediately to bright pink. This solution was cooled in an ice bath to which triethylsilane (0.3 mL, 1.96 mmol, 2 eq) was added dropwise to form a light blue solution that gradually turned colorless. The reaction vessel was allowed to warm to room temperature and the mixture was kept stirring for 7 days. A new non-polar spot was observed under TLC and the reaction did not go to completion (hexane/EtOAc). The yellow solution formed was quenched with sat. aq. NaHCO₃ (10 mL), extracted with EtOAc (30 mL) and the organic layer was evaporated to afford a yellow residue. To the residue MeOH and celite were added and the resultant mixture was evaporated to dryness in vacuo to afford a plug. The plug was loaded onto a silica gel column and flash chromatographed with hexane followed by gradual increase in polarity to 100% EtOAc. The fractions with the required R_f were collected and evaporated to afford **377** (88 mg, 48%) as a yellow syrup. TLC R_f = 0.5 (hexane/EtOAc 3:1); ¹H NMR (400 MHz, DMSO-*d*₆): δ 2.98-3.02 (m, 3 H, CH₂, CH), 3.87 (s, 3 H, COOCH₃), 6.17-6.2 (t, *J* = 6.10, 6.10 Hz, 1 H, O-CH), 7.62-7.64 (d, *J* = 8.29 Hz, 2 H, Ar), 8.0-8.02 (d, *J* = 8.32 Hz, 2 H, Ar). The intermediate **377** was not characterized further.

2-Amino-6-methyl-3,7-dihydro-4H-pyrrolo[2,3-*d*]pyrimidin-4-one (378).

To a suspension of 2,4-diamino-6-hydroxypyrimidine **22** (10g, 80 mmol, 1 eq) in water (200 mL), sodium acetate (6.5 g, 80 mmol, 1 eq) was added and refluxed. After the addition of chloroacetone (7.66 ml, 95 mmol, 1.2 eq) in portions (1.5 h), the solution cleared up and was stirred at reflux for 3.5 h until the reaction went to completion a new non-polar spot was observed on TLC (CHCl₃/MeOH). The reaction mixture was

cooled at 4 °C overnight and the precipitate that formed was filtered, washed with cold water and dried in vacuo. The crude product **378** (9 g, 69%) was obtained as a pink powder. TLC R_f = 0.06 (CHCl₃/MeOH, 5:1); mp 213 °C. ¹H NMR (400 MHz, DMSO-*d*₆): δ 2.15 (a, 3 H, Ar-CH₃), 5.84 (s, 1 H, C5-CH), 5.98 (s, 2 H, 2-NH₂, exch), 10.14 (s, 1 H, 3-NH, exch), 10.8 (s, 1 H, 7-NH, exch). ¹H NMR matches with the ¹H NMR of reported compound.³⁹⁸

***N*-(6-methyl-4-oxo-4,7-dihydro-3*H*-pyrrolo[2,3-*d*]pyrimidin-2-yl)pivalamide (379).**

A solution of **378** (5 g, 30 mmol) in trimethylacetic anhydride (16 mL, 82 mmol, 2.7 eq) stirred at 120 °C for 12 h until the reaction went to completion and a new non-polar spot was observed under TLC (CHCl₃/MeOH). The reaction mixture was brought to room temperature and then cooled in an ice bath. Freezer cold ether (100 ml) was added to give a precipitate which was filtered and dried on high vacuum to afford crude **379** (7 g, 6.83 mmol, 93% yield) as a light brown powder. TLC R_f = 0.25 (CHCl₃/MeOH, 5:1); mp 293 °C dec.³⁹⁹ ¹H NMR (400 MHz, DMSO-*d*₆) δ 1.24 (s, 9 H, (CH₃)₃), 2.26 (s, 3 H, Ar-CH₃), 6.08 (s, 1 H, C5-CH), 10.78 (s, 1 H, 2-NH, exch), 11.37 (s, 1 H, 3-NH, exch), 11.8 (s, 1 H, 7-NH, exch). ¹H NMR matches with the ¹H NMR of reported compound.³⁹⁹

***N*-(5-iodo-6-methyl-4-oxo-4,7-dihydro-3*H*-pyrrolo[2,3-*d*]pyrimidin-2-yl)pivalamide (373).**

To the suspension of **379** (6 g, 24 mmol, 1 eq) in CH₂Cl₂ (300 mL), NIS (3 mL, 29 mmol, 1.2 eq) was added and the resulting solution was stirred at 40 °C for 0.5 h until the disappearance of starting material and formation of a non-polar spot (CHCl₃/MeOH). The reaction was cooled to room temperature which was washed with aqueous Na₂S₂O₃

followed by brine. The combined organic layers were filtered through a plug of silica, and rinsed with CH₂Cl₂/MeOH (95/5). The solvent was evaporated to obtain crude product **373** (8.3 g, 93%) as a light brown powder. TLC R_f = 0.3 (CHCl₃/MeOH, 5:1); mp 180.4 °C. ¹H NMR (400 MHz, DMSO-*d*₆): δ 1.22 (s, 9 H, (CH₃)₃), 2.22 (s, 3 H, CH₃), 10.79 (s, 1 H, 2-NH, exch), 11.82 (s, 1 H, 3-NH, exch), 11.88 (s, 1 H, 7-NH, exch). The intermediate **373** was used for the next reaction without further characterization.

***N*-(5-bromo-6-methyl-4-oxo-4,7-dihydro-3*H*-pyrrolo[2,3-*d*]pyrimidin-2-yl)pivalamide (380).**

To the suspension of **379** (500 mg, 2 mmol, 1 eq) in CH₂Cl₂ (300 mL), NBS (430 mg, 2.42 mmol, 1.2 eq) was added and the resulting solution was stirred at 40 °C for 0.5 h until the disappearance of starting material and formation of a non-polar spot (CHCl₃/MeOH). The reaction was cooled to room temperature which was washed with aqueous Na₂S₂O₃ followed by brine. The combined organic layers were filtered through a plug of silica, and rinsed with CH₂Cl₂/MeOH (95/5). The solvent was evaporated to obtain crude product **380** (611 mg, 93%) as a light brown powder. TLC R_f = 0.3 (CHCl₃/MeOH, 5:1); mp >161 °C. ¹H NMR (400 MHz, DMSO-*d*₆): δ 1.24 (s, 9 H, (CH₃)₃), 2.21 (s, 3 H, CH₃), 10.85 (s, 1 H, 2-NH, exch), 11.8 (s, 1 H, 3-NH, exch), 11.85 (s, 1 H, 7-NH, exch). The intermediate **380** was used for the next reaction without further characterization.

Methyl 4-(1-hydroxy-4-(6-methyl-4-oxo-2-pivalamido-4,7-dihydro-3*H*-pyrrolo[2,3-*d*]pyrimidin-5-yl)but-3-yn-1-yl)benzoate (381).

To a solution of **373** (50 mg, 0.13 mmol, 1 eq), dissolved in anhydrous THF (3 mL), copper(I) iodide (10 mg, 0.05 mmol, 0.4 eq), **376** (163 mg, 0.8 mmol, 6 eq), and

tetrakis(triphenylphosphine)palladium(0) (15 mg, 0.013 mmol, 0.1 eq) and triethylamine (0.02 mL, 0.13 mmol, 1 eq) were added. The solution was stirred at room temperature for 72 h under nitrogen until a new polar spot was observed on the TLC (CHCl₃/MeOH). The solvent mixture was evaporated in vacuo and the residue was dissolved in MeOH. To the methanolic solution, celite was added and the solution was concentrated under reduced pressure to afford a celite plug. The plug was loaded onto a silica gel column and flash chromatographed with CHCl₃ followed by gradual increase in polarity to 5% MeOH in CHCl₃. The fractions with the required R_f were collected and evaporated to afford **381** (42 mg, 70%) as a sticky pink solid. TLC R_f = 0.3 (CHCl₃/ MeOH 5:1); ¹H NMR (400 MHz, DMSO-*d*₆): δ 1.2 (s, 9 H, (CH₃)₃), 2.4 (s, 3H, Ar-CH₃), 3.2-3.3 (m, 2 H, CH₂), 3.84 (s, 3 H, COOCH₃), 4.61-4.66 (td, *J* = 4.87, 4.87, 9.37 Hz, 1 H, OH-CH), 5.36-5.37 (d, *J* = 4.60 Hz, 1 H, OH), 7.45-7.47 (d, *J* = 8.29 Hz, 2 H, Ar), 7.89-7.91 (d, *J* = 8.25 Hz, 2 H, Ar), 10.9 (s, 1 H, 2-NH, exch), 11.97 (s, 1 H, 3-NH, exch), 12.03 (s, 1 H, 7-NH, exch). The intermediate **381** was used for the next reaction without further characterization.

(5-(4-(2-amino-4-oxo-4,7-dihydro-3H-pyrrolo[2,3-*d*]pyrimidin-6-yl)but-1-yn-1-yl)pyrimidine-2-carbonyl)glutamic acid (202).

Compound **202** was prepared using the general method described for the preparation of **179-180** from **297** (80 mg, 0.16 mmol) to give **202** (40 mg, 56%) as an orange powder. mp 114.1 °C dec. ¹H NMR (400 MHz, DMSO-*d*₆): δ 1.97-2.17 (m, 2 H, β-CH₂), 2.3-2.32 (m, 2 H, γ-CH₂), 4.44-4.49 (m, 1 H, α-CH), 6.0 (s, 2 H, 2-NH₂, exch), 6.03-6.04 (d, *J* = 1.99 Hz, 1 H, C5-CH), 8.97 (s, 2 H, Ar) 9.0-9.01 (d, *J* = 8.07 Hz, 1 H, CONH, exch), 10.16 (s, 1H, 3-NH, exch) 10.91 (s, 7-NH, exch). Anal. Calcd for (C₂₀H₁₉N₇O₆ · 0.95 H₂O) C, 51.04; H, 4.47; N, 20.83. Found C, 51.12; H, 4.60; N, 20.68.

Docking protocol for the molecular modeling of pyrrolo[2,3-*d*]pyrimidine classical antifolates inhibitors of GARFTase/AICARFTase/TS with selectivity for FRs and/or PCFT over RFC:

The X-ray crystal structures of hFR α (PDB: 5IZQ, 3.6 Å), hFR β (PDB: 4KN2, 2.6 Å), hGARFTase (PDB: 5J9F, 2.1 Å), hAICARFTase (1P4R, 2.55 Å) were obtained from protein database. Docking studies were performed using LeadIT 2.1.6. Default settings were used to calculate the protonation state of the proteins and the ligands, and the free rotation of water molecules in the active site (defined by amino acids 6.5 Å from the crystal structure ligand) were permitted. The ligands for docking were sketched in Maestro 11.2 and prepared using the Ligprep (4) application. The docking was performed in LeadIT 2.1.6 using the triangle matching placement method and scored using default settings. The docked poses were visualized in Maestro 11.2. To validate the docking process using LeadIT 2.1.6, the crystallized ligands were sketched in Maestro 11.2, prepared using Ligprep and docked as described. The RMSD of the docked crystal structures were <2, thus validating LeadIT 2.1.6 for docking in FR α , FR β , GARFTase and AICARFTase.

Table 23. Docked scores of proposed compounds in crystal structures of FR α FR β GARFTase AICARFTase and TS

	FRα	FRβ	GARFTase	AICARFTase	TS
179	-52.08	-62.52	-52.8	NA	NA
180	-56.6	-57.3	-53.2	NA	NA
181	-57.12	-57.8	-53.09	NA	NA
182	-58.25	-57.76	-49.74	NA	NA
183	-56.38	-60.3	-57.1	NA	NA

184	-50.75	-54.48	-50.28	NA	NA
185	-53.07	-57.55	-55.07	NA	NA
186	-53.58	-60.6	-50.8	NA	NA
187	-55.5	-61.76	-53.1	NA	NA
188	-54.07	-59.58	-52.8	NA	NA
189	-55.6	-63.7	-56.3	NA	NA
191	-54.2	-60.26	-54.7	NA	NA
192	-51.95	-61.13	-54.34	NA	NA
193	-55.08	-63.96	-43.5	-42.11	NA
194	-57.8	-70.52	-52.68	-39.32	NA
195	-58.1	-63.3	-46.35	-34.99	NA
196	-58.12	-66.15	-50.03	-32.24	NA
197	-58	-68.18	-52.45	-41.12	NA
198	-57.78	-65.99	-50.5	-39.17	NA
200	-49.2	-63.88	-40.9	-30.49	-38.23
202	54.97	62.36	-44.07	NA	NA
PMX	-48.73	-58.25	-44.25	-37.69	-40.45
2	-55	-60.4	-50.7	NA	NA
3	-54.74	-56.96	-56.4	NA	NA
4	-51	-62.2	-52.82	NA	NA
7	-50.65	-52.14	-52.8	NA	NA
9	-52.18	-59.14	-50.26	NA	NA
13	-56.13	-64.05	-48.06	-36.52	NA

IV. SUMMARY

The dissertation describes the design and synthesis of 6- and/or 5-substituted, 2-amino-4-oxo pyrrolo[2,3-*d*]pyrimidine- GARFTase/ AICARFTase inhibitors with selectivity for FRs and/or PCFT over RFC for targeted cancer chemotherapy. The novel compounds synthesized as part of this study are listed below:

1. (4-(4-(2-Amino-4-oxo-4,7-dihydro-3*H*-pyrrolo[2,3-*d*]pyrimidin-6-yl)butyl)-2-fluorobenzoyl)-L-glutamic acid (**179**)
2. (4-(4-(2-Amino-4-oxo-4,7-dihydro-3*H*-pyrrolo[2,3-*d*]pyrimidin-6-yl)butyl)-3-fluorobenzoyl)-L-glutamic acid (**180**)
3. (4-(3-(2-Amino-4-oxo-4,7-dihydro-3*H*-pyrrolo[2,3-*d*]pyrimidin-6-yl)propyl)-2-fluorobenzoyl)-L-glutamic acid (**181**)
4. (5-(3-(2-amino-4-oxo-4,7-dihydro-3*H*-pyrrolo[2,3-*d*]pyrimidin-6-yl)propyl)-3-fluoropicolinoyl)-L-glutamic acid (**182**)
5. (5-(4-(2-Amino-4-oxo-4,7-dihydro-3*H*-pyrrolo[2,3-*d*]pyrimidin-6-yl)butyl)-3-fluoropicolinoyl)-L-glutamic acid (**183**)
6. (4-(3-(2-Amino-4-oxo-4,7-dihydro-3*H*-pyrrolo[2,3-*d*]pyrimidin-6-yl)propyl)-3-fluorothiophene-2-carbonyl)-L-glutamic acid (**184**)
7. (5-(4-(2-Amino-4-oxo-4,7-dihydro-3*H*-pyrrolo[2,3-*d*]pyrimidin-6-yl)butyl)-2-fluorothiophene-3-carbonyl)-L-glutamic acid (**185**)
8. (4-(4-(2-amino-4-oxo-4,7-dihydro-3*H*-pyrrolo[2,3-*d*]pyrimidin-6-yl)butyl)-2,6-difluorobenzoyl)-L-glutamate (**186**)

9. (4-(4-(2-amino-4-oxo-4,7-dihydro-3*H*-pyrrolo[2,3-*d*]pyrimidin-6-yl)butyl)-2,5-difluorobenzoyl)-L-glutamate (**187**)
10. (4-(4-(2-amino-4-oxo-4,7-dihydro-3*H*-pyrrolo[2,3-*d*]pyrimidin-6-yl)butyl)-2,3-difluorobenzoyl)-L-glutamate (**188**)
11. (4-(4-(2-amino-4-oxo-4,7-dihydro-3*H*-pyrrolo[2,3-*d*]pyrimidin-6-yl)butyl)-2-methylbenzoyl)-L-glutamic acid (**189**)
12. (4-(4-(2-amino-4-oxo-4,7-dihydro-3*H*-pyrrolo[2,3-*d*]pyrimidin-6-yl)butyl)-2-(trifluoromethyl)benzoyl)-L-glutamate (**191**)
13. (5-(4-(2-amino-4-oxo-4,7-dihydro-3*H*-pyrrolo[2,3-*d*]pyrimidin-6-yl)butyl)pyrimidine-2-carbonyl)-L-glutamic acid (**192**)
14. (3-(4-(2-amino-4-oxo-4,7-dihydro-3*H*-pyrrolo[2,3-*d*]pyrimidin-5-yl)butyl)benzoyl)-L-glutamic acid (**193**)
15. (4-((3-(2-amino-4-oxo-4,7-dihydro-3*H*-pyrrolo[2,3-*d*]pyrimidin-5-yl)propyl)amino)benzoyl)-L-glutamate (**194**)
16. (4-(3-(2-amino-4-oxo-4,7-dihydro-3*H*-pyrrolo[2,3-*d*]pyrimidin-5-yl)propoxy)benzoyl)-L-glutamic acid (**195**)
17. (4-((3-(2-amino-4-oxo-4,7-dihydro-3*H*-pyrrolo[2,3-*d*]pyrimidin-5-yl)propyl)thio)benzoyl)-L-glutamic acid (**196**)
18. (4-((3-(2-amino-4-oxo-4,7-dihydro-3*H*-pyrrolo[2,3-*d*]pyrimidin-5-yl)butyl)amino)benzoyl)-L-glutamate (**197**)
19. (4-(4-(2-amino-4-hydroxy-7*H*-pyrrolo[2,3-*d*]pyrimidin-5-yl)butyl)-2-fluorobenzoyl)-L-glutamate (**198**)

20. (5-(4-(2-amino-4-oxo-4,7-dihydro-3*H*-pyrrolo[2,3-*d*]pyrimidin-6-yl)but-1-yn-1-yl)pyrimidine-2-carbonyl)glutamic acid (**202**).

Biological evaluation of proposed compounds were carried out in engineered CHO cell lines that overexpressing RFC, FR α , FR β , and PCFT. The aim for this dissertation was to obtain compounds with potent tumor-targeted activity via uptake by FRs and PCFT over RFC and intracellular inhibition of one or more folate metabolizing enzymes. Majority of the proposed compounds showed improved selectivity compared to the lead compounds. Using traditional bioisosteric and regioisomeric substitutions, we were able to successfully incorporate selectivity and improve potency. The major contributions of the current study are the (1) substitution of sidechain aryl CH (sp) with CF (sp) which successfully improved uptake by PCFT and incorporated intracellular inhibition of a new target (identification studies are underway), and (2) substitution of scaffold C6-CH (sp) with C6-C(CH₃) (sp) for successful incorporation of selectivity in **PMX** analogs.

VI. BIBLIOGRAPHY

1. Ducker, G. S.; Rabinowitz, J. D., One-carbon metabolism in health and disease. *Cell Metab.* **2017**, *25*, 27-42.
2. Copp, A. J.; Adzick, N. S.; Chitty, L. S.; Fletcher, J. M.; Holmbeck, G. N.; Shaw, G. M., Spina bifida. *Nat. Rev. Dis. Primers* **2015**, *1*, 15007.
3. Lucock, M., Folic acid: Nutritional biochemistry, molecular biology, and role in disease processes. *Mol. Genet. Metab.* **2000**, *71*, 121-138.
4. Stokstad, E. L. R., Historical perspective on key advances in the biochemistry and physiology of folates. *Contemp. Issues Clin. Nutr.* **1990**, *13*, 1-21.
5. Wright, A. J. A.; Dainty, J. R.; Finglas, P. M., Folic acid metabolism in human subjects revisited: Potential implications for proposed mandatory folic acid fortification in the UK. *Br. J. Nutr.* **2007**, *98*, 667-675.
6. V., H. A.; G., W. D., The history of folic acid. *Br. J. Haematol.* **2001**, *113*, 579-589.
7. Desmoulin, S. K.; Hou, Z.; Gangjee, A.; Matherly, L. H., The human proton-coupled folate transporter: Biology and therapeutic applications to cancer. *Cancer Biol. Ther.* **2012**, *13*, 1355-1373.
8. Bailey, L. B.; Berry, R. J., Folic acid supplementation and the occurrence of congenital heart defects, orofacial clefts, multiple births, and miscarriage. *Am. J. Clin. Nutr.* **2005**, *81*, 1213S-1217S.
9. Wang, J.; Alexander, P.; Wu, L.; Hammer, R.; Cleaver, O.; McKnight, S. L., Dependence of mouse embryonic stem cells on threonine catabolism. *Science (New York, N.Y.)* **2009**, *325*, 435-439.
10. Di Pietro, E.; Sirois, J.; Tremblay, M. L.; MacKenzie, R. E., Mitochondrial NAD-dependent methylenetetrahydrofolate dehydrogenase-methenyltetrahydrofolate cyclohydrolase is essential for embryonic development. *Mol. Cell Biol.* **2002**, *22*, 4158-4166.
11. Ron-Harel, N.; Santos, D.; Ghergurovich, J. M.; Sage, P. T.; Reddy, A.; Lovitch, S. B.; Dephoure, N.; Satterstrom, F. K.; Sheffer, M.; Spinelli, J. B.; Gygi, S.; Rabinowitz, J. D.; Sharpe, A. H.; Haigis, M. C., Mitochondrial biogenesis and proteome remodeling promotes one carbon metabolism for T cell activation. *Cell metabol.* **2016**, *24*, 104-117.
12. Narisawa, A.; Komatsuzaki, S.; Kikuchi, A.; Niihori, T.; Aoki, Y.; Fujiwara, K.; Tanemura, M.; Hata, A.; Suzuki, Y.; Relton, C. L.; Grinham, J.; Leung, K.-Y.; Partridge, D.; Robinson, A.; Stone, V.; Gustavsson, P.; Stanier, P.; Copp, A. J.; Greene, N. D. E.; Tominaga, T.; Matsubara, Y.; Kure, S., Mutations in genes encoding the glycine cleavage system predispose to neural tube defects in mice and humans. *Hum Mol. Genet.* **2012**, *21*, 1496-1503.
13. Momb, J.; Lewandowski, J. P.; Bryant, J. D.; Fitch, R.; Surman, D. R.; Vokes, S. A.; Appling, D. R., Deletion of MTHFD1L causes embryonic lethality and neural tube and craniofacial defects in mice. *Proc. Natl. Acad. Sci. USA* **2013**, *110*, 549-554.
14. Brosnan, M. E.; MacMillan, L.; Stevens, J. R.; Brosnan, J. T., Division of labour: how does folate metabolism partition between one-carbon metabolism and amino acid oxidation? *Biochem. J.* **2015**, *472*, 135-146.

15. Giovannucci, E., Epidemiologic studies of folate and colorectal neoplasia: A review. *J. Nutr.* **2002**, *132*, 2350S-2355S.
16. Ericson, U.; Sonestedt, E.; Gullberg, B.; Olsson, H.; Wirfält, E., High folate intake is associated with lower breast cancer incidence in postmenopausal women in the Malmö Diet and Cancer cohort. *Am. J. Clin. Nutr.* **2007**, *86*, 434-443.
17. Larsson, S. C.; Håkansson, N.; Giovannucci, E.; Wolk, A., Folate intake and pancreatic cancer incidence: A prospective study of swedish women and men. *J. Natl. Cancer Inst.* **2006**, *98*, 407-413.
18. Chae, Y.; Yun, J., Folic acid and prevention of colorectal adenomas. *JAMA* **2007**, *298*, 1397-1397.
19. Farber, S.; Diamond, L. K.; Mercer, R. D.; Sylvester, R. F.; Wolff, J. A., Temporary remissions in acute leukemia in children produced by folic acid antagonist, 4-aminopteroyl-glutamic acid (aminopterin). *N. Engl. J. Med.* **1948**, *238*, 787-793.
20. Burchenal, J. H.; Karnofsky, D. A.; Kingsley-Pillers, E. M.; Southam, C. M.; Laird Myers, W. P.; Escher, G. C.; Craver, L. F.; Dargeon, H. W.; Rhoads, C. P., Effects of the folic acid antagonists and 2,6-diaminopurine on neoplastic disease-with special reference to acute leukemia. *Cancer* **1951**, *4*, 549-569.
21. Huennekens, F. M., The methotrexate story: A paradigm for development of cancer chemotherapeutic agents. *Adv. Enzyme Regul.* **1994**, *34*, 397-419.
22. Visentin, M.; Zhao, R.; Goldman, I. D., The antifolates. *Hematol. Oncol. Clin. North Am.* **2012**, *26*, 629-ix.
23. Jackman, A. L.; Theti, D. S.; Gibbs, D. D., Antifolates targeted specifically to the folate receptor. *Adv. Drug Deliv. Rev.* **2004**, *56*, 1111-1125.
24. Gibbs, D. D.; Theti, D. S.; Wood, N.; Green, M.; Raynaud, F.; Valenti, M.; Forster, M. D.; Mitchell, F.; Bavetsias, V.; Henderson, E.; Jackman, A. L., BGC 945, a novel tumor-selective thymidylate synthase inhibitor targeted to α -folate receptor-overexpressing tumors. *Cancer Res.* **2005**, *65*, 11721-11728.
25. DeVita, V. T.; Chu, E., A History of Cancer Chemotherapy. *Cancer Res.* **2008**, *68*, 8643-8653.
26. Hazarika, M.; White, R. M.; Johnson, J. R.; Pazdur, R., FDA drug approval summaries: pemetrexed (Alimta). *Oncologist* **2004**, *9*, 482-488.
27. Cohen, M. H.; Justice, R.; Pazdur, R., Approval summary: Pemetrexed in the initial treatment of advanced/metastatic non-small cell lung cancer. *The Oncologist* **2009**, *14*, 930-935.
28. Chu, E.; Callender, M. A.; Farrell, M. P.; Schmitz, J. C., Thymidylate synthase inhibitors as anticancer agents: from bench to bedside. *Cancer Chemother. Pharmacol.* **2003**, *52*, 80-89.
29. Thompson, C. A., FDA approves pralatrexate for treatment of rare lymphoma. *Am. J. Health-Syst. Pharm.* **2009**, *66*, 1890-1890.
30. Avallone, A.; Gennaro, E. D.; Silvestro, L.; Iaffaioli, V. R.; Budillon, A., Targeting thymidylate synthase in colorectal cancer: critical re-evaluation and emerging therapeutic role of raltitrexed. *Expert Opin. Drug Saf.* **2014**, *13*, 113-129.
31. Matherly, L. H.; Goldman, I. D., Membrane transport of folates. *Vitam. Horm. (San Diego, CA, U. S.)* **2003**, *66*, 403-456.
32. Zhao, R.; Diop-Bove, N.; Visentin, M.; Goldman, I. D., Mechanisms of membrane transport of folates into cells and across epithelia. *Annu. Rev. Nutr.* **2011**, *31*, 177-201.

33. Zhao, R.; Goldman, I. D., Folate and thiamine transporters mediated by facilitative carriers (SLC19A1-3 and SLC46A1) and folate receptors. *Mol. Aspects Med.* **2013**, *34*, 373-385.
34. Matherly, L. H.; Hou, Z.; Deng, Y., Human reduced folate carrier: translation of basic biology to cancer etiology and therapy. *Cancer Metastasis Rev.* **2007**, *26*, 111-128.
35. Matherly, L. H.; Hou, Z., Structure and function of the reduced folate carrier: A paradigm of a major facilitator superfamily mammalian nutrient transporter. *Vitamins and hormones* **2008**, *79*, 145-184.
36. Goldman, I. D.; Lichtenstein, N. S.; Oliverio, V. T., Carrier-mediated transport of the folic acid analogue, methotrexate, in the L1210 leukemia cell. *J. Biol. Chem.* **1968**, *243*, 5007-5017.
37. Goldman, I. D., Transport energetics of the folic acid analogue, methotrexate, in L1210 leukemia cells: Enhanced accumulation by metabolic inhibitors. *J. Biol. Chem.* **1969**, *244*, 3779-3785.
38. D., G. I., The characteristics of the membrane transport of amethopterin and the naturally occurring folates. *Ann. N Y Acad. Sci.* **1971**, *186*, 400-422.
39. Zhao, R.; Matherly, L. H.; Goldman, I. D., Membrane transporters and folate homeostasis: intestinal absorption and transport into systemic compartments and tissues. *Expert Rev. Mol. Med.* **2009**, *11*, e4.
40. Zhao, R.; Goldman, I. D., The molecular identity and characterization of a Proton-Coupled Folate Transporter—PCFT; biological ramifications and impact on the activity of pemetrexed—12 06 06. *Cancer Metastasis Rev.* **2007**, *26*, 129-139.
41. Sierra, E. E.; Brigle, K. E.; Spinella, M. J.; Goldman, I. D., pH Dependence of methotrexate transport by the reduced folate carrier and the folate receptor in L1210 leukemia cells: Further evidence for a third route mediated at low pH. *Biochem. Pharmacol.* **1997**, *53*, 223-231.
42. Henderson, G. B.; Zevely, E. M., Structural requirements for anion substrates of the methotrexate transport system in L1210 cells. *Arch. Biochem. Biophys.* **1983**, *221*, 438-446.
43. Whetstine, J. R.; Flatley, R. M.; Matherly, L. H., The human reduced folate carrier gene is ubiquitously and differentially expressed in normal human tissues: identification of seven non-coding exons and characterization of a novel promoter. *Biochem. J.* **2002**, *367*, 629-640.
44. Wang, Y.; Zhao, R.; Russell, R. G.; Goldman, I. D., Localization of the murine reduced folate carrier as assessed by immunohistochemical analysis. *Biochim. Biophys. Acta, Rev. Biomembr.* **2001**, *1513*, 49-54.
45. Zhao, R.; Russell, R. G.; Wang, Y.; Liu, L.; Gao, F.; Kneitz, B.; Edelmann, W.; Goldman, I. D., Rescue of embryonic lethality in reduced folate carrier-deficient mice by maternal folic acid supplementation reveals early neonatal failure of hematopoietic organs. *J. Biol. Chem.* **2001**, *276*, 10224-10228.
46. Matherly, L. H.; Wilson, M. R.; Hou, Z., The major facilitative folate transporters solute carrier 19A1 and solute carrier 46A1: Biology and role in antifolate chemotherapy of cancer. *Drug Metab. Disp.* **2014**, *42*, 632-649.
47. Saier, M. H., Jr.; Beatty, J. T.; Goffeau, A.; Harley, K. T.; Heijne, W. H. M.; Huang, S.-C.; Jack, D. L.; Jahn, P. S.; Lew, K.; Liu, J.; Pao, S. S.; Paulsen, I. T.; Tseng, T.-T.;

- Virk, P. S., The major facilitator superfamily. *J. Mol. Microbiol. Biotechnol.* **1999**, *1*, 257-279.
48. Chang, A. B.; Lin, R.; Studley, W. K.; Tran, C. V.; Saier, J. M. H., Phylogeny as a guide to structure and function of membrane transport proteins (Review). *J. Membr. Biol.* **2004**, *21*, 171-181.
49. Marchant, J. S.; Subramanian, V. S.; Parker, I.; Said, H. M., Intracellular trafficking and membrane targeting mechanisms of the human reduced folate carrier in mammalian epithelial cells. *J. Biol. Chem.* **2002**, *277*, 33325-33333.
50. Liu, X. Y.; Witt, T. L.; Matherly, L. H., Restoration of high-level transport activity by human reduced folate carrier/ThTr1 thiamine transporter chimaeras: role of the transmembrane domain 6/7 linker region in reduced folate carrier function. *Biochem. J.* **2003**, *369*, 31-37.
51. Witt, T. L.; Stapels, S. E.; Matherly, L. H., Restoration of Transport Activity by Co-expression of Human Reduced Folate Carrier Half-molecules in Transport-impaired K562 Cells: LOCALIZATION OF A SUBSTRATE BINDING DOMAIN TO TRANSMEMBRANE DOMAINS 7-12. *J. Biol. Chem.* **2004**, *279*, 46755-46763.
52. Matherly, L. H.; Czajkowski, C. A.; Angeles, S. M., Identification of a highly glycosylated methotrexate membrane carrier in K562 human erythroleukemia cells up-regulated for tetrahydrofolate cofactor and methotrexate transport. *Cancer Res.* **1991**, *51*, 3420-3426.
53. Wong, S. C.; Zhang, L.; Proefke, S. A.; Matherly, L. H., Effects of the loss of capacity for *N*-glycosylation on the transport activity and cellular localization of the human reduced folate carrier. *Biochimica et Biophysica Acta (BBA) - Biomembranes* **1998**, *1375*, 6-12.
54. Liu, X. Y.; Matherly, L. H., Functional interactions between arginine-133 and aspartate-88 in the human reduced folate carrier: evidence for a charge-pair association. *Biochem. J.* **2001**, *358*, 511-516.
55. Sharina, I. G.; Zhao, R.; Wang, Y.; Babani, S.; Goldman, I. D., Mutational analysis of the functional role of conserved arginine and lysine residues in transmembrane domains of the murine reduced folate carrier. *Mol. Pharmacol.* **2001**, *59*, 1022-1028.
56. Sadlish, H.; Williams, F. M. R.; Flintoff, W. F., Functional role of arginine 373 in substrate translocation by the reduced folate carrier. *J. Biol. Chem.* **2002**, *277*, 42105-42112.
57. Deng, Y.; Hou, Z.; Wang, L.; Cherian, C.; Wu, J.; Gangjee, A.; Matherly, L. H., Role of lysine 411 in substrate carboxyl group binding to the human reduced folate carrier, as determined by site-directed mutagenesis and affinity inhibition. *Mol. Pharmacol.* **2008**, *73*, 1274-1281.
58. Hou, Z.; Matherly, L. H., Oligomeric structure of the human reduced folate carrier: Identification of homo-oligomers and dominant-negative effects on carrier expression and function. *J. Biol. Chem.* **2009**, *284*, 3285-3293.
59. Hou, Z.; Cherian, C.; Drews, J.; Wu, J.; Matherly, L. H., Identification of the minimal functional unit of the homo-oligomeric human reduced folate carrier. *J. Biol. Chem.* **2010**, *285*, 4732-4740.
60. Kugel Desmoulin, S.; Wang, L.; Hales, E.; Polin, L.; White, K.; Kushner, J.; Stout, M.; Hou, Z.; Cherian, C.; Gangjee, A.; Matherly, L. H., Therapeutic targeting of a novel 6-substituted pyrrolo [2,3-*d*]pyrimidine thienoyl antifolate to human solid tumors based on

selective uptake by the proton-coupled folate transporter. *Mol. Pharmacol.* **2011**, *80*, 1096-1107.

61. Sirotnak, F. M.; DeGraw, J. I.; Colwell, W. T.; Piper, J. R., A new analogue of 10-deazaaminopterin with markedly enhanced curative effects against human tumor xenografts in mice. *Cancer Chemother. Pharmacol.* **1998**, *42*, 313-318.

62. Visentin, M.; Unal, E. S.; Zhao, R.; Goldman, I. D., The membrane transport and polyglutamation of pralatrexate, a new-generation dihydrofolate reductase inhibitor. *Cancer Chemother. Pharmacol.* **2013**, *72*, 597-606.

63. Mendelsohn, L. G.; Worzalla, J. F.; Walling, J. M. In *Preclinical and clinical evaluation of the glycinamide ribonucleotide formyltransferase inhibitors lometrexol and LY309887*, Humana: 1999; pp 261-280.

64. Ray, M. S.; Muggia, F. M.; Leichman, C. G.; Grunberg, S. M.; Nelson, R. L.; Dyke, R. W.; Moran, R. G., Phase I study of (6R)-5,10-dideazatetrahydrofolate: a folate antimetabolite inhibitory to de novo purine synthesis. *J. Natl. Cancer Inst.* **1993**, *85*, 1154-1159.

65. Zhao, R.; Goldman, I. D., Resistance to antifolates. *Oncogene* **2002**, *22*, 7431.

66. Gonen, N.; Assaraf, Y. G., Antifolates in cancer therapy: Structure, activity and mechanisms of drug resistance. *Drug Resist. Updat.* **2012**, *15*, 183-210.

67. Elnakat, H.; Ratnam, M., Distribution, functionality and gene regulation of folate receptor isoforms: implications in targeted therapy. *Adv. Drug Deliv. Rev.* **2004**, *56*, 1067-1084.

68. Kamen, B. A.; Smith, A. K., A review of folate receptor alpha cycling and 5-methyltetrahydrofolate accumulation with an emphasis on cell models in vitro. *Adv. Drug Deliv. Rev.* **2004**, *56*, 1085-1097.

69. Kamen, B. A.; Wang, M. T.; Streckfuss, A. J.; Peryea, X.; Anderson, R. G., Delivery of folates to the cytoplasm of MA104 cells is mediated by a surface membrane receptor that recycles. *J. Biol. Chem.* **1988**, *263*, 13602-13609.

70. Antony, A. C.; Utley, C.; Van Horne, K. C.; Kolhouse, J. F., Isolation and characterization of a folate receptor from human placenta. *J. Biol. Chem.* **1981**, *256*, 9684-9692.

71. Ratnam, M.; Marquardt, H.; Duhring, J. L.; Freisheim, J. H., Homologous membrane folate binding proteins in human placenta: cloning and sequence of a cDNA. *Biochemistry* **1989**, *28*, 8249-8254.

72. Antony, A. C., Folate receptors: reflections on a personal odyssey and a perspective on unfolding truth. *Adv. Drug Deliv. Rev.* **2004**, *56*, 1059-1066.

73. Parker, N.; Turk, M. J.; Westrick, E.; Lewis, J. D.; Low, P. S.; Leamon, C. P., Folate receptor expression in carcinomas and normal tissues determined by a quantitative radioligand binding assay. *Anal. Biochem.* **2005**, *338*, 284-293.

74. Shen, F.; Ross, J. F.; Wang, X.; Ratnam, M., Identification of a novel folate receptor, a truncated receptor, and receptor type .beta. in hematopoietic cells: cDNA cloning, expression, immunoreactivity, and tissue specificity. *Biochemistry* **1994**, *33*, 1209-1215.

75. Lacey, S. W.; Sanders, J. M.; Rothberg, K. G.; Anderson, R. G.; Kamen, B. A., Complementary DNA for the folate binding protein correctly predicts anchoring to the membrane by glycosyl-phosphatidylinositol. *J. Clin. Invest.* **1989**, *84*, 715-720.

76. Maziarz, K. M.; Monaco, H. L.; Shen, F.; Ratnam, M., Complete mapping of divergent amino acids responsible for differential ligand binding of folate receptors α and β . *J. Biol. Chem.* **1999**, *274*, 11086-11091.
77. Wu, M.; Fan, J.; Gunning, W.; Ratnam, M., Clustering of GPI-anchored folate receptor independent of both cross-linking and association with caveolin. *J. Membr. Biol.* **1997**, *159*, 137-147.
78. Sabharanjak, S.; Mayor, S., Folate receptor endocytosis and trafficking. *Adv. Drug Deliv. Rev.* **2004**, *56*, 1099-1109.
79. Spector, R.; Lorenzo, A. V., Folate transport by the choroid plexus in vitro. *Science* **1975**, *187*, 540-542.
80. Geller, J.; Kronn, D.; Jayabose, S.; Sandoval, C., Hereditary folate malabsorption: Family report and review of the literature. *Medicine* **2002**, *81*, 51-68.
81. Cario, H.; Bode, H.; Debatin, K.-M.; Opladen, T.; Schwarz, K., Congenital null mutations of the *FOLR1* gene: A progressive neurologic disease and its treatment. *Neurology* **2009**, *73*, 2127-2129.
82. Steinfeld, R.; Grapp, M.; Kraetzner, R.; Dreha-Kulaczewski, S.; Helms, G.; Dechent, P.; Wevers, R.; Grosso, S.; Gärtner, J., Folate receptor alpha defect causes cerebral folate transport deficiency: A treatable neurodegenerative disorder associated with disturbed myelin metabolism. *Am. J. Human Genet.* **2009**, *85*, 354-363.
83. Salazar, M.; Ratnam, M., The folate receptor: What does it promise in tissue-targeted therapeutics? *Cancer Metastasis Rev.* **2007**, *26*, 141-152.
84. Puig-Kröger, A.; Sierra-Filardi, E.; Domínguez-Soto, A.; Samaniego, R.; Corcuera, M. T.; Gómez-Aguado, F.; Ratnam, M.; Sánchez-Mateos, P.; Corbí, A. L., Folate Receptor β Is Expressed by Tumor-Associated Macrophages and Constitutes a Marker for M2 Anti-inflammatory/Regulatory Macrophages. *Cancer Res.* **2009**, *69*, 9395-9403.
85. F., R. J.; K., C. P.; M., R., Differential regulation of folate receptor isoforms in normal and malignant tissues in vivo and in established cell lines. Physiologic and clinical implications. *Cancer* **1994**, *73*, 2432-2443.
86. Reddy, J. A.; Haneline, L. S.; Srour, E. F.; Antony, A. C.; Clapp, D. W.; Low, P. S., Expression and functional characterization of the β -isoform of the folate receptor on CD34(+) cells. *Blood* **1999**, *93*, 3940-3948.
87. Shen, F.; Wu, M.; Ross, J. F.; Miller, D.; Ratnam, M., Folate receptor type γ . Is primarily a secretory protein due to lack of an efficient signal for glycosylphosphatidylinositol modification: Protein characterization and cell type specificity. *Biochemistry* **1995**, (16), 5660-5665.
88. Rijnboutt, S.; Jansen, G.; Posthuma, G.; Hynes, J. B.; Schornagel, J. H.; Strous, G. J., Endocytosis of GPI-linked membrane folate receptor- α . *J. Cell Biol.* **1996**, *132*, 35-47.
89. Ross, J. F.; Wang, H.; Behm, F. G.; Mathew, P.; Wu, M.; Booth, R.; Ratnam, M., Folate receptor type β is a neutrophilic lineage marker and is differentially expressed in myeloid leukemia. *Cancer* **1999**, *85*, 348-357.
90. Chancy, C. D.; Kekuda, R.; Huang, W.; Prasad, P. D.; Kuhnel, J.-M.; Sirotnak, F. M.; Roon, P.; Ganapathy, V.; Smith, S. B., Expression and differential polarization of the reduced-folate transporter-1 and the folate receptor α in mammalian retinal pigment epithelium. *J. Biol. Chem.* **2000**, *275*, 20676-20684.

91. Chen, C.; Ke, J.; Zhou, X. E.; Yi, W.; Brunzelle, J. S.; Li, J.; Yong, E.-L.; Xu, H. E.; Melcher, K., Structural basis for molecular recognition of folic acid by folate receptors. *Nature* **2013**, *500*, 486-489.
92. Antony, A. C.; Kincade, R. S.; Verma, R. S.; Krishnan, S. R., Identification of high affinity folate binding proteins in human erythrocyte membranes. *J. Clin. Invest.* **1987**, *80*, 711-723.
93. Yang, J.; Chen, H.; Vlahov, I. R.; Cheng, J.-X.; Low, P. S., Characterization of the pH of folate receptor-containing endosomes and the rate of hydrolysis of internalized acid-labile folate-drug conjugates. *J. Pharmacol. Exp. Ther.* **2007**, *321*, 462-468.
94. Sabharanjak, S.; Sharma, P.; Parton, R. G.; Mayor, S., GPI-anchored proteins are delivered to recycling endosomes via a distinct cdc42-regulated, clathrin-independent pinocytotic pathway. *Dev. Cell* **2002**, *2*, 411-423.
95. Wibowo, A. S.; Singh, M.; Reeder, K. M.; Carter, J. J.; Kovach, A. R.; Meng, W.; Ratnam, M.; Zhang, F.; Dann, C. E., Structures of human folate receptors reveal biological trafficking states and diversity in folate and antifolate recognition. *Proc. Natl. Acad. Sci. USA* **2013**, *110*, 15180-15188.
96. Goldman, I. D.; Chattopadhyay, S.; Zhao, R.; Moran, R. G., The antifolates: Evolution, new agents in the clinic, and how targeting delivery via specific membrane transporters is driving the development of a next generation of folate analogs. *Curr. Opin. Investig. Drugs* **2010**, *11*, 1409-1423.
97. Zhao, R.; Min, S. H.; Wang, Y.; Campanella, E.; Low, P. S.; Goldman, I. D., A role for the proton-coupled folate transporter (PCFT-SLC46A1) in folate receptor-mediated endocytosis. *J. Biol. Chem.* **2009**, *284*, 4267-4274.
98. Toffoli, G.; Cernigoi, C.; Russo, A.; Gallo, A.; Bagnoli, M.; Boiocchi, M., Overexpression of folate binding protein in ovarian cancers. *Int. J. Cancer* **1997**, *74*, 193-198.
99. Wu, M.; Gunning, W.; Ratnam, M., Expression of folate receptor type α in relation to cell type, malignancy, and differentiation in ovary, uterus, and cervix. *Cancer Epidemiol. Biomarkers Prev.* **1999**, *8*, 775-782.
100. Bueno, R.; Appasani, K.; Mercer, H.; Lester, S.; Sugarbaker, D., The α folate receptor is highly activated in malignant pleural mesothelioma. *J. Thorac. Cardiovasc. Surg.* **2001**, *121*, 225-233.
101. Pan, X. Q.; Zheng, X.; Shi, G.; Wang, H.; Ratnam, M.; Lee, R. J., Strategy for the treatment of acute myelogenous leukemia based on folate receptor β -targeted liposomal doxorubicin combined with receptor induction using all-trans retinoic acid. *Blood* **2002**, *100*, 594-602.
102. Xia, W.; Low, P. S., Folate-targeted therapies for cancer. *J. Med. Chem.* **2010**, *53*, 6811-6824.
103. Leamon, C. P.; Jackman, A. L., Chapter 7 exploitation of the folate receptor in the management of cancer and inflammatory disease. In *Vitamins & Hormones*, Academic Press: 2008; Vol. 79, pp 203-233.
104. Wang, L.; Desmoulin, S. K.; Cherian, C.; Polin, L.; White, K.; Kushner, J.; Fulterer, A.; Chang, M.-H.; Mitchell, S.; Stout, M.; Romero, M. F.; Hou, Z.; Matherly, L. H.; Gangjee, A., Synthesis, biological and antitumor activity of a highly potent 6-substituted pyrrolo[2,3-d]pyrimidine thienoyl antifolate inhibitor with proton-coupled folate

- transporter and folate receptor selectivity over the reduced folate carrier that inhibits β -glycinamide ribonucleotide formyltransferase. *J. Med. Chem.* **2011**, *54*, 7150-7164.
105. Yang, J.; Vlashi, E.; Low, P. S., Folate-linked drugs for the treatment of cancer and inflammatory diseases. In *Water Soluble Vitamins: Clinical Research and Future Application*, Stanger, O., Ed. Springer Netherlands: Dordrecht, 2012; pp 163-179.
106. Low, P. S.; Antony, A. C., Folate receptor-targeted drugs for cancer and inflammatory diseases. *Adv. Drug Deliv. Rev.* **2004**, *56*, 1055-1058.
107. Wang, L.; Cherian, C.; Kugel Desmoulin, S.; Polin, L.; Deng, Y.; Wu, J.; Hou, Z.; White, K.; Kushner, J.; Matherly, L. H.; Gangjee, A., Synthesis and antitumor activity of a novel series of 6-substituted pyrrolo[2,3-*d*]pyrimidine thienoyl antifolate inhibitors of purine biosynthesis with selectivity for high affinity folate receptors and the proton-coupled folate transporter over the reduced folate carrier for cellular entry. *J. Med. Chem.* **2010**, *53*, 1306-1318.
108. Assaraf, Y. G.; Leamon, C. P.; Reddy, J. A., The folate receptor as a rational therapeutic target for personalized cancer treatment. *Drug Resist. Updat.* **2014**, *17*, 89-95.
109. Zhao, X. B.; Lee, R. J., Tumor-selective targeted delivery of genes and antisense oligodeoxyribonucleotides via the folate receptor. *Adv. Drug Deliv. Rev.* **2004**, *56*, 1193-1204.
110. Kim, S. H.; Jeong, J. H.; Chun, K. W.; Park, T. G., Target-specific cellular uptake of PLGA nanoparticles coated with poly(l-lysine)-poly(ethylene glycol)-folate conjugate. *Langmuir* **2005**, *21*, 8852-8857.
111. van Dam, G. M.; Themelis, G.; Crane, L. M. A.; Harlaar, N. J.; Pleijhuis, R. G.; Kelder, W.; Sarantopoulos, A.; de Jong, J. S.; Arts, H. J. G.; van der Zee, A. G. J.; Bart, J.; Low, P. S.; Ntziachristos, V., Intraoperative tumor-specific fluorescence imaging in ovarian cancer by folate receptor- α targeting: first in-human results. *Nat. Med.* **2011**, *17*, 1315-1319.
112. Deng, Y.; Zhou, X.; Desmoulin, S. K.; Wu, J.; Cherian, C.; Hou, Z.; Matherly, L. H.; Gangjee, A., Synthesis and biological activity of a novel series of 6-substituted thieno[2,3-*d*]pyrimidine antifolate inhibitors of purine biosynthesis with selectivity for high affinity folate receptors over the reduced folate carrier and proton-coupled folate transporter for cellular entry. *J. Med. Chem.* **2009**, *52*, 2940-2951.
113. Picciano, M. F.; Stokstad, E. L. R.; Gregory, J. F., *Contemporary issues in clinical nutrition, vol. 13: Folic acid metabolism in health and disease*. Wiley-Liss: 1990; p 299 pp.
114. Ravindra, M.; Wilson, M. R.; Tong, N.; O'Connor, C.; Karim, M.; Polin, L.; Wallace-Povirk, A.; White, K.; Kushner, J.; Hou, Z.; Matherly, L. H.; Gangjee, A., Fluorine-substituted pyrrolo[2,3-*d*]pyrimidine analogues with tumor targeting via cellular uptake by folate receptor α and the proton-coupled folate transporter and inhibition of de novo purine nucleotide biosynthesis. *J. Med. Chem.* **2018**, *61*, 4228-4248.
115. Ravindra, M.; Wallace-Povirk, A.; Karim, M. A.; Wilson, M. R.; O'Connor, C.; White, K.; Kushner, J.; Polin, L.; George, C.; Hou, Z.; Matherly, L. H.; Gangjee, A., Tumor targeting with novel pyridyl 6-substituted pyrrolo[2,3-*d*]pyrimidine antifolates via cellular uptake by folate receptor α and the proton-coupled folate transporter and inhibition of de novo purine nucleotide biosynthesis. *J. Med. Chem.* **2018**, *61*, 2027-2040.
116. Wang, L.; Cherian, C.; Kugel Desmoulin, S.; Mitchell-Ryan, S.; Hou, Z.; Matherly, L. H.; Gangjee, A., Synthesis and biological activity of 6-substituted pyrrolo[2,3-

- d*]pyrimidine thienoyl regioisomers as inhibitors of de novo purine biosynthesis with selectivity for cellular uptake by high affinity folate receptors and the proton-coupled folate transporter over the reduced folate carrier. *J. Med. Chem.* **2012**, *55*, 1758-1770.
117. Wang, Y.; Mitchell-Ryan, S.; Raghavan, S.; George, C.; Orr, S.; Hou, Z.; Matherly, L. H.; Gangjee, A., Novel 5-substituted pyrrolo[2,3-*d*]pyrimidines as dual inhibitors of glycinamide ribonucleotide formyltransferase and 5-aminoimidazole-4-carboxamide ribonucleotide formyltransferase and as potential antitumor agents. *J. Med. Chem.* **2015**, *58*, 1479-1493.
118. Deng, Y.; Wang, Y.; Cherian, C.; Hou, Z.; Buck, S. A.; Matherly, L. H.; Gangjee, A., Synthesis and discovery of high affinity folate receptor-specific glycinamide ribonucleotide formyltransferase inhibitors with antitumor activity. *J. Med. Chem.* **2008**, *51*, 5052-5063.
119. Desmoulin, S. K.; Wang, Y.; Wu, J.; Stout, M.; Hou, Z.; Fulterer, A.; Chang, M.-H.; Romero, M. F.; Cherian, C.; Gangjee, A.; Matherly, L. H., Targeting the proton-coupled folate transporter for selective delivery of 6-substituted pyrrolo[2,3-*d*]pyrimidine antifolate inhibitors of de novo purine biosynthesis in the chemotherapy of solid tumors. *Mol. Pharmacol.* **2010**, *78*, 577-587.
120. Mitchell-Ryan, S.; Wang, Y.; Raghavan, S.; Ravindra, M. P.; Hales, E.; Orr, S.; Cherian, C.; Hou, Z.; Matherly, L. H.; Gangjee, A., Discovery of 5-substituted pyrrolo[2,3-*d*]pyrimidine antifolates as dual-acting inhibitors of glycinamide ribonucleotide formyltransferase and 5-aminoimidazole-4-carboxamide ribonucleotide formyltransferase in de novo purine nucleotide biosynthesis: Implications of inhibiting 5-aminoimidazole-4-carboxamide ribonucleotide formyltransferase to AMPK activation and antitumor activity. *J. Med. Chem.* **2013**, *56*, 10016-10032.
121. Wang, L.; Wallace, A.; Raghavan, S.; Deis, S. M.; Wilson, M. R.; Yang, S.; Polin, L.; White, K.; Kushner, J.; Orr, S.; George, C.; O'Connor, C.; Hou, Z.; Mitchell-Ryan, S.; Dann, C. E.; Matherly, L. H.; Gangjee, A., 6-Substituted Pyrrolo[2,3-*d*]pyrimidine Thienoyl Regioisomers as Targeted Antifolates for Folate Receptor α and the Proton-Coupled Folate Transporter in Human Tumors. *Journal of Medicinal Chemistry* **2015**, *58* (17), 6938-6959.
122. Qiu, A.; Jansen, M.; Sakaris, A.; Min, S. H.; Chattopadhyay, S.; Tsai, E.; Sandoval, C.; Zhao, R.; Akabas, M. H.; Goldman, I. D., Identification of an intestinal folate transporter and the molecular basis for hereditary folate malabsorption. *Cell* **2006**, *127*, 917-928.
123. Zhao, R.; Aluri, S.; Goldman, I. D., The proton-coupled folate transporter (PCFT-SLC46A1) and the syndrome of systemic and cerebral folate deficiency of infancy: Hereditary folate malabsorption. *Mol. Aspects Med.* **2017**, *53*, 57-72.
124. Hou, Z.; Matherly, L. H., Chapter four - biology of the major facilitative folate transporters SLC19A1 and SLC46A1. In *Current Topics in Membranes*, Bevenssee, M. O., Ed. Academic Press: 2014; Vol. 73, pp 175-204.
125. Nakai, Y.; Inoue, K.; Abe, N.; Hatakeyama, M.; Ohta, K.-y.; Otagiri, M.; Hayashi, Y.; Yuasa, H., Functional characterization of human proton-coupled folate transporter/heme carrier protein 1 heterologously expressed in mammalian cells as a folate transporter. *J. Pharmacol. Exp. Ther.* **2007**, *322*, 469-476.
126. Katsuhisa, I.; Yasuhiro, N.; Sayaka, U.; Shunsuke, K.; Kin-ya, O.; Mai, H.; Yayoi, H.; Masaki, O.; Hiroaki, Y., Functional characterization of PCFT/HCP1 as the molecular

- entity of the carrier-mediated intestinal folate transport system in the rat model. *Am. J. Physiol. Gastrointest. Liver Physiol.* **2008**, *294*, G660-G668.
127. Chattopadhyay, S.; Tamari, R.; Min, S. H.; Zhao, R.; Tsai, E.; Goldman, I. D., Commentary: A case for minimizing folate supplementation in clinical regimens with pemetrexed based on the marked sensitivity of the drug to folate availability. *Oncologist* **2007**, *12*, 808-815.
128. Qiu, A.; Min, S. H.; Jansen, M.; Malhotra, U.; Tsai, E.; Cabelof, D. C.; Matherly, L. H.; Zhao, R.; Akabas, M. H.; Goldman, I. D., Rodent intestinal folate transporters (SLC46A1): secondary structure, functional properties, and response to dietary folate restriction. *Am. J. Physiol. Cell Physiol.* **2007**, *293*, C1669-C1678.
129. Yun, C. H.; Tse, C. M.; Nath, S. K.; Levine, S. A.; Brant, S. R.; Donowitz, M., Mammalian Na⁺/H⁺ exchanger gene family: structure and function studies. *Am. J. Physiol. Gastrointest Liver Physiol.* **1995**, *269*, G1-G11.
130. Wollack, J. B.; Makori, B.; Ahlawat, S.; Koneru, R.; Picinich, S. C.; Smith, A.; Goldman, I. D.; Qiu, A.; Cole, P. D.; Glod, J.; Kamen, B., Characterization of folate uptake by choroid plexus epithelial cells in a rat primary culture model. *J. Neurochem.* **2008**, *104*, 1494-1503.
131. Umopathy, N. S.; Gnana-Prakasam, J. P.; Martin, P. M.; Mysona, B.; Dun, Y.; Smith, S. B.; Ganapathy, V.; Prasad, P. D., Cloning and functional characterization of the proton-coupled electrogenic folate transporter and analysis of its expression in retinal cell types. *Invest. Ophthalmol. Vis. Sci.* **2007**, *48*, 5299-5305.
132. Zhao, R.; Qiu, A.; Tsai, E.; Jansen, M.; Akabas, M. H.; Goldman, I. D., The proton-coupled folate transporter: Impact on pemetrexed transport and on antifolates activities compared to the reduced folate carrier. *Mol. Pharmacol.* **2008**, *74*, 854-862.
133. Wang, L.; Cherian, C.; Desmoulin, S. K.; Polin, L.; Deng, Y.; Wu, J.; Hou, Z.; White, K.; Kushner, J.; Matherly, L. H.; Gangjee, A., Synthesis and biological activity of a novel series of 6-substituted pyrrolo[2,3-*d*]pyrimidine thienoyl antifolate inhibitors of purine biosynthesis with selectivity for high affinity folate receptors and the proton-coupled folate transporter over the reduced folate carrier for cellular entry(†). *J. Med. Chem.* **2010**, *53*, 1306-1318.
134. Lasry, I.; Berman, B.; Straussberg, R.; Sofer, Y.; Bessler, H.; Sharkia, M.; Glaser, F.; Jansen, G.; Drori, S.; Assaraf, Y. G., A novel loss-of-function mutation in the proton-coupled folate transporter from a patient with hereditary folate malabsorption reveals that Arg 113 is crucial for function. *Blood* **2008**, *112*, 2055-2061.
135. Min, S. H.; Oh, S. Y.; Karp, G. I.; Poncz, M.; Zhao, R.; Goldman, I. D., The clinical course and genetic defect in the PCFT gene in a 27-year old woman with hereditary folate malabsorption. *J. Pediatr.* **2008**, *153*, 435-437.
136. Atabay, B.; Turker, M.; Ozer, E. A.; Mahadeo, K.; Diop-Bove, N.; Goldman, I. D., Mutation of the proton-coupled folate transporter gene (PCFT-SLC46A1) in turkish siblings with hereditary folate malabsorption. *J. Pediatr. Hematol. Oncol.* **2010**, *27*, 614-619.
137. Mahadeo, K.; Diop-Bove, N.; Shin, D. S.; Unal, E. S.; Teo, J.; Zhao, R.; Chang, M.-H.; Fulterer, A.; Romero, M. F.; Goldman, I. D., Properties of the Arg376 residue of the proton-coupled folate transporter (PCFT-SLC46A1) and a glutamine mutant causing hereditary folate malabsorption. *Am. J. Physiol. Cell Physiol.* **2010**, *299*, C1153-C1161.

138. Meyer, E.; Kurian, M. A.; Pasha, S.; Trembath, R. C.; Cole, T.; Maher, E. R., A novel PCFT gene mutation (p.Cys66LeufsX99) causing hereditary folate malabsorption. *Mol. Genet. Metab. Rep.* **2010**, *99*, 325-328.
139. Shin, D. S.; Min, S. H.; Russell, L.; Zhao, R.; Fiser, A.; Goldman, I. D., Functional roles of aspartate residues of the proton-coupled folate transporter (PCFT-SLC46A1); a D156Y mutation causing hereditary folate malabsorption. *Blood* **2010**, *116*, 5162-5169.
140. Diop-Bove, N.; Jain, M.; Scaglia, F.; Goldman, I. D., A novel deletion mutation in the proton-coupled folate transporter (PCFT; SLC46A1) in a Nicaraguan child with hereditary folate malabsorption. *Gene* **2013**, *527*, 673-674.
141. Salojin, K. V.; Cabrera, R. M.; Sun, W.; Chang, W. C.; Lin, C.; Duncan, L.; Platt, K. A.; Read, R.; Vogel, P.; Liu, Q.; Finnell, R. H.; Oravec, T., A mouse model of hereditary folate malabsorption: deletion of the *PCFT* gene leads to systemic folate deficiency. *Blood* **2011**, *117*, 4895-4904.
142. Unal, E. S.; Zhao, R.; Chang, M.-H.; Fiser, A.; Romero, M. F.; Goldman, I. D., The functional roles of the his(247) and his(281) residues in folate and proton translocation mediated by the human proton-coupled folate transporter SLC46A1. *J. Biol. Chem.* **2009**, *284*, 17846-17857.
143. Zhao, R.; Unal, E. S.; Shin, D. S.; Goldman, I. D., Membrane topological analysis of the proton-coupled folate transporter (PCFT-SLC46A1) by the substituted cysteine accessibility method. *Biochemistry* **2010**, *49*, 2925-2931.
144. Unal, E. S.; Zhao, R.; Goldman, I. D., Role of the glutamate 185 residue in proton translocation mediated by the proton-coupled folate transporter SLC46A1. *Am. J. Physiol. Cell Physiol.* **2009**, *297*, C66-C74.
145. Veedamali, S. S.; Jonathan, S. M.; Hamid, M. S., Apical membrane targeting and trafficking of the human proton-coupled transporter in polarized epithelia. *Am. J. Cell Physiol.* **2008**, *294*, C233-C240.
146. Zhao, R.; Shin, D. S.; Diop-Bove, N.; Ovits, C. G.; Goldman, I. D., Random mutagenesis of the proton-coupled folate transporter (SLC46A1), clustering of mutations, and the bases for associated losses of function. *J. Biol. Chem.* **2011**, *286*, 24150-24158.
147. Shin, D. S.; Zhao, R.; Yap, E. H.; Fiser, A.; Goldman, I. D., A P425R mutation of the proton-coupled folate transporter causing hereditary folate malabsorption produces a highly selective alteration in folate binding. *Am. J. Physiol. Cell Physiol.* **2012**, *302*, C1405-C1412.
148. Zhao, R.; Shin, D. S.; Fiser, A.; Goldman, I. D., Identification of a functionally critical GXXG motif and its relationship to the folate binding site of the proton-coupled folate transporter (PCFT-SLC46A1). *Am. J. Physiol. Cell Physiol.* **2012**, *303*, C673-C681.
149. Shin, D. S.; Zhao, R.; Fiser, A.; Goldman, I. D., Role of the fourth transmembrane domain in proton-coupled folate transporter function as assessed by the substituted cysteine accessibility method. *Am. J. Physiol. Cell Physiol.* **2013**, *304*, C1159-C1167.
150. Hou, Z.; Kugel Desmoulin, S.; Etnyre, E.; Olive, M.; Hsiung, B.; Cherian, C.; Wloszczynski, P. A.; Moin, K.; Matherly, L. H., Identification and functional impact of homo-oligomers of the human proton-coupled folate transporter. *J. Biol. Chem.* **2012**, *287*, 4982-4995.
151. Wilson, M. R.; Kugel, S.; Huang, J.; Wilson, L. J.; Wloszczynski, P. A.; Ye, J.; Matherly, L. H.; Hou, Z., Structural determinants of human proton-coupled folate

- transporter oligomerization: role of GXXXG motifs and identification of oligomeric interfaces at transmembrane domains 3 and 6. *Biochem. J.* **2015**, *469*, 33-44.
152. K., D. P.; P., N.; P., B. M.; M., J., The monomeric state of the proton-coupled folate transporter represents the functional unit in the plasma membrane. *The FEBS Journal* **2013**, *280*, 2900-2915.
153. Gallagher, F. A.; Kettunen, M. I.; Day, S. E.; Hu, D.-E.; Ardenkjær-Larsen, J. H.; Zandt, R.; Jensen, P. R.; Karlsson, M.; Golman, K.; Lerche, M. H.; Brindle, K. M., Magnetic resonance imaging of pH in vivo using hyperpolarized ¹³C-labelled bicarbonate. *Nature* **2008**, *453*, 940.
154. Webb, B. A.; Chimenti, M.; Jacobson, M. P.; Barber, D. L., Dysregulated pH: a perfect storm for cancer progression. *Nat. Rev. Cancer* **2011**, *11*, 671-677.
155. Gatenby, R. A.; Gillies, R. J., Why do cancers have high aerobic glycolysis? *Nat. Rev. Cancer* **2004**, *4*, 891.
156. Hanahan, D.; Weinberg, R. A., Hallmarks of Cancer: The Next Generation. *Cell* **2011**, *144*, 646-674.
157. Gillies, R. J.; Robey, I.; Gatenby, R. A., Causes and consequences of increased glucose metabolism of cancers. *J. Nucl. Med.* **2008**, *49*, 24S-42S.
158. Wilson, M. R.; Hou, Z.; Yang, S.; Polin, L.; Kushner, J.; White, K.; Huang, J.; Ratnam, M.; Gangjee, A.; Matherly, L. H., Targeting nonsquamous nonsmall cell lung cancer via the proton-coupled folate transporter with 6-substituted pyrrolo[2,3-*d*]pyrimidine thienoyl antifolates. *Mol. Pharmacol.* **2016**, *89*, 425-434.
159. Hou, Z.; Gattoc, L.; O'Connor, C.; Yang, S.; Wallace-Povirk, A.; George, C.; Orr, S.; Polin, L.; White, K.; Kushner, J.; Morris, R. T.; Gangjee, A.; Matherly, L. H., Dual targeting of epithelial ovarian cancer via folate receptor α and the proton-coupled folate transporter with 6-substituted pyrrolo[2,3-*d*]pyrimidine antifolates. *Mol. Cancer Ther.* **2017**, *16*, 819-830.
160. Giovannetti, E.; Zucali, P. A.; Assaraf, Y. G.; Funel, N.; Gemelli, M.; Stark, M.; Thunnissen, E.; Hou, Z.; Muller, I. B.; Struys, E. A.; Perrino, M.; Jansen, G.; Matherly, L. H.; Peters, G. J., Role of proton-coupled folate transporter in pemetrexed resistance of mesothelioma: clinical evidence and new pharmacological tools. *Ann. Oncol.* **2017**, *28*, 2725-2732.
161. Gonen, N.; Bram, E. E.; Assaraf, Y. G., PCFT/SLC46A1 promoter methylation and restoration of gene expression in human leukemia cells. *Biochem. Biophys. Res. Commun.* **2008**, *376*, 787-792.
162. Menter, A.; Thrash, B.; Cherian, C.; Matherly, L. H.; Wang, L.; Gangjee, A.; Morgan, J. R.; Maeda, D. Y.; Schuler, A. D.; Kahn, S. J.; Zebala, J. A., Intestinal transport of aminopterin enantiomers in dogs and humans with psoriasis is stereoselective: Evidence for a mechanism involving the proton-coupled folate transporter. *J. Pharmacol. Exp. Ther.* **2012**, *342*, 696-708.
163. Sirotnak, F. M.; Donsbach, R. C., Comparative studies on the transport of aminopterin, methotrexate, and methasquin by the L1210 leukemia cell. *Cancer Res.* **1972**, *32*, 2120-2126.
164. Zhao, R.; Hanscom, M.; Chattopadhyay, S.; Goldman, I. D., Selective preservation of pemetrexed pharmacological activity in HeLa cells lacking the reduced folate carrier. *Association with the Presence of a Secondary Transport Pathway* **2004**, *64*, 3313-3319.

165. Chattopadhyay, S.; Moran, R. G.; Goldman, I. D., Pemetrexed: biochemical and cellular pharmacology, mechanisms, and clinical applications. *Mol. Cancer. Ther.* **2007**, *6*, 404-417.
166. Cherian, C.; Desmoulin, S. K.; Wang, L.; Polin, L.; White, K.; Kushner, J.; Stout, M.; Hou, Z.; Gangjee, A.; Matherly, L. H., Therapeutic targeting malignant mesothelioma with a novel 6-substituted pyrrolo[2,3-*d*]pyrimidine thienoyl antifolate via its selective uptake by the proton-coupled folate transporter. *Cancer Chemother. Pharmacol.* **2013**, *71*, 999-1011.
167. Golani, L. K.; Wallace-Povirk, A.; Deis, S. M.; Wong, J. E.; Ke, J.; Gu, X.; Raghavan, S.; Wilson, M. R.; Li, X.; Polin, L.; de Waal, P. W.; White, K.; Kushner, J.; O'Connor, C.; Hou, Z.; Xu, H. E.; Melcher, K.; Dann, C. E.; Matherly, L. H.; Gangjee, A., Tumor Targeting with Novel 6-Substituted Pyrrolo [2,3-*d*] Pyrimidine Antifolates with Heteroatom Bridge Substitutions Via Cellular Uptake by Folate Receptor α and the Proton-coupled Folate Transporter and Inhibition of De Novo Purine Nucleotide Biosynthesis. *Journal of medicinal chemistry* **2016**, *59*, 7856-7876.
168. Wright, A. J. A.; Dainty, J. R.; Finglas, P. M., Folic acid metabolism in human subjects revisited: potential implications for proposed mandatory folic acid fortification in the UK. *British Journal of Nutrition* **2007**, *98* (4), 667-675.
169. Stover, P. J.; Field, M. S., Trafficking of intracellular folates. *Adv. Nutr* **2011**, *2*, 325-331.
170. Lin, B. F.; Huang, R. F.; Shane, B., Regulation of folate and one-carbon metabolism in mammalian cells. III. Role of mitochondrial folylpoly-gamma-glutamate synthetase. *J. Biol. Chem.* **1993**, *268*, 21674-21679.
171. McCarthy, E. A.; Titus, S. A.; Taylor, S. M.; Jackson-Cook, C.; Moran, R. G., A mutation inactivating the mitochondrial inner membrane folate transporter creates a glycine requirement for survival of Chinese hamster cells. *J. Biol. Chem.* **2004**, *279*, 33829-33836.
172. Shane, B., Folylpolyglutamate synthesis and role in the regulation of one-carbon metabolism. In *Vitamins & Hormones*, Aurbach, G. D.; McCormick, D. B., Eds. Academic Press: 1989; Vol. 45, pp 263-335.
173. Moran, R. G., Characterization of the function of mammalian folylpolyglutamate synthetase (FPGS). In *Folyl and Antifolyl Polyglutamates*, Goldman, I. D.; Chabner, B. A.; Bertino, J. R., Eds. Springer US: Boston, MA, 1983; pp 327-339.
174. Shane, B.; Bognar, A. L.; Goldfarb, R. D.; LeBowitz, J. H., Regulation of folylpoly-gamma-glutamate synthesis in bacteria: in vivo and in vitro synthesis of pteroylpoly-gamma-glutamates by *Lactobacillus casei* and *Streptococcus faecalis*. *J. Bacteriol.* **1983**, *153*, 316-325.
175. McGuire, J. J.; Hsieh, P.; Bertino, J. R., Enzymatic synthesis of polyglutamate derivatives of 7-hydroxymethotrexate. *Biochem. Pharmacol.* **1984**, *33*, 1355-1361.
176. Baldwin, S. W.; Tse, A.; Gossett, L. S.; Taylor, E. C.; Rosowsky, A.; Shih, C.; Moran, R. G., Structural features of 5,10-dideaza-5,6,7,8-tetrahydrofolate that determine inhibition of mammalian glycinamide ribonucleotide formyltransferase. *Biochemistry* **1991**, *30*, 1997-2006.
177. Moran, R. G., Roles of folylpoly-gamma-glutamate synthetase in therapeutics with tetrahydrofolate antimetabolites: An overview. *Semin. Oncol.* **1999**, *26*, 24-32.

178. Freemantle, S. J.; Taylor, S. M.; Krystal, G.; Moran, R. G., Upstream organization of and multiple transcripts from the human folylpoly--glutamate synthetase gene. *J. Biol. Chem.* **1995**, *270*, 9579-9584.
179. Sun, X.; Bogнар, A. L.; Baker, E. N.; Smith, C. A., Structural homologies with ATP- and folate-binding enzymes in the crystal structure of folylpolyglutamate synthetase. *Proc. Natl. Acad. Sci. U S A* **1998**, *95*, 6647-6652.
180. Shih, C.; Thornton, D. E., Preclinical pharmacology studies and the clinical development of a novel multitargeted antifolate, MTA (LY231514). In *Antifolate Drugs in Cancer Therapy*, Jackman, A. L., Ed. Humana Press: Totowa, NJ, 1999; pp 183-201.
181. Lubin, M.; Lubin, A., Selective killing of tumors deficient in methylthioadenosine phosphorylase: A novel strategy. *PLoS ONE* **2009**, *4*, e5735.
182. Shih, C.; Chen, V. J.; Gossett, L. S.; Gates, S. B.; MacKellar, W. C.; Habeck, L. L.; Shackelford, K. A.; Mendelsohn, L. G.; Soose, D. J.; Patel, V. F.; Andis, S. L.; Bewley, J. R.; Rayl, E. A.; Moroson, B. A.; Beardsley, G. P.; Kohler, W.; Ratnam, M.; Schultz, R. M., LY231514, a pyrrolo[2,3-*d*]pyrimidine-based antifolate that inhibits multiple folate-requiring enzymes. *Cancer Res.* **1997**, *57*, 1116-1123.
183. Liani, E.; Rothem, L.; Bunni, M. A.; Smith, C. A.; Jansen, G.; Assaraf, Y. G., Loss of folylpoly- γ -glutamate synthetase activity is a dominant mechanism of resistance to polyglutamylated novel antifolates in multiple human leukemia sublines. *Int. J. Cancer* **2003**, *103*, 587-599.
184. An, S.; Kumar, R.; Sheets, E. D.; Benkovic, S. J., Reversible compartmentalization of de novo purine biosynthetic complexes in living cells. *Science* **2008**, *320*, 103-106.
185. French, J. B.; Jones, S. A.; Deng, H.; Pedley, A. M.; Kim, D.; Chan, C. Y.; Hu, H.; Pugh, R. J.; Zhao, H.; Zhang, Y.; Huang, T. J.; Fang, Y.; Zhuang, X.; Benkovic, S. J., Spatial colocalization and functional link of purinosomes with mitochondria. *Science (New York, N.Y.)* **2016**, *351*, 733-737.
186. Tucker, E. J.; Hershman, S. G.; Köhrer, C.; Belcher-Timme, C. A.; Patel, J.; Goldberger, O. A.; Christodoulou, J.; Silberstein, J. M.; McKenzie, M.; Ryan, M. T.; Compton, A. G.; Jaffe, J. D.; Carr, S. A.; Calvo, S. E.; RajBhandary, U. L.; Thorburn, D. R.; Mootha, V. K., Mutations in MTFMT underlie a human disorder of formylation causing impaired mitochondrial translation. *Cell metabol.* **2011**, *14*, 428-434.
187. Krupenko, N. I.; Dubard, M. E.; Strickland, K. C.; Moxley, K. M.; Oleinik, N. V.; Krupenko, S. A., ALDH1L2 is the mitochondrial homolog of 10-formyltetrahydrofolate dehydrogenase. *J. Biol. Chem.* **2010**, *285*, 23056-23063.
188. Fan, J.; Ye, J.; Kamphorst, J. J.; Shlomi, T.; Thompson, C. B.; Rabinowitz, J. D., Quantitative flux analysis reveals folate-dependent NADPH production. *Nature* **2014**, *510*, 298-302.
189. Piskounova, E.; Agathocleous, M.; Murphy, M. M.; Hu, Z.; Huddleston, S. E.; Zhao, Z.; Leitch, A. M.; Johnson, T. M.; DeBerardinis, R. J.; Morrison, S. J., Oxidative stress inhibits distant metastasis by human melanoma cells. *Nature* **2015**, *527*, 186-191.
190. Ducker, G. S.; Chen, L.; Morscher, R. J.; Ghergurovich, J. M.; Esposito, M.; Teng, X.; Kang, Y.; Rabinowitz, J. D., Reversal of cytosolic one-carbon flux compensates for loss of the mitochondrial folate pathway. *Cell Metab.* **2016**, *23*, 1140-1153.
191. Stead, L. M.; Brosnan, J. T.; Brosnan, M. E.; Vance, D. E.; Jacobs, R. L., Is it time to reevaluate methylation balance in humans? *Am. J. Clin. Nutr.* **2006**, *83*, 5-10.

192. Finkelstein, J. D., Methionine metabolism in mammals. *J. Nutr. Biochem.* **1990**, *1*, 228-237.
193. Mudd, S. H.; Brosnan, J. T.; Brosnan, M. E.; Jacobs, R. L.; Stabler, S. P.; Allen, R. H.; Vance, D. E.; Wagner, C., Methyl balance and transmethyltion fluxes in humans. *Am. J. Clin. Nutr.* **2007**, *85*, 19-25.
194. Su, X.; Wellen, K. E.; Rabinowitz, J. D., Metabolic control of methylation and acetylation. *Curr Opin. Chem. Biol.* **2016**, *30*, 52-60.
195. S., J. R.; D., H. J.; W., P. E., Structure, dynamics, and catalytic function of dihydrofolate reductase. *Annu. Rev. Biophys. Biomol. Struct.* **2004**, *33*, 119-140.
196. Oefner, C.; D'Arcy, A.; Winkler, F. K., Crystal structure of human dihydrofolate reductase complexed with folate. *Eur. J. Biochem.* **1988**, *174*, 377-385.
197. **Schrödinger Release 2018-2**: Maestro, Schrödinger, LLC, New York, NY, 2018.
198. Blakeley, R. L.; Benkovic, S. J., *Folates and pterins, vol. 1: Chemistry and biochemistry of folates*. John Wiley and Sons: 1984; p 628 pp.
199. Domin, B. A.; Cheng, Y. C.; Hakala, M. T., Properties of dihydrofolate reductase from a methotrexate-resistant subline of human KB cells and comparison with enzyme from KB parent cells and mouse S180 AT/3000 cells. *Mol. Pharmacol.* **1982**, *21*, 231-238.
200. Davies, J. F.; Delcamp, T. J.; Prendergast, N. J.; Ashford, V. A.; Freisheim, J. H.; Kraut, J., Crystal structures of recombinant human dihydrofolate reductase complexed with folate and 5-deazafofolate. *Biochemistry* **1990**, *29*, 9467-9479.
201. Charlton, P. A.; Young, D. W.; Birdsall, B.; Feeney, J.; Roberts, G. C. K., Stereochemistry of reduction of folic acid using dihydrofolate reductase. *J. Chem. Soc., Chem. Commun.* **1979**, (20), 922-924.
202. Gready, J. E., Theoretical studies on the activation of the pterin cofactor in the catalytic mechanism of dihydrofolate reductase. *Biochemistry* **1985**, *24*, 4761-4766.
203. Gready, J. E., Dihydrofolate reductase: binding of substrates and inhibitors and catalytic mechanism. *Adv. Pharmacol. Chemother.* **1980**, *17*, 37-102.
204. Polshakov, V. I., Dihydrofolate reductase: structural aspects of mechanisms of enzyme catalysis and inhibition. *Russ. Chem. Bull.* **2001**, *50*, 1733-1751.
205. Smith, G. K.; Mueller, W. T.; Wasserman, G. F.; Taylor, W. D.; Benkovic, S. J., Characterization of the enzyme complex involving the folate-requiring enzymes of de novo purine biosynthesis. *Biochemistry* **1980**, *19*, 4313-4321.
206. Askari, B. S.; Krajinovic, M., Dihydrofolate reductase gene variations in susceptibility to disease and treatment outcomes. *Curr. Genomics* **2010**, *11*, 578-583.
207. Carreras, C. W.; Santi, D. V., The catalytic mechanism and structure of thymidylate synthase. *Annu. Rev. Biochem.* **1995**, *64*, 721-762.
208. Hardy, L. W.; Finer-Moore, J. S.; Montfort, W. R.; Jones, M. O.; Santi, D. V.; Stroud, R. M., Atomic structure of thymidylate synthase: target for rational drug design. *Science (Washington, D. C., 1883-)* **1987**, *235*, 448-55.
209. Sayre, P. H.; Finer-Moore, J. S.; Fritz, T. A.; Biermann, D.; Gates, S. B.; MacKellar, W. C.; Patel, V. F.; Stroud, R. M., Multi-targeted antifolates aimed at avoiding drug resistance form covalent closed inhibitory complexes with human and Escherichia coli thymidylate synthases. *J. Biol. Chem.* **2001**, *313*, 813-829.
210. Matthews, D. A.; Villafranca, J. E.; Janson, C. A.; Smith, W. W.; Welsh, K.; Freer, S., Stereochemical mechanism of action for thymidylate synthase based on the X-ray

- structure of the covalent inhibitory ternary complex with 5-fluoro-2'-deoxyuridylate and 5,10-methylenetetrahydrofolate. *J. Mol. Biol.* **1990**, *214*, 937-948.
211. Montfort, W. R.; Perry, K. M.; Fauman, E. B.; Finer-Moore, J. S.; Maley, G. F.; Hardy, L. W.; Maley, F.; Stroud, R. M., Structure, multiple site binding, and segmental accommodation in thymidylate synthase on binding dUMP and an anti-folate. *Biochemistry* **1990**, *29*, 6964-6977.
212. Matthews, D. A.; Appelt, K.; Oatley, S. J.; Xuong, N. H., Crystal structure of Escherichia coli thymidylate synthase containing bound 5-fluoro-2'-deoxyuridylate and 10-propargyl-5,8-dideazafolate. *J. Mol. Biol.* **1990**, *214*, 923-936.
213. Santi, D. V.; McHenry, C. S.; Raines, R. T.; Ivanetich, K. M., Kinetics and thermodynamics of the interaction of 5-fluoro-2'-deoxyuridylate with thymidylate synthase. *Biochemistry* **1987**, *26*, 8606-8613.
214. Kamb, A.; Finer-Moore, J. S.; Stroud, R. M., Cofactor triggers the conformational change in thymidylate synthase: implications for an ordered binding mechanism. *Biochemistry* **1992**, *31*, 12876-12884.
215. Fontecilla-Camps, J. C.; Bugg, C. E.; Temple, C. J.; Rose, J. D.; Montgomery, J. A.; Kisliuk, R. L., Absolute configuration of biological tetrahydrofolates. A crystallographic determination. *J. Am. Chem. Soc.* **1979**, *101*, 6114-6115.
216. Chen, D.; Jansson, A.; Sim, D.; Larsson, A.; Nordlund, P., Structural analyses of human thymidylate synthase reveal a site that may control conformational switching between active and inactive states. *J. Biol. Chem.* **2017**, *292*, 13449-13458.
217. Davisson, V. J.; Sirawaraporn, W.; Santi, D. V., Expression of human thymidylate synthase in Escherichia coli. *J. Biol. Chem.* **1989**, *264*, 9145-9148.
218. Davisson, V. J.; Sirawaraporn, W.; Santi, D. V., Expression of human thymidylate synthase in Escherichia coli. *J. Biol. Chem.* **1994**, *269*, 30740.
219. Kamb, A.; Finer-Moore, J.; Calvert, A. H.; Stroud, R. M., Structural basis for recognition of polyglutamyl folates by thymidylate synthase. *Biochemistry* **1992**, *31*, 9883-9890.
220. Edler, D.; Hallstrom, M.; Johnston, P. G.; Magnusson, I.; Ragnhammar, P.; Blomgren, H., Thymidylate synthase expression: an independent prognostic factor for local recurrence, distant metastasis, disease-free and overall survival in rectal cancer. *Clin Cancer Res* **2000**, *6*, 1378-84.
221. Mizutani, Y.; Wada, H.; Yoshida, O.; Fukushima, M.; Nonomura, M.; Nakao, M.; Miki, T., Significance of Thymidylate Synthase Activity in Renal Cell Carcinoma. *Am. J. Clin. Cancer Res.* **2003**, *9*, 1453-1460.
222. Nomura, T.; Nakagawa, M.; Fujita, Y.; Hanada, T.; Mimata, H.; Nomura, Y., Clinical significance of thymidylate synthase expression in bladder cancer. *Int J. Urol.* **2002**, *9*, 368-376.
223. Pestalozzi, B. C.; Peterson, H. F.; Gelber, R. D.; Goldhirsch, A.; Gusterson, B. A.; Trihia, H.; Lindtner, J.; Cortés-Funes, H.; Simmoncini, E.; Byrne, M. J.; Golouh, R.; Rudenstam, C. M.; Castiglione-Gertsch, M.; Allegra, C. J.; Johnston, P. G., Prognostic importance of thymidylate synthase expression in early breast cancer. *J. Clin. Oncol.* **1997**, *15*, 1923-1931.
224. Shintani, Y.; Ohta, M.; Hirabayashi, H.; Tanaka, H.; Iuchi, K.; Nakagawa, K.; Maeda, H.; Kido, T.; Miyoshi, S.; Matsuda, H., New prognostic indicator for non-small-

- cell lung cancer, quantitation of thymidylate synthase by real-time reverse transcription polymerase chain reaction. *Int. J. Cancer* **2003**, *104*, 790-795.
225. Houghton, J. A.; Harwood, F. G.; Houghton, P. J., Cell cycle control processes determine cytostasis or cytotoxicity in thymineless death of colon cancer cells. *Cancer Res.* **1994**, *54*, 4967-4973.
226. Rahman, L.; Voeller, D.; Rahman, M.; Lipkowitz, S.; Allegra, C. J.; Barrett, J. C.; Kaye, F. J.; Zajac-Kaye, M., Thymidylate synthase as an oncogene: A novel role for an essential DNA synthesis enzyme. *Cancer Cell* **2004**, *5*, 341-351.
227. Zhao, H.; French, J. B.; Fang, Y.; Benkovic, S. J., The purinosome, a multi-protein complex involved in the de novo biosynthesis of purines in humans. *Chem. Commun.* **2013**, *49*, 4444-4452.
228. Yamaoka, T.; Kondo, M.; Honda, S.; Iwahana, H.; Moritani, M.; Ii, S.; Yoshimoto, K.; Itakura, M., Amidophosphoribosyltransferase limits the rate of cell growth-linked de novo purine biosynthesis in the presence of constant capacity of salvage purine biosynthesis. *J. Biol. Chem.* **1997**, *272*, 17719-17725.
229. Yamaoka, T.; Yano, M.; Kondo, M.; Sasaki, H.; Hino, S.; Katashima, R.; Moritani, M.; Itakura, M., Feedback inhibition of amidophosphoribosyltransferase regulates the rate of cell growth via purine nucleotide, DNA, and protein syntheses. *J. Biol. Chem.* **2001**, *276*, 21285-21291.
230. Natsumeda, Y.; Prajda, N.; Donohue, J. P.; Glover, J. L.; Weber, G., Enzymic capacities of purine de novo and salvage pathways for nucleotide synthesis in normal and neoplastic tissues. *Cancer Research* **1984**, *44*, 2475-2479.
231. Weber, G.; Lui, M. S.; Natsumeda, Y.; Faderan, M. A., Salvage capacity of hepatoma 3924A and action of dipyridamole. *Adv. Enzyme Regul.* **1983**, *21*, 53-69.
232. Buchanan, J. M.; Hartman, S. C., Enzymic reactions in the synthesis of the purines. *Adv. Enzymol. Relat. Areas Mol. Biol.* **1959**, *21*, 199-261.
233. Hartman, S. C.; Buchanan, J. M., Nucleic acids, purines, pyrimidines (nucleotide synthesis). **1959**, *28* (Annu. Rev. Biochem.), 365-410.
234. Dahms, T. E. S.; Sainz, G.; Giroux, E. L.; Caperelli, C. A.; Smith, J. L., The apo and ternary complex structures of a chemotherapeutic target: Human glycinamide ribonucleotide transformylase. *Biochemistry* **2005**, *44*, 9841-9850.
235. Welin, M.; Grossmann, J. G.; Flodin, S.; Nyman, T.; Stenmark, P.; Trésaugues, L.; Kotenyova, T.; Johansson, I.; Nordlund, P.; Lehtiö, L., Structural studies of tri-functional human GART. *Nucleic Acids Res.* **2010**, *38*, 7308-7319.
236. Zhang, Y.; Desharnais, J.; Greasley, S. E.; Beardsley, G. P.; Boger, D. L.; Wilson, I. A., Crystal structures of human GAR Tfase at low and high pH and with substrate β -GAR. *Biochemistry* **2002**, *41*, 14206-14215.
237. Greasley, S. E.; Horton, P.; Ramcharan, J.; Beardsley, G. P.; Benkovic, S. J.; Wilson, I. A., Crystal structure of a bifunctional transformylase and cyclohydrolase enzyme in purine biosynthesis. *Nat. Struct. Mol. Biol.* **2001**, *8*, 402-406.
238. Wolan, D. W.; Greasley, S. E.; Beardsley, G. P.; Wilson, I. A., Structural Insights into the Avian AICAR Transformylase Mechanism. *Biochemistry* **2002**, *41*, 15505-15513.
239. Kim, J.-W.; Dang, C. V., Cancer's molecular sweet tooth and the Warburg effect. *Cancer Res.* **2006**, *66*, 8927-8930.

240. Keller, K. E.; Tan, I. S.; Lee, Y.-S., SAICAR stimulates pyruvate kinase isoform M2 and promotes cancer cell survival in glucose -limited conditions. *Science (New York, N.Y.)* **2012**, *338*, 1069-1072.
241. Towler, M. C.; Hardie, D. G., AMP-activated protein kinase in metabolic control and insulin signaling. *Circ. Res.* **2007**, *100*, 328-341.
242. Hardie, D. G.; Ross, F. A.; Hawley, S. A., AMPK - a nutrient and energy sensor that maintains energy homeostasis. *Nat. Rev. Mol. Cell Biol.* **2012**, *13*, 251-262.
243. O'Neill, L. A. J.; Hardie, D. G., Metabolism of inflammation limited by AMPK and pseudo-starvation. *Nature* **2013**, *493*, 346.
244. Dev, I. K.; Harvey, R. J., N10-Formyltetrahydrofolate is the formyl donor for glycinamide ribotide transformylase in Escherichia coli. *J. Biol. Chem.* **1978**, *253*, 4242-4244.
245. Aimi, J.; Qiu, H.; Williams, J.; Zalkin, H.; Dixon, J. E., De novo purine nucleotide biosynthesis: cloning of human and avian cDNAs encoding the trifunctional glycinamide ribonucleotide synthetase-aminoimidazole ribonucleotide synthetase-glycinamide ribonucleotide transformylase by functional complementation in E.coli. *Nucleic Acids Res.* **1990**, *18*, 6665-6672.
246. Caperelli, C. A., Mammalian glycinamide ribonucleotide transformylase. Kinetic mechanism and associated de novo purine biosynthetic activities. *J. Biol. Chem.* **1989**, *264*, 5053-5057.
247. Inglese, J.; Johnson, D. L.; Benkovic, S. J.; Shiau, A.; Smith, J. M., Subcloning, characterization, and affinity labeling of Escherichia coli glycinamide ribonucleotide transformylase. *Biochemistry* **1990**, *29*, 1436-1443.
248. Smith, G. K.; Mueller, W. T.; Benkovic, P. A.; Benkovic, S. J., On the cofactor specificity of glycinamide ribonucleotide and 5-aminoimidazole-4-carboxamide ribonucleotide transformylase from chicken liver. *Biochemistry* **1981**, *20*, 1241-1245.
249. Zhang, Y.; Desharnais, J.; Marsilje, T. H.; Li, C.; Hedrick, M. P.; Gooljarsingh, L. T.; Tavassoli, A.; Benkovic, S. J.; Olson, A. J.; Boger, D. L.; Wilson, I. A., Rational design, synthesis, evaluation, and crystal structure of a potent inhibitor of human GAR Tfase: 10-(trifluoroacetyl)-5,10-dideazaacyclic-5,6,7,8-tetrahydrofolic acid. *Biochemistry* **2003**, *42*, 6043-6056.
250. Varney, M. D.; Palmer, C. L.; Romines, W. H.; Boritzki, T.; Margosiak, S. A.; Almasy, R.; Janson, C. A.; Bartlett, C.; Howland, E. J.; Ferre, R., Protein structure-based design, synthesis, and biological evaluation of 5-thia-2,6-diamino-4(3H)-oxopyrimidines: Potent inhibitors of glycinamide ribonucleotide transformylase with potent cell growth inhibition. *J. Med. Chem.* **1997**, *40*, 2502-2524.
251. Deis, S. M.; Doshi, A.; Hou, Z.; Matherly, L. H.; Gangjee, A.; Dann, C. E., Structural and enzymatic analysis of tumor-targeted antifolates that inhibit glycinamide ribonucleotide formyltransferase. *Biochemistry* **2016**, *55*, 4574-4582.
252. Caperelli, C. A.; Giroux, E. L., The human glycinamide ribonucleotide transformylase domain: Purification, characterization, and kinetic mechanism. *Arch. Biochem. Biophys.* **1997**, *341*, 98-103.
253. Shim, J. H.; Benkovic, S. J., Catalytic mechanism of escherichia coli glycinamide ribonucleotide transformylase probed by site-directed mutagenesis and pH-dependent studies. *Biochemistry* **1999**, *38*, 10024-10031.

254. Sanghani, S. P.; Moran, R. G., Tight binding of folate substrates and inhibitors to recombinant mouse glycinamide ribonucleotide formyltransferase. *Biochemistry* **1997**, *36*, 10506-10516.
255. Marsilje, T. H.; Labroli, M. A.; Hedrick, M. P.; Jin, Q.; Desharnais, J.; Baker, S. J.; Gooljarsingh, L. T.; Ramcharan, J.; Tavassoli, A.; Zhang, Y.; Wilson, I. A.; Beardsley, G. P.; Benkovic, S. J.; Boger, D. L., 10-Formyl-5,10-dideaza-acyclic-5,6,7,8-tetrahydrofolic acid (10-Formyl-DDACTHF): A potent cytotoxic agent acting by selective inhibition of human GAR Tfase and the de novo purine biosynthetic pathway. *Bioorg. Med. Chem.* **2002**, *10*, 2739-2749.
256. Cong, X.; Lu, C.; Huang, X.; Yang, D.; Cui, X.; Cai, J.; Lv, L.; He, S.; Zhang, Y.; Ni, R., Increased expression of glycinamide ribonucleotide transformylase is associated with a poor prognosis in hepatocellular carcinoma, and it promotes liver cancer cell proliferation. *Hum. Pathol.* **2014**, *45*, 1370-1378.
257. .
258. Cheong, C.-G.; Wolan, D. W.; Greasley, S. E.; Horton, P. A.; Beardsley, G. P.; Wilson, I. A., Crystal structures of human bifunctional enzyme aminoimidazole-4-carboxamide ribonucleotide transformylase/imp cyclohydrolase in complex with potent sulfonyl-containing antifolates. *J. Biol. Chem.* **2004**, *279*, 18034-18045.
259. Wolan, D. W.; Greasley, S. E.; Wall, M. J.; Benkovic, S. J.; Wilson, I. A., Structure of avian aicar transformylase with a multisubstrate adduct inhibitor β -DADf identifies the folate binding site. *Biochemistry* **2003**, *42*, 10904-10914.
260. Baggott, J. E.; Vaughn, W. H.; Hudson, B. B., Inhibition of 5-aminoimidazole-4-carboxamide ribotide transformylase, adenosine deaminase and 5'-adenylate deaminase by polyglutamates of methotrexate and oxidized folates and by 5-aminoimidazole-4-carboxamide riboside and ribotide. *Biochem. J.* **1986**, *236*, 193-200.
261. Allegra, C. J.; Drake, J. C.; Jolivet, J.; Chabner, B. A., Inhibition of phosphoribosylaminoimidazolecarboxamide transformylase by methotrexate and dihydrofolic acid polyglutamates. *Proc. Natl. Acad. Sci. U S A* **1985**, *82*, 4881-4885.
262. Beardsley, G. P.; Rayl, E. A.; Gunn, K.; Moroson, B. A.; Seow, H.; Anderson, K. S.; Vergis, J.; Fleming, K.; Worland, S.; Condon, B.; Davies, J. F., Structure and functional relationships in human pur H. *Adv. Exp. Med. Biol.* **1998**, *431*, 221-226.
263. Smith, G. K.; Mueller, W. T.; Sliker, L. J.; DeBrosse, C. W.; Benkovic, S. J., Direct transfer of one-carbon units in the transformylations of de novo purine biosynthesis. *Biochemistry* **1982**, *21*, 2870-2874.
264. Sugita, T.; Aya, H.; Ueno, M.; Ishizuka, T.; Kawashima, K., Characterization of molecularly cloned human 5-aminoimidazole-4-carboxamide ribonucleotide transformylase. *J. Biochem.* **1997**, *122*, 309-313.
265. Shim, J. H.; Wall, M.; Benkovic, S. J.; Diaz, N.; Suarez, D.; Merz, K. M., Jr., Evaluation of the catalytic mechanism of AICAR TRANSFORMYLASE BY pH-dependent kinetics, mutagenesis, and quantum chemical calculations. *J. Am. Chem. Soc.* **2001**, *123*, 4687-4696.
266. <https://www.proteinatlas.org/ENSG00000138363-ATIC/pathology> Accessed on 06/15/18.
267. Christopherson, R. I.; Lyons, S. D.; Wilson, P. K., Inhibitors of de novo nucleotide biosynthesis as drugs. *Acc. Chem. Res.* **2002**, *35*, 961-971.

268. Parker, W. B., Enzymology of purine and pyrimidine antimetabolites used in the treatment of cancer. *Chem. rev.* **2009**, *109*, 2880-2893.
269. Zain, J.; O'Connor, O., Pralatrexate: basic understanding and clinical development. *Expert Opin. Pharmacother.* **2010**, *11*, 1705-1714.
270. Racanelli, A. C.; Rothbart, S. B.; Heyer, C. L.; Moran, R. G., Therapeutics by cytotoxic metabolite accumulation: Pemetrexed causes ZMP accumulation, AMPK activation, and mTOR inhibition. *Cancer Res.* **2009**, *69*, 5467-5474.
271. Rothbart, S. B.; Racanelli, A. C.; Moran, R. G., Pemetrexed indirectly activates the metabolic kinase AMPK in human carcinomas. *Cancer res.* **2010**, *70*, 10299-10309.
272. John, J. M., Anticancer antifolates: Current status and future directions. *Curr. Pharm. Des.* **2003**, *9*, 2593-2613.
273. Beardsley, G. P.; Moroson, B. A.; Taylor, E. C.; Moran, R. G., A new folate antimetabolite, 5,10-dideaza-5,6,7,8-tetrahydrofolate is a potent inhibitor of de novo purine synthesis. *J. Biol. Chem.* **1989**, *264*, 328-333.
274. Moran, R. G.; Baldwin, S. W.; Taylor, E. C.; Shih, C., The 6*S*- and 6*R*-diastereomers of 5, 10-dideaza-5, 6, 7, 8-tetrahydrofolate are equiactive inhibitors of de novo purine synthesis. *J. Biol. Chem.* **1989**, *264*, 21047-21051.
275. Boritzki, T. J.; Barlett, C. A.; Zhang, C.; Howland, E. F.; Margosiak, S. A.; Palmer, C. L.; Romines, W. H.; Jackson, R. C., AG2034: a novel inhibitor of glycinamide ribonucleotide formyltransferase. *Invest. New Drugs* **1996**, *14*, 295-303.
276. Budman, D. R.; Johnson, R.; Barile, B.; Bowsher, R. R.; Vinciguerra, V.; Allen, S. L.; Koltz, J.; Ernest, S. C.; Kreis, W.; Zervos, P.; Walling, J., Phase I and pharmacokinetic study of LY309887: a specific inhibitor of purine biosynthesis. *Cancer Chemother. Pharmacol.* **2001**, *47*, 525-531.
277. Bissett, D.; McLeod, H. L.; Sheedy, B.; Collier, M.; Pithavala, Y.; Paradiso, L.; Pitsiladis, M.; Cassidy, J., Phase I dose-escalation and pharmacokinetic study of a novel folate analogue AG2034. *Br. J. Cancer* **2001**, *84*, 308-312.
278. Faessel, H. M.; Slocum, H. K.; Jackson, R. C.; Boritzki, T. J.; Rustum, Y. M.; Nair, M. G.; Greco, W. R., Super in vitro synergy between inhibitors of dihydrofolate reductase and inhibitors of other folate-requiring enzymes: The critical role of polyglutamylation. *Cancer Res.* **1998**, *58*, 3036-3050.
279. Agarwal, S.; Bell, C. M.; Rothbart, S. B.; Moran, R. G., AMP-activated protein kinase (AMPK) control of mTORC1 is p53- and TSC2-independent in pemetrexed-treated carcinoma cells. *J. Biol. Chem.* **2015**, *290*, 27473-27486.
280. W., N. C.; K., R. R., Aromaticity in heterocyclic systems. II. the application of N.M.R. in a study of the synthesis and structure of certain Imidazo[1,2-*c*]pyrimidines and related pyrrolo[2,3-*d*]pyrimidines. *J. Heterocycl. Chem.* **1964**, *1*, 34-41.
281. Gibson, C. L.; Ohta, K.; Paulini, K.; Suckling, C. J., Specific inhibitors in vitamin biosynthesis. Part 10. Synthesis of 7- and 8-substituted 7-deazaguanines. *J. Chem. Soc.* **1998**, 3025-3032.
282. Yoneda, F.; Higuchi, M.; Senga, K.; Kanahori, M.; Nishigaki, S., Syntheses and Properties of Some Pyrrolo [2, 3-*d*] pyrimidine Derivatives. *Chem. Pharm. Bull.* **1973**, *21*, 473-477.
283. Davoll, J., 26. Pyrrolo[2,3-*d*]pyrimidines. *J. chem. Soc.* **1960**, 131-138.
284. Gangjee, A.; Yu, J.; McGuire, J. J.; Cody, V.; Galitsky, N.; Kisliuk, R. L.; Queener, S. F., Design, synthesis, and X-ray crystal structure of a potent dual inhibitor of thymidylate

- synthase and dihydrofolate reductase as an antitumor agent. *J. Med. Chem.* **2000**, *43*, 3837-3851.
285. Gangjee, A.; Dubash, N. P.; Kisliuk, R. L., Synthesis of novel, nonclassical 2-amino-4-oxo-6-(arylthio)ethylpyrrolo[2,3-*d*] pyrimidines as potential inhibitors of thymidylate synthase. *J. Heterocycl. Chem.* **2001**, *38*, 349-354.
286. Gangjee, A.; Vidwans, A.; Elzein, E.; McGuire, J. J.; Queener, S. F.; Kisliuk, R. L., Synthesis, antifolate, and antitumor activities of classical and nonclassical 2-amino-4-oxo-5-substituted-pyrrolo[2,3-*d*]pyrimidines. *J. Med. Chem.* **2001**, *44*, 1993-2003.
287. Miwa, T.; Hitaka, T.; Akimoto, H., A novel synthetic approach to pyrrolo[2,3-*d*]pyrimidine antifolates. *J. Org. Chem.* **1993**, *58*, 1696-1701.
288. Taylor, E. C.; Liu, B., A simple and concise synthesis of LY231514(MTA). *Tetrahedron Lett.* **1999**, *40*, 4023-4026.
289. Barnett, C. J.; Wilson, T. M.; Kobierski, M. E., A practical synthesis of multitargeted antifolate LY231514. *Org. Process Res. Dev.* **1999**, *3*, 184-188.
290. Johnson, A. L.; Price, W. A.; Wong, P. C.; Vavala, R. F.; Stump, J. M., Synthesis and pharmacology of the potent angiotensin-converting enzyme inhibitor *N*-[1(*S*)-(ethoxycarbonyl)-3-phenylpropyl]-(*S*)-alanyl-(*S*)-pyroglutamic acid. *J. Med. Chem.* **1985**, *28*, 1596-1602.
291. Sakamoto, T.; Satoh, C.; Kondo, Y.; Yamanaka, H., Condensed heteroaromatic ring systems. XXI. Synthesis of pyrrolo[2,3-*d*]pyrimidines and pyrrolo[3,2-*d*]pyrimidines. *Chem. Pharm. Bull.* **1993**, *41*, 81-86.
292. Kondo, Y.; Watanabe, R.; Sakamoto, T.; Yamanaka, H., Condensed heteroaromatic ring systems. XVI. Synthesis of pyrrolo[2,3-*d*]pyrimidine derivatives. *Chem. Pharm. Bull.* **1989**, *37*, 2933-2936.
293. Crooks, P. A.; Robinson, B., Thermal indolization of 4-pyrimidinylhydrazones and 4-pyridylhydrazones. *Chem. Ind. (London)* **1967**, (13), 547-8.
294. Senda, S.; Hirota, K., Pyrimidine derivatives and related compounds. XXII. Synthesis and pharmacological properties of 7-deazaxanthine derivatives. *Chem. Pharm. Bull.* **1974**, *22*, 1459-67.
295. Senda, S.; Hirota, K., Novel synthesis of 2,4-dioxo-1,2,3,4-tetrahydropyrrolo[2,3-*d*]pyrimidine derivatives. *Chem. Lett.* **1972**, 367-8.
296. Wright, G. E., 9*H*-Pyrimido[4,5-*b*]indole-2,4-diones. The acid-catalyzed cyclization of 6-(phenylhydrazino)uracils. *J. Heterocycl. Chem.* **1976**, *13*, 539-44.
297. Duffy, T. D.; Wibberley, D. G., Pyrrolo[2,3-*d*]pyrimidines. Synthesis from 4-pyrimidylhydrazones, a 2-bis(methylthio) methyleneaminopyrrole-3-carbonitrile, and a pyrrolo[2,3-*d*][1,3]thiazine-2(1*H*)-thione. *J. Chem. Soc., Perkin Trans. 1* **1974**, 1921-1629.
298. Secrist, J. A.; Liu, P. S., Studies directed toward a total synthesis of nucleoside Q. Annulation of 2,6-diaminopyrimidin-4-one with .alpha.-halo carbonyls to form pyrrolo[2,3-*d*]pyrimidines and furo[2,3-*d*]pyrimidines. *J. Org. Chem.* **1978**, *43*, 3937-3941.
299. Taylor, E. C.; Patel, H. H.; Jun, J.-G., A one-step ring transformation/ring annulation approach to pyrrolo[2,3-*d*]pyrimidines. A new synthesis of the potent dihydrofolate reductase inhibitor TNP-351. *J. Org. Chem.* **1995**, *60*, 6684-6687.
300. Middleton, W. J.; Engelhardt, V. A.; Fisher, B. S., Cyanocarbon chemistry. VIII. Heterocyclic compounds from tetracyanoethylene. *J. Am. Chem. Soc.* **1958**, *80*, 2822-2829.

301. Taylor, E. C.; Hendess, R. W., Synthesis of pyrrolo[2,3-*d*]pyrimidines. The aglycon of toyocamycin. *J. Am. Chem. Soc.* **1965**, *87*, 1995-2003.
302. Tolman, R. L.; Robins, R. K.; Townsend, L. B., Pyrrolopyrimidine nucleosides. III. Total synthesis of toyocamycin, sangivamycin, tubercidin, and related derivatives. *J. Amer. Chem. Soc.* **1969**, *91*, 2102-2108.
303. Swayze, E. E.; Hinkley, J. M.; Townsend, L. B. In *2-Amino-5-bromo-3,4-dicyanopyrrole. The improved preparation of a versatile synthon for the synthesis of pyrrolo[2,3-*d*]pyrimidines*, Wiley: 1991; pp 16-18.
304. Pichler, H.; Folkers, G.; Roth, H. J.; Eger, K., Synthesis of 7-unsubstituted 7*H*-pyrrolo[2,3-*d*]pyrimidines. *Liebigs Ann. Chem.* **1986**, 1485-505.
305. Eger, K.; Pfahl, J. G.; Folkers, G.; Roth, H. J., Selected reactions on the o-aminonitrile system of substituted pyrroles. *J. Heterocycl. Chem.* **1987**, *24*, 425-430.
306. Chen, Y. L.; Mansbach, R. S.; Winter, S. M.; Brooks, E.; Collins, J.; Corman, M. L.; Dunaiskis, A. R.; Faraci, W. S.; Gallaschun, R. J.; Schmidt, A.; Schulz, D. W., Synthesis and oral efficacy of a 4-(butylethylamino)pyrrolo[2,3-*d*]pyrimidine: A centrally active corticotropin-releasing factor1 receptor antagonist. *J. Med. Chem.* **1997**, *40*, 1749-1754.
307. Girgis, N. S.; Joergensen, A.; Pedersen, E. B., Phosphorus pentoxide in organic synthesis; XI. A new synthetic approach to 7-deazahypoxanthines. *Synthesis* **1985**, 101-104.
308. Wamhoff, H.; Wehling, B., Heterocyclic β -enamino esters; 18. Synthesis of 2-aminopyrrole-3-carboxylic acid derivatives. *Synthesis* **1976**, 51.
309. Yumoto, M.; Kawabuchi, T.; Sato, K.; Takashima, M. 2-Aminopyrrole derivatives and method for their preparation. JP10316654A, 1998.
310. Taylor, E. C.; Liu, B., A new route to 7-substituted derivatives of *N*-{4-[2-(2-Amino-3,4-dihydro-4-oxo-7*H*-pyrrolo[2,3-*d*]pyrimidin-5-yl)-ethyl]benzoyl}-L-glutamic Acid [ALIMTA (LY231514, MTA)]. *J. Org. Chem.* **2001**, *66*, 3726-3738.
311. Galeazzi, R.; Mobbili, G.; Orena, M., A convenient approach to diastereomerically pure 1,3,4-trisubstituted pyrrolidin-2-ones by intramolecular cyclization of *N*-(2-alken-1-yl)amides mediated by Mn(III). An entry to both (*R*)- and (*S*)-3-pyrrolidineacetic acid. *Tetrahedron* **1996**, *52*, 1069-1084.
312. Barnett, C. J.; Wilson, T. M.; Grindey, G. B., Synthesis and antitumor activity of LY288601, the 5,6-dihydro analog of LY231514. *Adv. Exp. Med. Biol.* **1993**, *338* (Chemistry and biology of pteridines and folates), 409-412.
313. Dave, K. G.; Shishoo, C. J.; Devani, M. B.; Kalyanaraman, R.; Ananthan, S.; Ullas, G. V.; Bhadti, V. S., Reaction of nitriles under acidic conditions. Part I. A general method of synthesis of condensed pyrimidines. *J. Heterocycl. Chem.* **1980**, *17*, 1497-500.
314. Bookser, B. C.; Ugarkar, B. G.; Matelich, M. C.; Lemus, R. H.; Allan, M.; Tsuchiya, M.; Nakane, M.; Nagahisa, A.; Wiesner, J. B.; Erion, M. D., Adenosine kinase inhibitors. 6. Synthesis, water solubility, and antinociceptive activity of 5-phenyl-7-(5-deoxy- β -d-ribofuranosyl)pyrrolo[2,3-*d*]pyrimidines substituted at C4 with glycinamides and related compounds. *J. Med. Chem.* **2005**, *48*, 7808-7820.
315. Chinchilla, R.; Najera, C., Recent advances in Sonogashira reactions. *Chem. Soc. Rev.* **2011**, *40*, 5084-5121.
316. Chinchilla, R.; Najera, C., The Sonogashira reaction: a booming methodology in synthetic organic chemistry. *Chem. Rev. (Washington, DC, U. S.)* **2007**, *107*, 874-922.

317. Sonogashira, K.; Tohda, Y.; Hagihara, N., Convenient synthesis of acetylenes. Catalytic substitutions of acetylenic hydrogen with bromo alkenes, iodo arenes, and bromopyridines. *Tetrahedron Lett.* **1975**, (50), 4467-4470.
318. Gangjee, A.; Yu, J.; Copper, J. E.; Smith, C. D., Discovery of novel antitumor antimetabolic agents that also reverse tumor resistance. *J. Med. Chem.* **2007**, *50*, 3290-3301.
319. Heck, R. F.; Nolley, J. P., Jr., Palladium-catalyzed vinylic hydrogen substitution reactions with aryl, benzyl, and styryl halides. *J. Org. Chem.* **1972**, *37*, 2320-2322.
320. Mizoroki, T.; Mori, K.; Ozaki, A., Arylation of olefin with aryl iodide catalyzed by palladium. *Bull. Chem. Soc. Jap.* **1971**, *44*, 581.
321. Melpolder, J. B.; Heck, R. F., Palladium-catalyzed arylation of allylic alcohols with aryl halides. *J. Org. Chem.* **1976**, *41*, 265-72.
322. Chalk, A. J.; Magennis, S. A., Palladium-catalyzed vinyl substitution reactions. I. New synthesis of 2- and 3-phenyl-substituted allylic alcohols, aldehydes, and ketones from allylic alcohols. *J. Org. Chem.* **1976**, *41*, 273-8.
323. Larock, R. C.; Leung, W.-Y.; Stolz-Dunn, S., Synthesis of aryl-substituted aldehydes and ketones via palladium-catalyzed coupling of aryl halides and non-allylic unsaturated alcohols. *Tetrahedron Lett.* **1989**, *30*, 6629-6632.
324. Taylor, E. C.; Wang, Y., Synthesis of 7-methyl derivatives of 5,10-dideaza-5,6,7,8-tetrahydrofolic acid (DDATHF), 5,10-dideaza-5,6,7,8-tetrahydrohomofolic acid (HDDATHF), and LY254155. *Heterocycles* **1998**, *48*, 1537-1554.
325. Belley, M.; Gallant, M.; Roy, B.; Houde, K.; Lachance, N.; Labelle, M.; Trimble, L. A.; Charet, N.; Li, C.; Sawyer, N.; Tremblay, N.; Lamontagne, S.; Carriere, M.-C.; Denis, D.; Greig, G. M.; Slipetz, D.; Metters, K. M.; Gordon, R.; Chan, C. C.; Zamboni, R. J., Structure-activity relationship studies on ortho-substituted cinnamic acids, a new class of selective EP3 antagonists. *Bioorg. Med. Chem. Lett.* **2005**, *15*, 527-530.
326. Kim, H.; Sohn, J.; Wijewickrama, G. T.; Edirisinghe, P.; Gherezghiher, T.; Hemachandra, M.; Lu, P.-Y.; Chandrasena, R. E.; Molloy, M. E.; Tonetti, D. A.; Thatcher, G. R. J., Click synthesis of estradiol-cyclodextrin conjugates as cell compartment selective estrogens. *Bioorg. Med. Chem.* **2010**, *18*, 809-821.
327. Tamaru, Y.; Yamada, Y.; Yoshida, Z. I., Palladium catalyzed thienylation of allylic alcohols with 3-bromothiophene. *Tetrahedron Lett.* **1977**, 3365-8.
328. Yoshida, Z. I.; Yamada, Y.; Tamaru, Y., Palladium-catalyzed thienylation of allylic alcohols. *Chem. Lett.* **1977**, 423-424.
329. Giorgio, V. S.; Purvish, P.; Joachim, v. P.; Bonne, B.; Johan, V.; Christian, M.; Piotr, S.; Ulrich, G.; Raghunadharao, D.; Mauro, Z.; Jin, S. L.; Anders, M.; Keunchil, P.; Shekhar, P.; Janusz, R.; Tuncay, G.; Filippo, d. M.; Lorinda, S.; Katherine, P. S.; David, G., Phase iii study comparing cisplatin plus gemcitabine with cisplatin plus pemetrexed in chemotherapy-naïve patients with advanced-stage non-small-cell lung cancer. *J. Clin. Oncol.* **2008**, *26*, 3543-3551.
330. H., S.; T., C., Profound methyl effects in drug discovery and a call for new C-H methylation reactions. *Angew. Chem., Int. Ed.* **2013**, *52*, 12256-12267.
331. Pendergast, W.; Dickerson, S. H.; Dev, I. K.; Ferone, R.; Duch, D. S.; Smith, G. K., Benzo[*f*]quinazoline inhibitors of thymidylate synthase: Methyleneamino-linked aroylglutamate derivatives. *J. Med. Chem.* **1994**, *37*, 838-844.
332. Duch, D. S.; Banks, S.; Dev, I. K.; Dickerson, S. H.; Ferone, R.; Heath, L. S.; Humphreys, J.; Knick, V.; Pendergast, W.; Singer, S.; Smith, G. K.; Waters, K.; Wilson,

- H. R., Biochemical and cellular pharmacology of 1843U89, a novel benzoquinazoline inhibitor of thymidylate synthase. *Cancer Res.* **1993**, *53*, 810-818.
333. Habeck, L. L.; Mendelsohn, L. G.; Shih, C.; Taylor, E. C.; Colman, P. D.; Gossett, L. S.; Leitner, T. A.; Schultz, R. M.; Andis, S. L.; Moran, R. G., Substrate specificity of mammalian folylpolyglutamate synthetase for 5,10-dideazatetrahydrofolate analogs. *Mol. Pharmacol.* **1995**, *48*, 326-333.
334. Wang, J.; Sánchez-Roselló, M.; Aceña, J. L.; del Pozo, C.; Sorochinsky, A. E.; Fustero, S.; Soloshonok, V. A.; Liu, H., Fluorine in pharmaceutical industry: Fluorine-containing drugs introduced to the market in the last decade (2001–2011). *Chem. Rev. (Washington, DC, U. S.)* **2014**, *114*, 2432-2506.
335. Zhou, Y.; Wang, J.; Gu, Z.; Wang, S.; Zhu, W.; Aceña, J. L.; Soloshonok, V. A.; Izawa, K.; Liu, H., Next generation of fluorine-containing pharmaceuticals, compounds currently in phase II–III clinical trials of major pharmaceutical companies: New structural trends and therapeutic areas. *Chem. Rev.* **2016**, *116*, 422-518.
336. Böhm, H. J.; Banner, D.; Bendels, S.; Kansy, M.; Kuhn, B.; Müller, K.; Obst-Sander, U.; Stahl, M., Fluorine in medicinal chemistry. *ChemBioChem* **2004**, *5*, 637-643.
337. Kirk, K. L., Fluorine in medicinal chemistry: Recent therapeutic applications of fluorinated small molecules. *J. Fluor. Chem.* **2006**, *127*, 1013-1029.
338. Purser, S.; Moore, P. R.; Swallow, S.; Gouverneur, V., Fluorine in medicinal chemistry. *Chem. Soc. Rev.* **2008**, *37*, 320-330.
339. Gillis, E. P.; Eastman, K. J.; Hill, M. D.; Donnelly, D. J.; Meanwell, N. A., Applications of fluorine in medicinal chemistry. *J. Med. Chem.* **2015**, *58*, 8315-8359.
340. Huchet, Q. A.; Kuhn, B.; Wagner, B.; Kratochwil, N. A.; Fischer, H.; Kansy, M.; Zimmerli, D.; Carreira, E. M.; Müller, K., Fluorination patterning: A study of structural motifs that impact physicochemical properties of relevance to drug discovery. *J. Med. Chem.* **2015**, *58*, 9041-9060.
341. Meanwell, N. A., Fluorine and fluorinated motifs in the design and application of bioisosteres for drug design. *J. Med. Chem.* **2018**, *61*, 5822–5880.
342. Hagmann, W. K., The many roles for fluorine in medicinal chemistry. *J. Med. Chem.* **2008**, *51*, 4359-4369.
343. Müller, K.; Faeh, C.; Diederich, F., Fluorine in pharmaceuticals: Looking beyond intuition. *Science* **2007**, *317*, 1881-1886.
344. Shah, P.; Westwell, A. D., The role of fluorine in medicinal chemistry. *J. Enzyme Inhib. Med. Chem.* **2007**, *22*, 527-540.
345. Maienfisch, P.; Hall, R. G., The importance of fluorine in the life science industry. *CHIMIA International Journal for Chemistry* **2004**, *58*, 93-99.
346. Manjunatha Reddy, G. N.; Vasantha Kumar, M. V.; Guru Row, T. N.; Suryaprakash, N., N-H...F hydrogen bonds in fluorinated benzanilides: NMR and DFT study. *Phys. Chem. Chem. Phys.* **2010**, *12*, 13232-13237.
347. Divya, K.; Hebbar, S.; Suryaprakash, N., Intra-molecular hydrogen bonding with organic fluorine in the solution state: Deriving evidence by a two dimensional NMR experiment. *Chem. Phys. Lett.* **2012**, *525-526*, 129-133.
348. Chaudhari, S. R.; Mogurampelly, S.; Suryaprakash, N., Engagement of CF₃ group in N–H...F–C hydrogen bond in the solution state: NMR spectroscopy and md simulation studies. *J. Phys. Chem. Biophys.* **2013**, *117*, 1123-1129.

349. Zheng, Y.; Tice, C. M.; Singh, S. B., Conformational control in structure-based drug design. *Bioorg. Med. Chem. Lett.* **2017**, *27*, 2825-2837.
350. Zengjun, F.; Yu'ning, S.; Peng, Z.; Qingzhu, Z.; Xinyong, L., Conformational restriction: an effective tactic in 'follow-on'-based drug discovery. *Future Med. Chem.* **2014**, *6*, 885-901.
351. *Molecular Operating Environment (MOE)*, Chemical Computing 1201 Group Inc. 1010 Sherbooke St. West, Suite #910, Montreal, QC, 1202 Canada, H3A 2R7, 2017.
352. *LeadIT 2.1.6*, BioSolveIT GmbH: Sankt Augustin, Germany. Available at the following: www.biosolveit.de.
353. Pennington, L. D.; Moustakas, D. T., The necessary nitrogen atom: A versatile high-impact design element for multiparameter optimization. *J. Med. Chem.* **2017**, *60*, 3552-3579.
354. Desmoulin, S. K.; Wang, L.; Polin, L.; White, K.; Kushner, J.; Stout, M.; Hou, Z.; Cherian, C.; Gangjee, A.; Matherly, L. H., Functional loss of the reduced folate carrier enhances the antitumor activities of novel antifolates with selective uptake by the proton-coupled folate transporter. *Mol. Pharmacol.* **2012**, *82*, 591-600.
355. **Schrödinger Release 2018-2**: QikProp, Schrödinger, LLC, New York, NY, 2018.
356. Dalvit, C.; Vulpetti, A., Fluorine-protein interactions and ¹⁹F NMR isotropic chemical shifts: An empirical correlation with implications for drug design. *ChemMedChem* **2011**, *6*, 104-114.
357. Barreiro, E. J.; Kümmerle, A. E.; Fraga, C. A. M., The methylation effect in medicinal chemistry. *Chem. Rev.* **2011**, *111*, 5215-5246.
358. Bissantz, C.; Kuhn, B.; Stahl, M., A medicinal chemist's guide to molecular interactions. *J. Med. Chem.* **2010**, *53*, 5061-5084.
359. Leung, C. S.; Leung, S. S. F.; Tirado-Rives, J.; Jorgensen, W. L., Methyl effects on protein-ligand binding. *J. Med. Chem.* **2012**, *55*, 4489-4500.
360. Yu, J.; Gangjee, A.; Matherly, L. H., Unpublished results.
361. Swain, M., chemicalize.org. *Journal of Chemical Information and Modeling* **2012**, *52*, 613-615.
362. Hunsen, M., Pyridinium chlorochromate catalyzed oxidation of alcohols to aldehydes and ketones with periodic acid. *Tetrahedron Lett.* **2005**, *46*, 1651-1653.
363. Vugts, D. J.; Veum, L.; al-Mafraji, K.; Lemmens, R.; Schmitz, R. F.; de Kanter, F. J. J.; Groen, M. B.; Hanefeld, U.; Orru, R. V. A., A mild chemo-enzymatic oxidation-hydrocyanation protocol. *Eur. J. Org. Chem.* **2006**, *2006*, 1672-1677.
364. Steffel, L. R.; Cashman, T. J.; Reutershan, M. H.; Linton, B. R., Deuterium exchange as an indicator of hydrogen bond donors and acceptors. *J. Am. Chem. Soc.* **2007**, *129*, 12956-12957.
365. E., K. E.; G., H. S., Structural elucidation with NMR spectroscopy: Practical strategies for organic chemists. *Eur. J. Org. Chem.* **2008**, *2008*, 2671-2688.
366. Roberts, E. C.; Shealy, Y. F., Folic acid analogs. Modifications in the benzene-ring region. 5. 2',6'-diazafolic acid. *J. Heterocycl. Chem.* **1974**, *11*, 547-550.
367. Garrett, C. E.; Jiang, X.; Prasad, K.; Repič, O., New observations on peptide bond formation using CDMT. *Tetrahedron Lett.* **2002**, *43*, 4161-4165.
368. Gangjee, A.; Yu, J.; Kisliuk, R. L., 2-Amino-4-oxo-6-substituted-pyrrolo[2,3-*d*]pyrimidines as potential inhibitors of thymidylate synthase. *J. Heterocycl. Chem.* **2002**, *39*, 833-840.

369. Stokmaier, D.; Khorev, O.; Cutting, B.; Born, R.; Ricklin, D.; Ernst, T. O. G.; Böni, F.; Schwingruber, K.; Gentner, M.; Wittwer, M.; Spreafico, M.; Vedani, A.; Rabbani, S.; Schwardt, O.; Ernst, B., Design, synthesis and evaluation of monovalent ligands for the asialoglycoprotein receptor (ASGP-R). *Bioorg. Med. Chem.* **2009**, *17*, 7254-7264.
370. Taylor, E. C.; Jennings, L. D.; Mao, Z.; Hu, B.; Jun, J.-G.; Zhou, P., Synthesis of conformationally-constrained glutamate analogues of the antitumor agents DDATHF, LY254155, and LY231514. *J. Org. Chem.* **1997**, *62*, 5392-5403.
371. J., B. C.; E., K. M., A convenient method for regioselective C-5 halogenation of 4(3H)-oxo-7H-pyrrolo[2,3-d]pyrimidines. *Journal of Heterocyclic Chemistry* **1994**, *31* (5), 1181-1183.
372. Evano, G.; Blanchard, N.; Toumi, M., Copper-mediated coupling reactions and their applications in natural products and designed biomolecules synthesis. *Chemical Rev.* **2008**, *108*, 3054-3131.
373. Stuart, D. R.; Bertrand-Laperle, M.; Burgess, K. M. N.; Fagnou, K., Indole synthesis via rhodium catalyzed oxidative coupling of acetanilides and internal alkynes. *J. Am. Chem. Soc.* **2008**, *130*, 16474-16475.
374. Salvatore, R. N.; Shin, S. I.; Nagle, A. S.; Jung, K. W., Efficient carbamate synthesis via a three-component coupling of an amine, CO₂, and alkyl halides in the presence of Cs₂CO₃ and tetrabutylammonium iodide. *J. Org. Chem.* **2001**, *66*, 1035-1037.
375. Salvatore, R. N.; Flanders, V. L.; Ha, D.; Jung, K. W., Cs₂CO₃-promoted efficient carbonate and carbamate synthesis on solid phase. *Organic Lett.* **2000**, *2*, 2797-2800.
376. Salvatore, R. N.; Ledger, J. A.; Jung, K. W., An efficient one-pot synthesis of *N*-alkyl carbamates from primary amines using Cs₂CO₃. *Tetrahedron Lett.* **2001**, *42*, 6023-6025.
377. Salvatore, R. N.; Smith, R. A.; Nischwitz, A. K.; Gavin, T., A mild and highly convenient chemoselective alkylation of thiols using Cs₂CO₃-TBAI. *Tetrahedron Lett.* **2005**, *46*, 8931-8935.
378. Xin, L.; Chen, Y.-Z.; Niu, L.-Y.; Wu, L.-Z.; Tung, C.-H.; Tong, Q.-X.; Yang, Q.-Z., A selective turn-on fluorescent probe for Cd²⁺ based on a boron difluoride [small beta]-dibenzoyl dye and its application in living cells. *Org. Biomol. Chem.* **2013**, *11*, 3014-3019.
379. Uetake, Y.; Niwa, T.; Nakada, M., Synthesis of cycloalkanone-fused cyclopropanes by Au(I)-catalyzed oxidative ene-yne cyclizations. *Tetrahedron Lett.* **2014**, *55*, 6847-6850.
380. Hagishita, S.; Seno, K., Thromboxane A₂ receptor antagonists. I. Synthesis and pharmacological activity of 7-oxabicyclo[2.2.1]heptane derivatives with the benzenesulfonylamino group. *Chem. Pharm. Bull.* **1989**, *37*, 327-35.
381. Taylor, E. C.; Hu, B., A Fischer-indole approach to pyrrolo[2,3-*d*]pyrimidines. *Heterocycles* **1996**, *43*, 323-338.
382. Gangjee, A.; Mavandadi, F.; Kisliuk, R. L.; McGuire, J. J.; Queener, S. F., 2-Amino-4-oxo-5-substituted-pyrrolo[2,3-*d*]pyrimidines as nonclassical antifolate inhibitors of thymidylate synthase. *J. Med. Chem.* **1996**, *39*, 4563-4568.
383. Umaña, C. A.; Cabezas, J. A., Palladium-catalyzed one-pot conversion of aldehydes and ketones into 4-substituted homopropargyl alcohols and 5-en-3-yn-1-ols. *J. Org. Chem.* **2017**, *82*, 9505-9514.
384. Singer, M.; Nierth, A.; Jaeschke, A., Photochromism of diarylethene-functionalized 7-deazaguanosines. *Eur. J. Org. Chem.* **2013**, *2013*, 2766-2769.

385. Gangjee, A.; Yu, J.; Kisliuk, R. L.; Haile, W. H.; Sobrero, G.; McGuire, J. J., Design, synthesis, and biological activities of classical *N*-{4-[2-(2-amino-4-ethylpyrrolo[2,3-*d*]pyrimidin-5-yl)ethyl]benzoyl}-L-glutamic acid and its 6-methyl derivative as potential dual inhibitors of thymidylate synthase and dihydrofolate reductase and as potential antitumor agents. *J. Med. Chem.* **2003**, *46*, 591-600.
386. Seela, F.; Luepke, U., Mannich reaction at 2-amino-3,7-dihydropyrrolo[2,3-*d*]pyrimidin-4-one, the chromophore of the ribonucleoside "Q". *Chem. Ber.* **1977**, *110*, 1462-1469.
387. Klepper, F.; Jahn, E.-M.; Hickmann, V.; Carell, T., Synthesis of the transfer-RNA nucleoside queuosine by using a chiral allyl azide intermediate. *Angew. Chem., Int. Ed.* **2007**, *46*, 2325-2327.
388. Taylor, E. C.; Kuhnt, D.; Shih, C.; Rinzel, S. M.; Grindey, G. B.; Barredo, J.; Jannatipour, M.; Moran, R. G., A dideazatetrahydrofolate analog lacking a chiral center at C-6: *N*-[4-[2-(2-amino-3,4-dihydro-4-oxo-7*H*-pyrrolo[2,3-*d*]pyrimidin-5yl)ethyl]benzoyl]-L-glutamic acid is an inhibitor of thymidylate synthase. *J. Med. Chem.* **1992**, *35*, 4450-4454.
389. Barnett, C. J.; Kobierski, M. E., A convenient method for regioselective C-5 halogenation of 4(3*H*)-oxo-7*H*-pyrrolo[2,3-*d*]pyrimidines. *J. Heterocycl. Chem.* **1994**, *31*, 1181-1183.
390. Berscheid, R.; Voegtle, F., Concave dyestuffs: a triply bridged triphenylmethyl dication. *Synthesis* **1992**, 58-62.
391. Negishi, K.; Mashiko, Y.; Yamashita, E.; Otsuka, A.; Hasegawa, T., Cellulose chemistry meets click chemistry: Syntheses and properties of cellulose-based glycoclusters with high structural homogeneity. *Polymers (Basel, Switz.)* **2011**, *3*, 489-508.
392. Yao, Z.; Wei, X., Amidation of aryl halides catalyzed by the efficient and recyclable Cu₂O nanoparticles. *Chin. J. Chem.* **2010**, *28*, 2260-2268.
393. Wang, X.-J.; Yang, Q.; Liu, F.; You, Q.-D., Microwave-assisted synthesis of amide under solvent-free conditions. *Synth. Commun.* **2008**, *38*, 1028-1035.
394. Ohtaka, J.; Sakamoto, T.; Kikugawa, Y., A one-pot procedure for trifluoroacetylation of arylamines using trifluoroacetic acid as a trifluoroacetylating reagent. *Tetrahedron Lett.* **2009**, *50*, 1681-1683.
395. Nguyen, T. T.; Hull, K. L., Rhodium-catalyzed oxidative amidation of sterically hindered aldehydes and alcohols. *ACS Catal.* **2016**, *6*, 8214-8218.
396. Klumphu, P.; Lipshutz, B. H., "Nok": A phytosterol-based amphiphile enabling transition-metal-catalyzed couplings in water at room temperature. *J. Org. Chem.* **2014**, *79*, 888-900.
397. Ye, L.; Cui, L.; Zhang, G.; Zhang, L., Alkynes as equivalents of α -diazo ketones in generating α -oxo metal carbenes: A gold-catalyzed expedient synthesis of dihydrofuran-3-ones. *J. Am. Chem. Soc.* **2010**, *132*, 3258-3259.
398. Gangjee, A.; Jain, H. D.; Kisliuk, R. L., Novel 2-amino-4-oxo-5-arylthio-substituted-pyrrolo[2,3-*d*]pyrimidines as nonclassical antifolate inhibitors of thymidylate synthase. *Bioorg. Med. Chem. Lett.* **2005**, *15*, 2225-2230.
399. Gangjee, A.; Devraj, R.; McGuire, J. J.; Kisliuk, R. L., 5-arylthio substituted 2-amino-4-oxo-6-methylpyrrolo[2,3-*d*]pyrimidine antifolates as thymidylate synthase inhibitors and antitumor agents. *J. Med. Chem.* **1995**, *38*, 4495-4502.

400. Deng, Y.; Zhou, X.; Kugel Desmoulin, S.; Wu, J.; Cherian, C.; Hou, Z.; Matherly, L. H.; Gangjee, A., Synthesis and biological activity of a novel series of 6-substituted thieno[2,3-*d*]pyrimidine antifolate inhibitors of purine biosynthesis with selectivity for high affinity folate receptors over the reduced folate carrier and proton-coupled folate transporter for cellular entry. *J. Med. Chem.* **2009**, *52*, 2940-2951.
401. Flintoff, W. F.; Davidson, S. V.; Siminovitch, L., Isolation and partial characterization of three methotrexate-resistant phenotypes from Chinese hamster ovary cells. *Somatic Cell Genet.* **1976**, *2*, 245-261.
402. Wong, S. C.; Proefke, S. A.; Bhushan, A.; Matherly, L. H., Isolation of human cDNAs that restore methotrexate sensitivity and reduced folate carrier activity in methotrexate transport-defective Chinese hamster ovary cells. *J. Biol. Chem.* **1995**, *270*, 17468-17475.
403. Flintoff, W. F.; Nagainis, C. R., Transport of methotrexate in Chinese hamster ovary cells: a mutant defective in methotrexate uptake and cell binding. *Arch. Biochem. Biophys.* **1983**, *223*, 433-440.
404. Golani, L. K.; George, C.; Zhao, S.; Raghavan, S.; Orr, S.; Wallace, A.; Wilson, M. R.; Hou, Z.; Matherly, L. H.; Gangjee, A., Structure-activity profiles of novel 6-substituted pyrrolo[2,3-*d*]pyrimidine thienoyl antifolates with modified amino acids for cellular uptake by folate receptors alpha and beta and the proton-coupled folate transporter. *J. Med. Chem.* **2014**, *57*, 8152-8166.
405. Wang, L.; Kugel Desmoulin, S.; Cherian, C.; Polin, L.; White, K.; Kushner, J.; Fulterer, A.; Chang, M. H.; Mitchell-Ryan, S.; Stout, M.; Romero, M. F.; Hou, Z.; Matherly, L. H.; Gangjee, A., Synthesis, biological, and antitumor activity of a highly potent 6-substituted pyrrolo[2,3-*d*]pyrimidine thienoyl antifolate inhibitor with proton-coupled folate transporter and folate receptor selectivity over the reduced folate carrier that inhibits beta-glycinamide ribonucleotide formyltransferase. *J. Med. Chem.* **2011**, *54*, 7150-7164.
406. Wang, L.; Wallace, A.; Raghavan, S.; Deis, S. M.; Wilson, M. R.; Yang, S.; Polin, L.; White, K.; Kushner, J.; Orr, S.; George, C.; O'Connor, C.; Hou, Z.; Mitchell-Ryan, S.; Dann, C. E., 3rd; Matherly, L. H.; Gangjee, A., 6-Substituted pyrrolo[2,3-*d*]pyrimidine thienoyl regioisomers as targeted antifolates for folate receptor alpha and the proton-coupled folate transporter in human tumors. *J. Med. Chem.* **2015**, *58*, 6938-6959.
407. Lowry, O. H.; Rosebrough, N. J.; Farr, A. L.; Randall, R. J., Protein measurement with the Folin phenol reagent. *J. Biol. Chem.* **1951**, *193*, 265-275.
408. Kugel Desmoulin, S.; Wang, Y.; Wu, J.; Stout, M.; Hou, Z.; Fulterer, A.; Chang, M. H.; Romero, M. F.; Cherian, C.; Gangjee, A.; Matherly, L. H., Targeting the proton-coupled folate transporter for selective delivery of 6-substituted pyrrolo[2,3-*d*]pyrimidine antifolate inhibitors of de novo purine biosynthesis in the chemotherapy of solid tumors. *Mol. Pharmacol.* **2010**, *78*, 577-587.
409. Polin, L.; Valeriote, F.; White, K.; Panchapor, C.; Pugh, S.; Knight, J.; LoRusso, P.; Hussain, M.; Liversidge, E.; Peltier, N.; Golakoti, T.; Patterson, G.; Moore, R.; Corbett, T. H., Treatment of human prostate tumors PC-3 and TSU-PR1 with standard and investigational agents in SCID mice. *Invest. New Drugs* **1997**, *15*, 99-108.
410. Golani, L. K.; Wallace-Povirk, A.; Deis, S. M.; Wong, J. E.; Ke, J.; Gu, X.; Raghavan, S.; Wilson, M. R.; Li, X.; Polin, L.; de Waal, P. W.; White, K.; Kushner, J.; O'Connor, C.; Hou, Z.; Xu, H. E.; Melcher, K.; Dann, C. E.; Matherly, L. H.; Gangjee, A.,

Tumor Targeting with Novel 6-Substituted Pyrrolo [2,3-*d*] Pyrimidine Antifolates with Heteroatom Bridge Substitutions Via Cellular Uptake by Folate Receptor α and the Proton-coupled Folate Transporter and Inhibition of De Novo Purine Nucleotide Biosynthesis. *J. Med. Chem.* **2016**, *59*, 7856-7876.

411. Varela-Moreiras, G.; Selhub, J., Long-term folate deficiency alters folate content and distribution differentially in rat tissues. *J. Nutr.* **1992**, *122*, 986-991.

412. Alati, T.; Worzalla, J. F.; Shih, C.; Bewley, J. R.; Lewis, S.; Moran, R. G.; Grindey, G. B., Augmentation of the therapeutic activity of lometrexol [(6-*R*)5,10-dideazatetrahydrofolate] by oral folic acid. *Cancer Res.* **1996**, *56*, 2331-2335.

VII. APPENDIX

Biological evaluation. The biological evaluation of all the analogs listed in the following tables were performed by Dr. Larry H. Matherly (Molecular Therapeutics Program, Barbara Ann Karmanos Cancer Institute, Department of Oncology, Wayne State University School of Medicine, Department of Pharmacology, Wayne State University School of Medicine).

Reagents for biological studies. [3', 5', 7-³H]MTX (20 Ci/mmol), [3', 5', 7, 9-³H], folic acid (25 Ci/mmol), and [¹⁴C(U)]-glycine (87 mCi/mmol) were purchased from Moravек Biochemicals (Brea, CA). Unlabeled folic acid was purchased from Sigma-Aldrich (St. Louis, MO). LCV [(6*R,S*)5-formyl tetrahydrofolate] and MTX were provided by the Drug Development Branch, National Cancer Institute (Bethesda, MD). PMX [N-[4-[2-(2-amino-3,4-dihydro-4-oxo-7H-pyrrolo[2,3-*d*]pyrimidin-5-yl)ethyl]benzoyl]-L-glutamic acid] (Alimta) was provided by Eli Lilly and Co. (Indianapolis, IN). PT523 [N(α)-(4-amino-4-deoxypteroyl)-N(δ)-hemiphthaloyl-L-ornithine] was a gift from A. Rosowsky (Boston, MA). Other chemicals were obtained from commercial sources in the highest available purities.

Cell lines. The engineered CHO sublines including RFC-, PCFT- and FRα-null MTXRIIOua^R2-4 (R2), and RFC- (PC43-10), PCFT- (R2/PCFT4), FRα- (RT16) and FRβ- (D4) expressing CHO sublines were previously described.^{118, 400-403} The CHO cells were grown in α-minimal essential medium (MEM) supplemented with 10% bovine calf serum

(Invitrogen, Carlsbad, CA), L-glutamine (2 mM), penicillin (1000 U/ml), and streptomycin (1000 µg/ml) at 37° C with 5% CO₂. R2 transfected cells (PC43-10, RT16, D4, R2/PCFT4) were cultured in complete α -MEM media plus G418 (1 mg/ml). Prior to the cell proliferation assays (*below*), RT16 and D4 cells were cultured in complete folate-free RPMI 1640 (without added folate), plus 10% dialyzed fetal bovine serum (FBS) (Sigma-Aldrich) and penicillin/streptomycin for 3 days.

KB human nasopharyngeal carcinoma cells were obtained from the American Type Culture Collection (Manassas, VA). IGROV1 (NCI-IGROV1) (passage 5) epithelial ovarian cancer cells were obtained from the Division of Cancer Treatment and Diagnosis, National Cancer Institute (Frederich, MD). KB cells were cultured in folate-free RPMI 1640 medium, supplemented with 10% FBS, penicillin-streptomycin solution, and 2 mM L-glutamine at 37°C with 5% CO₂.

For growth inhibition studies, cells (CHO, KB, IGROV1) were plated in 96 well dishes (~2000 cells/well, total volume of 200 µl) and treated with a range of drug concentrations (0-1000 nM) in complete folate-free RPMI 1640 medium with 10% dialyzed FBS, supplemented with 2 nM (RT16, D4 CHO cells, KB and IGROV1) or 25 nM (all others) LCV, as described.^{118, 159, 400} To confirm FR-mediated drug uptake, 200 nM folic acid was added to parallel incubations for RT16 and D4 cells. After 96 h, viable cells were assayed with Cell-Titer Blue™ reagent (Promega, Madison, WI) and fluorescence measured with a fluorescence plate reader. Fluorescence measurements were used for calculations of

IC₅₀s, corresponding to the drug concentrations at which cells showed 50% loss of proliferation.

To confirm the targeted pathway/enzyme, *in vitro* growth inhibition of IGROV1 tumor cells was measured in the presence of thymidine (10 μ M) or adenosine (60 μ M).^{107, 116, 118, 120, 158, 400, 404-406} For *de novo* purine biosynthesis inhibitors, additional protection experiments used AICA (320 μ M) to distinguish inhibitory effects at GARFTase from those at AICARFTase.

Folate receptor binding assays. To determine relative binding affinities of the 6-substituted pyrrolo[2,3-*d*]pyrimidine analogues to FR α and FR β , engineered CHO cells (RT16 and D4, respectively) were used.^{107, 116, 118, 120, 159, 400, 404-406} Cells were plated in 60 mm dishes (7.5 x 10⁵ cell/dish). After 2 days (~80% confluency), the cells were sequentially washed with PBS at 4° C (3x), followed by acidic buffer (10 mM sodium acetate, 150 mM NaCl, pH 3.5) (2x) to remove FR-bound folates, and finally HEPES-buffered saline (20 mM HEPES, 140 mM NaCl, 5 mM KCl, 2 mM MgCl₂, 5 mM glucose, pH7.4) (HBS). Cells were treated with [³H]folic acid (50 nM, specific activity, 0.5 Ci/mmol) in HBS in the presence and absence of unlabeled folic acid, MTX (negative control), or the 6-substituted pyrrolo[2,3-*d*]pyrimidine antifolates (10 to 1000 nM) for 15 min at 4° C. Dishes were washed with HBS at 4° C (3x), after which the cells were solubilized with 0.5 N NaOH. Aliquots of the alkaline homogenates were measured for radioactivity and protein contents. Protein concentrations were measured using Folin-phenol reagent.⁴⁰⁷ FR-bound [³H]folic acid was calculated in units of pmol/mg protein, and binding affinities were

calculated as the inverse molar ratios of unlabeled ligands required to inhibit [³H]folic acid binding by 50%. The relative binding affinity of unlabeled folic acid was assigned a value of 1.

PCFT and RFC transport assays. R2 and R2/PCFT4 CHO sublines and R1-11 and R1-11-RFC2 HeLa sublines were grown in suspension as spinner cultures at densities of 2-5 x 10⁵ cells/mL.^{121, 408} Cells were isolated by centrifugation, washed with PBS (3x), and the cell pellets (~1 x 10⁷ cells) were suspended in transport buffer (2 ml) for cellular uptake assays. PCFT-dependent uptake of 0.5 μM [³H]MTX was assayed in cell suspension over 2 min at 37° C (in a shaking water bath) in 4-morpholinopropane sulfonic (MES)-buffered saline (20 mM MES, 140 mM NaCl, 5 mM KCl, 2 mM MgCl₂, and 5 mM glucose) at pH 5.5, or in HBS at pH 6.8 in the presence or 1 or 10 μM inhibitor, while RFC-dependent uptake was measured over 2 min at 37° C in pH 7.2 HBS. Transport was quenched with ice-cold PBS after 2 min and cells were washed three times with ice-cold PBS. Cellular proteins were solubilized with 0.5 N NaOH (3 h, 37° C). Transport levels were expressed as pmol/mg protein, calculated from direct measurements of radioactivity and protein contents of the cell homogenates. Protein concentrations were measured using Folin-phenol reagent.⁴⁰⁷ Transport levels were normalized to levels in untreated (R2/PCFT4 or R1-11-RFC2) controls. To determine K_i values for the 6-pyrrolo[2,3-*d*]pyrimidine antifolates, transport was measured over 2 min with 0.5 μM [³H]MTX and 0.05-1 μM of unlabeled antifolate competitor.⁴⁰⁸ Dixon plots were used to analyze data.

Protection experiments. IGROV1 cells were plated (2000 cells/well) in folate-free RPMI 1640 medium with 10% dialyzed FBS, antibiotics, L-glutamine, and 25 nM LCV with a

range of drug concentrations in the presence of adenosine (60 μ M), thymidine (10 μ M), AICA (320 μ M) or glycine (130 μ M). Cell proliferation was assayed with Cell Titer Blue (Promega) using a fluorescence plate reader. Data are representative of at least triplicate experiments. Error bars represent the standard errors.

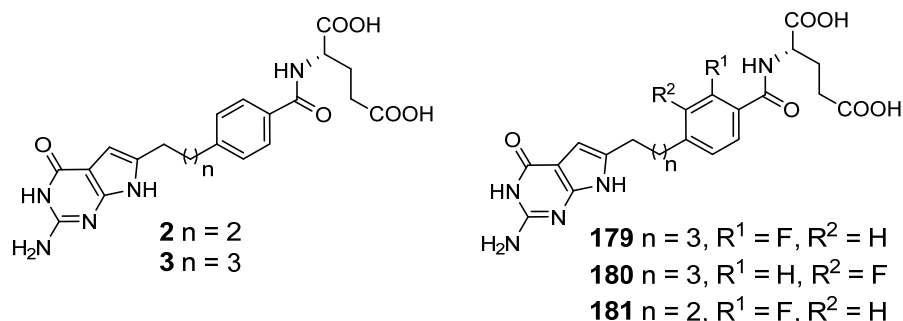
***In vivo* efficacy study with IGROV1 human EOC xenografts.** The methods for maintenance of the IGROV1 transplantable tumor xenografts, drug treatments, toxicity evaluations, and data analysis have been described previously.^{107, 405-406, 409-410} All animal studies were approved by the Institutional Animal Care and Use Committee of the Wayne State University. Briefly IGROV1 human EOC cells were implanted subcutaneously (5 x 10⁶ cells/flank) to establish a tumor xenograft model in female NCR SCID mice (NCI Animal Production Program). Mice were 10 weeks old on day 0 (tumor implant) with an average body weight of 20 g. For the study, the mice were maintained on either a folate-deficient diet from Harlan-Teklad (TD.00434) or a folate-replete diet from Lab Diet (5021; autoclavable mouse breeder diet) starting 14 days before subcutaneous tumor implant to ensure serum folate levels would approximate those of humans. Mice were supplied with food and water *ad libitum*. Folate serum levels were determined prior to tumor implant and post study via *Lactobacillus casei* bioassay.⁴¹¹ The animals on both diets were respectively pooled and implanted bilaterally subcutaneously with 30-60 mg tumor fragments with a 12 gauge trocar. Mice were again respectively pooled before unselective distribution to the various treatment and control groups. Chemotherapy began 3 days post-tumor implantation. Tumors were measured with a caliper two-to-three times weekly; mice were sacrificed when the cumulative tumor burden reached 1500 mg. Tumor weights were

estimated from two-dimensional measurements [i.e., tumor mass (in mg) = (a x b²)/2, where a and b are the tumor length and width in mm, respectively]. For calculation of end points, both tumors on each mouse were added together, and the total mass per mouse was used. Quantitative end points to assess antitumor activity include: (i) tumor growth delay [T-C, where T is the median time in days required for the treatment group tumors to reach a predetermined size (e.g., 1000 mg), and C is the median time in days for the control group tumors to reach the same size; tumor-free survivors are excluded from these calculations]; and (ii) T/C (in percent) for each treatment group when treatment (T) and control (C) groups for the control groups reached 700 mg in size (exponential growth phase). The median of each group was determined (including zeros).

C.1.1. 6-substituted, 2-amino-4-oxo pyrrolo[2,3-*d*]pyrimidine-fluorophenyl classical antifolates

The pyrrolo[2,3-*d*]pyrimidine compounds **179-181** were designed based on the 6-substituted parents pyrrolo[2,3-*d*]pyrimidine analogs **1-3** (Table 24). The synthesized analogs showed a considerable improvement in FRs and PCFT assays. While the 3C linker analog **181** has the best PCFT uptake, it also has significant uptake by RFC. The 4C linker analogs show reduced uptake by RFC by a substantial amount while maintaining/improving potent activity against PCFT-expressing cells. Between the *o*- and *m*- fluorine substitution to the L-glutamate, *o*-substitution improved the overall activity, suggesting that in the 6-substituted, 2-amino-4-oxo pyrrolo[2,3-*d*]pyrimidine classical antifolates, a 4C linker with *o*- fluorine substitution is optimal for improved activity and selectivity.

Table 24. IC₅₀ Values (nM) and protection studies of 6-substituted pyrrolo[2,3-*d*]pyrimidine antifolates **179-180**



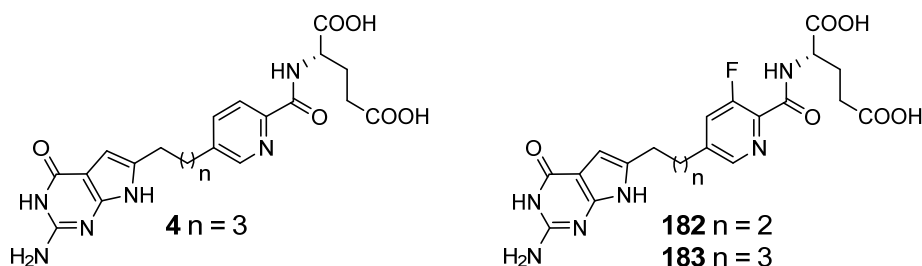
	CHO (IC ₅₀ s) (nM)					KB (IC ₅₀ s) (nM)	IGROV1 (+Thd/Ade/AICA)
	RFC PC43-10	R2	FR α RT16	FR β D4	PCFT R2/PCFT4	hRFC/hFR α /FR β /hPCFT	
2	304 (89)	>1000	4.1 (1.6)	5.6 (1.2)	23 (3.3)	1.7 (0.4)	Ade/AICA
3	>1000	>1000	6.3 (1.6)	10.0 (2)	213 (28)	1.9 (0.7)	Ade/AICA
179	>1000	>1000	0.58 (0.12)	1.6 (0.44)	23 (2)	0.59	Ade/AICA
180	>1000	>1000	1.4	0.93	207	1.67	ND
181	62 (12)	140 (27)	1.12 (0.37)	3.87 (0.14)	3.82 (0.27)	2.6	Ade/AICA

C.1.2. 6-substituted, 2-amino-4-oxo pyrrolo[2,3-*d*]pyrimidine-3'-fluoropyridyl classical antifolates

The pyrrolo[2,3-*d*]pyrimidine compounds **182** and **183** were designed based on the 6-substituted parent pyrrolo[2,3-*d*]pyrimidine analog **4** (Table 25). The 3C linker analog **182**

showed improved PCFT uptake and comparable activity in FRs, PCFT and KB cell assays. The 4C linker analog **183** showed similar activity as the parent **4** in FRs, PCFT and KB cell assays. Notably, fluorination of the pyridyl sidechain resulted in improved uptake by RFC and the 3C linker was more potent against RFC-expressing CHO cells over the 4C linker. This minimal SAR study suggests that any loss of selectivity incurred upon fluorine substitution can potentially be overcome by increasing the linker chain length.

Table 25. IC₅₀ Values (nM) and protection studies of 6-substituted pyrrolo[2,3-*d*]pyrimidine antifolates **182** and **183**

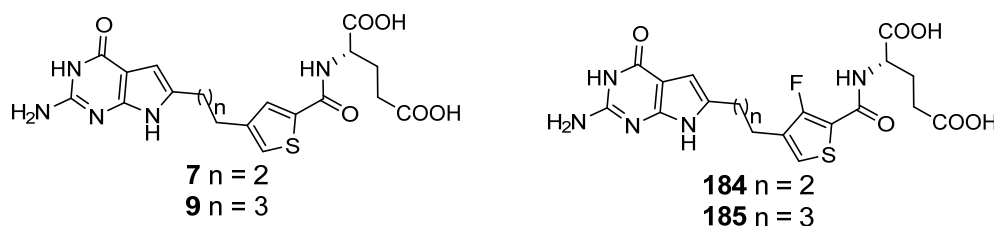


	CHO (IC ₅₀ s) (nM)					KB (IC ₅₀ s) (nM)	IGROV1 (+Thd/Ade/AICA)
	RFC PC43-10	R2	FR α RT16	FR β D4	PCFT R2/PCFT4	hRFC/hFR α /FR β /hPCFT	
4	>1000	>1000	1.3 (0.1)	0.51 (0.09)	30.4 (10.7)	0.37 (0.08)	Ade/AICA
182	45	ND	3.11	1.16	9	0.75	ND
183	468 (142)	>1000	0.69 (0.39)	0.44 (0.13)	67 (25)	0.27	Ade/AICA

C.1.3. 6-substituted, 2-amino-4-oxo pyrrolo[2,3-*d*]pyrimidine-3'-fluorothienyl classical antifolates

The pyrrolo[2,3-*d*]pyrimidine compounds **184** and **185** were designed based on the 6-substituted parent pyrrolo[2,3-*d*]pyrimidine analogs **7** and **9** (Table 26). The 3C linker analog **184** showed improved RFC and PCFT uptake and comparable activity in FRs and KB cell assays. The 4C linker analog **185** showed improved activity compared to the parent **9** in FR α and PCFT cell assays and comparable activity in FR β . Notably, fluorination of the thienyl sidechain in the 3C linker analog **184** resulted in improved uptake by RFC as well as PCFT. However, the 4C linker analog **185** showed improved PCFT activity along with selectivity over RFC. This suggests that fluorination in the 6-substituted, pyrrolo[2,3-*d*]pyrimidine thienyl series improves RFC and PCFT activity and the loss of selectivity upon fluorine substitution can potentially be overcome by increasing the linker chain length.

Table 26. IC₅₀ Values (nM) and protection studies of 6-substituted pyrrolo[2,3-*d*]pyrimidine antifolates **184** and **185**



	CHO (IC ₅₀ s) (nM)					KB (IC ₅₀ s) (nM)	IGROV1 (+Thd/Ade/AICA)
	RFC PC43-10	R2	FR α RT16	FR β D4	PCFT R2/PCFT4	hRFC/hFR α /FR β /hPCFT	
7	197 (49)	355 (10)	0.33 (0.15)	0.34 (0.03)	5.4 (1.3)	0.17 (0.05)	Ade/AICA

9	>1000	>1000	2.5 (0.5)	0.43 (0.14)	41.5 (3.1)	0.17 (0.02)	Ade/AICA
184	20.1 (6.2)	20.5 (1.6)	0.14 (0.03)	0.19 (0.02)	1.5 (0.4)	0.26	Ade/AICA
185	>1000	>1000	0.36 (0.13)	0.75 (0.42)	6.00 (0.94)	0.33	Ade/AICA

In vivo antitumor efficacy for compound 185 with IGROV1 EOC xenografts.

Based on the in vitro efficacies of **185** (Table 26), we extended our studies to an in vivo drug efficacy trial. The in vivo trial was performed with female NCR severe combined immunodeficient (SCID) mice bilaterally (subcutaneous) implanted with IGROV1 human EOC xenografts. In vivo efficacy for **185** was compared to that for **5**, the most active PCFT-targeted pyrrolo[2,3-*d*]pyrimidine analogue previously identified.^{158-159, 166, 405} For the trial, the mice were fed a folate-deficient diet *ad libitum* to reduce serum folate concentrations to levels approximating those reported in humans.⁴¹² A control cohort included tumor-bearing mice fed standard (folate-replete) chow. Mice were non-selectively randomized into control and treatment groups (5 mice/group). The pyrrolo[2,3-*d*]pyrimidine compounds were administered intravenously (IV) beginning on day 3 following tumor engraftment, using doses slightly below their respective maximum tolerated doses. Dosing was as follows: **185**, Q4dX4 at 95 mg/kg/inj, for a total dose of 380 mg/kg; and **5**, Q4dX3 at 32 mg/kg/inj, for a total dose of 96 mg/kg. The tumors were measured twice each week; overall health and body weights of the mice were recorded daily. For mice on the folate-deficient diet, both compounds **5** and **185** were efficacious. On day 60, the median tumor burdens were 700 mg (range, 259-1153 mg) for the control, 108 mg (range, 0-196 mg) for **5**, and 0 mg (range, 0-523 mg) for **185**, giving T/C values (based on median tumor

measurements) of 15% for **5** and 0% for **185**. Tumor growth delays (T-C to reach 1000 mg in days) of 28 days for **5** and 35 days for **185** were recorded (Figure 72). Treatments with **5** and **185** were generally well tolerated with moderate weight losses (15.7% median nadir on day 14 and 12.1% median nadir on day 18) that were completely reversible upon conclusion of therapy. For mice on the standard (high folate) diet, antitumor activities for **5** and **185** were ablated. No weight losses or other adverse symptoms were observed.

The results from the in vivo efficacy trial with FR α - and PCFT-expressing IGROV1 human EOC xenografts substantiate our in vitro antitumor efficacy results and establish that at equitoxic dose levels, **185** is more efficacious in vivo than **5**, as reflected in the T/C and T-C metrics, albeit with a higher dose requirement. For both **5** and **185**, there were no acute or long term toxicities other than completely reversible loss of weight.

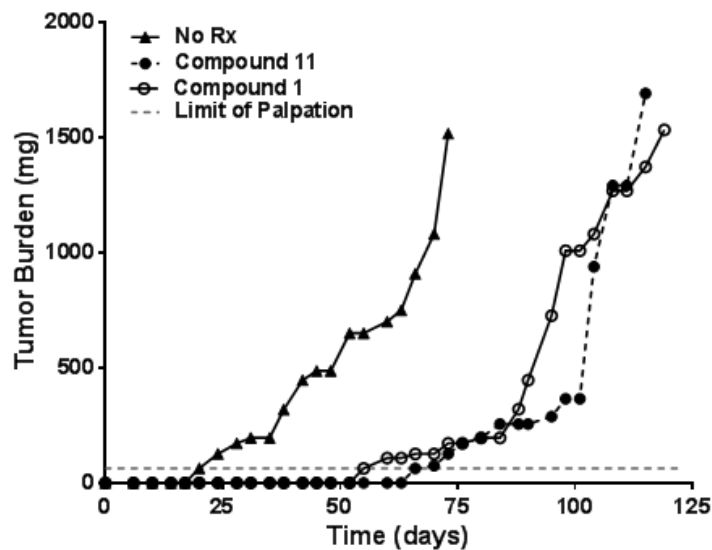


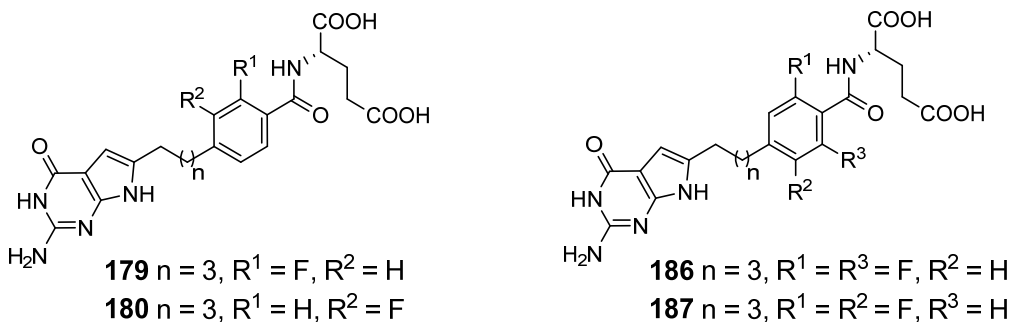
Figure 72. In vivo efficacies of compounds 185 and 5 toward the IGROV1 EOC xenografts. Female ICR SCID mice (10 weeks old; 20 g average body weight) were maintained on a folate-deficient diet *ad libitum* for 14 d prior to subcutaneous tumor

implant to decrease serum folate to a concentration approximating that in human serum. Human IGROV1 tumors were implanted bilaterally and mice were non-selectively randomized into 5 mice/group. Dosing began on day 3 following engraftment and was as follows: **11**, Q4dX4 at 95 mg/kg/inj, total dose of 380 mg/kg; and **1**, Q4dX3 at 32 mg/kg/inj, total dose of 96mg/kg. The drugs were dissolved in 5% ethanol (v/v), 1% Tween-80 (v/v), and 0.5% NaHCO₃ and were administered intravenously (0.2 ml/injection). The tumors were measured twice each week.

C.1.4. 6-substituted, 2-amino-4-oxo pyrrolo[2,3-*d*]pyrimidine-difluorophenyl classical antifolates

The pyrrolo[2,3-*d*]pyrimidine compounds **186** and **187** were designed based on the 6-substituted pyrrolo[2,3-*d*]pyrimidine 2'-fluorophenyl analogs **179-180** (Table 27). The most notable change in the activity brought about by difluorination is the loss of PCFT activity in all of the synthesized compounds. This implies that while mono fluorination improves PCFT activity as previously described, difluorination or fluorine scan with more than one fluorine atom substitution is detrimental towards uptake by PCFT.

Table 27. IC₅₀ Values (nM) and protection studies of 6-substituted pyrrolo[2,3-*d*]pyrimidine antifolates **186** and **187**.

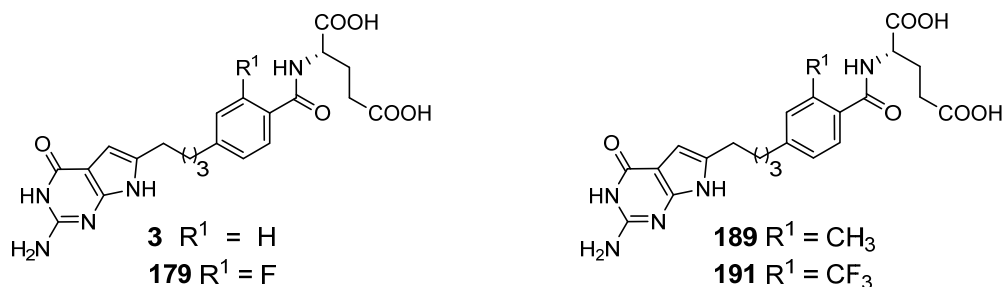


	CHO (IC50s) (nM)					KB (IC50s) (nM)	IGROV1 (+Thd/Ade /AICA)
	RFC PC43- 10	R2	FR α RT16	FR β D4	PCFT R2/PCFT4	hRFC/hFR α / FR β /hPCFT	
179	>1000	>1000	0.58 (0.12)	1.6 (0.44)	23 (2)	0.59	Ade/AICA
180	>1000	>1000	1.4	0.93	207	1.67	ND
181	62 (12)	140 (27)	1.12 (0.37)	3.87 (0.14)	3.82 (0.27)	2.6	Ade/AICA
186	>1000	>1000	1.45	1.28	769.3	2.37	ND
187	>1000	>1000	5.2	0.47	592	0.32	ND

C.1.5. 6-substituted, 2-amino-4-oxo pyrrolo[2,3-*d*]pyrimidine-2'-substitutedphenyl classical antifolates

The pyrrolo[2,3-*d*]pyrimidine compounds **189** and **191** were designed based on the 6-substituted pyrrolo[2,3-*d*]pyrimidine 2'-fluorophenyl analog **179** (Table 28). The important structure activity relationship obtained from this study is the importance of sterics at the 2'-position, as the activity is systematically reduced upon gradual increase in size. From the PCFT activity, it is also apparent that PCFT uptake is most sensitive to size of the side chain substitution, indicating a narrower pocket compared to the FRs.

Table 28. IC₅₀ Values (nM) and protection studies of 6-substituted pyrrolo[2,3-*d*]pyrimidine antifolates **189** and **191**



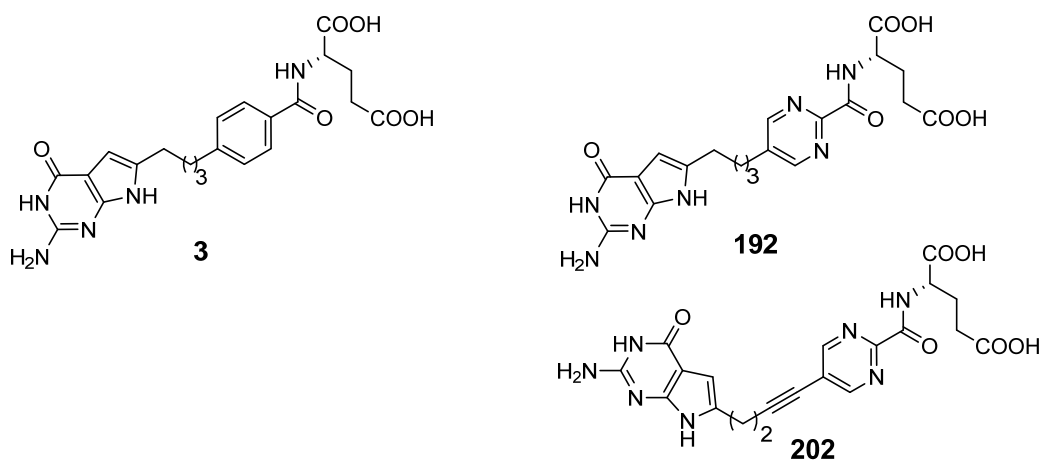
	CHO (IC ₅₀ s) (nM)					KB (IC ₅₀ s) (nM)	IGROV1 (+Thd/Ade/AICA)
	RFC PC43-10	R2	FR α RT16	FR β D4	PCFT R2/PCFT4	hRFC/hFR α /FR β /hPCFT	
3	>1000	>1000	6.3 (1.6)	10.0 (2)	213 (28)	1.9 (0.7)	Ade/AICA
179	>1000	>1000	0.58 (0.12)	1.6 (0.44)	23 (2)	0.59	Ade/AICA
189	>1000	>1000	2.23	7.16	>1000	0.67	ND
191	>1000	>1000	12	57.4	>1000	>1000	ND

C.1.6. 6-substituted, 2-amino-4-oxo pyrrolo[2,3-*d*]pyrimidine-pyrimidyl classical antifolates

The pyrrolo[2,3-*d*]pyrimidine compounds **192** was designed based on the 6-substituted pyrrolo[2,3-*d*]pyrimidine-phenyl analog **3** (Table 29). The important structure activity relationship obtained from this variation is the influence of electronics of the sidechain. We already know from previous SAR studies (Tables 2 and 4) that varying the sidechain (het)aryl ring significantly varies the tumor cell potency as well as transporter selectivities.

Replacing the sidechain phenyl with a pyrimidyl ring did not influence the RT16 and KB cell activities but brought about a considerable activity difference in D4 and R2/PCFT4 CHO cells. From the loss of R2/PCFT4 activity, it is apparent that along with sterics of the sidechain (Table 28), binding to/transport by PCFT is also influenced by the electronics of the side chain aryl ring.

Table 29. IC₅₀ Values (nM) of 6-substituted pyrrolo[2,3-*d*]pyrimidine antifolate **192**

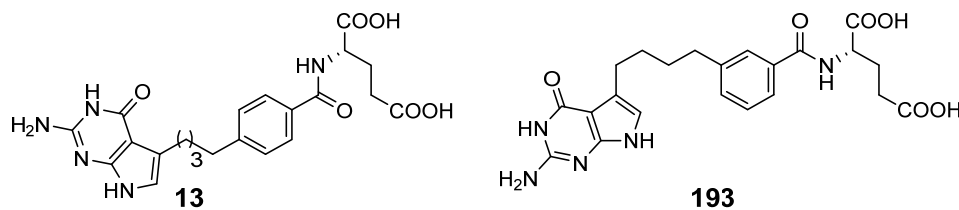


	CHO (IC ₅₀ s) (nM)					KB (IC ₅₀ s) (nM)	IGROV1 (+Thd/Ade/AICA)
	RFC PC43-10	R2	FR α RT16	FR β D4	PCFT R2/PCFT4	hRFC/hFR α / FR β /hPCFT	
3	>1000	>1000	6.3 (1.6)	10.0 (2)	213 (28)	1.9 (0.7)	Ade/AICA
192	>1000	>1000	6.33	1.96	>1000	0.56	ND
202	>1000	>1000	5.8	0.52	>1000	44.5	ND

C.2.1. 5-substituted, 2-amino-4-oxo pyrrolo[2,3-*d*]pyrimidine-3'-butylphenyl classical antifolates

The 1',3'-substituted, pyrrolo[2,3-*d*]pyrimidine compounds **193** was designed based on the 5-substituted pyrrolo[2,3-*d*]pyrimidine-phenyl analog **13** (Table 30). The anticipated loss of activity across all the cell lines, upon rearranging the relative substitution of the linker and the sidechain L-glutamate reestablished that the conformation of the scaffold and side-chain, as a consequence of linker length and flexibility, plays an important role in overall activity. The important structure activity relationship obtained from this variation is that in the 5-substituted pyrrolo[2,3-*d*]pyrimidine-phenyl analogs 1',3'-relative substitution of the glutamate tail and scaffold is detrimental to activity.

Table 30. IC₅₀ Values (nM) of 5-substituted pyrrolo[2,3-*d*]pyrimidine antifolate **193**

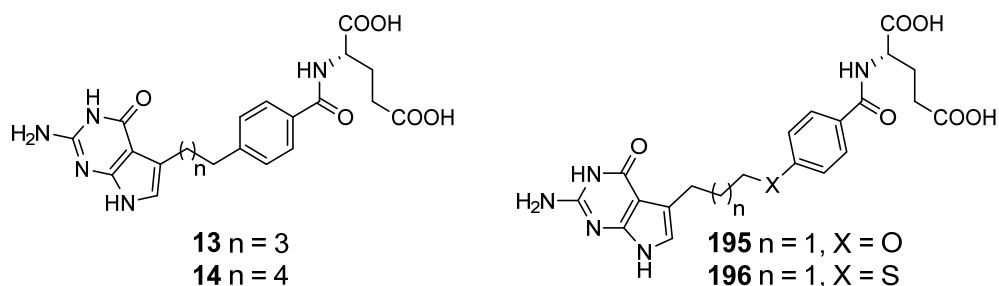


	CHO (IC ₅₀ s) (nM)					KB (IC ₅₀ s) (nM)	IGROV1 (+Thd/Ade/AICA)
	RFC PC43-10	R2	FR α RT16	FR β D4	PCFT R2/PCFT4	hRFC/hFR α / FR β /hPCFT	
13	56.6 (5.8)	>1000	8.6 (2.1)	6.99	840 (90)	12.7 (5.4)	Ade
194	608	>1000	>1000	>1000	>1000	>1000	ND

C.2.2. 5-substituted, 2-amino-4-oxo pyrrolo[2,3-*d*]pyrimidine-4'-propyloxy/propylthio/propylamino/butylaminophenyl classical antifolates

The compounds **195** and **196** with a heteroatom substitution of benzylic CH₂ was designed based on the 5-substituted pyrrolo[2,3-*d*]pyrimidine-phenyl analog **13** (Table 31) to evaluate the influence of varied bond angles of the benzylic position on selectivity and potency. Though heteroatom substitution resulted in reduced KB cell and RT16 potencies, there was a considerable improvement in activity against R2/PCFT4 cells. In **196** with a propyloxy linker, a significant improvement in FR β activity was also observed. Additionally, the loss of overall activity upon increasing the linker length from 4C in **13** to 5C in **14**, despite improved selectivity, was slightly compensated in **196** with a restoration of activity against R2/PCFT4 cells along with improved selectivity. It would be worthwhile to explore the role of heteroatom substitutions further in the 5-substituted, pyrrolo[2,3-*d*]pyrimidine analogs, especially for improved selectivity via increased uptake by FR β and PCFT and decreased uptake by RFC.

Table 31. IC₅₀ Values (nM) of 5-substituted pyrrolo[2,3-*d*]pyrimidine antifolates **195** and **196**



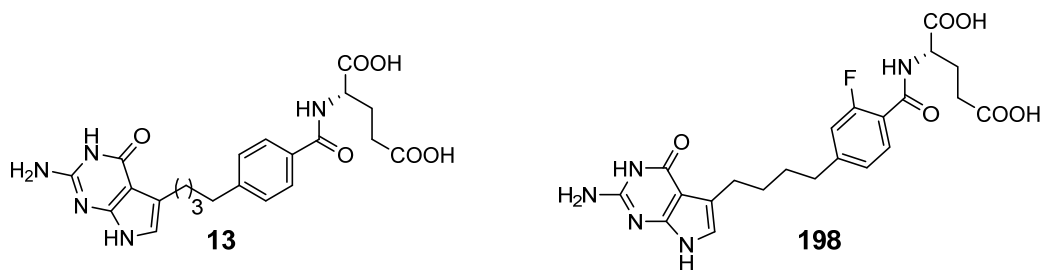
	CHO (IC _{50s}) (nM)	KB (IC _{50s}) (nM)	IGROV1

	RFC PC43- 10	R2	FRα RT16	FRβ D4	PCFT R2/PCFT 4	hRFC/hFRα/ FRβ/hPCFT	(+Thd/Ade /AICA)
13	56.6 (5.8)	>1000	8.6 (2.1)	6.99	840 (90)	12.7 (5.4)	Ade
14	196.4 (55)	>1000	33.5 (2.5)	ND	>1000	17.3 (8.9)	Ade/AICA
195	53.2	>1000	39.02	1.94	390	36.76	ND
196	>1000	>1000	291.5	78.5	549	46.01	ND

C.2.3. 5-substituted, 2-amino-4-oxo pyrrolo[2,3-*d*]pyrimidine-butyl-2'-fluorophenyl classical antifolates

The compound **198** with a 2'-fluorine substitution on the sidechain phenyl was designed based on the 5-substituted pyrrolo[2,3-*d*]pyrimidine-phenyl analog **13** (Table 32) to evaluate the influence on PCFT uptake. As observed in the 6-substituted pyrrolo[2,3-*d*]pyrimidines 2'-[ortho (o-) to the L-glutamate] fluorine substitution dramatically increased PCFT-mediated antiproliferative activity of R2/PCFT4 cells. The impact of 2'-fluorine substitution on potencies against all the other cell lines remained similar. This preliminary data encourages the design, synthesis and evaluation of novel fluorinated, 5-substituted pyrrolo[2,3-*d*]pyrimidine analogues.

Table 32. IC₅₀ Values (nM) of 5-substituted pyrrolo[2,3-*d*]pyrimidine antifolate **198**



	CHO (IC ₅₀ s) (nM)					KB (IC ₅₀ s) (nM)	IGROV1 (+Thd/Ade/AICA)
	RFC PC43-10	R2	FR α RT16	FR β D4	PCFT R2/PCFT4	hRFC/hFR α / FR β /hPCFT	
13	56.6 (5.8)	>1000	8.6 (2.1)	6.99	840 (90)	12.7 (5.4)	Ade
198	40	>1000	5.23	2.11	52.7	7.99	Ade

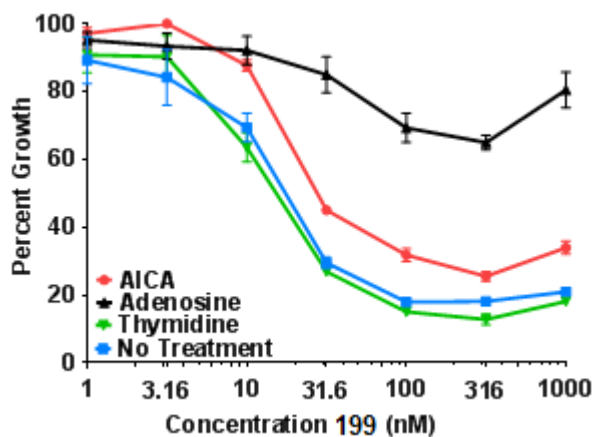


Figure 73. Growth inhibition assay of **198** in IGROV1 EOC cells and protection by nucleosides and AICA.

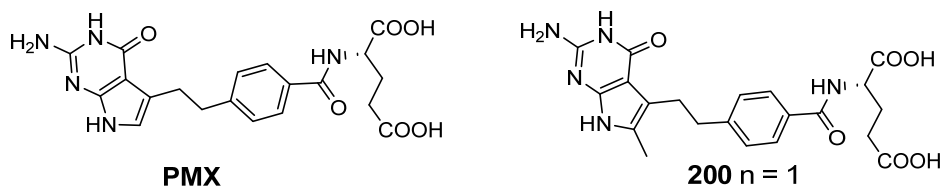
To investigate the intracellular targeted pathway/enzyme of **198**, in vitro growth inhibition of IGROV1 tumor cells was measured in the presence of thymidine (10 μ M) or adenosine (60 μ M), or glycine (). For de novo purine biosynthesis inhibitors, additional protection experiments used AICA (320 μ M) to distinguish inhibitory effects at GARFTase from those at AICARFTase. The results were normalized to those of untreated cells (no drug). The results shown are representative of triplicate experiments (Figure 73). The IGROV tumor cells were not protected by thymidine, suggesting that **199** is not a TS inhibitor. AICA only partially protected the cells, indicating a dual GARFTase and AICARFtase inhibition. However, partial protection by adenosine and complete protection by glycine at higher concentrations (data not shown) of **198**, suggests additional intracellular targets (SHMT inhibition). Further studies are underway to investigate the possible targets.

C.3.1. 5-substituted, 2-amino-4-oxo-6-methyl pyrrolo[2,3-*d*]pyrimidine classical antifolates

Based on the general trend of reduced RFC binding by the 6-substituted pyrrolo[2,3-*d*]pyrimidine series of analogs, compound **200** with a 6-methyl substitution was designed as a direct analog of 5-substituted pyrrolo[2,3-*d*]pyrimidine **PMX** (Table 33) to evaluate for selectivity over RFC. As expected, the activity against PC43-10 was drastically reduced, implying a loss of uptake by RFC. Additionally, activities against KB tumor cells and D4 cells also improved. While the activity against RT16 remained roughly similar, the uptake by PCFT was reduced as reflected by the \sim 8 fold loss in R2/PCFT4 activity. Nevertheless, the drastic improvement in selectivities for FRs and PCFT over RFC (Table 34) mainly due to the much needed loss of RFC uptake when compared with clinically

used **PMX** is a remarkable development and warrants future explorations of 6-alkylated, 5-substituted pyrrolo[2,3-*d*]pyrimidine classical antifolates.

Table 33. IC₅₀ Values (nM) and protection studies of 5-substituted, 6-methyl pyrrolo[2,3-*d*]pyrimidine antifolate **200**



	CHO (IC ₅₀ s) (nM)					KB (IC ₅₀ s) (nM)	IGROV1 (+Thd/Ade/AICA)
	RFC PC43-10	R2	FR α RT16	FR β D4	PCFT R2/PCFT4	hRFC/hFR α / FR β /hPCFT	
PMX	26.2 (5.5)	138 (13)	42 (9)	60 (8)	8.3 (2.7)	68 (12)	Thd/Ade
200	>1000	>1000	94.7	5.7	65	28.5	Ade/AICA

To investigate the intracellular targeted pathway/enzyme of **200**, in vitro growth inhibition of IGROV1 tumor cells was measured in the presence of thymidine (10 μ M) or adenosine (60 μ M), or glycine (130 μ M) (Figure 74). For de novo purine biosynthesis inhibitors, additional protection experiments used were, AICA (320 μ M) to distinguish inhibitory effects at GARFTase from those at AICARFTase. The results shown are representative of triplicate experiments. The IGROV tumor cells were not protected by thymidine, suggesting that **200** is not a TS inhibitor. Both adenosine and AICA completely protected the cells across the concentration range, indicating GARFTase inhibition. Unlike **PMX**, its

6-methylated analog **200** is not only a potential tumor-targeted inhibitor due to selectivity over RFC but primarily inhibits purine biosynthesis as a novel mechanism of action. As such, desirably, **200** is expected to not only circumvent the DLTs associated with **PMX** but also to overcome the PMX-associated drug-resistance due to its novel mechanism of action.

Table 34. Selectivity ratios of **PMX** and **200** for FR α (RT16) FR β (D4) and PCFT (PCFT4) over RFC (PC43-10)

	PC43-10/RT16	PC43-10/D4	PC43-10/PCFT4
PMX	0.62	0.43	3.15
200	10.5	175.4	>15

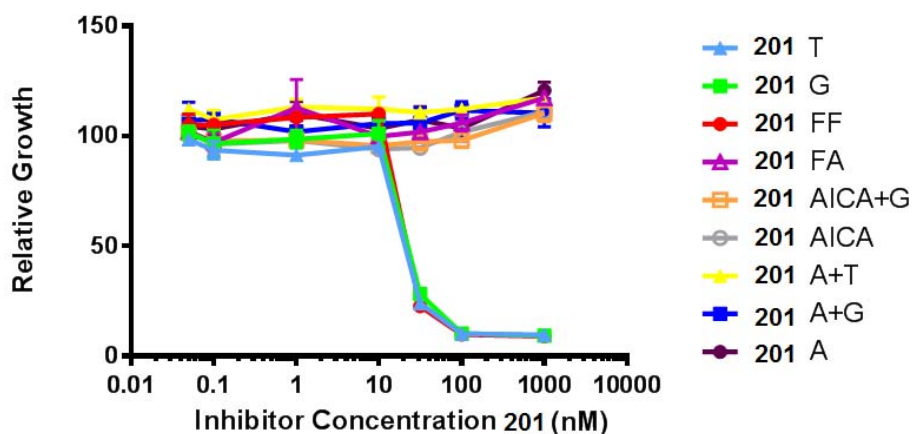


Figure 74. Growth inhibition assays of **200** against IGROV1 EOC cells and protection by excess folic acid, folate free media, nucleosides, glycine, and AICA.

Appendix bibliography:

1. Deng, Y.; Wang, Y.; Cherian, C.; Hou, Z.; Buck, S. A.; Matherly, L. H.; Gangjee, A., Synthesis and discovery of high affinity folate receptor-specific glycinamide ribonucleotide formyltransferase inhibitors with antitumor activity. *J. Med. Chem.* **2008**, *51*, 5052-5063.
2. Deng, Y.; Zhou, X.; Kugel Desmoulin, S.; Wu, J.; Cherian, C.; Hou, Z.; Matherly, L. H.; Gangjee, A., Synthesis and biological activity of a novel series of 6-substituted thieno[2,3-*d*]pyrimidine antifolate inhibitors of purine biosynthesis with selectivity for high affinity folate receptors over the reduced folate carrier and proton-coupled folate transporter for cellular entry. *J. Med. Chem.* **2009**, *52*, 2940-2951.
3. Flintoff, W. F.; Davidson, S. V.; Siminovitch, L., Isolation and partial characterization of three methotrexate-resistant phenotypes from Chinese hamster ovary cells. *Somatic Cell Genet.* **1976**, *2*, 245-261.
4. Wong, S. C.; Proefke, S. A.; Bhushan, A.; Matherly, L. H., Isolation of human cDNAs that restore methotrexate sensitivity and reduced folate carrier activity in methotrexate transport-defective Chinese hamster ovary cells. *J. Biol. Chem.* **1995**, *270*, 17468-17475.
5. Flintoff, W. F.; Nagainis, C. R., Transport of methotrexate in Chinese hamster ovary cells: a mutant defective in methotrexate uptake and cell binding. *Arch. Biochem. Biophys.* **1983**, *223*, 433-440.
6. Hou, Z.; Gattoc, L.; O'Connor, C.; Yang, S.; Wallace-Povirk, A.; George, C.; Orr, S.; Polin, L.; White, K.; Kushner, J.; Morris, R. T.; Gangjee, A.; Matherly, L. H., Dual targeting of epithelial ovarian cancer via folate receptor α and the proton-coupled folate transporter with 6-substituted pyrrolo[2,3-*d*]pyrimidine antifolates. *Mol. Cancer. Ther.* **2017**, *16*, 819-830.
7. Golani, L. K.; George, C.; Zhao, S.; Raghavan, S.; Orr, S.; Wallace, A.; Wilson, M. R.; Hou, Z.; Matherly, L. H.; Gangjee, A., Structure-activity profiles of novel 6-substituted pyrrolo[2,3-*d*]pyrimidine thienoyl antifolates with modified amino acids for cellular uptake by folatereceptors alpha and beta and the proton-coupled folate transporter. *J. Med. Chem.* **2014**, *57*, 8152-8166.
8. Mitchell-Ryan, S.; Wang, Y.; Raghavan, S.; Ravindra, M. P.; Hales, E.; Orr, S.; Cherian, C.; Hou, Z.; Matherly, L. H.; Gangjee, A., Discovery of 5-substituted pyrrolo[2,3-*d*]pyrimidine antifolates as dual-acting inhibitors of glycinamide ribonucleotide formyltransferase and 5-aminoimidazole-4-carboxamide ribonucleotide formyltransferase in de novo purine nucleotide biosynthesis: Implications of inhibiting 5-aminoimidazole-4-carboxamide ribonucleotide formyltransferase to AMPK activation and antitumor activity. *J. Med. Chem.* **2013**, *56*, 10016-10032.
9. Wang, L.; Cherian, C.; Kugel Desmoulin, S.; Mitchell-Ryan, S.; Hou, Z.; Matherly, L. H.; Gangjee, A., Synthesis and biological activity of 6-substituted pyrrolo[2,3-*d*]pyrimidine thienoyl regioisomers as inhibitors of de novo purine biosynthesis with

selectivity for cellular uptake by high affinity folate receptors and the proton-coupled folate transporter over the reduced folate carrier. *J. Med. Chem.* **2012**, *55*, 1758-1770.

10. Wang, L.; Cherian, C.; Kugel Desmoulin, S.; Polin, L.; Deng, Y.; Wu, J.; Hou, Z.; White, K.; Kushner, J.; Matherly, L. H.; Gangjee, A., Synthesis and antitumor activity of a novel series of 6-substituted pyrrolo[2,3-*d*]pyrimidine thienoyl antifolate inhibitors of purine biosynthesis with selectivity for high affinity folate receptors and the proton-coupled folate transporter over the reduced folate carrier for cellular entry. *J. Med. Chem.* **2010**, *53*, 1306-1318.

11. Wang, L.; Kugel Desmoulin, S.; Cherian, C.; Polin, L.; White, K.; Kushner, J.; Fulterer, A.; Chang, M. H.; Mitchell-Ryan, S.; Stout, M.; Romero, M. F.; Hou, Z.; Matherly, L. H.; Gangjee, A., Synthesis, biological, and antitumor activity of a highly potent 6-substituted pyrrolo[2,3-*d*]pyrimidine thienoyl antifolate inhibitor with proton-coupled folate transporter and folate receptor selectivity over the reduced folate carrier that inhibits beta-glycinamide ribonucleotide formyltransferase. *J. Med. Chem.* **2011**, *54*, 7150-7164.

12. Wang, L.; Wallace, A.; Raghavan, S.; Deis, S. M.; Wilson, M. R.; Yang, S.; Polin, L.; White, K.; Kushner, J.; Orr, S.; George, C.; O'Connor, C.; Hou, Z.; Mitchell-Ryan, S.; Dann, C. E., 3rd; Matherly, L. H.; Gangjee, A., 6-Substituted pyrrolo[2,3-*d*]pyrimidine thienoyl regioisomers as targeted antifolates for folate receptor alpha and the proton-coupled folate transporter in human tumors. *J. Med. Chem.* **2015**, *58*, 6938-6959.

13. Wilson, M. R.; Hou, Z.; Yang, S.; Polin, L.; Kushner, J.; White, K.; Huang, J.; Ratnam, M.; Gangjee, A.; Matherly, L. H., Targeting nonsquamous nonsmall cell lung cancer via the proton-coupled folate transporter with 6-substituted pyrrolo[2,3-*d*]pyrimidine thienoyl antifolates. *Mol. Pharmacol.* **2016**, *89*, 425-434.

14. Lowry, O. H.; Rosebrough, N. J.; Farr, A. L.; Randall, R. J., Protein measurement with the Folin phenol reagent. *J. Biol. Chem.* **1951**, *193*, 265-275.

15. Kugel Desmoulin, S.; Wang, Y.; Wu, J.; Stout, M.; Hou, Z.; Fulterer, A.; Chang, M. H.; Romero, M. F.; Cherian, C.; Gangjee, A.; Matherly, L. H., Targeting the proton-coupled folate transporter for selective delivery of 6-substituted pyrrolo[2,3-*d*]pyrimidine antifolate inhibitors of de novo purine biosynthesis in the chemotherapy of solid tumors. *Mol. Pharmacol.* **2010**, *78*, 577-587.

16. Wang, L.; Wallace, A.; Raghavan, S.; Deis, S. M.; Wilson, M. R.; Yang, S.; Polin, L.; White, K.; Kushner, J.; Orr, S.; George, C.; O'Connor, C.; Hou, Z.; Mitchell-Ryan, S.; Dann, C. E.; Matherly, L. H.; Gangjee, A., 6-Substituted Pyrrolo[2,3-*d*]pyrimidine Thienoyl Regioisomers as Targeted Antifolates for Folate Receptor α and the Proton-Coupled Folate Transporter in Human Tumors. *Journal of Medicinal Chemistry* **2015**, *58* (17), 6938-6959.

17. Polin, L.; Valeriote, F.; White, K.; Panchapor, C.; Pugh, S.; Knight, J.; LoRusso, P.; Hussain, M.; Liversidge, E.; Peltier, N.; Golakoti, T.; Patterson, G.; Moore, R.; Corbett, T. H., Treatment of human prostate tumors PC-3 and TSU-PR1 with standard and investigational agents in SCID mice. *Invest. New Drugs* **1997**, *15*, 99-108.

18. Golani, L. K.; Wallace-Povirk, A.; Deis, S. M.; Wong, J. E.; Ke, J.; Gu, X.; Raghavan, S.; Wilson, M. R.; Li, X.; Polin, L.; de Waal, P. W.; White, K.; Kushner, J.; O'Connor, C.; Hou, Z.; Xu, H. E.; Melcher, K.; Dann, C. E.; Matherly, L. H.; Gangjee, A., Tumor Targeting with Novel 6-Substituted Pyrrolo [2,3-*d*] Pyrimidine Antifolates with Heteroatom Bridge Substitutions Via Cellular Uptake by Folate Receptor α and the Proton-coupled Folate Transporter and Inhibition of De Novo Purine Nucleotide Biosynthesis. *J. Med. Chem.* **2016**, *59*, 7856-7876.
19. Varela-Moreiras, G.; Selhub, J., Long-term folate deficiency alters folate content and distribution differentially in rat tissues. *J. Nutr.* **1992**, *122*, 986-991.
20. Cherian, C.; Desmoulin, S. K.; Wang, L.; Polin, L.; White, K.; Kushner, J.; Stout, M.; Hou, Z.; Gangjee, A.; Matherly, L. H., Therapeutic targeting malignant mesothelioma with a novel 6-substituted pyrrolo[2,3-*d*]pyrimidine thienoyl antifolate via its selective uptake by the proton-coupled folate transporter. *Cancer Chemother. Pharmacol.* **2013**, *71*, 999-1011.
21. Alati, T.; Worzalla, J. F.; Shih, C.; Bewley, J. R.; Lewis, S.; Moran, R. G.; Grindey, G. B., Augmentation of the therapeutic activity of lometrexol [(6-*R*)5,10-dideazatetrahydrofolate] by oral folic acid. *Cancer Res.* **1996**, *56*, 2331-2335.